CENTRAL RESEARCH LIBRARY

ORNL-5112

Cy 1

# Mechanical Properties Test Data for Structural Materials Quarterly Progress Report for Period Ending January 31, 1976

[redacted]

OAK RIDGE NATIONAL LABORATORY
CENTRAL RESEARCH LIBRARY
DOCUMENT COLLECTION
LIBRARY LOAN COPY
DO NOT TRANSFER TO ANOTHER PERSON
If you wish someone else to see this document, send in name with document and the library will arrange a loan.
UCN-7969
(3 3-67)

OAK RIDGE NATIONAL LABORATORY
OPERATED BY UNION CARBIDE CORPORATION FOR THE ENERGY RESEARCH AND DEVELOPMENT ADMINISTRATION

Printed in the United States of America. Available from
the Energy Research and Development Administration,
Technical Information Center
P.O. Box 62, Oak Ridge, Tennessee 37830
Price: Printed Copy $11.00 ; Microfiche $2.25

This report was prepared as an account of work sponsored by the United States Government. Neither the United States nor the Energy Research and Development Administration, nor any of their employees, nor any of their contractors, subcontractors, or their employees, makes any warranty, express or implied, or assumes any legal liability or responsibility for the accuracy, completeness or usefulness of any information, apparatus, product or process disclosed, or represents that its use would not infringe privately owned rights.

ORNL-5112
UC-79-b, -h, -k
(Liquid Metal Fast
Breeder Reactors)

Contract No. W-7405-eng-26

METALS AND CERAMICS DIVISION

# MECHANICAL PROPERTIES TEST DATA FOR STRUCTURAL MATERIALS QUARTERLY PROGRESS REPORT FOR PERIOD ENDING JANUARY 31, 1976

Aerojet Nuclear Company
Argonne National Laboratory
Oak Ridge National Laboratory
Naval Research Laboratory
Hanford Engineering Development Laboratory
Westinghouse Advanced Reactors Division
University of Cincinnati
University of California at Los Angeles
General Electric Company

Compiled by M. R. Hill

MARCH 1976

OAK RIDGE NATIONAL LABORATORY
Oak Ridge, Tennessee 37830
operated by
UNION CARBIDE CORPORATION
for the
ENERGY RESEARCH AND DEVELOPMENT ADMINISTRATION

## FOREWORD

This is the tenth in a series of progress reports, the purpose of which is to record and distribute quarterly the collected results of all structural materials mechanical properties test programs sponsored by the Reactor Research and Development Division of the Energy Research and Development Administration.

To be useful as resource documents, the reports in this series must be published and distributed in a timely manner to those in the reactor design and materials technology community who have a need of mechanical property test data for nuclear reactor and power plant applications. A test and material index is included to increase the effectiveness of the report.

Reports previously issued in this series are as follows: ORNL-4936, period ending October 31, 1973; ORNL-4948, period ending January 31, 1974; ORNL-4963, period ending April 30, 1974; ORNL-4998, period ending July 31, 1974; ORNL-5103, period ending October 31, 1974; ORNL-5104, period ending January 31, 1975; ORNL-5105 for period ending April 30, 1975; ORNL-5106 for period ending July 31, 1975, and ORNL-5107 for period ending October 31, 1975. The next quarterly report will be for the period ending April 30, 1976, and contributions are due at ORNL by May 15, 1976.

W. R. Martin
Metals and Ceramics Division
Oak Ridge National Laboratory

CONTENTS

SUMMARY . . . . . ix

1. AEROJET NUCLEAR COMPANY . . . . . 1

1.1 INTRODUCTION . . . . . 1

1.2 MECHANICAL PROPERTY PROGRAM OF ALLOY 718 . . . . . 1

1.2.1 Low Cycle Fatigue Tests . . . . . 1

1.2.2 Mean Stress Effects on High Cycle Fatigue . . . . 6

1.2.3 Stress Rupture Tests . . . . . 11

1.3 REFERENCES . . . . . 18

2. ARGONNE NATIONAL LABORATORY . . . . . 19

2.1 INTRODUCTION . . . . . 19

2.2 SODIUM EFFECTS ON LMFBR MATERIALS . . . . . 19

2.2.1 Influence of Sodium Environment on the Low-cycle Fatigue Behavior of Austenitic Stainless Steels . . . . . 19

2.2.2 Uniaxial Creep-Rupture Properties of Austenitic Stainless Steels . . . . . 21

2.2.2.1 Creep-Rupture Correlations . . . . . 30

2.3 REFERENCES . . . . . 35

3. OAK RIDGE NATIONAL LABORATORY . . . . . 37

3.1 INTRODUCTION . . . . . 37

3.2 MECHANICAL PROPERTIES AND BEHAVIOR FOR STRUCTURAL MATERIALS . . . . . 37

3.2.1 Mechanical Property Characterization of Type 304 Stainless Steel Reference Heat . . . . . 37

3.2.1.1 Creep and Rupture Properties of the 51-mm (2-in.) Plate of Reference Heat. . 37

3.2.2 Heat-to-Heat Variations of Mechanical Properties of Austenitic Stainless Steels of Types 304 and 316 . . . . . 44

3.2.2.1 Relation Between Tensile and Creep Properties . . . . . 44

3.2.2.2 Effect of Thermal Aging on Tensile and Creep Properties of Types 304 and 316 Stainless Steel . . . . . 56

3.2.3 Materials Behavior in Support of Development and Evaluation of Failure Criteria for Materials . . . . . 67

3.2.3.1 Development of Creep Equation for Type 304 Stainless Steel . . . . . 67

3.2.4 Computerized Data Management System . . . . . 74

3.2.5 Elastic Properties of Engineering Construction Materials . . . . . 75

3.2.5.1 Elastic Properties Determined by Static Tests . . . . . 77

3.3 MECHANICAL AND METALLURGICAL BEHAVIOR OF WELDMENTS FOR LMFBR . . . . . 80

3.3.1 Preliminary Report on Effect of Postweld Heat Treatment on Type 308 Stainless Steel Submerged-Arc Welds . . . . . 80

3.3.2 Studies of Strain Distribution in Weldments and Room-Temperature Elastic Constants . . . . . 85

3.3.2.1 Summary of Applicable Formulae Used to Determine Elastic Compliances. . . . . 86

3.3.2.2 Elastic Compliance and Stiffness Results . . . . . 88

3.3.2.3 Remarks on Results and Test Procedures . 90

3.4 MECHANICAL PROPERTIES OF STEAM GENERATOR MATERIALS . . . 91

3.4.1 Strain-Rate Effects on the Tensile Properties of Annealed 2 1/4 Cr-1 Mo Steel . . . . . 91

3.4.2 Heat-to-Heat Variation of 2 1/4 Cr-1 Mo Steel . . 92

3.4.3 Fatigue Behavior of 2 1/4 Cr-1 Mo Steel . . . . . 101

3.4.3.1 Fatigue Curve Development. . . . . 101

3.4.3.2 Bilinear Cyclic Stress-Strain Constants. 103

3.4.4 Mechanical Property Correlations of 2 1/4 Cr-1 Mo Steel for LMFBR Steam Generators . . . . . 103

3.4.4.1 Rupture Life . . . . . 103

3.4.4.2 Minimum Creep Rate . . . . . 122

3.4.4.3 Uniform Elongation . . . . . 124

3.4.4.4 Diamond Pyramid Hardness . . . . . 126

3.4.4.5 Time to Tertiary Creep . . . . . 127

3.4.5 Elastic Constants in Weldment Structures . . . . 133

3.4.5.1 Dynamic Elastic Constants of Weld Deposits . . . . . 133

3.4.5.2 Future Work . . . . . 137

3.4.6 Mechanical Properties of a Weld-Overlaid Stainless Steel Forging . . . . . 142

3.5 HIGH-TEMPERATURE DESIGN . . . . . 143

3.5.1 Exploratory Studies in Support of Structural Design Methods . . . . . 143

3.5.1.1 Exploratory Testing of Type 304 Stainless Steel to Identify Behavior Features . . . . . 144

3.5.1.2 Exploratory Testing of Type 316 Stainless Steel. . . . . 146

3.5.1.3 Exploratory Testing of 2 1/4 Cr-1 Mo Steel . . . . . 148

3.5.2 Investigations of Creep Failure Under Uniaxial and Multiaxial Conditions . . . . . 151

3.5.2.1 Uniaxial Tests . . . . . 151

3.5.2.2 Multiaxial Testing . . . . . 151

3.6 MECHANICAL PROPERTIES OF HTGR STEAM GENERATOR AND PRIMARY CIRCUIT MATERIALS . . . . . 160

3.6.1 Tensile Testing . . . . . 161

3.6.2 Environmental Creep Testing . . . . . 161

3.6.3 Fatigue-Life Testing . . . . . 162

3.6.4 Subcritical Crack Growth Studies . . . . . 168

3.6.4.1 Testing in Air . . . . . 168

3.6.4.2 Testing in Steam . . . . . 170

3.6.4.3 Testing in HTGR Helium . . . . . 171

3.7 REFERENCES . . . . . 172

4. NAVAL RESEARCH LABORATORY . . . . . 179

4.1 INTRODUCTION . . . . . 179

4.2 EFFECT OF SPECIMEN THICKNESS ON FATIGUE CRACK GROWTH IN TYPE 304 STAINLESS STEEL . . . . . 179

4.2.1 Background . . . . . 179

4.2.2 Experimental Procedure . . . . . 180

4.2.3 Results and Discussion . . . . . 180

4.2.4 References. . . . . 184

4.3 THE EFFECT OF HOLD TIME ON THE FATIGUE CRACK GROWTH BEHAVIOR OF TYPE 316 STAINLESS STEEL . . . . . 186

4.3.1 Background . . . . . 186

4.3.2 Materials and Test Procedures . . . . . 186

4.3.3 Results . . . . . 187
4.3.4 References . . . . . 187
5. HANFORD ENGINEERING DEVELOPMENT LABORATORY (No report) . . . 193
6. WESTINGHOUSE ADVANCED REACTORS DIVISION . . . . . 195
6.1 INTRODUCTION . . . . . 195
6.2 BASIC SPECIMEN TESTING . . . . . 196
6.2.1 Strain Distribution in Weldments . . . . . 197
6.2.1.1 Test Models . . . . . 197
6.2.1.2 Test Results . . . . . 198
6.2.2 Notched Bars . . . . . 206
6.3 TUBULAR SPECIMEN TESTING . . . . . 206
6.4 SODIUM EFFECTS ON MECHANICAL PROPERTIES OF STRUCTURAL MATERIALS . . . . . 209
6.4.1 Type 316 Stainless Steel . . . . . 209
6.4.2 Inconel 718 . . . . . 216
6.5 REFERENCES . . . . . 222
7. UNIVERSITIES . . . . . 223
7.1 UNIVERSITY OF CINCINNATI . . . . . 223
7.1.1 Introduction . . . . . 223
7.1.2 Experimental Program . . . . . 223
7.1.2.1 High Temperature Fatigue Substructure for Incoloy 800 . . . . . 224
7.1.3 References . . . . . 246
7.2 UNIVERSITY OF CALIFORNIA, LOS ANGELES . . . . . 249
7.2.1 The Influence of (0—10%) Cold Work on the Creep Behavior of AISI Type 304 Stainless Steel . . . . . 249
7.2.2 Introduction . . . . . 249
7.2.3 Materials and Experimental Procedure . . . . . 250
7.2.4 Experimental Results . . . . . 251
7.2.4.1 Creep Curves and the Creep Parameters . 251
7.2.4.2 Rupture Life, $t_r$ . . . . . 259
7.2.4.3 Activation Energy . . . . . 260
7.2.5 Discussion of Results . . . . . 261
7.2.5.1 Initial Creep Rate, $\dot{\varepsilon}_i$ . . . . . 261

7.2.5.2 The Instantaneous Loading Strain ($\varepsilon_0$) and the Limiting Transient Creep Strain ($\hat{\varepsilon}_t$) . . . . . 267

7.2.5.3 The Transient Creep Parameter r . . . . 270

7.2.5.4 The Steady State Creep Rate, $\dot{\varepsilon}_s$ . . . . 270

7.2.6 Conclusions . . . . . 271

7.2.7 References . . . . . 272

8. GENERAL ELECTRIC COMPANY . . . . . 275

8.1 INTRODUCTION . . . . . 275

8.2 MECHANICAL PROPERTIES OF STAINLESS STEEL IN CARBURIZING SODIUM . . . . . 276

8.2.1 Fatigue Crack Growth Studies . . . . . 276

8.2.2 Creep/Fatigue Studies . . . . . 280

8.3 DECARBURIZATION KINETICS AND DESIGN METHODS VERIFICATION TESTING . . . . . 287

8.3.1 Objective . . . . . 287

8.3.2 Decarburization Kinetics . . . . . 287

8.3.3 Mechanical Properties of 2 1/4 Cr-1 Mo Steel in Decarburizing Sodium . . . . . 289

8.4 METALLURGICAL CHARACTERIZATION OF VAR AND ESR 2 1/4 Cr-1 Mo ALLOY STEEL . . . . . 304

8.4.1 Heat Treatment . . . . . 304

8.4.2 Tensile Tests . . . . . 304

8.4.3 Charpy V-Notch Tests . . . . . 306

8.4.4 Creep-Rupture Tests . . . . . 336

8.4.5 Isothermal Transformation Study . . . . . 336

8.4.6 Fracture Toughness Testing of VAR Materials . . . 347

8.4.7 CRBRP Prototype and Plant Tubesheet Forgings. . . 349

8.4.8 Correction to the Previously Reported Chemical Analysis . . . . . 350

8.5 FRACTURE TOUGHNESS OF LMFBR STEAM GENERATOR MATERIALS. . 351

8.6 REFERENCES . . . . . 375

INDEX . . . . . 377

## SUMMARY

### 1. AEROJET NUCLEAR COMPANY

Low cycle fatigue tests of base and weld Alloy 718 given the INEL heat treatment are reported and compared to fatigue behavior of 1750°F conventional heat treated material at 700K (800°F), 811K (1000°F), and 922K (1200°F). Preliminary data is reported on the effects of mean stress on the high cycle fatigue of Alloy 718 with conventional heat treatments at room temperature and 922K (1200°F).

Stress rupture tests of base and weld Alloy 718 given the INEL heat treatment are also reported and compared with 1750°F conventional heat treat data.

### 2. ARGONNE NATIONAL LABORATORY

Additional low-cycle fatigue tests have been conducted on annealed Type 304 stainless steel in 600°C sodium. A comparison of data obtained from tests in sodium with data reported in the literature for tests in an air environment at 593°C shows good agreement at strain ranges of $\lesssim$1%. At higher strain ranges (>1%), the fatigue lifetimes are slightly decreased when the tests are conducted in sodium. Low-cycle fatigue data were also obtained on Type 304 stainless steel after a 1512-h exposure to sodium that produced a carburized surface region to a depth of 0.01 cm. Unlike Type 316 stainless steel, the result of the exposure increased fatigue lifetimes at all strain ranges of concern.

Uniaxial creep-rupture tests have been conducted on Type 304 stainless steel specimens in the solution-annealed condition and after exposure to flowing sodium of controlled, nonmetallic element concentrations. In general, the data obtained at 700, 650, and 600°C show that, for the range of carburization attained in the present investigation, the exposure of this stainless steel to a sodium environment results in an increase in rupture life and a decrease in minimum creep rate when compared with material in the solution-annealed condition. Creep correlations have been developed that relate rupture life with minimum creep rate and with time to onset of tertiary creep.

### 3. OAK RIDGE NATIONAL LABORATORY

Creep and creep-rupture testing of type 304 stainless steel reference heat (9T2796) is continuing. Conditions for creep testing have been reviewed with respect to the conditions for which data are available in the literature and to the design requirements. Creep test conditions and the stress-rupture curves from the ASME code case are compared with the various regions of deformation maps.

Creep and creep-rupture strengths of austenitic stainless steels have been related to ultimate tensile strength at the creep testing temperature.

Tensile data on specimens tested at aging temperatures are presented for several heats of types 304 and 316 stainless steel. These data were compared with *Nuclear Systems Materials Handbook* minimum value curves. Aging had less influence on tensile ductility of specimens tested at the aging temperature than of specimens tested at other temperatures.

Data on long-term creep tests in progress on aged specimens of various heats of type 304 stainless steel are presented. Thus far the data show either an increase in time to rupture or no influence.

The development of an improved design creep equation for type 304 stainless steel has begun. Initial results for heat 9T2796, 51 mm (2-in.) plate indicate that a single rational polynominal creep equation describes the data well.

Development and expansion of a computerized Mechanical Property Data Storage and Retrieval System (DSRS) is continuing. Current efforts are being centered on development of computer programs for analysis of data in the system.

The results of a comprehensive evaluation of the Young's Modulus of 2 1/4 Cr-1 Mo steel (Heat 20017) and type 304 stainless steel (Heat 9T2796) are presented as functions of temperature and strain rate as determined by the "repetitive" specimen technique with LVDT strain sensors. Use of a single specimen causes only a slight lowering of Young's modulus, and strain rate (0.1 to 0.001/hr) was not a significant variable within the use temperature ranges ordinarily prescribed for these alloys.

Creep-rupture testing at 649°C (1200°F) of a submerged-arc type 308 stainless steel weld in three conditions — as-welded, stress-relief annealed, and solution annealed — is in progress. Initial results indicate that sigma phase results in low ductility in the first two conditions. Possible improvement in ductility after solution annealing is being explored.

Static measurements of the room-temperature elastic compliance matrix for type 308 stainless steel electroslag-deposited weld metal have been completed and are reported. Orthotropic behavior is observed.

A report was issued on studies of the tensile properties of annealed 2 1/4 Cr-1 Mo steel over the range of 25 to 593°C. The results from that report are summarized.

Studies on the effect of heat treatment on the tensile properties of annealed 2 1/4 Cr-1 Mo steel were continued. The effect of the

cooling rate on the dynamic strain aging response was explained in terms of the amounts of carbon and molybdenum removed from solution by precipitation during the anneal.

Revised mean curves for fatigue cycle life as a function of imposed strain range for 2 1/4 Cr-1 Mo steel are presented. Comparisons with previous mean curves show no reasons to change the currently recommended design curves.

Development of interim curves showing the bilinear stress-strain constants $\kappa_0$, $\kappa_1$, $\kappa_2$, $\kappa_3$, $E_m$, and $C$ as functions of maximum strain, $\varepsilon_{max}$, for 2 1/4 Cr-1 Mo steel at various temperatures has been completed.

Mathematical descriptions of rupture life, minimum creep rate, uniform elongation, and hardness are given for annealed and isothermally annealed 2 1/4 Cr-1 Mo steel. Alternate models for rupture life and minimum creep rate are also presented. The lower limits of stress to cause rupture are compared with corresponding minimum stress values from Code Case 1592. A revised equation for time to tertiary creep, $t_3$, for 2 1/4 Cr-1 Mo steel as a function of stress ($\sigma$) and temperature ($T$) has been obtained by expressing rupture life, $t_r$, as a function of $\sigma$ and $T$ and then predicting $t_3$ by $t_3 = 0.28 t_r^{1.07}$.

Dynamic elastic constants ($E$, $G$, and $\nu$) at room temperature were determined for two weld deposits in Inconel 82, for one in 18-8-2, and for Inconel 606 (wrought version of Inconel 82) by sonic methods that assume isotropy. Also elastic constants were established for the latter two materials from 24 to 732°C (75—1350°F). Except for the information developed for Inconel 606 the data do not appear valid as a result of the sonic methods used. For a 47-pass weld deposit, we plan future tests in Inconel 82 that employ sonic methods appropriate to anisotropic bodies.

A final report has been prepared on the experimental studies of the creep-rupture properties of a type 304 stainless steel forging overlaid with type 308 stainless steel weld metal. A summary of the results from this report is presented.

Results from a study of the influence of thermomechanical history on the rupture strength of type 304 stainless steel at 593°C indicate that cooling rate from the annealing temperature is more significant than cold working. Initial results from tensile tests on type 316 stainless steel show an inversion in the influence of strain rate on flow stress at 593°C. The relaxation strength to 100 hr was significantly greater than predicted from the *Nuclear Systems Materials Handbook* creep equation. The results of creep, cyclic creep, and relaxation tests on 2 1/4 Cr-1 Mo steel at 538°C are reported. Results of uniaxial and multiaxial creep tests at Babcock and Wilcox Company on type 304 stainless steel at 593°C are reported. Data include rupture times as great as 25,942 hr for uniaxial tests and 3336 hr for multiaxial conditions.

Tensile specimens of Inconel 617 are ready to test. Hastelloy X creep specimens in simulated HTGR coolant failed in 159 hr with 57% elongation at 760°C (1400°F) and 152 MPa (22 ksi) and in 554 hr with 35% elongation at 871°C (1600°F) and 62 MPa (9 ksi). Additional specimens of Hastelloy X and 2 1/4 Cr-1 Mo steel under test in HTGR coolant and in air are listed. Low-cycle strain-controlled fatigue testing of Hastelloy X began, and results to date are presented. Hastelloy X and Inconel 617 are being aged to scope their thermal stability in relation to creep and fatigue behavior. Design of system for conducting fatigue tests in a helium atmosphere or vacuum is being reviewed. Heat-to-heat, frequency, and environmental effects on subcritical crack growth of 2 1/4 Cr-1 Mo steel are reported. Preliminary data on Hastelloy X are presented.

## 4. NAVAL RESEARCH LABORATORY

Fatigue crack propagation rates were determined as a function of stress intensity factor using single-edge-notch cantilever specimens. No significant effect of test section thickness in the range from 7.6 to 25.4 mm (0.30 to 1.0 in.) was evident on crack propagation rates in Type 304 stainless steel at 24, 427, and 593°C (75, 800, and 1100°F).

Comparisons have been made of the fatigue crack growth behavior of solution-annealed and 20 percent cold-worked Type 316 stainless steel at 427°C (800°F) tested at 5 cpm with and without tensile hold times. A 0.1 minute tensile hold period produced no significant effect on crack growth rate for either material condition. Comparison of the present 5 cpm zero hold time data with previous 10 cpm results showed no effect of frequency for this frequency range. The results indicated that the cyclic loading rather than the static loading was responsible for the crack growth behavior observed for annealed and cold-worked Type 316 stainless steel at 427°C (800°F).

## 5. HANFORD ENGINEERING DEVELOPMENT LABORATORY

(No Report)

## 6. WESTINGHOUSE ADVANCED REACTORS DIVISION

Testing of weld specimens has shown that the rupture strength of type CRE 308 welds for lives of up to 5000 hours is equal to or greater than that of the base type 304 material. Cracks initiate in the HAZ of welds perpendicular to the direction of maximum principal stress at about the same time as that observed for the base metal. The crack growth rate in the weld metal is much lower than that in the base metal or HAZ. The growth rate is nearly proportional to the creep rate in

the same plane in front of the crack tip. The rupture life of a welded model or component is therefore a function of the direction of the maximum principal stress and the creep strain. For crack initiation the critical strain limit at creep rates near $10^{-3}$/h is about 4%.

All creep testing of Type 304 SS for tubular specimens has been completed and the resulting data have been processed and corrections made for variability in the extensometer responses. The data were fitted to a single exponential creep equation and the constants determined.

Progress in sodium effects on mechanical properties has been made in the following areas: (1) creep-rupture tests in flowing sodium for solution annealed Type 316 stainless steel with various pre-treatments, (2) low cycle fatigue tests of solution annealed Type 316 stainless steel in flowing sodium, with and without hold-time, and (3) low cycle fatigue tests of Inconel 718 conducted in air. Progress on the sodium pre-exposure and thermal aging of additional mechanical property samples is also described.

## 7. UNIVERSITIES

### UNIVERSITY OF CINCINNATI

Work on the observation and the preliminary evaluation of the dislocation substructure of the fatigue specimens of Incoloy 800 were completed. Incoloy 800 push-pull fatigue specimens were examined after being tested at various test conditions at 538, 649, 704, and 760°C. Substructure parameters such as cell or subgrain intercept size, dislocation density, were evaluated and correlated with the observed fatigue properties. Cells or subgrains were observed to form in Incoloy 800 after LCF at all testing temperatures. The subboundary intercept size and the dislocation density were found to be related to both the saturation stress and the plastic strain range. Subboundaries were also found to lie on the low index crystallographic planes with mixed, tilt and twist nature.

### UNIVERSITY OF CALIFORNIA, LOS ANGELES

The effect of cold work on the creep strength of AISI Type 304 stainless steel is being investigated. The maximum improvement resulted from 8% prestrain. Prior cold work enhances the creep strength only for the low-strain-rate tests where recovery is not rapid enough to eliminate the benefit of cold work.

## 8. GENERAL ELECTRIC COMPANY

Programs designed to study the effects of high temperature sodium environments on the mechanical properties of stainless steels and 2¼Cr-1Mo are continuing. The results of a program evaluating the effect of heat treatment and melting practice on the mechanical behavior of 2¼Cr-1Mo are also reported.

The planned post weld heat treatment considered for 2¼Cr-1Mo used in the CRBR steam generators has been shown to produce a stable microstructure. Above 454°C (850°F) the yield strength of VAR and ESR material generally fell below the ASME Code Case 1592 expected minimum value. Full anneal plus post weld heat treatment provides the more resistance to brittle fracture than several other heat treatments tested. Safe behavior of VAR 2¼Cr-1Mo with respect to fracture has been demonstrated provided the $K_{IR}$ curve of Appendix G of Section III of the ASME Code is followed.

Fatigue crack propagation rates of Type 316 stainless steel are being determined at 510°C (950°F) in air and in carburizing sodium. Preliminary results for annealed base material are reported for both environments. GTA weld specimens are currently being prepared for testing.

Fracture toughness properties of 2¼Cr-1Mo steel are being determined through the use of J-Integral test methods. Room temperature test results for base material in several conditions are reported, along with charpy, drop-weight, and tensile characterizations. Elevated temperature testing and the evaluation of SMAW weldments, currently being prepared, are planned.

The results of the first phase of creep testing of 2¼Cr-1Mo in a strongly decarburizing environment are summarized in this report. Uniaxial creep specimens tested in titanium gettered sodium fail in much less time (approximate order of magnitude effect) than control specimens, but the same fracture strain is observed. Influence of the decarburizing environment is noted over the entire creep history for tests exhibiting a minimum 400 hour rupture time. In the next phase of testing major effort will be concentrated in quantifying decarburization influence under monotonic creep stress conditions.

Severe weld porosity occured in tubular 2¼Cr-1Mo weld metal specimens exposed to titanium gettered sodium. These specimens were part of a test matrix to characterize the creep properties of 2¼Cr-1Mo weld metal. The sodium/weld metal interaction responsible for the porosity is being investigated.

Creep data summarizing the results of the first phase of testing 316H stainless steel in a strongly carburizing sodium environment are included in this report. Data representing the main experimental

parameters (mode of loading and environment) fall within a common scatterband. All data fall above the minimum expected value for stress rupture approximated from ASME Code Case 1592 data.

# 1. AEROJET NUCLEAR COMPANY

D. D. KEISER

## 1.1 INTRODUCTION

Aerojet Nuclear Company is conducting mechanical properties investigations under a program sponsored by ERDA Division of Reactor Development and Demonstration. Program IA-009, Alloy 718 Mechanical Property Program, has as its primary objective the acquisition of the necessary mechanical property data to permit safe, efficient use of this material in LMFBR service. The specific immediate application is for selected structural components of the Clinch River Breeder Reactor Project. Other reactor service applications which require high levels of mechanical properties at temperatures up to 922K (1200°F) are also expected to make use of this material.

What have been considered standard heat treatments for Alloy 718 have not consistently yielded acceptable ductility values for the welded material. Current work involves fatigue and stress-rupture testing of material subjected to a modified thermal treatment designated as the INEL Heat Treatment*.

## 1.2 MECHANICAL PROPERTY PROGRAM OF ALLOY 718

G. E. Korth and G. R. Smolik

### 1.2.1 Low Cycle Fatigue Tests

Test specimens from 12.7 mm (1/2 inch) plate, 12.7 mm (1/2 inch) weldment, and 15.9 mm (5/8 inch) weldment were tested at 700K (800°F), 811K (1000°F), and 922K (1200°F). The weld specimens tested to date were taken transverse to the welding direction. The weld joint was prepared by butt welding two plates together containing J-Grooves of slightly more than half the plate thickness. After the joint was partially

---

* INEL heat treatment: 1366K (2000°F) solution anneal 1 h, slow cool to 991K (1325°F) at 83K (150°F) ± 28K (50°F)/h, age at 991K (1325°F) for 4 h, FC to 894K (1150°F) and age 16h, AC.

filled with weld deposit, the weldment was back-machined into the original weld and then both sides were filled with weld deposit using the GTAW process. The resulting joint contained a minimum thickness in the center equal to the plate thickness as illustrated in Figure 1.1. The uniform gage length of the transverse weld fatigue test specimens was short enough that it contained only weld deposit. Longitudinal weld specimens have also been prepared but none of these have been tested yet. Figure 1.2 illustrates the orientation of transverse and longitudinal specimens with respect to the weldment. Uniform gage fatigue specimens were utilized for the majority of weld metal testing since this geometry is much less prone to give poor test results when the potentional for anisotropy exists as it does in weldments. Base metal tests were conducted using an hourglass geometry in the test section. The degree of anisotropy in a transverse weld metal specimen was measured on two specimens and is shown in Figure 1.3. From the anisotropy measurements taken, the variations are seen not to be large and the trends are consistent. It is believed that valid tests can be run by carefully positioning the diametral extensometer on a weld hourglass specimen where its mean diametral strain coincides very closely with base metal values ( $\sim 75°$, see Figure 1.3). A few hourglass weld metal specimens were run with no apparent problems where the strains were totally elastic and previous scans could identify the optimum orientation for the extensometer placement.

The base metal 811K (1000°F) fatigue tests have been reported previously[1]. Therefore, only current test results for weld metal at this temperature are listed in Table 1.1. Fatigue test results for base and weld metal at 700K (800°F) and 922K (1200°F) tests are also listed in Table 1.1 where:

$\Delta\varepsilon_t$ = total strain range

$\Delta\varepsilon_p$ = plastic strain range at $N_f/2$

$\Delta\sigma$ = stress range

$\sigma_t$ = tensile stress amplitude

$N_o$ = cycles at crack initiation (first sign of tensile load decrease)

$N_f$ = cycles at failure

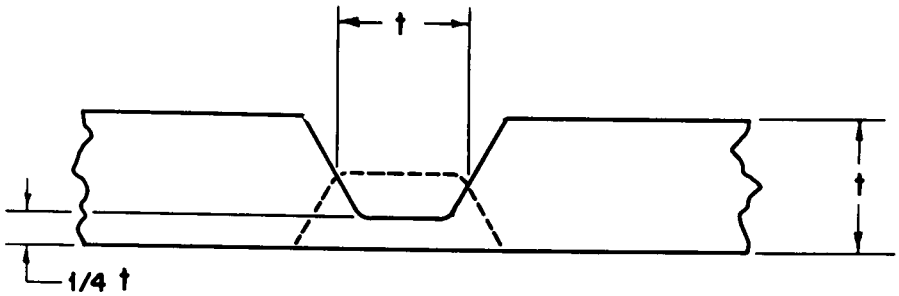


Fig. 1.1. Weld Joint Design Used for Test Specimen Material.

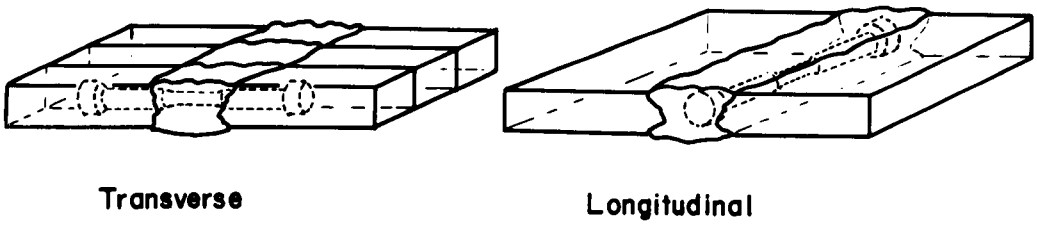


Fig. 1.2. Orientation of Transverse and Longitudinal Specimens with respect to the weld seam.

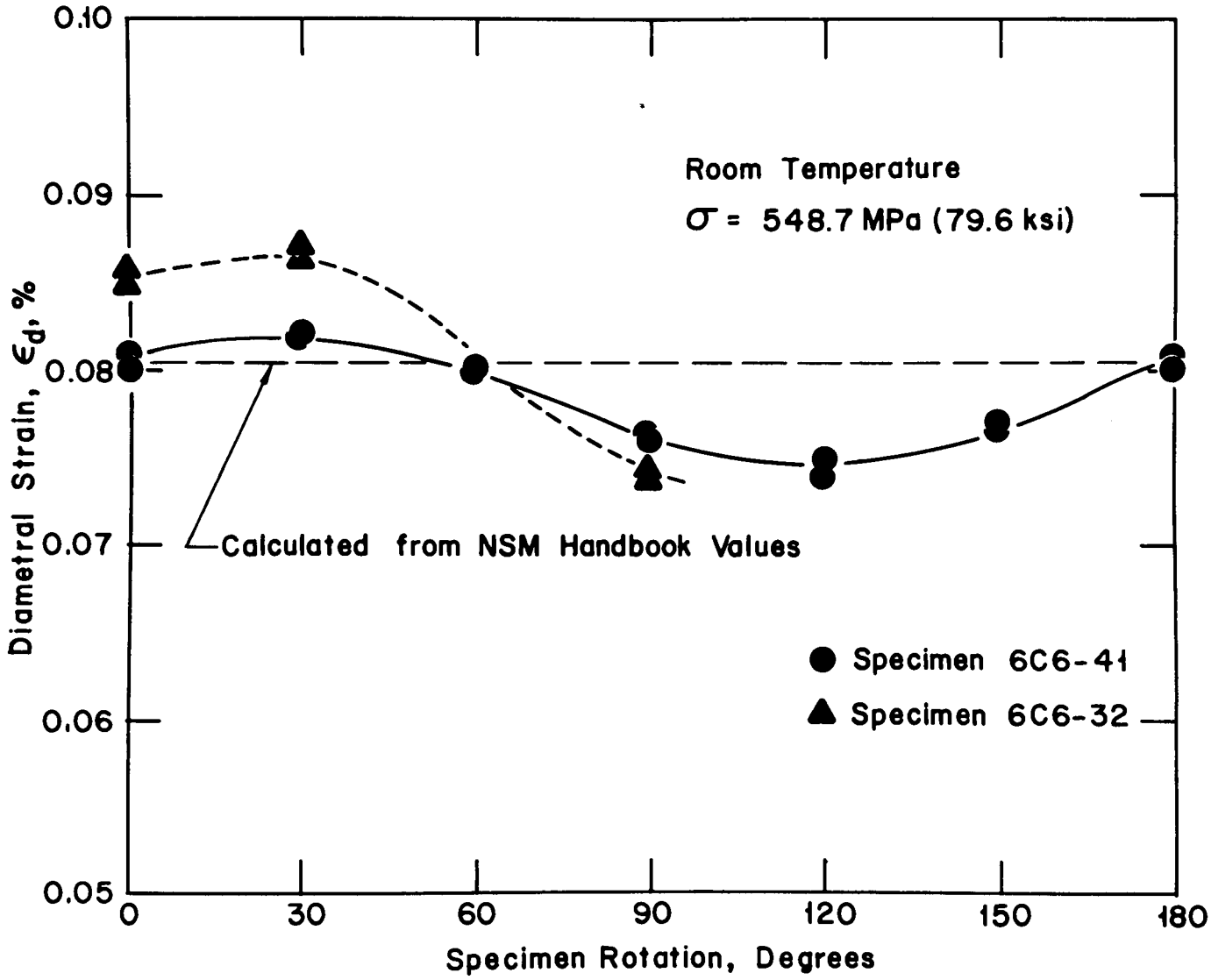


Fig. 1.3. Elastic Diametral Strain vs Orientation for Two Alloy 718 Transverse Fatigue Specimens.

Table 1.1 Strain Fatigue[a] of Base and Weld Alloy 718 Given the INEL Heat Treatment

| Specimen No. | Type | Heat[b] | $\Delta\varepsilon_t$, % | $\Delta\varepsilon_p$, % | $\Delta\sigma$ at $N_f/2$ MPa | (ksi) | $\sigma_t$ at $N_f/2$ MPa | (ksi) | $N_o$ | $N_f$ | Test Temperature K | (F) |
|---|---|---|---|---|---|---|---|---|---|---|---|---|
| 1A1-11 | Trans. Weld | A | 3.25 | 1.86 | 2302 | (333.9) | 1129 | (163.8) | 189 | 197 | 700 | (800) |
| 318-48 | Base | 3 | 3.06 | 1.46 | 2281 | (330.9) | 1124 | (163.0) | 235 | 249 | 700 | (800) |
| 6C6-3 | Trans. Weld | C | 2.04 | 0.88 | 2022 | (293.3) | 997 | (144.6) | 546 | 572 | 700 | (800) |
| 318-47 | Base | 3 | 2.08 | 0.68 | 1962 | (284.6) | 973 | (141.1) | 1,061 | 1,101 | 700 | (800) |
| 1A1-2 | Trans. Weld | A | 1.50 | 0.39 | 1989 | (288.5) | 978 | (141.9) | 941 | 941 | 700 | (800) |
| 318-46 | Base | 3 | 1.56 | 0.35 | 1900 | (275.6) | 942 | (136.6) | 2,285 | 2,375 | 700 | (800) |
| 6C6-1 | Trans. Weld | C | 1.25 | 0.28 | 1837 | (266.4) | 898 | (130.3) | 1,931 | 1,977 | 700 | (800) |
| 6C6-34 | Trans. Weld | C | 1.21 | 0.16 | 1837 | (266.4) | 889 | (129.0) | 4,473 | 4,512 | 700 | (800) |
| 318-45 | Base | 3 | 1.04 | 0.05 | 1650 | (239.3) | 778 | (112.9) | 5,969 | 6,394 | 700 | (800) |
| 1A1-4 | Trans. Weld | A | 1.02 | 0.11 | 1772 | (257.0) | 856 | (124.2) | 4,710 | 4,710 | 700 | (800) |
| 6C6-2 | Trans. Weld | C | 0.84 | 0.02 | 1536 | (222.8) | 778 | (112.8) | 9,808 | 10,202 | 700 | (800) |
| 318-49 | Base | 3 | 0.83 | 0.00 | 1404 | (203.6) | 702 | (101.9) | 16,628 | 16,904 | 700 | (800) |
| 318-44 | Base | 3 | 0.74 | 0.00 | 1215 | (176.2) | 614 | (89.0) | 21,842 | 24,861 | 700 | (800) |
| 6C6-35 | Trans. Weld | C | 0.64 | 0.00 | 1102 | (159.9) | 542 | (78.6) | 69,690 | 70,318 | 700 | (800) |
| 318-51 | Base | 3 | 0.63 | 0.00 | 1053 | (152.8) | 508 | (73.7) | 83,152 | 86,013 | 700 | (800) |
| 318-50 | Base | 3 | 0.63 | 0.00 | 1093 | (158.5) | 532 | (77.1) | 87,058 | 94,563 | 700 | (800) |
| 6C6-36 | Trans. Weld | C | 0.59 | 0.00 | 1054 | (152.9) | 538 | (78.0) | — | 77,537 | 700 | (800) |
| 6C6-37 | Trans. Weld | C | 0.53 | 0.00 | 920 | (133.4) | 445 | (64.6) | 252,254 | 252,470 | 700 | (800) |
| 1A1-12 | Trans. Weld | A | 3.39 | 1.96 | 2232 | (323.8) | 1081 | (156.8) | 101 | 110 | 811 | (1000) |
| 1A1-175 | Trans. Weld | A | 1.70 | 0.65 | 1863 | (270.2) | 918 | (133.1) | 714 | 775 | 811 | (1000) |
| 1A1-158 | Trans. Weld | A | 0.98 | 0.09 | 1582 | (229.5) | 649 | (94.1) | 4,446 | 4,549 | 811 | (1000) |
| 1A1-162 | Trans. Weld | A | 0.77 | 0.01 | 1400 | (203.0) | 685 | (99.3) | 11,574 | 11,767 | 811 | (1000) |
| 6C6-41 | Trans. Weld | C | 0.65 | 0.00 | 1104 | (160.2) | 532 | (77.1) | — | 265,670[c] | 811 | (1000) |
| 1A1-17 | Trans. Weld | A | 2.52 | 1.24 | 2041 | (296.1) | 991 | (143.7) | 51 | 61 | 922 | (1200) |
| 318-40 | Base | 3 | 2.48 | 1.16 | 2099 | (304.4) | 1034 | (149.9) | 199 | 232 | 922 | (1200) |
| 6C6-10 | Trans. Weld | C | 2.02 | 0.82 | 1951 | (283.0) | 960 | (139.2) | 93 | 100 | 922 | (1200) |
| 318-38 | Base | 3 | 1.76 | 0.50 | 1930 | (279.9) | 947 | (137.3) | 514 | 615 | 922 | (1200) |
| 6C6-9 | Trans. Weld | C | 1.50 | 0.39 | 1844 | (267.4) | 908 | (131.7) | 187 | 271 | 922 | (1200) |
| 318-36 | Base | 3 | 1.31 | 0.22 | 1751 | (253.9) | 783 | (113.6) | 1,198 | 1,322 | 922 | (1200) |
| 1A1-5 | Trans. Weld | A | 1.25 | 0.23 | 1703 | (247.0) | 833 | (120.8) | 290 | 338 | 922 | (1200) |
| 6C6-4 | Trans. Weld | C | 1.05 | 0.14 | 1490 | (216.1) | 736 | (106.8) | 758 | 876 | 922 | (1200) |
| 1A1-1 | Trans. Weld | A | 1.00 | 0.12 | 1519 | (220.3) | 751 | (108.9) | — | 910 | 922 | (1200) |
| 318-37 | Base | 3 | 1.00 | 0.04 | 1469 | (213.1) | 714 | (103.6) | 3,344 | 4,280 | 922 | (1200) |
| 1A1-10 | Trans. Weld | A | 0.90 | 0.09 | 1426 | (206.9) | 706 | (102.4) | 1,624 | 1,646 | 922 | (1200) |
| 1A1-8 | Trans. Weld | A | 0.89 | 0.10 | 1352 | (196.1) | 674 | (97.8) | — | 1,748 | 922 | (1200) |
| 6C6-6 | Trans. Weld | C | 0.88 | 0.08 | 1329 | (192.7) | 668 | (96.9) | 1,252 | 1,456 | 922 | (1200) |
| 6C6-5 | Trans. Weld | C | 0.77 | 0.09 | 1222 | (177.2) | 612 | (88.8) | — | 5,752 | 922 | (1200) |
| 6C6-7 | Trans. Weld | C | 0.72 | 0.00 | 1134 | (164.5) | 578 | (83.9) | 7,986 | 8,877 | 922 | (1200) |
| 6C6-33 | Trans. Weld | C | 0.71 | 0.00 | 1123 | (162.9) | 547 | (79.3) | — | 39,215 | 922 | (1200) |
| 318-41 | Base | 3 | 0.70 | 0.00 | 1171 | (169.8) | 550 | (79.8) | 25,450 | 26,024 | 922 | (1200) |
| 318-42 | Base | 3 | 0.65 | 0.00 | 1079 | (156.5) | 547 | (79.3) | 59,320 | 60,129 | 922 | (1200) |
| 6C6-40 | Trans. Weld | C | 0.62 | 0.00 | 1056 | (153.2) | 523 | (75.8) | 335,411 | 336,644 | 922 | (1200) |
| 318-43 | Base | 3 | 0.60 | 0.00 | 978 | (141.8) | 442 | (64.1) | 306,030 | 307,932 | 922 | (1200) |

[a] - Tested in strain control, fully reversed push-pull with ramp waveform and a strain rate of $4 \times 10^{-3}$ s.$^{-1}$

[b] - Weld Batch A is 1.57mm (.062 inch) HAPD Ht. 60C7E
Weld Batch C is 1.14mm (.045 inch) HAPD Ht. 52B0E
Base Heat 3 is 12.7mm (1/2 inch) VIM-ESR plate, HAPD Ht. 52C9EK

[c] - Specimen did not fail

Figures 1.4, 1.5, and 1.6 show the data plotted. Conventional heat treat* test data are also plotted for comparison with the INEL heat treated material.

At test temperatures of 811K (1000°F) and 922K (1200°F) where 1750°F conventional heat treat data are available, it can be seen that the INEL heat treatment is slightly inferior in the high cycle regime but compares very favorably with the 1900°F conventional heat treatment at all three test temperatures where data are available. The transverse weld metal given the INEL heat treatment shows fatigue behavior very near that of the base metal given the same heat treatment at 700K (800°F) and 811K (1000°F). However, at 922K (1200°F) the weld metal does exhibit a lower fatigue life below approximately 2 x $10^4$ cycles-to-fail. Above this value in the high cycle regime the data show the base and weld metal to be equivalent in fatigue behavior.

The stress behavior of strain controlled fatigue tests was quite different between the two heat treatments as illustrated in Figure 1.7 where two identical tests were conducted on identical specimens except for the heat treatment. The cyclic softening of the conventional heat treat material is much more pronounced. Evidently the finer hardening precipitate observed in the conventional heat treated material is more conclusive to flow, even though it has a higher yield strength, once plastic strain cycling is introduced. At lower strain ranges the difference between the cyclic flow behavior of the two heat treatments is not as dramatic but still significant.

### 1.2.2 Mean Stress Effects on High Cycle Fatigue

Mean stress effects on the high cycle fatigue of Alloy 718 given the 1750°F conventional heat treatment are being investigated. The investigation reported here is preliminary in nature but does give some

---

* 1900°F Conventional Heat Treat = 1311K (1900°F) Sol. An. 2h, AC, 1033K (1400°F) age 10h, FC to 922K (1200°F) hold for total duplex aging time of 20 h.

* 1750°F Conventional Heat Treat = 1228K (1750°F) Sol. An. 2h, AC, 991K (1325°F) age 8h, FC to 894K (1150°F) hold for total duplex aging time of 18h.

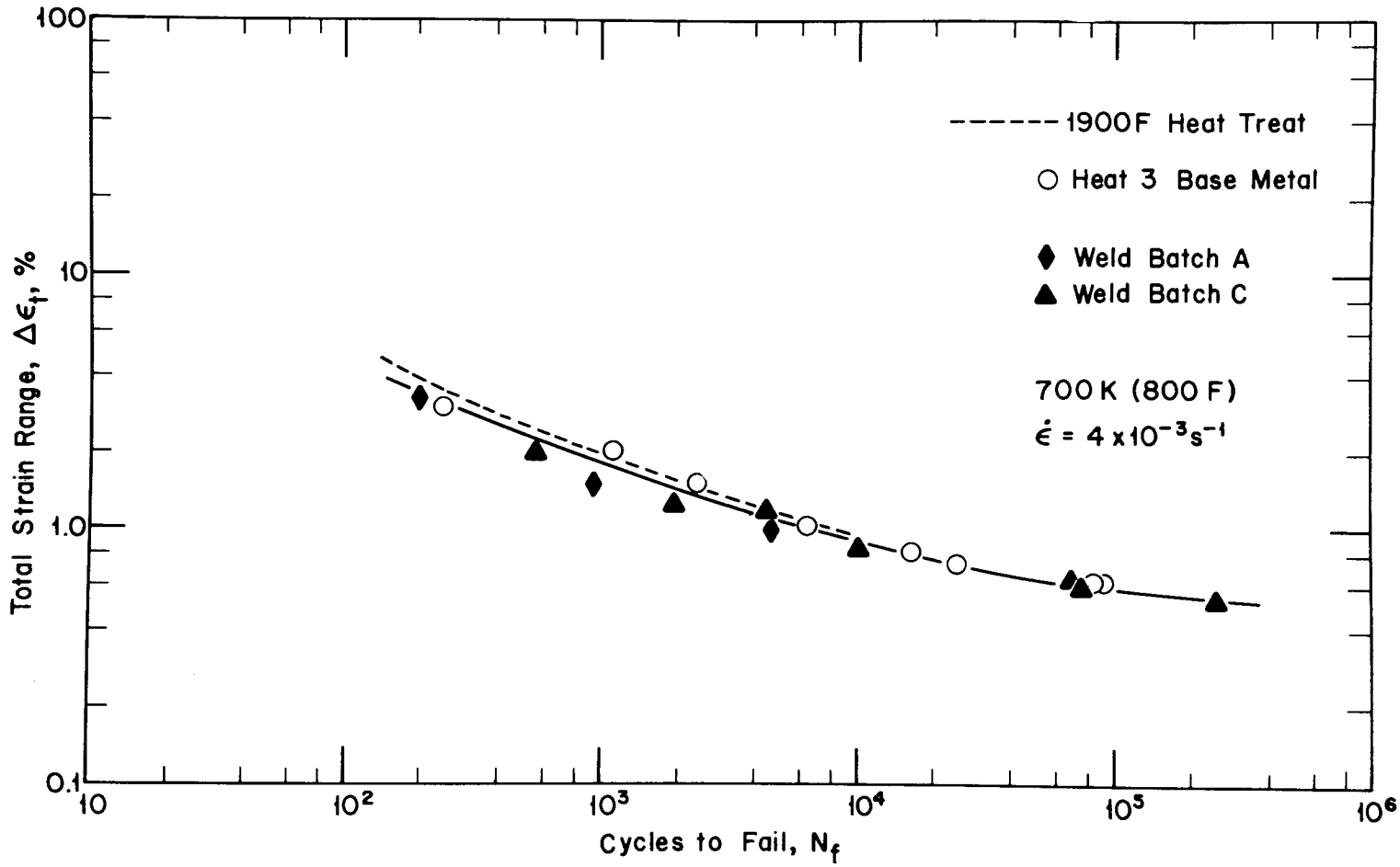


Fig. 1.4. Strain Fatigue of Alloy 718 at 700K (800°F) Comparing INEL and 1900°F Conventional Heat Treatments.

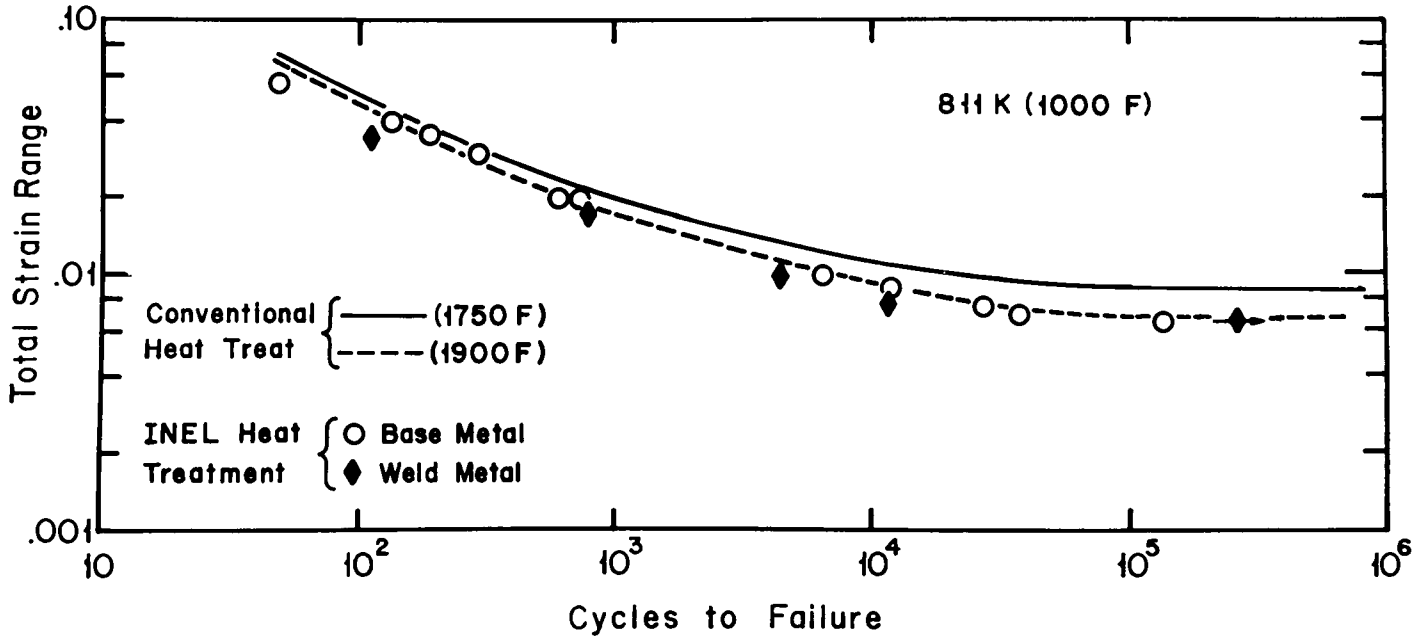


Fig. 1.5. Strain Fatigue of Alloy 718 at 811K (1000°F) Comparing INEL and Conventional Heat Treatments.

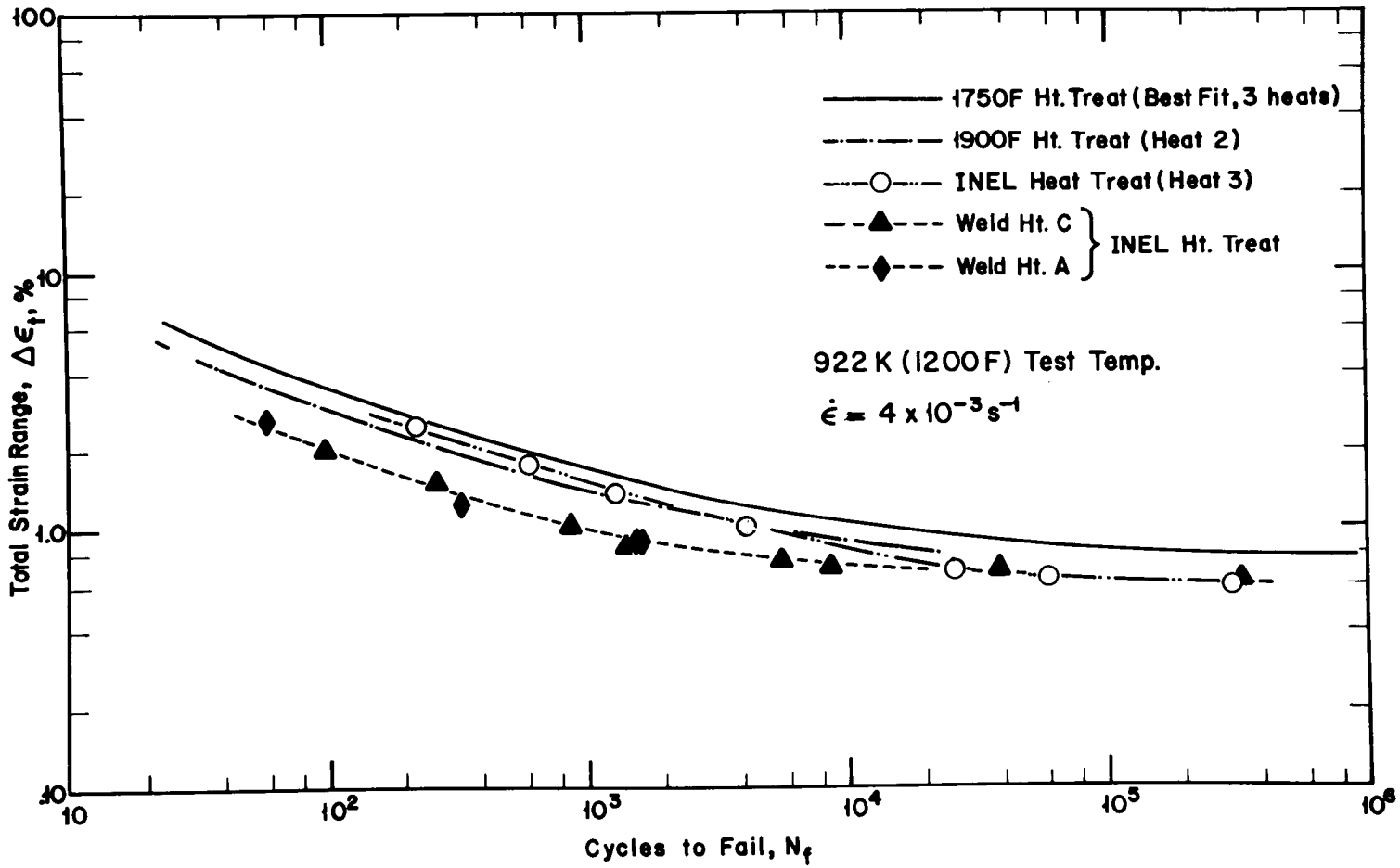


Fig. 1.6. Strain Fatigue of Alloy 718 at 922K (1200°F) Comparing INEL and Conventional Heat Treatments.

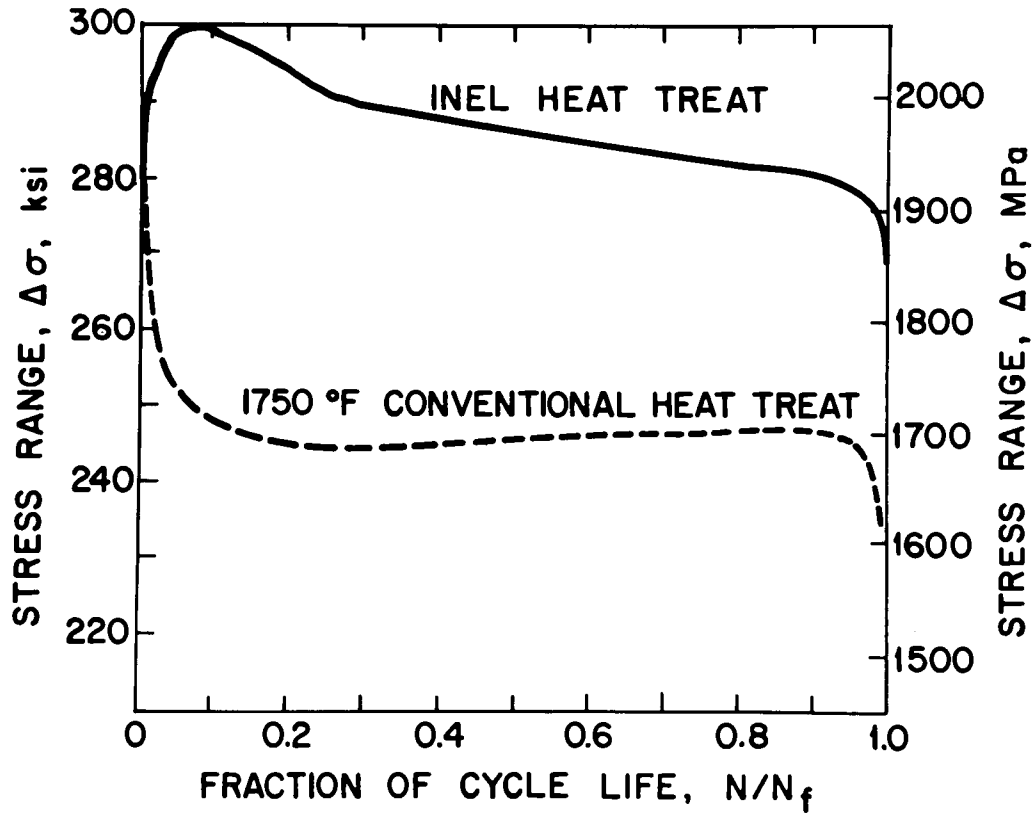


Fig. 1.7. Stress Range vs Cycle Life of Alloy 718 Strain Fatigue Cycled at a Total Strain Range of 2% at 811K (1000°F) Comparing Two Heat Treatments.

direction as to the expected behavior of Alloy 718 when mean stresses are present.

An hourglass specimen geometry was utilized and testing was performed in a servo-hydraulic, closed loop system using push-pull axial loading. Heat 2 [Cabot Ht. 2180-2-9247, 19 mm (3/4 inch) VIM-VAR plate] was the material used for the tests. All data of this preliminary investigation are listed in Table 1.2. The room temperature data are plotted in Figure 1.8 and compared to data previously generated. The stress amplitude is reduced approximately 25% in the $10^5$ cycles-to-fail region when the maximum stress (mean stress plus stress amplitude) approaches the proportional limit; but as the mean stress is reduced such that the maximum stress approaches 80% of the proportional limit, the mean stress effect becomes minimal. These conclusions are based on rather limited data but the trend appears consistent. Tests were conducted at various cycle rates in both load and strain control. There was an indication that the strain controlled tests did yield slightly lower cycle lives but any effect of cycling frequency was not apparent. There was no relaxation of the mean strain in the strain controlled tests nor any ratcheting observed in the load controlled tests at room temperature. At 922K (1200°F) however, mean strain relaxation and ratcheting were significant as illustrated in Figure 1.9.

### 1.2.3 Stress Rupture Tests

Scoping stress-rupture tests of notched and smooth specimens at 922K (1200°F) were reported previously[3]. Additional smooth bar base and transverse weld metal data have been generated since then and are reported in Table 1.3 and compared with 1750°F conventional heat treat data[4] in Figures 1.10 and 1.11. The weldment specimens were taken transverse to the weld seam so the gage length contained base metal, heat-affected-zone (HAZ), and weld deposit. Two specimens failed in the weld and one in the HAZ.

Comparing rupture ductility of the INEL heat treatment with conventional heat treatment data[4] shows that the INEL heat treatment exhibits 1.2 to 3 times better elongation at 922K (1200°F) and equivalent or slightly better at 978K (1300°F). Reduction in area values are quite

Table 1.2 Mean Stress Effects on Fatigue of Alloy 718 Plate Given the 1750°F Conventional Heat Treatment

| Specimen No. | Test Temp, K (F) | Control Mode | Freq. Hz | Stress Amplitude, MPa (ksi) | Mean Stress MPa (ksi) | Cycles to Fail | $\sigma_{max}/\sigma_p$[a] | Remarks |
|---|---|---|---|---|---|---|---|---|
| 2-1-3-10 | RT | Load | 10 | 483 (70) | 386 (56) | 118,300 | 0.97 | 1900°F Heat Treat |
| 2-1-3-3 | RT | Load | 10 | 448 (65) | 358 (52) | 2,420,000[b] | 0.84 | Did not fail |
| 2-1-4-12 | RT | Load | 10 | 448 (65) | 517 (75) | 148,620 | 1.00 | Mean strain remained constant |
| 2-1-5-20 | RT | Strain | 0.42 | 439 (63.7) | 519 (75.3) | 119,214 | 0.99 | Mean stress remained constant |
| 2-1-4-2 | RT | Strain | 1.08 | 439 (63.7) | 439 (63.7) | 154,839 | 0.91 | Mean stress remained constant |
| 2-1-3-42 | RT | Load | 0.83 | 448 (65) | 396 (57.5) | 451,054 | 0.88 | Strain remained constant |
| 2-1-4-4 | 922 (1200) | Strain | 0.45 | .22% Strain amplitude | .22% Strain | 442,056[b] | 0.87 initally | Did not fail, mean stress relaxed significantly |
| 2-1-4-49 | 922 (1200) | Load | 0.36 | 448 (65) | 379 (55) | 990,010[b] | 1.00 | Did not fail, mean strain increased |
| 2-1-4-48 | 922 (1200) | Load | 0.36 | 448 (65) | 448 (65) | 699,674 | 1.08 | Mean strain increased |
| 2-1-4-14 | 922 (1200) | Load | 0.36 | 448 (65) | 517 (75) | 327,674 | 1.17 | Mean strain increased |

[a] - Ratio of maximum stress (= Stress amplitude + mean stress) to proportional limit [$\sigma_p$ = 965 MPa (140 ksi) at RT and 827 MPa (120 ksi) at 922K (1200°F)]

[b] - Specimen did not fail, test stopped intentionally

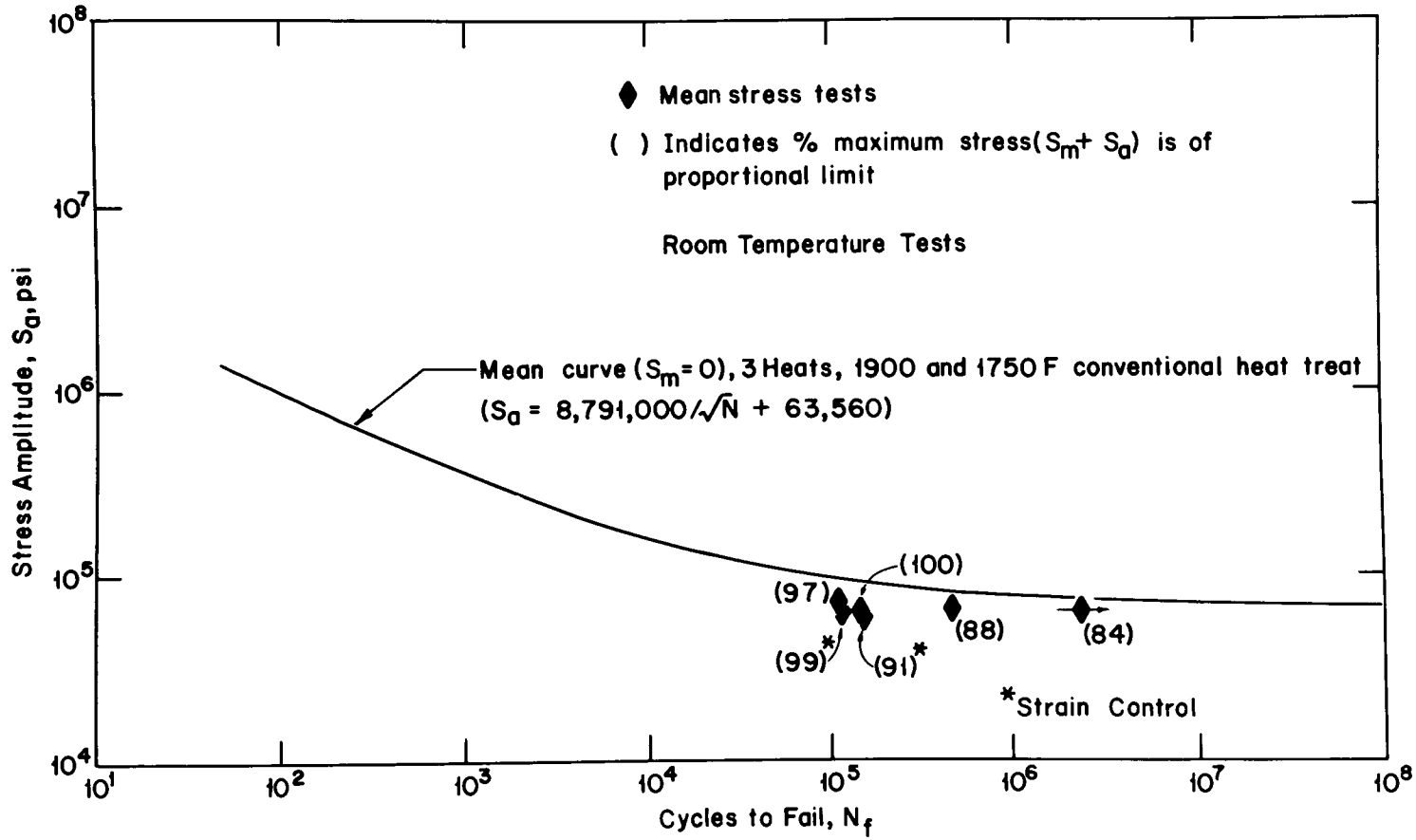


Fig. 1.8. Mean Stress Fatigue Data of Alloy 718 at Room Temperature Compared to Mean Curve of Data Without Mean Stress.

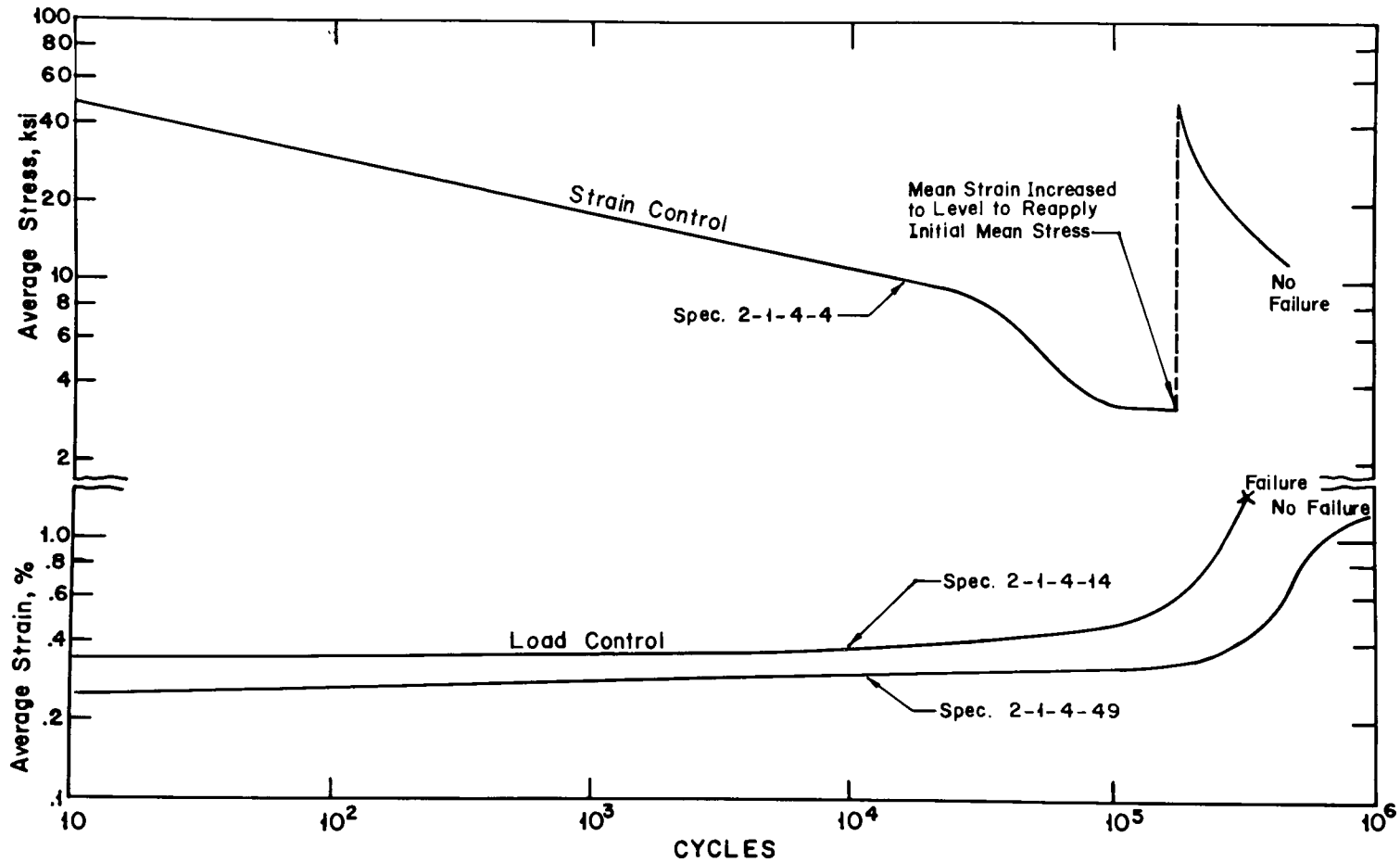


Fig. 1.9. Relaxation and Ratcheting Associated with Mean Strain and Mean Stress Fatigue Testing of Alloy 718 at 922K (1200°F). ($\dot{\varepsilon} = 4 \times 10^{-3}\ s^{-1}$).

Table 1.3 Stress-rupture of Alloy 718 Weld and Base Metal Given the INEL Heat Treatment

| Specimen No. | Type | Test Temperature K | (F) | Applied Stress MPa | (ksi) | Rupture Life, h | Elong. in 5.08mm,% | Red. in Area, % |
|---|---|---|---|---|---|---|---|---|
| 319-5 | Base-3[a] | 811 | (1000) | 966 | (140.1) | 156.4 | 6.8 | 9.4 |
| 319-2 | Base-3 | 922 | (1200) | 861 | (124.9) | 0.8 | 11.2 | 10.3 |
| 319-4 | Base-3 | 922 | (1200) | 813 | (117.9) | 10.8 | 9.2 | 9.5 |
| 319-26 | Base-3 | 922 | (1200) | 759 | (110.1) | 51.9 | 15.7 | 31.1 |
| 318-30 | Base-3 | 922 | (1200) | 723 | (104.8) | 94.7 | 15.0 | 27.2 |
| 319-6 | Base-3 | 922 | (1200) | 690 | (100.1) | 194.7 | 10.6 | 22.4 |
| 319-1 | Base-3 | 922 | (1200) | 621 | (90.0) | 427.0 | 11.7 | 15.4 |
| 319-3 | Base-3 | 922 | (1200) | 552 | (80.0) | 2253.0 | 14.3 | 27.7 |
| 6C6-71[c] | Weld-C[b] | 922 | (1200) | 691 | (100.2) | 20.5 | 2.8 | 8.4 |
| 6C6-73[c] | Weld-C | 922 | (1200) | 655 | (95.0) | 217.1 | 2.4 | 6.3 |
| 6C6-72[d] | Weld-C | 922 | (1200) | 621 | (90.0) | 309.1 | 2.1 | 5.8 |
| 319-9 | Base-3 | 978 | (1300) | 517 | (75.0) | 128.1 | 10.8 | 23.7 |
| 319-7 | Base-3 | 978 | (1300) | 448 | (65.0) | 363.7 | 8.9 | 16.1 |
| 319-8 | Base-3 | 978 | (1300) | 414 | (60.0) | 593.7 | 8.2 | 26.0 |

[a] - Heat 3 (52C9EK, 1/2 inch VIM-ESR plate)

[b] - Heat 6 (2180-4-9478, 1/2 inch VIM-ESR plate) welded with weld wire batch C (Ht. 52 BOE). Gage length was 50.8mm long and contained ∿ 12.7mm weld deposit.

[c] - Failed in weld

[d] - Failed in HAZ

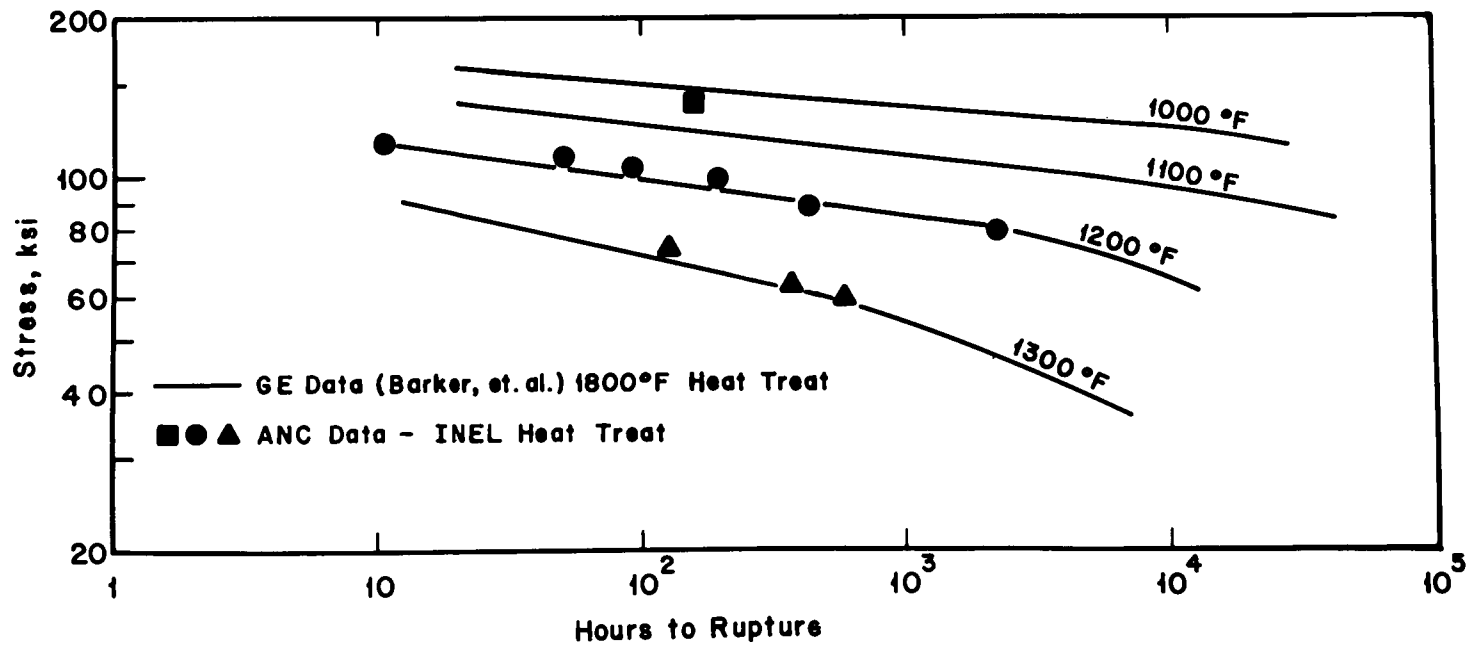


Fig. 1.10. Stress-Rupture Data of Alloy 718 given the INEL Heat Treatment Compared with Conventionally Heat Treated Material.[4]

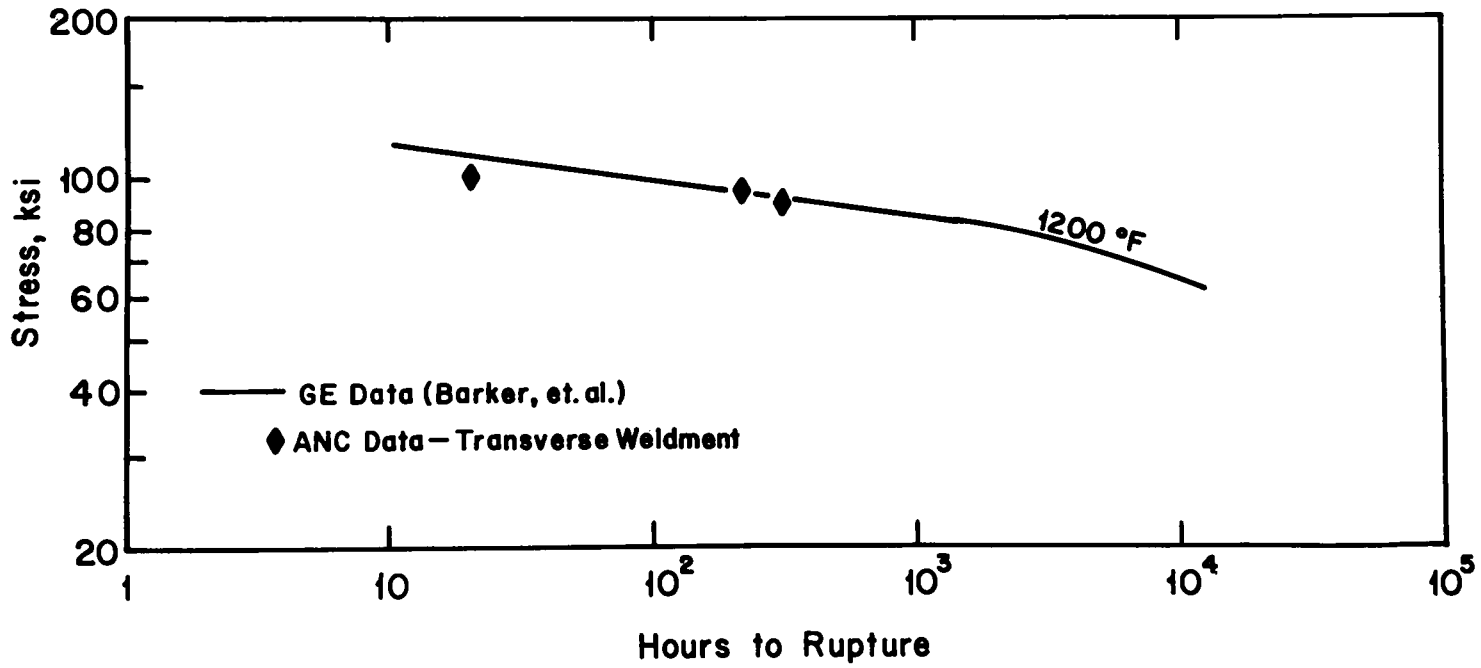


Fig. 1.11. Stress-Rupture Data of Transverse Weldment of Alloy 718 given the INEL Heat Treatment Compared with Conventionally Heat Treated Material.[4]

variable for both heat treatments making comparisons much more difficult but trends show the INEL heat treatment values to be equivalent or perhaps better than the 1750°F conventional heat treatment.

## 1.3 REFERENCES

1. D. D. Keiser, et. al, Mechanical Property Test Data for Structural Materials Quarterly Progress Report for Period Ending July 31, 1974, ORNL-4998, Section 1.3.

2. C. R. Brinkman and G. E. Korth, "Strain Fatigue and Tensile Behavior of Inconel 718 from Room Temperature to 650°C," JTEVA, Vol. 2, No. 4, July 1974, (249-259).

3. G. E. Korth and G. R. Smolik, Mechanical Property Test Data for Structural Materials Quarterly Progress Report for Period Ending July 31, 1975, ORNL-5106 (14-16).

4. J. F. Barker, et. al, "Long Time Stability of Inconel 718," J. Metals, January 1970, (31-41).

# 2. ARGONNE NATIONAL LABORATORY

R. W. Weeks

## 2.1 INTRODUCTION

Argonne National Laboratory (ANL) is conducting extensive programs to provide elevated-temperature, low-cycle fatigue data on Types 304 and 316 stainless steel and to study the effects of sodium environment on the elevated-temperature mechanical properties of these materials. Both programs are in support of LMFBR component design. The present report describes the results of low-cycle fatigue tests conducted on Type 304 stainless steel at 600°C in flowing sodium, and includes creep-rupture data on Type 304 stainless steel in the solution-annealed and sodium-preexposed conditions.

## 2.2 SODIUM EFFECTS ON LMFBR MATERIALS -- T. F. Kassner

### 2.2.1 Influence of Sodium Environment on the Low-cycle Fatigue Behavior of Austenitic Stainless Steels -- D. L. Smith and G. J. Zeman

The effects of a high-temperature sodium environment on the low-cycle fatigue behavior of AISI Types 304 and 316 stainless steel are being investigated. The tests have been formulated to determine (a) the effect of testing in a sodium environment, and (b) the effect of long-term sodium exposure on the fatigue properties of these steels. The fatigue tests are performed in sodium of controlled purity (∿1 ppm oxygen and 0.3 ppm carbon) at a strain rate of $4 \times 10^{-3}$ $s^{-1}$. The experimental equipment and testing procedures have been described previously.[1,2]

Limited low-cycle fatigue data obtained for annealed Type 304 stainless steel tested in air at 600°C are given in Fig. 2.1. More extensive data of Weeks et al.[3] and Brinkman and Korth[4] at 593°C are shown for comparison. The fatigue response of annealed Type 304 stainless steel tested in sodium at 600°C is indicated in Fig. 2.2. At total strain ranges below 1%, the fatigue lifetime in sodium is in excellent agreement with the base-line air data from Fig. 2.1. At

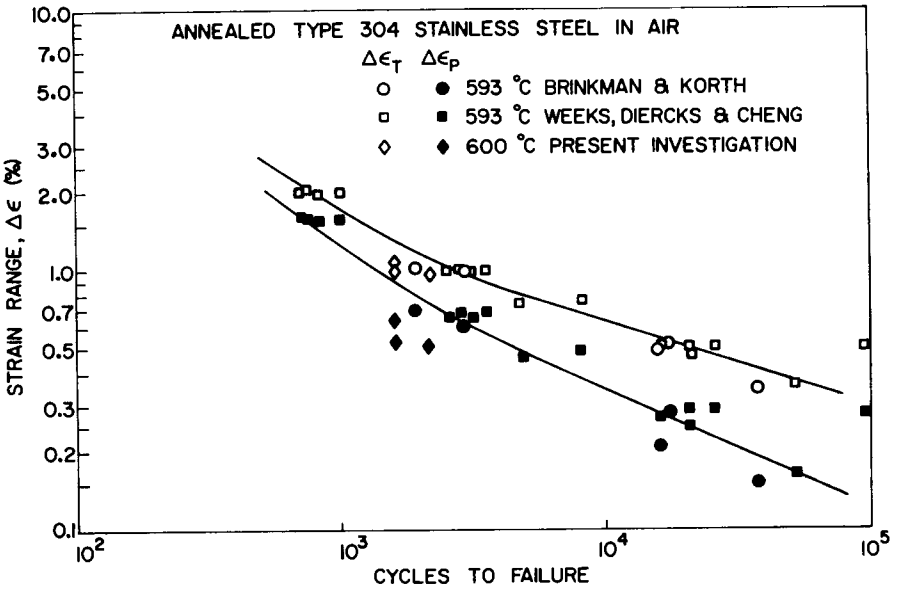


Fig. 2.1. Fatigue Data Obtained on Annealed Type 304 Stainless Steel in an Air Environment. Neg. No. MSD-62378.

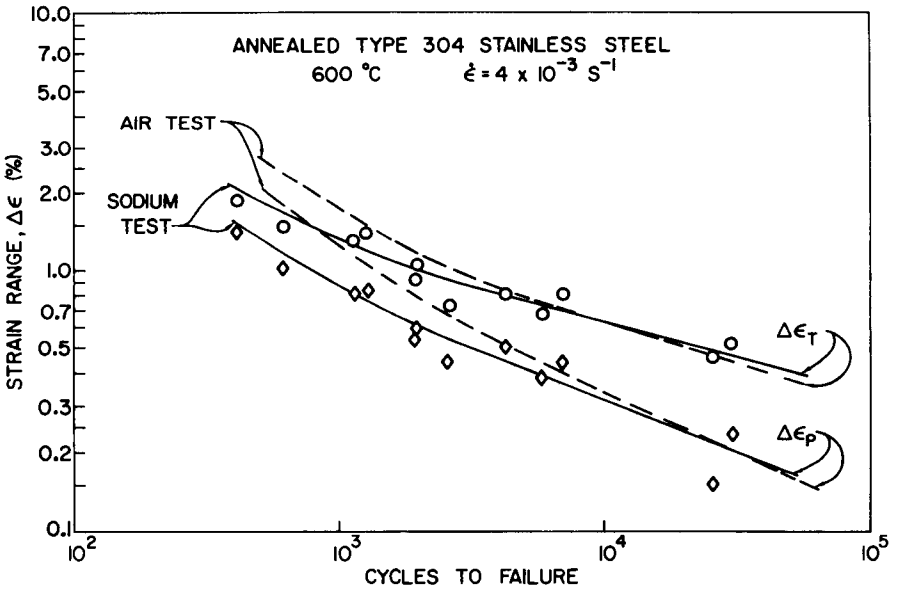


Fig. 2.2. Comparison of Fatigue Data Obtained on Annealed Type 304 Stainless Steel Tested in Air and in Sodium. Neg. No. MSD-62379.

higher strain ranges (i.e., $\Delta\varepsilon_t > 1\%$), the fatigue lifetime in sodium is slightly lower than that in air. These results differ from previous results for Type 316 stainless steel at 600°C.[2] The lifetime of this steel tested in sodium was significantly greater (by a factor of four at $\Delta\varepsilon_t = 1\%$) than when tested in air. The reasons for the differences in fatigue behavior of the two steels are being investigated.

Fatigue tests were also conducted on Type 304 stainless steel samples preexposed to 600°C sodium for 1512 h. The long-term exposure to sodium containing 0.4 ppm carbon produced a carbon gradient near the surface of the material. The carbon concentration ranged from 0.30 wt% at the surface to the bulk concentration of 0.05 wt% at a depth of ∿4 mils. Results for the sodium-exposed material are shown in Fig. 2.3. The fatigue lifetime for the sodium-exposed specimens is about a factor of four greater than that for the annealed specimens at a total strain range of 1%. This result for Type 304 stainless steel also differs from that observed for Type 316 stainless steel in that the 1512-h sodium exposure had little effect on the fatigue lifetime of Type 316 stainless steel.[2]

The cyclic stress-strain response for Type 304 stainless steel is shown in Fig. 2.4. The results obtained for annealed material in both sodium and air are in agreement with literature data. Some softening of the sodium-exposed specimens was observed, which is in qualitative agreement with data for Type 316 stainless steel.

### 2.2.2 Uniaxial Creep-rupture Properties of Austenitic Stainless Steels -- K. Natesan and O. K. Chopra

The effect of carburization of the creep-rupture properties of Types 304, 316, and Ti-modified 316 stainless steel, after exposure to well-characterized sodium at temperatures between 550 and 700°C, is being determined. The mechanical-property changes in the carburized material will be correlated with the sodium purity, which will be helpful in establishing better design and performance criteria for components that operate in a sodium environment.

Data have been obtained on the uniaxial creep-rupture properties of Type 304 stainless steel specimens in the solution-annealed condition

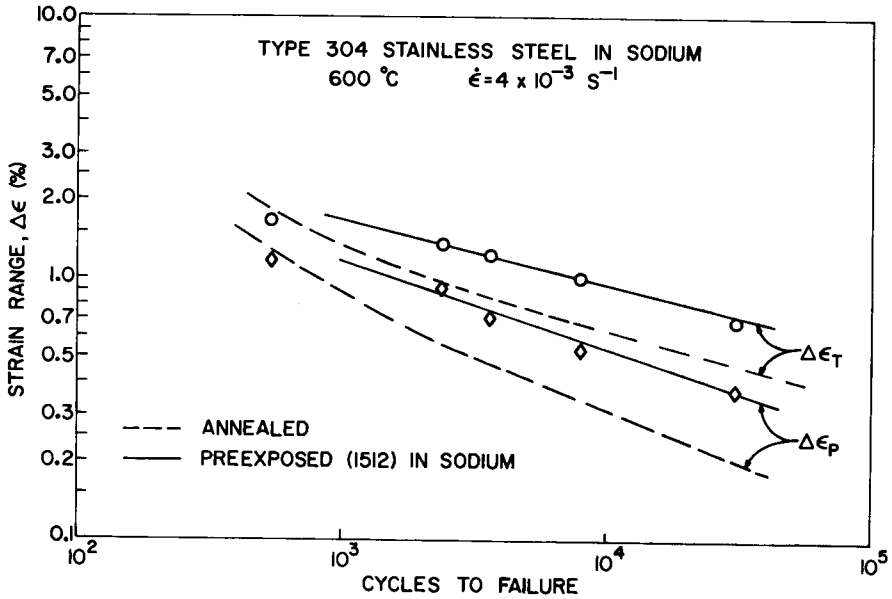


Fig. 2.3. Fatigue Data Obtained on Type 304 Stainless Steel Tested in Sodium after a 1500-h Exposure to Sodium at 600°C Compared with Data for Annealed Material Tested in Sodium. Neg. No. MSD-62380.

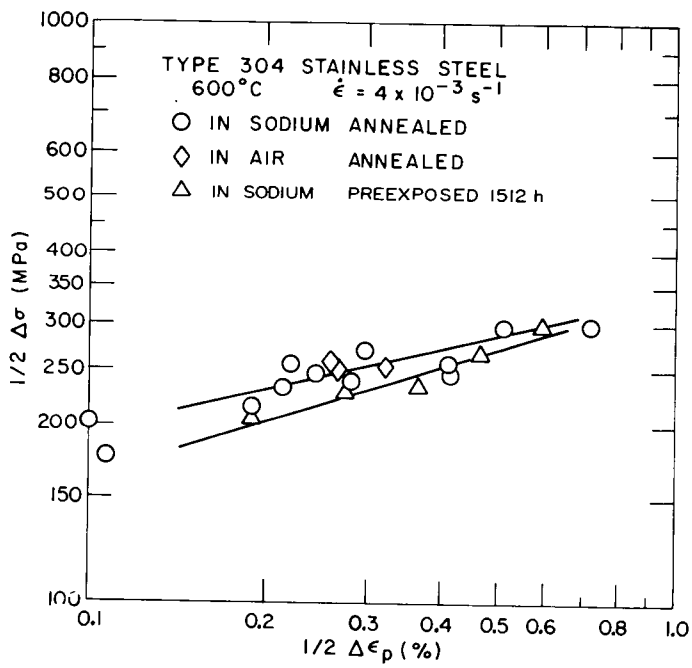


Fig. 2.4. Cyclic Stress-Strain Response of Type 304 Stainless Steel to a Change in Environment and a Change in Material Condition. Neg. No. MSD-62377.

and after exposure to a flowing sodium environment at temperatures of 700, 650, and 600°C. The specimens were exposed to sodium for times between 120 and 5012 h to produce carbon penetration depths of ∿0.01, 0.02, and 0.038 cm. The specimens were subsequently used in uniaxial creep-rupture tests in an argon environment to obtain the creep curves and creep-rupture times. The creep strain in the specimens was measured by a linear-variable-differential transducer, in which displacements of $5 \times 10^{-4}$ cm could be accurately determined. A schematic of a creep curve that is obtained from a constant-load creep test is shown in Fig. 2.5. Strain values $\varepsilon_1$ and $\varepsilon_2$ and times $t_1$ and $t_2$ were determined, respectively, from the beginning and end of the secondary creep stage. At rupture, elongation $\varepsilon_r$ and rupture time $t_r$ were determined. The minimum creep rate $\dot{\varepsilon}_m$, that is, the slope of the linear portion between $t_1$ and $t_2$, was also obtained from the creep-rupture curve. These quantities are listed in Tables 2.1-2.3 for specimens tested in the solution-annealed condition and after exposure to a flowing sodium environment. The average carbon concentrations in the mechanical test specimens were determined from combustion analysis of the specimens subsequent to creep testing, and the surface carbon concentrations in the specimens were determined from analysis of 2-mil-thick foils of the same material equilibrated in sodium during the specimen-exposure period. The values for surface and average carbon concentrations for various specimens are also listed in Tables 2.1-2.3.

Figures 2.6, 2.7, and 2.8 show the variations in rupture life and minimum creep rate with applied stress at 700, 650, and 600°C, respectively, for specimens tested in the solution-annealed condition and after exposure to a flowing sodium environment for different times. In general, the data show that, for the range of carburization attained in the present investigation, the exposure of the stainless steel to the sodium environment results in an increase in rupture life and a decrease in minimum creep rate when compared with material in the solution-annealed condition. The carbon concentration in sodium is such that Type 304 stainless steel with an initial carbon content of 0.046 wt% is almost in thermodynamic equilibrium with the carbon in sodium at 700°C.

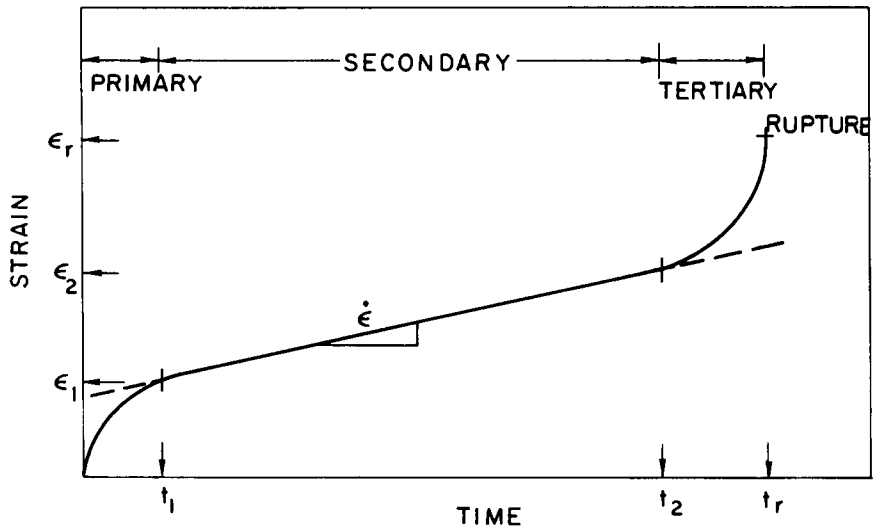


Fig. 2.5. Schematic of a Creep Curve from a Constant-load Creep Test. Neg. No. MSD-62370.

Table 2.1. Uniaxial Creep Behavior of AISI Type 304 Stainless Steel in Solution-annealed Condition

| Test Temperature, °C | Applied Stress, ksi | $t_1$, h | $\varepsilon_1$, % | $t_2$, h | $\varepsilon_2$, % | $t_r$, h | $\varepsilon_r$, % | $\dot{\varepsilon}_m$, %/h |
|---|---|---|---|---|---|---|---|---|
| 600 | 40 | 0.01 | 0.1 | 2.89 | 12.9 | 4.1 | 20.7 | 4.44 |
| | 35 | 0.95 | 2.4 | 9.6 | 14.0 | 14.7 | 24.7 | 1.34 |
| | 30 | 9.0 | 2.9 | 55.0 | 10.9 | 85.8 | 20.2 | 0.174 |
| | 25 | 20.0 | 2.0 | 75.5 | 8.7 | 139.3 | 14.8 | 0.121 |
| | 20 | 30.0 | 1.3 | 896.0 | 13.9 | 1223.0 | 20.9 | 0.0146 |
| | 16 | 50.0 | 0.08 | - | - | (a) | - | - |
| 650 | 30 | 0.4 | 4.8 | 2.23 | 18.4 | 3.4 | 34.2 | 7.43 |
| | 25 | 1.6 | 2.2 | 15.00 | 12.2 | 24.6 | 25.4 | 0.746 |
| | 20 | 5.0 | 3.3 | 46.50 | 15.5 | 68.3 | 27.1 | 0.294 |
| | 16 | 38.0 | 4.1 | 188.00 | 14.4 | 350.6 | 27.4 | 0.069 |
| | 14 | 165.0 | 8.2 | - | - | (a) | - | - |
| | 12 | 1070.0 | 4.2 | 2880.00 | 7.8 | (a) | (a) | 0.002 |
| 700 | 20 | 1.2 | 5.3 | 3.3 | 12.2 | 8.6 | 44.1 | 3.286 |
| | 16 | 8.5 | 3.2 | 55.0 | 17.0 | 86.0 | 32.0 | 0.297 |
| | 11 | 12.0 | 2.6 | 111.0 | 15.2 | 231.5 | 38.2 | 0.127 |
| | 10 | 100.0 | 8.8 | 281.0 | 21.8 | 386.3 | 33.7 | 0.072 |
| | 8 | 142.0 | 4.1 | 1010.0 | 19.6 | 1091.2 | 22.8 | 0.018 |

[a]Test terminated prior to fracture.

Table 2.2. Uniaxial Creep Behavior of AISI Type 304 Stainless Steel upon Exposure to Sodium Environment at 700°C

| Sodium Exposure | | Carbon Penetration Depth, μm | Carbon Concentration, wt% | | Test Temperature, °C | Applied Stress, ksi | $t_1$, h | $\varepsilon_1$, % | $t_2$, h | $\varepsilon_2$, % | $t_r$, h | $\varepsilon_r$, % | $\dot{\varepsilon}_m$, %/h |
|---|---|---|---|---|---|---|---|---|---|---|---|---|---|
| Temperature, °C | Time, h | | Surface | Average | | | | | | | | | |
| 700 | 120 | ∿100 | 0.046 | 0.043-0.046 | 700 | 20 | - | 3.5 | - | 17.8 | - | 47.7 | 2.295 |
| | | | | | 700 | 18 | - | 1.1 | 103.5 | 12.8 | 125.5 | 16.4 | 0.134 |
| | | | | | 700 | 13 | 250.0 | 9.4 | 460.0 | 12.6 | 678.0 | 17.2 | 0.0145 |
| | | | | | 700 | 11 | 436.0 | 15.8 | 1028.0 | 22.6 | 1052.0 | 22.9 | 0.0115 |
| | | | | | 700 | 9 | 2000.0 | 8.8 | 4210.0 | 14.9 | 4902.7 | 19.4 | 0.003 |
| | | | | | 650 | 20 | 25.0 | 7.5 | 77.0 | 18.3 | 125.0 | 36.5 | 0.205 |
| | | | | | 650 | 20 | 510.0 | 11.8 | 1460.0 | 25.8 | 1891.3 | 37.3 | 0.015 |
| 700 | 504 | ∿200 | | | 700 | 18 | 1.2 | 5.0 | 7.4 | 20.8 | 12.5 | 47.0 | 2.55 |
| | | | | | 700 | 16 | 3.2 | 4.8 | 22.0 | 22.3 | 36.5 | 52.4 | 0.931 |
| | | | | | 700 | 13 | 25.0 | 7.6 | 95.0 | 21.2 | 159.5 | 44.0 | 0.190 |
| | | | | | 700 | 10 | 195.0 | 10.8 | 330.0 | 17.2 | 600.8 | 42.0 | 0.045 |
| | | | | | 700 | 8 | 510.0 | 9.4 | 1830.0 | 20.6 | 2418.0 | 33.0 | 0.009 |
| 700 | 1512 | ∿375 | | | 700 | 20 | 0.4 | 1.0 | 4.3 | 21.5 | 6.2 | 41.9 | 4.97 |
| | | | | | 700 | 13 | 12.5 | 4.0 | 88.0 | 21.4 | 135.5 | 44.0 | 0.218 |
| | | | | | 700 | 11 | 30.0 | 6.6 | 134.0 | 23.0 | 182.2 | 35.6 | 0.128 |
| | | | | | 700 | 10 | 250.0 | 11.2 | 480.0 | 19.2 | 822.0 | 42.6 | 0.043 |
| | | | | | 700 | 8 | 800.0 | 14.4 | 2010.0 | 24.8 | 2338.0 | 31.9 | 0.011 |
| | | | | | 650 | 20 | 10.0 | 6.5 | 42.0 | 21.8 | 72.5 | 52.3 | 0.466 |
| | | | | | 650 | 20 | 150.0 | 5.2 | 680.0 | 17.8 | 1133.0 | 35.1 | 0.0236 |

Table 2.3. Uniaxial Creep Behavior of AISI Type 304 Stainless Steel upon Exposure to Sodium Environment at 650 and 600°C

| Sodium Exposure | | Carbon Penetration Depth, μm | Carbon Concentration, wt% | | Test Temperature, °C | Applied Stress, ksi | $t_1$, h | $\varepsilon_1$, % | $t_2$, h | $\varepsilon_2$, % | $t_r$, h | $\varepsilon_r$, % | $\dot{\varepsilon}_m$, %/h |
|---|---|---|---|---|---|---|---|---|---|---|---|---|---|
| Temperature, °C | Time, h | | Surface | Average | | | | | | | | | |
| 650 | 312 | 100 | 0.095 | 0.078 | 650 | 30 | 4.1 | 4.6 | 13.1 | 12.8 | 22.9 | 28.3 | 1.00 |
| | | | | | | 20 | 6.5 | 3.2 | 54.0 | 14.6 | 105.9 | 28.9 | 0.201 |
| | | | | | | 20 | 5.5 | 2.2 | 44.0 | 12.4 | 96.1 | 33.5 | 0.268 |
| | | | | | | 15 | 281.0 | 8.5 | 752.0 | 19.7 | 760.5 | 19.8 | 0.023 |
| | | | | | | 12 | 540.0 | 8.4 | 1860.0 | 22.4 | 2298.3 | 30.2 | 0.011 |
| | | | | | 700 | 20 | 1.2 | 5.5 | 3.2 | 11.8 | 7.8 | 42.0 | 3.76 |
| 650 | 1512 | 200 | 0.25±0.02 | 0.122±0.01 | 650 | 25 | 4.0 | 2.8 | 24.4 | 13.4 | 39.9 | 31.2 | 0.515 |
| | | | | | | 20 | 18.5 | 7.8 | 47.0 | 15.6 | 90.0 | 35.9 | 0.268 |
| | | | | | | 15 | 95.0 | 8.4 | 432.0 | 22.7 | 493.6 | 28.8 | 0.0424 |
| | | | | | | 12 | 200.0 | 3.0 | 2200.0 | 12.7 | 2546.9 | 17.4 | 0.0056 |
| | | | | | 700 | 20 | 1.2 | 5.8 | 6.6 | 21.8 | 9.7 | 42.6 | 2.963 |
| | | | | | 600 | 20 | 220.0 | 5.0 | 1270.0 | 17.8 | 1811.5 | 28.9 | 0.012 |
| 650 | 5012 | 375 | 0.25±0.02 | 0.195±0.01 | 650 | 20 | 14.0 | 2.3 | 94.0 | 9.6 | 203.7 | 28.0 | 0.091 |
| | | | | | 700 | 20 | 0.8 | 1.0 | 7.3 | 7.8 | 15.9 | 22.9 | 1.046 |
| | | | | | 600 | 20 | 190.0 | 2.8 | 1440.0 | 15.6 | 2124.7 | 28.0 | 0.010 |
| 600 | 1512 | 100 | 0.30±0.02 | 0.145±0.01 | 600 | 35 | 11.8 | 6.3 | 25.2 | 10.7 | 34.7 | 14.9 | 0.328 |
| | | | | | | 30 | 38.0 | 3.7 | 215.0 | 7.9 | 251.0 | 9.5 | 0.024 |
| | | | | | | 25 | 148.0 | 4.4 | 433.0 | 8.5 | 631.4 | 13.2 | 0.014 |
| | | | | | | 22 | 1440.0 | 2.2 | 2600.0 | 2.8 | (a) | - | 0.0005 |
| | | | | | 700 | 20 | 13.0 | 2.6 | 96.0 | 12.8 | 16.1 | 26.7 | 1.221 |
| | | | | | 650 | 20 | 18.0 | 1.8 | 104.0 | 6.6 | 215.1 | 16.6 | 0.055 |

[a]Test terminated prior to fracture.

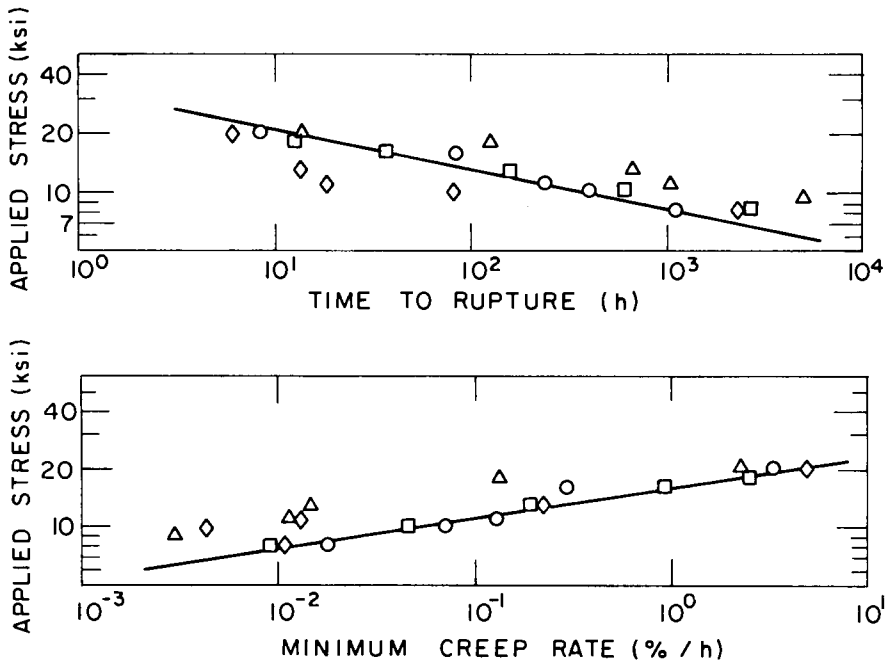


Fig. 2.6. Variations in Time to Rupture and Minimum Creep Rate with Applied Stress at 700°C. o solution-annealed; carburization depths; Δ 100 μm, ◻ 200 μm, and ◇ 375 μm. Neg. No. MSD-62368.

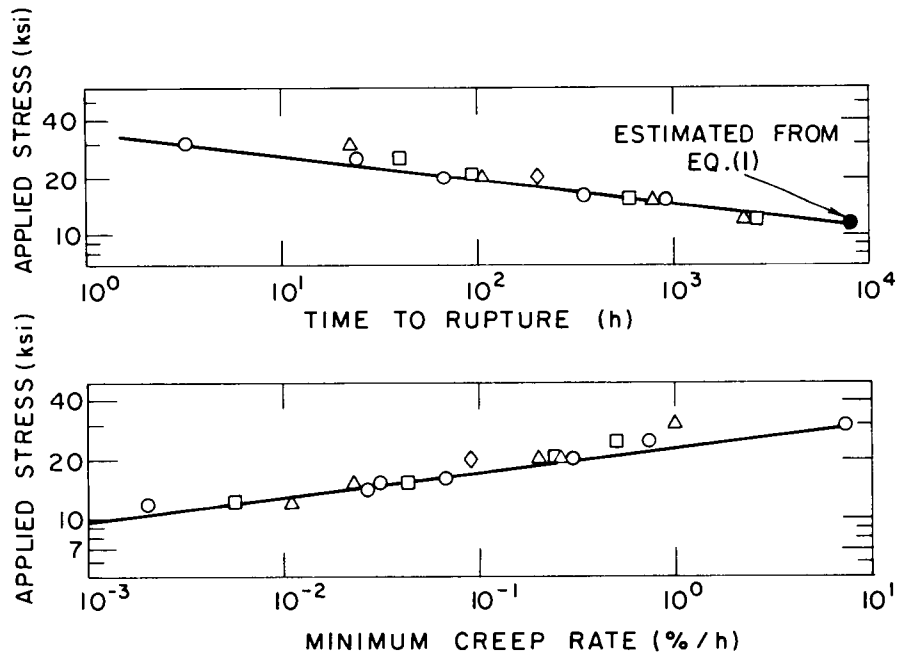


Fig. 2.7. Variations in Time to Rupture and Minimum Creep Rate with Applied Stress at 650°C. o Solution-annealed; carburization depths; Δ 100 μm, ◻ 200 μm, and ◇ 375 μm. Neg. No. MSD-62367.

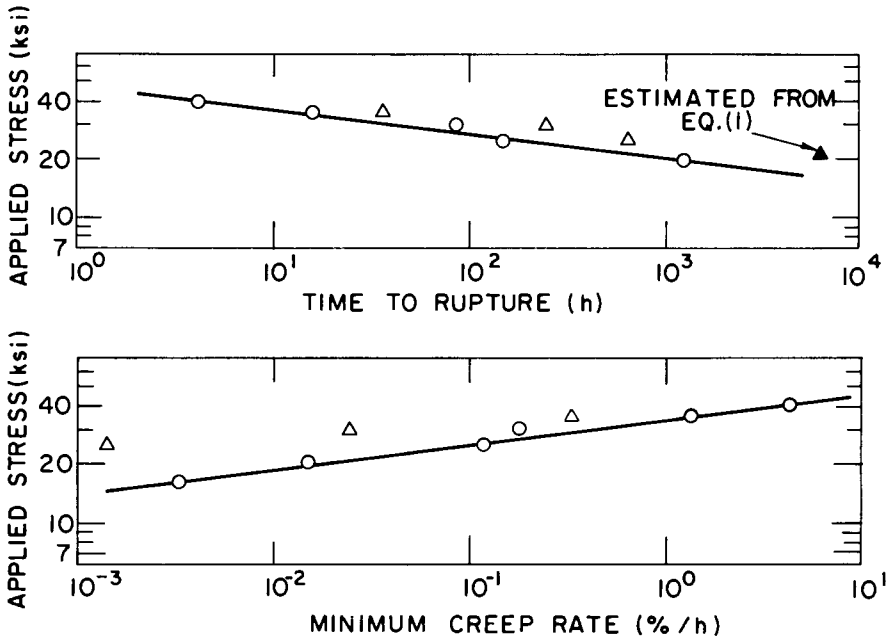


Fig. 2.8. Variations in Time to Rupture and Minimum Creep Rate with Applied Stress at 600°C. o Solution-annealed; carburization depths; Δ 100 μm, □ 200 μm, and ◇ 375 μm. Neg. No. MSD-62366.

Within the limits of uncertainty in carbon analysis and maintenance of constant carbon concentration in sodium, the steel at 700°C may have undergone slight carburization during the 120-h exposure, whereas it could have decarburized slightly during 1512-h exposure. This could account for the increase in rupture life for the shorter exposure and the decrease in life for the longer exposure at 700°C.

At sodium-exposure temperatures of 650 and 600°C, the steel carburizes, the amount depending on the time of exposure. The creep test results at these temperatures clearly show the beneficial effect of carburization in the stress range of our investigation.

2.2.2.1 Creep-rupture Correlations

To understand creep-rupture behavior more fully, various correlations between rupture life and other quantities determined from the creep-rupture curve were attempted. Relationships between rupture life and minimum creep rate or time for onset of tertiary creep are useful if they describe the creep behavior of the material over a wide range of temperatures and applied stresses. Furthermore, such relationships, if developed, can be used to evaluate the necessary creep quantities from standard stress-rupture tests. Tertiary creep is generally indicative of material cracking and void formation and therefore may be metallurgically related to material damage. Also, tertiary creep results in material instability, since an increase in strain rate occurs with an increase in strain and strain concentrations induced by creep are accelerated. As a result, a correlation between the rupture life and the time-to-tertiary creep will be useful to establish the onset of instability in design studies.

The variation of $t_r$ as a function of $\dot{\varepsilon}_m$ can be written as

$$t_r = C \left( \frac{1}{\dot{\varepsilon}_m} \right)^{\alpha}, \tag{1}$$

where C and $\alpha$ are constants. Figure 2.9 shows a plot of $\ln t_r$ versus $\ln \dot{\varepsilon}_m$ for specimens tested in the solution-annealed condition and after exposure to flowing sodium at 700, 650, and 600°C. In general, the

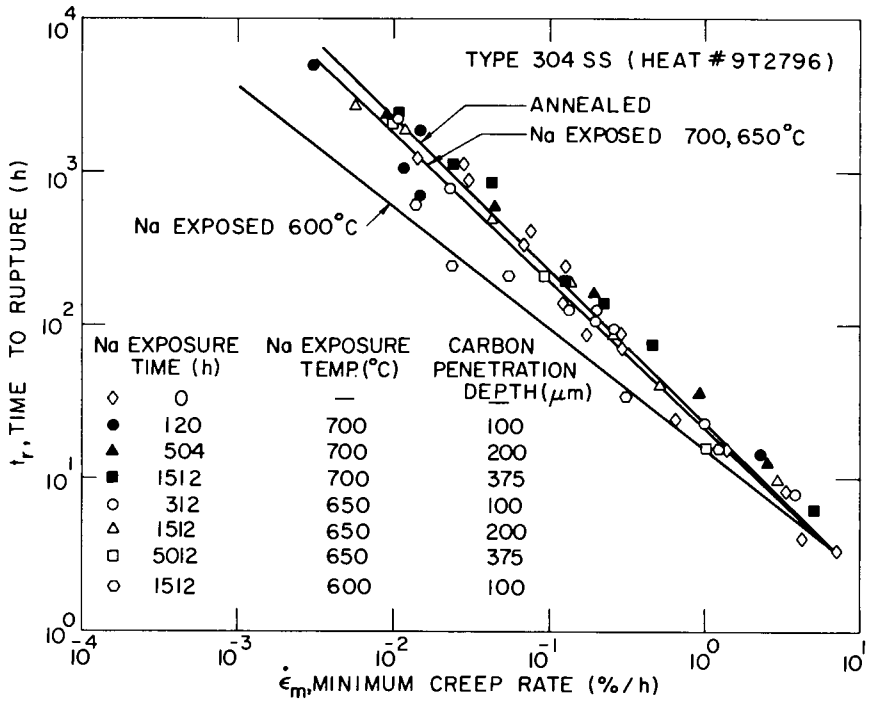


Fig. 2.9. Plot of Rupture Life vs Minimum Creep Rate for Specimens in Solution-annealed and Sodium-exposed Conditions. Neg. No. MSD-62369.

results indicate that, for a given rupture time, the minimum creep rate decreases as the amount of carburization increases. The evaluations of constants C and $\alpha$, for different sets of data in Fig. 2.9, are given in Table 2.4. The correlations developed here are used to estimate the rupture lives of specimens for tests terminated prior to fracture (data in Tables 2.1 and 2.2 identified with a). The calculated values, the solid symbols in Figs. 2.7 and 2.8, are in excellent agreement with extrapolations based on data obtained at the higher stresses.

The time for the onset of tertiary creep can be correlated with rupture life by the expression

$$t_2 = B(t_r)^{\beta} \tag{2}$$

where B and $\beta$ are constants. Figure 2.10 shows a plot of $\ln t_2$ versus $\ln t_r$ for specimens tested in the solution-annealed condition and after exposure to flowing sodium at 700, 650, and 600°C. The constants B and $\beta$ evaluated for different sets of data are given in Table 2.4. The results show that the time to initiation of tertiary creep is a fixed fraction of the time for rupture for the annealed and carburized conditions in the temperature range 600-700°C. The rate of coalescence of voids and growth of cracks during tertiary creep should be related to quantity B in Eq. (2). Since $\beta$ is almost unity, $B = t_2/t_r$. From the values of B reported in Table 2.4 for specimens in the solution-annealed condition and after exposure to sodium, it can be concluded that the void coalescence rates in carburized specimens are slower than in the annealed specimens.

The effect of carburization on the creep and rupture behavior of Type 304 stainless steel is dependent on the influence of the carbide-precipitate particles on the creep mechanism. In this regard, applicability of high-temperature steady-state creep theories, such as recovery-controlled creep and thermally activated dislocation glide theory, to second stage creep behavior is being examined for both solution-annealed and sodium-exposed specimens.

Table 2.4. Correlations Relating Time to Rupture with Minimum Creep Rate and Time to Tertiary Creep

$$t_r = C(\dot{\varepsilon}_m)^{-\alpha}$$

| Treatment | $\alpha$ | C |
|---|---|---|
| Solution Annealed | 0.99 | 22.16 |
| Na Exposed at 650 and 700°C | 0.95 | 22.45 |
| Na Exposed at 600°C | 0.79 | 17.90 |

$$t_2 = B(t_r)^{\beta}$$

| Treatment | $\beta$ | B |
|---|---|---|
| Solution Annealed | 1.025 | 0.558 |
| Na Exposed (All Temperatures) | 1.061 | 0.475 |
| All Data | 1.05 | 0.501 |

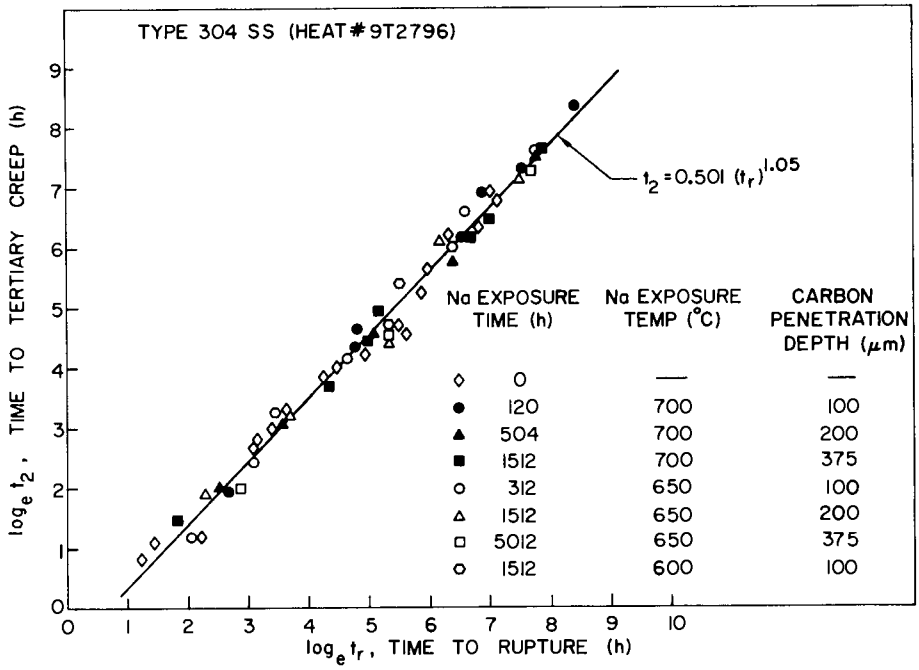


Fig. 2.10. Plot of Rupture Life vs Time to Tertiary Creep for Specimens in Solution-annealed and Sodium-exposed Conditions. Neg. No. MSD-62365.

## 2.3 REFERENCES

1. Mechanical Properties Test Data for Structural Materials Quarterly Progress Report for Period Ending October 31, 1974, Oak Ridge National Laboratory, ORNL-5103, pp. 13-17.

2. D. L. Smith, K. Natesan, T. F. Kassner, and G. J. Zeman, "Effects of Sodium on the Low-cycle Fatigue Behavior of Austenitic Stainless Steel," in Structural Materials for Service at Elevated Temperatures in Nuclear Power Generation, ASME MPC-1, 1975, pp. 290-301.

3. R. W. Weeks, D. R. Diercks, and C. F. Cheng, "ANL Low-cycle Fatigue Studies -- Program, Results, and Analysis," Argonne National Laboratory, ANL-8009 (November 1973).

4. C. R. Brinkman and G. E. Korth, "Heat-to-heat Variations in the Fatigue and Creep-Fatigue Behavior of AISI Type 304 Stainless Steel at 593°C," J. Nucl. Mater., 48, 293-306 (1973).

# 3. OAK RIDGE NATIONAL LABORATORY

W. R. Martin

## 3.1 INTRODUCTION

The ORNL mechanical properties effort comprises several programs. The program Mechanical Properties and Behavior for Structural Materials deals with materials of general applicability to the LMFBR program. Other programs are concerned with the mechanical properties of weldments in LMFBR components, the specific materials of interest for LMFBR steam generators, collection and correlation of mechanical data needed for design on high-temperature LMFBR systems, and materials for the primary circuit and steam generators of HTGR systems.

## 3.2 MECHANICAL PROPERTIES AND BEHAVIOR FOR STRUCTURAL MATERIALS — C. R. Brinkman

The objective of this program is to collect mechanical property data and material behavior for LMFBR structural and component materials. Included in the scope of this effort are the following: (1) basic tensile, creep, creep-rupture, and relaxation base-line data that are directly applicable to design criteria and methods for types 304 and 316 stainless steel reference heats and cyclic stress-strain tests performed with emphasis on loading and aging history effects, (2) variations in properties for several heats of types 304 and 316 stainless steel determined to allow establishment of minimum and average values of specific properties and the equations parameters required for design purposes. This work will include determination of property variation of samples from different mill products within a given heat of stainless steel.

### 3.2.1 Mechanical Property Characterization of Type 304 Stainless Steel Reference Heat — V. K. Sikka, R. H. Baldwin, and E. B. Patton

#### 3.2.1.1 Creep and Rupture Properties of the 51-mm (2-in.) Plate of Reference Heat

Several creep tests on 51-mm (2-in.) plate of the reference heat of type 304 stainless steel (9T2796) continued. The test times and strains

for all tests have been updated and are summarized in Table 3.1. Creep stresses and test temperatures of various specimens being tested are plotted in Fig. 3.1. Included in the figure are also the curves for ASME code case minimum stress to rupture in $3 \times 10^4$, $10^5$, and $3 \times 10^5$ hr. We have also included the stress and temperature conditions for pressure vessel, sodium input pipe, and inner reactor skirt for fast breeder reactors, calculated by Frost and Ashby.[1] Figure 3.2 shows stresses and temperature conditions for which creep and creep-rupture data are available in the literature for type 304 stainless steel. Note that most of the data available in the literature are at stresses and temperatures significantly higher than fast breeder design conditions. Only 12 creep test data points are below the $3 \times 10^4$-hr stress-rupture curve in Fig. 3.2, as opposed to 26 such points for the ongoing program at ORNL shown in Fig. 3.1. Another point to note from Fig. 3.1 is that the position of stress-rupture curves with respect to the test conditions provides guidance on the possibility of a specimen rupture. We can see from Fig. 3.1 that out of 26 test conditions below the rupture curve for $3 \times 10^4$ hr, 19 tests will possibly rupture at periods approaching $10^5$ hr or greater.

Figure 3.3 shows a partial deformation map[1,2] for type 304 stainless steel. This map has been drawn from the work of Frost and Ashby. Superimposed on the deformation map are the ASME stress-rupture points for various times. Minimum stress-rupture curves for periods of 1, $3 \times 10^4$, $1 \times 10^5$, and $3 \times 10^5$ hr are also shown. The deformation map shows the areas of dislocation glide, dislocation creep, and diffusional flow. It can be noted from Fig. 3.3 that the stress-rupture data for periods of 1 to $3 \times 10^5$ hr fall within one deformation mechanism area (dislocation creep) for test temperatures up to 538°C (1000°F). Since these stresses represent only minimum values, the average values can be expected to fall within one deformation mechanism for higher temperatures than 538°C (1000°F). For higher temperatures the stress-rupture mechanism crosses from dislocation creep to diffusional flow. Stresses at which the deformation mechanism changes at various

Table 3.1 Creep Tests on Type 304 Stainless Steel Reference Heat 9T2796 51-mm-Thick (2-in.) Plate[a]

| Test | Temperature (°C) | Temperature (°F) | Stress (MPa) | Stress (ksi) | Time in Test (hr) | Strain, % Loading | Strain, % Creep | Ratio of Creep Stress to Yield Stress[b] | Comments[c] |
|---|---|---|---|---|---|---|---|---|---|
| 11595 | 427 | 800 | 138 | 20.0 | 22,361 | 2.67 | 0.081 | 1.57 | |
| 12368 | 427 | 800 | 124 | 18.0 | 19,109 | 1.91 | 0.0216 | 1.42 | |
| 12472 | 427 | 800 | 110 | 16.0 | 17,816 | 1.17 | 0.069 | 1.26 | |
| 12570 | 427 | 800 | 97 | 14.0 | 17,477 | 0.83 | 0.048 | 1.10 | |
| 15319 | 482 | 900 | 207 | 30.0 | 5,852 | 7.86 | 0.168 | 2.54 | |
| 15268 | 482 | 900 | 138 | 20.0 | 6,714 | 3.38 | 0.068 | 1.70 | |
| 11569 | 482 | 900 | 138 | 20.0 | 15,455 | 3.27 | 0.141 | 1.70 | Discontinued |
| 12375 | 482 | 900 | 124 | 18.0 | 12,376 | 2.40 | 0.072 | 1.53 | Discontinued |
| 11675 | 482 | 900 | 110 | 16.0 | 2,451 | 1.48 | 0.032 | 1.36 | Discontinued |
| 11693 | 482 | 900 | 97 | 14.0 | 97 | 0.92 | 0.14 | 1.19 | Discontinued |
| 11830 | 482 | 900 | 83 | 12.0 | 83 | 0.35 | 0.04 | 1.02 | Discontinued |
| 13152 | 482 | 900 | 69 | 10.0 | 15,881 | 0.089 | 0.015 | 0.85 | |
| 13020 | 482 | 900 | 69 | 10.0 | 16,329 | 0.085 | 0.030 | 0.85 | |
| 10489 | 538 | 1000 | 138 | 20.0 | 26,729 | 3.80 | 0.762 | 1.80 | |
| 12250 | 538 | 1000 | 124 | 18.0 | 19,709 | 2.62 | 0.317 | 1.62 | |
| 11625 | 538 | 1000 | 110 | 16.0 | 19,656 | 1.79 | 0.262 | 1.44 | Discontinued |
| 10491 | 538 | 1000 | 97 | 14.0 | 27,726 | 1.16 | 0.276 | 1.26 | |
| 12444 | 538 | 1000 | 97 | 14.0 | 18,297 | 1.18 | 0.223 | 1.26 | |
| 12445 | 538 | 1000 | 97 | 14.0 | 4,498 | 1.17 | 0.090 | 1.26 | Discontinued |
| 11568 | 538 | 1000 | 83 | 12.0 | 22,472 | 0.53 | 0.119 | 1.08 | |
| 11626 | 538 | 1000 | 69 | 10.0 | 22,161 | 0.071 | 0.118 | 0.90 | |
| 11641 | 538 | 1000 | 55 | 8.0 | 3,170 | 0.040 | 0.027 | 0.72 | Discontinued |
| 10853 | 593 | 1100 | 124 | 18.0 | 4,547 | 2.84 | 5.94 | 1.65 | Ruptured |
| 10852 | 593 | 1100 | 110 | 16.0 | 14,647 | 2.29 | 3.55 | 1.47 | Ruptured |
| 13947 | 593 | 1100 | 110 | 16.0 | 10,000 | 2.13 | 1.54 | 1.47 | Discontinued |
| 10554 | 593 | 1100 | 97 | 14.0 | 8,710 | 1.40 | 0.65 | 1.28 | Discontinued |
| 11596 | 593 | 1100 | 83 | 12.0 | 22,329 | 0.52 | 0.52 | 1.10 | |
| 10490 | 593 | 1100 | 69 | 10.0 | 27,148 | 0.22 | 0.403 | 0.92 | |
| 13710 | 593 | 1100 | 69 | 10.0 | 2,010 | 0.096 | 0.204 | 0.92 | Discontinued |
| 14163 | 593 | 1100 | 69 | 10.0 | 9,980 | 0.228 | 0.230 | 0.92 | |
| 11227 | 593 | 1100 | 55 | 8.0 | 6,103 | 0.041 | 0.080 | 0.73 | Discontinued |
| 12459 | 593 | 1100 | 34 | 5.0 | 18,017 | 0.024 | 0.170 | 0.46 | |
| 10855 | 649 | 1200 | 110 | 16.0 | 304 | 2.41 | 12.0 | 1.57 | Ruptured |
| 13764 | 649 | 1200 | 110 | 16.0 | 245 | 2.42 | 14.53 | 1.57 | Ruptured |
| 10854 | 649 | 1200 | 97 | 14.0 | 761 | 1.60 | 13.0 | 1.37 | Ruptured |
| 11563 | 649 | 1200 | 83 | 12.0 | 2,674 | 0.59 | 13.0 | 1.18 | Ruptured |
| 11226 | 649 | 1200 | 69 | 10.0 | 7,278 | 0.18 | 7.0 | 0.98 | Ruptured |
| 10851 | 649 | 1200 | 55 | 8.0 | 20,059 | 0.044 | 5.03 | 0.78 | Ruptured |
| 12255 | 649 | 1200 | 34 | 5.0 | 992 | 0.030 | 0.08 | 0.49 | Discontinued |
| 12443 | 649 | 1200 | 34 | 5.0 | 17,843 | 0.024 | 0.188 | 0.49 | |
| 12460 | 649 | 1200 | 21 | 3.0 | 18,139 | 0.020 | 0.240 | 0.29 | |
| 10856 | 704 | 1300 | 69 | 10.0 | 568 | 0.067 | 15.60 | 0.90 | Ruptured |
| 11562 | 704 | 1300 | 69 | 10.0 | 653 | 0.12 | 22.50 | 0.90 | Ruptured |
| 11222 | 704 | 1300 | 55 | 8.0 | 2,760 | 0.031 | 16.40 | 0.72 | Ruptured |
| 12254 | 704 | 1300 | 34 | 5.0 | 19,174 | 0.030 | 3.63 | 0.45 | |
| 12461 | 704 | 1300 | 21 | 3.0 | 18,129 | 0.018 | 0.35 | 0.27 | |
| 12462 | 704 | 1300 | 14 | 2.0 | 17,772 | 0.010 | 0.223 | 0.18 | |

[a]Annealed 0.5 hr at 1093°C before testing. All tests loaded at a strain rate of 0.004/min.

[b]Yield stresses used in this ratio were 12,700 psi (88 MPa) at 427°C (800°F), 11,800 psi (81 MPa) at 482°C (900°F), 11,100 psi (77 MPa) at 538°C (1000°F), 10,900 psi (75 MPa) at 593°C (1100°F), 10,200 psi (70 MPa) at 649°C (1200°F). 11,000 psi (77 MPa) at 704°C (1300°F).

[c]Unless otherwise noted, tests in progress.

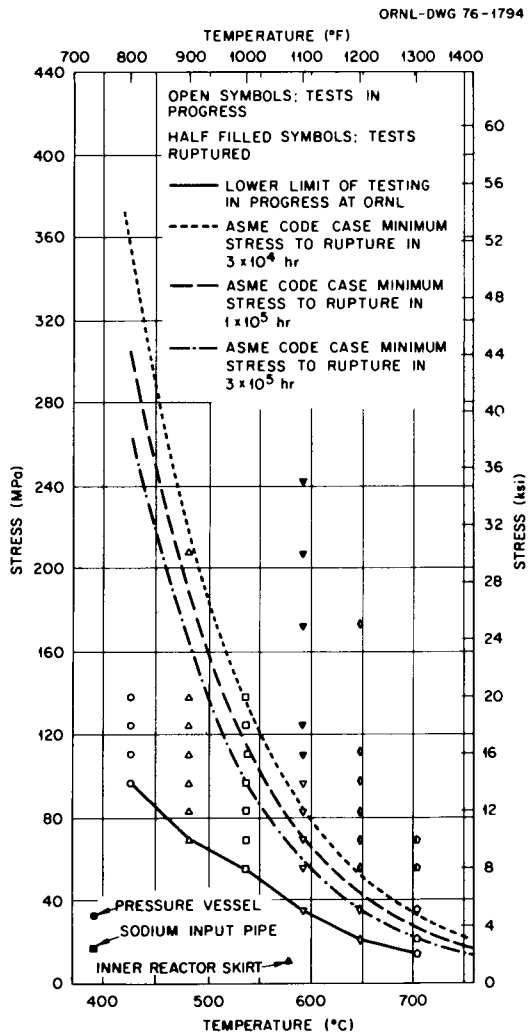


Fig. 3.1. Stress Versus Test Temperature for Various Creep Testing Conditions for the Reference Heat of Type 304 Stainless Steel.

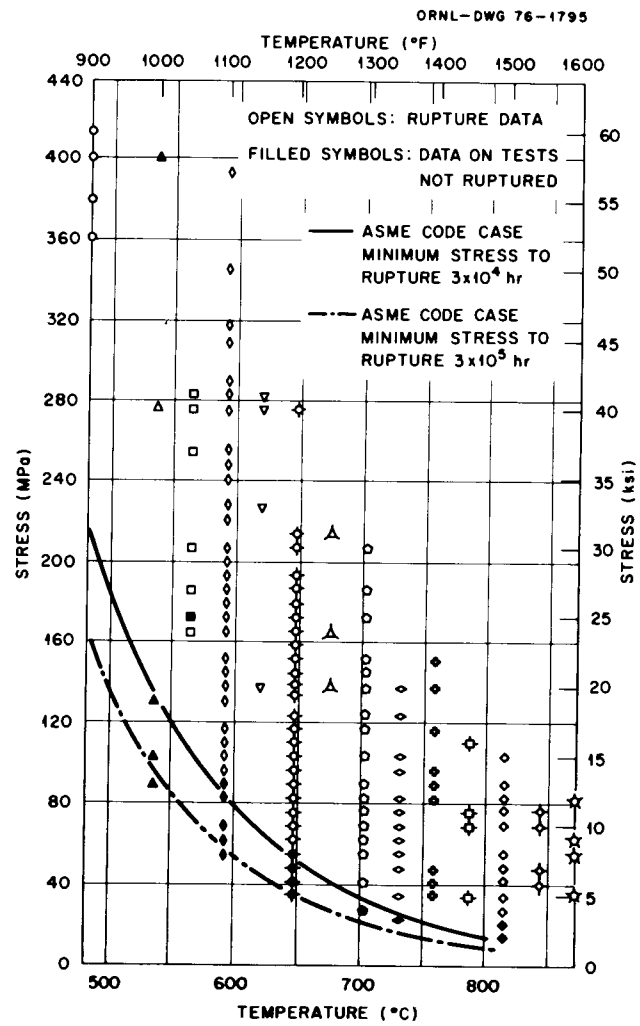


Fig. 3.2. Stress Versus Test Temperature for Various Testing Conditions for which Creep Data are Available in Literature for Type 304 Stainless Steel.

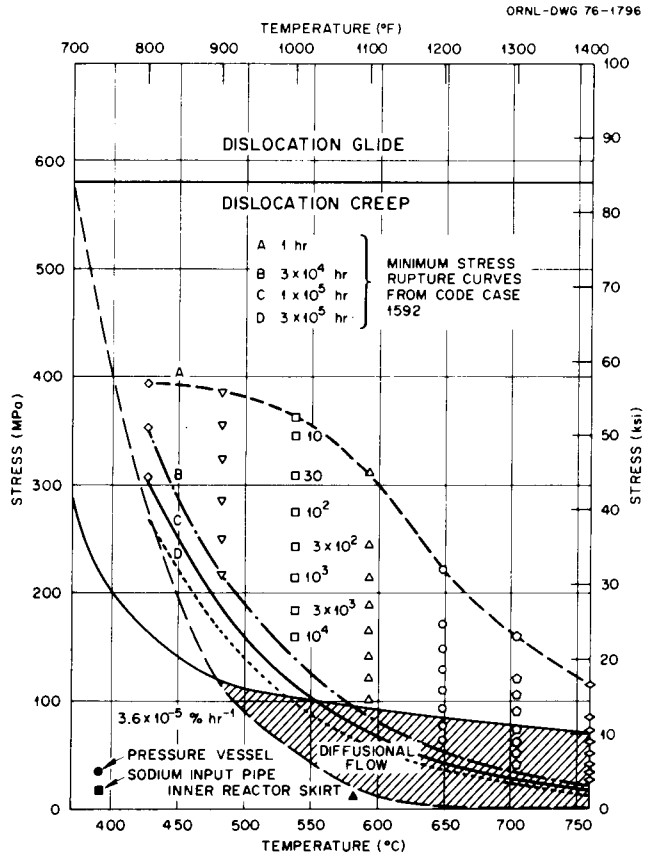


Fig. 3.3 Deformation Map of Type 304 Stainless Steel.

temperatures are summarized below:

| | | | | |
|---|---|---|---|---|
| Temperature, °C(°F) | 565(1050) | 593(1100) | 649(1200) | 704(1300) |
| Stress, MPa(ksi) | 97(14) | 93(13.5) | 83(12) | 77(11) |
| Time, hr | $3 \times 10^4$ to $1 \times 10^5$ | $10^4$ to $3 \times 10^4$ | $10^3$ to $3 \times 10^3$ | $10^2$ to $3 \times 10^2$ |

Frost and Ashby[1] represented the dislocation creep by a power-law creep equation of the form:

$$\dot{\gamma} = A_s \frac{D\mu b}{kT} \left(\frac{\sigma_s}{\mu}\right)^n , \tag{1a}$$

where

$D$ = lattice diffusion coefficient,

$A_s$ and $n$ = dimensionless constants,

$\mu$ = shear modulus,

$b$ = Burger's vector,
$k$ = Boltzmann constant,
$\dot{\gamma}$ = steady-state shear strain rate = $\dot{\varepsilon}_m/\sqrt{3}$,
$\sigma_s$ = applied shear stress = $\sigma/\sqrt{3}$,
$\dot{\varepsilon}_m$ = uniaxial minimum creep rated,
$\sigma$ = uniaxial stress.

Frost and Ashby[1] used a value of 7.5 for $n$ in Eq. (1a) for the construction of the deformation map for type 304 stainless steel. Results described in Fig. 3.3 would indicate that Eq. (1a) can be used to extrapolate the creep rate data for test temperatures up to 593°C (1100°F) from the high-stress range (stress less than dislocation glide and dislocation creep boundary) to stresses where rupture is anticipated at $3 \times 10^5$ hr. Furthermore, from a relationship between minimum creep rate and stress to rupture, Eq. (1a) can be modified to a form that should be capable of extrapolation of even time to rupture data:

$$\frac{1}{t_r} = A_s' \frac{D\mu b}{kT} \left(\frac{\sigma_s}{\mu}\right)^{n_r} , \tag{1b}$$

where

$A_s' = A_s a$ = constant,
$t_r$ = time to rupture,
$\dot{\gamma} = a/t_r$, $a$ = constant,
$n_r$ = stress exponent for rupture.

Attention should be drawn to Figs. 3.1 and 3.3, where design conditions for various components of the fast breeder reactor are included. Note that the design conditions are well inside the diffusional flow field, in the regime controlled by grain boundary diffusion. It should be noted from Fig. 3.2 that almost no data from the literature lie in this field, and thus available data are of almost no help in predicting the steady-state creep rates of the hypothetical components. Frost and Ashby[1] have concluded that experiments in the diffusional field are urgently needed. Reexamining Figs. 3.1 and 3.3 shows that at least 26

of the tests needed in the diffusion-controlled region are in progress at ORNL. Furthermore, because all these tests are in an area where a single deformation mechanism controls, the results should be extrapolatable to near the design conditions.

Frost and Ashby[1] used the following equations to draw the diffusional controlled area in the map:

$$\dot{\gamma} = \frac{42\sigma_s \Omega}{kTD^2} D_{\text{eff}} \quad , \tag{2}$$

where

$$D_{\text{eff}} = D_v \left(1 + \frac{\pi\delta}{d} \frac{D_B}{D_v}\right) , \tag{3}$$

and

$\Omega$ = atomic volume,

$d$ = grain diameter,

$\delta$ = grain boundary width,

$D_B$ = grain boundary diffusion coefficient,

$D_v$ = lattice diffusion coefficient.

At high temperatures, when lattice diffusion controls the rate, the flow is known as Nabarro-Herring creep and given by combining Eqs. (2) and (3):

$$\dot{\gamma}_{\text{NH}} = \frac{42\sigma_s \Omega}{kTd^2} D_v \quad . \tag{4}$$

At lower temperatures, when grain boundary diffusion takes over, it is called Coble creep and given by:

$$\dot{\gamma}_{\text{c}} = \frac{42\sigma_s \Omega \pi\delta}{kTd^3} D_B \quad . \tag{5}$$

In conclusion, then, we have shown the need for more definite fast breeder design-oriented data and how ORNL tests in progress fill the need. Furthermore, we have shown the possibility of power law

extrapolation of stress-rupture data to rupture times of $3 \times 10^5$ hr for test temperatures up to 538°C (1000°F). For the design condition range, diffusion-controlled equations are thought to be more appropriate.

### 3.2.2 Heat-to-Heat Variations of Mechanical Properties of Austenitic Stainless Steels of Types 304 and 316 — V. K. Sikka

#### 3.2.2.1 Relation Between Tensile and Creep Properties

Heat-to-heat variation in 20 heats of type 304 and 7 heats of type 316 stainless steels were presented in a recent paper.[3] Since that paper, a closer examination of creep and creep-rupture properties of type 304 stainless steels in terms of detailed chemical analysis was performed and reported.[4,5] We showed that increasing the niobium content from 10 to 200 ppm increases the creep strength. A further examination of heat-to-heat variation in tensile and creep properties showed that heats with higher niobium contents had higher elevated-temperature ultimate tensile strength.

Figure 3.4 shows an example of creep curves of seven heats of type 304 stainless steels. The niobium content of these heats increased from 20 to 100 ppm and ultimate tensile strength of the same heats varied from 336 to 364 MPa (48.7—52.8 ksi). Figure 3.5 shows $10^3$- and $10^4$-hr creep-rupture strengths of various heats at 593°C (1100°F) plotted as functions of ultimate tensile strength of these heats at 593°C (1100°F) and a strain rate of 0.04/min. Note a definite trend of increasing creep rupture strength with increasing ultimate tensile strength. The trend in Fig. 3.5 is consistent with a relation between creep-rupture strength, $S_R^t$, and ultimate tensile strength, $S_u$, of the following form:

$$S_R^t = \alpha \exp(\beta S_u) \quad , \tag{6}$$

where $\alpha$ and $\beta$ are constants.

The importance of ultimate tensile strength in creep-rupture strength is not exactly a new concept. It has been suggested from time to time by various investigators. For example, Bens[6] showed that an increase in

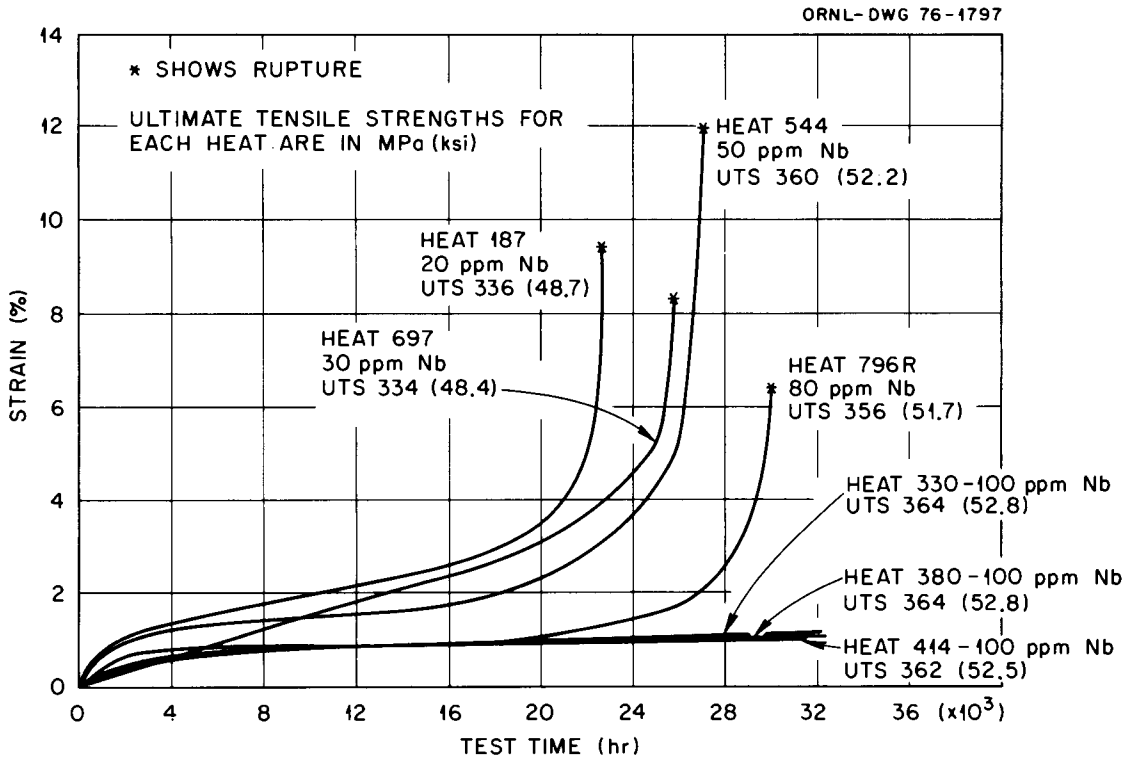


Fig. 3.4. Comparison of Long-Term Creep Behavior at 593°C (1100°F) and 117 MPa (17 ksi) for Seven Heats of Type 304 Stainless Steel.

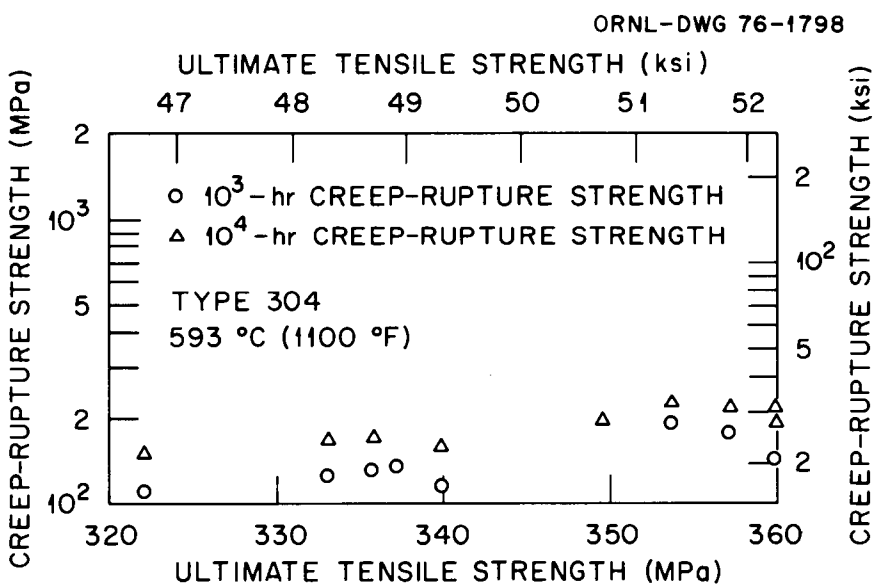


Fig. 3.5. Creep-Rupture Strength as a Function of Ultimate Tensile Strength at Creep Test Temperature for Various Heats of Type 304 Stainless Steel.

hot hardness at 871°C (1600°F) of various chromium-base alloys produced an increase in time to rupture for fixed stresses of 138 and 165 MPa (20 and 24 ksi). The trend observed by Bens could be expressed by an alternate form of Eq. (6). Garofalo et al.[7] showed that an increase in hot hardness increased the creep and creep-rupture strength of 18-8 stainless steels and carbon steels in the temperature range 454 to 816°C (850–1500°F). They did not suggest any relationship of the type given in Eq. (6). Our plot of their trend data in Fig. 3.6 indeed shows the trend suggested by Eq. (6). For comparison, we have also plotted the slope of our $10^3$-hr line obtained for several austenitic stainless steels. Note that the slope of our line is quite similar to that obtained by replotting the data of Garofalo et al. Next, we present the results of applying Eq. (6) to ORNL data and data collected from the literature on various types of austenitic stainless steels. Figure 3.7 shows the plot of creep-rupture strength as a function of ultimate tensile strength for various

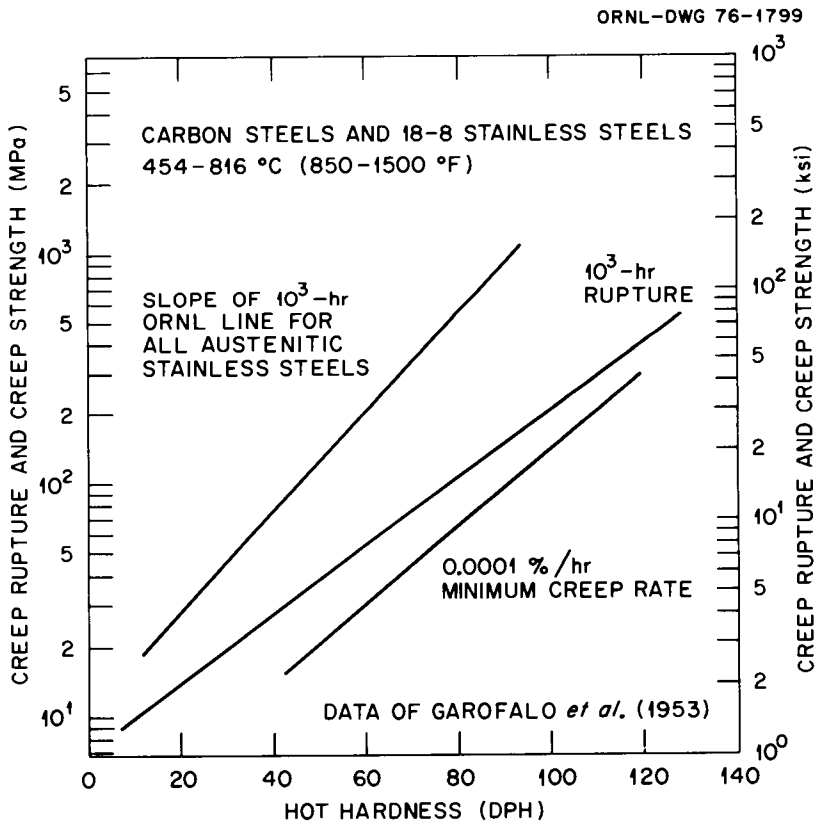


Fig. 3.6. Creep and Creep-Rupture Strength as a Function of Hot Hardness for Carbon Steels and 18-8 Stainless Steels. Data of Garofalo et al. *Trans. Am. Soc. Met.* 45: 377–96 (1953).

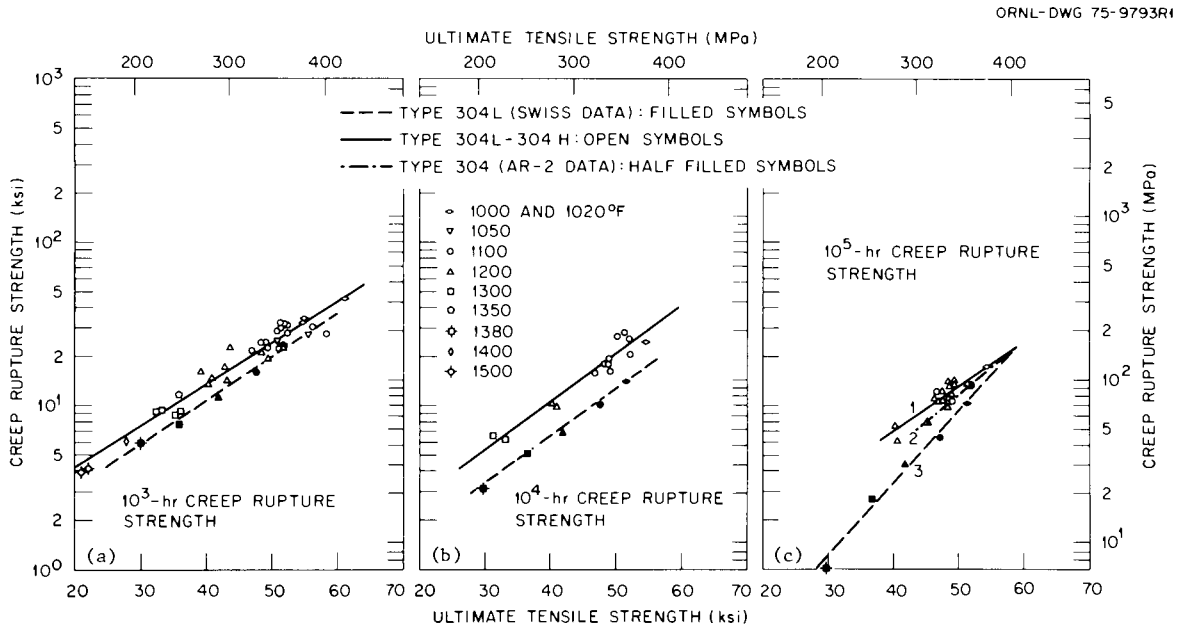


Fig. 3.7. Creep-Rupture Strength as a Function of Ultimate Tensile Strength at the Creep Test Temperature for Various Heats and Variations of Type 304 Stainless Steel. (a) $10^3$ hr. (b) $10^4$ hr. (c) $10^5$ hr. Lines 1, 2, and 3 in (c) represent extrapolated values from 10,000 to 20,000 hr, from 50,000 to 60,000 hr, and nonextrapolated data, respectively. In °C, the temperatures listed are 538, 549, 566, 593, 649, 704, 732, 749, 760, and 816.

heats of type 304 stainless steels, tested in the temperature range 538 to 816°C (1000–1500°F). Note that Eq. (6) describes the variation in creep-rupture strength both among different heats and due to the test temperature. A detailed description of Fig. 3.7 is available in another report.[8] Similar plots for types 316, 347, 321, and 201, 202, and 303 stainless steel are presented in Figs. 3.8 through 3.11. The least square lines are drawn through the data points, and the constants $\alpha$ and $\beta$ calculated for various austenitic stainless steels are summarized in Table 3.2.

Further investigation showed that the creep strength (stress required to cause a specified secondary creep rate) also can be related to ultimate tensile strength by Eq. (6). Figures 3.12 through 3.15 show examples of creep strength versus ultimate tensile strength plots for various types of austenitic stainless steels. Constants $\alpha$ and $\beta$ from the creep strength plots are summarized in Table 3.3. Since constants $\alpha$ and $\beta$ were not very

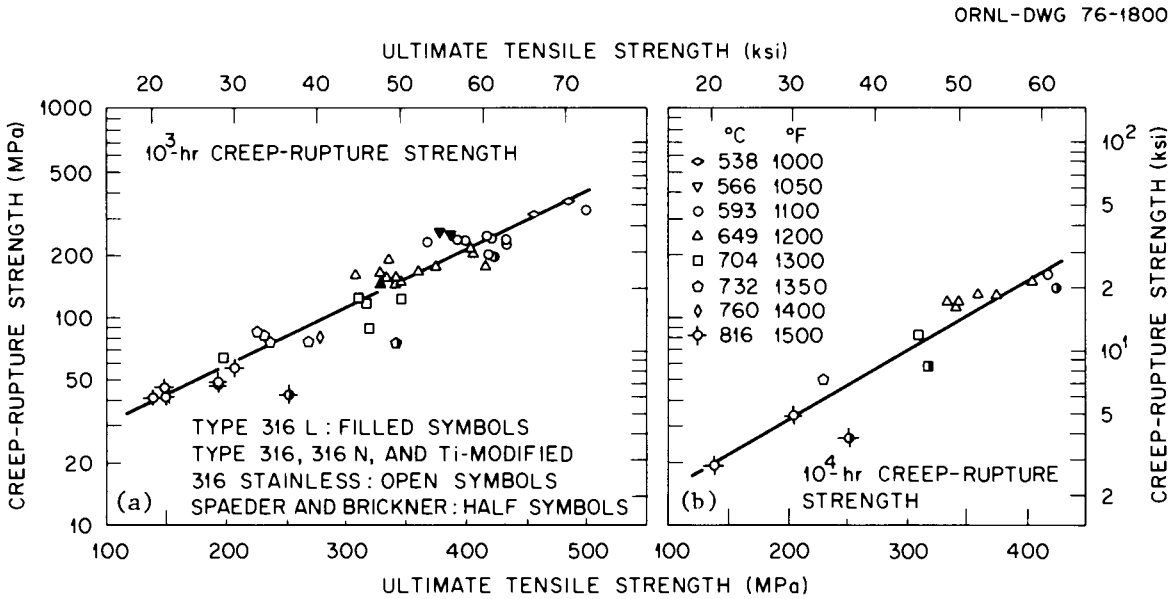


Fig. 3.8. Creep-Rupture Strength as a Function of Ultimate Tensile Strength at the Creep-Test Temperature for Various Heats and Variations of Type 316 Stainless Steel. (a) $10^3$ hr. (b) $10^4$ hr.

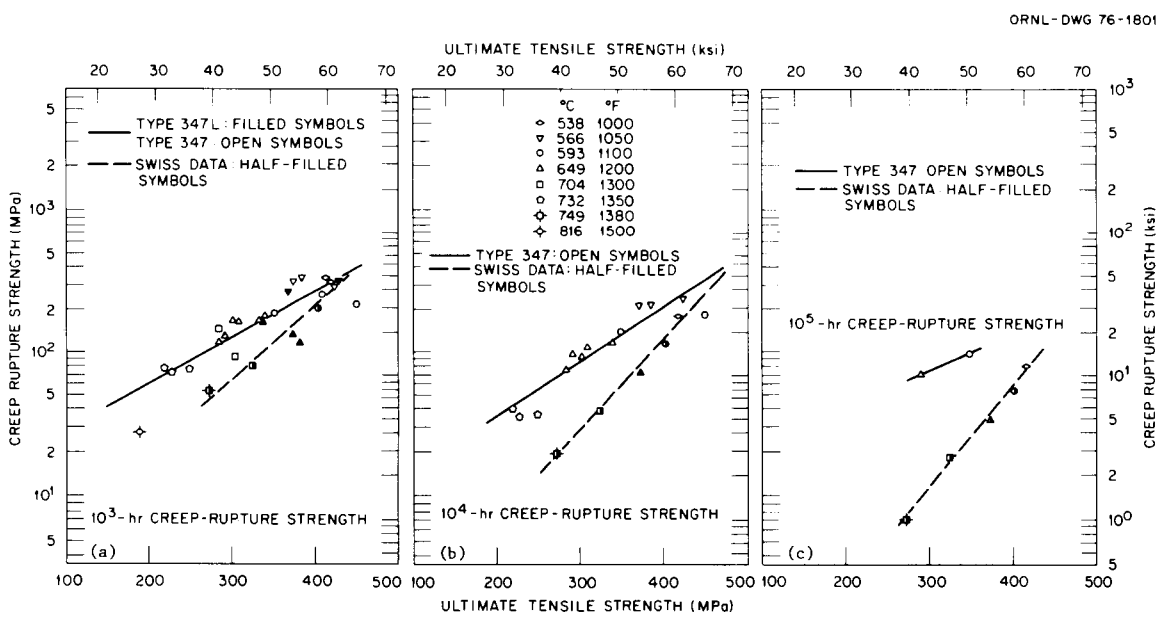


Fig. 3.9. Creep-Rupture Strength as a Function of Ultimate Tensile Strength at the Creep-Test Temperature for Various Heats and Variations of Type 347 Stainless Steel. (a) $10^3$ hr. (b) $10^4$ hr. (c) $10^5$ hr.

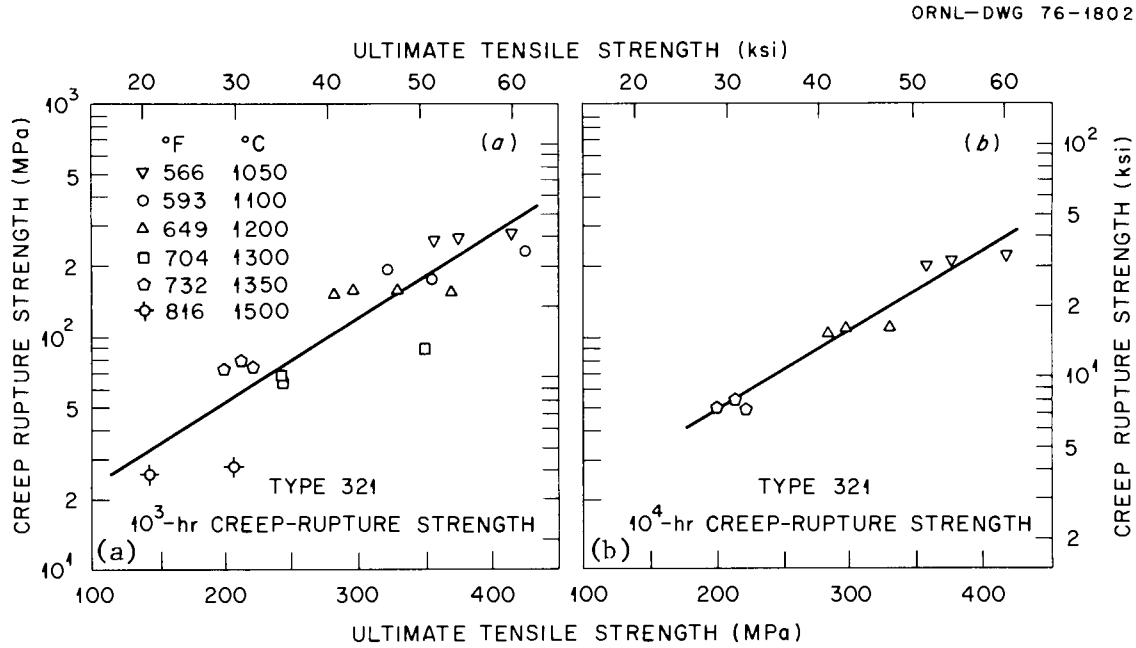


Fig. 3.10. Creep-Rupture Strength as a Function of Ultimate Tensile Strength at the Creep-Test Temperature for Various Heats and Variations of Type 321 Stainless Steel. (a) $10^3$ hr. (b) $10^4$ hr.

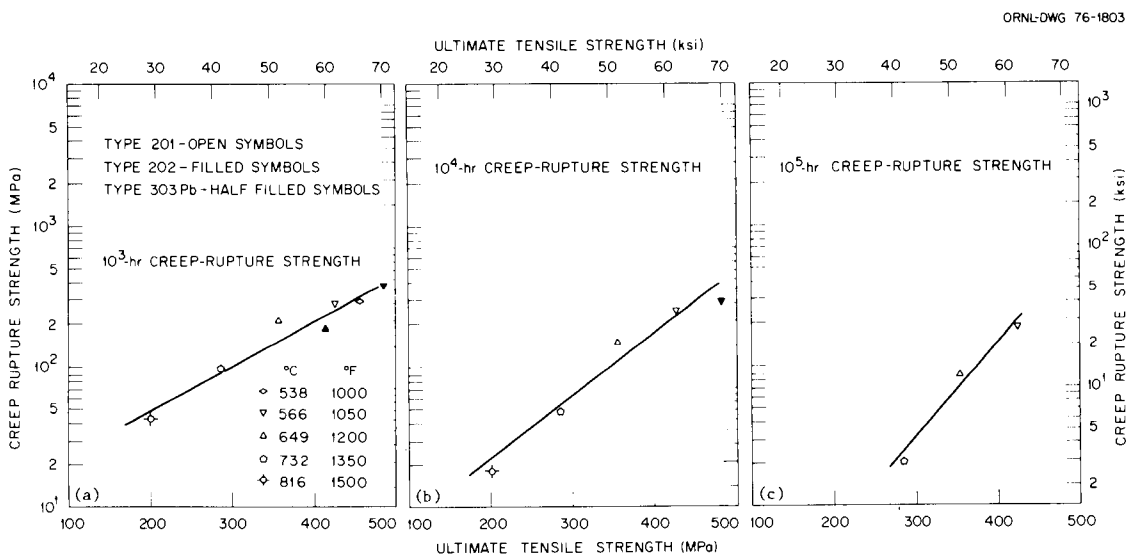


Fig. 3.11. Creep-Rupture Strength as a Function of Ultimate Tensile Strength at the Creep-Test Temperature for Various Heats and Variations of Types 201, 202, and 303 Stainless Steels. (a) $10^3$ hr. (b) $10^4$ hr. (c) $10^5$ hr.

Table 3.2. Summary of Creep-Rupture Strength Constants in Equation $S_R^t = \alpha \exp(\beta S_u)$ for Several Austenitic Stainless Steels

| Stainless Steel Type | Number of Data Points | Temperature Range (°C) | Temperature Range (°F) | Constants[a] α (ksi) | Constants[a] β ($ksi^{-1}$) |
|---|---|---|---|---|---|
| | | $10^3$-hr Rupture Strength | | | |
| 304, 304L, 304H, 304N | 38 | 538–816 | 1000–1500 | 1.3198 | 0.05807 |
| 304L[b] | 5 | 550–750 | 1020–1380 | 0.9088 | 0.06111 |
| 316L, 316N, 316 (Ti modified) | 45 | 538–816 | 1000–1500 | 2.3761 | 0.04352 |
| 347, 347L | 23 | 538–816 | 1000–1500 | 1.9154 | 0.05151 |
| 347[b] | 5 | 550–750 | 1020–1380 | 0.2439 | 0.08335 |
| 321 | 21 | 566–816 | 1050–1500 | 1.4670 | 0.05720 |
| 201, 202, 303 | 7 | 538–816 | 1000–1500 | 1.6753 | 0.04980 |
| | | $10^4$-hr Rupture Strength | | | |
| 304, 304L, 304H, 304N | 14 | 538–704 | 1000–1300 | 0.6919 | 0.06774 |
| 304L[b] | 5 | 550–750 | 1020–1380 | 0.4449 | 0.06680 |
| 316L, 316N | 14 | 593–816 | 1100–1500 | 0.9753 | 0.05330 |
| 347, 347L | 13 | 566–732 | 1050–1350 | 0.8981 | 0.06001 |
| 347[b] | 5 | 550–750 | 1020–1380 | 0.0536 | 0.09961 |
| 321 | 9 | 566–732 | 1050–1350 | 1.4942 | 0.05413 |
| 201, 202, 303 | 5 | 566–816 | 1050–1500 | 0.3999 | 0.07004 |
| | | $10^5$-hr Rupture Strength | | | |
| 304, 304H[c] | 19 | 538–704 | 1000–1300 | 0.5745 | 0.06224 |
| 304[d] | 2 | 593–649 | 1100–1200 | 0.2558 | 0.07634 |
| 304L[b] | 5 | 550–750 | 1020–1320 | 0.0596 | 0.10055 |
| 347[c] | 2 | 593–649 | 1100–1200 | 1.8965 | 0.03958 |
| 347[b] | 5 | 550–750 | 1020–1380 | 0.0131 | 0.11110 |
| 201[c] | 3 | 566–732 | 1050–1350 | 0.0392 | 0.10705 |

[a]To convert to MPa, multiply α and divide β by 6.895.

[b]Creep-rupture strength was from 11 years of creep testing, but tensile strength values were obtained by multiplying average room-temperature value listed by Smith with his tensile strength ratio.

[c]Creep-rupture strength obtained by extrapolation.

[d]AR-2 data extrapolated from test times of 50,000 to 65,000 hr.

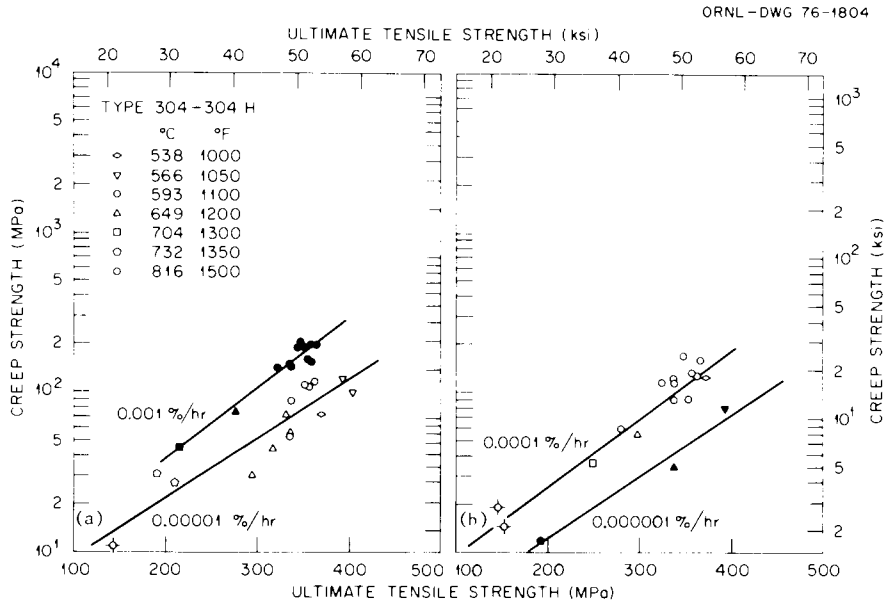


Fig. 3.12. Creep Strength as a Function of Ultimate Tensile Strength at the Creep-Test Temperature for Various Heats and Variations of Type 304 Stainless Steel. (a) 0.001%/hr and 0.00001%/hr. (b) 0.0001%/hr and 0.000001%/hr.

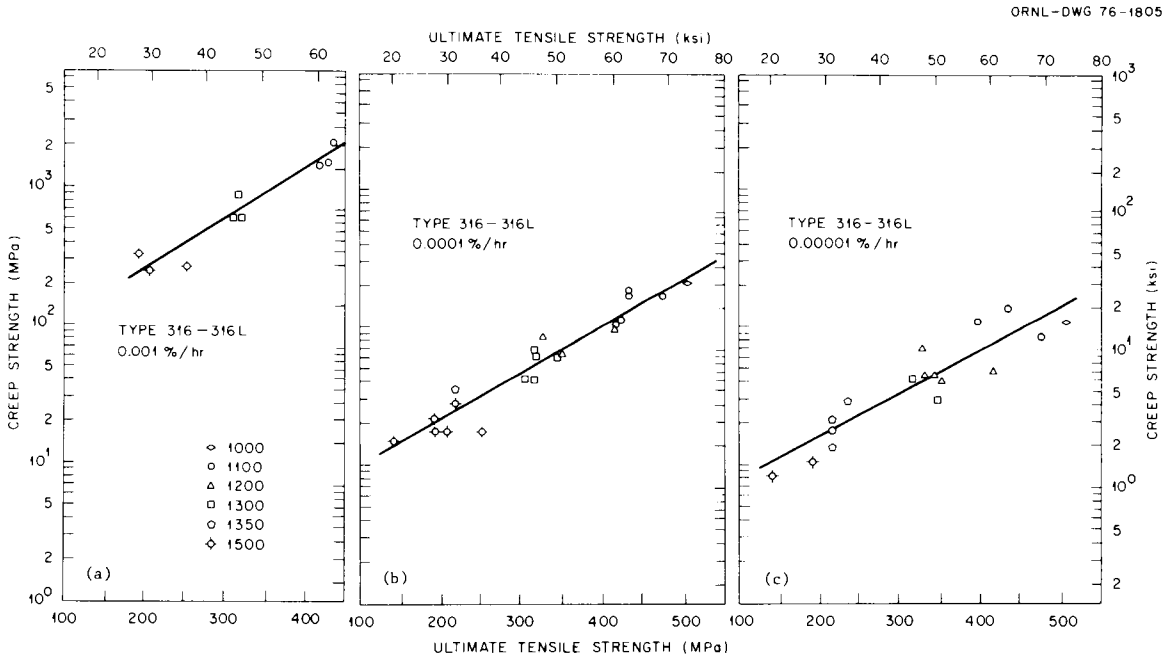


Fig. 3.13. Creep Strength as a Function of Ultimate Tensile Strength at the Creep-Test Temperature for Various Heats and Variations of Type 316 Stainless Steel. (a) 0.001%/hr. (b) 0.0001%/hr. (c) 0.00001%/hr.

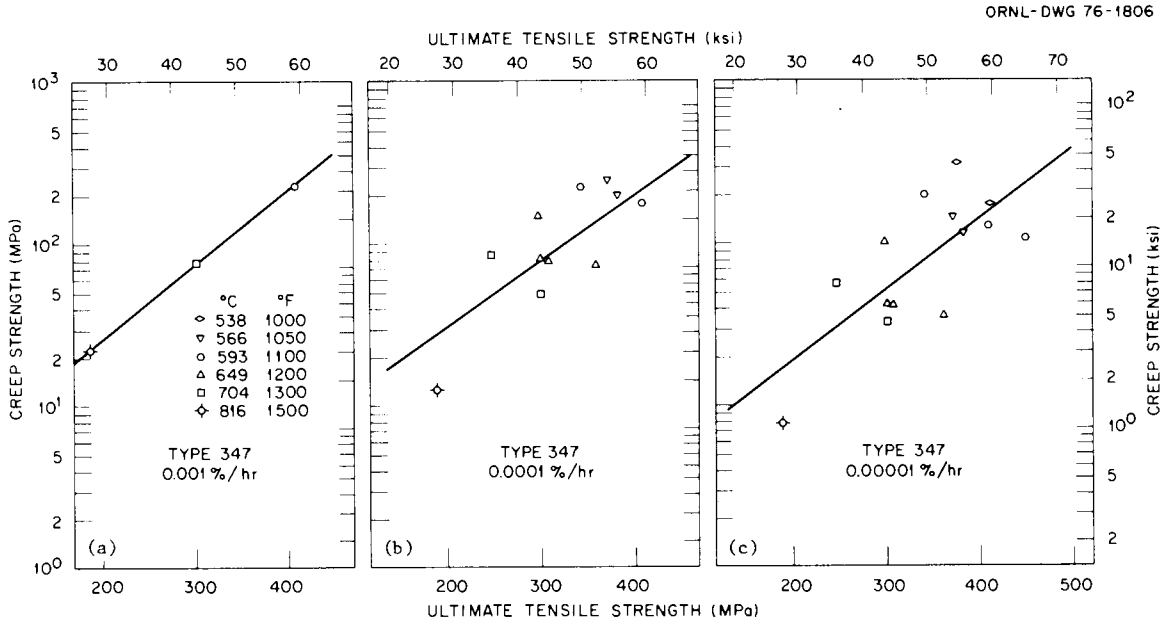


Fig. 3.14. Creep Strength as a Function of Ultimate Tensile Strength at the Creep-Test Temperature for Various Heats and Variations of Type 347 Stainless Steel. (a) 0.001%/hr. (b) 0.0001%/hr. (c) 0.00001%/hr.

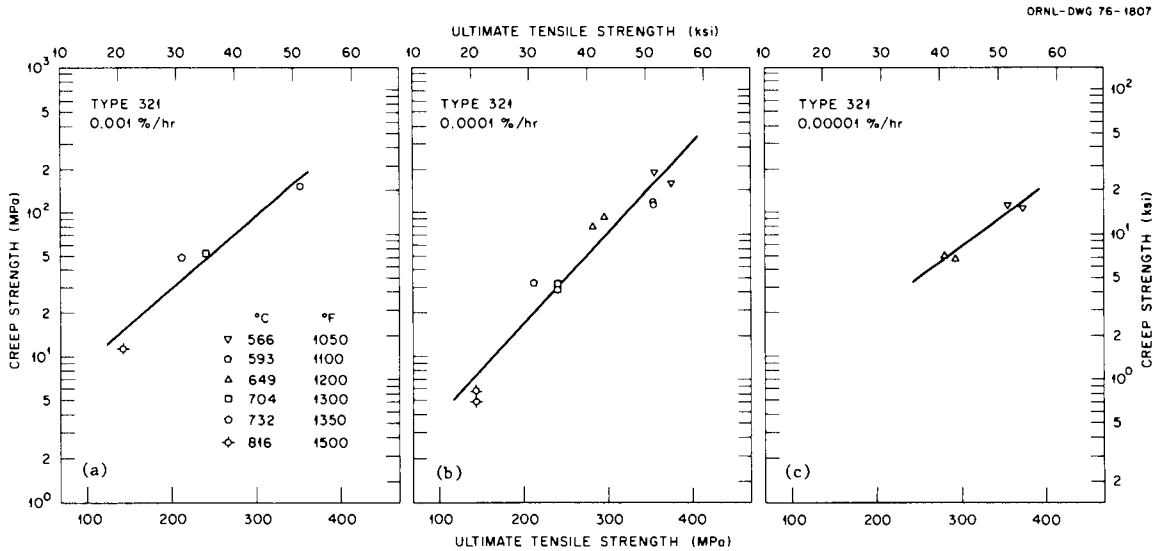


Fig. 3.15. Creep Strength as a Function of Ultimate Tensile Strength at the Creep-Test Temperature for Various Heats and Variations of Type 321 Stainless Steel. (a) 0.001%/hr. (b) 0.0001%/hr. (c) 0.00001%/hr.

Table 3.3. Summary of Creep Strength Constants in Equation $S_R^t = \alpha \exp(\beta S_u)$ for Several Austenitic Stainless Steels

| Stainless Steel Type | Number of Data Points | Temperature Range (°C) | Temperature Range (°F) | Constants α (ksi) | Constants α (MPa) | Constants β (1/ksi) | Constants β (1/MPa) |
|---|---|---|---|---|---|---|---|
| | | 0.001%/hr Creep Strength | | | | | |
| 304[a] | 12 | 593–704 | 1100–1300 | 0.7498 | 5.1697 | 0.06917 | 0.010032 |
| 316[a] | 9 | 593–816 | 1100–1500 | 0.7149 | 4.9291 | 0.05689 | 0.008251 |
| 347 | 3 | 593–816 | 1100–1500 | 0.4235 | 2.9199 | 0.07344 | 0.010652 |
| 321 | 4 | 593–816 | 1100–1500 | 0.4066 | 2.8034 | 0.08020 | 0.011632 |
| | | 0.0001%/hr Creep Strength | | | | | |
| 304 | 15 | 593–816 | 1100–1500 | 0.5272 | 3.6349 | 0.06698 | 0.009715 |
| 316 | 21 | 538–816 | 1000–1500 | 0.6686 | 4.5823 | 0.05304 | 0.007693 |
| 347 | 12 | 593–816 | 1100–1500 | 0.6949 | 4.7912 | 0.06232 | 0.009039 |
| 321 | 11 | 565–816 | 1050–1500 | 0.1323 | 0.9122 | 0.09963 | 0.014450 |
| | | 0.00001%/hr Creep Strength | | | | | |
| 304 | 15 | 538–816 | 1000–1500 | 0.6032 | 4.1589 | 0.05753 | 0.008344 |
| 316 | 17 | 538–816 | 1000–1500 | 0.5408 | 3.7287 | 0.04913 | 0.007126 |
| 347 | 14 | 538–816 | 1000–1500 | 0.3579 | 2.4676 | 0.06966 | 0.010103 |
| 321 | 4 | 565–649 | 1050–1500 | 0.4295 | 2.9613 | 0.06813 | 0.009881 |
| | | 0.000001%/hr Creep Strength | | | | | |
| 304 | 3 | 565–732 | 1050–1350 | 0.2971 | 2.0484 | 0.06120 | 0.008876 |

[a]Including modification with controlled carbon or titanium.

different for different types of stainless steel, we tried to treat all data together. Plots of the combined data are shown in Fig. 3.16. The upper and lower central tolerance limits are also included in Fig. 3.16. The central tolerance limits are such that with 90% confidence, 95% of the data will fall above the lower limit and 95% will fall below the upper limit. The values of constants α and β for all austenitic stainless steels treated together are presented in Table 3.4. As can be seen from previous figures, Eq. (6) appears to hold true for various heats, stainless steels, and test temperatures for data collected from sources in the United States. We have also attempted to check the validity of Eq. (6) and the constants calculated for individual and combined steels for creep-rupture strength data reported by the British Steelmakers Creep Committee.[9] Plots in Fig. 3.17 show the data for type 316 stainless steel for a temperature range of 550 to 700°C (1022–1292°F). Note that the lines drawn based on ORNL combined data fit the data points quite well. Thus,

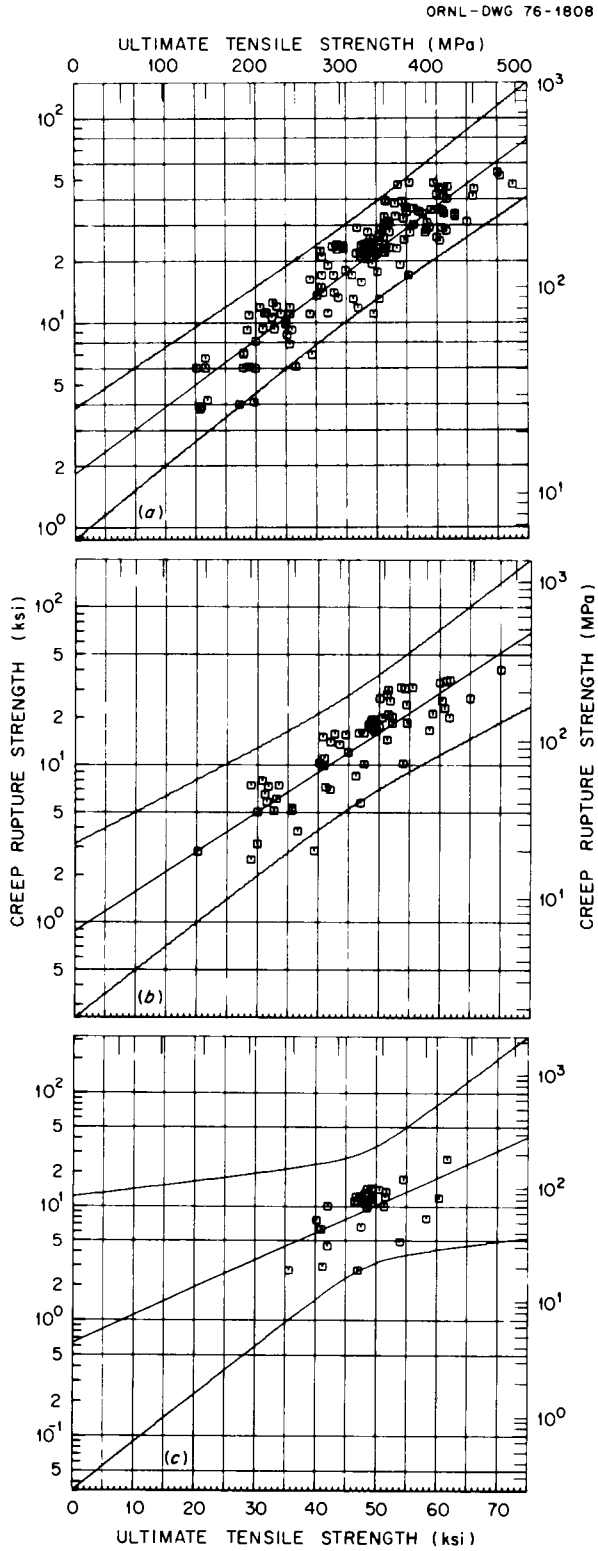


Fig. 3.16 Creep-Rupture Strength as a Function of Ultimate Tensile Strength at the Creep-Test Temperature for Various Heats and Variations of Several Austenitic Stainless Steels. (a) $10^3$ hr. (b) $10^4$ hr. (c) $10^5$ hr.

Table 3.4. Summary of Constants in Equation $S_R^t = \alpha \exp(\beta S_u)$ for Data on Types 304, 316, 347, 321, 201, 202, and 303 Austenitic Stainless Steel

| Rupture Life (hr) | Number of Data Points | Temperature Range | | Constants in Equation for Creep-Rupture Strength | | | | $R^2$ [a] (%) |
|---|---|---|---|---|---|---|---|---|
| | | (°C) | (°F) | α, MPa | β, $MPa^{-1}$ | α, ksi | β, $ksi^{-1}$ | |
| $10^3$ | 144 | 538–816 | 1000–1500 | 12.639 | 0.007259 | 1.833 | 0.05005 | 83.5 |
| $10^4$ | 65 | 538–816 | 1000–1500 | 6.061 | 0.008434 | 0.879 | 0.05815 | 74.9 |
| $10^5$ | 32 | 538–732 | 1000–1350 | 4.371 | 0.008051 | 0.634 | 0.05551 | 34.2 |

[a] $R^2$ is the coefficient of determination (square of the multiple correlation coefficient).

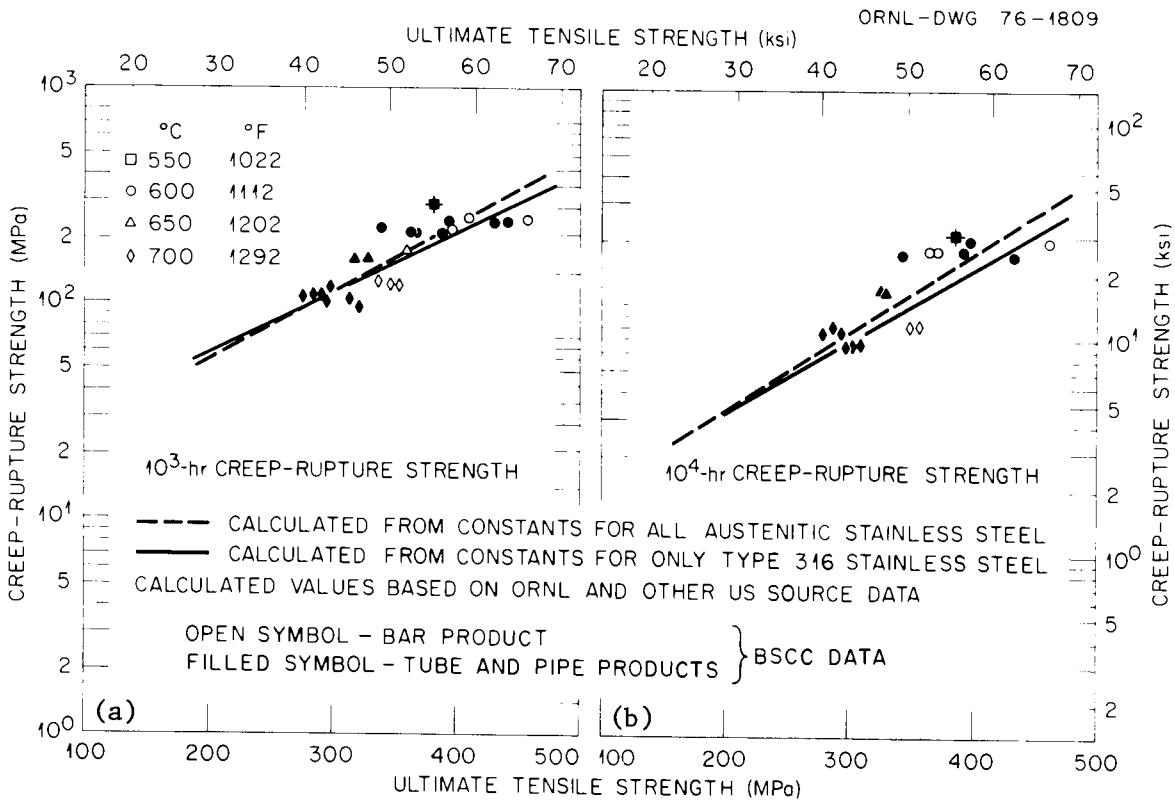


Fig. 3.17. British Steelmakers Creep Committee Values of Creep-Rupture Strength of Type 316 Stainless Steel as a Function of Ultimate Tensile Strength at the Creep Test Temperature, Compared with Eq. (6) Constants for All Austenitic Stainless Steels and for Type 316 Stainless Steel. (a) $10^3$ hr. (b) $10^4$ hr.

we have noted that ultimate tensile strength at the creep test temperature can describe the creep behavior of a given heat or type of stainless steel. This finding is true for both creep and creep-rupture strengths of austenitic stainless steels. More work is continuing in this area.

### 3.2.2.2 Effect of Thermal Aging on Tensile and Creep Properties of Types 304 and 316 Stainless Steel

Tensile and creep properties of several heats of types 304 and 316 stainless steel have been reported[10–12] at a test temperature of 593°C (1100°F) on specimens aged for periods up to 10,000 hr at temperatures of 482, 593, and 649°C (900, 1100, and 1200°F). The test temperatures used in previous work were higher than, equal to, and lower than the aging temperatures. During the last quarter we have completed tensile

testing of aged specimens at the aging temperatures. Results from this study are presented here.

Tables 3.5 and 3.6 summarize the tensile data on several heats of types 304 and 316 stainless steel. The average values of various tensile properties (0.2% yield, ultimate tensile strength, uniform and total elongation, and reduction of area) are plotted as functions of aging and test temperature in Figs. 3.18 through 3.20. Error bands for each data point represent the spread in data due to heat-to-heat variations. The

Table 3.5. Tensile Properties of Several Heats of Type 304 Stainless Steel Tested at Aging Temperature and a Strain Rate of 0.040/min

| Condition[a] | Test Temperature | | Stress, MPa (ksi) | | Elongation (%) | | Reduction of Area (%) |
|---|---|---|---|---|---|---|---|
| | (°C) | (°F) | Yield | Ultimate | Uniform | Total in 1-in. (25.4-mm) | |
| | | | | Heat 807 | | | |
| Reannealed | 482 | 900 | 89 (13.0) | 380 (55.11) | 39.2 | 46.9 | 61.9 |
| Reannealed, aged | 482 | 900 | 110 (15.9) | 389 (56.4) | 31.9 | 43.0 | 65.8 |
| Reannealed | 593 | 1100 | 90 (13.0) | 330 (47.9) | 36.0 | 45.7 | 74.9 |
| Reannealed, aged | 593 | 1100 | 106 (15.4) | 295 (42.8) | 29.1 | 44.3 | 55.7 |
| Reannealed | 649 | 1200 | 78 (11.3) | 271 (39.3) | 31.9 | 43.0 | 65.8 |
| Reannealed, aged | 649 | 1200 | 112 (16.3) | 262 (38.0) | 26.1 | 46.4 | 63.7 |
| | | | | Reference Heat, 796K | | | |
| Reannealed | 482 | 900 | 84 (12.2) | 385 (55.8) | 46.4 | 51.5 | 71.4 |
| Reannealed, aged | 482 | 900 | 127 (18.4) | 359 (52.0) | 27.2 | 38.7 | 57.2 |
| Reannealed | 593 | 1100 | 70 (10.1) | 322 (46.7) | 43.0 | 49.6 | 63.3 |
| Reannealed, aged | 593 | 1100 | 95 (13.8) | 323 (46.9) | 34.5 | 46.8 | 55.7 |
| Reannealed | 649 | 1200 | 72 (10.4) | 277 (40.2) | 36.0 | 48.3 | 49.2 |
| Reannealed, aged | 649 | 1200 | 100 (14.5) | 277 (40.2) | 25.7 | 44.7 | 60.0 |
| | | | | Heat 926 | | | |
| A 240[b] | 482 | 900 | | | | | |
| A 240, aged | 482 | 900 | 125 (18.1) | 416 (60.3) | 37.1 | 50.2 | 71.7 |
| A 240 | 593 | 1100 | 132 (19.1) | 359 (52.0) | 39.0 | 45.1 | 71.0 |
| A 240, aged | 593 | 1100 | 142 (20.6) | 357 (51.8) | 27.6 | 41.2 | 64.1 |
| A 240 | 649 | 1200 | 117 (16.9) | 276 (40.1) | 31.8 | 40.6 | 44.2 |
| A 240, aged | 649 | 1200 | 139 (20.2) | 308 (44.7) | 23.0 | 46.6 | 64.5 |
| | | | | Heat 845 | | | |
| A 240 | 482 | 900 | 124 (18.0) | 414 (60.1) | 40.8 | 51.5 | 73.6 |
| A 240, aged | 482 | 900 | 139 (20.1) | 416 (60.3) | 35.1 | 48.8 | 71.0 |
| A 240 | 593 | 1100 | 140 (20.3) | 357 (51.8) | 39.2 | 48.8 | 68.1 |
| A 240, aged | 593 | 1100 | 157 (22.8) | 350 (50.8) | 25.6 | 41.9 | 66.1 |
| A 240 | 649 | 1200 | 128 (18.6) | 296 (43.0) | 32.0 | 51.8 | 67.7 |
| A 240, aged | 649 | 1200 | 139 (20.2) | 294 (42.7) | 21.1 | 45.9 | 67.3 |
| | | | | Heat 813 | | | |
| Reannealed | 593 | 1100 | 82 (11.9) | 354 (51.3) | 43.4 | 51.6 | 71.9 |
| Reannealed, aged | 593 | 1100 | 110 (15.9) | 345 (50.1) | 28.6 | 44.2 | 61.4 |
| Reannealed | 649 | 1200 | 79 (11.4) | 300 (43.5) | 36.0 | 56.6 | 68.2 |
| Reannealed, aged | 649 | 1200 | 130 (18.8) | 301 (43.7) | 23.2 | 45.8 | 64.7 |

[a]Reannealed is 0.5 hr at 1065°C (1950°F). Aged is 10,000 hr at the test temperature.

[b]Test incomplete.

Table 3.6. Tensile Properties of Several Heats of Type 316 Stainless Steel Tested at Aging Temperature and a Strain Rate of 0.040/min

| Condition[a] | Aging and Test Temperature | | Stress, MPa (ksi) | | Elongation (%) | | Reduction of Area (%) |
|---|---|---|---|---|---|---|---|
| | (°C) | (°F) | Yield | Ultimate | Uniform | Total in 1-in. (25.4-mm) | |
| | | | | Heat 686 | | | |
| Reannealed | 482 | 900 | 216 (31.3) | 544 (78.9) | 36.2 | 47.2 | 66.8 |
| Reannealed, aged | 482 | 900 | 216 (31.3) | 555 (80.5) | 31.1 | 45.5 | 63.9 |
| Reannealed | 593 | 1100 | 199 (28.8) | 501 (72.6) | 38.4 | 48.8 | 60.5 |
| Reannealed, aged | 593 | 1100 | 209 (30.3) | 481 (69.8) | 23.7 | 36.2 | 52.8 |
| Reannealed | 649 | 1200 | 193 (28.0) | 430 (62.3) | 36.0 | 54.3 | 60.2 |
| Reannealed, aged | 649 | 1200 | 205 (29.7) | 423 (61.3) | 15.7 | 44.4 | 68.3 |
| | | | | Heat 212 | | | |
| Reannealed | 482 | 900 | 117 (17.0) | 463 (67.1) | 44.8 | 52.9 | 61.2 |
| Reannealed, aged | 482 | 900 | 136 (19.7) | 495 (71.8) | 36.9 | 45.1 | 63.7 |
| Reannealed | 593 | 1100 | 100 (14.5) | 418 (60.6) | 49.6 | 51.0 | 60.7 |
| Reannealed, aged | 593 | 1100 | 133 (19.3) | 429 (62.3) | 28.1 | 40.4 | 46.3 |
| Reannealed | 649 | 1200 | 98 (14.2) | 350 (50.7) | 40.0 | 59.5 | 64.8 |
| Reannealed, aged | 649 | 1200 | 176 (25.5) | 391 (56.7) | 18.0 | 50.7 | 64.2 |
| | | | | Heat 613 | | | |
| Reannealed | 482 | 900 | 127 (18.4) | 481 (69.8) | 43.3 | 49.2 | 57.0 |
| Reannealed, aged | 482 | 900 | 143 (20.8) | 499 (72.4) | 39.6 | 48.1 | 66.1 |
| Reannealed | 593 | 1100 | 112 (16.3) | 438 (63.5) | 45.6 | 53.9 | 53.9 |
| Reannealed, aged | 593 | 1100 | 149 (21.6) | 429 (62.2) | 29.0 | 41.7 | 52.9 |
| Reannealed | 649 | 1200 | 111 (16.1) | 366 (53.1) | 36.0 | 56.4 | 53.7 |
| Reannealed, aged | 649 | 1200 | 165 (24.0) | 373 (54.1) | 18.5 | 48.6 | 68.4 |
| | | | | Heat 509 | | | |
| A 312 | 482 | 900 | 138 (19.95) | 467 (67.7) | 43.1 | 48.8 | 58.8 |
| A 312, aged | 482 | 900 | 139 (20.1) | 467 (67.8) | 34.9 | 39.5 | 66.7 |
| A 312 | 649 | 1200 | 117 (17.0) | 350 (50.7) | 34.7 | 44.8 | 63.5 |
| A 312, aged | 649 | 1200 | 185 (26.9) | 383 (55.6) | 15.4 | 33.85 | 60.78 |

[a]Reannealed is 0.5 hr at 1065°C (1950°F). Aged is 10,000 hr at the test temperature.

*Nuclear Systems Materials (NSM) Handbook* minimum property curves are also included in Figs. 3.18 and 3.19. Following are some important observations from these plots.

1. The average yield strength values of several heats for both types 304 and 316 stainless steel [Fig. 3.18(a)] are either close to or slightly below the *NSM Handbook* minimum curve. Aging at the tensile test temperatures increased the yield strength for all three test temperatures. The increase in yield strength increased with aging temperature and was much more for type 316 than for type 304 stainless steel. The average yield strength values for aged materials were above the *NSM Handbook* minimum curve for all three test temperatures.

2. In contrast with the 0.2% yield strength results, average ultimate tensile strength values for several heats of both types 304 and 316 stainless steel in the unaged condition were above the *NSM Handbook* minimum

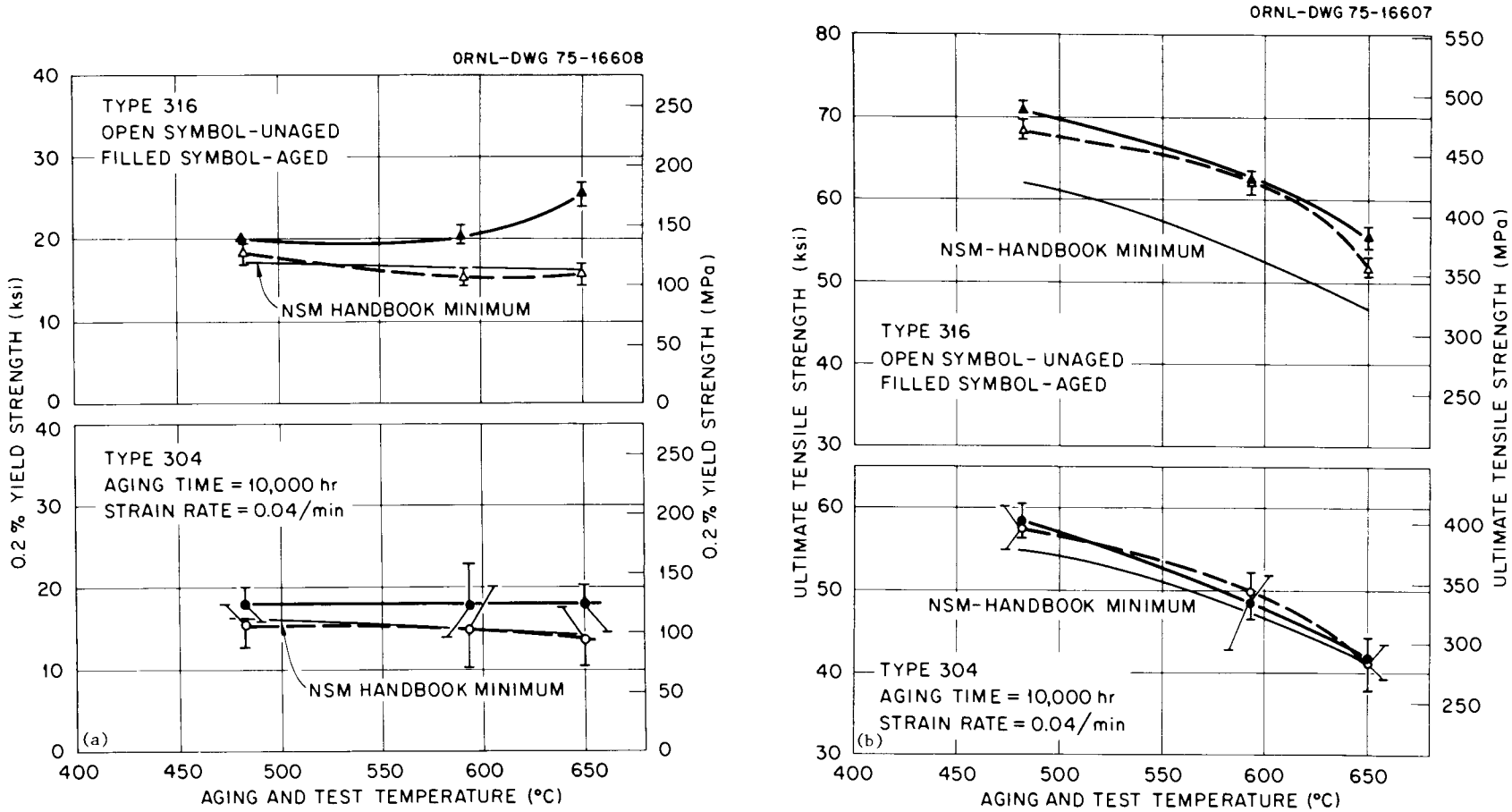


Fig. 3.18. Effect of Aging and Test Temperature on the Strength of Several Heats of Types 304 and 316 Stainless Steel. (a) 0.2% yield strength. (b) Ultimate tensile strength.

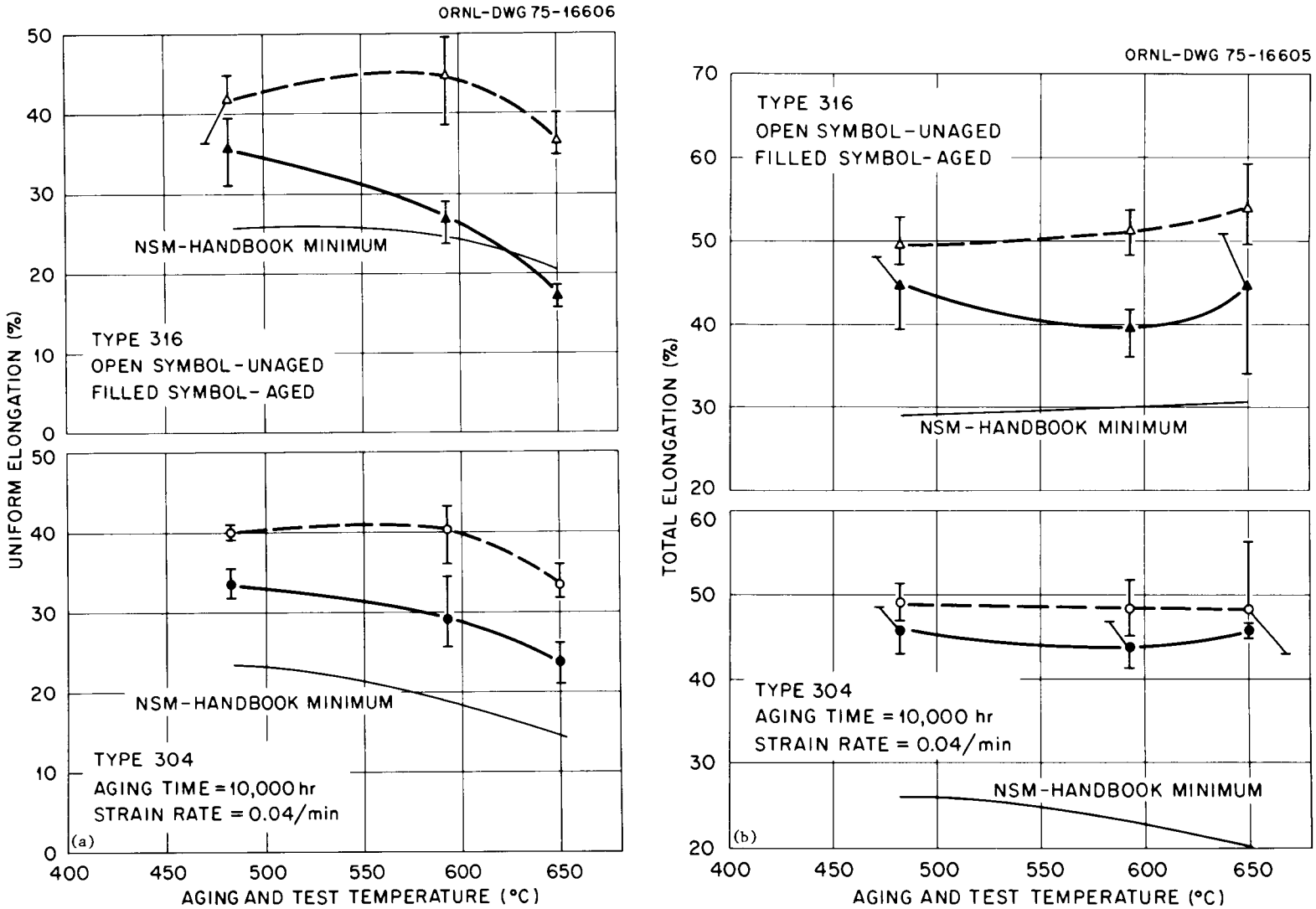


Fig. 3.19. Effect of Aging and Test Temperature on the Elongation of Several Heats of Types 304 and 316 Stainless Steel. (a) Uniform. (b) Total.

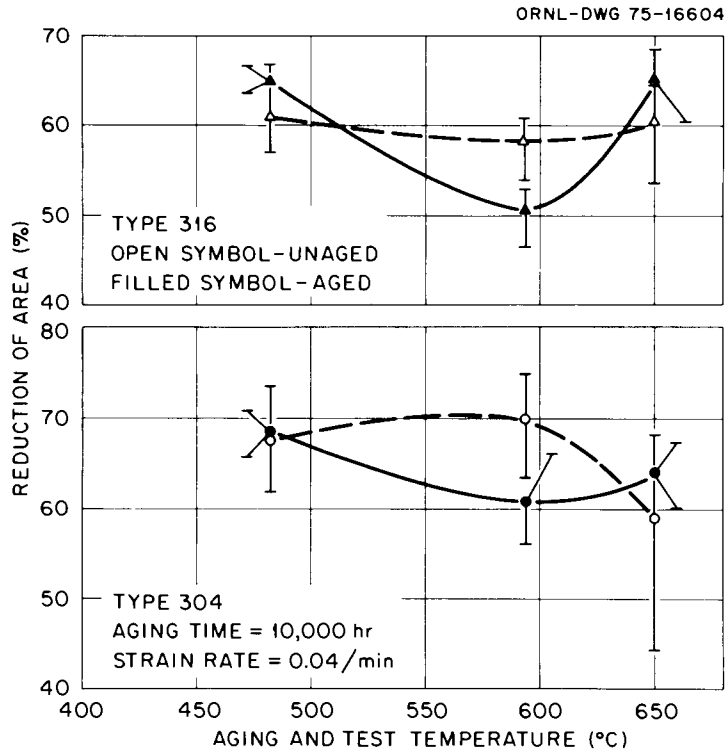


Fig. 3.20. Effect of Aging and Test Temperature on the Reduction of Area of Several Heats of Types 304 and 316 Stainless Steel.

curve [Fig. 3.18(b)]. Aging at the tensile test temperature did not alter the ultimate tensile strength to any significant amount. However, the changes produced on aging were again more pronounced for type 316 than for type 304 stainless steel.

3. The average uniform elongation values for several heats of both types 304 and 316 stainless steel in the unaged condition were significantly above the *NSM Handbook* minimum curve. Aging at the test temperature lowered the uniform elongation for all test temperatures. For type 304 stainless steel, the uniform elongation curve for aged material was still above the *NSM Handbook* minimum curve, whereas for type 316 there was a crossover, and uniform elongation values at 649°C (1200°F) fell below the minimum curve.

4. The average total elongation values for several heats of types 304 and 316 stainless steel in the unaged condition were well above the *NSM Handbook* minimum curves in Fig. 3.19(b). The total elongation curve for the aged material was below that for the unaged, but still significantly

above the minimum. Note again that the changes produced in total elongation of several heats of type 316 stainless steel were far more pronounced than for type 304. A comparison of Fig. 3.19(b) with data presented earlier[10,11] shows that testing at an aging temperature of 649°C (1200°F) produces less loss in total elongation than testing at 593°C (1100°F) after aging at 649°C (1200°F). In either event, total elongation after aging for 10,000 hr at temperatures of 482, 593, and 649°C (900, 1100, and 1200°F) remains at least 40%.

5. The reduction of area curve for aged specimens is interesting in that it shows a maximum loss on aging and testing at 593°C (1100°F) and an increase on aging and testing at 649°C (1200°F). Once again, data presented earlier[10,11] showed that aging at 649°C (1200°F) and testing at room temperature and 593°C (1100°F) produced a loss in reduction of area, as opposed to an increase observed for aging and testing at 649°C (1200°F).

Microstructural changes produced after aging for 10,000 hr at temperatures of 482, 593, and 649°C (900, 1100, and 1200°F) were studied with the transmission electron microscope and reported previously.[13] No resolvable precipitates were observed in specimens aged at 482°C (900°F), whereas aging temperatures of 593 and 649°C (1100 and 1200°F) produced precipitates at all sites (matrix, twin, and grain boundaries). The increase in yield strength of the aged specimens is then expected[11,12] to result from the contributions from matrix and grain boundary precipitates. At 482°C (900°F), where resolvable precipitates were absent, the increase in yield strength is expected to have originated primarily through the changes in grain boundary configuration.

Little or no change in ultimate tensile strength on aging was believed to be the result of balance between work hardening due to precipitates and work softening through decreased dynamic strain aging caused by matrix depletion of interstitial carbon and nitrogen. The changes in ductility indices (uniform and total elongation, reduction of area), are all probably related to precipitates in the matrix and at grain boundaries through a complex mechanism.

One possible reason for the increase in reduction of area for specimens aged and tested at 649°C (1200°F) is the occurrence of grain boundary

migration[6] at this test temperature. Furthermore, the globular precipitate formed at 649°C (1200°F) probably enhances the grain boundary migration. On the other hand, a test temperature of 593°C (1100°F) is too low for any significant grain boundary migration. Furthermore, aging at 649°C (1200°F) produces a relatively high intragranular strength[11,12] (due to a more uniform distribution of a fine precipitate), as opposed to intergranular strength and thus produces a loss in reduction of area and other ductility indices due to concentrated deformation along the grain boundaries.

In conclusion, aging and testing at the same temperature appear to have less deleterious influence on tensile ductility than aging above the test temperature.

Several long-term creep tests are in progress on aged specimens of various heats of type 304 stainless steel. Creep data from these tests are summarized in Table 3.7. Creep curves for unaged and aged specimens are plotted in Figs. 3.21 through 3.24. These curves are for reference heat, a weak heat, and heat 845, a strong heat. Note also that in Figs. 3.22 and 3.24 duplicate creep curves for the unaged material have also been plotted to show the reproducibility of testing and creep behavior. One common influence of aging in all cases was the decrease in loading strain. The influence of aging on creep behavior cannot be generalized from one heat to another and therefore it is described individually for each case.

Figure 3.21 shows the creep curves at 124 MPa (18 ksi) and 593°C (1100°F) for unaged and aged specimens of the reference heat of type 304 stainless steel. The rupture time for the aged specimen is approximately 3 times that for the unaged specimen, even though the aged specimen showed higher creep strain than the unaged specimen for corresponding times nearly up to the rupture life of the latter. Furthermore, no significant difference was observed in the total elongation or reduction of area between unaged and aged specimens.

Figure 3.22 shows the creep curves for unaged and aged specimens of the reference heat tested at 110 MPa (16 ksi) and 593°C (1100°F). Note that the duplicate tests in the unaged condition show excellent reproducibility. The aged specimen is showing a higher creep strain than the unaged specimen for test times available thus far. Furthermore, the

Table 3.7. Summary of Long-Term Creep Tests on Aged Specimens of Several Heats of Type 304 Stainless Steel

| Test | Heat | Treatment | | | Test Temperature | | Stress | | Time in Test[a] (hr) | Strain (%) | |
|---|---|---|---|---|---|---|---|---|---|---|---|
| | | Time (hr) | Temperature (°C) | Temperature (°F) | (°C) | (°F) | (MPa) | (ksi) | | Loading | Creep |
| 13806 | 796K | 4,000 | 482 | 900 | 593 | 1100 | 97 | 14 | 12155 | 0.50 | 1.10 |
| 13804 | 796K | 4,000 | 482 | 900 | 593 | 1100 | 124 | 18 | 12516 | 2.42 | 7.11 |
| 13790 | 796K | 4,000 | 649 | 1200 | 482 | 900 | 207 | 30 | 12670 | 3.84 | 0.99 |
| 15433 | 796K | 10,000 | 593 | 1100 | 593 | 1100 | 69 | 10 | 4229 | 0.056 | 0.15 |
| 15383 | 796K | 10,000 | 593 | 1100 | 593 | 1100 | 110 | 16 | 4772 | 1.12 | 2.21 |
| 13866 | 807 | 4,000 | 482 | 900 | 593 | 1100 | 97 | 14 | 12020 | 0.092 | 0.36 |
| 13889 | 807 | 4,000 | 482 | 900 | 593 | 1100 | 117 | 17 | 11852 | 0.992 | 2.65 |
| 13867 | 807 | 4,000 | 482 | 900 | 593 | 1100 | 138 | 20 | 7444[b] | 1.430 | 6.89 |
| 14184 | 845 | 4,000 | 593 | 1100 | 593 | 1100 | 69 | 10 | 10671 | 0.0788 | 0.10 |
| 15423 | 845[c] | 10,000 | 593 | 1100 | 593 | 1100 | 172 | 25 | 4244 | 0.43 | 6.42 |

[a]Unless otherwise noted tests are in progress.

[b]Discontinued.

[c]As-received and aged, as opposed to all other specimens, which were reannealed and aged.

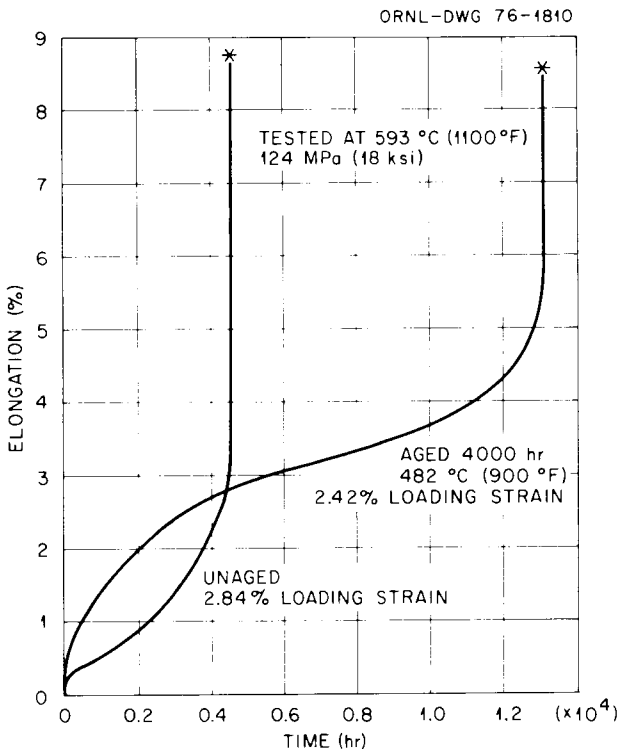


Fig. 3.21. Creep Curves at 18 ksi (124 MPa) and 593°C (1100°F) for Unaged and Aged Specimens of the Reference Heat (796K) of Type 304 Stainless Steel.

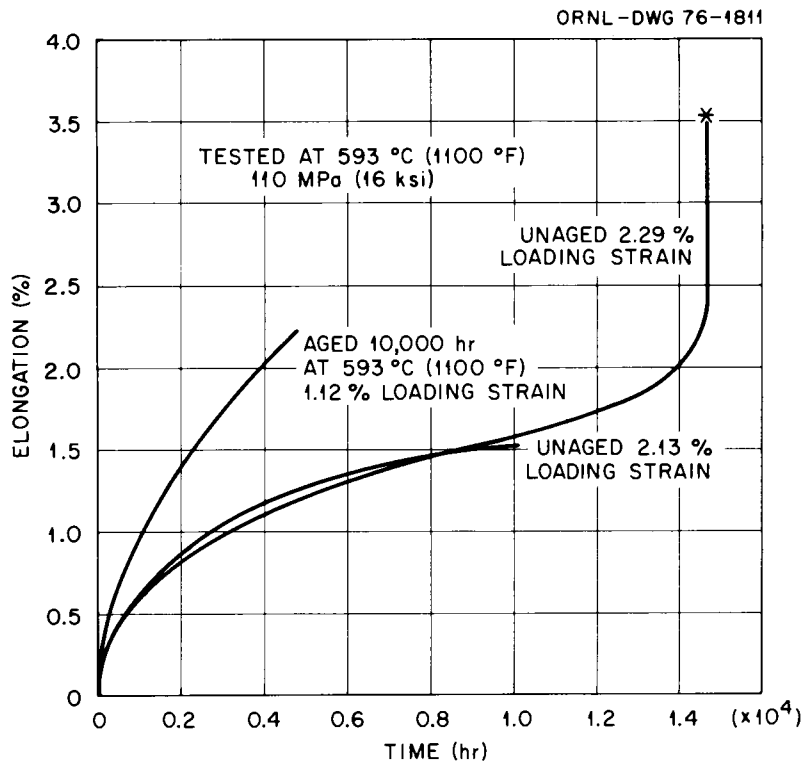


Fig. 3.22. Creep Curves at 16 ksi (110 MPa) and 593°C (1100°F) for Unaged and Aged Specimens of the Reference Heat (796K) of Type 304 Stainless Steel.

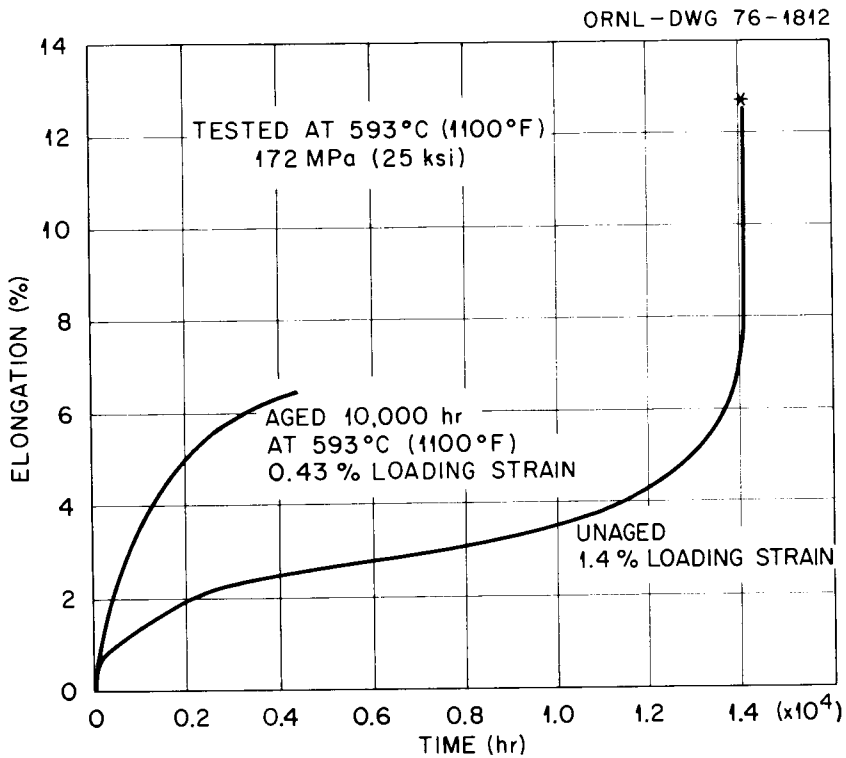


Fig. 3.23. Creep Curves at 25 ksi (172 MPa) and 593°C (1100°F) for Unaged and Aged Specimens of Heat 845 of Type 304 Stainless Steel.

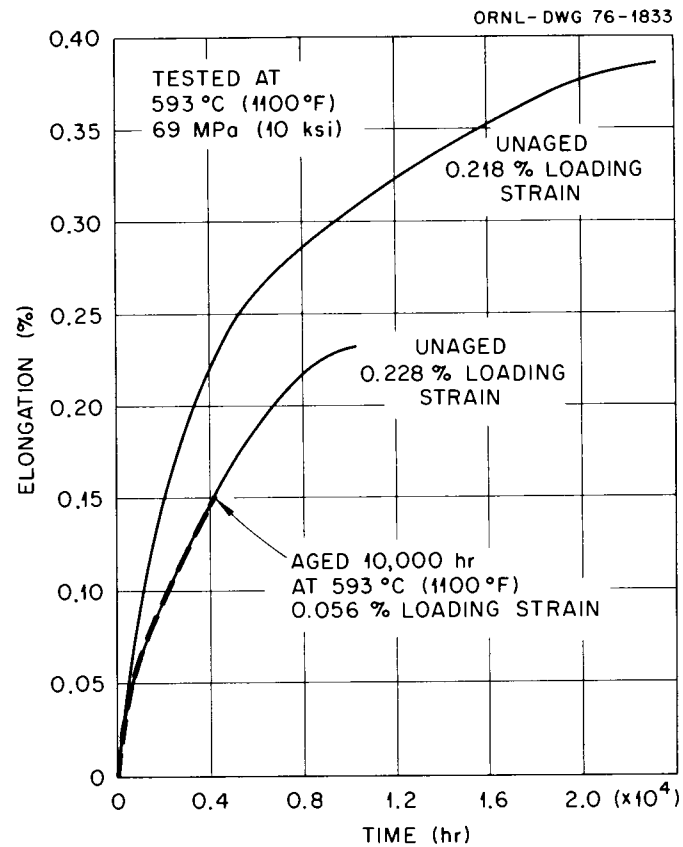


Fig. 3.24. Creep Curves at 10 ksi (69 MPa) and 593°C (1100°F) for Unaged and Aged Specimens of Heat 845 of Type 304 Stainless Steel.

creep curve for the aged specimen has not yet entered the second stage creep and thus might show a behavior similar to one observed at 124 MPa (18 ksi) in Fig. 3.21.

Figure 3.23 shows the creep curves for specimens of heat 845 of type 304 stainless steel tested at 172 MPa (25 ksi) and 593°C (1100°F). Note that for the longest test time available thus far, the aged specimen has already acquired three times the creep strain of the unaged specimen.

Figure 3.24 shows the creep curves for specimens of heat 845 tested at 69 MPa (10 ksi) and 593°C (1100°F). The creep curves on two unaged specimens show excellent reproducibility. Furthermore, unlike Figs. 3.21 through 3.23, the creep data on aged specimens at 69 MPa (10 ksi) cannot be differentiated from that for the unaged specimens.

In conclusion, the long-term creep tests in progress on aged specimens are showing either an increase in time to rupture or no effect. More long-term data will be presented as it becomes available.

### 3.2.3 Materials Behavior in Support of Development and Evaluation of Failure Criteria for Materials

#### 3.2.3.1 Development of Creep Equation for Type 304 Stainless Steel — M. K. Booker

The existing double-exponential creep equation for type 304 stainless steel[14] contains several problems and inconsistencies, similar to those reported earlier[15] for type 316 stainless steel. In addition, the problem of heat-to-heat variations can be quite severe in this material. It is hoped that the creep data obtained through the ORNL heat-to-variations program (Sec. 3.2.2) will allow some measure of heat-to-heat variation to be accounted for by the creep equation. Thus, the current development of an improved creep equation for type 304 stainless steel is aimed at (1) reducing the complexity and analytical awkwardness of the current equation, and (2) accounting for heat-to-heat variations.

As a first step, a base-line equation is being developed for the 51-mm (2-in.) plate of heat 9T2796, the ORNL "reference heat" (Sect. 3.2.1). This equation will represent creep strain as a function of

time ($t$), stress ($\sigma$), and temperature ($T$) during the primary and secondary portions of a uniaxial constant-load isothermal creep test. Several analytical models for creep strain as a function of time have been developed through the years.[16] Of these models, those commonly used[14,17,18] for austenitic stainless steels have been the so-called exponential equations, which consist of a linear secondary term and one or two transient primary terms:

$$e_c = e_t(1 - e^{-rt}) + \dot{e}_m t \tag{7}$$

or

$$e_c = e_t(1 - e^{-rt}) + e_x(1 - e^{-st}) + \dot{e}_m t \ . \tag{8}$$

However, these equations [especially Eq. (8)] can be cumbersome to work with in design and design analysis. Far superior in utility and simplicity is the single rational polynomial equation, which was used in a recent similar study of 2 1/4 Cr-1 Mo steel.[19] This equation is of the form

$$e_c = t/(a + bt) + \dot{e}_m t \ . \tag{9}$$

where $e_c$ is the total creep strain, $\dot{e}_m$ is the minimum creep rate, $1/b$ is the total primary creep strain, and $1/a$ is the initial slope of the primary term (see Fig. 3.25). Thus the equation is simple in form, and its constants all have clear physical meanings. Moreover, the equation can readily be solved for time as a function of strain:

$$t = \frac{be_c - a\dot{e}_m - 1 \pm \sqrt{(a\dot{e}_m + 1 - be_c)^2 + 4ae_c b\dot{e}_m}}{2b\dot{e}_m} \ . \tag{10}$$

Thus the equation can be used for strain-hardening type analyses of variable load-temperature and relaxation behavior without need for the iterative procedures required by the current double-exponential equation.

ORNL-DWG 76-1871

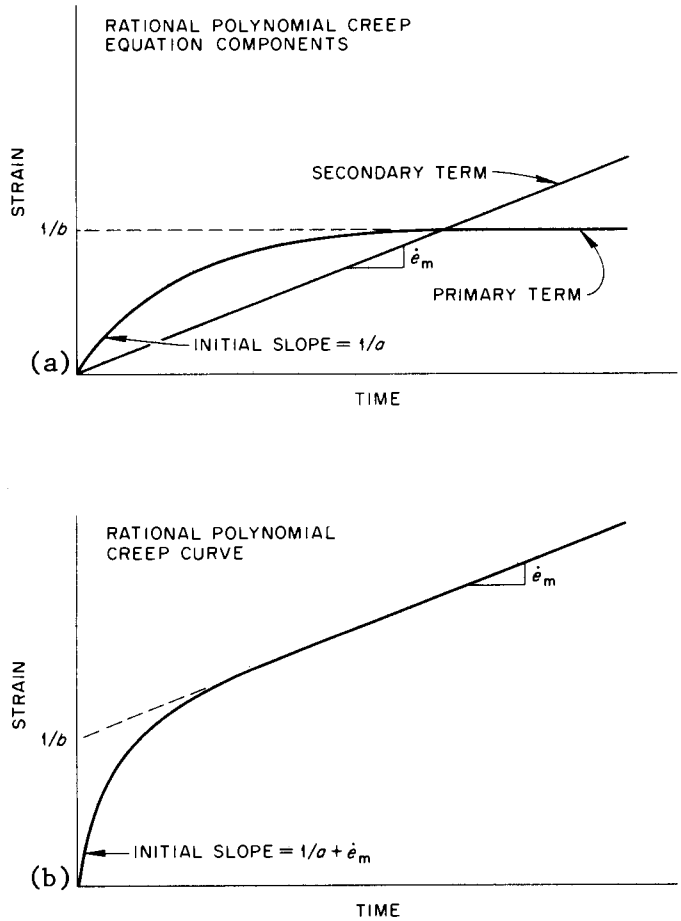


Fig. 3.25. Schematic Diagrams of Creep Curves Showing (a) the Components of the Rational Polynomial Creep Equation, and (b) a Rational Polynomial Creep Curve.

Metallurgically, Eq. (9) can be derived from a treatment of self-diffusion theory as outlined by Oding.[20] Therefore, the equation has a firm analytical and physical basis. The only remaining question is whether it accurately describes individual experimental creep curves.

Equation (9) may be fit to experimental data by methods of non-linear least squares optimization. Alternatively, Oding[21] has cited a semi-graphical solution, which is much simpler to perform and allows more engineering judgment on the part of the analyst.

Rewriting Eq. (9) as

$$e_c = \dot{e}_m t + Cpt/(1 + pt) \ , \tag{11}$$

the coefficients $p$ and $\dot{e}_m$ can be determined[21] by:

$$p = \frac{\frac{t_1 - t_2}{t_3 - t_2}\left(\frac{e_3 - e_2}{t_3 - t_2}\right) + \left(\frac{e_2 - e_1}{t_2 - t_1}\right)}{\frac{t_1 - t_2}{t_3 - t_2}(e_2 - e_3) + e_1 - e_2} \tag{12}$$

and

$$\dot{e}_m = \frac{1}{t_1 - t_2}\left(\frac{e_1}{pt_1} - \frac{e_2}{pt_2} + e_1 - e_2\right) , \tag{13}$$

where $(t_1,e_1)$, $(t_2,e_2)$, and $(t_3,e_3)$ are the coordinates of three strain-time points read from the experimental creep curve. Then, $C$, the total primary creep strain, is given by

$$C = (e - \dot{e}_{mt})(1 + pt)/pt , \tag{14}$$

where $t$ and $e$ are the coordinates of any strain-time point. (In the current calculations $C$ has been computed at $t_1$, $t_2$, and $t_3$ above, and then averaged. Values of $C$ do not vary much with time, however, as should be the case.)

Note that Eqs. (9) and (11) are related by

$$C = 1/b , \tag{15}$$

$$Cp = 1/a , \tag{16}$$

so that the constants allow calculation by either Eq. (9) or (11). Preliminary results show that Eq. (11) provides an excellent fit to experimental data, as illustrated in Figs. 3.26 through 3.30.

Having established that the single rational polynomial equation does indeed accurately describe the strain-time behavior of type 304 stainless steel, the next step in the development of a base-line creep equation is to express the constants $e_m$, $C$, and $p$ as functions of stress ($\sigma$) and temperature ($T$). Also, since the equation is valid only up to the onset of tertiary creep, an expression relating time to

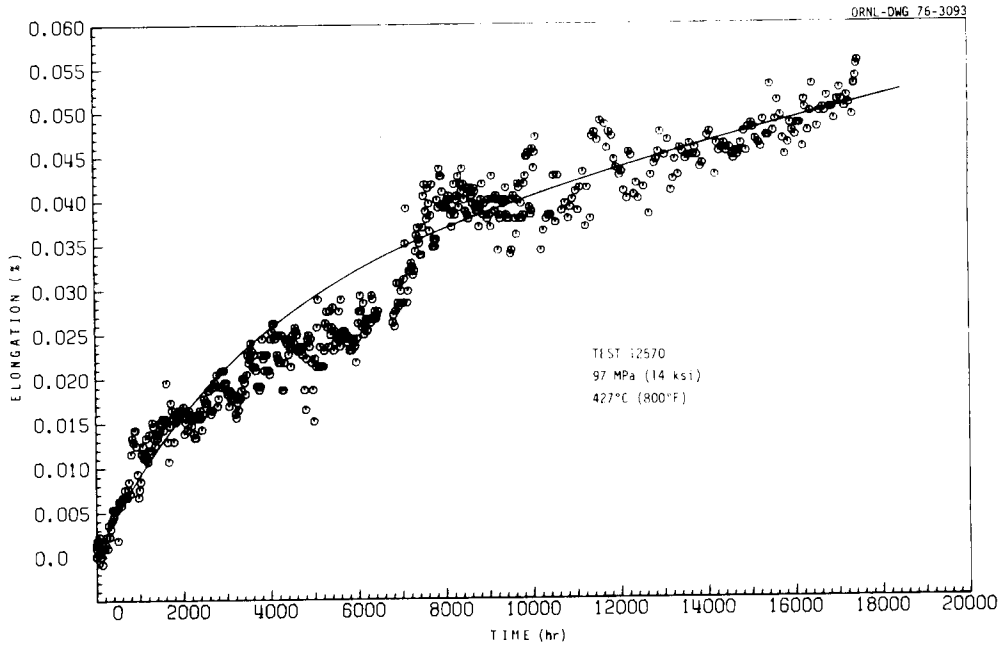


Fig. 3.26. Fit of the Rational Polynomial Creep Equation to an Experimental Curve at 427°C (800°F).

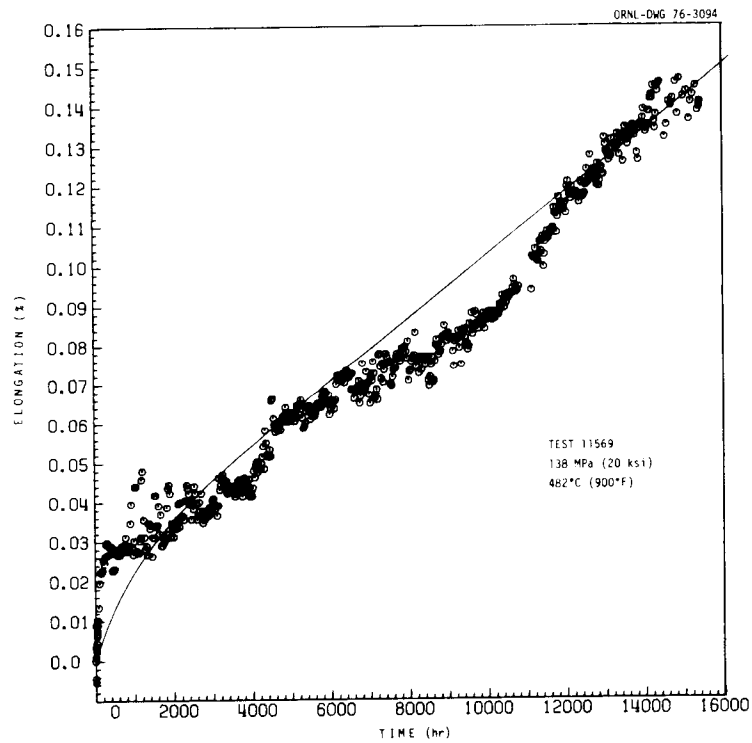


Fig. 3.27. Fit of the Rational Polynomial Creep Equation to an Experimental Curve at 482°C (900°F).

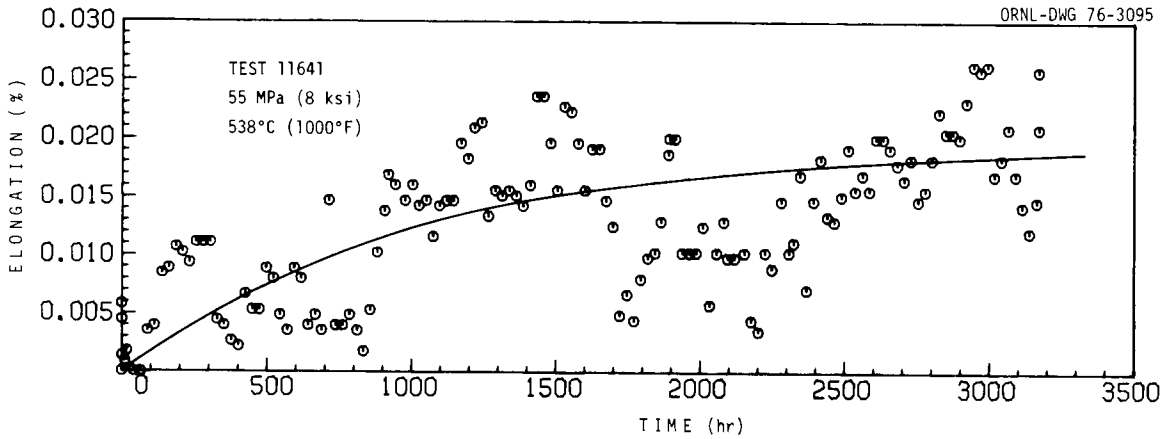


Fig. 3.28. Fit of the Rational Polynomial Creep Equation to an Experimental Curve at 538°C (1000°F).

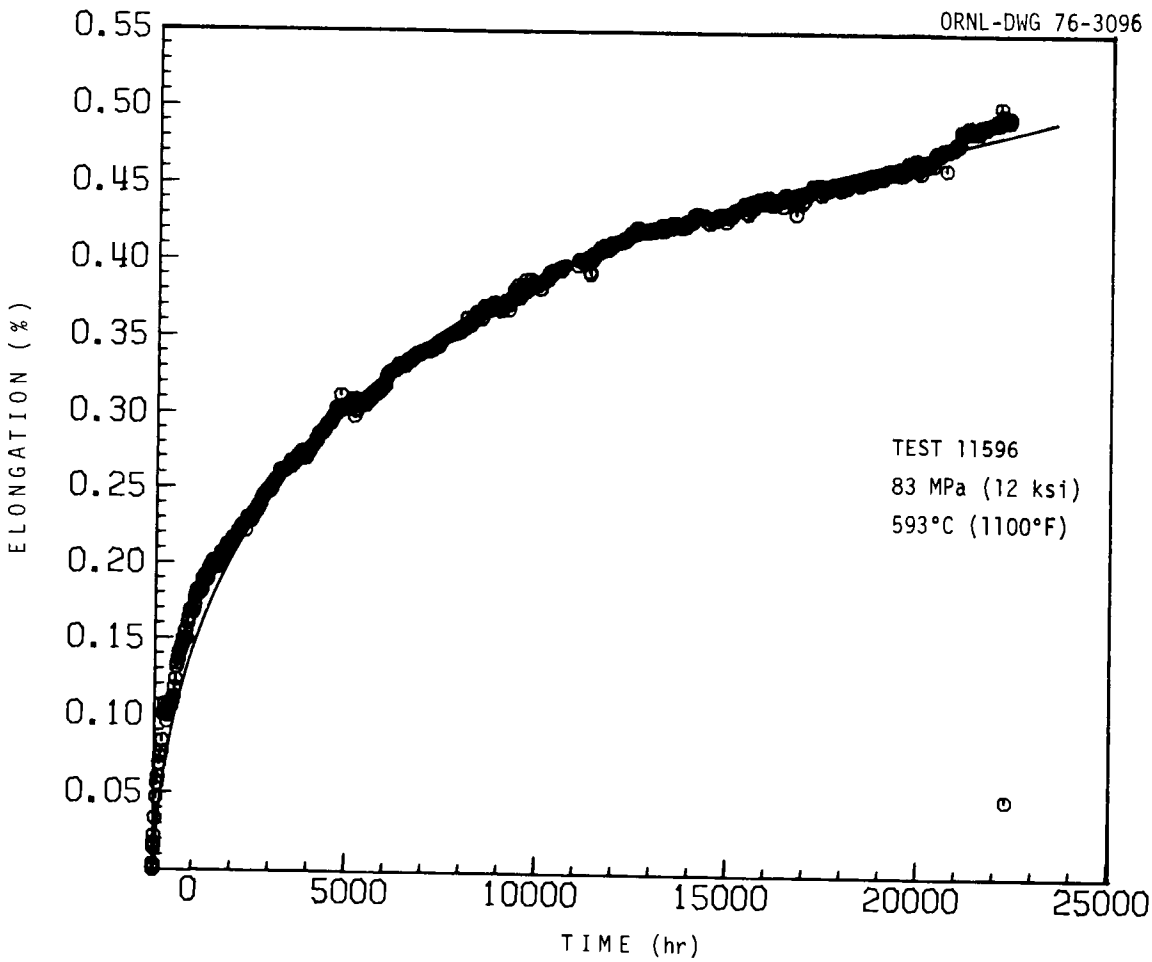


Fig. 3.29. Fit of the Rational Polynomial Creep Equation to an Experimental Curve at 593°C (1100°F).

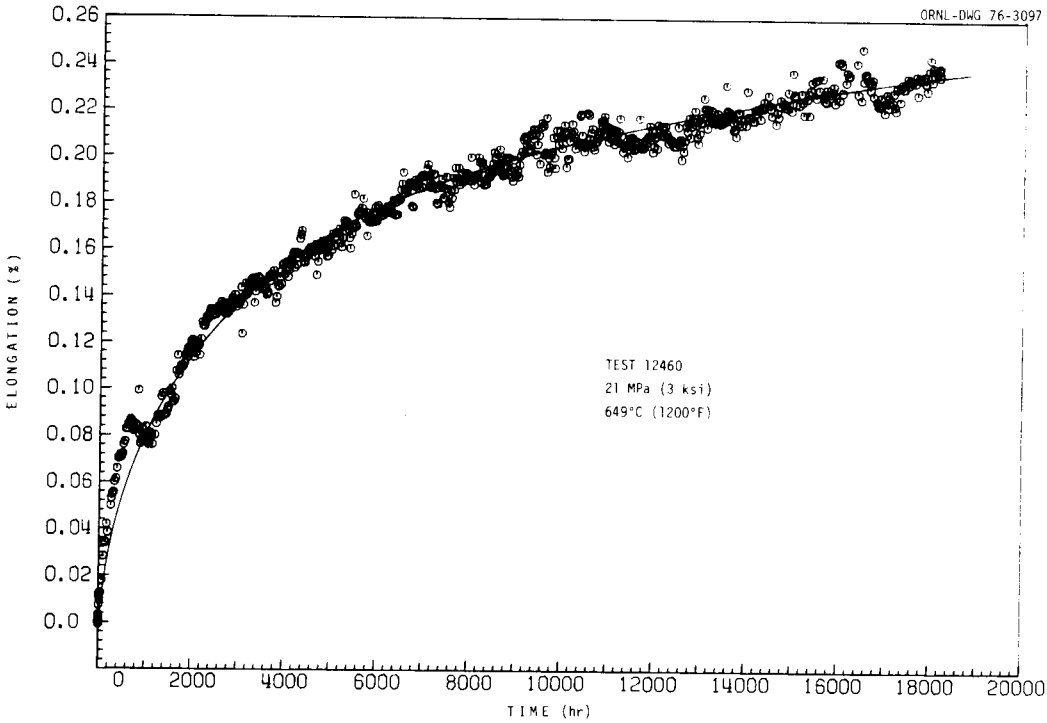


Fig. 3.30. Fit of the Rational Polynomial Creep Equation to an Experimental Curve at 649°C (1200°F).

tertiary creep, $t_3$, to $\sigma$ and $T$ is also needed. Work in this area is proceeding.

Variations in creep behavior make it impossible (and not necessary desirable) for the final creep equation to precisely fit every experimental creep curve. The two criteria that must be met are: (1) that the predicted curves have shapes accurately depicting material behavior and (2) that the magnitudes of predicted strains well represent average material behavior. This second criterion may be checked by several means, including that shown in Fig. 3.31. In this figure, the nominal stress is plotted against the time to reach various levels of creep strain at a given temperature (here 593°C). Comparison of predictions from a creep equation with a plot such as Fig. 3.31 allows a determination of the general accuracy of such an equation. Analysis of the data shown in Fig. 3.31 by parametric or other means also provides an analytical comparison with the creep equation. For instance, isochronous stress-strain curves[22] can be constructed by parametric means[23,24] for

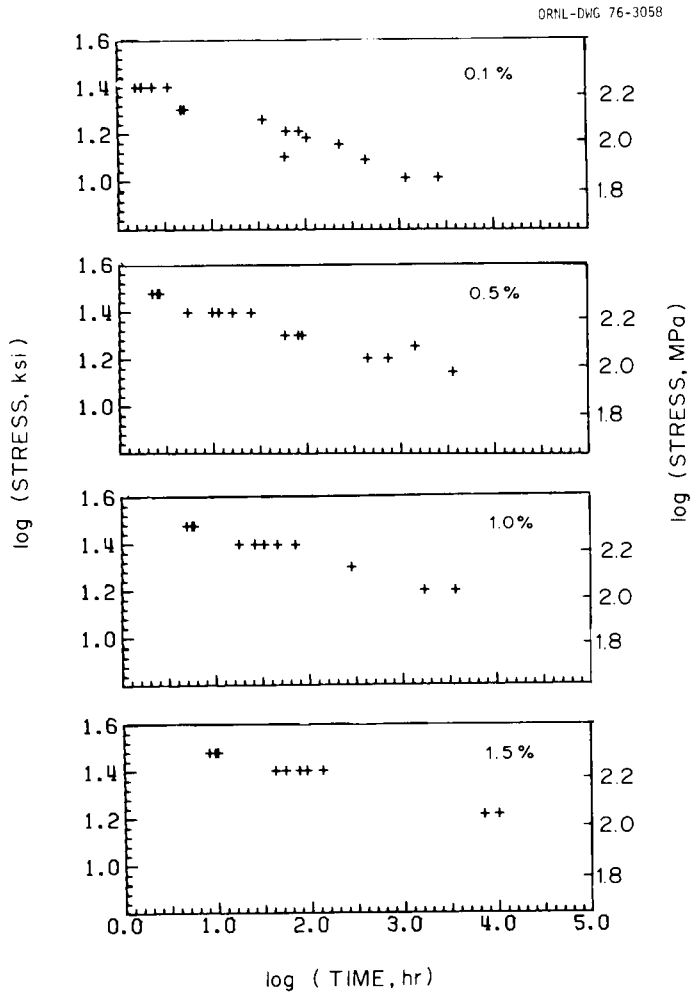


Fig. 3.31. Nominal Stress Versus Time to the Accummulation of 0.1%, 0.5%, 1.0%, and 1.5% Creep Strain at 593°C; Heat 9T2796, 51-mm (2-in.) Plate, Type 304 Stainless Steel.

comparison with isochronous curves constructed from the creep equation. The results of such calculations and comparisons will be described in later reports.

### 3.2.4 Computerized Data Management System — M. K. Booker and B.L.P. Booker

Development and expansion of a computerized Mechanical Properties Data Storage and Retrieval System (DSRS) is continuing. Current efforts are being centered on the development of computer programs for the analysis of data stored in DSRS. Thus, the system serves not merely

as a passive depository for data, but as a dynamic active system for data handling and analysis.

Data analysis will be done mainly through two programs that are currently under development, APEND and ASEND. The Analytical Program for Edited Numerical Data (APEND) directly accesses on-line data sets and allows least squares regression analysis, plotting, and statistical analysis of relationships between two variables. The Analytical System for Edited Numerical Data (ASEND) performs the same functions, except that it can handle several variables, performing multiple regression analyses and a variety of flexible plotting and statistical functions.

Figure 3.32 illustrates results obtained through APEND for 2 1/4 Cr-1 Mo steel, where the lines shown are mean regression lines (cubic polynomials in temperature). Calculation of statistical limits (tolerance limits, confidence limits, etc.) is presently being implemented.

The Analytical System for Edited Numerical Data is currently being implemented, and initial results should be available this quarter. This program will allow a variety of data analyses, including parametric analysis of creep data etc.

### 3.2.5 Elastic Properties of Engineering Construction Materials — J. P. Hammond

Precise measurements show that for metals the "elastic" stress-strain relationships are not perfectly linear, even at low stresses and strain levels, and they become progressively more nonlinear as stress increases. Discrepancies thus often occur between elastic constants determined at different strain levels and rates of strain (for example, constants determined by dynamic and static techniques).

The purpose of this program is to correlate the two separate categories of elastic constants (dynamic and static) for reactor materials of interest, giving specific attention to temperature and other significant test variables. In addition to elastic constants (Young's modulus, $E$; shear modulus, $G$; and Poisson's ratio, $\nu$), elastic and proportional limits (E.L. and P.L.) will be determined. This information is needed to enable more exact and enlightened use of this class of information in engineering design and structural verification work.

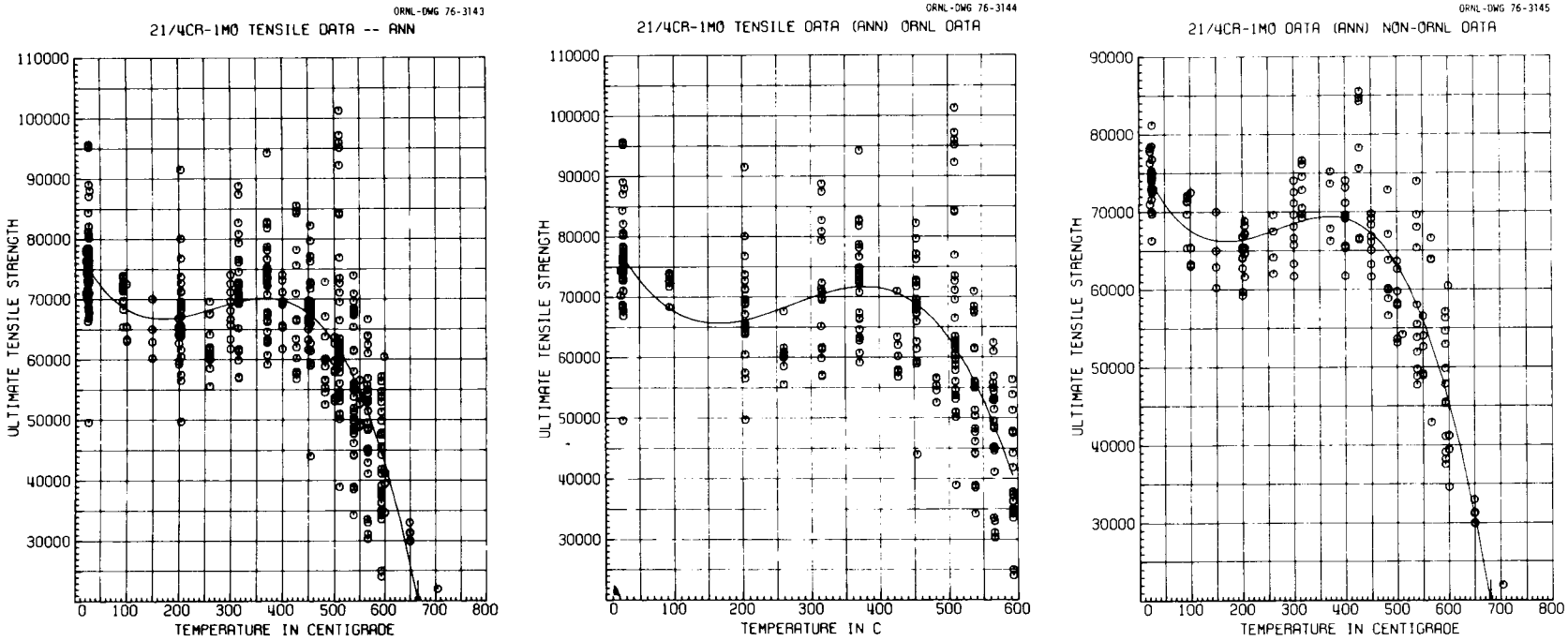


Fig. 3.32. Ultimate Tensile Strength (psi) vs Temperature (°C) Data for Annealed 2 1/4 Cr-1 Mo Steel as Stored in DSRS: Plot Output from APEND Computer Program.

3.2.5.1 Elastic Properties Determined by Static Tests

Previously we described[25] a method employing MG-425 resistance strain gages for accurately determining elastic constants ($E$, $G$, and $\nu$) as functions of temperature by repetitively using a single test specimen for gathering the bulk of the data. Key features of the method include (1) confining test runs to strain levels well within the elastic range ($<120 \times 10^{-6}$) and (2) correcting for stress misalignment in the specimen. Qualifying runs were conducted on 2 1/4 Cr-1 Mo steel, heat 20017 (isothermally annealed), and type 304 stainless steel, heat 9T2796 (mill annealed), to establish the effects of repetitively using a single specimen for gathering elevated-temperature data, as opposed to employing a separate specimen for each data point. For economy, LVDT strain sensors were used for these preliminary tests. In the process of conducting these runs, additional data on the static Young's moduli of these materials were obtained and are reported here.

Tests were made in quadruplicate at each of the strain rates 0.1, 0.01, and 0.001/hr at room temperature (RT) and generally at 55°C (100°F) increments at elevated temperature. To obtain accurate RT values of Young's modulus, numerous sets of data were acquired and averaged. Cubic polynomials were established by regression analysis from the combined data to normalize the high-resolution but less accurate elevated-temperature data to the accurate RT values. Best estimates of Young's modulus as a function of temperature were determined for the materials with the equations.

Constants for the polynomial model,

$$E = E_0 \; 1 + A(T - T_0) + B(T - T_0)^2 + C(T - T_0)^3 \; ,$$

are given in Table 3.8, and the results are shown graphically in Figs. 3.33 and 3.34.

The repetitive use of a single specimen proved to cause moderate lowering of the Young's modulus for both 2 1/4 Cr-1 Mo steel and type 304 stainless steel at the high temperatures, but in the temperature ranges ordinarily prescribed for use of the materials the effect

Table 3.8. Constants in Cubic Equation Describing Elevated-Temperature Static Young's Modulus of 2 1/4 Cr-1 Mo Steel and Type 304 Stainless Steel

| Constant | 2 1/4 Cr-1 Mo | Type 304 SS |
|---|---|---|
| $E_0$,[a] GPa | 208 ± 1.4 | 196 ± 1.4 |
| psi | (30.1 ± 0.2) × $10^6$ | (28.5 ± 0.2) × $10^6$ |
| $A$, °$C^{-1}$(°$F^{-1}$) | 0.185 (0.103) | 0.431 (0.239) |
| $B$, °$C^{-2}$(°$F^{-2}$) | 2.33 (0.720) | 0.356 (0.110) |
| $C$, °$C^{-3}$(°$F^{-3}$) | 3.34 (0.573) | 1.389 (0.238) |

[a]Tolerance shown is standard deviation.

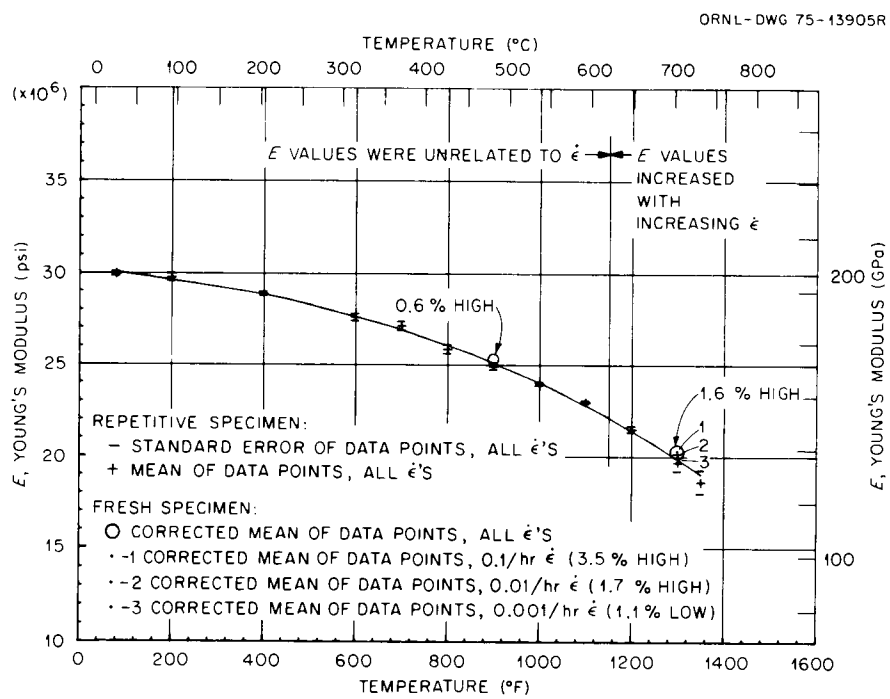


Fig. 3.33. Static Young's Modulus of 2 1/4 Cr-1 Mo Steel, Heat 20017.

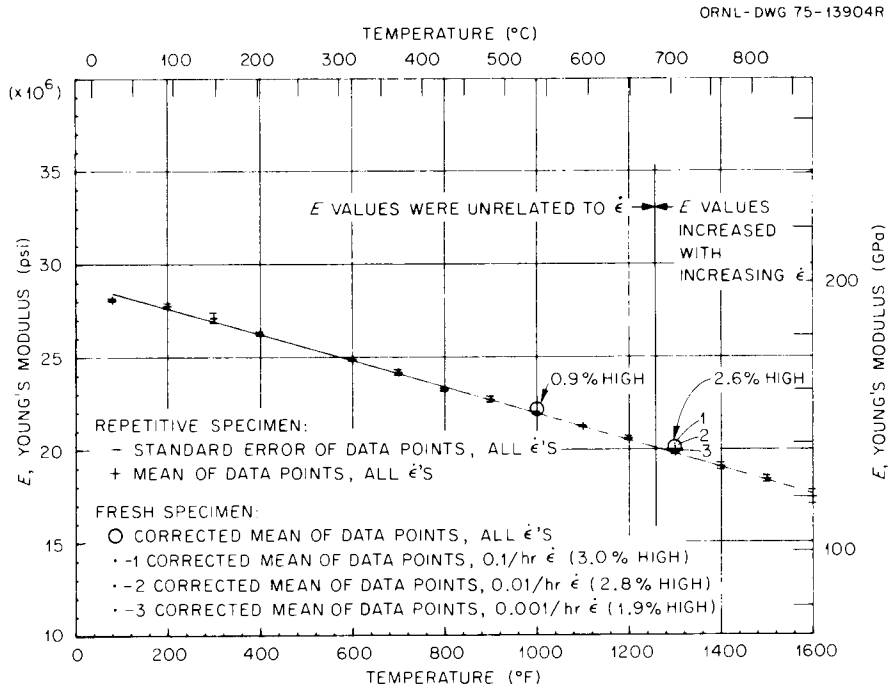


Fig. 3.34. Static Young's Modulus of Type 304 Stainless Steel, Heat 9T2796.

was hardly appreciable. The effect was established by comparing the property determined at a selected test temperature on a "fresh" specimen with that obtained on the "repetitive" specimen (value estimated with the polynomial). A bias correction factor was applied in determining the values for the "fresh" specimen to correct for stress misalignment,[25] to enable a valid comparison.

Corrected values for the "fresh" specimen at the check temperatures are shown in Figs. 3.33 and 3.34 as circles. They indicate some softening but, as earlier indicated, the effect is slight, only 0.6% at 482°C (900°F) for 2 1/4 Cr-1 Mo steel and 0.9% for type 304 stainless steel at 538°C (1000°F). Strain rate did not prove to be a significant factor in the tests conducted on 2 1/4 Cr-1 Mo steel below about 621°C (1150°F) or below about 677°C (1250°F) for type 304 stainless steel.

Having qualified the test schedules for determining the elastic constants on these two materials, we have mounted weldable MC-425 strain gages on square specimens of the stainless steel alloy in the manner described earlier,[26] and the equipment was readied for test runs. Foil

gages of the type EA-09-125BB-120 have been temporarily fastened to the specimen to check the temperature-compensated gage factors supplied by the vendors of the weldable gages and calibrate the results of test runs.

## 3.3 MECHANICAL AND METALLURGICAL BEHAVIOR OF WELDMENTS FOR LMFBR — P. Patriarca, G. M. Slaughter, W. R. Martin, and C. R. Brinkman

### 3.3.1 Preliminary Report on Effect of Postweld Heat Treatment on Type 308 Stainless Steel Submerged-Arc Welds — E. Bolling and R. T. King

In principle, annealing austenitic weld metal to dissolve and agglomerate ferrite should improve the elevated-temperature creep ductility of weld metal, all other factors being equal. Previous work[27] has demonstrated that conventional type 308 submerged-arc (SA) stainless steel weld metal can have low creep-rupture ductility at 649°C (1200°F). At about 649°C (1200°F), the ferrite in the weld metal transforms to sigma phase,[28] and the austenite-sigma phase boundary provides ready paths for crack propagation at relatively low strain. Other corroborating work[29] has shown that the tendency for low-ductility creep fractures is decreased when the continuity of the austenite-sigma phase boundaries is reduced for type 308 stainless steel shielded metal-arc welds (although weld composition was a confounding variable in the experiment). Limited data[30] from an earlier experiment demonstrate improved creep ductility for austenitic welds that were solution annealed, with an accompanying loss of creep-rupture strength. It should be noted, however, that there are many welds for which the process of high-temperature annealing and quenching to avoid sensitization of base metal is not feasible, particularly for large components, intricate shapes, and field welds. Postweld heat treatment thus can not be viewed as a panacea for improving the creep ductility of welds, in a practical sense.

Cole et al.[28] have published data on the effect of annealing time and temperature on the ferrite morphology in selected welds. The purpose of the work reported here was to demonstrate the feasibility of improving the ductility of a type 308 SA weld in thick (51 mm, 2.0 in.) type 304 stainless steel plate, for a weld made to ASME Sect. III and RDT

specifications. The test welds were provided by Westinghouse Electric Corporation, Advanced Reactors Division, in approximately 0.25- by 0.10 to 0.15-m plate (10 by 4–6 in.). Exact procedures by which the welds were made are not available yet. Sections were supplied in the as-welded condition, after stress relief annealing 4 hr at 607°C (1125°F) and water quenching, and after "solution" annealing 2 hr at 982°C (1800°F).

Preliminary metallography revealed that the welds were made in a double-U or double-V joint configuration, being about 10 mm (0.4 in.) wide in the root and about 25 mm (1.0 in.) wide at the surface, exclusive of cosmetic passes. The root pass region is one pass wide, while the surface region is two or three passes wide. Detailed optical investigations of the microstructures are in progress; hardness traverses will be performed. Transmission microscopy will be employed to the extent justified by other observations.

Longitudinal (L), all-weld-metal and transverse (T) specimens were cut from locations having center lines approximately 9.5 mm (0.38 in.) below the surface (L1- and T1-type), 16.6 mm (0.65 in.) below the surface (L2- and T2-type), and 27.6 mm (1.09 in.) below the surface (L3- and T3-type). The 6.3-mm-diam by 31.7-mm-long (0.25 by 1.25 in.) gage, threaded-end specimen design has been reported before.[31] The specimens were continuously loaded at about 0.004/min strain rate, and strains were monitored by averaging extensometers mounted on the shoulders of the specimens, so as not to damage the gage section. Creep-rupture tests were performed at 649 ± 2°C (1200°F) at 172 and 138 MPa (25 and 20 ksi); initial tests were performed first on the more numerous L1, T1, L2, and T2 specimens. The test strain data are reported in Table 3.9. Listed are strains on loading, during Stage I creep, during Stage II creep to departure from linearity and by the 0.2% offset methods; also strain rates, reductions of area (for assumed elliptical fracture cross section), rupture times, and the fraction of the total strain that occurred before the onset of tertiary creep. The latter quantity was below 0.25 for the as-welded and stress-relieved welds, and between 0.25 and 0.5 for the solution-annealed specimens. The times to various events are given in Table 3.10 together with the fraction of the total test

Table 3.9. Creep Test Strain Data for Type 308 Stainless Steel Submerged-Arc Welds Tested at 649°C (1200°F)

| Specimen Type | Stress (MPa) | Stress (ksi) | Strain, % | | | | | | | Strain Rate, %/hr | | | Reduction of Area (%) | Rupture Time, $\varepsilon_r$ (hr) | $\frac{\varepsilon_{III}}{\varepsilon_r}$ |
|---|---|---|---|---|---|---|---|---|---|---|---|---|---|---|---|
| | | | Loading $\varepsilon_L$ | $\varepsilon_{Stage\ I}$ | $\varepsilon_{Stage\ II}$ Real | $\varepsilon_{Stage\ II}$ Offset | $\varepsilon_{Stage\ III}$ Real | $\varepsilon_{Stage\ III}$ Offset | Rupture $\varepsilon_r$ | $\dot{\varepsilon}_{Stage\ II}$ Real | $\dot{\varepsilon}_{Stage\ II}$ Offset | $\varepsilon_r/t_r$ | | | |
| Annealed 4 hr at 607°C (1125°F), Water Quenched | | | | | | | | | | | | | | | |
| L2 | 172 | 25 | 0.35 | 0.27 | 1.14 | 1.82 | 24.4 | 23.1 | 25.5 | 0.039 | 0.044 | 0.17 | 25.7 | 147.9 | 0.096 |
| L2 | 138 | 20 | 0.26 | 0.30 | 0.54 | 0.87 | 6.0 | 5.7 | 7.1 | 0.00098 | 0.00124 | 0.0074 | 5.0 | 957.0 | 0.20 |
| L1 | 172 | 25 | | | | | | | 30.3 | | | | 33.4 | 71.9 | |
| L1 | 138 | 20 | | | | | | | | | | | | | |
| T2 | 172 | 25 | 0.31 | 0.21 | 0.57 | 1.3 | 8.3 | 7.6 | 9.4 | 0.0098 | 0.0116 | 0.043 | 14.0 | 217.1 | 0.19 |
| T2 | 138 | 20 | | | | | | | >0.75 | | | | | 1190.4 | |
| As Welded | | | | | | | | | | | | | | | |
| L2 | 172 | 25 | 0.29 | 0.56 | 0.90 | 1.85 | 17.2 | 16.3 | 19.0 | 0.033 | 0.039 | 0.13 | 26.7 | 144.9 | 0.14 |
| L2 | 138 | 20 | 0.31 | 0.38 | 0.16 | 0.66 | 7.1 | 6.5 | 7.6 | 0.00096 | 0.00125 | 0.0106 | 7.9 | 786.4 | 0.18 |
| L1 | 172 | 25 | 0.32 | 0.44 | 1.8 | 3.0 | 33.7 | 32.6 | 36.3 | 0.200 | 0.21 | 0.53 | 29.1 | 69.1 | 0.10 |
| L1 | 138 | 20 | | | | | | | | | | | | | |
| T1 | 172 | 25 | 0.37 | 0.13 | 0.52 | 1.12 | 7.4 | 6.8 | 8.4 | 0.0093 | 0.111 | 0.041 | 8.0 | 204.5 | 0.19 |
| T1 | 138 | 20 | 0.18 | 0.24 | 0.21 | 0.50 | 3.2 | 2.9 | 3.8 | 0.00057 | 0.00092 | 0.0061 | 2.5 | 623.9 | 0.24 |
| Annealed 2 hr at 982°C (1800°F), Water Quenched | | | | | | | | | | | | | | | |
| L2 | 172 | 25 | 1.50 | 2.19 | 12.5 | 13.8 | 40.9 | 39.5 | 57.0 | 0.163 | 0.149 | 0.34 | 42.43 | 166.2 | 0.31 |
| L2 | 138 | 20 | | | | | | | 12.6 | | | | 10.9 | 1320.4 | |
| L1 | 172 | 25 | 0.8 | 3.1 | 4.85 | 7.3 | 33.4 | 30.9 | 42.1 | 0.27 | 0.29 | 0.53 | 36.5 | 79.2 | 0.27 |
| L1 | 138 | 20 | | | | | | | | | | | | >50 | |
| T1 | 172 | 25 | 1.5 | 3.7 | 6.0 | 8.0 | | | 28.0 | 0.075 | 0.077 | 0.13 | 46.0 | 211.4 | 0.47 |
| T1 | 138 | 20 | | | | | | | >4.3 | | | | | >1171 | |

Table 3.10. Creep Test Times to Various Events for Type 308 Stainless Steel Submerged-Arc Welds Tested at 649°C (1200°F)

| Stress (MPa) | Stress (ksi) | Approximate Time, hr, to Various Events: End First Stage | End Second Stage | 0.2% Offset Third Stage | Fracture | 0.5% Creep Strain | 1% Creep Strain | 2% Creep Strain | 0.5% Total Strain | 1% Total Strain | 2% Total Strain | $t_{III}/t_r$ |
|---|---|---|---|---|---|---|---|---|---|---|---|---|
| | | | | | Annealed 4 hr at 607°C (1125°F), Water Quenched | | | | | | | |
| 172 | 25 | 2.4 | 31.6 | 43.5 | 147.9 | 7.5 | 20 | 42 | 0.8 | 12 | 36 | 0.29 |
| 138 | 20 | 100 | 650 | 800 | 957.0 | 315 | 737 | 950 | 40 | 563 | 923 | 0.84 |
| 172 | 25 | | | | 71.9 | | | | | | | |
| 138 | 20 | | | | | | | | | | | |
| 172 | 25 | 7.5 | 66.2 | 120 | 217.1 | 35.8 | 86 | 142 | 6.2 | 57 | 125 | 0.55 |
| 138 | 20 | | | | 1190.4 | | | | | | | |
| | | | | | As Welded | | | | | | | |
| 172 | 25 | 8.0 | 35.0 | 56.0 | 144.9 | 6.7 | 22 | 48.5 | 0.8 | 13 | 43.1 | 0.39 |
| 138 | 20 | 65.1 | 233.2 | 593.3 | 786.4 | 183 | 569 | 780 | 5 | 353 | 770 | 0.75 |
| 172 | 25 | 1.0 | 10.2 | 15.0 | 69.1 | 1.2 | 4 | 9 | 0.3 | 2 | 7.5 | 0.22 |
| 138 | 20 | | | | | | | | | | | |
| 172 | 25 | 2.0 | 58.2 | 102.7 | 204.5 | 40 | 86 | 140 | 1.5 | 55 | 123 | 0.50 |
| 138 | 20 | | | | 623.9 | | | | | | | |
| | | | | | Annealed 2 hr at 982°C (1800°F), Water Quenched | | | | | | | |
| 172 | 25 | 6 | 82.3 | 89.7 | 166.2 | 0.5 | 1.7 | 5.1 | 0 | 0 | 0.5 | 0.54 |
| 138 | 20 | 74.5 | 444.9 | 620 | 1320.4 | 620 | a | a | 200 | 622 | a | 0.47 |
| 172 | 25 | 7.1 | 25.0 | 32.5 | 79.2 | 0.25 | 1.1 | 4 | 0 | 0.1 | 1.5 | 0.41 |
| 138 | 20 | | | | >50 | | | | | | | |
| 172 | 25 | 27.8 | 107.5 | 131.5 | 211.4 | 0.9 | 3.1 | 9.8 | 0 | 0 | 0.9 | 0.62 |
| 138 | 20 | | | | >498 | | | | | | | |

[a]Failed before reaching indicated strain.

time that occurred before the onset of tertiary creep. These values varied widely, from 0.22 to 0.84.

The stress-rupture time data for L2 welds have been plotted with average expected values and $-1.645\sigma$ ($\sigma$ = standard deviation) curves[14] for type 304 stainless steel base metal. For specimens oriented in the longitudinal and transverse directions, rupture times tended to be above the average expected values for type 304 stainless steel base metal, but below the "+1.645 standard deviation curve."

Total elongation measured after test and reduction of area for Level 2 specimens are plotted against rupture time in Fig. 3.35 (a) and (b), respectively. Both measures of ductility decrease significantly with rupture time from about 100 to 1000 hr for as-welded and stress-relieved material. (Trends have not yet been established for solution-annealed specimens, but the solution-annealed specimens that showed about 100-hr rupture lives were more ductile than comparable specimens of as-welded or stress-relieved material.) For the former materials, total strains as low as 3.8% and reductions of area of 2.5% have been recorded.

All longitudinal specimens failed by substructural tearing in the weld metal, as identified under low-power magnification. Scanning

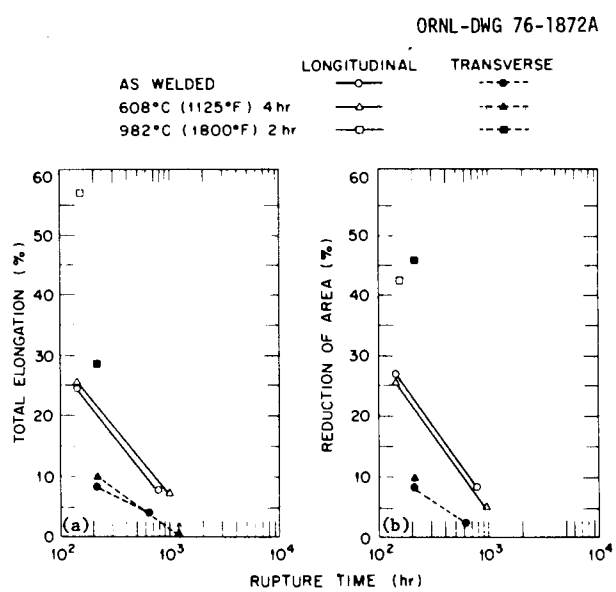


Fig. 3.35. Comparison of Creep-Rupture Properties for Type 308 Stainless Steel Submerged-Arc Welds in Different Conditions; Longitudinal and Transverse, Level 2. (a) Strains. (b) Reductions of area.

electron microscopy and optical metallography are planned. All transverse specimens except one failed in the weld metal by substructural tearing. The exception was a transverse weld test on solution-annealed material that reduced in area about 35% where the elongated subgrains were essentially parallel to the tensile axis, but only 7% where the elongated subgrains were nearly normal to the tensile axis. (The failure occurred close to the fusion line.) Further testing is in progress.

### 3.3.2 Studies of Strain Distribution in Weldments and Room-Temperature Elastic Constants — B. R. Dewey* and R. T. King

Elastic constant determinations continue for an electroslag weldment having type 308 stainless steel weld metal with type 304 base metal. Longitudinal and lateral strain data from 28 tensile specimens having a nominal 3.18-mm (0.125-in.) diameter and 28.6-mm (1.125-in.) reduced section length have now been analyzed and selected tests have been repeated.

Data from longitudinal strain measurements, reported previously,[32] have shown the directional variation of the apparent elastic modulus and the apparent yield strength of the weld metal. Now, with the completion of lateral strain measurements, the elastic compliance and elastic stiffness matrices for the weld metal have been computed.

As this work progressed, considerable scatter in data became apparent. Repeating all measurements four (or more) times revealed that the contribution of measurement error to scatter was significantly less than that of material variation from one specimen to another. Material variation includes (1) the error in judging the orientation of the grain axis with respect to the specimen axis and (2) the occurrence of weld metal of unusual grain orientations or solidification directions within the test section. As a result, the standard deviation (estimated as $\sqrt{\Sigma(x - \bar{x})^2/(n - 1)}$, where $x$ = observed values, $\bar{x}$ = mean value, and $n$ = number of measurements) of each compliance component was computed, and data that fell more than one standard deviation from the mean were rejected. All rejected data were from specimens containing nonregular material structure.

---

*Consultant from the Department of Engineering Science and Mechanics, University of Tennessee, Knoxville.

The approximate standard deviations for the directly observed compliances are given in Table 3.11.

Table 3.11. Approximate Standard Deviations in the Nine Directly Observed Compliances

| Compliance | Number of Different Specimens | Total Number of Observations | Standard Deviation of All Data (%) |
|---|---|---|---|
| $S_{11}$ | 2 | 11 | 9.0 |
| $S_{22}$ | 2 | 10 | 2.2 |
| $S_{33}$ | 2 | 15 | 3.5 |
| $S_{12} = S_{21}$ | 4 | 8 | 41.9 |
| $S_{13} = S_{31}$ | 4 | 8 | 4.2 |
| $S_{23} = S_{32}$ | 4 | 8 | 11.0 |

### 3.3.2.1 Summary of Applicable Formulae Used to Determine Elastic Compliances

When tensile specimens are tested, the components of elastic compliances are the most directly obtained for specimens with orientations in the principal directions, as shown in Fig. 3.36, longitudinal stress-strain measurements produce

$$\begin{aligned} S_{11} &= \varepsilon_1/\sigma_1 \ , \\ S_{22} &= \varepsilon_2/\sigma_2 \ , \\ S_{33} &= \varepsilon_3/\varepsilon_3 \ , \end{aligned} \tag{17}$$

where $S_{ij}$ are compliance components, $\varepsilon_i$ is measured strain in the $i$ direction, and $\sigma_i$ is the load divided by area in the $i$ direction. From lateral strain measurements we have

$$\begin{aligned} S_{12} &= \varepsilon_1/\sigma_2 \ , \\ S_{13} &= \varepsilon_1/\sigma_3 \ , \\ S_{23} &= \varepsilon_2/\sigma_3 \ , \\ S_{21} &= \varepsilon_2/\sigma_1 \ , \\ S_{31} &= \varepsilon_3/\sigma_1 \ , \\ S_{32} &= \varepsilon_3/\sigma_2 \ . \end{aligned} \tag{18}$$

ORNL-DWG 75-13166

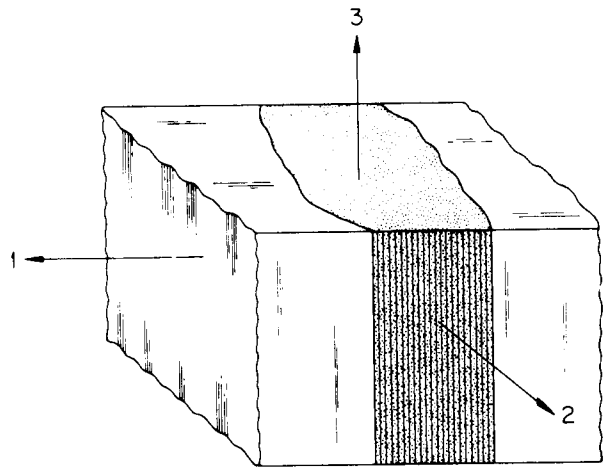


Fig. 3.36. Orientation of Axes in Weldment.

Symmetry dictates that

$$
\begin{aligned}
S_{21} &= S_{12} \ , \\
S_{23} &= S_{32} \ , \\
S_{31} &= S_{13} \ .
\end{aligned}
\tag{19}
$$

Furthermore, for orthotropic symmetry $S_{44}$, $S_{55}$, and $S_{66}$ are the only remaining nonzero compliances. These are computed from longitudinal stress-strain measurements on specimens oriented in nonprincipal directions. The appropriate transformation equations are

$$
\begin{aligned}
S_{66} &= m^{-2}n^{-2}(S'_{11} - m^4 S_{11} - 2m^2n^2 S_{12} - n^4 S_{22}) \ , \\
S_{55} &= m^{-2}n^{-2}(S'_{33} - m^4 S_{33} - 2m^2n^2 S_{31} - n^4 S_{11}) \ , \\
S_{44} &= m^{-2}n^{-2}(S'_{33} - n^4 S_{22} - 2m^2n^2 S_{23} - m^4 S_{33}) \ ,
\end{aligned}
\tag{20}
$$

where $m = \cos\theta$, $n = \sin\theta$, and the primed compliances are those measured at angle $\theta$ to the subscripted principal direction.

The compliances also lead directly to engineering constants as follows:

$$
\begin{aligned}
E_{11} &= 1/S_{11} \ , \\
E_{22} &= 1/S_{22} \ , \\
E_{33} &= 1/S_{33} \ , \\
\nu_{12} &= -S_{12}E_{11} \ , \\
\nu_{21} &= -S_{12}E_{22} \ , \\
\nu_{23} &= -S_{23}E_{22} \ , \\
\nu_{32} &= -S_{23}E_{33} \ , \\
\nu_{13} &= -S_{13}E_{11} \ , \\
\nu_{31} &= -S_{13}E_{33} \ , \\
G_{12} &= 1/S_{66} \ , \\
G_{13} &= 1/S_{55} \ , \\
G_{23} &= 1/S_{44} \ .
\end{aligned}
\tag{21}
$$

Also, with reference to Fig. 3.36 one might expect that the 1-2 plane is a plane of isotropy. In this case, the compliance matrix is further simplified to

$$
[S] = \begin{bmatrix}
S_{11} & S_{12} & S_{13} & 0 & 0 & 0 \\
 & S_{11} & S_{13} & 0 & 0 & 0 \\
 & & S_{33} & 0 & 0 & 0 \\
 & & & S_{44} & 0 & 0 \\
 & & & & S_{44} & 0 \\
\text{(Sym)} & & & & & 2(S_{11} - S_{12})
\end{bmatrix} \ , \tag{22}
$$

which contains five independent constants. The seven engineering constants for this symmetry follow from Eq. (21).

### 3.3.2.2 Elastic Compliance and Stiffness Results

From the slopes of load-deformation curves, and with the statistical criterion previously stated, the following compliance matrix has been computed with Eqs. (17) through (20):

$$[S] = 10^{-8} \begin{bmatrix} 4.58 & -1.23 & -2.19 & 0 & 0 & 0 \\ & 4.93 & -2.61 & 0 & 0 & 0 \\ & & 6.18 & 0 & 0 & 0 \\ & & & 7.32 & 0 & 0 \\ & & & & 6.41 & 0 \\ (\text{Sym}) & & & & & 13.06 \end{bmatrix} \text{psi}^{-1}$$

$$= 10^{-12} \begin{bmatrix} 6.43 & -1.73 & -3.07 & 0 & 0 & 0 \\ & 6.93 & -3.66 & 0 & 0 & 0 \\ & & 8.69 & 0 & 0 & 0 \\ & & & 10.28 & 0 & 0 \\ & & & & 9.00 & 0 \\ (\text{Sym}) & & & & & 18.35 \end{bmatrix} \text{Pa}^{-1} \tag{23}$$

The compliance matrix may be inverted to give the stiffness matrix:

$$[C] = 10^{7} \begin{bmatrix} 3.85 & 2.16 & 2.27 & 0 & 0 & 0 \\ & 3.82 & 2.37 & 0 & 0 & 0 \\ & & 3.42 & 0 & 0 & 0 \\ & & & 1.37 & 0 & 0 \\ & & & & 1.56 & 0 \\ (\text{Sym}) & & & & & 0.77 \end{bmatrix} \text{psi}$$

$$= 10^{11} \begin{bmatrix} 2.74 & 1.54 & 1.62 & 0 & 0 & 0 \\ & 2.72 & 1.69 & 0 & 0 & 0 \\ & & 2.43 & 0 & 0 & 0 \\ & & & 0.97 & 0 & 0 \\ & & & & 1.11 & 0 \\ (\text{Sym}) & & & & & 0.54 \end{bmatrix} \text{Pa} \tag{24}$$

For the simplest use of the above data in design, it is frequently convenient to use a two-dimensional stress analysis such as plane stress,

plane strain, or axisymmetry. By averaging the appropriate terms of Eq. (23) or (24) to give the symmetry of Eq. (22), and subsequently using Eq. (21) to obtain engineering constants, we have

$$
\begin{aligned}
E_{11} &= E_{22} = 14.6 \times 10^{10}\ \text{Pa} = 21.1 \times 10^{6}\ \text{psi}\ , \\
E_{33} &= 11.2 \times 10^{10}\ \text{Pa} = 16.2 \times 10^{6}\ \text{psi}\ , \\
\nu_{12} &= \nu_{21} = 0.260\ , \\
\nu_{23} &= \nu_{13} = 0.503\ , \\
\nu_{32} &= \nu_{31} = 0.387\ , \\
G_{12} &= 4.82 \times 10^{10}\ \text{Pa} = 6.99 \times 10^{6}\ \text{psi}\ , \\
G_{13} &= G_{23} = 10.1 \times 10^{10}\ \text{Pa} = 14.6 \times 10^{6}\ \text{psi}\ .
\end{aligned}
\tag{25}
$$

3.3.2.3 Remarks on Results and Test Procedures

The results such as those given in Eqs. (23) through (25) definitely show that this particular weld metal may not be assumed to be isotropic for computational purposes. The use of these results, however, is routine in finite element programs. In some programs, orthotropic engineering constants may be entered directly. All programs convert engineering constants into stiffness or compliance matrices internally, hence the appropriate matrix may be entered.

The procedure as described here is equally valid for multipass welds, where a form of macroscopic orthotropy is assumed. One of the principal directions is the local solidification direction. The other two principal directions may be deduced by symmetry in the weld pattern. As the number of weld passes increases, the assumption of macroscopic orthotropy improves for many weld configurations over much of the weld.

When the nonprincipal-direction specimens are used to determine the off-axis compliances $S'_{11}$, $S'_{22}$, or $S'_{33}$, end constraint could induce shear stresses in addition to the normal stress. This effect has been ignored; it can be shown that as the reduced section length increases, the effect of end constraint decreases. Because of this, the longest possible reduced section length is recommended for off-axis specimens.

Metallurgical variations relative to measurement errors may necessitate the use of a statistical procedure to reject data. Thus, it is implied that a large number of specimens should be tested to characterize the elastic property matrix for weld metal.

An alternate method of elastic constant determination is the ultrasonic velocity measurement method. The ultrasonic method permits direct measurement of the diagonal terms in the stiffness matrix, and the off-diagonal terms must be calculated from transformation equations. Thus, it might appear that a hybrid method may be advantagous whereby the shear terms are determined ultrasonically and the Poisson terms are found by static tensile testing. Of course, the distinction between dynamic and static constants still needs to be made.

## 3.4 MECHANICAL PROPERTIES OF STEAM GENERATOR MATERIALS — C. R. Brinkman

### 3.4.1 Strain-Rate Effects on the Tensile Properties of Annealed 2 1/4 Cr-1 Mo Steel — R. L. Klueh

We have now completed our studies on the high-strain-rate tensile properties of annealed 2 1/4 Cr-1 Mo steel.[33,34] A report has been issued[35] and is summarized here.

The tensile properties of annealed 2 1/4 Cr-1 Mo steel were studied over the temperature range 25 to 566°C (77—1050°F) and the strain rate range $2.67 \times 10^{-6}$ to 144/sec. The following observations and conclusions were made:

1. Except at 25°C, the 0.2% yield stress was little affected by strain rate. Above about 0.1/sec at 25°C, there was a large increase in yield stress with increasing strain rate. The only other effect was a minor peak at intermediate temperatures and strain rates.

2. At 25°C, the effect of strain rate on ultimate tensile stress was similar to the effect on yield strength: there was a large increase above 0.1/sec, though the ultimate tensile strength also showed a smaller rate of increase at lower strain rates. The ultimate tensile strength as a function of temperature exhibited a dynamic strain-aging peak, which was a maximum at about 350°C (660°F) and $2.67 \times 10^{-6}$/sec.

In this temperature range, the ultimate tensile strength increased with decreasing strain rate. A strain aging peak occurred at each strain rate, but as the strain rate was increased, the peak height decreased and occurred at progressively higher temperatures. At the highest temperatures, 510 and 566°C (950 and 1050°F), the ultimate tensile strength increased with increasing strain rate.

3. Except at 510 and 566°C, ductility was little affected by strain rate. At these temperatures, the total elongation and the reduction of area increased with decreasing strain rate, while the uniform elongation decreased with decreasing strain rate.

### 3.4.2 Heat-to-Heat Variation of 2 1/4 Cr-1 Mo Steel — R. L. Klueh

As explained previously,[36] for a ferritic material such as 2 1/4 Cr-1 Mo steel, where a phase transformation occurs during the heat treatment, differences in the heat treatment process (by different vendors etc.) can give rise to heat-to-heat variations in mechanical properties over and above differences due to variations in composition. For this reason, along with the fact that several different methods are used to heat-treat ferritic steels, we are determining the effect of heat treatment on mechanical properties.

We previously reported[36] on the effect of heat treatment on the tensile properties taken from sections of 25-mm-thick (1-in.) plate (heat 20017) that had been annealed differently. Two sections of plate were furnace cooled (fully annealed) at different rates after austenitization [1 hr at 927°C (1700°F)]. These two plates were referred to as AN-1 and AN-2; AN-1 was cooled to 700°C (1292°F) (most of the transformation to proeutectoid ferrite is complete by the time the temperature reaches 700°C) in about 3.5 hr, AN-2 in about 4.8 hr. We also tested a section of plate that had been isothermally annealed [after 1 hr at 927°C it was cooled at about 83°C/hr (150°F/hr) to 704°C (1300°F), held for 2 hr, then furnace cooled]; this heat treatment was referred to as IA. Specimens taken from these plates were tensile tested between 25 and 593°C (77 and 1100°F) at strain rates of $2.67 \times 10^{-6}$, $6.67 \times 10^{-5}$, $6.67 \times 10^{-4}$, and $6.67 \times 10^{-3}$/sec. Over this range

of test variables, we observed significant differences in properties, which must be attributed to the heat treatment.[36] The major differences were in the dynamic strain aging effects, which are best illustrated by plots of the ultimate tensile strength as a function of temperature. Such plots are shown in Fig. 3.37 for AN-1, AN-2, and IA, along with one for a normalized-and-tempered plate, the microstructure of which was entirely bainite.

All three annealing heat treatments resulted in microstructures that were primarily proeutectoid ferrite. Although AN-2 contained more bainite than the other two heat treatments, this difference in microstructure cannot be used to account for the strength differences, since

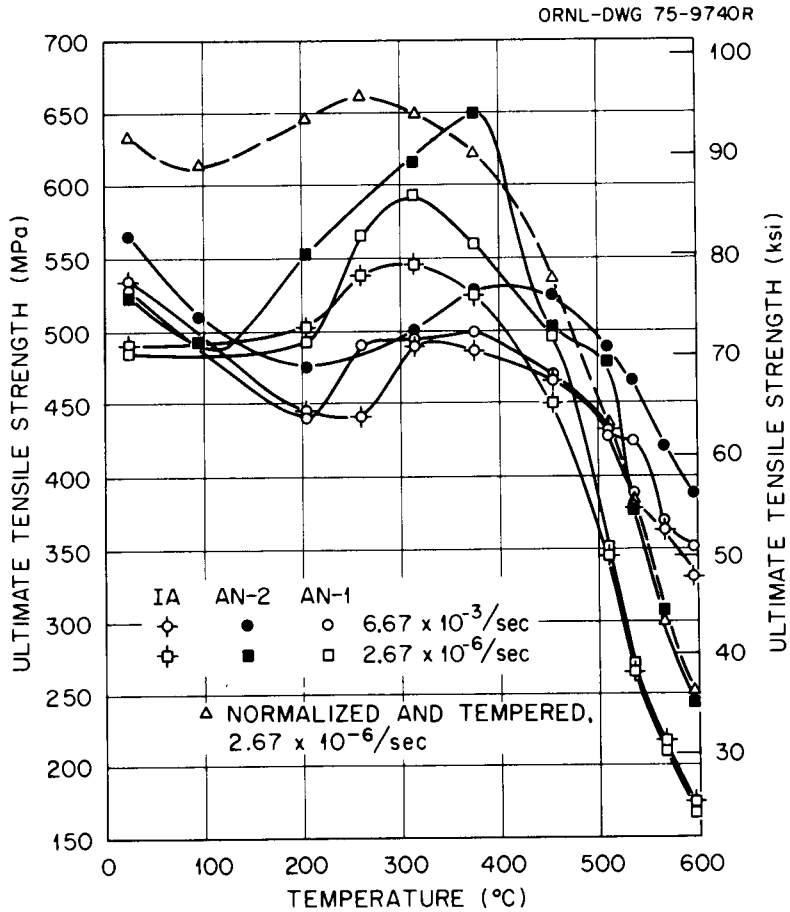


Fig. 3.37. The Ultimate Tensile Strength for the Three Different Annealing Heat Treatments AN-1, AN-2, and IA as a Function of Temperature at Strain Rates of $6.67 \times 10^{-3}$ and $2.67 \times 10^{-6}$/sec. Also shown is the curve for this same steel in the normalized-and-tempered condition at a strain rate of $2.67 \times 10^{-6}$/sec.

even in AN-2, only 15% of the microstructure was bainite. Hence, the explanation must involve the proeutectoid ferrite, which makes up the bulk of the microstructure for both AN-1 and AN-2. In the following, we will discuss possible explanations for these differences.

We previously discussed the dynamic strain aging peaks for AN-1 and the normalized-and-tempered steel,[37] relying on the work by Baird and Jamieson,[38] for our explanations. These same explanations also apply for the present results.

According to Baird,[39] who has reviewed the subject, two types of solute-dislocation interactions give rise to hardening by dynamic strain aging. The most commonly discussed effect is associated with the interaction of carbon or nitrogen atoms with dislocations and is observed at lower temperatures (100 to 300°C, the "blue brittleness" range). However, in ferritic alloys containing chromium and/or molybdenum along with carbon and/or nitrogen, a second effect is observed, which extends the dynamic strain aging peak to higher temperatures. Baird and Jamieson[38] termed this second effect "interaction solid-solution hardening" and attributed it to a strengthening that results from the simultaneous presence in solution of substitutional and interstitial atoms with an affinity for each other (e.g., carbon and molybdenum or carbon and chromium). The exact nature of the hardening is not completely understood, and it will depend upon whether the interstitial atoms are bound more strongly to the substitutional atoms or the dislocations.[38]

Previously, we concluded that the dynamic strain aging that occurred in AN-1 was the result of interaction solid-solution hardening, probably involving the interaction of dislocations with carbon and molybdenum.[35] The similarity between the ultimate tensile strength versus temperature curves of Fig. 3.37 for AN-1 and isothermally annealed plate IA would indicate that the same reactions must also occur in the latter, and the previous conclusions for AN-1 apply. Comparison of the curves for AN-1 and AN-2 indicates that the curve shapes for these heat treatments are also similar. The primary difference is that the peak height for AN-2 is greater than that for

AN-1 and IA, and it is shifted to a higher temperature. Thus, apparently the dynamic strain aging reaction that gives rise to the peak for AN-2 is also due to interaction solid-solution hardening in proeutectoid ferrite, similar to that occurring in AN-1 and IA. [Note that the fact that the relative peak height for AN-2 is greater and occurs at a higher temperature than for the all-bainitic normalized-and-tempered steel (Fig. 3.37) cannot be used as direct evidence that the larger amount of bainite in AN-2 is not causing the difference between AN-2 and AN-1 and IA, because the bainite in AN-2 is untempered.]

In Fig. 3.37 decided differences are seen between the dynamic strain aging in the tempered bainite of the normalized-and-tempered plate and the proeutectoid ferrite of the annealed plate. If we base our comparisons on the strength at room temperature, we note the following: (1) the strengthening for the bainitic steel begins at a lower temperature, (2) the relative height of the peak is less for the bainitic steel, and (3) the dynamic strain aging effect for the bainitic steel does not extend to temperatures as high as those for the annealed steel.

To explain the difference between the effect of dynamic strain aging in the tempered bainite of the normalized-and-tempered plate and the proeutectoid ferrite of the annealed plate (AN-1), we previously[35] referred to the precipitation studies of Baker and Nutting,[40] who showed that different carbide reaction sequences occur in these different microstructures. In proeutectoid ferrite, the first precipitate to form is $Mo_2C$, and it forms quite slowly. For bainite, however, a complex reaction sequence takes place, with the first precipitate to form being $M_3C$, followed rather quickly — almost simultaneously — by $Mo_2C$. In both proeutectoid ferrite and bainite, the $Mo_2C$ is not stable. In the proeutectoid ferrite $Mo_2C$ is replaced by $M_6C$, while in bainite $M_{23}C_6$, $M_7C_3$, and $M_6C$ result.[40] The replacement of $Mo_2C$ by the more stable carbides is much more rapid for the bainite than the proeutectoid ferrite.

To explain the observations in the different microstructural constituents, we suggested[35] that the exclusive formation of $Mo_2C$ in

proeutectoid ferrite is preceded by the agglomeration of molybdenum and carbon atoms in solution before incorporation in $Mo_2C$ precipitate, and this gives rise to the interaction solid-solution hardening in AN-1. That is, interaction occurs before the completion of precipitation, and it implies that once all the carbon in solution is incorporated in the precipitate, strengthening by dynamic strain aging will cease.[38]

Since $Mo_2C$ does form in bainite, the possibility of pre-precipitation agglomeration in this constituent also exists. However, Baker and Nutting[40] found that because of the more complicated precipitation sequence in bainite, $Mo_2C$ formation and eventual dissolution are much more rapid than in ferrite. Furthermore, after tempering the bainite microstructure has a larger density of precipitate particles present than proeutectoid ferrite; in addition to $M_3C$ and $Mo_2C$, $M_7C_3$ and $M_{23}C_6$ are also found.[41] As a result of these differences, the pre-precipitation agglomeration of molybdenum and carbon would be expected to be much less likely in bainite. That is, because of the greater precipitate density, a carbon atom is much more likely to be incorporated in a precipitate than to be associated with a molybdenum atom, which would lead to interaction solid-solution hardening. Therefore, for bainite interaction solid-solution hardening would be expected to occur over a smaller temperature range and at lower temperatures, because at higher temperatures where diffusion (required for precipitate formation) is more rapid, the associated molybdenum and carbon atoms could be rapidly incorporated into precipitate, making them unavailable for hardening.

The difference between AN-1 and AN-2 must be the difference of the amount of precipitate formed and the degree of pre-precipitation agglomeration that occurs for the different cooling rates. In related work, we extracted the carbides from these same heat-treated conditions.[41] After extraction, the amount of carbide was weighed, and the supernate from the extraction was analyzed for chromium and molybdenum to determine the amount of these elements that remained in solid solution (i.e., not in the precipitate). The results, which should provide qualitative information on the distribution of molybdenum and

chromium, are shown in Table 3.12 and support the above suggested explanation. In Fig. 3.37, the peak heights for a strain rate of $2.67 \times 10^{-6}$/sec decrease in the order AN-2, AN-1, and IA, which corresponds to the order of decreasing molybdenum in solution and increasing amount of carbide formed. That is, the higher the cooling rate, the less precipitate formed, and thus, the more molybdenum remaining in solution and being available for interaction solid-solution hardening. The fact that the peak for AN-2 moved to a higher temperature could mean that some further agglomeration is required before optimum hardening can occur (the faster cooling rate has not allowed for maximum agglomeration). Such pre-precipiration agglomeration requires diffusion, which will be favored at a higher test temperature. Note that for the normalized-and-tempered plate, much more molybdenum remains in solution than for the annealed plates. As explained above, however, the more rapid precipitation in bainite favors the incorporation of carbon and molybdenum into existing precipitates rather than associations that would lead to interaction solid-solution hardening.

If the dynamic strain aging in 2 1/4 Cr-1 Mo steel is the result of interaction solid-solution hardening as postulated above, then further heat treatment should reduce the dynamiic strain aging peaks. For example, if the annealed specimens were tempered before testing,

Table 3.12. Effect of Heat Treatment on Amount of Precipitate and Estimate of Amount of Elements Remaining in Solution

| Heat Treatment | Amount of Precipitate in Steel (wt %) | Amount, wt %, in Ferrite Solid Solution[a] | |
|---|---|---|---|
| | | Cr | Mo |
| AN-1 | 1.43 | 1.65 | 0.49 |
| AN-2 | 1.12 | 1.57 | 0.54 |
| IA | 1.53 | 1.67 | 0.40 |
| Normalized and Tempered | 1.57 | 1.68 | 0.81 |

[a]Determined by analyzing the supernate; steel originally contained 2.2% Cr, 0.9% Mo.

the precipitation reactions, which remove molybdenum and carbon from solution, will proceed. Since less of these elements is then available for interaction solid-solution hardening, the strain aging peak should be lowered.

Specimens from AN-2, which showed the most pronounced peak (Fig. 3.37), were tempered for 1 hr at 704°C (1300°F) and then tested at 25 to 593°C (77—1100°F) at $6.67 \times 10^{-3}$ and $2.67 \times 10^{-6}$/sec. The results are given in Table 3.13. The tempering treatment affected both

Table 3.13. Tensile Properties of Annealed (AN-2) 2 1/4 Cr-1 Mo Steel After Tempering 1 hr at 704°C

| Temperature | | Strength, MPa (ksi) | | | Elongation, % | | Reduction of Area (%) |
|---|---|---|---|---|---|---|---|
| (°C) | (°F) | Yield | Ultimate | Fracture | Uniform | Total | |
| | | | Strain Rate — $6.67 \times 10^{-3}$/sec | | | | |
| 25 | 75 | 309 (44.9) | 537 (77.9) | 296 (42.9) | 13.3 | 28.2 | 74.2 |
| 204 | 400 | 269 (39.0) | 461 (66.9) | 274 (39.8) | 10.9 | 23.7 | 71.3 |
| 316 | 600 | 253 (36.7) | 495 (71.9) | 316 (45.8) | 9.1 | 22.2 | 66.4 |
| 371 | 700 | 255 (37.0) | 506 (73.5) | 345 (50.0) | 8.8 | 19.2 | 63.5 |
| 454 | 850 | 243 (35.2) | 471 (68.4) | 267 (38.7) | 9.2 | 23.2 | 67.3 |
| 510 | 950 | 226 (32.8) | 420 (61.0) | 209 (30.3) | 8.6 | 23.5 | 75.6 |
| 538 | 1000 | 221 (32.1) | 387 (56.2) | 175 (25.4) | 8.3 | 27.3 | 78.1 |
| 566 | 1050 | 219 (31.8) | 353 (51.3) | 134 (19.4) | 7.5 | 29.6 | 83.0 |
| 593 | 1100 | 205 (29.8) | 315 (45.7) | 99 (14.3) | 6.7 | 32.8 | 84.6 |
| | | | Strain Rate — $2.67 \times 10^{-6}$/sec | | | | |
| 25 | 75 | 287 (41.6) | 498 (72.3) | 291 (42.3) | 11.1 | 26.4 | 74.4 |
| 204 | 400 | 265 (38.5) | 533 (77.4) | 354 (51.4) | 9.4 | 20.5 | 66.9 |
| 316 | 600 | 243 (35.2) | 555 (80.5) | 368 (53.4) | 9.8 | 21.4 | 65.8 |
| 371 | 700 | 249 (36.2) | 509 (73.9) | 298 (43.3) | 9.3 | 23.0 | 69.5 |
| 454 | 850 | 229 (33.2) | 422 (61.3) | 173 (25.1) | 7.0 | 25.6 | 78.8 |
| 510 | 950 | 215 (31.2) | 307 (44.5) | 32 (4.6) | 4.3 | 35.8 | 88.1 |
| 538 | 1000 | 206 (29.9) | 244 (35.4) | 31 (4.5) | 3.3 | 52.8 | 89.7 |
| 566 | 1050 | 175 (25.4) | 200 (29.0) | 28 (4.0) | 4.5 | 51.9 | 88.1 |
| 593 | 1100 | 144 (20.9) | 166 (24.1) | 60 (8.7) | 5.2 | 49.9 | 87.4 |

the yield stress and the ultimate tensile strength; the elongations and reductions of area increased slightly with tempering and were similar to those of AN-1 and IA.

In Fig. 3.38, the yield stress results for the tempered steel are shown as a function of temperature; also shown are the results[36] for the untempered AN-2 at the same strain rates. The figure shows that the 1-hr temper at 704°C has raised the yield strength at room temperature and caused a drop at the higher temperatures, with the drop in yield stress increasing as temperature increases and strain rate decreases. At the highest temperatures, the yield stresses are now similar to those[36] for AN-1 and IA. The increase in yield stress at 25°C is probably due to static strain aging, since after tempering, we observed a yield point that was not present before tempering.

In Fig. 3.39, the ultimate tensile strength for AN-2 is compared before and after tempering. For both strain rates the dynamic strain aging peak height decreased significantly. Furthermore, tempering decreased the temperature of the peak. Comparing the curves in Fig. 3.39 with those for AN-1 and IA given in Fig. 3.37 shows that after tempering the properties for AN-2 rather closely resemble those of IA — the heat treatment that displayed the least dynamic strain aging effects. Note that the peak for AN-2 is now at about the same temperature as the peaks for AN-1 and IA, about 320°C (600°F), as opposed to 250°C (480°F) for the normalized-and tempered plate. If the larger amount of bainite in AN-2 were affecting the properties, then we would expect the peak to drop below those for AN-1 and IA after tempering. Hence, the above conclusion that the properties of AN-2 are determined by the proeutectoid ferrite appears correct.

All the above observations agree with the effects expected from the interaction solid-solution hardening model postulated by Baird and Jamieson.[38] The tempering at 704°C (1300°F) has continued the formation of $Mo_2C$, thus removing molybdenum and carbon from solid solution and making it unavailable for interaction with dislocations.

The above discussion assumed that the interaction solid-solution hardening was the result of interactions between molybdenum and carbon

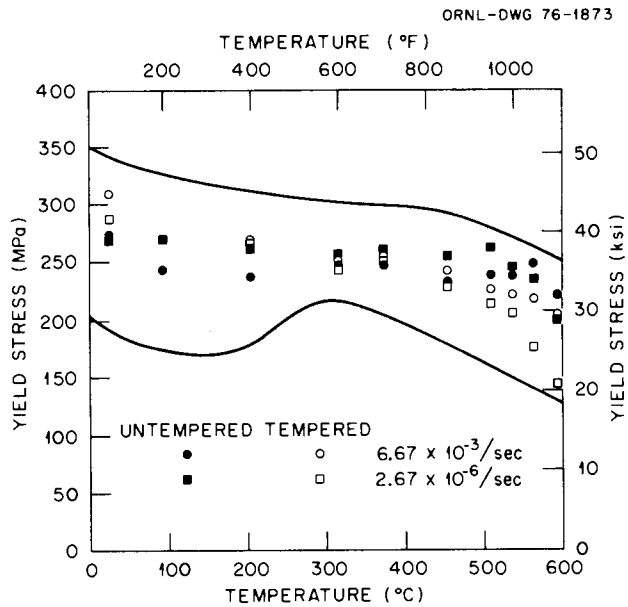


Fig. 3.38. Yield Strength as a Function of Temperature for AN-2 Before and After Tempering at 704°C. Also shown is a scatter band for the data on annealed 2 1/4 Cr-1 Mo steel compiled by Smith (ASTM Data Series DS 6-S2).

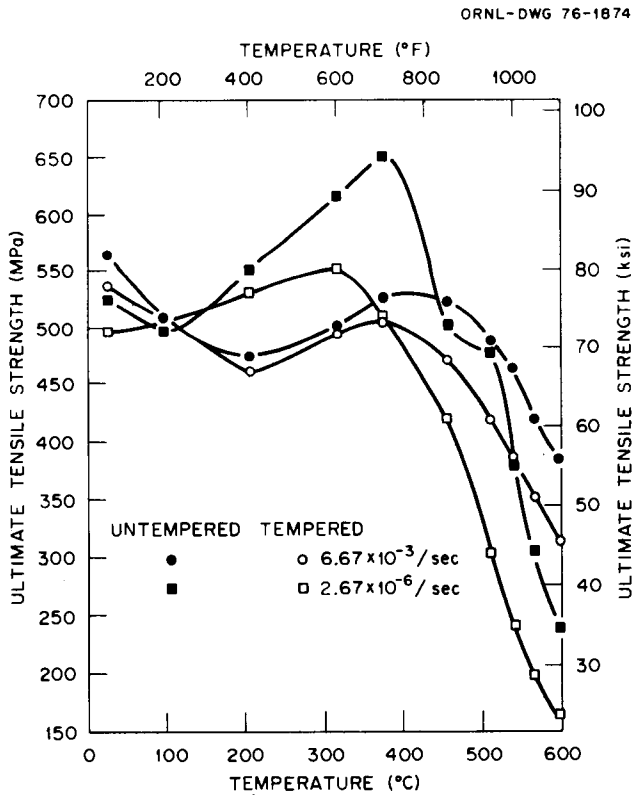


Fig. 3.39. The Ultimate Tensile Strength as a Function of Temperature for AN-2 Before and After Tempering at 704°C.

atoms or atom clusters with dislocations, although no direct proof was given for this assumption. Molybdenum, rather than chromium, is felt to cause the primary effect for two reasons. First, Baird and Jamieson[38] found that molybdenum displayed a much larger interaction solid-solution hardening effect than chromium in ternary Fe-Mo-C and Fe-Cr-C alloys. Secondly, $Mo_2C$ is the first precipitate to form in proeutectoid ferrite, and for prolonged periods at elevated temperatures it is the only precipitate present. Since the agglomeration of molybdenum and carbon is a required step for precipitation, the association of these species in the small atomic units required for interaction solid-solution hardening should be enhanced. In bainite (the normalized-and-tempered steel) $M_7C_3$ and $M_{23}C_6$, both chromium-rich precipitates, form rather early in the tempering process, and as seen previously (Fig. 3.37), the dynamic strain aging peak for this microstructure is much less pronounced.

### 3.4.3 Fatigue Behavior of 2 1/4 Cr-1 Mo Steel — C. R. Brinkman

#### 3.4.3.1 Fatigue Curve Development — M. K. Booker

Development of continuous cycling fatigue design curves for 2 1/4 Cr-1 Mo from room temperature to 593°C (1100°F) has been reported.[42] These design curves were constructed by applying the lesser of safety factors of 2 on strain range and 20 on cycles to failure from graphically constructed mean curves.

The graphically constructed mean curves were drawn through data at 427, 538, and 593°C (800, 1000, and 1100°F) by use of engineering judgment. The resultant curves were felt to be applicable for Room Temperature $\leqslant T \leqslant$ 427°C, 427°C $< T \leqslant$ 538°C, and 538°C $< T \leqslant$ 593°C respectively, where $T$ is test temperature.

Since the construction of the original curves, several new data have become available. To check the accuracy of the previous curves, new curves have been generated from the current data base. These curves, however, were obtained from least squares fits to the data, using data generated in the range of applicability of each curve. Figure 3.40 illustrates the resultant fits to the data (solid lines), given by:

427°C (800°F) $$\log N_f = 3.578 - 2.358 \log \Delta\varepsilon_t + 3.506(\log \Delta\varepsilon_t)^2 - 4.197(\log \Delta\varepsilon_t)^3 , \quad (26)$$

538°C (1000°F) $$\log N_f = 3.302 - 2.388 \log \Delta\varepsilon_t + 3.521(\log \Delta\varepsilon_t)^2 - 2.577(\log \Delta\varepsilon_t)^3 , \quad (27)$$

593°C (1100°F) $$\log N_f = 3.153 - 1.803 \log \Delta\varepsilon_t + 2.613(\log \Delta\varepsilon_t)^2 - 3.738(\log \Delta\varepsilon_t)^3 , \quad (28)$$

where

$N_f$ = cycles to failure,
$\Delta\varepsilon_t$ = total strain range, %.

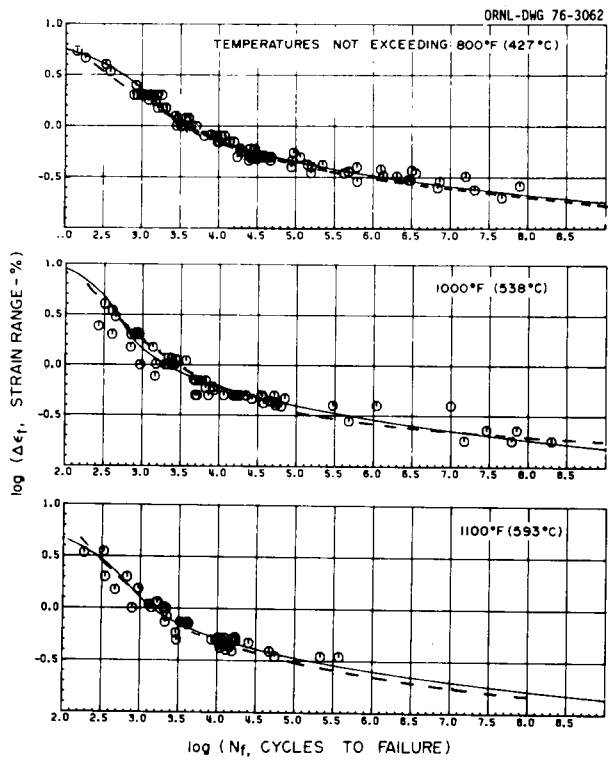


Fig. 3.40. Best-Fit Fatigue Curves for 2 1/4 Cr-1 Mo Steel. Solid lines are least squares fits to the data shown. Dashed lines are graphical fits from Brinkman et al., ORNL-TM-4993.

The dashed lines in Fig. 3.40 are the previous graphically constructed curves. The agreement is good, although the earlier curves appear slightly more conservative in general for $N_f > 10{,}000$. However, variations due to differences in composition, geometry, and other factors can be large. Therefore, at least until the availability of more information about such factors, no changes in the design curves are recommended. For applications involving only mean values, Eqs. (26) through (28) should be used, however.

3.4.3.2 Bilinear Cyclic Stress-Strain Constants — M. K. Booker

The development of interim curves showing the bilinear stress-strain constants $\kappa_0$, $\kappa_1$, $\kappa_2$, $E_m$, and $C$ as functions of maximum strain, $\varepsilon_{max}$, has been reported earlier.[43] These results are finalized in this report, where one change is made from the previous report. The $\kappa_2$ values used here were obtained from the first available hysteresis loop after 100 cycles, in accordance with current design recommendations.[44] The $N_f/2$ values of $\kappa$ are labelled $\kappa_3$. Otherwise, all background information was given before.[43] Figures 3.41 through 3.48 display the final results for the $\kappa$ values, while Fig. 3.49 shows the results for $C$ and $E_m$. As discussed,[43] Figs. 3.43 through 3.48 were derived from tests on heat 20017 of 2 1/4 Cr-1 Mo steel at a ramp strain rate of $4 \times 10^{-3}$/sec. Figures 3.41 and 3.42 reflect tensile data on this heat at a strain rate of $6.7 \times 10^{-3}$/sec. Figure 3.49 was derived from data for three heats at various strain rates.

Because of the limited scope of the data from which these curves were derived, they should be regarded as interim — subject to revision upon the availability of more data.

### 3.4.4 Mechanical Property Correlations of 2 1/4 Cr-1 Mo Steel for LMFBR Steam Generators

3.4.4.1 Rupture Life — T. L. Hebble*

A mathematical model for rupture life of annealed 2 1/4 Cr-1 Mo steel, reported previously,[45] was based on a data set that included

*Mathematics and Statistics Research Department.

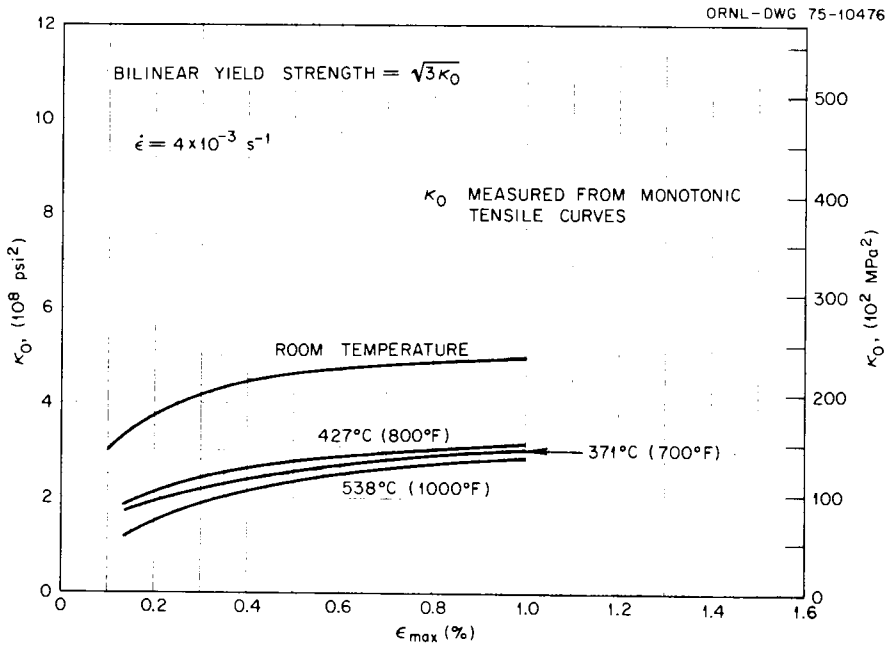


Fig. 3.41. Variation of Bilinear Stress-Strain Constant $\kappa_0$ with $\varepsilon_{max}$ for 2 1/4 Cr-1 Mo Steel.

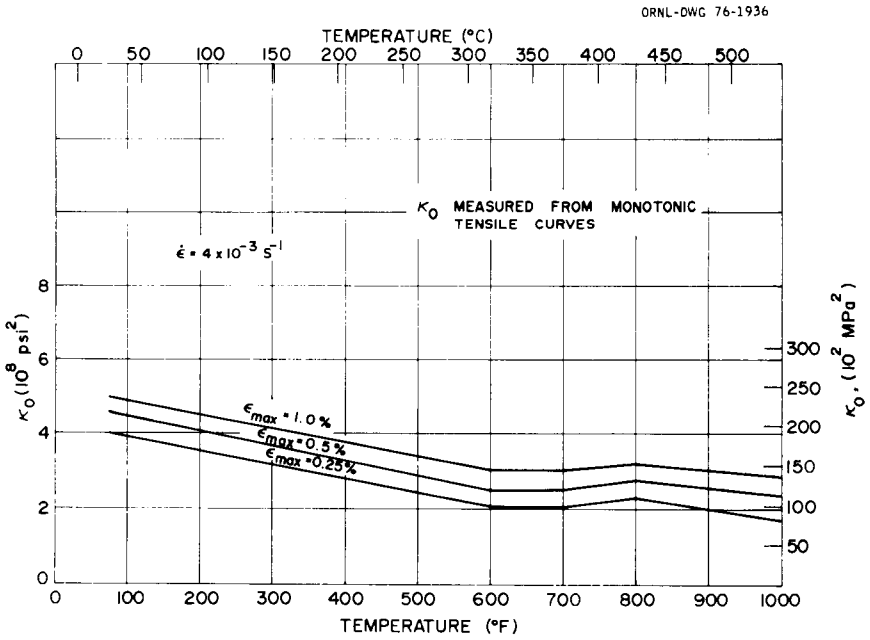


Fig. 3.42. Variation of Bilinear Stress-Strain Constant $\kappa_0$ with Temperature for 2 1/4 Cr-1 Mo Steel.

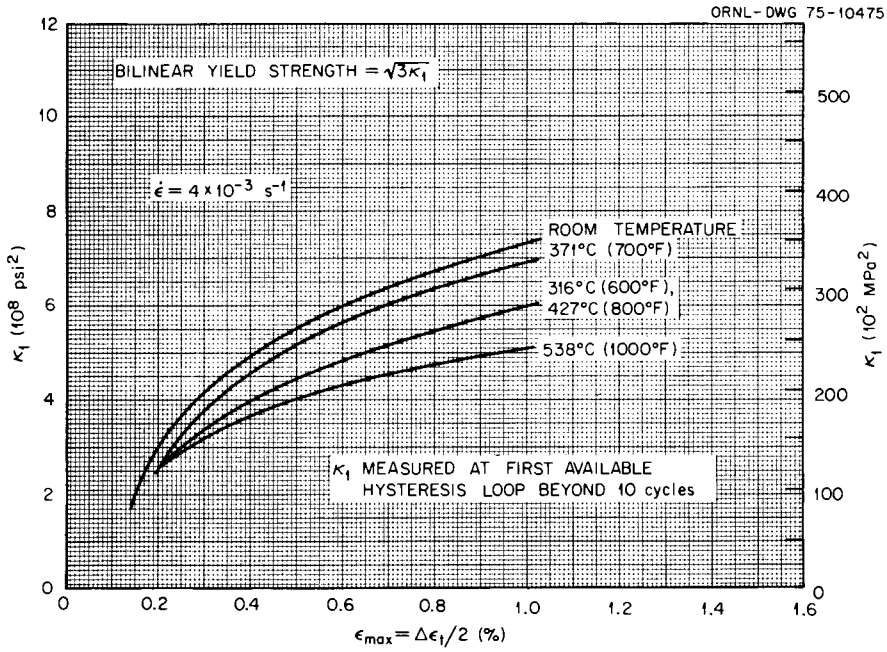


Fig. 3.43. Variation of Bilinear Cyclic Stress-Strain Constant $\kappa_1$ with $\varepsilon_{max}$ for 2 1/4 Cr-1 Mo Steel.

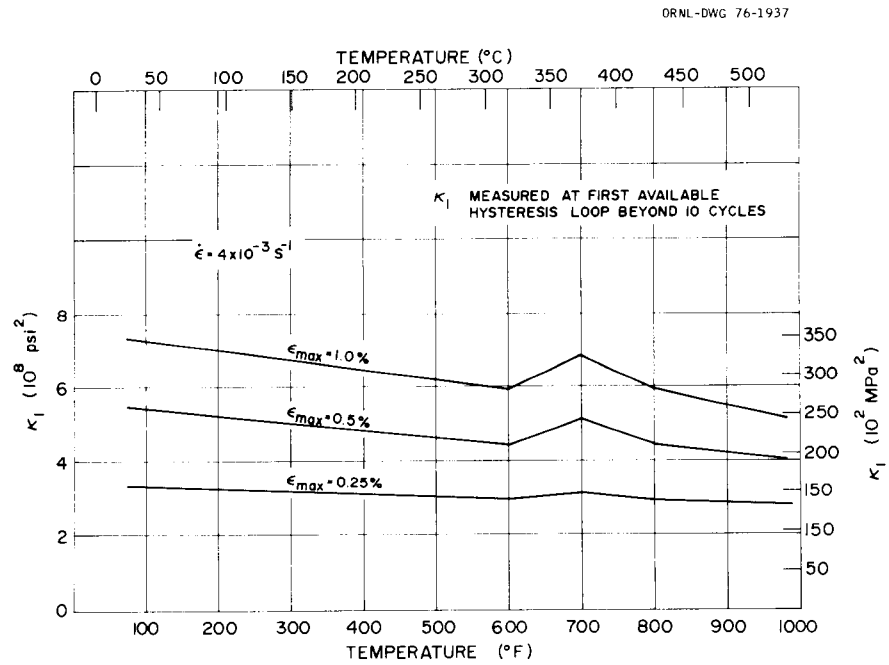


Fig. 3.44. Variation of Bilinear Cyclic Stress-Strain Constant $\kappa_1$ with Temperature for 2 1/4 Cr-1 Mo Steel.

ORNL-DWG 76-1938

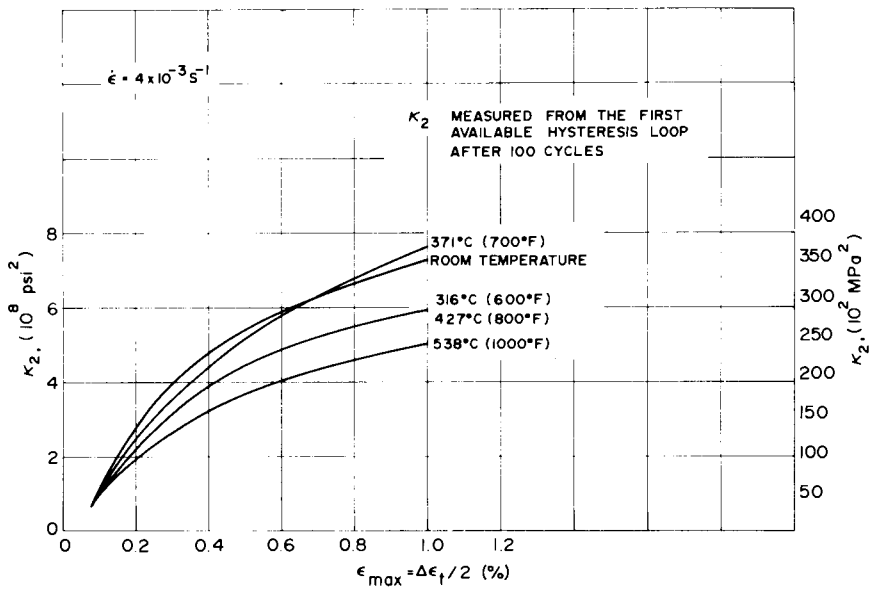


Fig. 3.45. Variation of Bilinear Cyclic Stress-Strain Constant $K_2$ with $\varepsilon_{max}$ for 2 1/4 Cr-1 Mo Steel.

ORNL-DWG 76-1939

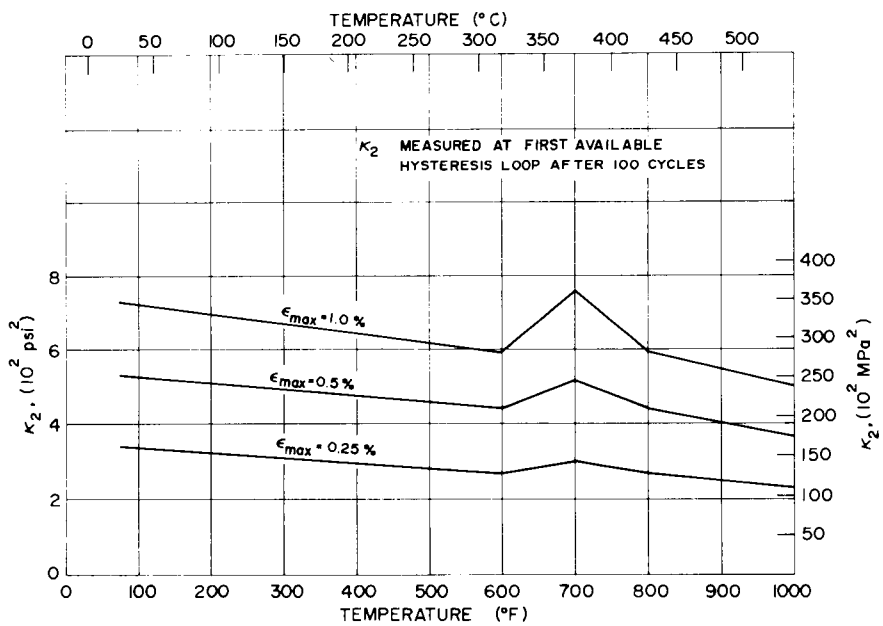


Fig. 3.46. Variation of Bilinear Cyclic Stress-Strain Constant $K_2$ with Temperature for 2 1/4 Cr-1 Mo Steel.

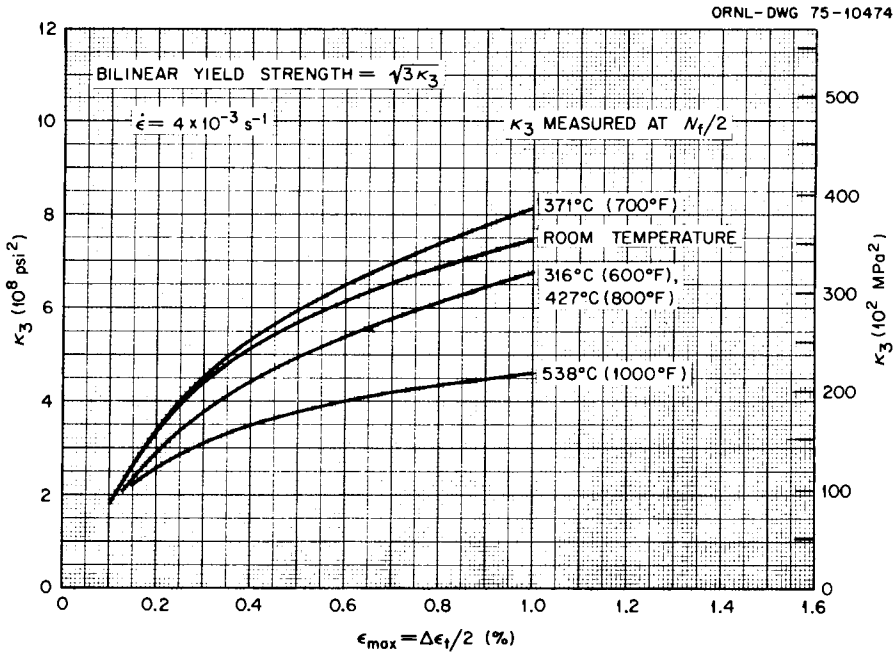


Fig. 3.47. Variation of Bilinear Cyclic Stress-Strain Constant $\kappa_3$ with $\varepsilon_{max}$ for 2 1/4 Cr-1 Mo Steel.

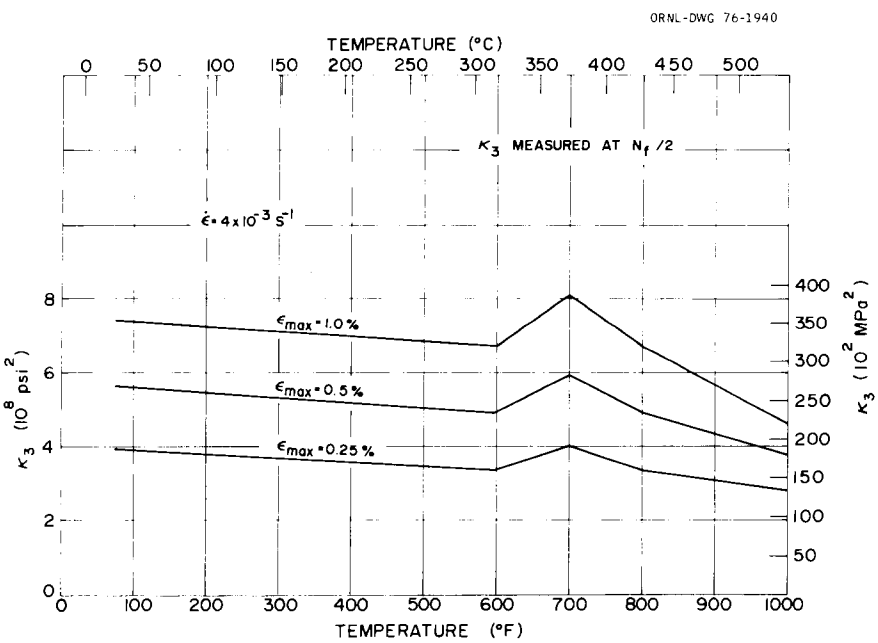


Fig. 3.48. Variation of Bilinear Cyclic Stress-Strain Constant $\kappa_3$ with Temperature for 2 1/4 Cr-1 Mo Steel.

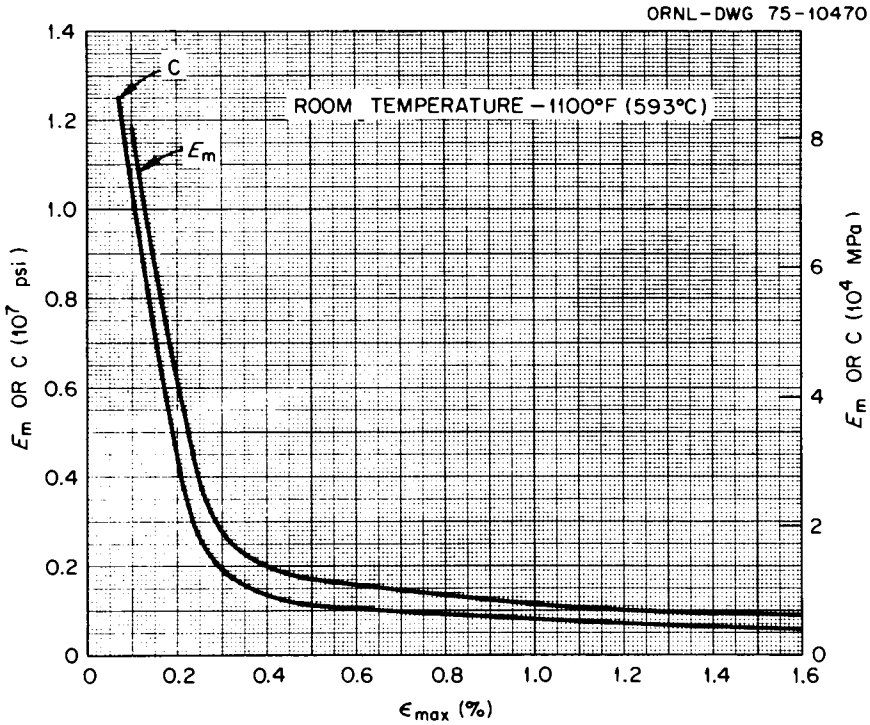


Fig. 3.49. Variation of Bilinear Cyclic Stress-Strain Parameters $C$ and $E_m$ with $\varepsilon_{max}$ for 2 1/4 Cr-1 Mo Steel.

short-time tests (<10 hr). Applying the same technique that led to the earlier model to a revised data set, which excluded tests rupturing in less than 10 hr, an equation was developed that was linear in the logarithm of stress. In this section we present the new model and discuss the data base. Then the limits of stress to cause rupture are compared with corresponding ASME Code Case 1592 minimum values. Also presented are two alternate models, which were developed from a data base that excluded Japanese tests performed at 600°C (1112°F).

3.4.4.1.1 Mathematical Description of Rupture Life. A mathematical description for the expected value of rupture life based on a data set that excluded tests rupturing in less than 10 hr, is given for annealed and isothermally annealed material:

$$\hat{t}_r = 10^{\log t_r} , \tag{29}$$

where

$\hat{t}_r \equiv$ expected value of rupture life (hr),

$$\log t_r = a_0 + a_1/T + a_2 \log \sigma + a_3 T \log \sigma \ , \tag{30}$$

where

$\log t_r$ = expected value of the common logarithm of rupture life,
$T$ = test temperature (K),
$\sigma$ = engineering stress (MPa),

and $a_0$, $a_1$, $a_2$, $a_3$ are unknown constants estimated by method of least squares from 563 observations. Parameter estimates are listed below with standard errors:

$$a_0 = -31.45 \pm 5.9 \ ,$$
$$a_1 = 3.932 \times 10^4 \pm 5.0 \times 10^3 \ ,$$
$$a_2 = -19.75 \pm 2.8 \ ,$$
$$a_3 = 1.642 \times 10^{-2} \pm 3.3 \times 10^{-3} \ .$$

Expected rupture lives are given in Table 3.14 at selected levels of stress and temperature. These values are shown graphically in Fig. 3.50 and with data at 538 and 593°C (1000 and 1100°F) in Fig. 3.51. The model predicts reasonable and consistent results within the following ranges of temperature, stress, and rupture life:

$$371°C\ (700°F) \leqslant T \leqslant 593°C\ (1100°F) \ ,$$
$$\sigma < 276\ \text{MPa}\ (40\ \text{ksi}) \ ,$$
$$t_r < 300{,}000\ \text{hr} \ .$$

It should be emphasized that the models presented in this section are empirical and that continued reliance on them or any other empirical model for extrapolated results without valid data in the extrapolated region cannot be justified.

Table 3.14. Expected Values of Rupture Life

| Temperature (°C) | Temperature (°F) | Expected Values and Lower Limits of Rupture Life,[a] hr, for Various Creep Stresses in MPa (ksi): 34 (5) | 69 (10) | 103 (15) | 138 (20) | 172 (25) | 207 (30) | 241 (35) | 276 (40) |
|---|---|---|---|---|---|---|---|---|---|
| 371 | 700 | | | | | | | | |
| 399 | 750 | | | | | | | (140,000) | (54,000) |
| 427 | 800 | | | | | (140,000) | (41,000) | 120,000 (14,000) | 38,000 (5,600) |
| 454 | 850 | | | | (77,000) | 140,000 (18,000) | 34,000 (5,300) | 10,000 (1,800) | 3,600 (700) |
| 482 | 900 | | | (73,000) | 78,000 (12,000) | 15,000 (2,800) | 3,900 (830) | 1,300 (280) | 480 (100) |
| 510 | 950 | | (150,000) | 76,000 (13,000) | 10,000 (2,100) | 2,200 (530) | 640 (160) | 220 (51) | 88 (19) |
| 538 | 1000 | | 160,000 (29,000) | 12,000 (2,700) | 1,900 (480) | 450 (120) | 140 (34) | 51 (12) | 22 (4.7) |
| 566 | 1050 | (300,000) | 28,000 (6,300) | 2,500 (650) | 440 (120) | 120 (29) | 39 (9.1) | 15 (3.4) | 7.0 (1.5) |
| 593 | 1100 | 280,000 (47,000) | 6,000 (1,400) | 640 (170) | 130 (31) | 38 (8.3) | 14 (2.8) | 5.9 (1.1) | 2.8 (0.5) |

[a]Rupture times exceeding 300,000 hr are omitted. This was the case for all values at 371°C (700°F).

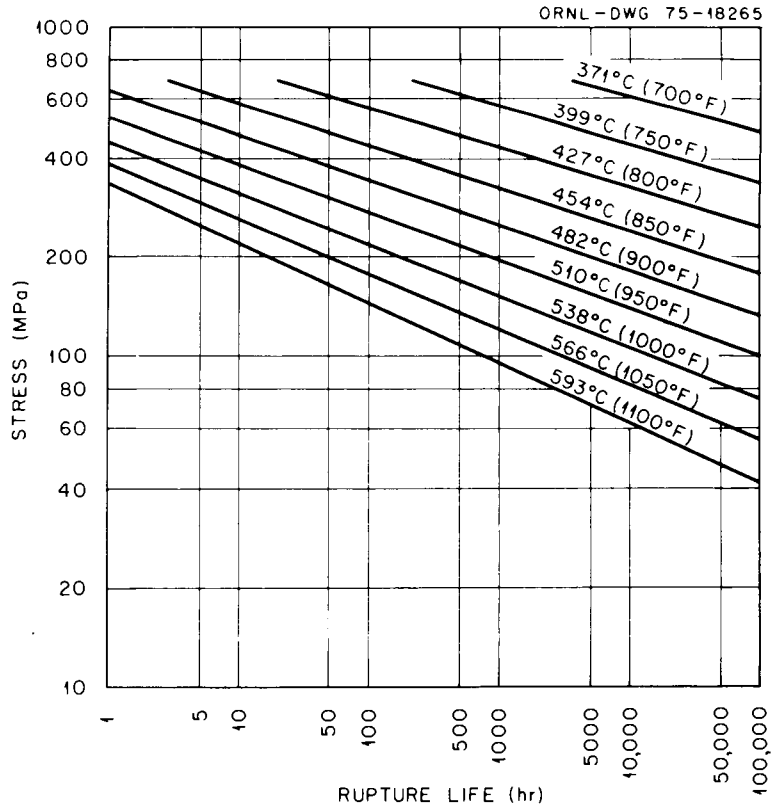


Fig. 3.50. Expected Value of Stress to Cause Rupture.

3.4.4.1.2 Expected Stress to Cause Rupture. The expected value of stress to cause rupture is defined to be

$$\hat{\sigma} = 10^{\log \sigma} ,$$

where

$$\log \sigma = (\log t_r - a_0 - a_1/T)/(a_2 + a_3 T) , \tag{31}$$

with remaining parameters being defined as for Eqs. (29) and (30). Equation (31) is obtained by solving Eq. (29) for stress. Expected stresses are given in Table 3.15.

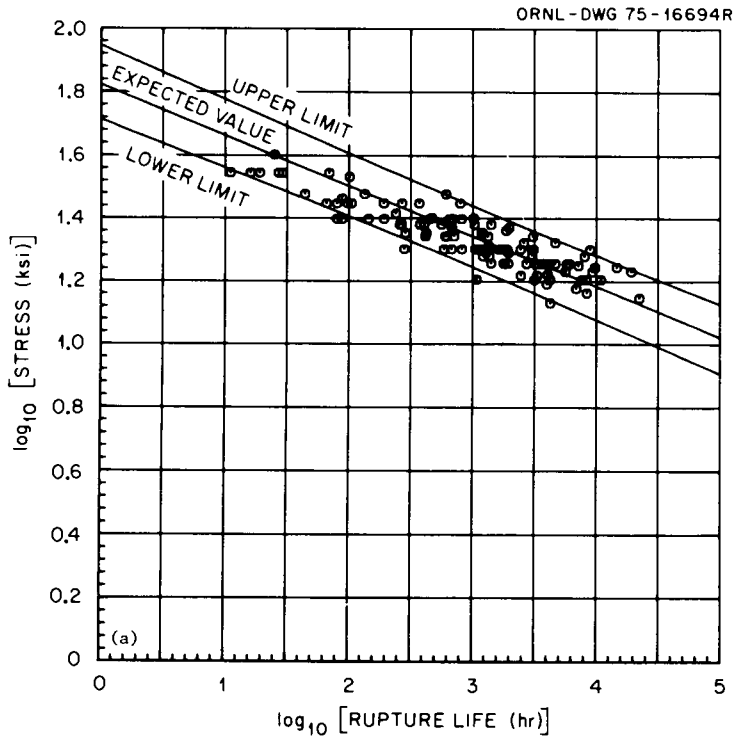


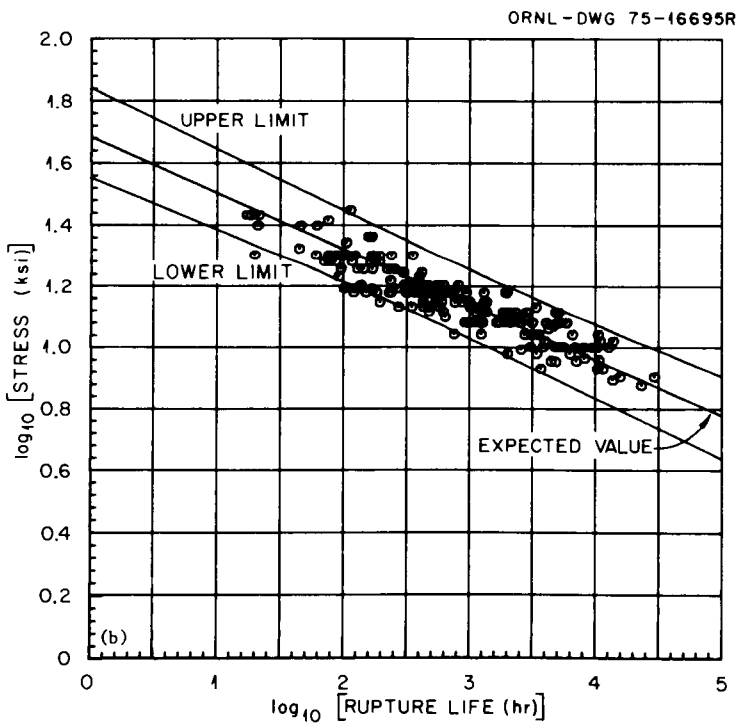


Fig. 3.51. Rupture Life of Annealed and Isothermally Annealed 2 1/4 Cr-1 Mo Steel. (a) 538°C (1000°F). (b) 593°C (1100°F).

Table 3.15. Expected Stress to Cause Rupture

| Temperature | | Stress, MPa [ksi], for each Rupture Life in hr | | | | | |
|---|---|---|---|---|---|---|---|
| (°C) | (°F) | 1000 | 3000 | 10,000 | 30,000 | 100,000 | 300,000 |
| 371 | 700 | 793[a] [115.0] | 703[a] [102.0] | 617[a] [89.5] | 547[a] [79.4] | 480[a] [69.6] | 425 [61.7] |
| 399 | 750 | 577[a] [83.7] | 509[a] [73.8] | 443 [64.2] | 391 [56.7] | 340 [49.3] | 300 [43.5] |
| 427 | 800 | 429 [62.2] | 376 [54.5] | 325 [47.1] | 284 [41.2] | 245 [35.6] | 215 [31.2] |
| 454 | 850 | 325 [47.1] | 282 [40.9] | 242 [35.1] | 210 [30.4] | 180 [26.1] | 156 [22.6] |
| 482 | 900 | 250 [36.2] | 215 [31.2] | 182 [26.4] | 157 [22.8] | 133 [19.3] | 115 [16.7] |
| 510 | 950 | 194 [28.1] | 165 [24.0] | 139 [20.1] | 119 [17.2] | 99 [14.4] | 85 [12.3] |
| 538 | 1000 | 152 [22.1] | 128 [18.6] | 106 [15.4] | 90 [13.0] | 74 [10.7] | 63 [9.1] |
| 566 | 1050 | 120 [17.4] | 100 [14.5] | 82 [11.9] | 68 [9.8] | 56 [8.1] | 46 [6.7] |
| 593 | 1100 | 95 [13.8] | 79 [11.4] | 63 [9.1] | 52 [7.5] | 42 [6.1] | 34 [4.9] |

[a]Exceeds expected value of ultimate tensile strength at temperature.

3.4.4.1.3 Data Base. Data are derived from 563 creep tests on annealed and isothermally annealed 2 1/4 Cr-1 Mo steel meeting the following restrictions:

carbon content: 0.07—0.15 wt %,

chromium content: 2.0—2.5 wt %,

molybdenum content: 0.9—1.1 wt %,

minimum room-temperature ultimate tensile strength: 414 MPa (60 ksi),

minimum room-temperature (0.2% offset) yield strength: 207 MPa (30 ksi).

Tests rupturing in less than 10 hr and tests performed on known aged or stress relieved material were excluded.

These data cover the following ranges of temperature, stress, and rupture life:

$$454°C\ (850°F) \leqslant T \leqslant 600°C\ (1112°F)\ ,$$

$$69\ MPa\ (10\ ksi) \leqslant \sigma \leqslant 448\ MPa\ (65\ ksi)\ ,$$

$$10\ hr \leqslant t_r \leqslant 50{,}200\ hr\ .$$

This coverage is not uniform over the above region since low stresses tended to be associated with high temperatures. In fact, the correlation between the independent variables, stress and temperature, is −0.75 whereas the correlation between the independent variable, log $\sigma$, and the dependent variable, log $t_r$, is −0.62.

These data are heavily weighted with short-time tests, as is seen in Fig. 3.52, which shows the distribution of tests over 1000-hr intervals. Further, it is seen that Japanese data are a substantial part of our longer time information. Although overall there are twice as many American tests as Japanese, at times greater than 11,000 hr there are twice as many Japanese tests as American.

3.4.4.1.4 Selection of Eq. (30). Equation (30) is considered the "best" linear combination of three terms (plus constant) as selected from terms in the following set of eight variables:
(1) $T$ = temperature, (2) $\sigma$ = stress, (3) $1/T$, (4) $\sigma T$, (5) $\sigma/T$, (6) log $\sigma$, (7) $(1/T)\log\sigma$, and (8) $T \log\sigma$.
Plots of the logarithm of rupture life against the logarithm of stress do not show the need for including higher degree terms in stress or log stress.

"Best" here is used in the sense of (1) ability to fit the data, (2) simplicity, and (3) behavior of the model in the extrapolated region. Ability to fit the data is measured by the coefficient of determination denoted $R^2$ (square of the multiple correlation coefficient):

$$R^2 = 1 - \mathrm{RSS/CTSS} ,$$

where

RSS = residual sum of squares,
CTSS = corrected total sum of squares.

Simplicity and model behavior are subjective criteria that must necessarily be based on metallurgical considerations.

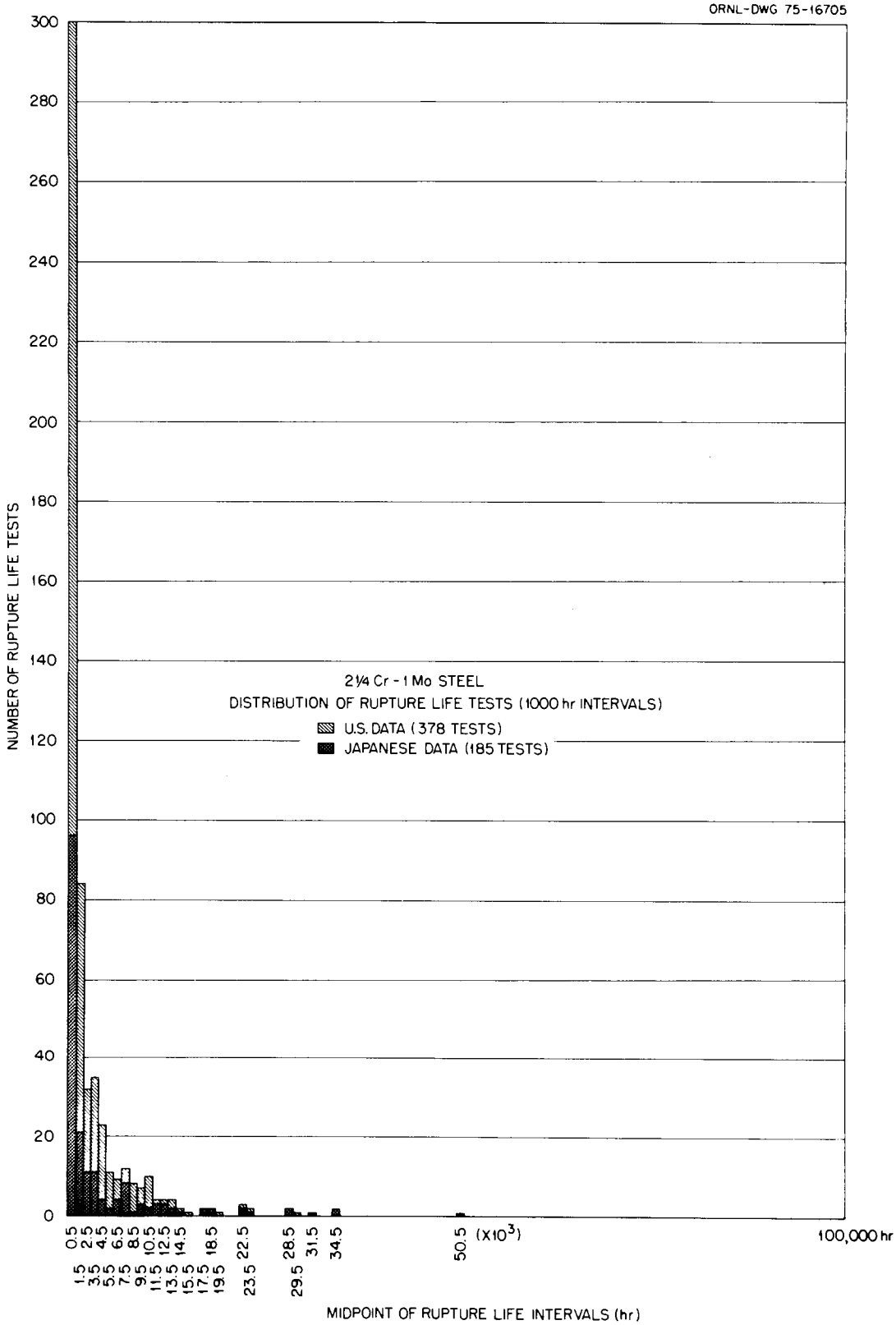


Fig. 3.52. Distribution of Rupture Life Tests for 2 1/4 Cr-1 Mo Steel.

3.4.4.1.5 Lower Limits. The lower limit of rupture life, denoted $L$, is based on the lower central tolerance ($P$ = 0.90, $\lambda$ = 0.95) about the expected value of log $t_r$ from Eq. (30).

Thus,

$$L = 10^{L*} , \tag{32}$$

where

$L*$ = log $t_r$ − $[\sqrt{11.24Z'VZ} + 0.548]$,

log $t_r$ = expected value of common logarithm of rupture life,

$t_r$ = rupture life (hr),

$V$ = variance-covariance matrix,

$$= \begin{bmatrix} 34.5515 & -2.91530 \times 10^4 & 16.2523 & -1.92718 \times 10^{-2} \\ -2.91530 \times 10^4 & 2.46380 \times 10^7 & -1.37269 \times 10^4 & 16.2501 \\ 16.2523 & -1.37269 \times 10^4 & 7.67066 & -9.08666 \times 10^{-3} \\ -1.92718 \times 10^{-2} & 16.2501 & -9.08666 \quad 10^{-3} & 1.07824 \times 10^{-5} \end{bmatrix} ,$$

$Z$ = vector representing point at which lower limit is sought ($Z'$ indicates transpose of $Z$),

= [1, $1/T$, log $\sigma$, $T$ log $\sigma$],

$T$ = test temperature (K),

$\sigma$ = engineering stress (MPa).

The tolerance statement means that at a confidence level of 0.95, 95% of all observed values are expected to fall above the lower limit. This limit is simultaneous in all levels of temperature and stress; that is, the limits may be calculated repeatedly for different levels of temperature and stress without affecting the level of confidence. The actual tolerance limit is based on the Bonferroni inequality and is discussed by Lieberman and Miller.[46] These limits are given in Table 3.14 and Fig. 3.53.

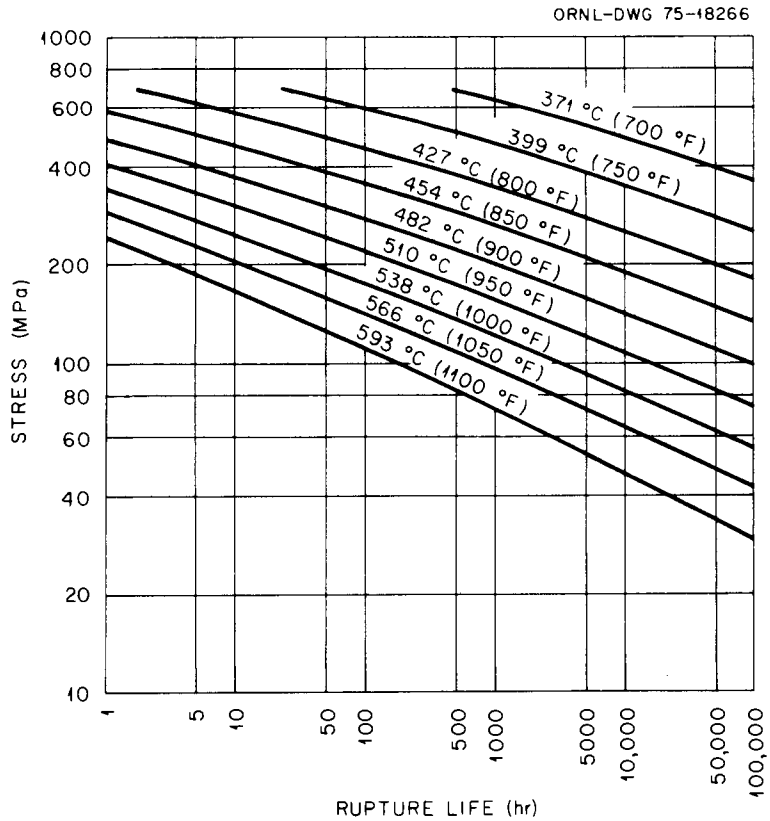


Fig. 3.53. Lower Limit of Stress to Cause Rupture.

3.4.4.1.6 Comparison of Results with ASME Code Case 1592. We define the lower limit to cause rupture to be that stress necessary for the lower limit of rupture life [from Eq. (32)] to equal a specified value. Table 3.16 and Fig. 3.54 compare these limits with ASME Code Case 1592 minimum stress values. In the lower stress and temperature region where no data exist, Code Case values tend to be less conservative.

3.4.4.1.7 Alternate Models on Reduced Data Base. The same procedures that led to Eq. (30) were applied to the subset of the 563 data base that excluded tests performed at temperatures above 600°C (1112°F). The excluded tests displayed curvature or a "break-downward" in plots of log $\sigma$ against log $t_r$ (see Fig. 3.55) while at lower temperatures the trend was linear. Although this curvature is considered real and is expected to occur at lower temperatures, such a "break" is not expected at temperatures below 510°C (950°F) until after 300,000 hr.

Table 3.16. Comparison of Lower Limits with ASME Code Case 1592 Minimum Values

| Rupture Life (hr) | Stress,[a] MPa [ksi], at each Temperature, °C(°F) | | | | | | | |
|---|---|---|---|---|---|---|---|---|
| | 427(800) | | 482(900) | | 538(1000) | | 593(1100) | |
| | A | B | A | B | A | B | A | B |
| 1,000 | 348 [50.4] | 296 [43.0] | 201 [29.2] | 193 [28.0] | 122 [17.7] | 123 [17.9] | 74 [10.7] | 74 [10.8] |
| 3,000 | 301 [43.6] | 259 [37.5] | 170 [24.7] | 172 [25.0] | 101 [14.7] | 105 [15.2] | 59 [8.6] | 63 [9.1] |
| 10,000 | 254 [36.8] | 238 [34.5] | 141 [20.5] | 149 [21.6] | 83 [12.0] | 90 [13.1] | 47 [6.8] | 52 [7.5] |
| 30,000 | 217 [31.4] | 210 [30.5] | 119 [17.2] | 131 [19.0] | 69 [10.0] | 76 [11.0] | 38 [5.5] | 43 [6.2] |
| 100,000 | 181 [26.3] | 186 [27.0] | 97 [14.3] | 113 [16.4] | 56 [8.1] | 65 [9.4] | 30 [4.3] | 34 [5.0] |
| 300,000 | 154 [22.3] | 165 [24.0] | 83 [12.0] | 97 [14.1] | 47 [6.8] | 54 [7.9] | 24 [3.5] | 28 [4.1] |

[a]A = lower limits from Eq. (32). B = ASME Code Case 1592 minimum values.

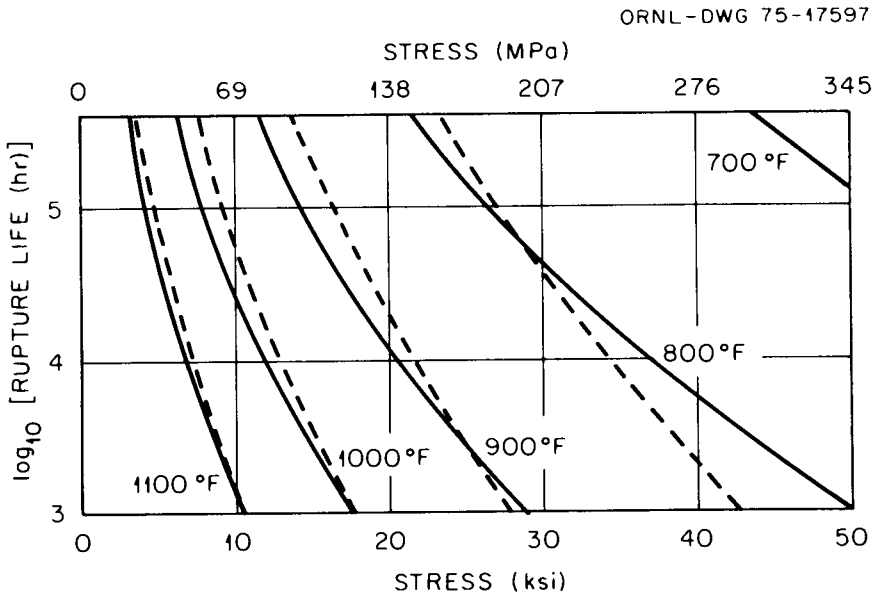


Fig. 3.54. Comparison of Lower Stress Limits (Solid Lines) with ASME Code Case 1592 Minimum Stress Values (Dashed Lines).

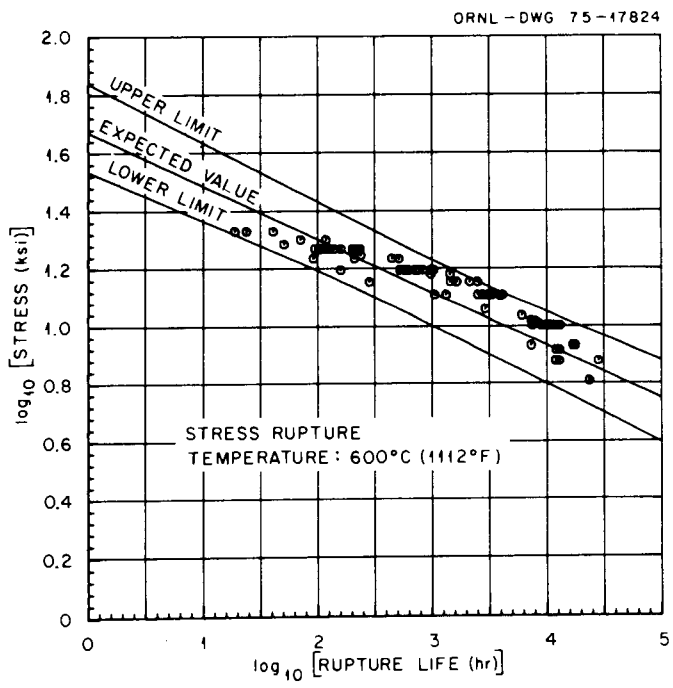


Fig. 3.55. Rupture Lives in 74 Tests of 2 1/4 Cr-1 Mo Steel Excluded from Data Base for Alternate Model.

The "best" linear model with three terms (plus constant) was of the same form as Eq. (30) but with different estimates for the coefficients.

$$\log t_r = \alpha_0 + \alpha_1 \, 1/T + \alpha_2 \log \sigma + \alpha_3 T \log \sigma \ , \tag{33}$$

where

$\log t_r$ = expected value of the logarithm of rupture life,
$T$ = temperature (K),
$\sigma$ = stress (MPa),

and $\alpha_0$, $\alpha_1$, $\alpha_2$, $\alpha_3$ are unknown constants estimated by the method of least squares from 489 observations. Parameter estimates are listed below with standard errors:

$$\alpha_0 = -42.19 \pm 6.4 \ ,$$
$$\alpha_1 = 4.807 \times 10^4 \pm 5.3 \times 10^3 \ ,$$
$$\alpha_2 = -24.45 \pm 3.0 \ ,$$
$$\alpha_3 = 2.218 \times 10^{-2} \pm 3.6 \times 10^{-3} \ .$$

A second alternate model based on the data base with 489 tests is the following form of the Larson-Miller[47] function:

$$\log t_r = \beta_0 + \beta_1/T + (\beta_2/T) \log \sigma \ , \tag{34}$$

where

$\log t_r$ = expected value of the logarithm of rupture life,
$\sigma$ = stress (MPa),
$T$ = temperature (K),

and $\beta_0$, $\beta_1$, $\beta_2$ are unknown constants estimated by the method of least squares. Parameter estimates are listed below with standard errors:

$$\beta_0 = -15.75 \pm 0.52 \ ,$$
$$\beta_1 = 2.597 \times 10^4 \pm 6.2 \times 10^2 \ ,$$
$$\beta_2 = -4.933 \times 10^3 \pm 1.0 \times 10^2 \ .$$

The Larson-Miller constant is equal to $|\beta_0|$. Expected values and lower tolerance limits of stress to cause rupture based on Eqs. (30), (33), and (34) are compared in Tables 3.17 and 3.18.

Table 3.17. Expected Value of Stress to Cause Rupture

| Rupture Life (hr) | Equation | Stress, MPa [ksi], at each Temperature, °C(°F) | | | |
|---|---|---|---|---|---|
| | | 427(800) | 482(900) | 538(1000) | 593(1100) |
| 1,000 | (30) | 429 [62.2] | 250 [36.2] | 152 [22.0] | 96 [13.9] |
| | (33) | 430 [62.3] | 250 [36.2] | 152 [22.0] | 92 [13.4] |
| | (34) | 403 [58.4] | 248 [36.0] | 152 [22.1] | 94 [13.6] |
| 10,000 | (30) | 325 [47.1] | 183 [26.2] | 106 [15.4] | 63 [9.1] |
| | (33) | 332 [48.1] | 185 [26.9] | 105 [15.3] | 60 [8.7] |
| | (34) | 290 [42.1] | 174 [25.3] | 104 [15.1] | 62 [9.0] |
| 100,000 | (30) | 245 [35.6] | 134 [19.4] | 74 [10.8] | 41 [5.9] |
| | (33) | 256 [37.1] | 137 [19.9] | 74 [10.8] | 39 [5.6] |
| | (34) | 210 [30.4] | 122 [17.7] | 72 [10.4] | 41 [6.0] |

Table 3.18. Lower Limit of Stress to Cause Rupture

| Rupture Life (hr) | Equation | Stress, MPa [ksi], at each Temperature, °C(°F) | | | |
|---|---|---|---|---|---|
| | | 427(800) | 482(900) | 538(1000) | 593(1100) |
| 1,000 | (30) | 348 [50.4] | 201 [29.2] | 122 [17.7] | 74 [10.7] |
| | (33) | 354 [51.4] | 205 [29.8] | 121 [17.6] | 70 [10.1] |
| | (34) | 314 [45.6] | 195 [28.3] | 121 [17.5] | 72 [10.5] |
| 10,000 | (30) | 254 [36.8] | 141 [20.5] | 83 [12.0] | 47 [6.8] |
| | (33) | 265 [38.5] | 146 [21.2] | 83 [12.1] | 43 [6.2] |
| | (34) | 225 [32.6] | 135 [19.6] | 81 [11.8] | 48 [6.9] |
| 100,000 | (30) | 181 [26.3] | 97 [14.3] | 56 [8.1] | 30 [4.3] |
| | (33) | 195 [28.3] | 103 [15.0] | 57 [8.2] | 26 [3.8] |
| | (34) | 161 [23.3] | 94 [13.6] | 54 [7.8] | 31 [4.5] |

3.4.4.2 Minimum Creep Rate — T. L. Hebble* and R. L. Klueh

Two models for describing minimum creep rate of annealed and isothermally annealed 2 1/4 Cr-1 Mo steel are given: the proposed model for the *Nuclear Systems Materials Handbook* and an alternate model based on a power law frequently used in describing such data.

A new feature is that both models include room-temperature ultimate tensile strength, denoted $\tau$. Stratification of test results due to $\tau$ occurs when considering the higher tensile strength data from tests on normalized-and-tempered and quenched-and-tempered material. Although not as readily apparent in the relatively narrow range of tensile strength for annealed material, this effect of $\tau$ is accounted for in the models. A numerical indication of its importance is shown by comparing the coefficient of determination, $R^2$, with and without $\tau$. For the alternate model described below, $R^2$ is 74.5% with $\tau$ and 66.6% without $\tau$. A more intuitively satisfying approach would be to consider ultimate tensile strength at temperature; however, sufficient tensile strength information over temperature for individual heats is not available.

The proposed model for calculating minimum creep rate is given by:

$$\hat{\dot{\varepsilon}}_m = 10^{\log \dot{\varepsilon}_m} , \tag{35}$$

where

$\hat{\dot{\varepsilon}}_m$ = expected value of minimum creep rate (%/hr),

$$\log \dot{\varepsilon}_m = \text{common logarithm of minimum creep rate} = a_0 + \tau[a_1 + a_2 T + a_3 \log \sigma], \tag{36}$$

$T$ = test temperature (K),

$\sigma$ = stress (MPa),

$\tau$ = room-temperature ultimate tensile strength (MPa),

and $a_0$, $a_1$, $a_2$, and $a_3$ are constants. Least squares estimates of these constants based on 131 observations are listed below with standard errors:

---

*Mathematics and Statistics Research Department.

$$a_0 = 1.909 \pm 0.72 \ ,$$
$$a_1 = -9.700 \times 10^{-2} \pm 5.2 \times 10^{-3} \ ,$$
$$a_2 = 6.978 \times 10^{-5} \pm 3.9 \times 10^{-6} \ ,$$
$$a_3 = 1.459 \times 10^{-2} \pm 7.6 \times 10^{-4} \ .$$

The alternate model for calculating expected values of minimum creep rate is given next:

$$\hat{\dot{\varepsilon}}_m = 10^{\log \dot{\varepsilon}_m} \ , \tag{37}$$

where

$$\log \dot{\varepsilon}_m = b_0 + b_1/T + (b_2/\tau)\log \sigma + b_3\tau \log \sigma \ , \tag{38}$$

and $b_0$, $b_2$, $b_2$, and $b_3$ are unknown constants. Least squares estimates of these constants are listed below with standard errors:

$$b_0 = 10.56 \pm 1.1 \ ,$$
$$b_1 = -2.380 \times 10^4 \pm 1.4 \times 10^3 \ ,$$
$$b_2 = 2.284 \times 10^3 \pm 1.5 \times 10^2 \ ,$$
$$b_3 = 5.393 \times 10^{-3} \pm 4.4 \times 10^{-4} \ .$$

Equation (37) may be rewritten in more familiar notation as

$$\dot{\varepsilon}_m = K\sigma^{n(\tau)}e^{-Q/RT} \ , \tag{39}$$

where

$$\begin{aligned} K &= 2.303 \times 10^{b_0} \\ &= 8.362 \times 10^{10}, \\ n(\tau) &= (b_2 + b_3\tau^2)/\tau, \\ Q &= \text{activation energy} = 455 \text{ kJ/mole} = 108.9 \text{ kcal/mole}, \\ R &= \text{gas constant} = 8.314 \text{ J mole}^{-1} \text{ K}^{-1} = 1.987 \text{ cal mole}^{-1} \text{ K}^{-1}, \end{aligned} \tag{40}$$

and $b_0$, $b_2$, $b_3$, $\varepsilon_m$, $\sigma$, $\tau$, and $T$ are defined already. The exponent of stress in Eq. (39), normally considered a constant, decreases with increasing room-temperature ultimate tensile strength:

| $\tau$ MPa (ksi) | $n(\tau)$ |
|---|---|
| 490 (70) | 7.34 |
| 517 (75) | 7.21 |
| 552 (80) | 7.12 |
| 586 (85) | 7.06 |

Since $n(\tau)$ reaches a minimum of 7.02 when $\tau \approx 650$ MPa (94 ksi), use of the model beyond $\tau = 650$ MPa is not recommended. This should not present any problems since the upper ($P = 0.90$, $\lambda = 0.95$) tolerance limit of tensile strength at room temperature for annealed material is 612 MPa (89 ksi).

Equation (37) is based on a fit of the model to a particular set of data combined with the notion of a constant activation energy and a decreasing $n(\tau)$ with increasing $\tau$. Another form for $n(\tau)$, such as

$$n^*(\tau) = \alpha/\tau + \beta ,$$

where $\alpha$ and $\beta$ are constants estimated from the data, may be more acceptable (if $\beta > 0$) since it preserves the same graphical shape as Eq. (40) but eliminates the minimum. Instead $n^*(\tau)$ approaches a constant $\beta$ as $\tau$ increases without limit.

Figures 3.56 and 3.57 show contours of constant temperature at two levels of $\tau$ for each model. In the lower stress region Eq. (38) is seen to generate substantially less conservative results than Eq. (36).

### 3.4.4.3 Uniform Elongation — T. L. Hebble*

A third-degree polynomial is used to predict uniform elongation over a temperature range of 20 to 600°C (68—1112°F) for annealed and

---

*Mathematics and Statistics Research Department.

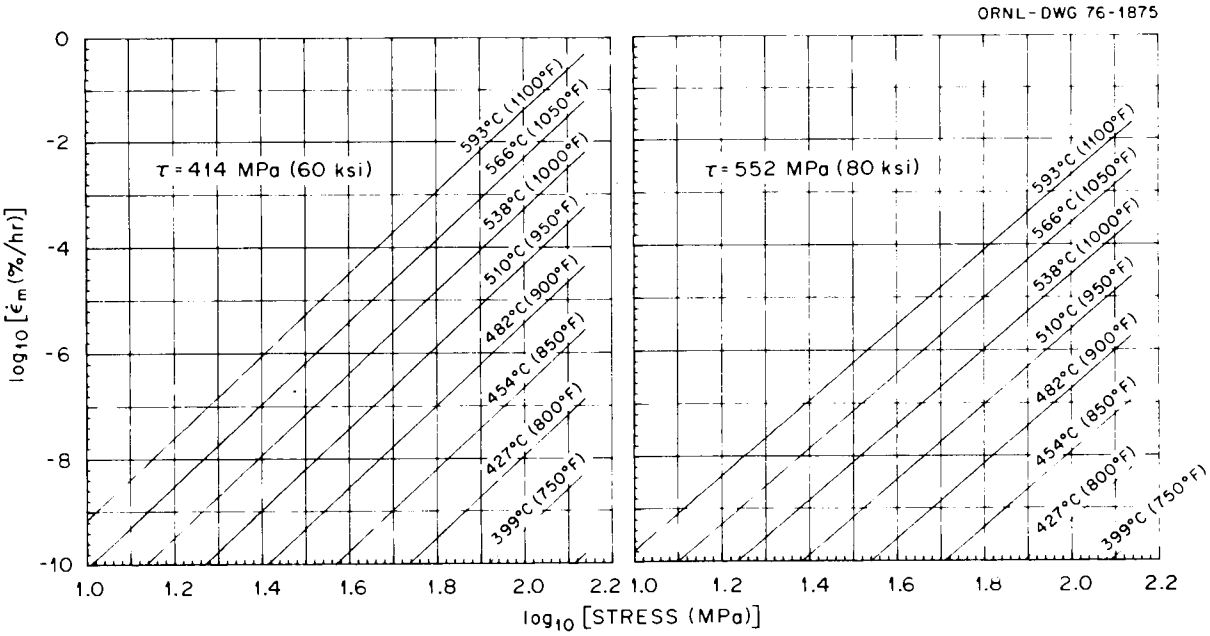


Fig. 3.56. Expected Values of Minimum Creep Rate from the Proposed Model.

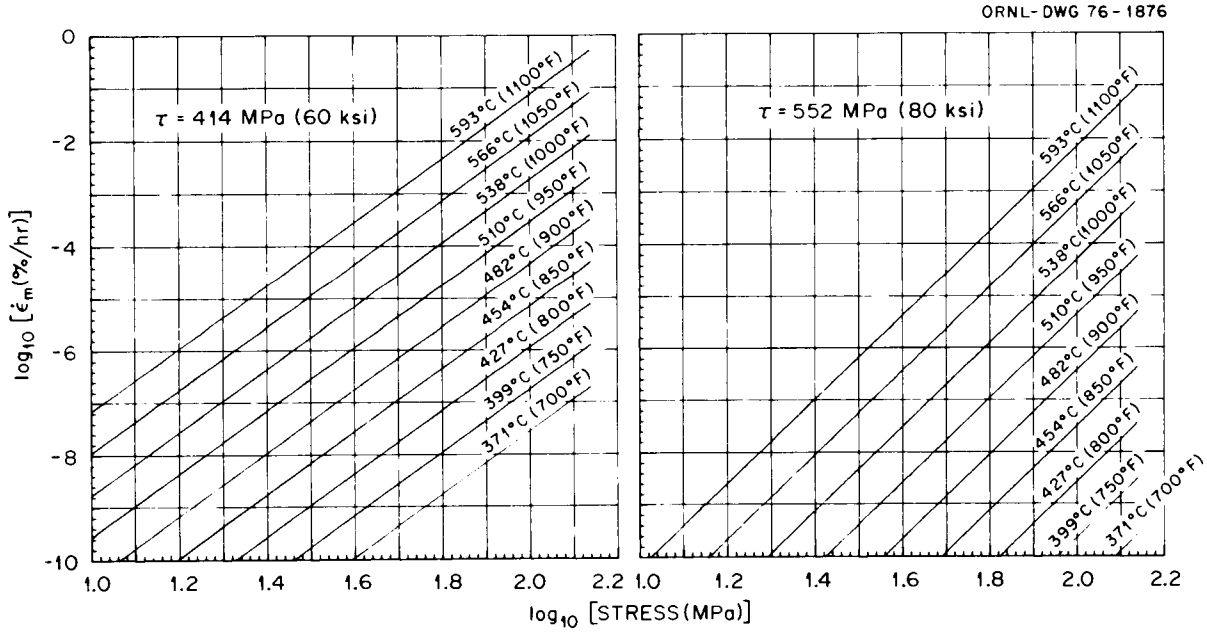


Fig. 3.57. Expected Values of Minimum Creep Rate from Alternate Model.

isothermally annealed 2 1/4 Cr-1 Mo steel in the form of tube or pipe and plate. Thus,

$$\widehat{UE} = b_0 + b_1 T + b_2 T^2 + b_3 T^3 ,$$

where

$\widehat{UE}$ = expected value of uniform elongation (%),

$T$ = test temperature (°C),

$b_0$, $b_1$, $b_2$, $b_3$ = unknown constants; estimates are listed below with standard errors:

$b_0 = 14 \pm 0.4$ ,

$b_1 = -4.8 \times 10^{-2} \pm 0.7 \times 10^{-2}$ ,

$b_2 = 1.74 \times 10^{-4} \pm 0.30 \times 10^{-4}$ ,

$b_3 = -1.94 \times 10^{-7} \pm 0.31 \times 10^{-7}$ .

Unknown constants were estimated by method of least squares from 234 observations. The small coefficient of determination ($R^2 = 0.535$) reflects a large variability in the data.

Klueh and Oakes[35] indicated that strain rate has relatively little effect on uniform elongation. They stated that a noticeable change did occur in the low-strain-rate ($2.7 \times 10^{-6}$/sec) high-temperature ($\geqslant$ 510°C) region, where uniform elongation decreases with strain rate.

Table 3.19 lists expected values of uniform elongation with corresponding ($P = 0.90$, $\lambda = 0.95$) tolerance limits.

3.4.4.4 Diamond Pyramid Hardness — T. L. Hebble* and M. K. Booker

The regression of room-temperature ultimate tensile strength on diamond pyramid hardness is used to predict tensile strength since both variables are subject to error and exhibit a high correlation ($r = 0.98$) between them:

$$\hat{\tau} = 40.9 + 3.12H ,$$

*Mathematics and Statistics Research Department.

Table 3.19. Expected Values and Tolerance Limits of Uniform Elongation of 2 1/4 Cr-1 Mo Steel

| Temperature | | Uniform Elongation, % | | |
|---|---|---|---|---|
| (°C) | (°F) | Lower Limit | Expected Value | Upper Limit |
| 25 | 77 | 9 | 13 | 17 |
| 50 | 122 | 8 | 12 | 16 |
| 100 | 212 | 7 | 11 | 15 |
| 150 | 302 | 6 | 10 | 15 |
| 200 | 392 | 5 | 10 | 14 |
| 250 | 482 | 6 | 10 | 14 |
| 300 | 572 | 6 | 10 | 14 |
| 350 | 662 | 6 | 10 | 14 |
| 400 | 752 | 6 | 10 | 14 |
| 450 | 842 | 6 | 10 | 14 |
| 500 | 932 | 5 | 9 | 13 |
| 550 | 1022 | 4 | 8 | 12 |
| 600 | 1112 | 1 | 6 | 10 |

where

$\hat{\tau}$ = expected (predicted) value of room-temperature ultimate tensile strength (MPa),

$H$ = diamond pyramid hardness number (at temperature).

Calculated values of $\hat{\tau}$ at various levels of $H$ are listed in Table 3.20.

3.4.4.5 Time to Tertiary Creep — M. K. Booker

Based on the data described herein, the time to the onset of tertiary creep, $t_3$, for annealed and isothermally annealed 2 1/4 Cr-1 Mo steel has been expressed as a function of stress and temperature. Both mean and lower limit values are included. This correlation has been established first by determining rupture life, $t_r$, as a function of

Table 3.20. Correlation of Hardness with Room-Temperature Ultimate Tensile Strength for 2 1/4 Cr-1 Mo Steel

| $H$, Hardness (DPH) | $\hat{\tau}$, Expected Room-Temperature Ultimate Tensile Strength | |
|---|---|---|
| | (MPa) | (ksi) |
| 125 | 431 | 62.5 |
| 150 | 509 | 73.8 |
| 175 | 587 | 85.1 |
| 200 | 665 | 96.4 |
| 225 | 743 | 107.7 |
| 250 | 821 | 119.1 |
| 275 | 899 | 130.4 |
| 300 | 977 | 141.7 |
| 325 | 1055 | 153.3 |
| 350 | 1133 | 164.3 |

stress and temperature, then by relating[48] $t_3$ and $t_r$ by $t_3 = At_r^{\beta}$. The quantity $t_3$ can be a useful design limit in itself, but it also serves as an upper limit in time on the applicability of the creep equation for this material.[19]

The number and distribution of available data are such that direct statistical analysis of time to the onset of tertiary creep, $t_3$, as a function of stress ($\sigma$) and temperature ($T$) is difficult. First, the data exhibit a large amount of scatter. Second, the data are available over a fairly narrow range of $\sigma$, $T$, and $t_3$. Figure 3.58 illustrates problems encountered with a typical analytical model.[45] This figure shows available data at 538°C (1000°F) with a mean best-fit line and upper and lower central tolerance limits[46] ($P = 0.90$, $\lambda = 0.95$). Clearly, the data can be fitted reasonably well, but the amount of uncertainty is so great as to force considerable "flaring" of the tolerance limits at long time. Because of this flaring, we feel that such tolerance limits, while statistically correct based on available data, do not yield physically realistic lower limit values.

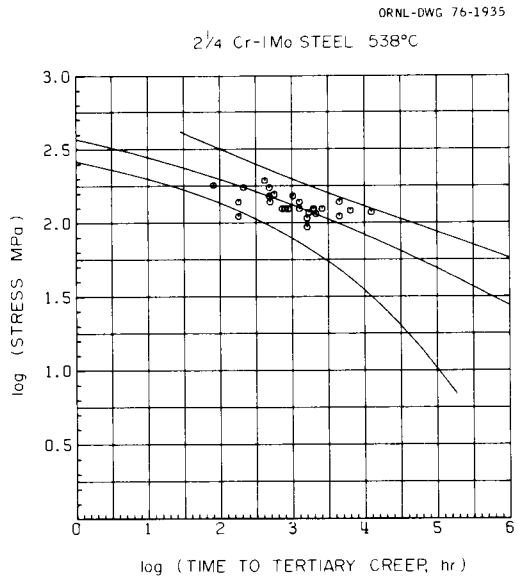


Fig. 3.58. Results Obtained by Direct Analysis of Time to Tertiary Creep as a Function of Stress and Temperature for 2 1/4 Cr-1 Mo Steel. Shown here are experimental data, a best fit line, and upper and lower tolerance limits at 538°C (1000°F). Note the extremely conservative lower limit.

To avoid the above problem we took an approach suggested elsewhere.[48] This approach allows consideration of available rupture life data in developing an expression for $t_3$. Such consideration is desirable, since many more rupture data, over a larger range of conditions, were available. Indeed, $t_r$ may be expressed successfully as a function of $\sigma$ and $T$ by

$$\log t_r = -31.45 + 3.932 \times 10^4/T - 19.75 \log \sigma + 0.01642T \log \sigma \ , \quad (41)$$

where

$T$ = temperature, K;

$\sigma$ = stress, MPa;

$t_r$ = rupture life, hr.

Details of this relationship may be found in Sect. 3.4.4.1.1 of this report. It should be noted that this relationship predicts linear log $\sigma$ vs log $t_r$ isothermals at all temperatures. However, some indications of long-term curvature are seen in these isothermals at temperatures above 566°C

(1050°F). Therefore, Eq. (41) must be used with some caution at these temperatures.

With $t_r = F(\sigma, T)$ established, $t_3$ was then expressed as $G(t_r)$, so that $t_3 = G[F(\sigma, T)] = H(\sigma, T)$. This was done by

$$t_3 = 0.28 t_r^{1.07} . \tag{42}$$

The fit of Eq. (42) to the available data is shown in Fig. 3.59, where it appears to be excellent. Included in this figure are upper and lower tolerance limits ($P = 0.90$, $\lambda = 0.95$). The linear correlation coefficent (in log $t_3$ vs log $t_r$) for this relationship was 0.98. The combination of Eqs. (41) and (42) yields a prediction for the mean value of $t_3$ as a function of $\sigma$ and $T$.

To calculate a lower limit for $t_3$, one must account for the variability in both Eqs. (41) and (42). A conservative way to do this is simply to determine a value $t_r'$ from the lower tolerance limit on Eq. (41) and to insert this value as the independent variable in Eq. (42). The lower limit time to the onset of tertiary creep, $t_3'$, is then given by the lower tolerance limit on Eq. (42) at this value. This approach

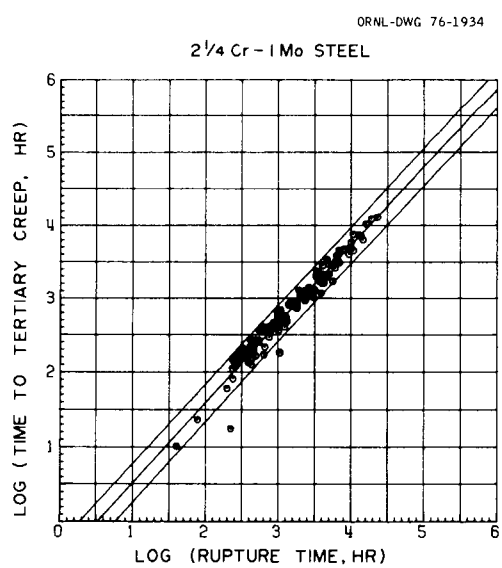


Fig. 3.59. Relationship Between Rupture Life, $t_r$, and Time to Tertiary Creep, $t_3$, for 2 1/4 Cr-1 Mo Steel From 454 to 593°C (850–1100°F). Mean line given by $t_3 = 0.28 t_r^{1.07}$; also included are upper and lower tolerance limits ($P = 0.90$, $\lambda = 0.95$).

was used to calculate the current lower limit values, although it should be noted that these resultant values are *not* lower tolerance limits in themselves, but should be conservative. Figure 3.60 compares predicted mean and lower limit values with actual data. Availability of more data in the future may change the current conclusions; for instance, direct analysis may become possible. At present, however, it is felt that the approach taken here is the best available. It should also be noted that these lower limits are not necessarily intended as definitions of "minimum" values per ASME Code Case 1592.

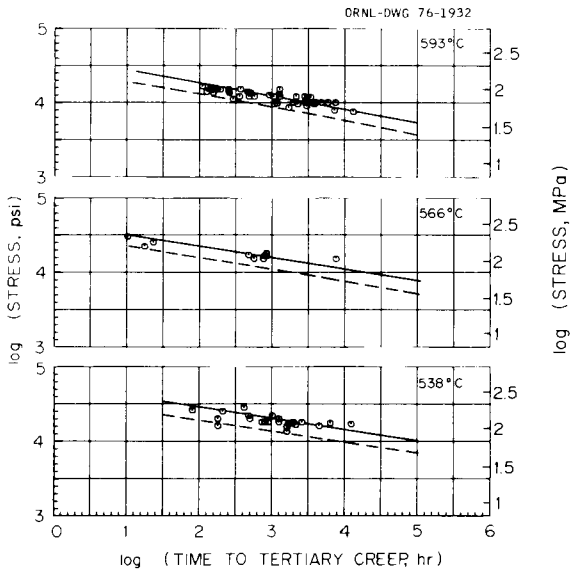


Fig. 3.60. Variation of Time to Tertiary Creep with Stress at Various Temperatures for 2 1/4 Cr-1 Mo Steel. Points are experimental data. Solid line indicates prediction from $t_3 = 0.28 t_r^{1.07}$, where $t_r = -31.45 + 3.932 \times 10^4/T - 19.75 \log \sigma + 0.01642T \log \sigma$. Dashed line is predicted lower limit.

Also, as shown in Figs. 3.61 and 3.62, predicted values for stress to cause onset of tertiary creep in a given time can fall above the ultimate tensile strength at temperatures not exceeding 427°C (800°F). This event is not physically reasonable but is a result of extrapolation of the data to lower temperatures than those for which data are available.

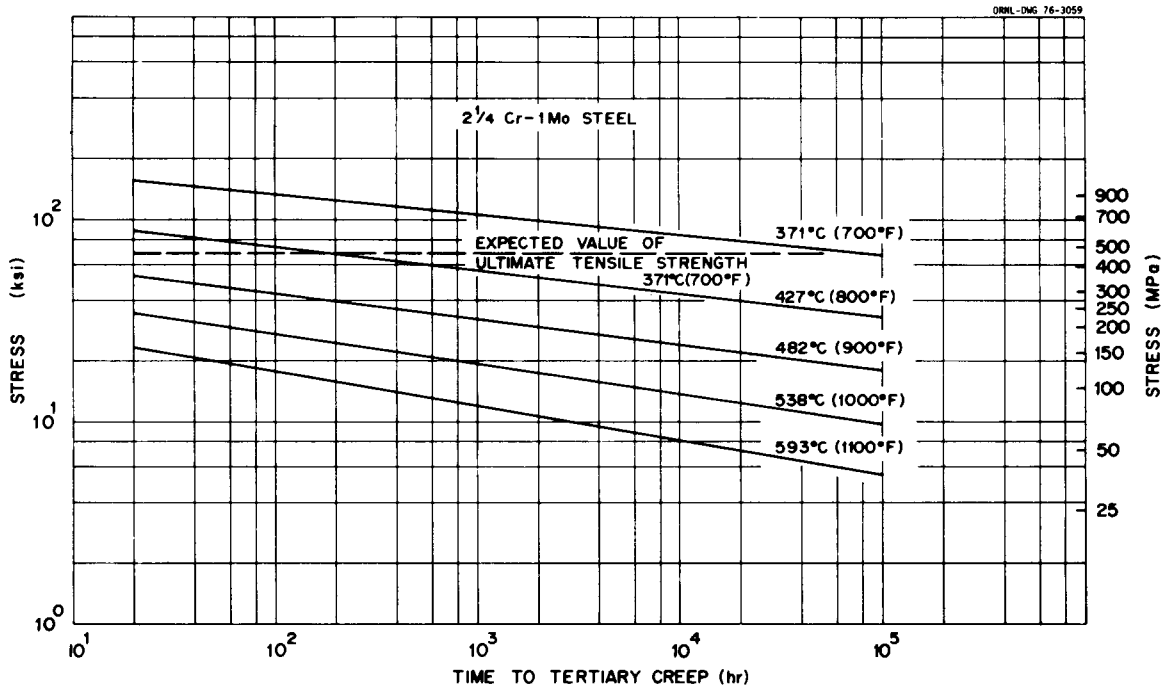


Fig. 3.61. Isothermals of Predicted Time to Tertiary Creep as a Function of Stress for 2 1/4 Cr-1 Mo Steel, Calculated from Eqs. (41) and (42).

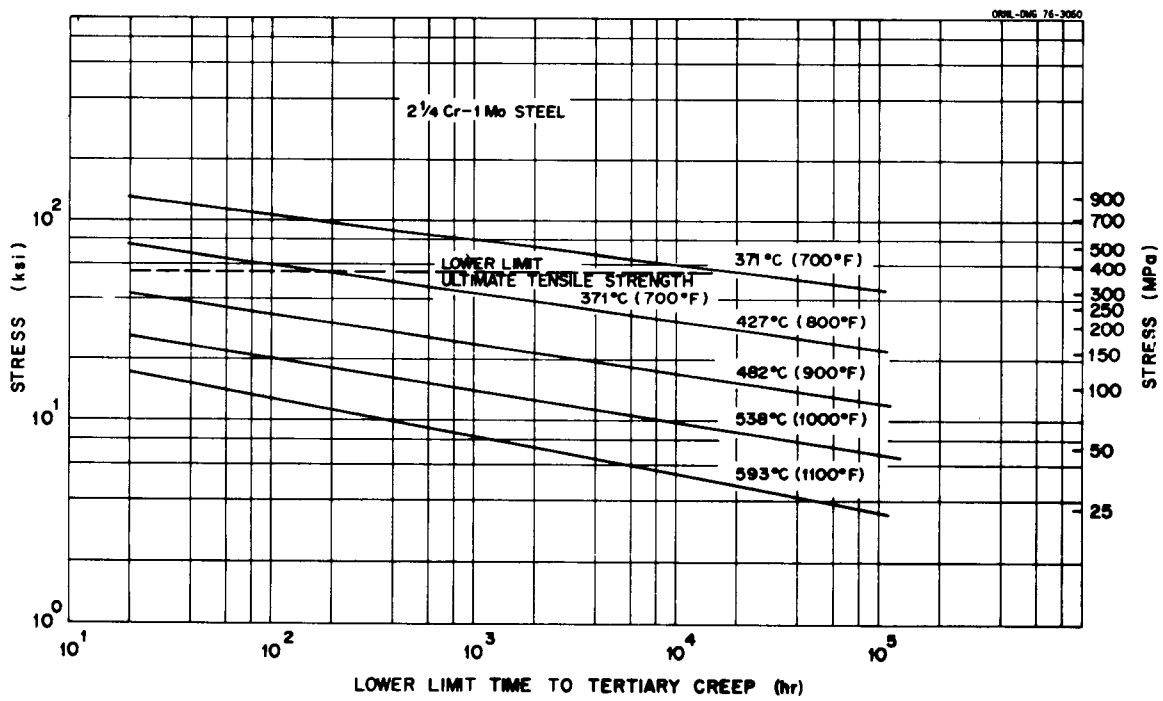


Fig. 3.62. Isothermals of Predicted Lower Limits on Time to Tertiary Creep as a Function of Stress for 2 1/4 Cr-1 Mo Steel, Predicted from Lower Tolerance Limits ($P$ = 0.90, $\lambda$ = 0.95) on Eqs. (41) and (42).

### 3.4.5 Elastic Constants in Weldment Structures — J. P. Hammond

Dynamic (sonic) elastic constants ($E$, $G$, and $\nu$) were determined at room temperature (RT) on three samples of Inconel 82 filler metal [two as weld deposits and one wrought (Inconel 606*)] and one type 16-8-2 stainless steel weld deposit. Dynamic moduli of the Inconel 606 and type 16-8-2 stainless weld deposit also were determined from 24 to 732°C (75—1350°F). The results of tests are presented below.

#### 3.4.5.1 Dynamic Elastic Constants of Weld Deposits

Descriptive information on the weldment samples examined is listed below:

Sample 21SR-1, Inconel 82

Weldment of eight passes by gas tungsten-arc (GTA) process; Incoloy 800 to 2 1/4 Cr-1 Mo steel butt joint in 13-mm-thick (1/2-in.) plate; V-groove of 90° included angle with zero root opening.

Sample 21SR-2, Inconel 82

Weldment of 17 passes by GTA process; Incoloy 800 to Incoloy 800 butt joint in 13-mm-thick (1/2-in.) plate; V-groove of 100° included angle with 0.8-mm (1/32-in.) root opening.

Sample 21W, Inconel 606

Wrought rod 6.4 mm (1/4 in.) in diameter.

Sample 22SR, type 16-8-2 stainless steel

Multipass weldment by GTA process; passes laid down on 6.4-mm-thick (1/4-in.) backing plate of Incoloy 800.

---

*Inconel 82 filler metal in structural forms is designated Inconel 606 by International Nickel Company.

All samples except Inconel 606 were stress relieved for 1 hr at 732°C (1350°F), the treatment generally prescribed for weldments in these alloys; this is indicated by "SR" in the sample numbers.

The acoustic data for determining elastic constants were acquired on wires 2.5 mm (0.1 in.) diam by 75 to 130 mm (3–5 in.) long by the transit-time method employing sound of 0.2 MHz frequency introduced with a magnetostrictive transducer. The wires were taken from the welds with their axes parallel to the weld direction, except of course for the Inconel 606 alloy, where it was parallel to the rod axis. Methods of determining sonic elastic constants appropriate to isotropic materials were used. The relationships for determining constants from sound velocities are given in the *Nondestructive Testing Handbook*.[49] Our procedures for treating the elastic constant statistically for obtaining estimates of the individual properties as functions of temperature were previously reported.[50] Generally the elastic constant data consisted of 52 or more data points. These were fitted with cubic polynomials by regression analysis. The equations are of a form that normalizes elevated-temperature data to the more accurate room-temperature values. However, in the present case, the room-temperature values do not have the usual high accuracy (0.7%), since they were established on wires instead of on the customary block samples.[50]

The elastic constants at RT established for the foregoing materials, along with the sonic data, are given in Table 3.21. Observe that the Poisson's ratios of the Inconel 82 weld deposits (Samples 21SR-1 and 21SR-2) are unrealistic, whereas Poisson's ratio of Inconel 606 [the wrought form of Inconel 82 (Sample 21W)] is reasonable.* The abnormally low values exhibited by these weldment samples indicate that the materials are anisotropic and the method used for obtaining their elastic properties is inappropriate. Whereas the Poisson's ratio for the type 16-8-2 stainless steel weld deposit (0.2888) is not greatly out of line, a test conducted on a type 308 stainless steel deposit

---

*Metals are expected to have Poisson's ratios in the region from 0.25 to somewhat below 0.50, the value rapidly approached on going from solid to the liquid state.

Table 3.21. Elastic Constants and Sound Velocities of Weldment Alloys at Room Temperature

| Property | Value for Each Test Material[a] | | | |
|---|---|---|---|---|
| | Inconel 82 21 SR-1 | Inconel 82 21 SR-2 | Inconel 606 21 W | 16-8-2 22 SR |
| $\nu$, Poisson's Ratio | 0.1840 ± 0.0154 | 0.1146 ± 0.0041 | 0.3462 ± 0.0030 | 0.2888 ± 0.0243 |
| $E$, Young's modulus | | | | |
| GPa | 213.8 ± 2.6 | 188.5 ± 0.15 | 214.3 ± 0.42 | 191.5 ± 3.0 |
| $10^6$ psi | 31.01 ± 0.37 | 27.34 ±0.02 | 31.09 ± 0.06 | 27.77 ± 0.43 |
| $G$, shear modulus | | | | |
| GPa | 90.30 ± 0.46 | 84.57 ± 0.31 | 79.60 ± 0.08 | 74.28 ± 0.80 |
| $10^6$ psi | 13.10 ± 0.07 | 12.27 ± 0.04 | 11.54 ± 0.01 | 10.77 ± 0.12 |
| $B$, bulk modulus | | | | |
| GPa | 112.8 ± 5.7 | 81.52 ± 0.88 | 232.27 ± 4.51 | 151.16 ± 17.54 |
| $10^6$ psi | 16.36 ± 0.82 | 11.82 ± 0.13 | 33.69 ± 0.65 | 21.92 ± 2.54 |
| Longitudinal velocity | | | | |
| m/sec | 5301.5 ± 95.0 | 4839.0 ± 11.5 | 6386.6 ± 80.4 | 5675.0 ± 354.7 |
| in./sec | 208721.4 ± 3740.1 | 190512.9 ± 452.9 | 251441.4 ± 3166.3 | 223424.2 ± 13964.4 |
| Shear velocity, | | | | |
| m/sec | 3299.2 ± 8.4 | 3192.6 ± 5.8 | 3097.6 ± 1.6 | 3092.2 ± 16.5 |
| in./sec | 129888.3 ± 329.3 | 125694.4 ± 227.4 | 121951.1 ± 62.6 | 121739.7 ± 651.6 |
| Extensional velocity | | | | |
| m/sec | 5076.8 ± 30.5 | 4766.7 ± 1.9 | 5082.6 ± 5.0 | 4964.6 ± 38.5 |
| in./sec | 199875.2 ± 1199.6 | 187666.6 ± 73.5 | 200104.3 ± 195.0 | 195457.1 ± 1514.9 |
| Density, g/cm$^3$ | 8.2965 ± 0.0004 | 8.2965 ± 0.0005 | 8.2965 ± 0.0005 | 7.7690 ± 0.0005 |

[a]Tolerance shown is standard deviation.

gave a value of −0.18, which is all the more unreasonable. Significantly, the Young's and shear moduli obtained for the Inconel 606 were close to those listed in an International Nickel Company catalogue for Inconel 600, which has the composition falling nearest Inconel 82 of those for which data was available.

A recent study by Kikuchi[51] on elastic anisotropy in single crystals of type 305 stainless steel (18% Cr, 12% Ni) showed extraordinarily large differences in elastic constants with crystallographic direction, a feature not uncommon to high-elasticity alloys of the fcc crystal structure.[52] Kikuchi[51] found an elastic anisotropy (defined as $E_{\langle 111 \rangle}/E_{\langle 100 \rangle}$) of 3.09 at RT, increasing to about 3.61 as temperature was increased to 500°C (932°F). Table 3.22 compares his values of the Young's and shear moduli in the three principal crystallographic directions with values for polycrystalline metal.

The large degree of elastic anisotropy cited above for alloys of the fcc crystal structure emphasizes the importance of employing

Table 3.22. Anistropy of Young's and Shear Moduli of Type 305 Stainless Steel

| Direction | *E*, Young's Modulus | | *G*, Shear Modulus | |
|---|---|---|---|---|
| | (GPa) | (psi) | (GPa) | (psi) |
| ⟨111⟩ | 313.8 | $45.51 \times 10^6$ | 48.6 | $7.05 \times 10^6$ |
| ⟨100⟩ | 101.4 | 14.71 | 138.6 | 20.10 |
| ⟨110⟩ | 205.9 | 29.86 | 58.1 | 8.42 |
| Polycrystal | 170.8 | 24.77 | 65.7 | 9.53 |

anisotropic methods when analyzing elastic properties in composite structure of such unique grain structure as the present weld deposits. A commendable beginning in this direction is the recent work of Dewey and King,[53] who endeavored to establish elastic constants in a weld deposit of type 308 stainless steel. (See also Sect. 3.3.2 of this report). However, they prepared their weld deposit by electroslag welding to give unidirectional solidification and thereby simplified the analysis of elastic coefficients. In principle, their weld deposit amounted to a single pass weld.

The weld deposit samples examined in the present work were anisotropic but far more unsymmetrical than the foregoing electroslag weld. Consequently, any valid method for determining elastic constants in the present welds would be much more intricate. Until suitable methods are devised, it would appear profitable to employ the elastic constants we established for the Inconel 82 filler metal in wrought form (Inconel 606) for interim studies of transitional joints. This is reasonable since the individual elastic constants ($E$, $G$, and $\nu$) of isotropic polycrystals in fcc alloys generally are intermediate in value to the highest and lowest of those represented by the principal crystallographic directions in their anisotropic single crystals.

The polynomial equations for the elastic constants we derived from the combined room- and elevated-temperature sonic data on the Inconel 606 alloy and type 16-8-2 stainless steel weld deposit samples (Samples 21W and 22SR) are given below:

$$x = x_0[1 + A_x(T - T_0) + B_x(T - T_0)^2 + C_x(T - T_0)^3] ,$$

where

$x$ = the property ($E$, $G$, or $\nu$),
$x_0$ = same at 24°C,
$T$ = temperature in °C,
$T_0$ = 24°C, and
$A_x$, $B_x$, and $C_x$ = constants.

Coefficients of the equations for the respective properties with the standard deviation of fit of data points are given in Table 3.23. The elastic constants from 24 to 732°C (75–1350°F) determined with the polynomials for the Inconel 606 alloy and type 16-8-2 stainless steel weld deposit are presented in Table 3.24 and 3.25, respectively.

3.4.5.2 Future Work — L. Adler* and J. P. Hammond

As a second step in the investigation of elastic constants in weldments, a multipass weld in Inconel 82 filler metal of the following description was prepared for elastic analysis by sonic methods that assume anisotropy.

Weld Geometry: "V" groove of 30° included angle with 32-mm (1 1/4-in.) root opening in 25-mm-thick (1-in.) plate of Incoloy 800.

Weld Parameters: Forty-seven passes by cold-wire, GTA processes; 1850 J/m (47,000 J/in.) power input; 0.85 mm/sec (2 in./min) travel speed; 21 mm/sec (50 in./min) rate of metal wire [1.1 mm (0.045 in.) diam] feed.

---

*Consultant from the University of Tennessee.

Table 3.23. Coefficients of Polynomials for Representing Elastic Constants of Inconel 606 and Type 16-8-2 Stainless Steel Weld Deposit

| Property | $x_0$ (GPa) | $x_0$ (psi) | $A_x$ (°C$^{-1}$) | $B_x$ (°C$^{-2}$) | $C_x$ (°C$^{-3}$) | Standard Deviation of Fit (GPa) | Standard Deviation of Fit (psi) |
|---|---|---|---|---|---|---|---|
| | | | | Inconel 606 | | | |
| $E$ | 214.2 | $31.09 \times 10^6$ | $-2.53523 \times 10^{-4}$ | $-5.80418 \times 10^{-8}$ | $-3.24092 \times 10^{-11}$ | 0.83 | $1.20 \times 10^5$ |
| $G$ | 79.6 | $11.55 \times 10^6$ | $-3.25918 \times 10^{-4}$ | $5.45774 \times 10^{-8}$ | $-6.69584 \times 10^{-11}$ | 0.46 | $6.7 \times 10^4$ |
| $\nu$ | 0.2462 | | $2.82884 \times 10^{-4}$ | $-3.58322 \times 10^{-7}$ | $4.18511 \times 10^{-11}$ | $7.0 \times 10^{-6}$ | |
| | | | | Type 16-8-2 Stainless Steel Weld Deposit | | | |
| $E$ | 191.5 | $27.77 \times 10^6$ | $-2.72504 \times 10^{-4}$ | $-3.50320 \times 10^{-7}$ | $2.58895 \times 10^{-10}$ | 0.97 | $1.41 \times 10^5$ |
| $G$ | 74.3 | $10.77 \times 10^6$ | $-2.68043 \times 10^{-4}$ | $-6.48569 \times 10^{-7}$ | $6.48934 \times 10^{-10}$ | 0.45 | $6.5 \times 10^4$ |
| $\nu$ | 0.2889 | | $-9.28133 \times 10^{-5}$ | $1.86679 \times 10^{-6}$ | $-2.29872 \times 10^{-9}$ | $5.7 \times 10^{-4}$ | |

Table 3.24. Elastic Constants of Inconel 606 as a Function of Temperature

| Temperature | | Young's Modulus | | Shear Modulus | | Poisson's Ratio |
|---|---|---|---|---|---|---|
| (°C) | (°F) | (GPa) | (psi) | (GPa) | (psi) | |
| 24 | 75 | 214.3 | $31.09 \times 10^6$ | 79.63 | $11.55 \times 10^6$ | 0.346 |
| 38 | 100 | 213.6 | 30.98 | 79.29 | 11.50 | 0.347 |
| 52 | 125 | 212.8 | 30.87 | 78.94 | 11.45 | 0.349 |
| 66 | 150 | 212.2 | 30.78 | 78.53 | 11.39 | 0.350 |
| 79 | 175 | 211.3 | 30.65 | 78.19 | 11.34 | 0.351 |
| 93 | 200 | 210.8 | 30.54 | 77.84 | 11.29 | 0.352 |
| 107 | 225 | 209.7 | 30.42 | 77.50 | 11.24 | 0.353 |
| 121 | 250 | 209.0 | 30.31 | 77.15 | 11.19 | 0.354 |
| 135 | 275 | 208.2 | 30.20 | 76.81 | 11.14 | 0.355 |
| 149 | 300 | 207.4 | 30.08 | 76.46 | 11.09 | 0.356 |
| 163 | 325 | 206.6 | 29.96 | 76.12 | 11.04 | 0.357 |
| 177 | 350 | 205.8 | 29.85 | 75.77 | 10.99 | 0.358 |
| 191 | 375 | 205.0 | 29.73 | 75.43 | 10.94 | 0.359 |
| 204 | 400 | 204.2 | 29.61 | 75.08 | 10.89 | 0.360 |
| 218 | 425 | 203.3 | 29.49 | 74.74 | 10.84 | 0.361 |
| 232 | 450 | 202.5 | 29.37 | 74.39 | 10.79 | 0.361 |
| 246 | 475 | 201.6 | 29.24 | 74.05 | 10.74 | 0.362 |
| 260 | 500 | 200.8 | 29.12 | 73.70 | 10.69 | 0.363 |
| 274 | 525 | 199.9 | 29.00 | 73.36 | 10.64 | 0.363 |
| 288 | 550 | 199.1 | 28.87 | 73.01 | 10.59 | 0.364 |
| 302 | 575 | 198.2 | 28.75 | 72.67 | 10.54 | 0.364 |
| 316 | 600 | 197.3 | 28.62 | 72.33 | 10.49 | 0.365 |
| 329 | 625 | 196.4 | 28.49 | 71.98 | 10.44 | 0.365 |
| 343 | 650 | 195.5 | 28.36 | 71.63 | 10.39 | 0.365 |
| 357 | 675 | 194.6 | 28.23 | 71.29 | 10.34 | 0.366 |
| 371 | 700 | 193.7 | 28.10 | 70.95 | 10.29 | 0.366 |
| 385 | 725 | 192.8 | 27.97 | 70.60 | 10.24 | 0.366 |
| 399 | 750 | 191.9 | 27.83 | 70.26 | 10.19 | 0.366 |
| 413 | 775 | 191.0 | 27.70 | 69.91 | 10.14 | 0.366 |
| 427 | 800 | 190.0 | 27.56 | 69.57 | 10.09 | 0.366 |
| 441 | 825 | 189.1 | 27.43 | 69.22 | 10.04 | 0.367 |
| 454 | 850 | 188.2 | 27.29 | 68.81 | 9.98 | 0.367 |
| 468 | 875 | 187.2 | 27.15 | 68.46 | 9.93 | 0.367 |
| 482 | 900 | 186.2 | 27.01 | 68.12 | 9.88 | 0.366 |
| 496 | 925 | 185.3 | 26.87 | 67.77 | 9.83 | 0.366 |
| 510 | 950 | 184.2 | 26.72 | 67.43 | 9.78 | 0.366 |
| 524 | 975 | 183.3 | 26.58 | 67.09 | 9.73 | 0.366 |
| 538 | 1000 | 182.4 | 26.43 | 66.74 | 9.68 | 0.366 |
| 552 | 1025 | 181.3 | 26.29 | 66.40 | 9.63 | 0.365 |
| 566 | 1050 | 180.2 | 26.14 | 65.98 | 9.57 | 0.365 |
| 579 | 1075 | 179.2 | 25.99 | 65.64 | 9.52 | 0.365 |
| 593 | 1100 | 178.2 | 25.84 | 65.29 | 9.47 | 0.364 |
| 607 | 1125 | 177.1 | 25.69 | 64.95 | 9.42 | 0.364 |
| 621 | 1150 | 176.0 | 25.53 | 64.53 | 9.36 | 0.364 |
| 635 | 1175 | 175.0 | 25.38 | 64.19 | 9.31 | 0.363 |
| 649 | 1200 | 173.9 | 25.22 | 63.84 | 9.26 | 0.363 |
| 663 | 1225 | 172.8 | 25.06 | 63.43 | 9.20 | 0.362 |
| 677 | 1250 | 171.7 | 24.90 | 63.09 | 9.15 | 0.361 |
| 691 | 1275 | 170.6 | 24.74 | 62.67 | 9.09 | 0.361 |
| 704 | 1300 | 169.5 | 24.58 | 62.33 | 9.04 | 0.360 |
| 718 | 1325 | 168.4 | 24.42 | 61.91 | 8.98 | 0.359 |
| 732 | 1350 | 167.2 | 24.25 | 61.57 | 8.93 | 0.359 |

Table 3.25. Elastic Constants of Type 16-8-2 Weld Deposit as a Function of Temperature

| Temperature | | Young's Modulus | | Shear Modulus | | Poisson's Ratio |
|---|---|---|---|---|---|---|
| (°C) | (°F) | (GPa) | (psi) | (GPa) | (psi) | |
| 24 | 75 | 191.5 | $27.78 \times 10^6$ | 74.32 | $10.78 \times 10^6$ | 0.289 |
| 38 | 100 | 190.8 | 27.67 | 74.05 | 10.74 | 0.289 |
| 52 | 125 | 190.0 | 27.56 | 73.70 | 10.69 | 0.289 |
| 66 | 150 | 189.2 | 27.45 | 73.43 | 10.65 | 0.289 |
| 79 | 175 | 188.4 | 27.33 | 73.08 | 10.60 | 0.290 |
| 93 | 200 | 187.6 | 27.21 | 72.74 | 10.55 | 0.290 |
| 107 | 225 | 186.8 | 27.09 | 72.33 | 10.49 | 0.291 |
| 121 | 250 | 185.9 | 26.96 | 71.98 | 10.44 | 0.292 |
| 135 | 275 | 185.0 | 26.83 | 71.57 | 10.38 | 0.292 |
| 149 | 300 | 184.1 | 26.70 | 71.15 | 10.32 | 0.293 |
| 163 | 325 | 183.1 | 26.58 | 70.74 | 10.26 | 0.294 |
| 177 | 350 | 182.2 | 26.43 | 70.33 | 10.20 | 0.295 |
| 191 | 375 | 181.3 | 26.29 | 69.91 | 10.14 | 0.297 |
| 204 | 400 | 180.2 | 26.14 | 69.43 | 10.07 | 0.298 |
| 218 | 425 | 179.3 | 26.00 | 69.02 | 10.01 | 0.299 |
| 232 | 450 | 178.2 | 25.85 | 68.53 | 9.94 | 0.301 |
| 246 | 475 | 177.2 | 25.70 | 68.05 | 9.87 | 0.302 |
| 260 | 500 | 176.2 | 25.55 | 67.57 | 9.80 | 0.304 |
| 274 | 525 | 175.1 | 25.40 | 67.09 | 9.73 | 0.305 |
| 288 | 550 | 174.0 | 25.24 | 66.60 | 9.66 | 0.307 |
| 302 | 575 | 173.0 | 25.09 | 66.12 | 9.59 | 0.308 |
| 316 | 600 | 171.9 | 24.93 | 65.64 | 9.52 | 0.310 |
| 329 | 625 | 170.8 | 24.77 | 65.09 | 9.44 | 0.311 |
| 343 | 650 | 169.7 | 24.61 | 64.60 | 9.37 | 0.313 |
| 357 | 675 | 168.6 | 24.45 | 64.12 | 9.30 | 0.314 |
| 371 | 700 | 167.5 | 24.29 | 63.64 | 9.23 | 0.316 |
| 385 | 725 | 166.3 | 24.12 | 63.09 | 9.15 | 0.317 |
| 399 | 750 | 165.2 | 23.96 | 62.60 | 9.08 | 0.319 |
| 413 | 775 | 164.0 | 23.79 | 62.12 | 9.01 | 0.320 |
| 427 | 800 | 162.9 | 23.63 | 61.64 | 8.94 | 0.322 |
| 441 | 825 | 161.8 | 23.46 | 61.16 | 8.87 | 0.323 |
| 454 | 850 | 160.6 | 23.30 | 60.67 | 8.80 | 0.324 |
| 468 | 875 | 159.5 | 23.13 | 60.19 | 8.73 | 0.325 |
| 482 | 900 | 158.4 | 22.97 | 59.71 | 8.66 | 0.326 |
| 496 | 925 | 157.2 | 22.80 | 59.23 | 8.59 | 0.327 |
| 510 | 950 | 156.0 | 22.63 | 58.81 | 8.53 | 0.327 |
| 524 | 975 | 154.9 | 22.47 | 58.33 | 8.46 | 0.328 |
| 538 | 1000 | 153.8 | 22.30 | 57.92 | 8.40 | 0.328 |
| 552 | 1025 | 152.6 | 22.14 | 57.50 | 8.34 | 0.328 |
| 566 | 1050 | 151.5 | 21.97 | 57.09 | 8.28 | 0.328 |
| 579 | 1075 | 150.4 | 21.81 | 56.67 | 8.22 | 0.327 |
| 593 | 1100 | 149.3 | 21.65 | 56.26 | 8.16 | 0.327 |
| 607 | 1125 | 148.2 | 21.49 | 55.85 | 8.10 | 0.326 |
| 621 | 1150 | 147.1 | 21.33 | 55.50 | 8.05 | 0.325 |
| 635 | 1175 | 146.0 | 21.17 | 55.16 | 8.00 | 0.323 |
| 649 | 1200 | 144.9 | 21.01 | 54.81 | 7.95 | 0.321 |
| 663 | 1225 | 143.8 | 20.85 | 54.47 | 7.90 | 0.319 |
| 677 | 1250 | 142.7 | 20.70 | 54.19 | 7.86 | 0.317 |
| 691 | 1275 | 141.3 | 20.55 | 53.92 | 7.82 | 0.314 |
| 704 | 1300 | 140.6 | 20.39 | 53.64 | 7.78 | 0.311 |
| 718 | 1325 | 139.5 | 20.24 | 53.36 | 7.74 | 0.307 |
| 732 | 1350 | 138.6 | 20.10 | 53.16 | 7.71 | 0.303 |

The solidification characteristics of the weld are shown in Fig. 3.63. This weld deposit has a structure similar to one understood to be under consideration by General Electric for making pipe-to-pipe joints of 2 1/4 Cr-1 Mo steel to Incoloy 800.

Early sonic tests on the weld structure will be designed to determine whether it can be analyzed by measurements that assume orthotropic symmetry and whether a heterogeneous specimen taken from any given region corresponds to that of another. Ultrasonic measurement techniques will be used to determine the longitudinal and transverse sound velocities in different directions of preferred crystallographic orientation. From the ultrasonic data, the elastic stiffness coefficients as well as the anisotropy will be determined. Subsequently the maximum and minimum values of the elastic constants ($E$, $G$, and $\nu$) in principal directions will be determined for engineering application.

Fig. 3.63. Macrostructure of 47-Pass Weld Made with Inconel 82 Filler Metal in Incoloy 800 Plate. Macrograph is normal to weld direction. Etched with equal parts $HCl$-$HNO_3$-$H_2SO_4$. 3.25×.

### 3.4.6 Mechanical Properties of a Weld-Overlaid Stainless Steel Forging — R. L. Klueh

We have completed our creep-rupture studies[54—58] on a type 304 stainless steel forging that was weld overlaid with type 308 stainless steel weld metal, and a report is being prepared.[59] A summary of that work follows.

Creep and rupture tests were made on specimens taken from a cylindrical forging of type 304 stainless steel weld overlaid by the submerged-arc process with six layers of type 308 stainless steel filler metal. Properties were determined at three locations: weld metal, forging adjacent to the fusion line, and forging farther than 50 mm (2 in.) from the fusion line (unaffected by the overlay process). Specimens of three different orientations (relative to the forging cylinder) were tested at 482, 538, and 593°C (900, 1000, and 1100°F).

The following observations and conclusions were made.

1. At all temperatures, creep-rupture strength of the forging just below the fusion line was slightly greater than that of the forging at a distance from the fusion line. Both types of base metal specimens were considerably stronger than the weld metal.

2. The rupture strengths of the weld metal tangential specimens were slightly greater than those of the radial specimens, though the properties of the two different orientations approached each other as the rupture stress was decreased. This difference was attributed to the inhomogeneous structure in the weld metal developed as a result of the overlay process. The type 304 stainless steel specimens showed no orientation effect.

3. The total elongation and reduction of area of the type 308 stainless steel weld metal at 538 and 593°C (1000 and 1100°F) decreased with increasing rupture life (decreasing stress). At 593°C, the ductility of the type 304 stainless steel specimens went through a minimum at a rupture life of approximately 1500 hr; at 538°C the ductility of the type 304 stainless steel continuously decreased with increasing rupture life.

4. The strength advantage of the type 304 stainless steel immediately adjacent to the fusion line was explained in terms of the stresses

generated in the overlay process by the shrinkage of the weld metal during solidification.

5. With two exceptions, the axial composite specimens that contained both type 308 stainless steel filler metal and type 304 stainless steel forging in the gage section failed in the weld metal. In two instances, however, failure started at the fusion line at defects introduced during the forging process.

## 3.5 HIGH-TEMPERATURE DESIGN — J. M. Corum* and C. E. Pugh*

### 3.5.1 Exploratory Studies in Support of Structural Design Methods — R. W. Swindeman

The objectives of these studies are (1) to perform exploratory uniaxial tests to identify basic inelastic high-temperature material behavior for constitutive equation development, (2) to provide characterization data needed as input into inelastic analyses of structural tests, (3) to provide limited information as needed in support of subcontracted activities, (4) to provide limited data from reference heats of materials in connection with failure criteria, and (5) to identify materials properties data for high-temperature design. The materials considered include a reference heat of type 304 stainless steel (9T2796) and a reference heat of type 316 stainless steel (8092297). Other alloys of interest for Liquid Metal Fast Breeder Reactor (LMFBR) components, such as 2 1/4 Cr-1 Mo steel, are being studied. Experiments are separated into studies of time-independent plasticity, time-dependent creep, and creep-plasticity interaction, with both monotonic and cyclic loadings included in each category. Data collected thus far have contributed to the establishment of interim constitutive equations for certain alloys, to the analyses of the simple structure tests that have been performed, to the characterization of the relative behavior of various product forms, and to various subcontractor and design-code-related activities.

---

*Reactor Division.

### 3.5.1.1 Exploratory Testing of Type 304 Stainless Steel to Identify Behavior Features

Constant-load creep and rupture testing of the reference heat of type 304 stainless steel has been completed, and current activities are concerned with the influence of history on the flow strength and ductility. As part of this effort we are examining hardening and recovery processes in creep. A group of variable-load creep-rupture experiments is being performed to supplement data produced by Babcock and Wilcox[60] at 593°C (1100°F). One series of tests involves cycling between two stress levels, with the minimum level being about 10% of the maximum. The wave shape is trapezoidal, and cycling periods range from $2 \times 10^{-3}$ to 336 hr. Creep curves, representing only the time under maximum stress, are plotted in log-log coordinates in Fig. 3.64 for the 336-hr cycle period. Generally, we find that the creep curves are not greatly influenced by recovery periods, although the plastic flow stress in some cases drops below the level of the maximum stress.

With respect to creep-rupture life, we have accumulated data showing the influence of several different histories, including both different thermomechanical treatments and prior creep exposures. These data are summarized by the composite Fig. 3.65. Generally, we find that

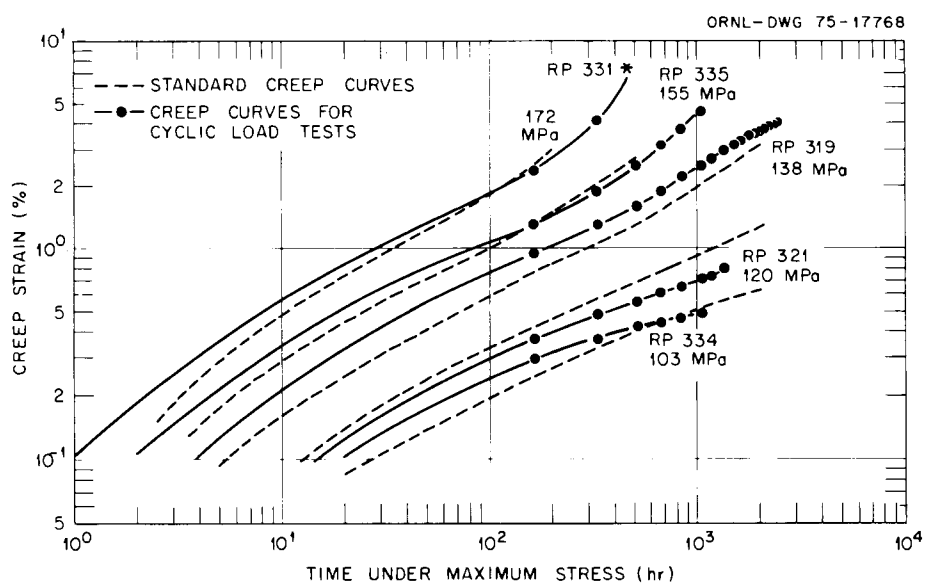


Fig. 3.64. Comparison of Standard Creep Curves for Type 304 Stainless Steel (Heat 9T2796) with Curves Obtained by Load Cycling with a 336-hr Cycling Period at 593°C (1100°F).

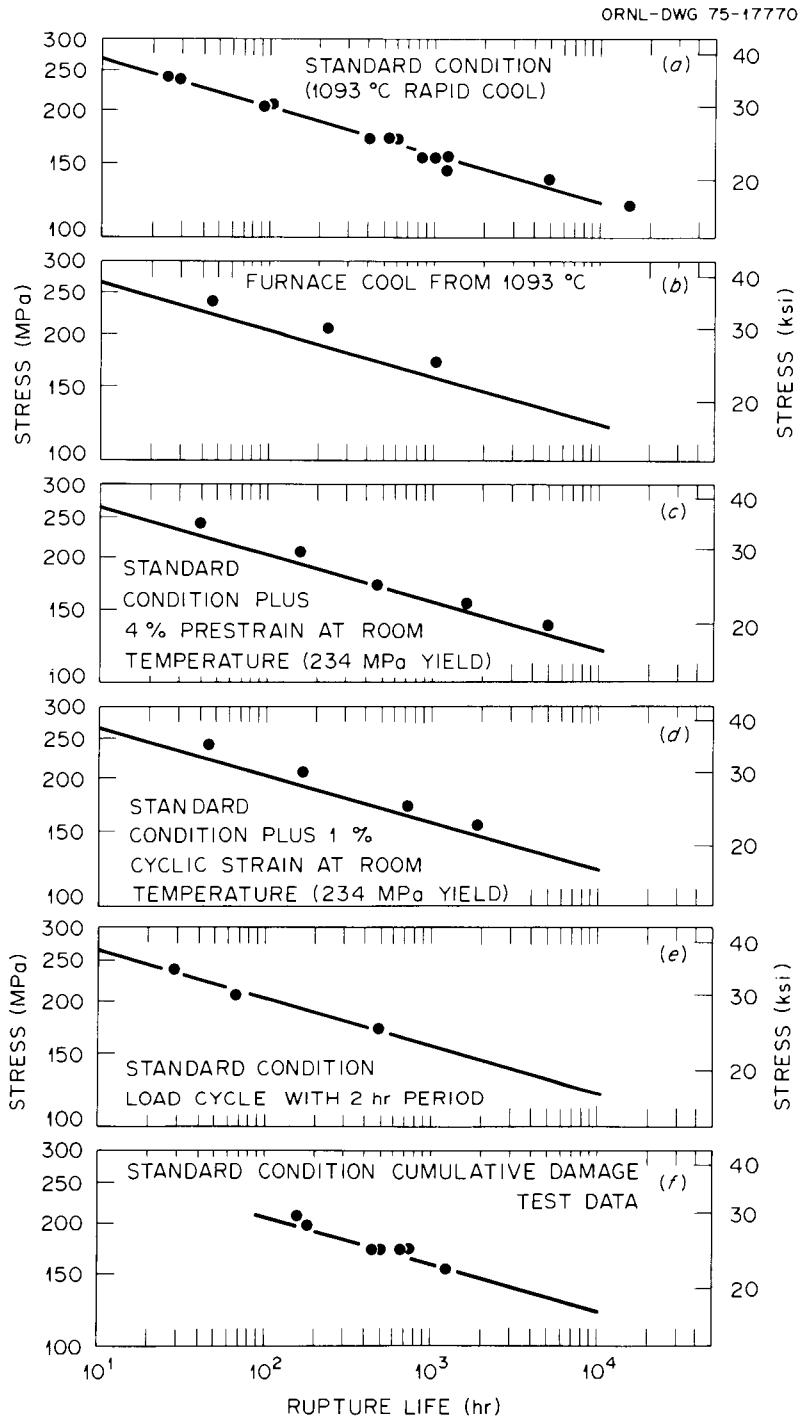


Fig. 3.65. Stress-Rupture Curves for Type 304 Stainless Steel (Heat 9T2796) Showing the Influence of Thermomechanical History at 593°C (1100°F). (a) Standard rapid cool (line shown on all subsequent graphs). (b) Anneal. (c) Cold work. (d) Cyclic cold work. (e) Slow cycling. (f) Cumulative damage.

the most significant "history" variable is the cooling rate from the annealing temperature. Slow cooling greatly extends the rupture life, as shown in Fig. 3.65(b). To a lesser extent, life is extended by prior tensile or cyclic cold work, as shown in Fig. 3.65(c) and (d). In Fig. 3.65(e) the rupture lives for specimens cycled with a 2-hr period are compared with the standard curve and we see that the data lie close to the curve. Finally, some cummulative damage data are provided in Fig. 3.65(f). To obtain the data we summed the life fraction ratios for all conditions up to, but not including, the final stress. This ratio was used to calculate the "equivalent" of hours consummed at the final stress. The actual time at the final stress was added to this calculated time. Generally, we find that the material surpasses the expected life. That is, our damage summations generally equal or exceed unity. However, data at 538°C (1000°F) are not included, and we find that damage summations are less than unity at this temperature.

3.5.1.2 Exploratory Testing of Type 316 Stainless Steel

In this reporting period characterization testing of the reference heat of type 316 stainless steel was initiated at 593°C (1100°F). Tensile curves for three strain rates are provided in Fig. 3.66 and show

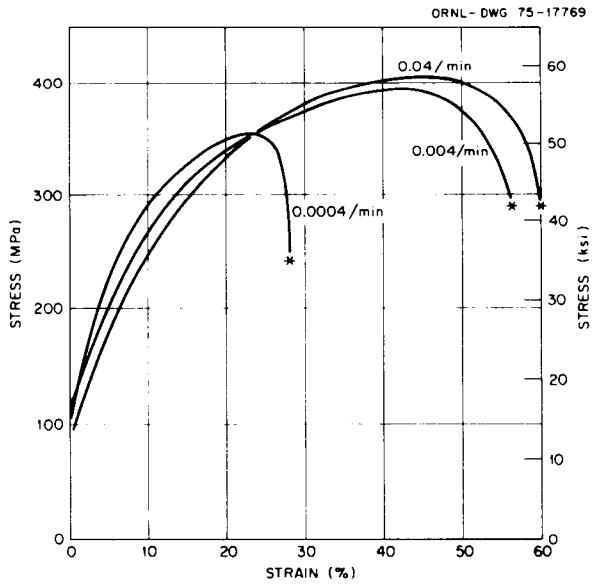


Fig. 3.66. Tensile Curves for Type 316 Stainless Steel (Heat 8092297) at 593°C (1100°F).

that the influence of strain rate is significantly inverted at strains below 20%. The ultimate tensile strengths follow the usual decrease with decreasing strain rates, however. Creep curves at five high stress levels are provided in Fig. 3.67. Examination of the data reveals some inconsistencies with respect to loading strains, transient strains, and general features of the curves. This varibility is about the same as we observed for the reference heat of type 304 stainless steel. The type 316 stainless steel is about 30% stronger than the type 304, however.

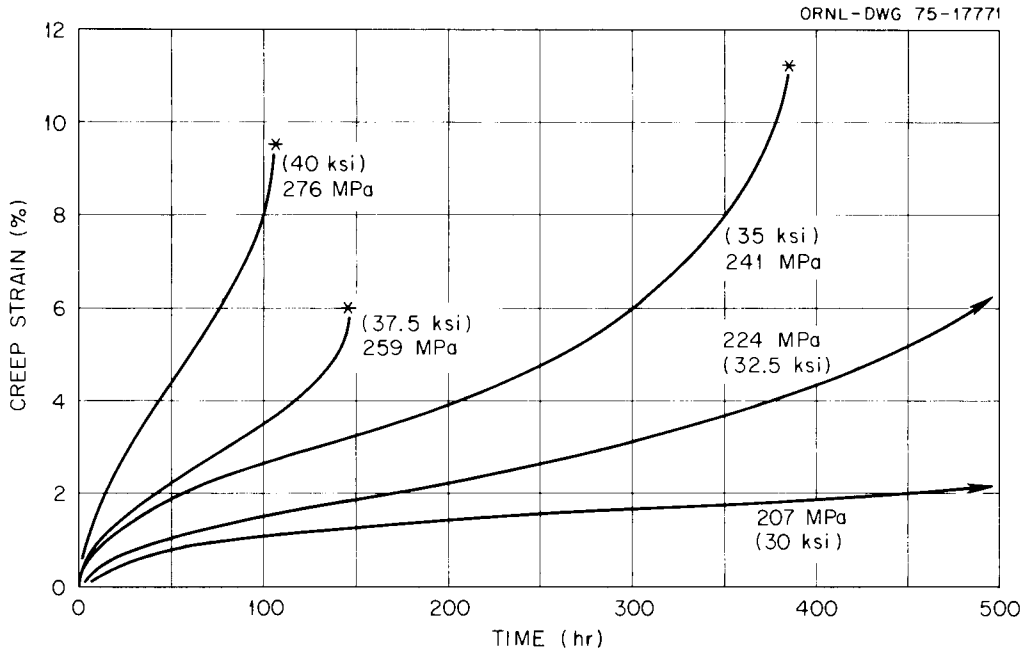


Fig. 3.67. Creep Curves for Type 316 Stainless Steel (Heat 8092297) at 593°C (1100°F).

Relaxation behavior of this material to 100 hr is shown for 593°C (1100°F) in Fig. 3.68. Data are compared with predictions based on the proposed *Nuclear Systems Materials Handbook* equation (double-exponential form). The relaxation strength appears substantially greater than that predicted for this material. The predicted strength for type 304 stainless steel is also included and is substantially greater than predicted for type 316 stainless steel.

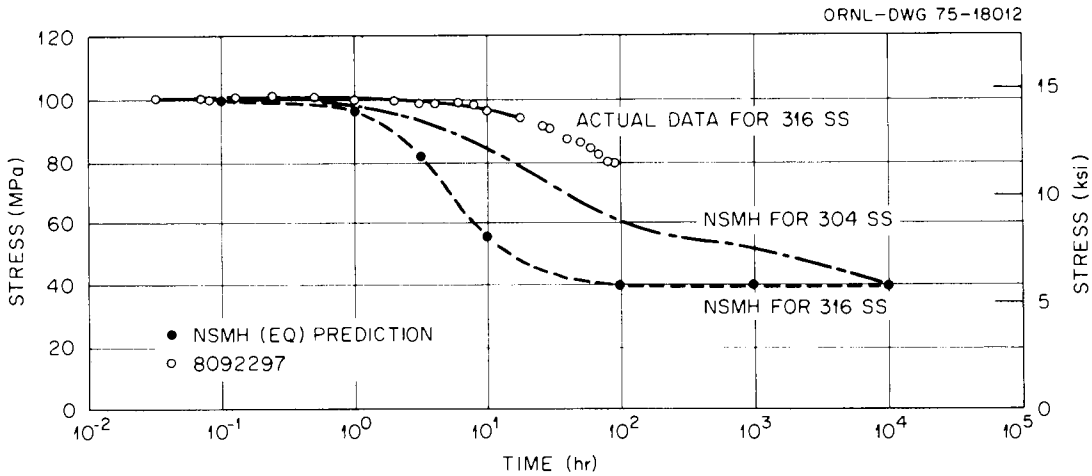


Fig. 3.68. Relaxation Behavior for Type 316 Stainless Steel (Heat 8092297) at 593°C (1100°F).

3.5.1.3 Exploratory Testing of 2 1/4 Cr-1 Mo Steel

Exploratory testing of 2 1/4 Cr-1 Mo steel has been greatly expanded in this reporting period. Three heats of material are involved. Early testing included relaxation and creep-plasticity studies of heat 20017 in the annealed condition, and currently we are examining a second heat, 3P5601, under conditions of creep, relaxation, and creep-plasticity at 538°C (1000°F). A third heat, which has been studied extensively in programs sponsored by the Metal Properties Council, is also being used at ORNL to fabricate a portion of the third Thermal Transient Test specimen. Our mechanical tests on this material will involve a few low-stress tests to supplement creep data produced by the Battelle Columbus Laboratory.[61]

Relaxation data for heat 20017 at temperature from 482 to 566°C (900–1050°F) have been reported previously.[62,63] Additional data for 450°C (842°F) are provided in Fig. 3.69.

Creep data for heat 3P5601 have been obtained for the stress range 86 to 207 MPa (12.5 to 30 ksi) and are plotted in Fig. 3.70. Above 103 MPa (15 ksi) the curves exhibit a relatively short primary stage followed by a prolonged tertiary stage. At 103 MPa (15 ksi), and below, gradual creep hardening is observed.

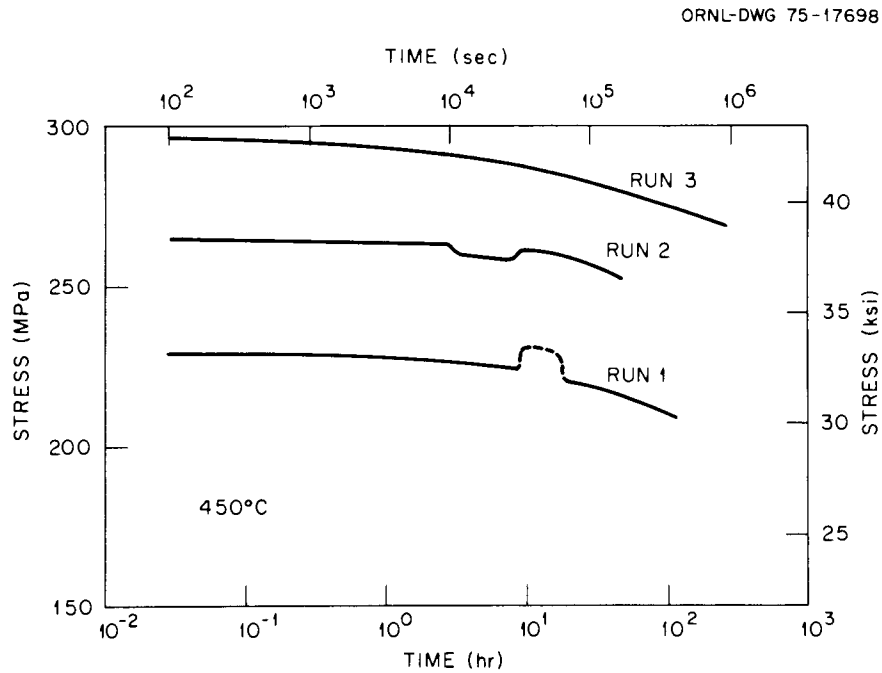


Fig. 3.69. Relaxation Behavior of 2 1/4 Cr-1 Mo Steel (Heat 20017) at 425°C (842°F).

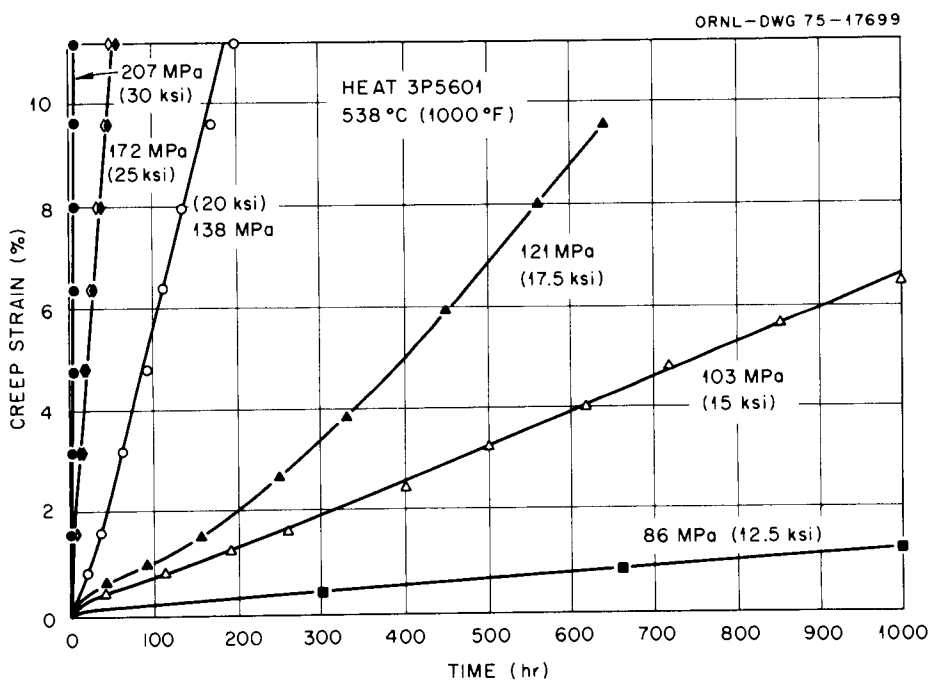


Fig. 3.70. Short-Time Creep Curves for 2 1/4 Cr-1 Mo Steel (Heat 3P5601) at 538°C (1000°F).

The results of a series of relaxation tests on heat 3P5601 at 538°C (1000°F) are shown in Fig. 3.71. Similar to heat 20017, the relaxation curves for the first and second loadings cross.

The results of a reversal creep test on heat 3P5601 at 538°C (1000°F) are shown in Fig. 3.72. The material shows an increase in the cyclic creep strain after the first loading period.

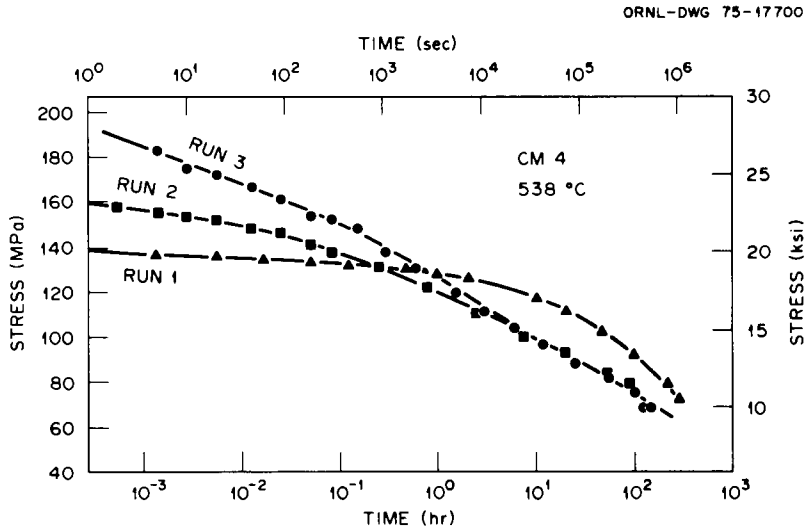


Fig. 3.71. Relaxation Behavior of 2 1/4 Cr-1 Mo Steel (Heat 3P5601) at 538°C (1000°F).

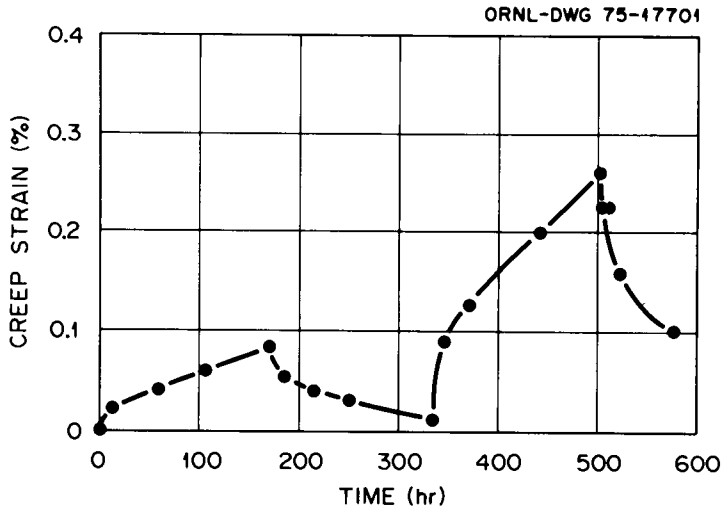


Fig. 3.72. Reversed Creep Behavior of 2 1/4 Cr-1 Mo Steel (Heat 3P5601) at 538°C (1000°F) and ±103 MPa (±15 ksi).

### 3.5.2 Investigations of Creep Failure Under Uniaxial and Multiaxial Conditions — C. C. Schultz (Babcock and Wilcox)

During this reporting period two uniaxial and three biaxial tests were in progress. All tests were at 593°C (1100°F).

#### 3.5.2.1 Uniaxial Tests

In test BWR-11 [117 MPa (17 ksi)] rupture occurred during August after 25,942 hr. Test BWR-7 [110 MPa (16 ksi)] is still under way after approximately 29,000 hr. The creep strain versus time data for both tests are shown in Fig. 3.73. The stress versus time-to-rupture data for all constant-load uniaxial tests are shown in Fig. 3.74. Tables 3.26 and 3.27 summarize the results for these tests. A detailed account of the variability observed in the uniaxial test results from the 16-mm-diam (5/8-in.) hot-rolled bar of heat 9T2796 has been reported.[64]

#### 3.5.2.2 Multiaxial Testing

Two biaxial specimens ruptured and a third test was started during this period. The stresses for each of the multiaxial tests are shown in Table 3.28. In that table, two sets of stresses are shown for each test. The first set of stresses was derived from the mean radius formula, and the second set consists of the average stresses. At this time, no effort has been made to determine the time history of the actual state of stress. After completion of stress redistribution, the actual stresses at the outside surface are more closely approximated by the stresses based on the mean radius formula than by the average stresses.

The stress versus time-to-rupture results for the biaxial specimens are compared with the uniaxial results in Fig. 3.75. In that figure, the stress plotted for the biaxial specimens is the maximum principal stress based on the mean radius formula.

In the two tests that were completed this period, BWTR-6 and BWTR-7, the radial displacement at the center of the gage length was monitored by six DCDT probes. This same procedure had been used during part of an earlier test, BWTR-3. As in all earlier tests, the axial extension over the center 0.13 m (5 in.) of the 0.2-m (8-in.) test section was monitored by means of extensometers, mounted on opposite sides of the specimen.

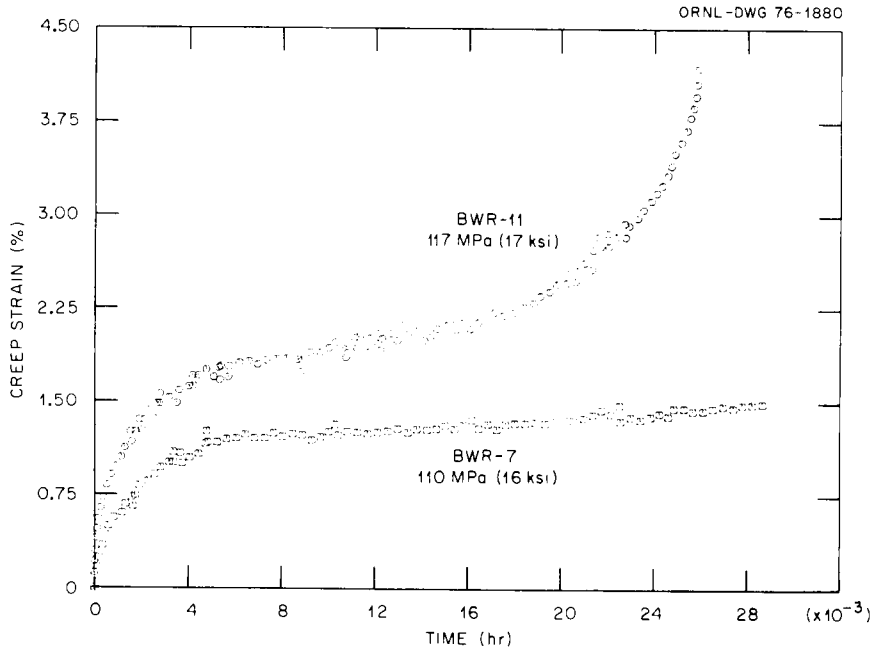


Fig. 3.73. Constant-Load Uniaxial Rupture Tests at 593°C (1100°F). Type 304 stainless steel, heat 9T2796, 16-mm (5/8-in.) bar, reannealed at 1093°C (2000°F) for 30 min.

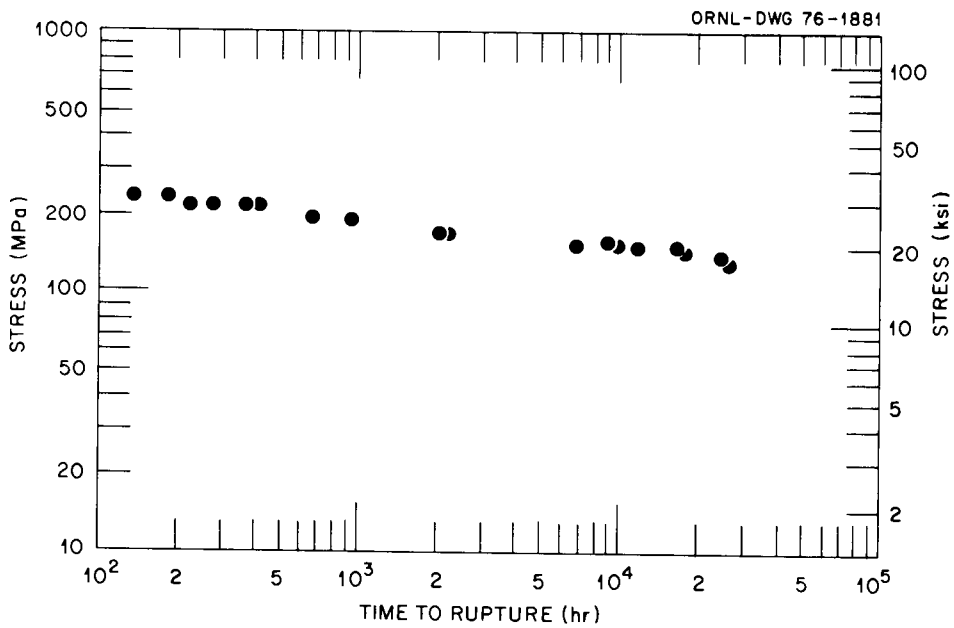


Fig. 3.74. Time to Rupture for Constant-Load Tests at 593°C (1100°F). Type 304 stainless steel, heat 9T2796, 16-mm (5/8-in.) bar, reannealed at 1093°C (2000°F) for 30 min.

Table 3.26. Constant-Load Uniaxial Creep-Rupture Tests at 593°C (1100°F), Type 304 Stainless Steel, Heat 9T2796

| Test | Specimen | Stress (MPa) | Stress (ksi) | Total[a] Strain on Loading (%) | Time to Secondary Creep (hr) | Minimum Creep Rate (%/hr) | Time to[b] Tertiary Creep (hr) | Intercept[c] Creep Strain (%) | Test[d] Time (hr) | Fracture[e] Elongation (%) | Reduction of Area (%) |
|---|---|---|---|---|---|---|---|---|---|---|---|
| BWC-1 | 7-15 | 207 | 30 | 5.0 | | | | | 187 R | 19.0 | 30.5 |
| BWR-1 | 7-1 | 207 | 30 | 7.80 | | | | | 138 R | 21.5 | 32.9 |
| BWC-2 | 2-22 | 193 | 28 | 6.35 | 40 | 0.016 | 195 | 0.50 | 227 R | 13.0 | 20.4 |
| BWR-2 | 2-1 | 193 | 28 | 5.75 | 40 | 0.022 | 230 | 0.65 | 368 R | 16.5 | 18.3 |
| BWR-13 | 7-13 | 193 | 28 | 6.57 | 60 | 0.023 | 215 | 0.88 | 276 R | 16.5 | 18.9 |
| BWC-9 | 7-25 | 193 | 28 | 4.25 | 85 | 0.021 | | 1.16 | 415 R | 18.3 | 25.2 |
| BWC-3[f] | 7-28 | 172 | 25 | 4.20 | 80 | 0.0065 | 500 | 0.45 | 667 R | 12.7 | 12.0 |
| BWR-3 | 7-8 | 172 | 25 | 3.90 | 100 | 0.0079 | 585 | 0.71 | 948 R | 17.0 | 23.2 |
| BWC-4 | 2-28 | 152 | 22 | 4.00 | 175 | 0.0014 | 1,400 | 0.60 | 2,130 R | 10.7 | 13.7 |
| BWR-4 | 7-7 | 152 | 22 | 3.30 | 160 | 0.0030 | 1,170 | 0.72 | 2,026 R | 12.5 | 16.6 |
| BWC-5[g] | 2-15 | 138 | 20 | | | | | | D | | |
| BWC-5B | 2-16 | 138 | 20 | 1.83 | 5,000 | 0.000165 | 8,700 | 1.84 | 9,584 R | 10.5 | 12.0 |
| BWR-5[h] | 2-14 | 138 | 20 | 2.02 | | | | | 4,842 D | | |
| BWR-14 | 2-9 | 138 | 20 | 2.02 | 3,200 | 0.00044 | 5,800 | 1.88 | 6,868 R | 8.5 | 13.1 |
| BWC-10 | 7-18 | 138 | 20 | 1.58 | 4,000 | 0.00021 | 8,000 | 2.30 | 9,450 R | 9.3 | 14.3 |
| BWR-6 | 7-14 | 131 | 19 | 1.48 | 6,000 | 0.000073 | 13,500 | 2.90 | 17,547 R | 9.5 | 12.6 |
| BWR-9 | 7-11 | 124 | 18 | 1.15 | 7,500 | 0.000036 | 18,000 | 2.40 | 24,495 R | 8.5 | 13.8 |
| BWR-11[i] | 2-12 | 117 | 17 | | | | | | 94 D | | |
| BWR-11 | 2-10 | 117 | 17 | 1.35 | 6,000 | 0.000033 | 20,000 | 1.60 | 25,942 R | 7.5 | 13.2 |
| BWR-7 | 2-4 | 110 | 16 | 0.60 | 6,000 | 0.000009 | | 1.15 | 29,000 I | | |

[a]All specimens were step-loaded 12.9 MPa (1.87 ksi) increments, except test BWC-5B, which was step-loaded 10.3 MPa (1.49 ksi) increments.

[b]Based on the 0.2% offset from the minimum rate line.

[c]Intercept creep strain does not include the elastic and initial plastic components.

[d]R = ruptured; D = discontinued; I = in test.

[e]Elongation over 76.2 mm (3 in.) in BWC series; over 50.8 mm (2 in.) in BWR series.

[f]Failure occurred near end of gage length.

[g]Temperature excursion to 704°C (1300°F) before loading; replaced by test BWC-5B.

[h]Temperature excursion to 749°C (1380°F) at 4842 hr; terminated.

[i]Temperature excursion to 704°C (1300°F) at 94 hr; replaced by test BWR-11B.

Table 3.27. Interrupted Uniaxial Tests at 593°C (1100°F) and 134 MPa (19.5 ksi), Type 304 Stainless Steel, Heat 9T2796

| Test | Specimen | Total[a] Strain on Loading (%) | Time to Secondary Creep (hr) | Minimum Creep Rate (%/hr) | Time to[b] Tertiary Creep (hr) | Intercept[c] Creep Strain (%) | Test[d] Time (hr) | Fracture[e] Elongation (%) | Reduction of Area (%) |
|---|---|---|---|---|---|---|---|---|---|
| BWI-1 | 6-4 | 0.98 | 5600 | 0.00008 | 13,000 | 3.3 | 15,788 D | | |
| BWI-2 | 6-5 | 1.07 | 5400 | 0.00010 | 13,000 | 3.2 | 16,891 R | 13.0 | 11.5 |
| BWI-3 | 6-6 | 1.50 | 4800 | 0.00019 | 9,000 | 3.2 | 11,608 R | 11.0 | 13.3 |
| BWI-4 | 6-1 | 0.98 | 7000 | 0.00005 | N.A. | 3.5 | 12,100 D | | |
| BWI-5 | 6-2 | 1.65 | 3800 | 0.00026 | 8,300 | 2.7 | 9,072 D | | |
| BWI-6 | 6-3 | 1.30 | 3800 | 0.00023 | 7,500 | 2.8 | 9,049 D | | |

[a]All specimens were step-loaded in 12.9 MPa (1.87 ksi) increments.

[b]Time to tertiary creep based on the 0.2% offset from the minimum rate line.

[c]Intercept creep strain does not include the elastic and initial plastic components.

[d]R = ruptured; D = discontinued.

[e]Elongation over 50.8-mm (2-in.) gage length.

Table 3.28. Biaxial Creep Tests at 593°C (1100°F), Type 304 Stainless Steel, Heat 9T2796, 49-mm (1.9-in.) Bar

| Test | Specimen | Internal Pressure | | Additional Axial Load | | Stress,[a] MPa (ksi) | | | Estimated Rupture Time[b] (hr) | Test Time[c] (hr) |
|---|---|---|---|---|---|---|---|---|---|---|
| | | (MPa) | (psi) | (kN) | (lb) | Circumferential | Axial | Effective | | |
| BWTR-1 | 5R-37A | | | 32.63 | 7337 | | 150.7 (21.85)<br>150.7 (21.85) | 150.7 (21.85)<br>150.7 (21.85) | 2000 | 1997 R |
| BWTR-2 | 8R-5A | 15.86 | 2300 | | | 150.7 (21.85)<br>142.7 (20.70) | 75.36 (10.93)<br>67.57 (9.80) | 130.45 (18.92)<br>123.7 (17.94) | 2000 | 1713 R |
| BWTR-3 | 7R-5A | 15.86 | 2300 | 16.32 | 3668 | 150.7 (21.85)<br>142.7 (20.70) | 150.7 (21.85)<br>142.9 (20.73) | 150.7 (21.85)<br>142.8 (20.71) | 2000 | 584 R |
| BWTR-4 | 6R-37A | 7.93 | 1150 | 24.46 | 5500 | 75.33 (10.93)<br>71.36 (10.35) | 150.7 (21.85)<br>146.7 (21.28) | 130.5 (18.92)<br>127.1 (18.43) | 2000 | 3336 R |
| BWTR-5 | 9R-3A | 7.26 | 1053 | 22.40 | 5036 | 68.95 (10.00)<br>65.36 (9.48) | 137.9 (20.00)<br>134.4 (19.49) | 119.4 (17.32)<br>116.4 (16.88) | 5000 | 700 I |
| BWTR-6 | 10R-3A | 14.51 | 2105 | | | 137.9 (20.00)<br>130.7 (18.95) | 68.95 (10.00)<br>61.85 (8.97) | 119.4 (17.32)<br>113.1 (16.41) | 5000 | 3272 R |
| BWTR-7 | 8R-3A | 14.51 | 2105 | 14.94 | 3358 | 137.9 (20.00)<br>130.7 (18.95) | 137.9 (20.00)<br>130.9 (18.98) | 137.9 (20.00)<br>130.7 (18.96) | 5000 | 1925 R |

[a]The first set of stresses shown is based on the mean radius formula and the second set is average stresses, 38.1-mm (1.50-in.) OD and 1.91-mm (0.075-in.) wall thickness.

[b]The estimated rupture time is based on the maximum principal stress from the mean radius formula.

[c]R = ruptured, I = in test.

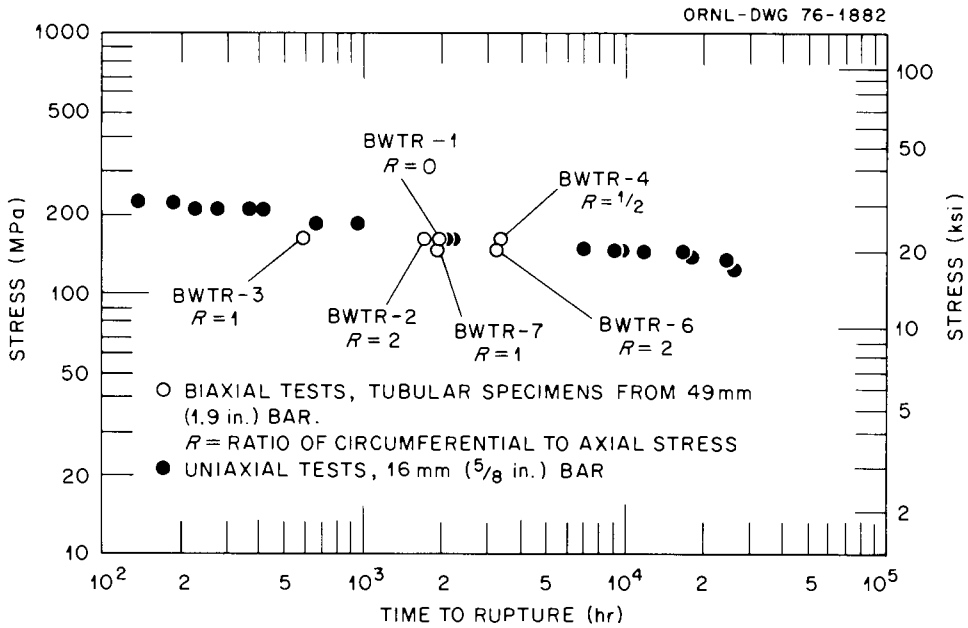


Fig. 3.75. Comparison of Uniaxial and Biaxial Rupture Tests at 593°C (1100°F). Type 304 stainless steel, heat 9T2796, reannealed at 1093°C (2000°F) for 30 min.

In Fig. 3.70 the creep strain-time data for test BWTR-3 [equal biaxial tension of 150.7 MPa (21.85 ksi)] are shown. The circumferential strain at the center of the gage length was measured by means of three pairs of opposed radial DCDTs. The outputs from both members of a pair were averaged to eliminate the effects of relative lateral motion between the specimen and the DCDT reference frame. The axial strain was obtained by averaging the outputs of the two opposed axial extensometers. Note that the creep strains in Fig. 3.76 have as their zero reference the strain at 100 hr. During the initial 100 hr of testing the diameters were not measured. It was expected that the measured axial and circumferential creep strains would be equal. Part of the difference between the axial and circumferential creep strains is attributed to the fact that the axial strain measurement was the average over 0.13 m (5 in.) and the circumferential strain was determined at a single axial location. Measurements of the specimen diameter taken when the test was interrupted (after 100 hr under load) and again upon completion of the test indicated good agreement with the in-test measurements made with the radial DCDTs.

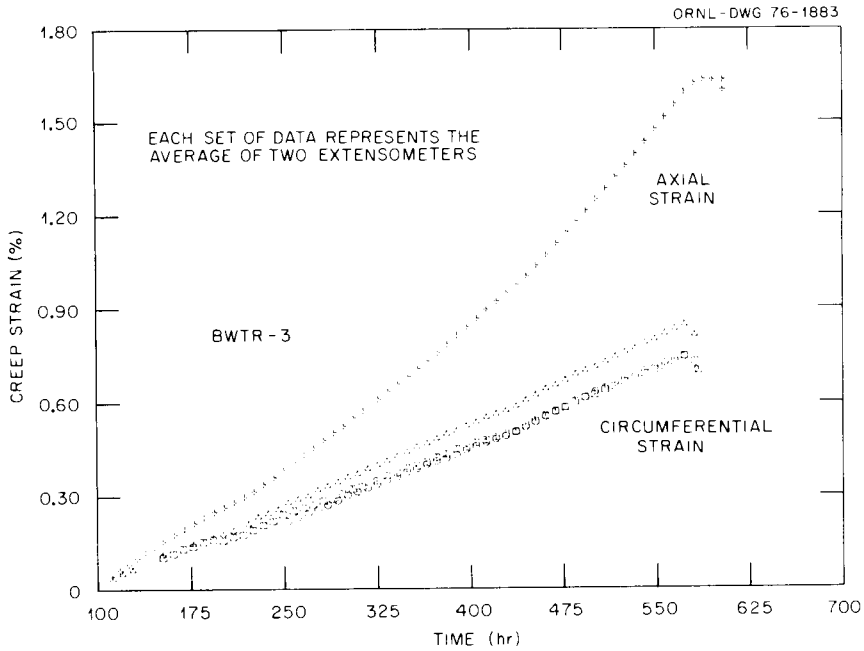


Fig. 3.76. Axial and Circumferential Creep Strains in a Constant-Load Biaxial Rupture Test. Tubular specimen with internal pressure and additional axial load. Equal biaxial tension of 150.7 MPa (21.85 ksi) at 593°C (1100°F). Outside diameter of 38.1 mm (1.50 in.) and wall thickness of 1.91 mm (0.075 in.). Type 304 stainless steel heat 9T2796, 49-mm (1.9-in.) bar.

Between 100 hr and the end of the test, the radial DCDTs indicated an average diametral growth of approximately 0.30 mm (0.012 in.). Similar out-of-test measurements at the same axial location showed an average diametral growth of approximately 0.28 mm (0.011 in.). The total end-of-test diametral growth at this same axial location was approximately 1.47 mm (0.058 in.), which corresponds to a permanent circumferential strain of 3.9%. At this same axial location the diameter was constant (with respect to angular location) to within ±0.03 mm (0.001 in.). The failure occurred approximately 3.8 cm (1 1/2 in.) from the center of the gage length. At this location the diametral growth was approximately 2.39 mm (0.094 in.), a permanent strain of 6.3%. At this axial location the diameter was constant to within ±0.05 mm (0.002 in.). We conclude that the extensometers functioned properly during the test and that the disparity between the average axial and local circumferential strains is probably due to nonuniformity of the strain over the test section.

Figure 3.77 is a similar representation of test BWTR-7, which was also loaded in equal biaxial tension [137.9 MPa (20.00 ksi)]. Note that the data are not complete to the end of the test. In this test the axial strain more closely approximated the circumferential strain than in test BWTR-3. This specimen was measured during an unscheduled test interruption after 1636 hr under load. It ruptured very recently and thus has not been measured in the final state. In-test measurements showed an average diametral growth at the center of the test section of 1.22 mm (0.048 in.) or 3.2% strain during the first 1636 hr of loading. Similar out-of-test measurements showed an average diametral increase of 1.09 mm (0.043 in.). At this location the diameter was constant to within ±0.03 mm (0.001 in.). The maximum diametral change (at a different axial loaction) after 1636 hr was 1.37 mm (0.054 in.) or 3.6% strain. At this location the diameter was constant to within ±0.03 mm (0.0001 in.).

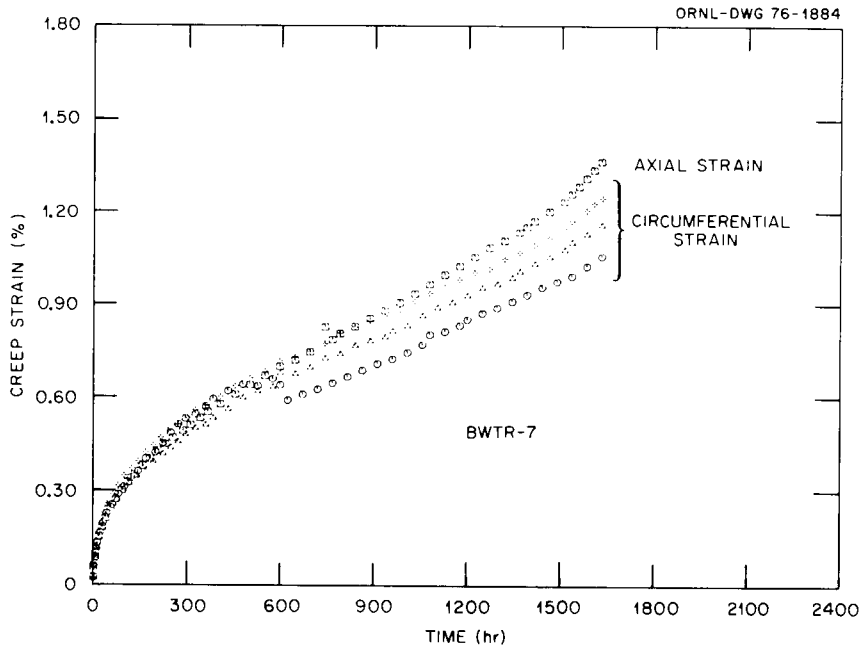


Fig. 3.77. Axial and Circumferential Creep Strains in a Constant-Load Biaxial Rupture Test. Tubular specimen with internal pressure and additional axial load. Equal biaxial tension of 137.9 MPa (20 ksi) at 593°C (1100°F). Outside diameter of 38.1 mm (1.50 in.) and wall thickness of 1.91 mm (0.075 in.). Type 304 stainless steel heat 9T2796, 49-mm (1.9-in.) bar.

The axial creep strain-time data for test BWTR-6 under internal pressure only are shown in Fig. 3.78. As in a previous test under internal pressure only (BWTR-2),[65] a small axial extension occurred that had a rapidly diminishing rate. The circumferential creep strain-time data are shown in Fig. 3.79. Out-of-test specimen measurements were made at the end of test and during an unscheduled test interruption after 416 hr under load. The average diametral growth measured in-test up to 416 hr was 0.86 mm (0.034 in.) or 2.3% strain. Out-of-test diametral measurements at the same location showed a diametral change of 0.91 mm (0.036 in.) Before testing and after 416 hr in test the diameter was constant to within ±0.03 mm (0.001 in.) at this axial location. The diameter varied very little with axial location after 416 hr of testing. At the end of the test, the in-test measurements showed an average diametral growth of 1.27 mm (0.050 in.) or 3.3% strain, and the out-of-test measurements showed an average growth of 1.40 mm (0.55 in.) at the center of the test

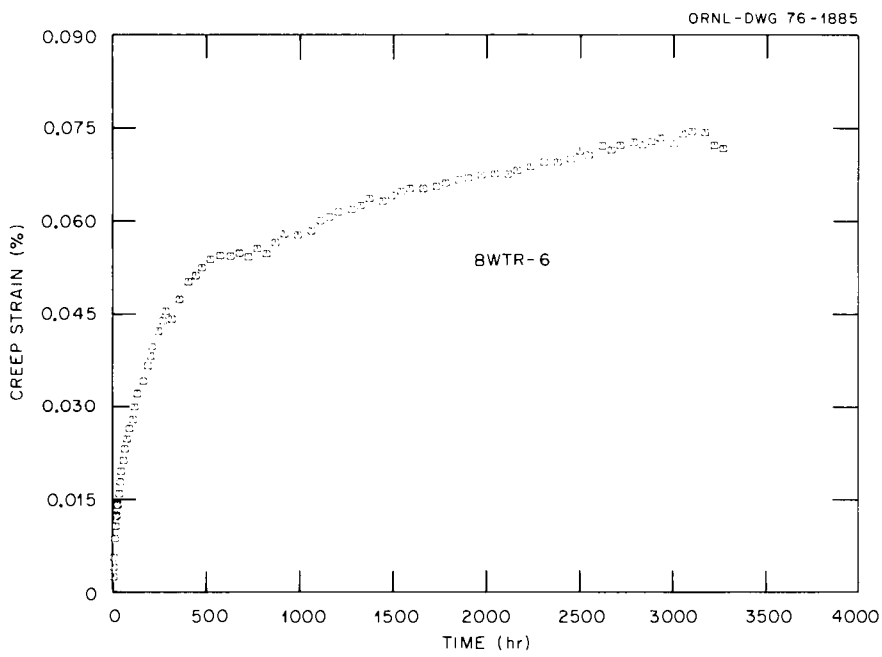


Fig. 3.78. Axial Creep Strain in a Constant-Load Biaxial Rupture Test. Tubular specimen with internal pressure. Axial stress of 68.95 MPa (10 ksi) and circumferential stress of 137.9 MPa (20 ksi) at 593°C (1100°F). Outside diameter of 38.1 mm (1.50 in.) and wall thickness of 1.91 mm (0.075 in.). Type 304 stainless steel, heat 9T2796, 49 mm (1.9 in.) bar.

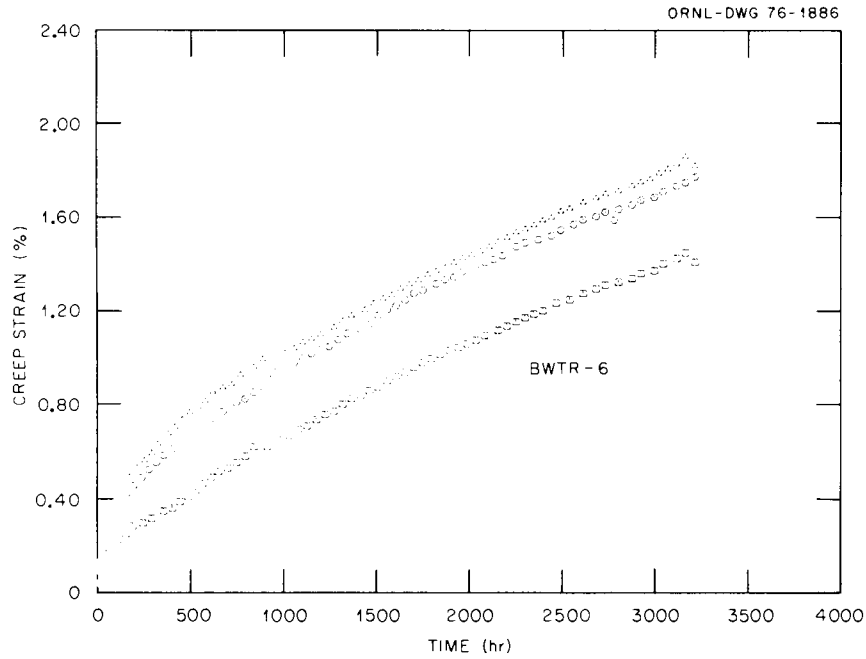


Fig. 3.79. Circumferential Creep Strain in a Constant-Load Biaxial Rupture Test. Tubular specimen with internal pressure. Axial stress of 68.95 MPa (10 ksi) and circumferential stress of 137.9 MPa (20 ksi) at 593°C (1100°F). Outside diameter of 38.1 mm (1.50 in.) and wall thickness of 1.91 mm (0.075 in.). Type 304 stainless steel heat 9T2796, 49 mm (1.9-in.) bar.

section. The diameter was constant to within ±0.08 mm (0.003 in.) at that location. The failure occurred approximately 3.8 mm (1.5 in.) from the center of the test section with an average diametral growth of 1.80 mm (0.071 in.) or 4.7% strain. At this location the diameter varied by ±0.08 mm (0.003 in.) around the circumference.

Preliminary axial creep strain versus time results for test BWTR-4 [axial stress of 137.9 MPa (20.00 ksi)] and circumferential stress of 68.95 MPa (10.00 ksi) are shown in Fig. 3.80. No in-test radial displacement measurements are being made during this test, nor has the test been interrupted for specimen measurements.

## 3.6 MECHANICAL PROPERTIES OF HTGR STEAM GENERATOR AND PRIMARY CIRCUIT MATERIALS — J. R. DiStefano

The major overall objectives of this program are to (1) determine the compatibility of alloys planned for use in the HTGR steam-cycle system with their environment and (2) determine, compile, and analyze

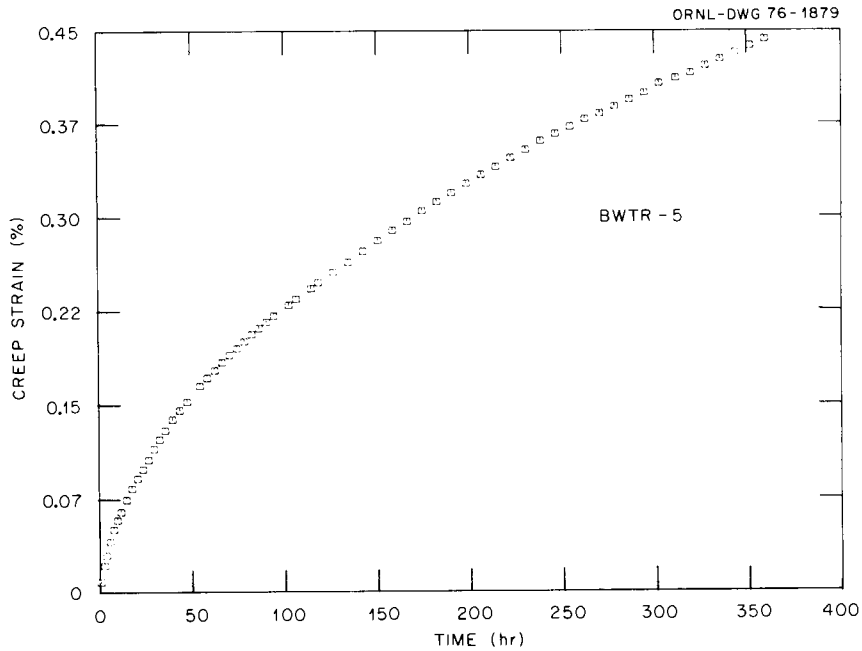


Fig. 3.80. Axial Creep Strain in a Constant-Load Biaxial Rupture Test. Tubular specimen with internal pressure and additional axial load. Axial stress of 137.9 MPa (20 ksi) and circumferential stress of 68.95 MPa (10 ksi) at 593°C (1100°F). Outside diameter of 38.1 mm (1.50 in.) and wall thickness of 1.91 mm (0.075 in.). Type 304 stainless steel heat 9T2796, 49 mm (1.9-in.) bar.

materials design data for the commercial HTGR. To achieve these objectives it is necessary to study the mechanical behavior (tensile, creep, low-cycle fatigue, and crack growth) of HTGR alloys at temperatures and in environments (helium and steam) appropriate to their service in the reactor.

### 3.6.1 Tensile Testing — A. Lystrup

Specimens from hot-rolled, solution-annealed 13-mm-thick (1/2-in.) Inconel 617 plate (Heat XX01H3US) have been fabricated and inspected, and they are now ready to be tested in the temperature range from 22 to 982°C (72–1800°F).

### 3.6.2 Environmental Creep Testing — A. Lystrup

The environmental creep tests of HTGR structural alloys in simulated primary coolant helium have continued during the quarter. Two

tests on Hastelloy X were completed during this period, and results are shown in Table 3.29. Cross sections of specimens from the two tests were examined metallographically. The specimen from test 16031 [Hastelloy X, 760°C (1400°F), 152 MPa (22 ksi), 159 hr] shows a 1-μm-thick discontinuous surface oxide and many 40–50-μm-deep grain boundary penetrations in the stressed part of the specimen. The surface on the unstressed part of the specimen (at the shoulder) is covered with a smooth green continuous 1-μm-thick oxide layer, and there is no grain boundary attack at all. The specimen from test 16054 [Hastelloy X, 871°C (1600°F), 62 MPa (9 ksi), 554 hr] shows a very thin, if any, surface film on the stressed portion of the specimen and only few 20–30-μm-deep penetrations. On the unstressed portion of the specimen there was also a very thin oxide layer but, as noted in the previous test, there was no grain boundary attack at all.

Table 3.29. Results of Environmental Creep Tests Completed During the Quarter

| Material and Heat | Test | Temperature | | Stress | | Rupture Life (hr) | Elongation at Rupture (%) |
|---|---|---|---|---|---|---|---|
| | | (°C) | (°F) | (MPa) | (ksi) | | |
| Hastelloy X 2600-3-2792 | 16031 | 760 | 1400 | 152 | 22 | 159 | 57 |
| Hastelloy X 2600-3-2792 | 16054 | 871 | 1600 | 62 | 9 | 554 | 35 |

The matrix of our current creep tests in simulated HTGR primary coolant is shown in Table 3.30. Maximum time in test is approaching 7500 hr (e.g., tests 15023, 15046, and 15047).

For comparison, six air creep machines have just been loaded and the test matrix is also shown in Table 3.30.

### 3.6.3 Fatigue-Life Testing — J. P. Strizak

Low-cycle strain-controlled fatigue testing of Hastelloy X material has recently begun. Tests are being conducted in air over the temperature

Table 3.30. Current Creep Tests on HTGR Structural Alloys

| Material | Heat | Test | Temperature (°C) | Temperature (°F) | Stress (MPa) | Stress (ksi) |
|---|---|---|---|---|---|---|
| | | Tests in Simulated Primary Coolant | | | | |
| 2 1/4 Cr-1 Mo | X-6216 | 15023 | 593 | 1100 | 69 | 10 |
| 2 1/4 Cr-1 Mo | X-6216 | 15046 | 538 | 1000 | 103 | 15 |
| 2 1/4 Cr-1 Mo | X-6216 | 15047 | 593 | 1100 | 69 | 10 |
| 9 Cr-1 Mo | 316381-1A | 15363 | 538 | 1000 | 103 | 15 |
| 2 1/4 Cr-1 Mo | 36202 | 15369 | 538 | 1000 | 103 | 15 |
| 2 1/4 Cr-1 Mo | 36202 | 15374 | 482 | 900 | 172 | 25 |
| Hastelloy X | 2600-3-4936 | 15772 | 649 | 1200 | 172 | 25 |
| Hastelloy X | 2600-3-4936 | 15792 | 704 | 1300 | 138 | 20 |
| Hastelloy X | 2600-3-4936 | 16125 | 760 | 1400 | 138 | 20 |
| Hastelloy X | 2600-3-4936 | 16126 | 871 | 1600 | 34 | 5 |
| | | Tests in Air | | | | |
| 2 1/4 Cr-1 Mo | 36202 | 16263 | 482 | 900 | 207 | 30 |
| 2 1/4 Cr-1 Mo | 36202 | 16264 | 538 | 1000 | 103 | 15 |
| 2 1/4 Cr-1 Mo | 72768 | 16266 | 593 | 1100 | 103 | 15 |
| Hastelloy X | 2600-3-4936 | 16267 | 649 | 1200 | 172 | 25 |
| Hastelloy X | 2600-3-4936 | 16268 | 704 | 1300 | 138 | 20 |
| Hastelloy X | 2600-3-4936 | 16269 | 816 | 1500 | 69 | 10 |

range from room temperature to 982°C (1800°F). The types of wave forms to be applied in these fully reversed strain-controlled tests include continuous cycling at constant strain rate and tensile and/or compressive hold periods introduced each cycle at peak strain values. These wave forms are shown in Fig. 3.81.

Hourglass-shaped specimens having a gage section with a minimum diameter of 5.08 mm (0.200 in.) and a radius to diameter ratio ($R/D$) of 6 were fabricated from a solution annealed heat (2600-3-4936, with ASTM specification B 435-71) of 12.7-mm-thick (0.5 in.) plate material; and the finished specimens were given no further heat treatment after

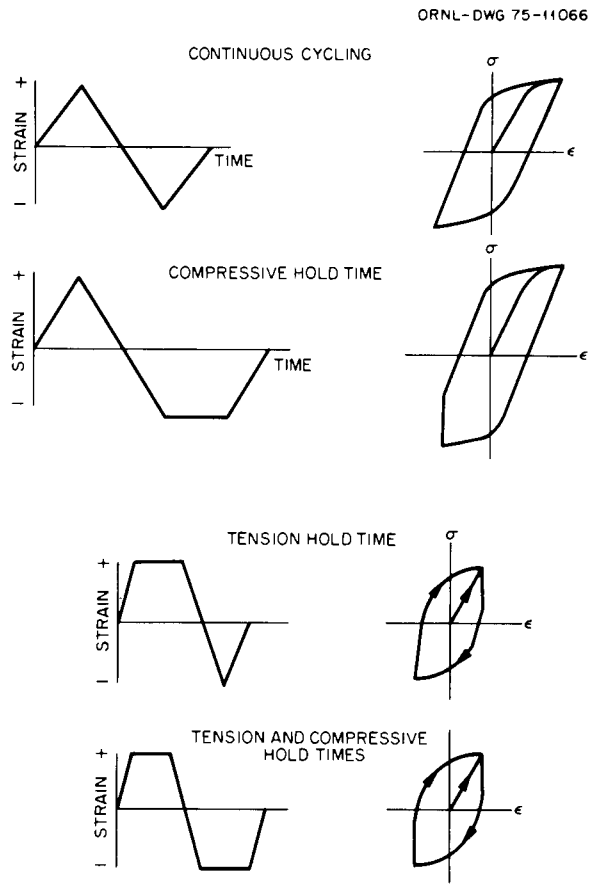


Fig. 3.81. Wave Forms Used for Completely Reversed Strain-Controlled Fatigue Tests.

machining. Chemical composition (ladle analysis) for this material is given in Table 3.31. The ASTM grain size is 4.

Strain-controlled push-pull tests were conducted with closed-loop electro-hydraulic testing systems incorporating: (1) hydraulically operated grips for the button-ended hourglass-shaped specimens in an integral die-set arrangement for rigidity and resistance to buckling, (2) a load cell located within the die set, (3) a diametral extensometer attached to the minimum diameter of the test specimen, (4) a simple analog computer to calculate and control total axial strain from load and diametral strain signals, and (5) a high-frequency induction unit for specimen heating. Thermocouples were spotwelded to the specimens approximately 6.4 mm (0.25 in.) above and below the minimum-diameter

Table 3.31. Chemical Composition of Hastelloy X, Heat 2600-3-4936

| Element | Content (wt %) | Element | Content (wt %) |
|---|---|---|---|
| Cr | 21.82 | Ni | bal |
| W | 0.63 | Mn | 0.58 |
| Fe | 19.09 | Mo | 9.42 |
| C | 0.07 | P | 0.016 |
| Si | 0.44 | S | <0.005 |
| Co | 1.68 | B | <0.002 |

test section of the specimen for temperature control and readout. A typical fatigue test system is shown in Fig. 3.82.

Continuous cycling tests completed to date over the temperature range from room temperature to 871°C (1600°F) are compared as a function of total strain range ($\Delta\varepsilon_t$) vs cycle life ($N_f$) in Fig. 3.83. Compilation and analysis of data are under way and will be reported later.

Low-cycle strain-controlled fatigue tests will be conducted later in a simulated HTGR primary coolant helium environment. Tests will also be conducted over the temperature range from room temperature to 982°C (1800°F) for direct comparison with data from current tests in air. Design of an environmental system to facilitate this testing is nearly complete and is presently being reviewed. The environmental system, which will have the capability of environmental fatigue testing in inert gas or in vacuum to 1.3 μPa ($10^{-8}$ torr), will include: (1) an environmental chamber, (2) specimen grips for hourglass-shaped specimens incorporating a die-set arrangement for rigidity and resistance to buckling, (3) a load cell located inside the chamber and die-set, (4) a diametral extensometer, and (5) vacuum equipment for purging the chamber before atmosphere flow or for testing in vacuum. The environmental chamber and specimen grip arrangement, which will be adapted to the existing testing system (Fig. 3.82), is shown schematically in Fig. 3.84. The completion date for fabrication of the environmental system is projected for

Y-130411

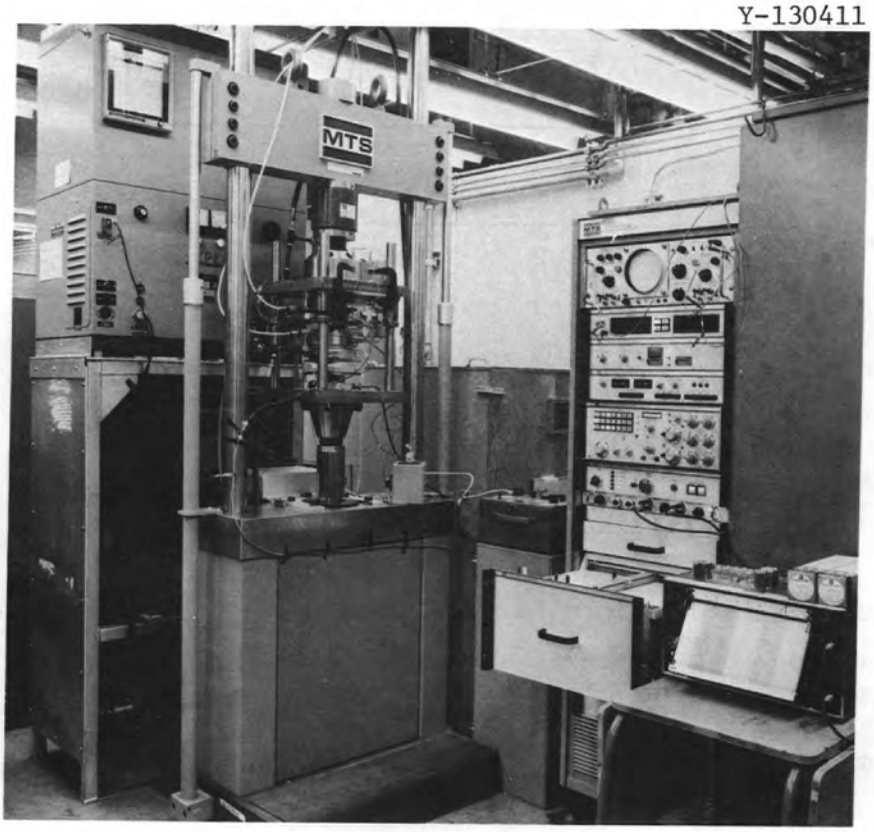


Y-130414

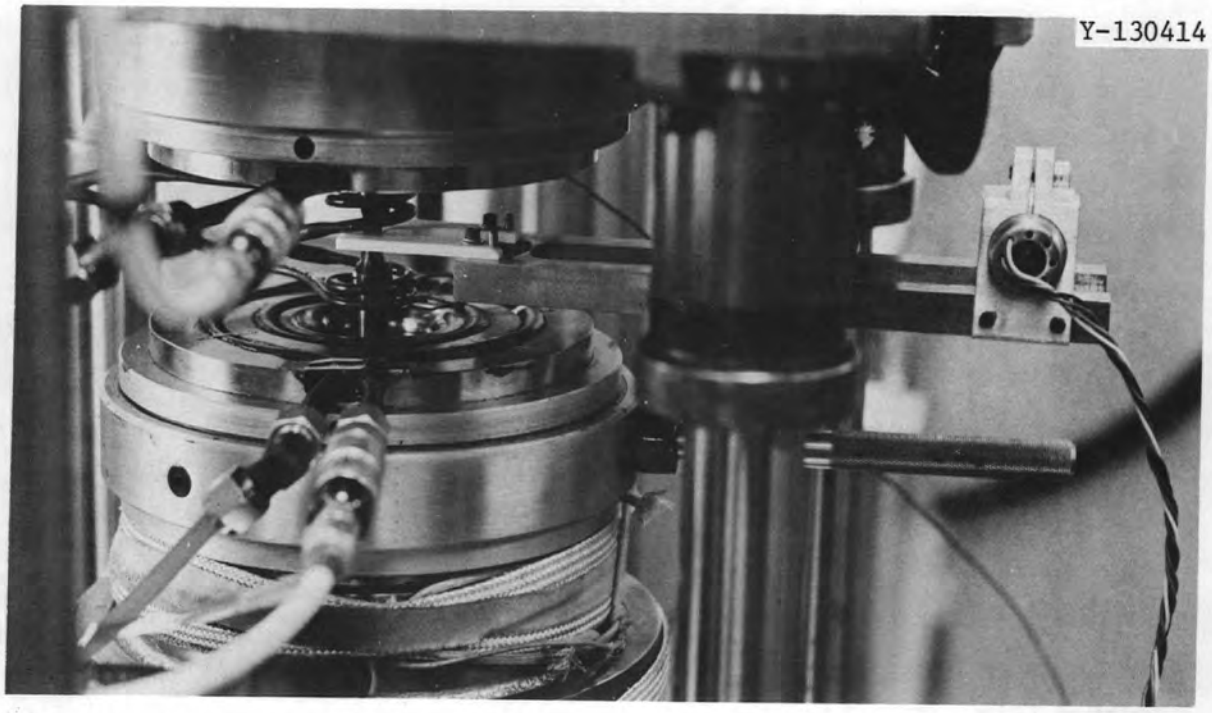

Fig. 3.82. Low-Cycle Strain-Controlled Push-Pull Fatigue Testing Facility.

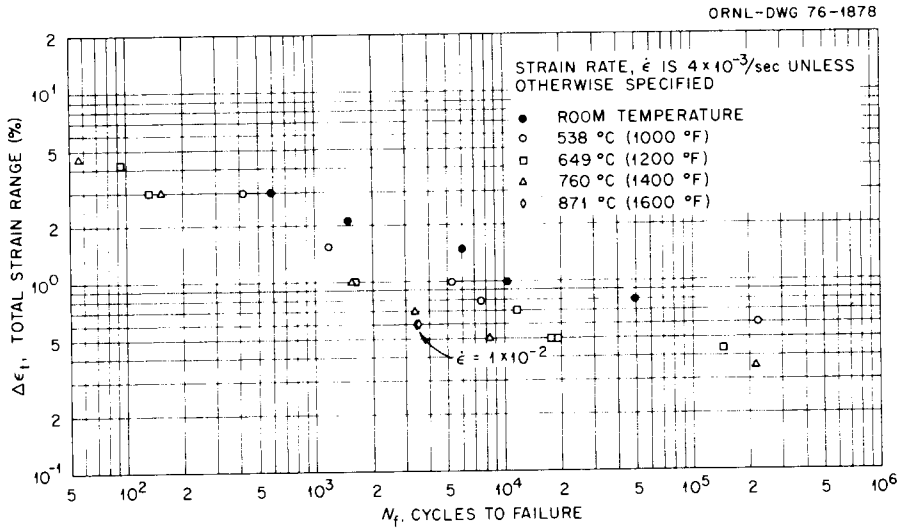


Fig. 3.83. Comparison of the Low-Cycle Strain-Controlled Fatigue Behavior of Hastelloy Alloy X (Heat 2600-3-4936) Over the Temperature Range of 23°C (74°F) to 871°C (1600°F).

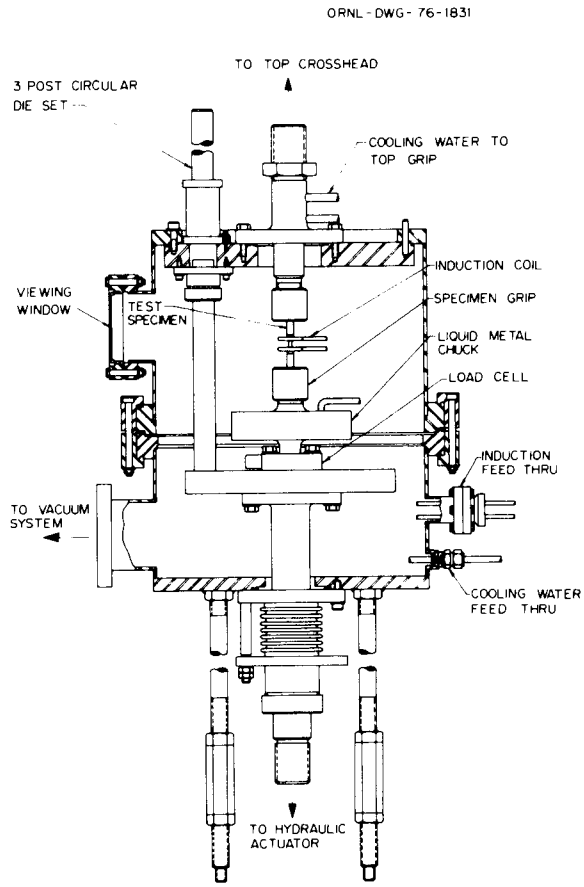


Fig. 3.84. Schematic of Environmental Chamber Design for Conducting Fatigue Tests in a Helium Atmosphere or Vacuum.

May 1, 1976 primarily because of two-month delivery dates on some vacuum flanges and other components. Installation and checkout of the system and establishment of standard operating procedure will follow.

Additional low-cycle fatigue tests will be conducted on aged material to characterize the thermal stability of Hastlloy X (Heat 2600-3-4936) as well as Inconel 617 (Heat XX01A3US). Material is presently being aged at 538, 704, and 871°C (1000, 1300, and 1600°F) for periods of 2500, 10,000, and 20,000 hr in closed capsules that had been back filled with argon. Completion of 2500 hr at 538 and 704°C is expected on March 10, 1976, with 2500 hr at 871°C following on April 5, 1976. Fabrication of fatigue and creep specimens and testing will begin as each aging period is reached.

### 3.6.4 Subcritical Crack Growth Studies — W. R. Corwin

The materials being used in this study are two Babcock and Wilcox heats 20017 and 3P5601 of 2 1/4 Cr-1 Mo ferritic steel and heat 2600-3-4936 of Hastelloy X from Cabot. Mechanical Properties of these materials have been reported previously.

#### 3.6.4.1 Testing in Air

During this quarter testing of 2 1/4 Cr-1 Mo steel in air was continued to determine the effects of cycle frequency and heat-to-heat variations in the material.

Specimens from heat 3P5601 were tested under conditions identical to those previously used for heat 20017. As shown in Fig. 3.85, fatigue crack propagation (FCP) behavior of both heats was essentially the same when they were tested at 510°C (950°F) and 40 cpm with $R = 0.05$. The only noticeable difference between the test results is more scatter in data from heat 3P5601. The average $da/dN$ vs $\Delta K$ curves were virtually identical. However, in tests at 371°C (700°F) and 400 cpm with $R = 0.05$, heat 20017 appears to exhibit greater cracking resistance at the higher levels of $\Delta K$. This could be due to a different temperature response to dynamic strain aging by the two heats. Preliminary work indicates that strengthening due to dynamic strain aging occurs at about 371°C (700°F)

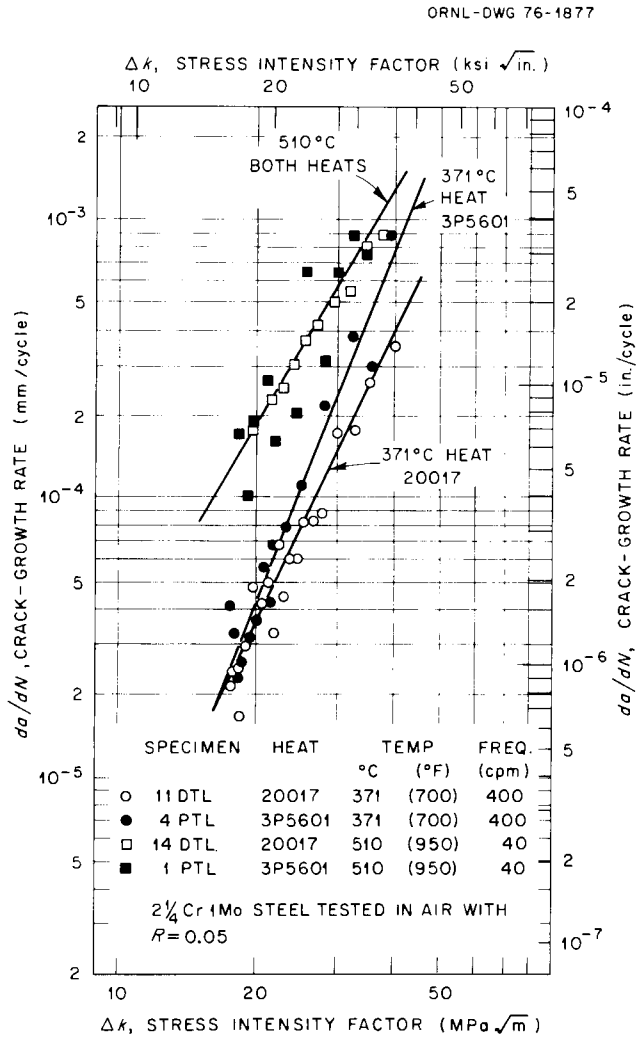


Fig. 3.85. Heat-to-Heat Effects on Fatigue Crack Growth.

in heat 20017, whereas in heat 3P5601 it may be 55 to 85°C (100 to 150°F) higher. More tests will be necessary to confirm this.

Studies to determine the effect of frequency on FCP were continued this quarter. With the completion of tests at 40 cpm at 510°C (950°F) with $R$ = 0.05, material behavior has now been determined at both 510 and 593°C (950 and 1100°F) with $R$ = 0.05 at frequencies of 4, 40, and 400 cpm, as shown in Fig. 3.86. Tests are currently under way at 510°C (950°F), $R$ = 0.05, and at a frequency of 0.4 cpm; a combination of conditions where creep effects become very prominent.

Testing of Hastelloy X began this quarter. Experimental difficulties in maintaining a straight crack front have been encountered.

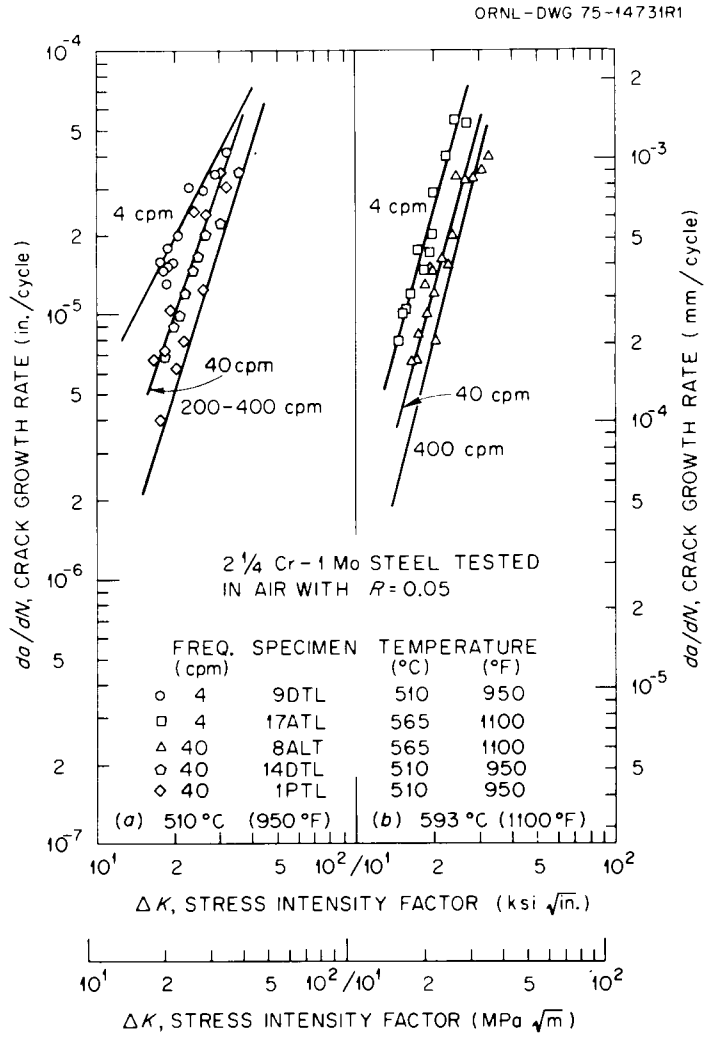


Fig. 3.86. Effect of Frequency on Crack Growth in 2 1/4 Cr-1 Mo Steel at 510 and 593°C (950 and 1100°F).

This is believed to be due to problems in specimen fabrication, which are currently being corrected. Nonetheless, limited data have been obtained at room temperature, 537°C (1000°F), and 648°C (1200°F).

### 3.6.4.2 Testing in Steam

Examination of the effects of a superheated steam environment on the FCP of 2 1/4 Cr-1 Mo steel continued intermittently last quarter. Limited machine availability prevented completion of comparative effects of steam at 593°C (1100°F); however, interim indications are that the crack growth rate is less in steam than in air. This corresponds with the data shown last quarter at 510°C (950°F).

3.6.4.3 Testing in HTGR Helium

Completion of comparison tests on 2 1/4 Cr-1 Mo steel in air at 510°C (950°F), 40 cpm, $R$ = 0.05 indicate (Fig. 3.87) that the simulated HTGR primary coolant does reduce the crack growth rate below that in air. Although data in the HTGR helium are still limited the trend is

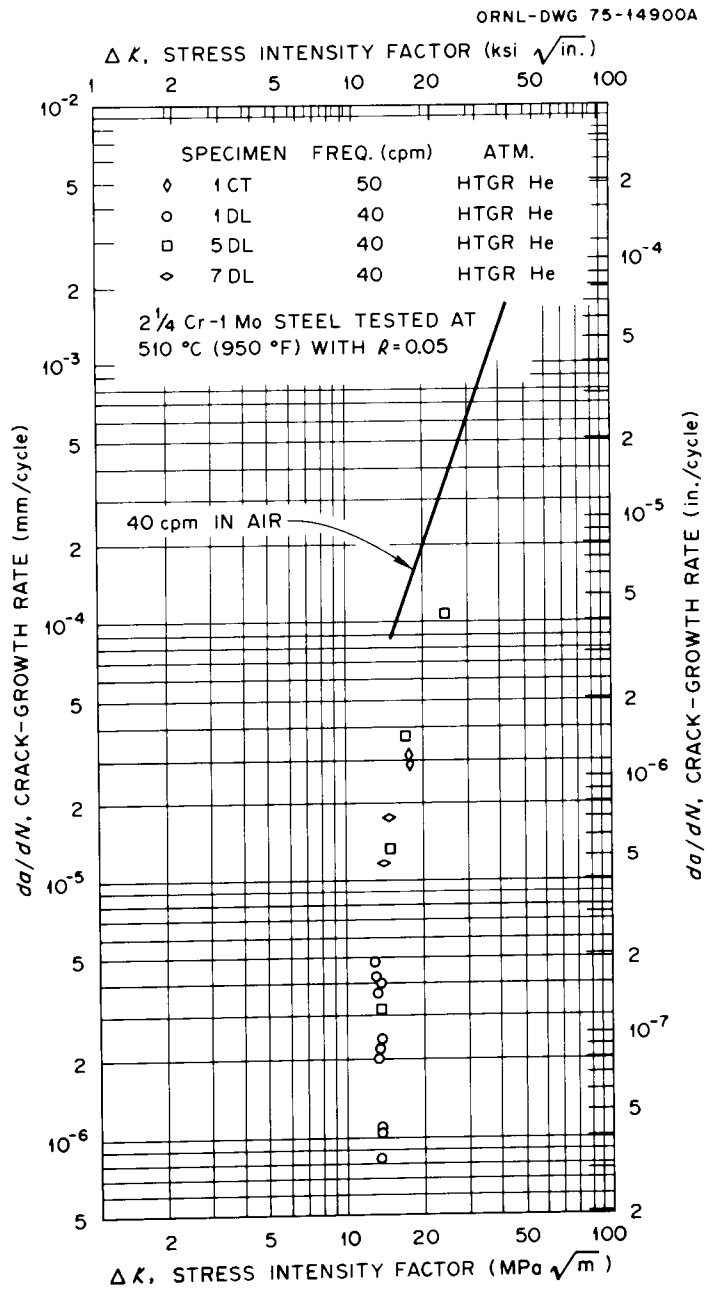


Fig. 3.87. Effects of Simulated HTGR Primary Coolant on Crack Growth in 2 1/4 Cr-1 Mo Steel at 510°C (950°F).

similar to that reported above for tests in steam and to the results in liquid sodium at Hanford reported by James.[66] It appears that air is a very aggressive environment for FCP.

Testing in HTGR He on 2 1/4 Cr-1 Mo steel was initiated this quarter, and limited data was acquired at 593°C (1100°F) prior to loss of environmental integrity in the test chamber. After repairs to the chamber testing of Hastelloy X at 648°C (1200°F) was initiated and is currently in progress.

## 3.7 REFERENCES


1. H. J. Frost and M. F. Ashby, private communication, July 1975.
2. M. F. Ashby, "A First Report on Deformation Mechanism Maps," *Acta Metall.* 20: 887–97 (1972).
3. V. K. Sikka, H. E. McCoy, M. K. Booker, and C. R. Brinkman, "Heat-to-Heat Variation in Creep Properties of Types 304 and 316 Stainless Steel," *J. Pressure Vessel Technol.* 93(4): 243 (1975).
4. V. K. Sikka, "Heat-to-Heat Variation and Its Relation with Chemical Composition," *Mechanical Properties Test Data for Structural Materials Quart. Progr. Rep. Apr. 30, 1975,* ORNL-5105, pp. 95–101.
5. V. K. Sikka, E. B. Patton, and R. H. Baldwin, "Creep Properties," *Mechanical Properties Test Data for Structural Materials Quart. Progr. Rep. Oct. 31, 1975,* ORNL-5107, pp. 61–66.
6. E. P. Bens, "Hardness Testing of Metals and Alloys at Elevated Temperatures," *Trans. Am. Soc. Met.* 38: 505–16 (1947).
7. F. Garofalo, P. R. Malenock, and G. V. Smith, "Hardness of Various Steels at Elevated Temperatures," *Trans. Am. Soc. Met.* 45: 377–96 (1953).
8. V. K. Sikka and C. R. Brinkman, "Relation Between Short- and Long-Term Elevated-Temperature Properties of Several Austenitic Stainless Steels," accepted for publication in *Scripta Metallurgica.*
9. The British Steelmakers Creep Committee, *BSCC High Temperature Data, British Long Term Creep Rupture and Elevated Temperature Tensile Data on Steels for High Temperature Service,* The Iron and Steel Institute, London.

10. V. K. Sikka, E. Lee, and E. B. Patton, "Effect of Aging on Tensile and Creep Properties of Type 304 Stainless Steel," *Mechanical Properties Test Data for Structural Materials Quart. Progr. Rep. Oct. 31, 1974,* ORNL-5103, pp. 126–37.

11. V. K. Sikka, "Effect of Thermal Aging on Tensile Properties of Types 304 and 316 Stainless Steels, *Mechanical Properties Test Data for Structural Materials Quart. Progr. Rep. July, 31, 1975,* ORNL-5106, pp. 72–86.

12. V. K. Sikka, C. R. Brinkman, and H. E. McCoy, "Effect of Thermal Aging on Tensile and Creep Properties of Types 304 and 316 Stainless Steel," pp. 316–50 in *Symposium on Structural Materials for Service at Elevated-Temperatures in Nuclear Power Generation,* MPC-1, ed. by A. O. Schaefer, American Society of Mechanical Engineers, New York, 1975.

13. V. K. Sikka, R. H. Baldwin, and E. B. Patton, "Tensile Tests Following Period of Creep," *Mechanical Properties Test Data for Structural Materials Quart. Progr. Rep. Oct. 31, 1975,* ORNL-5107, pp. 18–35.

14. L. D. Blackburn, "Isochronous Stress-Strain Curves for Austenitic Stainless Steels," pp. 15–48 in *The Generation of Isochronous Stress-Strain Curves,* ed. by A. O. Schaefer, American Society of Mechanical Engineers, New York, 1972.

15. W. E. Stillman, "Development of Creep Equation for Type 316 Stainless Steel," *Mechanical Properties Test Data for Structural Materials Quart. Progr. Rep. Oct. 31, 1975,* ORNL-5107, pp. 81–93.

16. J. B. Conway, *Numerical Methods for Creep and Rupture Analyses,* Gordon and Breach, New York, 1968.

17. F. Garofalo, C. Richmond, W. F. Domis, and F. Von Gemmingen, "Strain-Time, Rate-Stress, and Rate-Temperature Relations During Large Deformations in Creep," pp. 1–31 in *Joint International Conference on Creep,* Institution of Mechanical Engineers, London, 1963.

18. W. J. Evans and B. Wilshire, "Work-Hardening and Recovery During Transient and Steady-State Creep," *Trans. Met. Soc. AIME* 242: 2514 (1968).

19. M. K. Booker, T. L. Hebble, D. O. Hobson, and C. R. Brinkman, "Mechanical Property Correlations for 2 1/4 Cr-1 Mo Steel in Support of Nuclear Reactor Systems Design," paper F 8/9 in *Transactions of the 3rd International Conference on Structural Mechanics in Reactor Technology* (London, UK, 1–5 Sept. 1975), Vol. 2, Part F, Commission of the European Communities, Luxemborg, 1975.

20. I. A. Oding, ed., *Creep and Stress Relaxation in Metals,* transl. by E. Bishop, ed. by A. J. Kennedy, Oliver and Boyd, London, 1959, pp. 78–82.

21. Ibid., pp. 359–60.

22. A. O. Schaefer, ed., *The Generation of Isochronous Stress-Strain Curves,* American Society of Mechanical Engineers, New York, 1972.

23. D. I. Roberts and S. A. Sterling, "A Parametric Method for the Development of Isochronous Stress-Strain Curves," pp. 1–14 in *The Generation of Isochronous Stress-Strain Curves,* ed. by A. O. Schaefer, American Society of Mechanical Engineers, New York, 1972.

24. J. B. Conway, "Parametric Considerations Applied to Isochronous Stress-Strain Plots," pp. 55–66 in *The Generation of Isochronous Stress-Strain Curves,* ed. by A. O. Schaefer, American Society of Mechanical Engineers, New York, 1972.

25. J. P. Hammond, "Elastic Properties of Engineering Construction Materials," *Mechanical Properties Test Data for Structural Materials Quart. Progr. Rep. Oct. 31, 1975,* ORNL-5107, pp. 94–100.

26. Ibid., *July 31, 1975,* ORNL-5106, pp. 100–11.

27. G. M. Goodwin, N. C. Binkley, N. C. Cole, and R. G. Berggren, "Submerged-Arc Process," *Metals and Ceramics Div. Annu. Progr. Rep. June 30, 1971,* ORNL-4770, pp. 82–83.

28. N. C. Cole, G. M. Goodwin, and G. M. Slaughter, "Effect of Heat Treatments on the Microstructure of Stainless Steel Weld Metal," *Microstructural Science,* Vol. 3, ed. by P. M. French, R. J. Gray, and J. McCall, American Elsevier, New York, 1975, pp. 789–822.

29. R. G. Berggren, N. C. Cole, G. M. Goodwin, and R. T. King, "Properties and Structure of Type 308 Stainless Steel Welds with Varying Ferrite Contents," *Fuels and Materials Development Program Quart. Progr. Rep. June 30, 1973,* ORNL-TM-4355, pp. 138–47.

30. R. G. Berggren, N. C. Binkley, and G. M. Goodwin, "Investigation of Mechanical Properties," *Fuels and Materials Development Program Quart. Progr. Rep. Mar. 31, 1971,* ORNL-TM-3416, pp. 127–30.

31. R. T. King, J. O. Stiegler, and G. M. Goodwin, "Relation Between Mechanical Properties and Microstructure in a Thick Stainless Steel Weldment," *Weld. J. (Miami)* 53(7): 307-s–313-s (July 1974).

32. B. R. Dewey and R. T. King, "Studies of Strain Distribution in Weldments and Room-Temperature Elastic Constants," *Mechanical Properties Test Data for Structural Materials Quart. Progr. Rep. Oct. 31, 1975,* ORNL-5107, pp. 101–09.

33. R. L. Klueh, "High-Strain-Rate Tensile Properties of Annealed 2 1/4 Cr-1 Mo Steel," *Mechanical Properties Test Data for Structural Materials Quart. Progr. Rep. Jan. 31, 1975,* ORNL-5104, pp. 202–06.

34. R. L. Klueh, "Strain Rate Effects on the Tensile Properties of Annealed 2 1/4 Cr-1 Mo Steel," *Mechanical Properties Test Data for Structural Materials Quart. Progr. Rep. Apr. 30, 1975,* ORNL-5105, pp. 187–96.

35. R. L. Klueh and R. E. Oakes, Jr., *High-Strain-Rate Tensile Properties of Annealed 2 1/4 Cr-1 Mo Steel,* ORNL-TM-5028 (October 1975).

36. R. L. Klueh, "Heat-to-Heat Variations of 2 1/4 Cr-1 Mo Steel," *Mechanical Properties Test Data for Structural Materials Quart. Progr. Rep. July 31, 1975,* ORNL-5106, pp. 131–44.

37. R. L. Klueh, "High-Strain Rate Tensile Properties of 2 1/4 Cr-1 Mo Steel," *Mechanical Properties Test Data for Structural Materials Quart. Progr. Rep. July 31, 1975,* ORNL-5106, pp. 121–31.

38. J. D. Baird and A. Jamieson, "High-Temperature Tensile Properties of Some Synthesized Iron Alloys Containing Molybdenum and Chromium," *J. Iron Steel Inst.* 210: 841–46 (1972).

39. J. D. Baird, "The Effects of Strain-Aging Due to Interstitial Solutes on the Mechanical Properties of Metals," Metallurgical Review No. 149, *Metals Mater.* 5: 1–18 (February 1971).

40. R. G. Baker and J. Nutting, "The Tempering of 2 1/4 Cr-1 Mo Steel After Quenching and Normalizing," *J. Iron Steel Inst.* 192: 257–68 (1957).

41. J. M. Leitnaker and R. L. Klueh, *Characterization of the Microstructure of 2 1/4 Cr-1 Mo Steel,* report in preparation.

42. C. R. Brinkman, M. K. Booker, J. P. Strizak, W. R. Corwin, J. L. Frazier, and J. M. Leitnaker, *Interim Report on the Continuous Cycling Elevated-Temperature Fatigue and Subcritical Crack Growth Behavior of 2 1/4 Cr-1 Mo Steel,* ORNL-TM-4993 (December 1975).

43. M. K. Booker, "Bilinear Cyclic Stress-Strain Constants," *Mechanical Properties Test Data for Structural Materials Quart. Progr. Rep. Oct. 31, 1975,* ORNL-5107, pp. 158–71.

44. C. E. Pugh, K. C. Liu, J. M. Corum, and W. L. Greenstreet, *Currently Recommended Constitutive Equations for Inelastic Design Analysis of FFTF Components,* ORNL-TM-3602 (September 1972).

45. T. L. Hebble, "Mechanical Property Correlations of 2 1/4 Cr-1 Mo Steel for LMFBR Steam Generators," *Mechanical Properties Test Data for Structural Materials Quart. Progr. Rep. July 31, 1975,* ORNL-5106, pp. 155–65.

46. G. J. Lieberman and R. G. Miller, Jr., "Simultaneous Tolerance Intervals in Regression," *Biometrika* 50: 155–68 (1963).

47. F. R. Larson and J. Miller, "Time-Temperature Relationship for Rupture and Creep Stresses," *Trans. ASME* 74: 765 (1952).

48. M. K. Booker and V. K. Sikka, *Interrelationships Between Creep Life Criteria for Four Nuclear Structural Materials,* ORNL-TM-4997 (August 1975).

49. B. C. McMaster, *Nondestructive Testing Handbook,* Vol. 2, Roland Press, New York, 1963, p. 43.

50. J. P. Hammond and M. W. Moyer, "Elastic Properties Determined by Dynamic Tests," *Mechanical Properties Test Data for Structural Materials Quart. Progr. Rep. July 31, 1975,* ORNL-5106, pp. 100–11.

51. M. Kikuchi, "Elastic Anisotropy and Its Temperature Dependence of Single Crystals and Polycrystals of 18-2 Type Stainless Steel," *Trans. Japan Inst. Met.* 12: 417–21 (1971).

52. D. H. Chung and W. R. Buessen: *J. Appl. Phys.* 38 (1967), as cited by Kikuchi.[51]

53. M. D. Sullivan, General Electric, San Jose, California, private communication to J. F. King, ORNL, Jan. 6, 1976.

54. R. L. Klueh, "Mechanical Properties of Weld-Overlaid Stainless Steel," *Fuels and Materials Development Program Quart. Progr. Rep. June 30, 1974,* ORNL-TM-4688, pp. 68–74.

55. R. L. Klueh, "Mechanical Properties of Weld-Overlaid Forging," *Mechanical Properties Test Data for Structural Materials Quart. Progr. Rep. Oct. 31, 1974,* ORNL-5103, pp. 236–40.

56. Ibid., *Jan. 31, 1975,* ORNL-5104, pp. 236–39.

57. R. L. Klueh, "Mechanical Properties of Weld-Overlaid Stainless Steel Forging," *Mechanical Properties Test Data for Structural Materials Quart. Progr. Rep. Apr. 30, 1975,* ORNL-5105, pp. 232–41.

58. Ibid., *July 31, 1975,* ORNL-5106, pp. 165–71.

59. R. L. Klueh and D. A. Canonico, *The Creep-Rupture Properties of a Weld-Overlaid Type 304 Stainless Steel Forging,* ORNL-5058 (February 1976).

60. C. C. Schultz, "Investigations of Creep Failure Under Uniaxial and Multiaxial Conditions," *High-Temperature Structural Design Program Progr. Rep. Dec. 31, 1974,* ORNL-5048, pp. 117–39.

61. C. E. Jaske and M. Mindlin, "Elevated-Temperature Low-Cycle Fatigue Behavior of 2 1/4 Cr-1 Mo and 1 Cr-1 Mo-1/4 V Steels," pp. 137–210 in *Symposium on 2 1/4 Chrome-1 Molybdenum Steel in Pressure Vessels and Piping* (held Sept. 16–17, 1970, Denver, Colorado), ed. by A. O. Schaefer, The American Society of Mechanical Engineers, New York, 1971.

62. R. W. Swindeman and R. L. Klueh, "Exploratory Testing of 2 1/4 Cr-1 Mo Steel," *Mechanical Properties Test Data for Structural Materials Quart. Progr. Rep. July 31, 1975,* ORNL-5106, pp. 179–85.

63. Ibid., *Oct. 31, 1975,* ORNL-5107, pp. 182–85.

64. W. E. Leyda and C. C. Schultz, *Variability in Creep and Rupture Test Results in a Single Heat of Type 304 Stainless Steel,* The Babcock and Wilcox Company, ORNL-Sub-3654-3 (September 1975).

65. C. C. Schultz, "Investigations of Creep Failure Under Uniaxial and Multiaxial Conditions," *High-Temperature Structural Design Methods for LMFBR Components Progr. Rep. January–March 1974*, ORNL-4977, pp. 79–94.

66. L. A. James and R. L. Knecht, "Fatigue Crack Propagation Behavior of Type 304 Stainless Steel in a Liquid Sodium Environment," *Metall. Trans.* 6A(1): 109–16 (January 1975).

# 4. NAVAL RESEARCH LABORATORY

L. E. Steele

## 4.1 INTRODUCTION - L. E. Steele

The research program of the NRL Engineering Materials Division, Thermostructural Materials Branch, includes the study of the behavior of structural materials useful in reactor construction. Within the scope of the title above much unirradiated data are developed. This report is developed using such data to support the USERDA and USNRC objective of compiling structural materials properties data for use in national reactor development programs. The NRL program is sponsored by the Office of Naval Research, the U. S. Energy Research and Development Administration, the U. S. Nuclear Regulatory Commission, and the U. S. Army Engineer Power Group. The unirradiated materials properties data contributed here include that developed in the course of research in the areas of high temperature materials, radiation damage, and fracture mechanics.

## 4.2 EFFECT OF SPECIMEN THICKNESS ON FATIGUE CRACK GROWTH IN TYPE 304 STAINLESS STEEL - P. Shahinian

### 4.2.1 Background

The application of fatigue crack growth rate data with the fracture mechanics method to design requires knowledge of the influence of section thickness on crack growth. While much fatigue data have been generated for metals for high temperature service, little is known about the effect of thickness at these temperatures.

A number of investigators have examined the influence of specimen thickness (or section size) on fatigue crack growth rate at or near room temperature, but their findings are apparently inconsistent. Several investigators have reported no effect of thickness, while others have shown either an increase or decrease in crack growth rate with increasing specimen thickness. Some of the studies related the absence or presence of a thickness effect to plane strain or plane stress conditions, respectively, but yet other studies showed no such correlation.

It is difficult to reconcile the differences among the findings on the basis of thickness range or stress state. Because of the inconsistent findings, prediction of the thickness dependence of growth rate is not possible at this time. Therefore an investigation was undertaken to examine the effect of thickness on fatigue crack growth behavior of Type 304 stainless steel at room and elevated temperatures. Crack growth rates were compared on the basis of the crack-tip stress intensity factor.

### 4.2.2 Experimental Procedure

The chemical composition and tensile properties of the solution annealed Type 304 stainless steel plate (25.4 mm, 1 in.) are given in Table 1. Single-edge-notch cantilever specimens were machined from the plate with a L-T specimen orientation, having test section thicknesses of 7.6, 12.7, and 25.4 mm (0.3, 0.5, and 1.0 in.). The specimens were cycled at 0.17 Hz (10 cpm) in cantilever bending at a stress ratio, R = 0, in air at 24, 427, and 593°C (75, 800, and 1100°F). Additional experimental details are given elsewhere (1).

Stress intensity values were calculated from the formula,

$$K = \frac{6PL}{(B \cdot B_N)^{1/2} W^{3/2}} \cdot Y$$

where $Y = 1.99\ (a/W)^{1/2} - 2.47\ (a/W)^{3/2} + 12.97\ (a/W)^{5/2} - 23.17\ (a/W)^{7/2} + 24.80\ (a/W)^{9/2}$

P = maximum cyclic load

L = distance from crack plane to point of load application

a = total length of crack and notch

W = specimen width

B = specimen thickness, and

$B_N$ = net thickness at the groves.

### 4.2.3 Results and Discussion

The rates of fatigue crack growth are plotted as a function of the crack-tip stress intensity factor range on logarithmic coordinates in Figs. 1, 2, and 3 for 24, 427, and 593°C (75, 800, and 1100°F), respectively. At each temperature a single curve (obtained from regression analysis) represents the data reasonably well for the three thicknesses

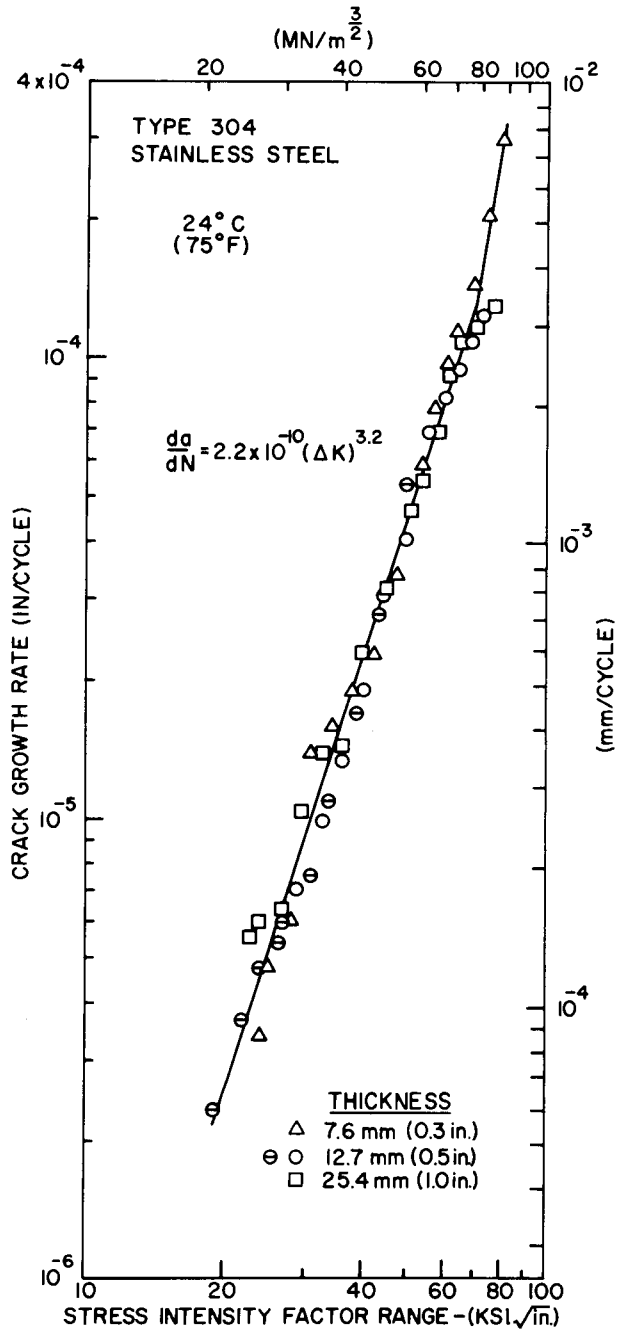


Fig. 1 - Fatigue crack growth rates as a function of stress intensity factor range for 7.6, 12.7, and 25.4 mm thickness specimens at 24°C.

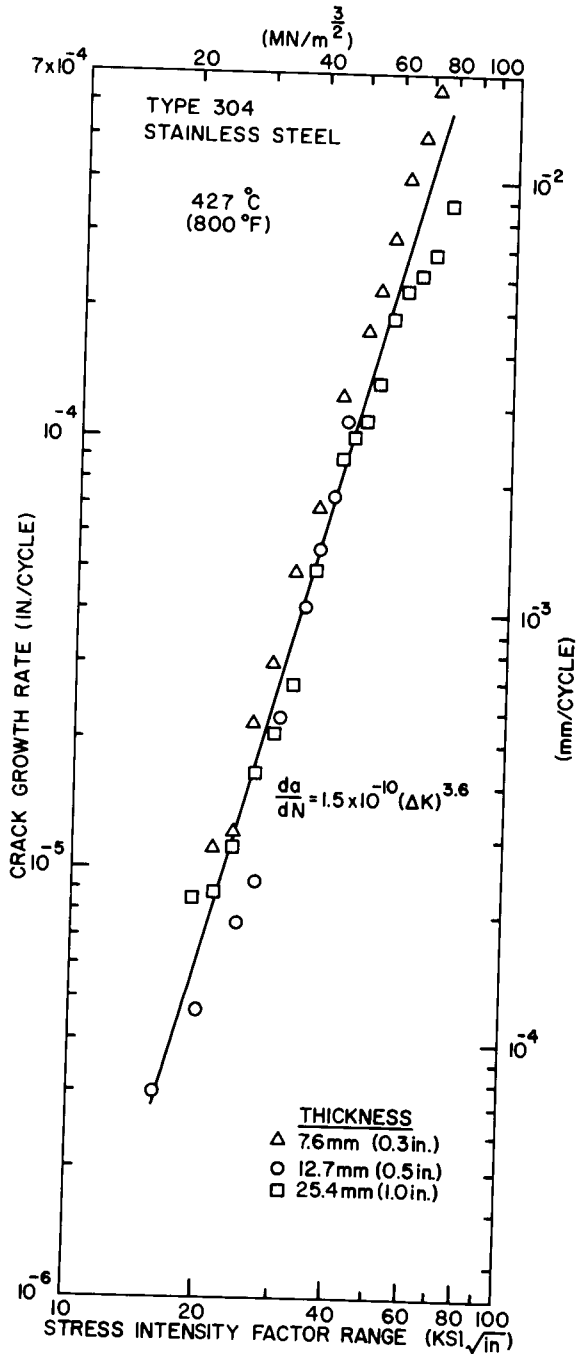


**Fig. 2 - Fatigue crack growth rates as a function of stress intensity factor range for 7.6, 12.7, and 25.4 mm thickness specimens at 427°C.**

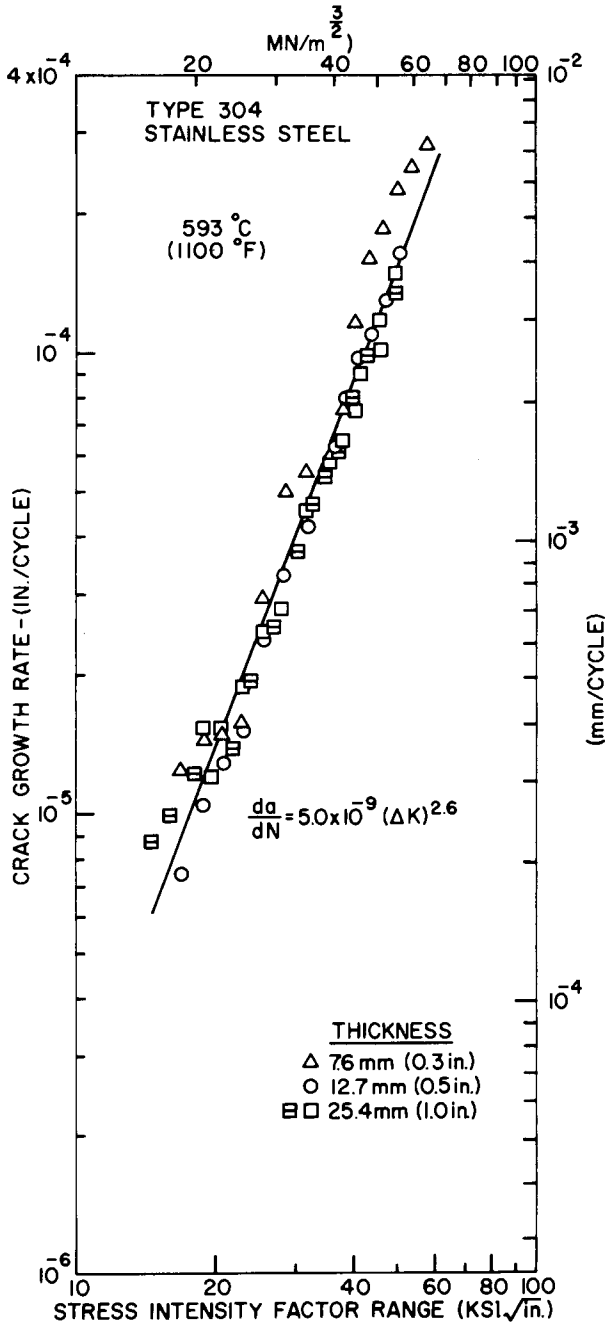


**Fig. 3 - Fatigue crack growth rates as a function of stress intensity factor range for 7.6, 12.7, and 25.4 mm thickness specimens at 593°C.**

(7.6, 12.7, and 25.4 mm). The data fall on a single straight line except for high $\Delta K$ values (>77 $MN/m^{3/2}$, >70 ksi$\sqrt{in.}$) at room temperature where a slope transition occurred. In general, the scatter in data was less at room temperature than at elevated temperatures and also less at intermediate crack growth rates than at either low or high rates. Good agreement was observed between data (da/dN versus $\Delta K$) obtained from tests run at different load levels but otherwise identical conditions.

The results show no significant effect of thickness on fatigue crack growth rate. However, it should be noted that, at a given stress intensity factor, the growth rate for the 7.6 mm (0.3 in.) specimen tend to lie on the high side of the data band at the elevated temperatures. Because the scatter in data among multiplicate tests is often about the magnitude of the observed difference, the apparent effect cannot be considered real. In any case, the change in crack growth rate that could possible be attributed to the reduction in thickness is small.

With regard to temperature dependence, crack growth rates for a given $\Delta K$ generally increased with increase in temperature. However, growth rates at 427°C and 593°C at high $\Delta K$ values were essentially equal, though considerably higher than rates for corresponding $\Delta K$ at room temperature.

The results indicate that available crack growth rate data on stainless steels obtained from specimens with thicknesses in the 7.6 to 25.4 mm range may confidently be used in the design and safety analysis of components having thickness within this same range and at temperatures of 24 to 593°C. It appears that for thicknesses less than 7.6 mm growth rates may possibly be higher although there is no direct evidence of this. Certainly caution should be exercised in applying these data to smaller thicknesses at the higher temperatures.

### 4.2.4 References

1. Shahinian, P., Smith, H. H., and Hawthorne, J.R.,"Fatigue Crack Propagation in Stainless Steel Weldments at High Temperature," Welding Journal, Research Supplement, Vol. 51, No. 11, November 1972, pp. 527s to 532s.

Table 4.1

Chemical Composition and Tensile Properties of AISI 304 Steel

Chemical Composition, weight percent

| C | Mn | P | S | Si | Cr | Ni |
|---|---|---|---|---|---|---|
| 0.048 | 1.48 | 0.025 | 0.015 | 0.52 | 18.57 | 9.45 |

Room Temperature Tensile Properties

| 0.2% Yield Strength | | Ultimate Strength | | Elongation | Reduction of Area |
|---|---|---|---|---|---|
| MPa | ksi | MPa | ksi | % | % |
| 255 | 37 | 572 | 83 | 57 | 72 |

## 4.3 THE EFFECT OF HOLD TIME ON THE FATIGUE CRACK GROWTH BEHAVIOR OF TYPE 316 STAINLESS STEEL - H. H. Smith, D. J. Michel, and H. E. Watson

### 4.3.1 Background

Previous elevated temperature fatigue studies have shown that the addition of tensile hold periods during cyclic loading can significantly increase fatigue crack propagation rates in austenitic stainless steels. The results from these studies indicate that hold time effects are related to material condition as well as being temperature dependent.[1] For example, tensile hold times of 0.1 and 1.0 minute do not produce any significant effect on crack growth rate in solution-annealed and 20 percent cold-worked Type 316 stainless steel tested in air at 427°C (800°F). At 593°C (1100°F), hold times again have no significant effect on cracking in solution-annealed specimens; however, crack growth rates in 20 percent cold-worked specimens were greatly increased with 0.1 and 1.0 minute hold times. For these results it was concluded that recovery processes rather than environmental effects contributed to the increased crack growth rates observed in the cold-worked material at 593°C (1100°F).

It is apparent that hold time effects can result from complex interactions between material factors such as strain rate, frequency, and environmental sensitivity, microstructural stability, and creep resistance. In this report, results are presented from experiments designed to compare zero and 0.1 minute hold time results at a common frequency of 5 cpm. This is in contrast to the experiments previously described in which frequency as well as hold time was a variable.

### 4.3.2 Materials and Test Procedures

The chemical composition of the Type 316 stainless steel, the specimen design, and the general test procedure have been previously reported.[2] Briefly, single-edge-notched cantilever specimens were cycled under zero-to-tension loading to a constant maximum load in air. In the present series of tests, the 5 cpm cyclic frequency was achieved by using two load wave forms and consequently different loading and unloading rates. Specimens utilized for zero hold time tests were loaded in a continuous sawtooth mode. For the hold time tests, tensile loads were imposed on the

specimen during each cycle by holding at the maximum load value for 0.1 minutes before returning to zero load.

### 4.3.3 Results

Comparisons have been made of the fatigue crack growth behavior of annealed and cold-worked Type 316 stainless steel at 427°C (800°F) tested at 5 cpm with and without tensile hold times. The experimental data were analyzed to yield crack growth rate, da/dN, as a function of the stress intensity factor range, $\Delta K$. From an examination of the results in Figs. 1 and 2, it is seen that there is no significant effect of hold time on crack growth rate at 427°C (800°F) for annealed and cold-worked Type 316 stainless steel. In Fig. 3, comparison of the 0.1 minute hold time data for annealed and cold-worked Type 316 stainless steel shows that the cold-worked material offers greater crack growth resistance at 427°C (800°F).

The similar da/dN fatigue response depicted in Figs. 1 and 2 for zero and 0.1 minute hold times suggests that the fatigue behavior at 427°C (800°F) is primarily cycle rather than time dependent. In addition, comparison of the 5 cpm zero hold time data with previously reported 10 cpm zero hold time data[1] shows identical fatigue behavior which indicates that there is a negligible effect of frequency and loading waveform in this frequency range at 427°C (800°F).

A similar series of tests are being conducted at 593°C (1100°F) and will be reported when the data become available. The present low temperature data will serve as baseline information to be used in the interpretation of the thermally activated behavior expected at higher temperatures.

### 4.3.4 References

1. Michel, D. J., Smith, H. H., and Watson, H. E., "Effect of Hold Time on Elevated Temperature Fatigue Crack Propagation in Fast Neutron Irradiated and Unirradiated Type 316 Stainless Steel," in Structural Materials for Service at Elevated Temperatures in Nuclear Power Generation, American Society of Mechanical Engineers, 1975, pp. 167-190.

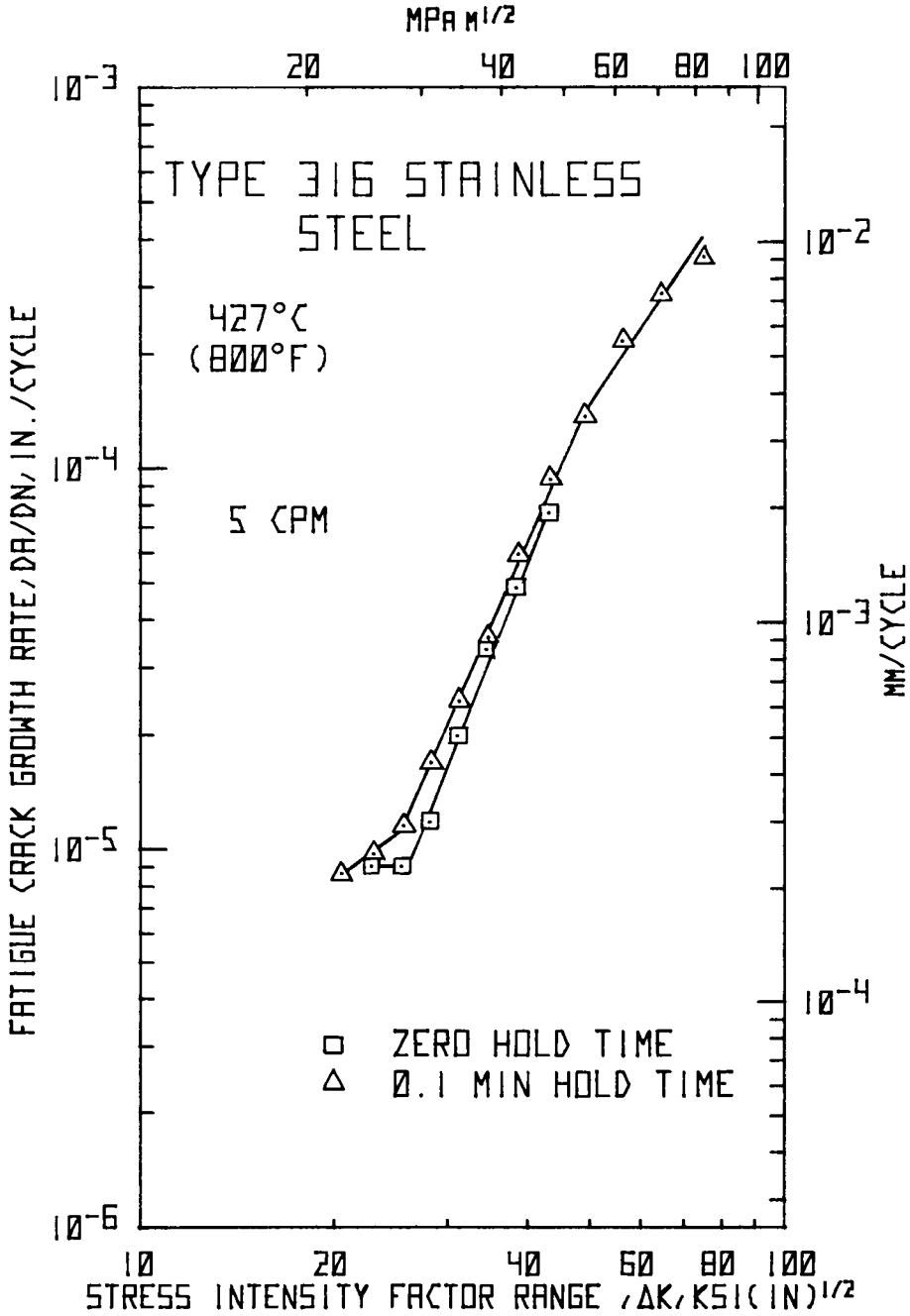


**Fig. 1 - The effect of hold time on fatigue crack growth rate, da/dN, in air at 427°C (800°F) for solution-annealed Type 316 stainless steel.**

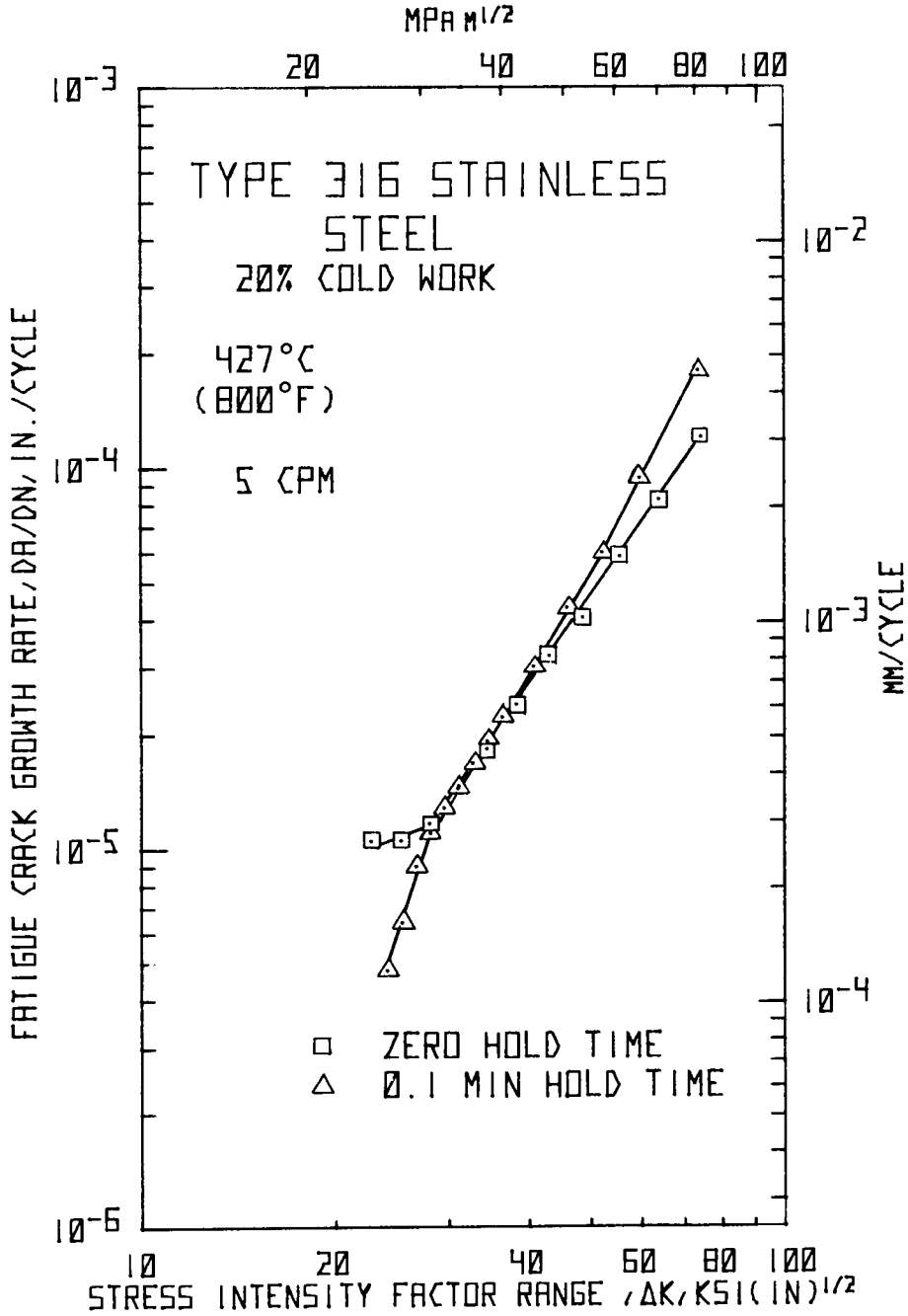


**Fig. 2 - The effect of hold time on fatigue crack growth rate, da/dN, in air at 427°C (800°F) for 20 percent cold-worked Type 316 stainless steel.**

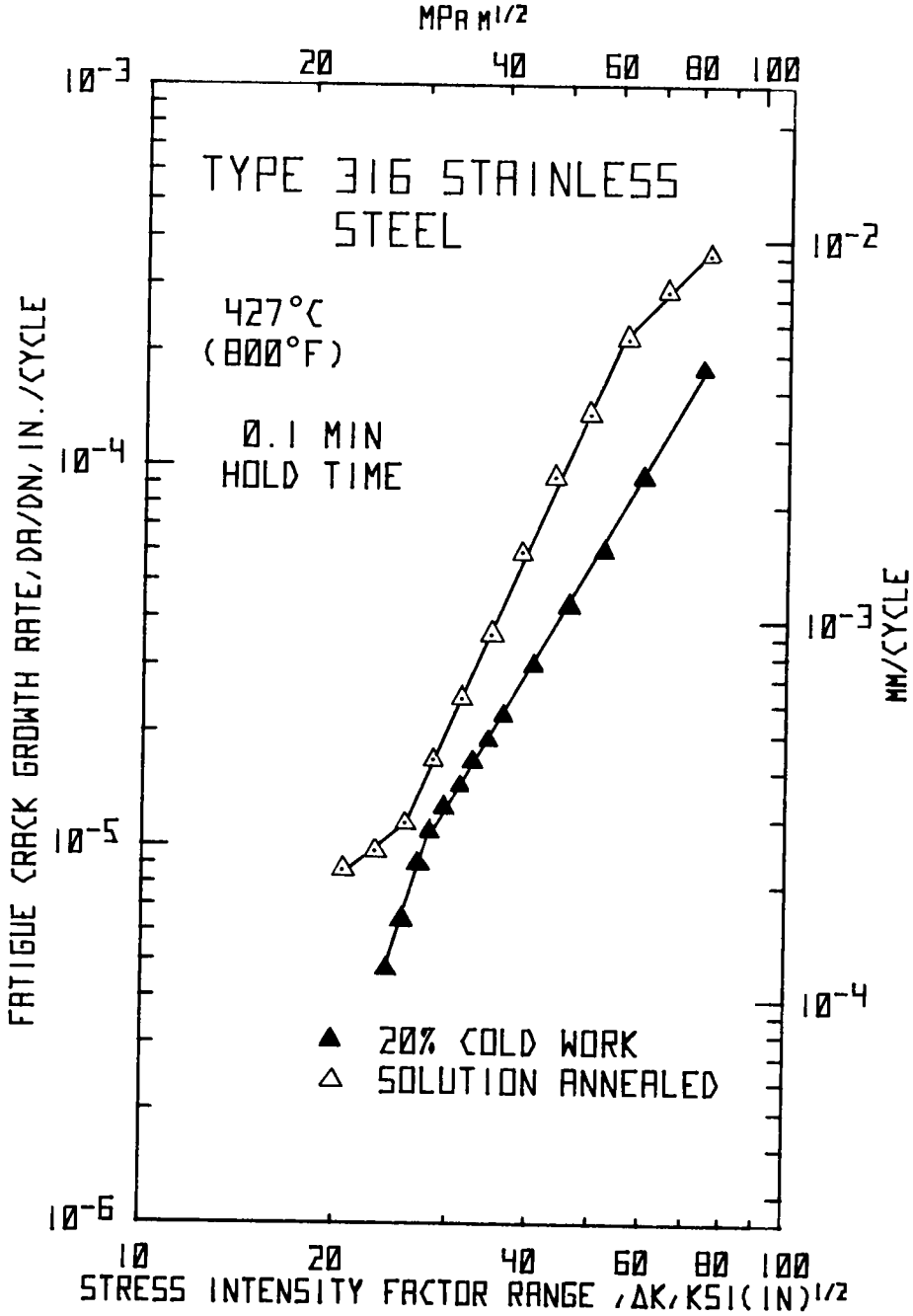


**Fig. 3 - Comparison of the fatigue crack growth behavior of solution-annealed and cold-worked Type 316 stainless steel at 427°C (800°F) for 0.1 minute hold time.**

2. Michel, D. J., Smith, H. H., and Watson, H. E., "Fatigue Crack Growth in Type 316 Stainless Steel," in Mechanical Properties Test Data for Structural Materials, Quarterly Progress Report, ORNL-4948, Oak Ridge National Laboratory, Oak Ridge, Tennessee, March 1974, pp. 157-163.

## 5. HANFORD ENGINEERING DEVELOPMENT LABORATORY

(Contribution not received in time for inclusion in this issue.)

# 6. WESTINGHOUSE ADVANCED REACTORS DIVISION

E. C. Bishop, W. E. Ray

## 6.1 INTRODUCTION

Two programs are being performed at Westinghouse Advanced Reactors Division (ARD). The first program is "Validation of High Temperature Design Methods and Criteria" (189a CW063). Two of the tasks in this program are "Basic Specimen Testing" and "Tubular Specimen Testing". The specimen material for both tasks was supplied from the ORNL reference heat of Type 304 stainless steel and future tests will include specimens from the reference heat of Type 316 stainless steel. The second program is "Component Materials Compatibility" (189a CW065). One of the tasks in this program is "Mechanical Properties."

The basic specimen tests are performed on plates and bars loaded at 1100°F (593°C). Specimen designs have been selected to provide nonuniform stress distributions (uniaxial, plane stress, and plane strain) and to determine the effects of holes, notches, and welds in various orientations. Uniform and stepped loading is applied at levels sufficient to cause significant creep strain in hundreds of hours and rupture in several thousand hours. Test data are used for: verification of constitutive equations for time-dependent material response, validation of analytical techniques for nonuniform stress states, and investigation of strain limits in base metal, welds, and at geometrical discontinuities.

The tubular specimen tests are being run at 1100°F (593°C) with various combinations of internal pressure and axial load to produce a uniform stress state with a range of biaxiality. Load levels have been selected to determine secondary creep rates in 2000 hours with both steady state and stepped loading. A limited number of tests will be continued to rupture with geometrical discontinuities. The test data are primarily used for verification of constitutive equations and validation of analytical techniques for shells under multiaxial states of stress.

Westinghouse ARD is performing experiments to identify the effects of a flowing sodium environment on the mechanical properties of LMFBR

structural components. The present scope of the program involves three materials: Type 316 stainless steel, Type 304 stainless steel, and Inconel 718. Work on these materials is in support of the CRBRP upper plenum and hot leg piping components design. Inconel 718 is also being evaluated on a limited basis, relative to the thermal transients to be experienced by the thermal baffles in the upper plenum of the FFTF reactor. More extensive evaluations of the material for the CRBRP will follow. Low-cycle fatigue, creep-fatigue, and creep-rupture experiments are being performed in flowing sodium at elevated temperatures on as-fabricated, aged, and sodium pre-exposed samples in order to identify the environmental effects. In addition, in-air experiments are being performed on the same materials to obtain baseline data.

This report covers the work performed during the period from August 1 to October 31, 1975.

## 6.2 BASIC SPECIMEN TESTING - M. J. Manjoine (Westinghouse Research Laboratories)

The tests in progress at 1100°F or under preparation are shown in Table 6.1

TABLE 6.1

TESTING STATUS

| Test No. and Description | Loading | Stress (ksi) | Accumulated test time, hours |
|---|---|---|---|
| CAW-1 Central hole in axial weld | Monotonic | 18 | 12,765 |
| BTW-2 Transverse weld | Monotonic | 19 | 4,720 |
| CTW-1 Central hole in transverse weld | Monotonic | 23 | In Preparation |
| DTW-1 Notched transverse weld | Monotonic | 29 | 4,795 |

| Test No. and Description | Loading | Stress (ksi) | Accumulated test time, hours |
|---|---|---|---|
| E-2 Combined tension & bending | Monotonic | 18(avg.) | 8,500 |
| C-4 Plate with hole | Monotonic | 18 | In Preparation |
| D-6 | Monotonic | 20 | 15,660 |

6.2.1 Strain Distribution in Weldments

Circumferential and longitudinal welds in pressure vessels and piping are usually loaded under conditions of plane strain, that is, the strain or creep rate in the longitudinal direction essentially vanishes. This report describes the creep and rupture characteristics at 1100°F (593°C) of type 304 models welded with type CRE 308 weld metal. These weldments contain zones of different compositions and thermal history, (Base metal, heat affected zone (HAZ), weld metal), therefore, the weld introduces a metallurgical and rheological discontinuity.

The purposes of this creep-rupture program are as follows:

a) Obtain the strain distributions of models with several states of stress as a function of stress and time.

b) Compare these distributions with the results of computer programs to validate and qualify the methods of analysis.

c) Determine the rupture initiation and propagation characteristics under the various states of stress and for the strain rates associated with different stress levels.

d) Investigate the strain instabilities and the magnitudes at rupture initiation for weldments under different states of stress.

e) Formulate damage criteria and strain limits under steady loading for axial and transverse welds.

6.2.1.1 Test Models

Model GAW is a flat plate whose width, w, is ten times the thickness, t, with a central axial weld of width 2t (20% of w) and loaded in the

axial direction where the effective length is about 4t. The heads at the ends of the axial length are reinforced and laterally constrained so that the plastic strain in the width direction is prevented and, therefore, a condition of plane strain is generated at the heads and is maintained over the short gauge length. Model BA is the same except that the uniform length is increased to 9t, about equal to the width. The degree of lateral constraint diminishes toward mid-length. These models with the weld and the maximum principal stress in the axial direction simulates a circumferential weld in a pipe under internal pressure.

Models GT and BT have the same type G and B gauge dimensions but the weld is transverse at mid-length. The maximum principal stress is perpendicular to the weld, thus, these models simulate a longitudinal weld in a pipe under internal pressure.

Models CA and CT have the type B geometry with a central hole of diameter t in an axial or transverse weld of width about 2t. The hole introduces a local stress and strain concentration in the weldment and enables a study of this effect on rupture initiation and propagation.

Model D is a round bar with a circumferential notch to produce multiaxial stress. Type DT has the notch root entirely within the weld. Type DTZ has the notch root at the heat affected zone for part of the circumference. Because of the irregular shape of the narrow HAZ it is difficult to locate the notch root for more than a part of its circumference.

#### 6.2.1.2 Test Results

The axial strain distribution at the centerline of the axial weld of specimen model GAW-1 is given in Fig. 6.1 for several time periods in a test at an average stress of 23 ksi (158.6 MPa). These measurements were taken from photographic records of grid lines on the model. Early in life the strain increases from the fillet and it levels off over the uniform section. The lateral stress increases with creep strain and is a minimum at mid-length. The strain, therefore, peaks near mid-length later in life.

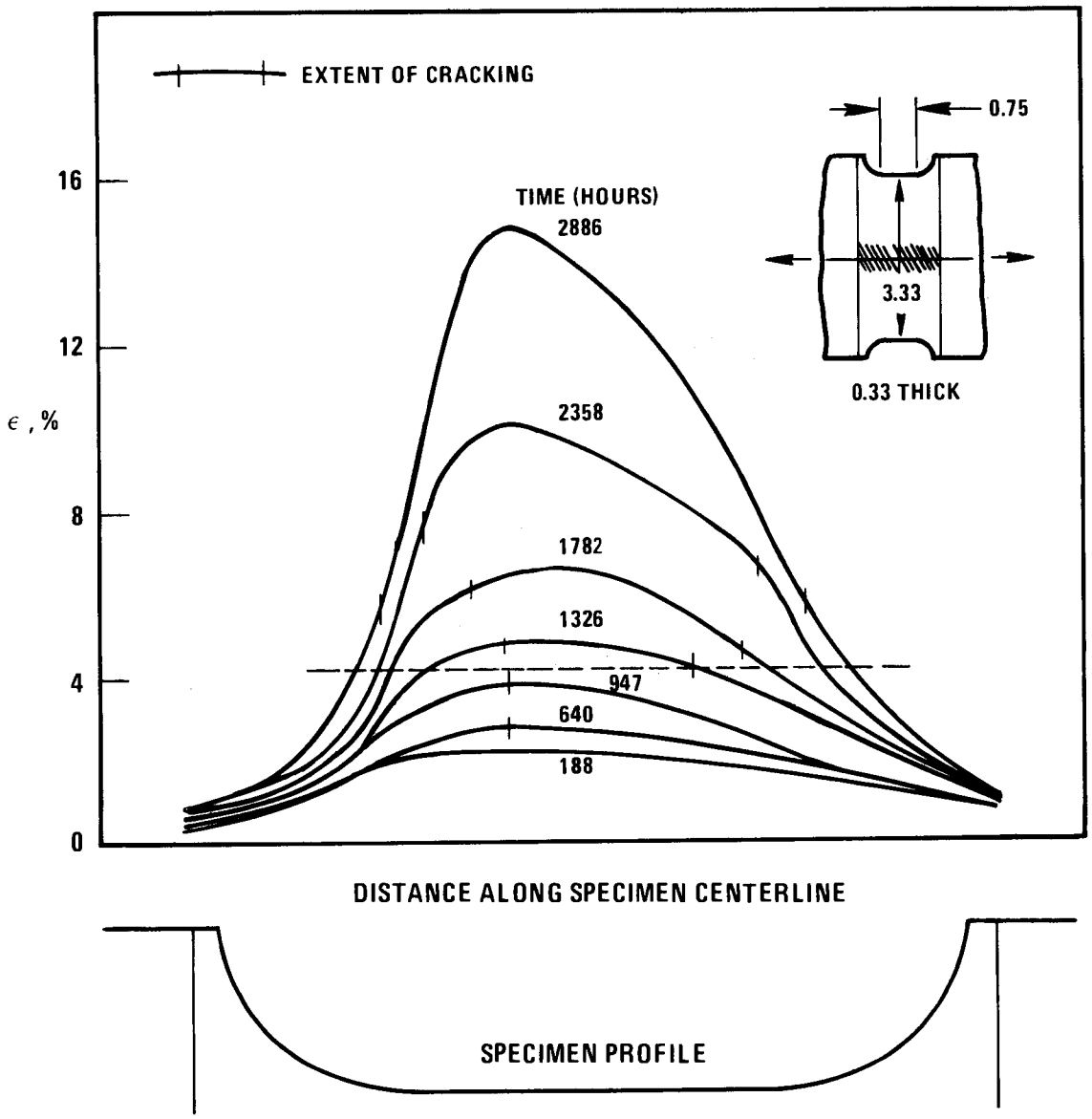


Figure 6.1. Axial Strain Distributions Along Centerline of Specimen GAW-1 (Plate With Central Axial Weld At 23 ksi And 1100°F

8307-1

Surface voids were observed at 640 hours (20% of life) in the HAZ near mid-length where the strain was the highest at about 3%. These voids grew with continued creep to form cracks which were oriented perpendicular to the maximum principal stress direction (axial), Fig. 6.2. The time estimated for these cracks to grow through the thickness is about 1000 hours (30% of life) which is the same time as that for rupture of the base metal at 23 ksi. As the creep continues additional cracks form in a regular axial spacing along each HAZ where the strain is over 4% for the average creep rate of $3 \times 10^{-3}$%/hour. The extent of cracking is marked for each time period in Fig. 6.1.

Crack propagation rate was very low in the direction of the weld and although the rate in the direction of the base metal was higher, it required 2/3 of the rupture life of 3096 hours to transverse the cross section. This latter propagation rate was nearly proportional to the creep rate of the base metal beyond the crack tip, Fig. 6.3. The rupture time of the axial weld model was about three times that estimated for the base metal.

Fig. 6.4 illustrates the crack pattern for the longer gauge length specimen, type BAW. The lighter area of the fracture face results from the slow crack propagation through the thickness and shows the crack front which progresses to the final overload rupture.

For the models GT or BT the voids and cracks again initiate in the HAZ in a direction perpendicular to the maximum principal stress and at about the same time as that estimated for an axial under the same loading. However, the cracks form at each edge of the transverse weld and propagate through the HAZ toward the axial center, Fig. 6.5, and at a higher rate than that estimated for the base metal of the axial weld. The propagation rate through the thickness was much slower for this transverse weld so that the initiated cracks met near the center of the cross section (which is ten times the thickness) while it propagated through the thickness. The rupture time of the transverse weld models are about the same or slightly less than that of the base metal.

The distributions of the strains at fracture are shown in Fig. 6.6 for a type B geometry with central transverse weld (BTW-1). Because of

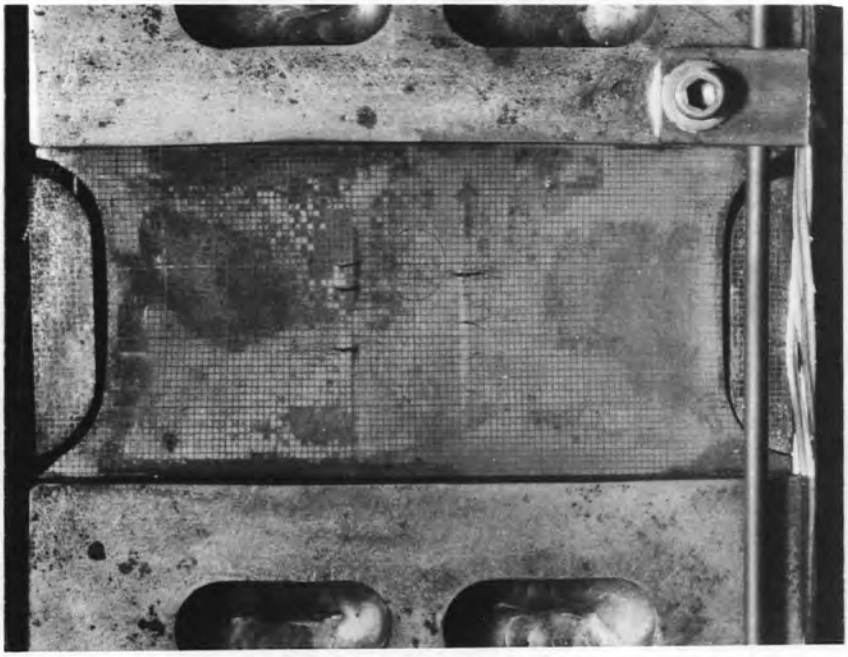

(a) VIEW OF CRACKING AT HEAT EFFECTED ZONES

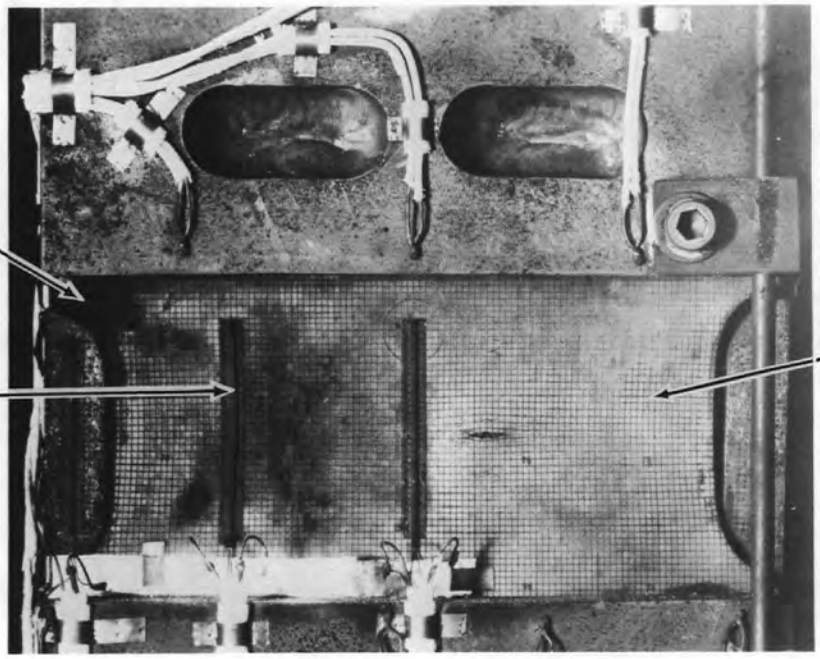


(b) VIEW OF CRACKING ON SIDE OPPOSITE (a)

Figure 6.2. Specimen GAW-1 After 2886 Hours At 23 ksi And 1100°F

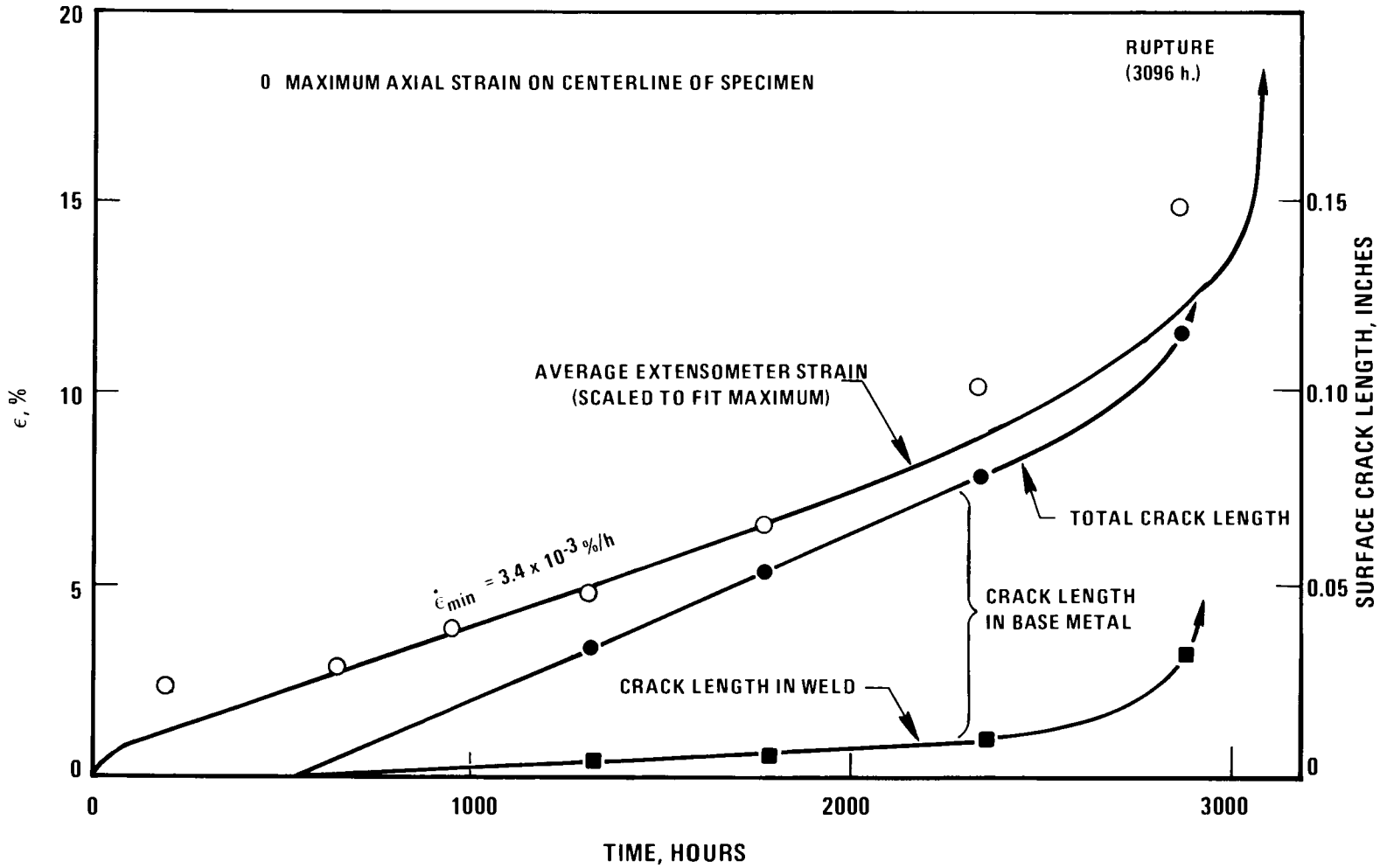


Figure 6.3. Increase Of Axial Strain And Surface Crack Length With Time In Specimen GAW-1 (Plate With Central Axial Weld At 23 ksi And 1100°F)

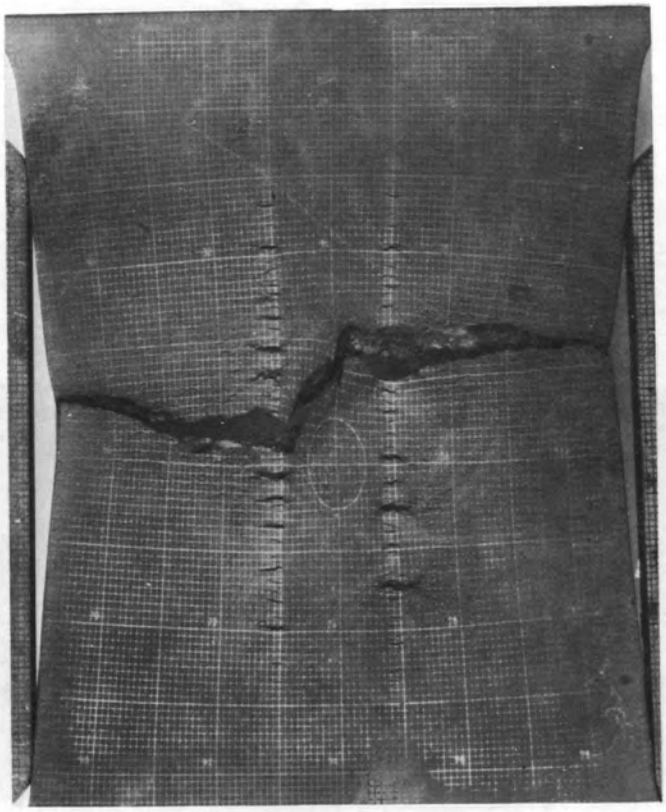

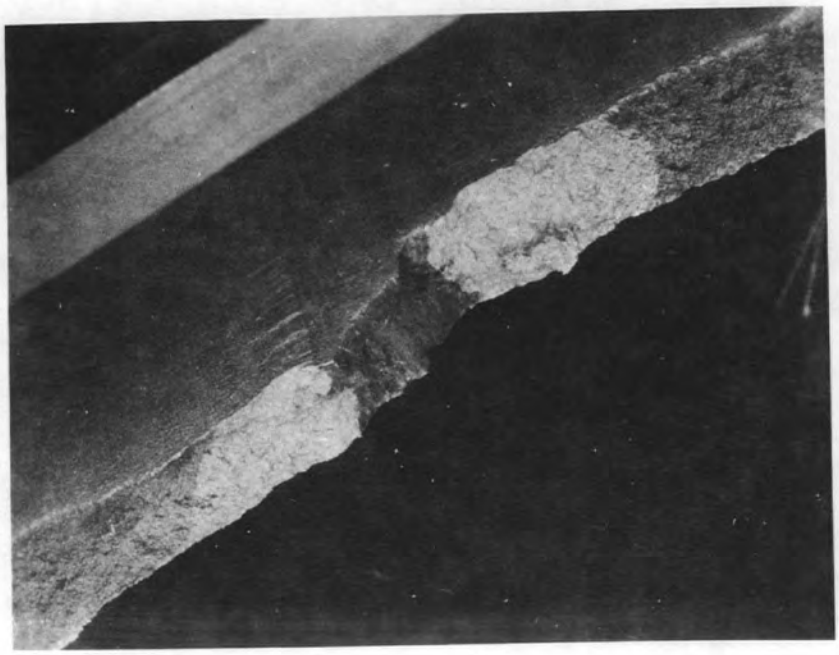

Figure 6.4. Fracture Of Axial Weld Model, BAW-1, After 1532 Hours At 25 ksi

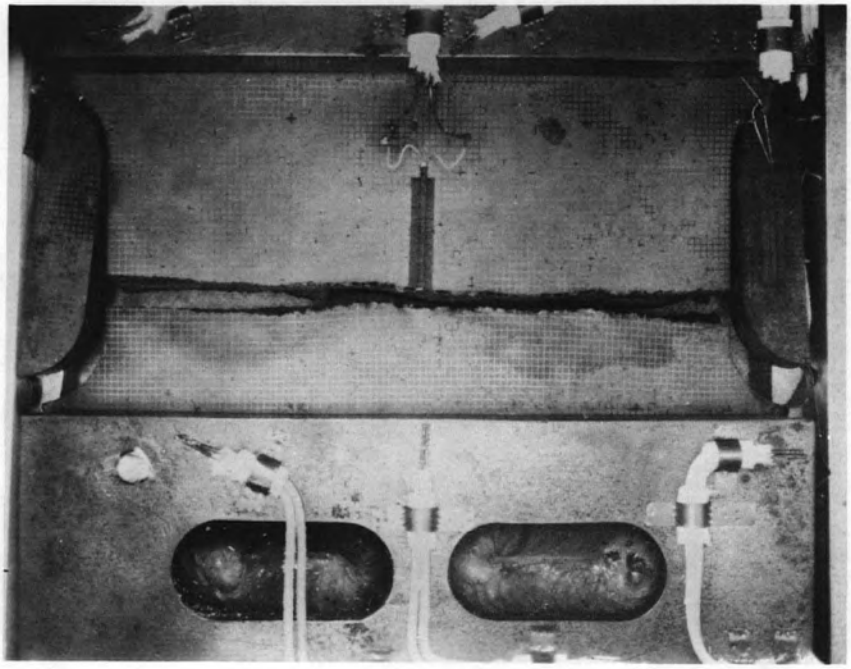

Figure 6.5. Fracture Of Transverse Weld, Model GTW-1, After 448 Hours At 25 ksi

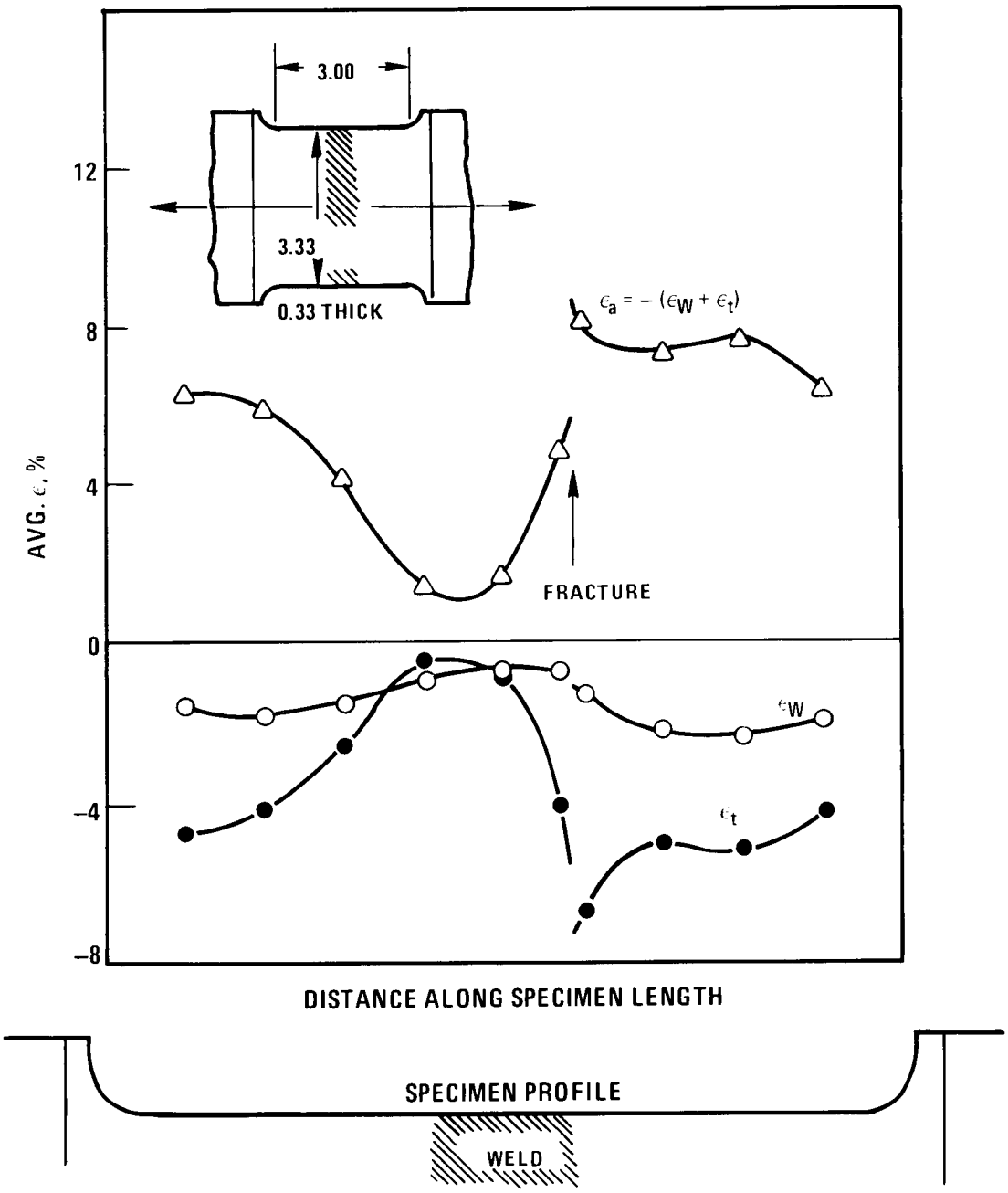


Figure 6.6. Distribution Of Average Strains Along The Length Of Specimen BTW 1 After Rupture At 1734 Hours (Plate With Central Transverse Weld At 21 ksi And 1100°F)

8307-3

lateral constraint at the heads and the higher creep strength of the weld, the lateral strain, $\varepsilon_W$, is small over the entire gauge length. The thickness and axial strains decrease from the heads to the center of the weld, except for the final failure line at the HAZ.

### 6.2.2 Notched Bars

Transverse weld specimens were prepared with circumferential notches whose roots were either entirely in the weld, type D7, or at some points along the HAZ, type DZT, Fig. 6.7.

The rupture life of the notch DT welds was about 20 times that of the unnotched base metal, about 8 times that of the notched base metal and greater than that of the all-weld metal, Fig. 6.8.

The average rupture lives of the notched HAZ were about the same as the unnotched base metal and the tests showed a high variability because of the difficulty of intersecting the HAZ around the circumference of the notch root.

In general the rupture strength of type CRE 308 welds for lives of up to 5000 hours is equal to or greater than that of the base type 304 material, Fig. 6.8. Cracks initiate in the HAZ of welds perpendicular to the direction of maximum principal stress at about the same time as that observed for the base metal. The crack growth rate in the weld metal is much lower than that in the base metal or HAZ. The growth rate is nearly proportional to the creep rate in the same plane in front of the crack tip. The rupture life of a welded model or component is therefore a function of the direction of the maximum principal stress and the creep strain. For crack initiation the critical strain limit at creep rates near $10^{-3}$%/h is about 4%.

## 6.3 TUBULAR SPECIMEN TESTING

All creep testing of Type 304 SS for tubular specimens has been completed. Three specimens with a creep duration of 2000 hours are currently being tested to failure. All 304 SS data have been processed and corrections made for variability in the extensometer responses. The data were fitted to a single exponential creep equation and the constants determined. Good correlation was observed between predicted and observed readings. 316 SS specimens are being prepared for testing with primary effort on heat treatment control.

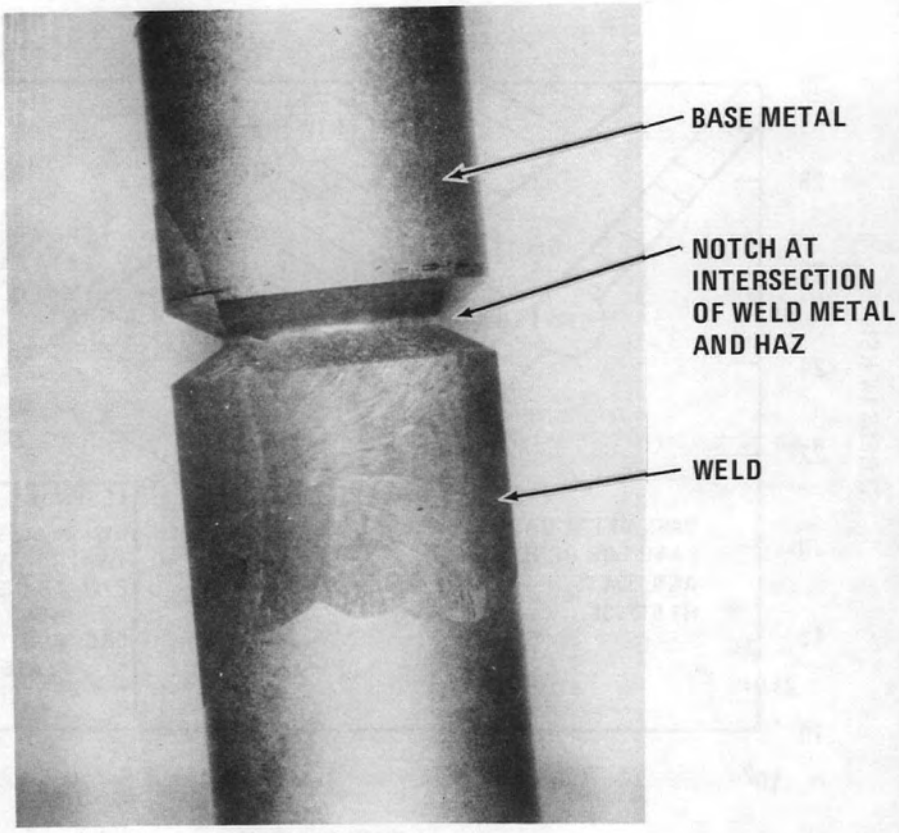


Figure 6.7. Specimen DZTW

6593-38

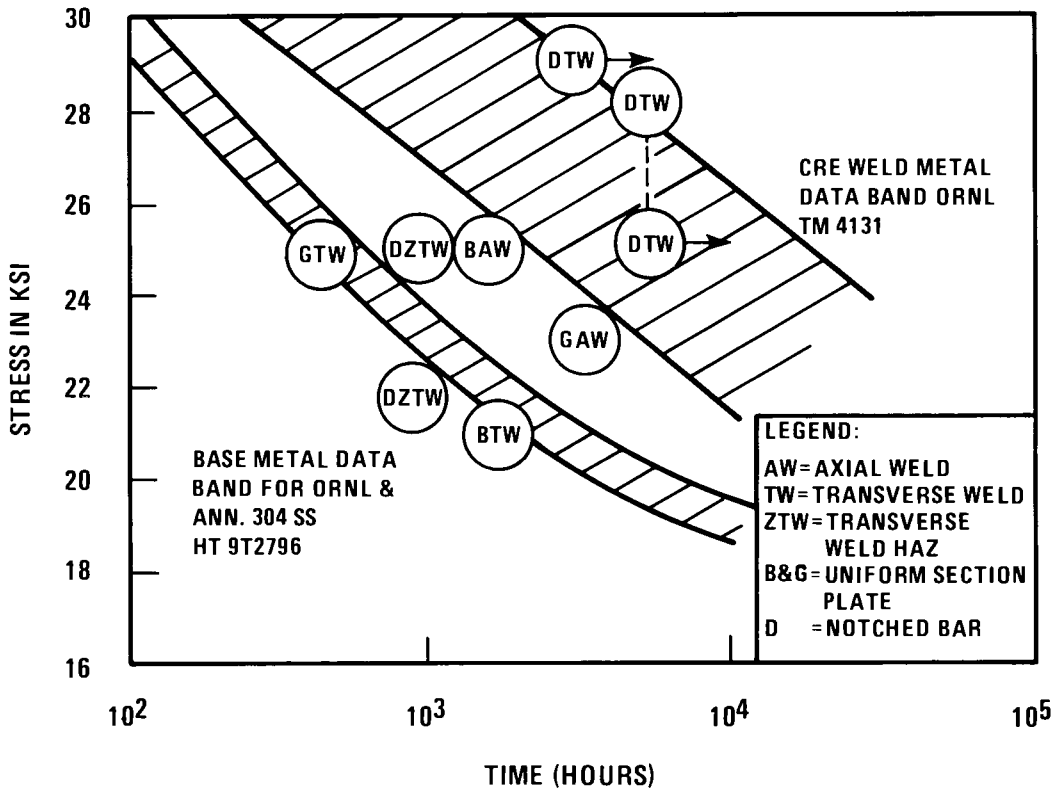


Figure 6.8. Basic Specimen Rupture Data for Welds at 1100°F

8037-5

## 6.4 SODIUM EFFECTS ON MECHANICAL PROPERTIES OF STRUCTURAL MATERIALS - S. L. Schrock, P. N. Flagella, J. Kahrs, J. Denne, P. Wu

### 6.4.1 Type 316 Stainless Steel

Mechanical property evaluations for solution annealed Type 316 stainless steel, as affected by a flowing sodium environment, involves two heats of the material. The first heat, purchased by Westinghouse ARD, involves a limited number of test samples fabricated from bar material. Sodium exposure and thermal aging of the samples was performed previously. Mechanical property tests in sodium of these samples provides an indication of the effect of the environment, including pre-treatment.

The second heat of solution-annealed Type 316 stainless steel to be used for the evaluations was obtained from the HEDL stockpile (Heat 65805) and is in plate form (1.0" thick). The larger number of test samples from this heat will allow a more detailed study on the mechanical effects of a sodium environment. Sodium exposure and thermal aging of samples at different temperatures for different amounts of time, prior to testing in sodium and in air, is presently in progress.

Creep-rupture tests of samples from the ARD heat of material were initiated early in this reporting period. Four samples, each with a different prior history, were creep-rupture tested in flowing sodium at 1100°F and 32.5 ksi. Table 6.2 lists the pre-treatment for each sample along with a summary of the test results. Figures 6.9.A and 6.9.B present the creep curves for each test in terms of both the total strain (including the strain-on-loading) and the creep strain. Although all four tests were performed on samples from the same heat of solution-annealed Type 316 stainless steel and at the same test conditions, significant differences are seen, obviously resulting from the different pre-treatments. Somewhat surprising is that the strain-on-loading for the as-fabricated sample is almost twice that of the pre-treated samples. This is apparently due to the fact that the as-fabricated sample is in the solution annealed condition and has a low dislocation density. This is also supported by the fact that the time to secondary creep is much longer for the as-fabricated sample. On the other hand, the pre-treated

Table 6.2 Creep-Rupture Data for Solution Annealed Type 316 SS[a] Tested in Flowing Sodium at 1100°F and 32.5 ksi[b]

| Sample Number | Pre-Treatment for 5,000 hr. | | Loading Strain, % | Hours to Indicated Creep Strain, % | | | | | | | Min. Creep Rate, %/hr. | 0.2% Offset | | Time to Rupture hr. | Total Elong. % | |
|---|---|---|---|---|---|---|---|---|---|---|---|---|---|---|---|---|
| | Envir. | Temp. °F | | 0.5 | 1.0 | 2.0 | 3.0 | 5.0 | 7.0 | 10.0 | | Time hr. | Creep Strain % | | Creep Curve | Post Test |
| 030 | As-Fabricated | | 8.10 | 1.7 | 5.1 | 16.0 | 36.0 | 125 | 268 | 446 | $1.80 \times 10^{-2}$ | 487 | 11.0 | 684 | 29.3 | 29.7 |
| 033 | Sodium | 1200 | 4.32 | 2.7 | 9.1 | 32.7 | 64.8 | 135 | 200 | 280 | $2.90 \times 10^{-2}$ | 218 | 7.7 | 705 | 72.3 | 75.0 |
| 037 | Sodium | 1325 | 4.62 | 3.2 | 10.3 | 27.0 | 46.2 | 82.0 | 117 | 168 | $5.60 \times 10^{-2}$ | 170 | 10.2 | 456 | 63.9 | 64.0 |
| 031 | Argon | 1325 | 3.40 | 2.9 | 7.1 | 18.4 | 37.0 | 77.0 | 118 | 185 | $5.38 \times 10^{-2}$ | 242 | 13.4 | 572 | 80.6 | 79.7 |

(a) WARD Heat
(b) Bar samples, 0.25" dia. x 1.00" lg. gage section

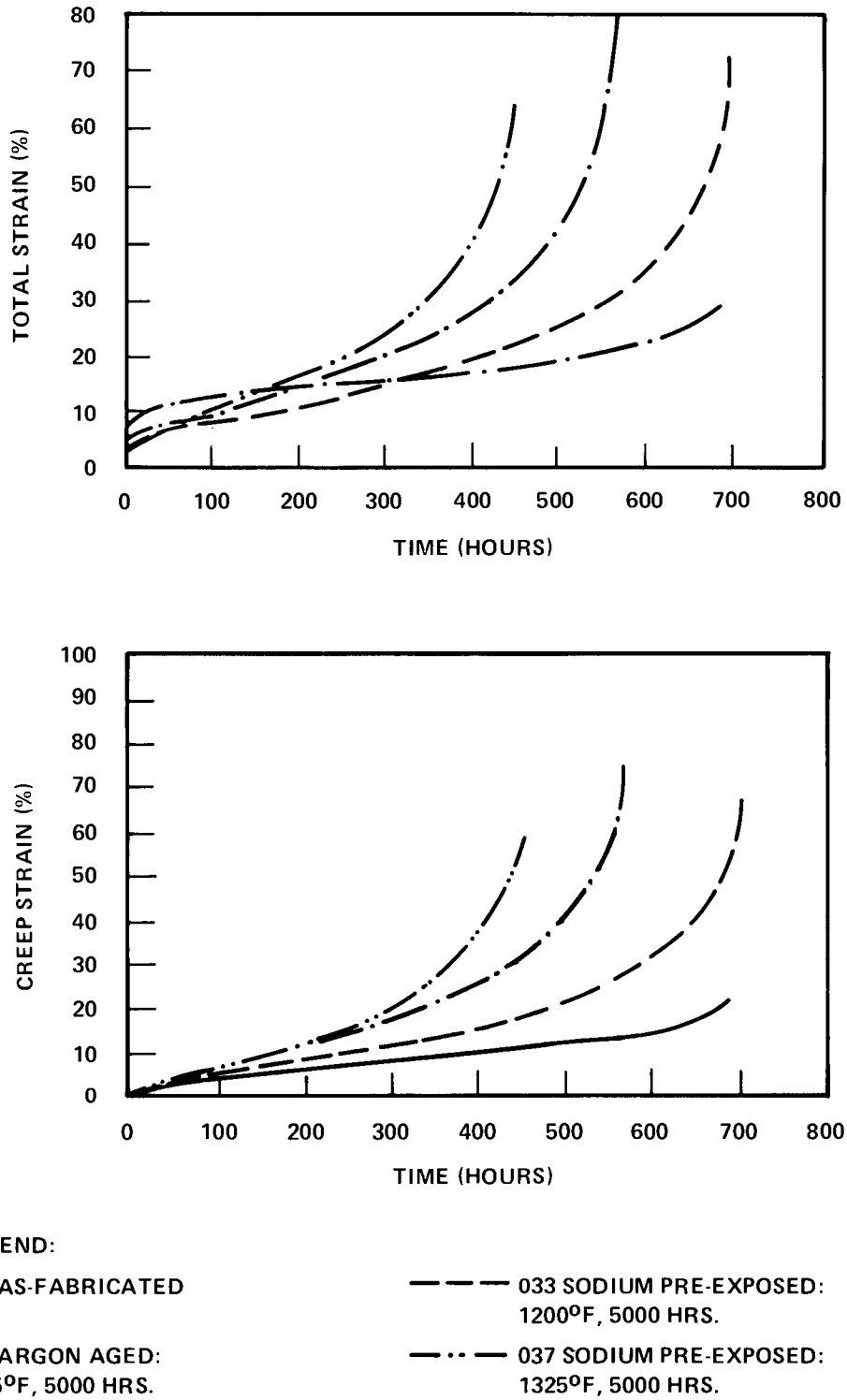


Figure 6.9.A. Creep Curves For S.A. Type 316 S.S. Tested In Flowing Sodium At 100°F And 32.5 KSI

8327-1

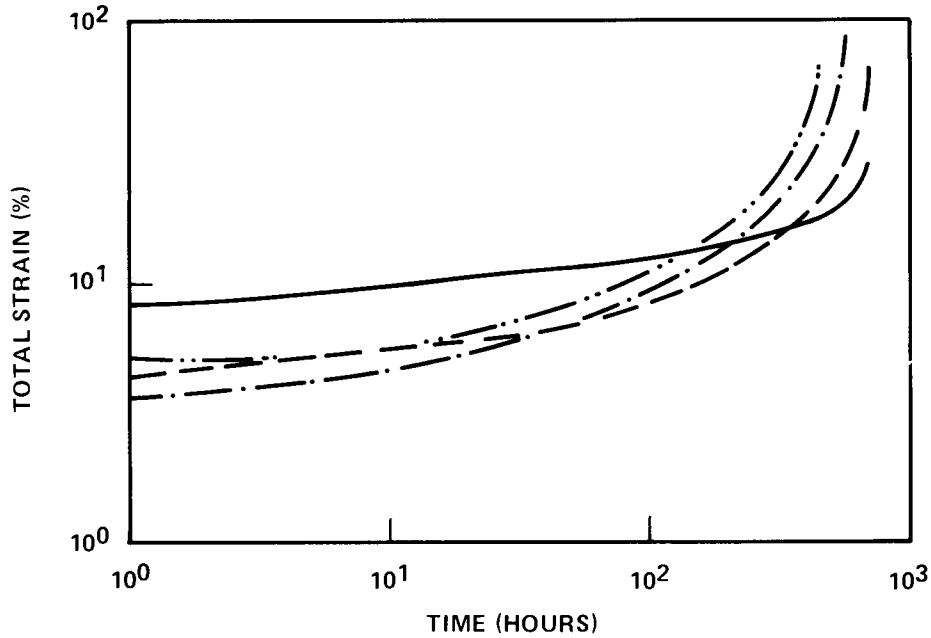


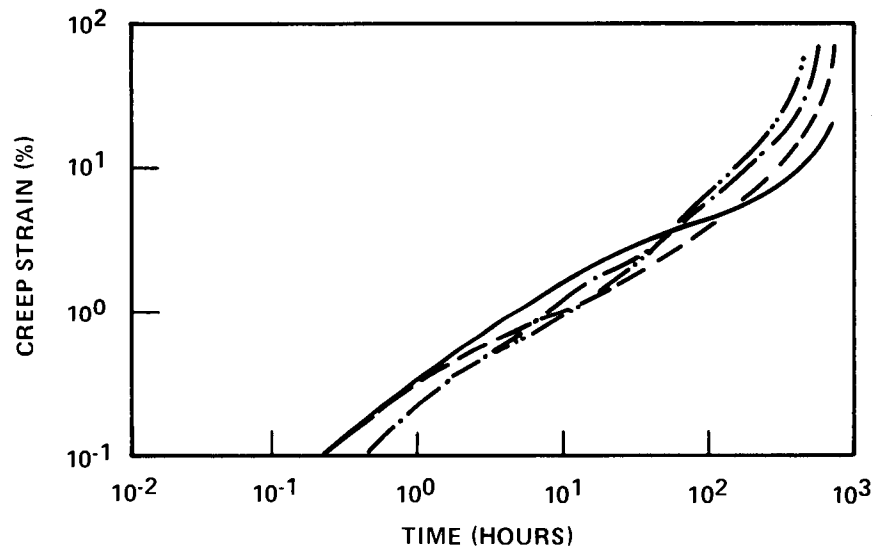


LEGEND:

——— 030 AS-FABRICATED

— — — 033 SODIUM PRE-EXPOSED: 1200°F, 5000 HRS.

—·— 031 ARGON AGED: 1325°F, 5000 HRS.

—··— 037 SODIUM PRE-EXPOSED: 1325°F, 5000 HRS.

Figure 6.9.B. Creep Curves For S.A. Type 316 S.S. Tested In Flowing Sodium At 1100°F And 32.5 KSI

8327-2

samples probably contain varying amounts of precipitates inhibiting dislocation motion during the loading. The minimum creep rate for the sample sodium pre-exposed at 1325°F is approximately three times that of the as-fabricated sample whereas the sample sodium pre-exposed at 1200°F is approximately twice that of the as-fabricated sample, indicating a strong influence of pre-treatment temperature on the minimum creep rate. The fact that the sample which was pre-exposed to sodium at 1325°F has a higher minimum creep rate than the sample which was argon aged at 1325°F indicates a possible sodium effect. Additional data will be required to confirm this observation. In terms of ductility, all pre-treated samples have a total elongation at rupture of more than twice that of the as-fabricated sample.

Additional creep-fatigue tests of the ARD heat of solution annealed Type 316 SS material were performed in flowing sodium at 1100°F during this reporting period. A summary of the test results (Sample Numbers 111, 041, and 131) are included in Table 6.3. Since this completes the fatigue and creep-fatigue testing of available samples from the ARD heat of material, Table 6.3 presents all the tests performed. A comparison of the in-sodium creep-fatigue results for zero and 0.1 hour hold times to in-air results for hold times to five hours reported in the literature[1] is shown in Figure 6.10. Hold times were performed in the tensile mode only. Test samples pre-treated for 5,000 hours prior to testing in sodium show significant increases in fatigue life in all cases when compared to both the in-air and in-sodium tests of as-fabricated samples, at the total strain range of 1%. The as-fabricated sample, tested in sodium with no hold time gave essentially the same fatigue life as the in-air data, whereas the 0.1 hour hold time test in sodium was almost 40% greater in fatigue life. This may be due to experimental scatter, but is more probably the environmental sodium effect, influenced by the test time. The in-sodium test with zero hold-time required only 3.2 hours of testing, whereas the 0.1 hours hold-time test involved 62 hours of testing.

In order to evaluate the in-air vs. in-sodium pure fatigue (zero hold time) results more accurately, an in-air test was performed at the same conditions, using an as-fabricated sample from the ARD heat of

Table 6.3 Low Cycle Fatigue Data for Solution Annealed Type 316 SS[a] Tested in Flowing Sodium at 1100°F[b]

| Sample Number | Pre-Treatment for 5000 hr. | | Strain Range,% | | Hold Time[c] (hours) | Stress Range[d] (ksi) | Fatigue Life ($N_f$) |
|---|---|---|---|---|---|---|---|
| | Environment | Temp. (°F) | $\Delta\varepsilon t$ | $\Delta\varepsilon p$ | | | |
| 122 | Sodium | 1325 | 0.51 | 0.25 | 0 | 47.9 | 56,201 |
| 114 | Argon | 1325 | 0.51 | 0.31 | 0 | 50.3 | 49,753 |
| 110 | Argon | 1200 | 0.51 | 0.24 | 0 | 50.9 | 43,419 |
| 118 | Sodium | 1200 | 0.51 | 0.27 | 0 | 51.1 | 38,765 |
| 130 | As-Fabricated | | 0.51 | 0.19 | 0 | 73.8 | 54,670 |
| 113 | Argon | 1325 | 1.03 | 0.69 | 0 | 68.2 | 9602 |
| 123 | Sodium | 1325 | 1.03 | 0.62 | 0 | 65.0 | 7950 |
| 119 | Sodium | 1200 | 1.01 | 0.66 | 0 | 70.0 | 5711 |
| 109 | Argon | 1200 | 1.01 | 0.62 | 0 | 67.8 | 4842 |
| 128 | As-Fabricated | | 1.00 | 0.61 | 0 | 86.8 | 2356 |
| 115 | Argon | 1325 | 1.01 | 0.69 | 0.1 | 70.0 | 2093 |
| 124 | Sodium | 1325 | 0.99 | 0.68 | 0.1 | 64.3 | 1744 |
| 111 | Argon | 1200 | 1.00 | 0.67 | 0.1 | 65.9 | 3132 |
| 117 | Sodium | 1200 | 1.02 | 0.67 | 0.1 | 71.0 | 2518 |
| 041 | As-Fabricated | | 0.99 | 0.61 | 0.1 | 84.4 | 616 |
| 131 | As-Fabricated | | 1.00 | 0.58 | 0 | 81.8 | 1842[e] |

(a) ARD Heat
(b) Strain Rate: $4 \times 10^{-3}$ $sec^{-1}$
Control Mode: Axial Strain
Wave Form: Triangular, zero mean strain

(c) Tension only
(d) At $N_f/2$ (maximum stress range for hold-time tests)
(e) Tested in air

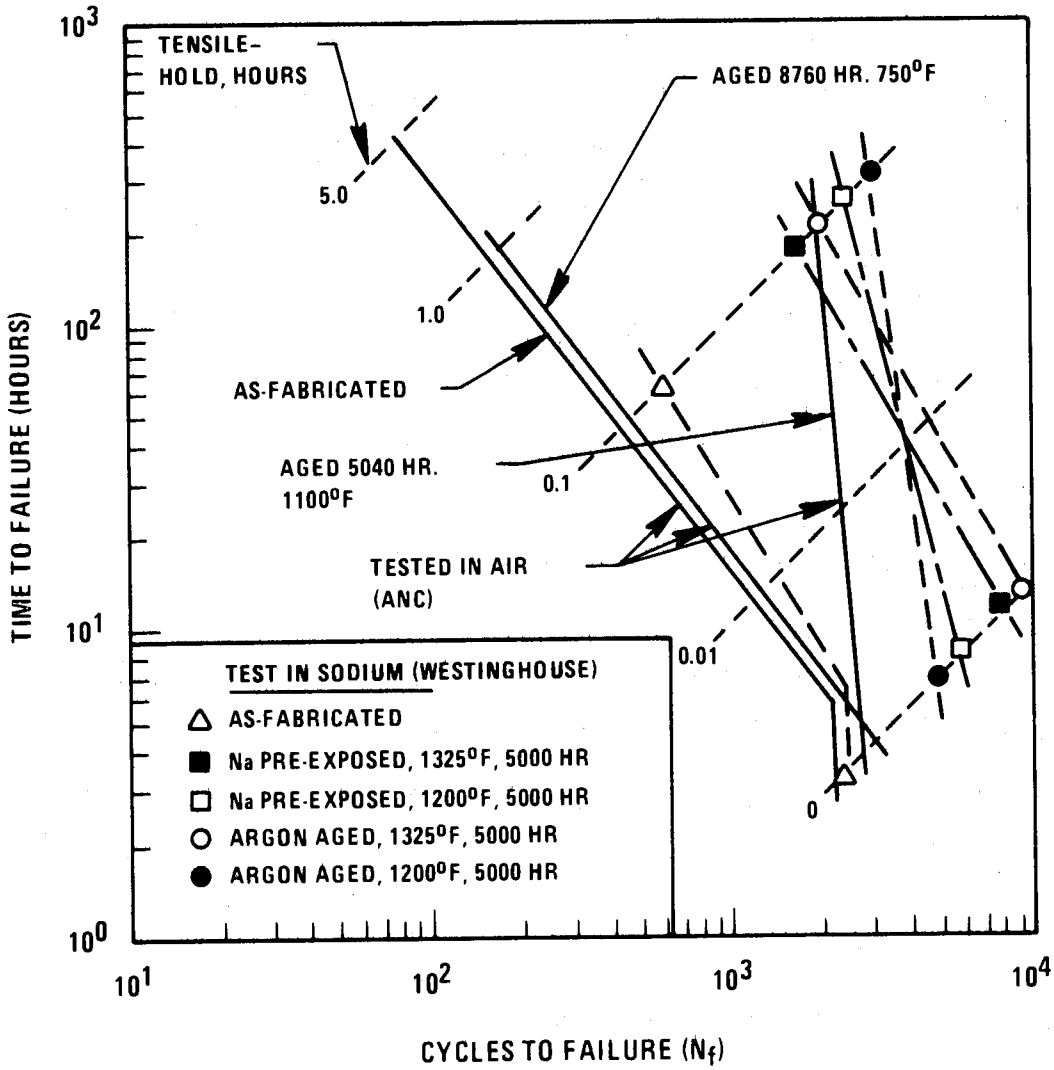


Figure 6.10. Comparison Of Creep-Fatigue Results For S.A. Type 316 SS Tested In Air And Sodium At 1100°F And $\Delta\epsilon_t \approx 1\%$ ($\dot{\epsilon} = 4 \times 10^{-3}$ Sec$^{-1}$)

8327-4

material. Results of the test are given in Table 6.3. The test was unique in that the same in-sodium test system was used with the sodium providing the test temperature. With the gage section of the test sample enclosed in a bellows, low-velocity air was allowed to flow past the gage section. Results of the test show good agreement with the in-sodium test (within experimental scatter) indicating no significant sodium effects for short time tests.

Although the sodium effect is not clear for the pre-treated samples with zero hold time (pure fatigue), the 0.1 hour hold-time tests for the sodium pre-exposed samples gave a lower fatigue life when compared to the argon aged samples. This may be related to the corrosion and interstitial transfer incurred during the sodium pre-exposure. Since the samples were located in the hot-leg of a flowing $\Delta T$ sodium loop during pre-exposure, chromium, nickel and carbon contents were decreased at the surfaces of the samples, causing a decrease in the strength of the material (and probably an increase in ductility) at the surface. This could cause a decrease in the creep life during the creep-fatigue tests. This is supported by the creep-rupture test results shown in Figure 6.9, where the time-to-rupture is lowest and the minimum creep rate highest for the sodium pre-exposed sample. Additional tests will be required to confirm this and relate it to other temperatures and times.

### 6.4.2 Inconel 718

Low-cycle fatigue testing of Inconel 718 in air is continuing. The results will be used as baseline data for tests of the same heat and heat treatment of material to be tested in sodium. Test sample geometry for the in-air and in-sodium tests consist of a 0.25 inch diameter x 0.50 inch long gage section. Axial strain control is obtained using an LVDT, measuring the load train deflection. Calibration of the load train compliance is accomplished by using a zero gage length sample at test temperature, with the same test environment.

Low-cycle fatigue results obtained in air at 1000°F for the plate material (Heat 2180-2-9247), heat treated per AMS-5596C (1725°F solution anneal + double age), are given in Tables 6.4 and 6.5 for

Table 6.4 Low-Cycle Fatigue Data[a] for Inconel 718[b] Tested at 1000°F in Air

| Sample Number | Strain Range, % | | Compressive Hold-Time, hr. | Stress Range,[c] ksi | Fatigue Life $N_f$ |
|---|---|---|---|---|---|
| | Total | Plastic | | | |
| 17 | 0.97 | 0.15 | 0 | 231.0 | 3,340 |
| 9 | 0.95 | 0.22 | 0 | 233.6 | 2,050 |
| 25 | 1.96 | 0.96 | 0 | 286.0 | 377 |
| 1 | 2.04 | 1.09 | 0 | 308.0 | 400 |
| 39[d] | 5.32 | 3.74 | 0 | 320.0 | 12 |
| 31 | 2.01 | 0.98 | 0.5 | 258.0 | 357 |
| 55 | 2.00 | 0.90 | 1.0 | 266.0 | 333 |

(a) Strain Rate: $4 \times 10^{-3}$ $sec^{-1}$
Control Mode: Axial Strain
Wave Form: Triangular, zero mean strain
(b) 1725 S.A. + double age (AMS-5596C)
(c) Stress range at $N_f/2$, maximum stress range for hold-time tests
(d) Sample showed slight buckling

Table 6.5 Low-Cycle Fatigue Data[a] for Inconel 718[b] Tested at 1000°F in Air After Vacuum Aging at 1000°F for 2000 hours

| Sample Number | Strain Range, % | | Compressive Hold-Time hr. | Stress Range,[c] ksi | Fatigue Life $N_f$ |
|---|---|---|---|---|---|
| | Total | Plastic | | | |
| 11 | 0.87 | 0.03 | 0 | 204.0 | >45,556[f] |
| 27[d] | 1.02 | 0.06 | 0 | 236.0 | 3,725 |
| 7 | 1.26 | 0.18 | 0 | 264.0 | 2,286 |
| 19 | 1.45 | 0.42 | 0 | 264.0 | 1,482 |
| 3[e] | 1.90 | 0.71 | 0 | 276.0 | 627 |
| 15 | 1.90 | 0.94 | 0 | 272.0 | 457 |
| 29 | 2.01 | 0.78 | 0.5 | 268.0 | 419 |
| 45 | 1.27 | 0.17 | 1.0[g] | 290.0 | 2,590 |

(a) Strain Rate: $4 \times 10^{-3}$ $sec^{-1}$
Control Mode: Axial Strain
Wave Form: Triangular, zero mean strain
(b) 1725°F S.A. + double age (AMS-5596C)
(c) Stress range at $N_f/2$, maximum stress range for hold-time tests
(d) Sample inadvertently compressed to 2% during the second cycle
(e) Sample was overheated to 1300°F for 30 minutes during heat up period
(f) Test terminated, no failure
(g) 1.0 hour hold-time in compression for the first 290 cycles, followed by zero hold-time for duration of test

as-fabricated and vacuum aged samples respectively. Based on the test data, Figure 6.11 presents the fatigue curves for each. The total strain range curves show that the fatigue life is somewhat increased as a result of the thermal aging at 1000°F for 2000 hours prior to test. This effect appears to decrease with increasing strain range. The difference appears to be related to the larger elastic strain range values obtained for the aged material, at the same fatigue life. When the elastic strain range values are correlated with the stress range values for each test, a different modulus value is indicated for the two materials. This difference will be investigated further. The slope of the plastic strain range curve in Figure 6.11 is quite high ($\approx 1$). More data in the high strain range region will be required to confirm this. Figure 6.12 presents the cyclic stress-strain response for the two material conditions. A lower strain hardening exponent is indicated for the aged material implying softening of the material as a result of the pre-treatment. Significant stress-relaxation due to the hold-time in compression was observed for the vacuum aged material.

Tables 6.4 and 6.5 present the results of testing with 0.5 and 1.0 hour hold-time in compression-only. Both the as-fabricated and the aged materials show no significant fatigue damage resulting from the compressive creep, for the test conditions involved. Sample Numbers 7 and 45 in Table 6.5 were both tested at essentially the same total strain range and show excellent agreement in the measured plastic strain range. However, the stabilized stress range, based on the $N_f/2$ criteria, is larger for sample number 45 and so is its fatigue life. Although sample number 45 was tested with a hold time of one hour in compression during the first 290 cycles, this should cause a slight decrease in fatigue life. The fact that this sample had a longer fatigue life than sample 7 appears to indicate that the difference is due to microstructural or material property variations. Post-test examination of the specimens will be conducted to analyze the microstructures.

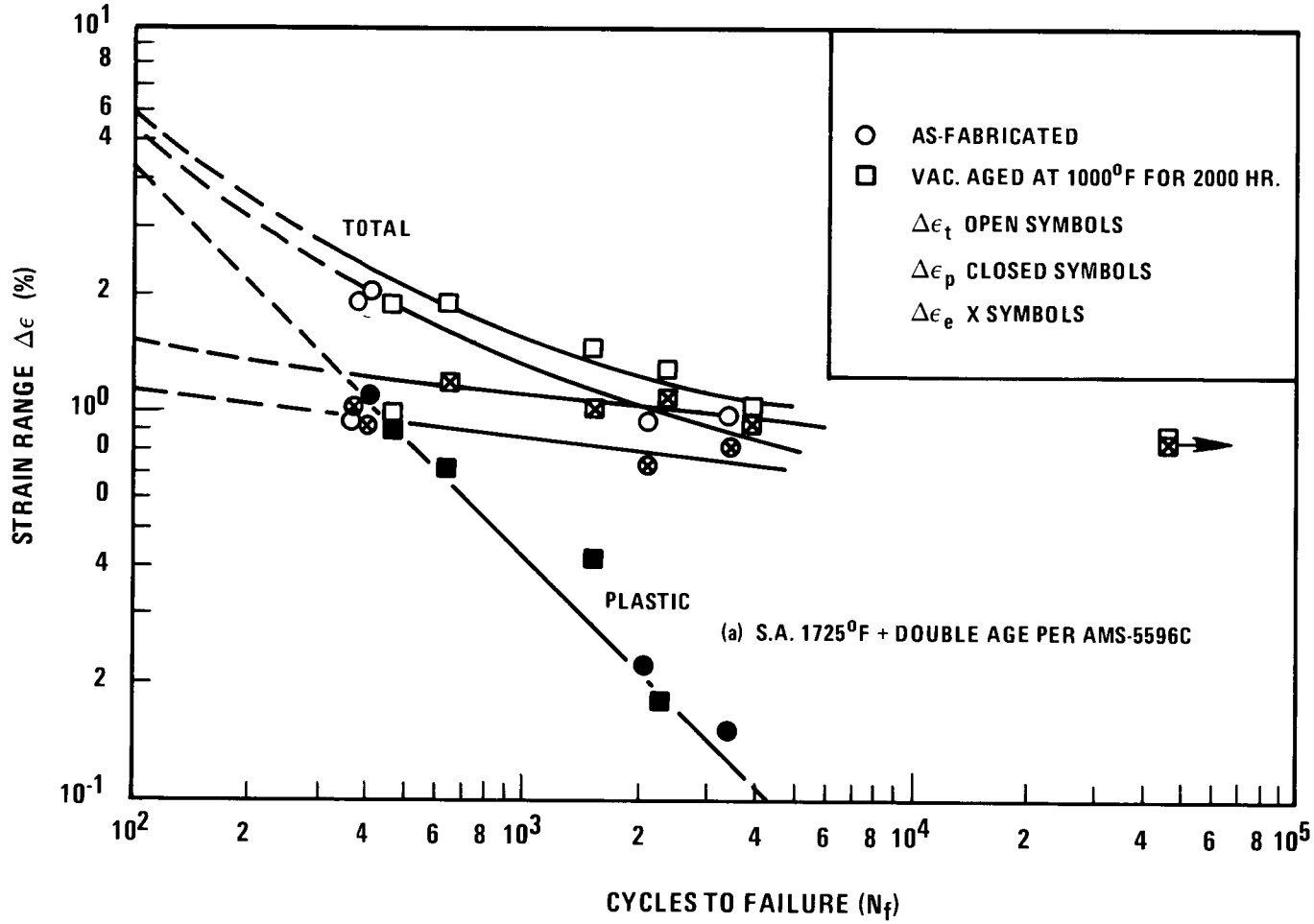


Figure 6.11. Low Cycle Fatigue Data For Inconel 718[a] Tested At 1000°F In Air ($\dot{\epsilon} = 4 \times 10^{-3}$ Sec$^{-1}$)

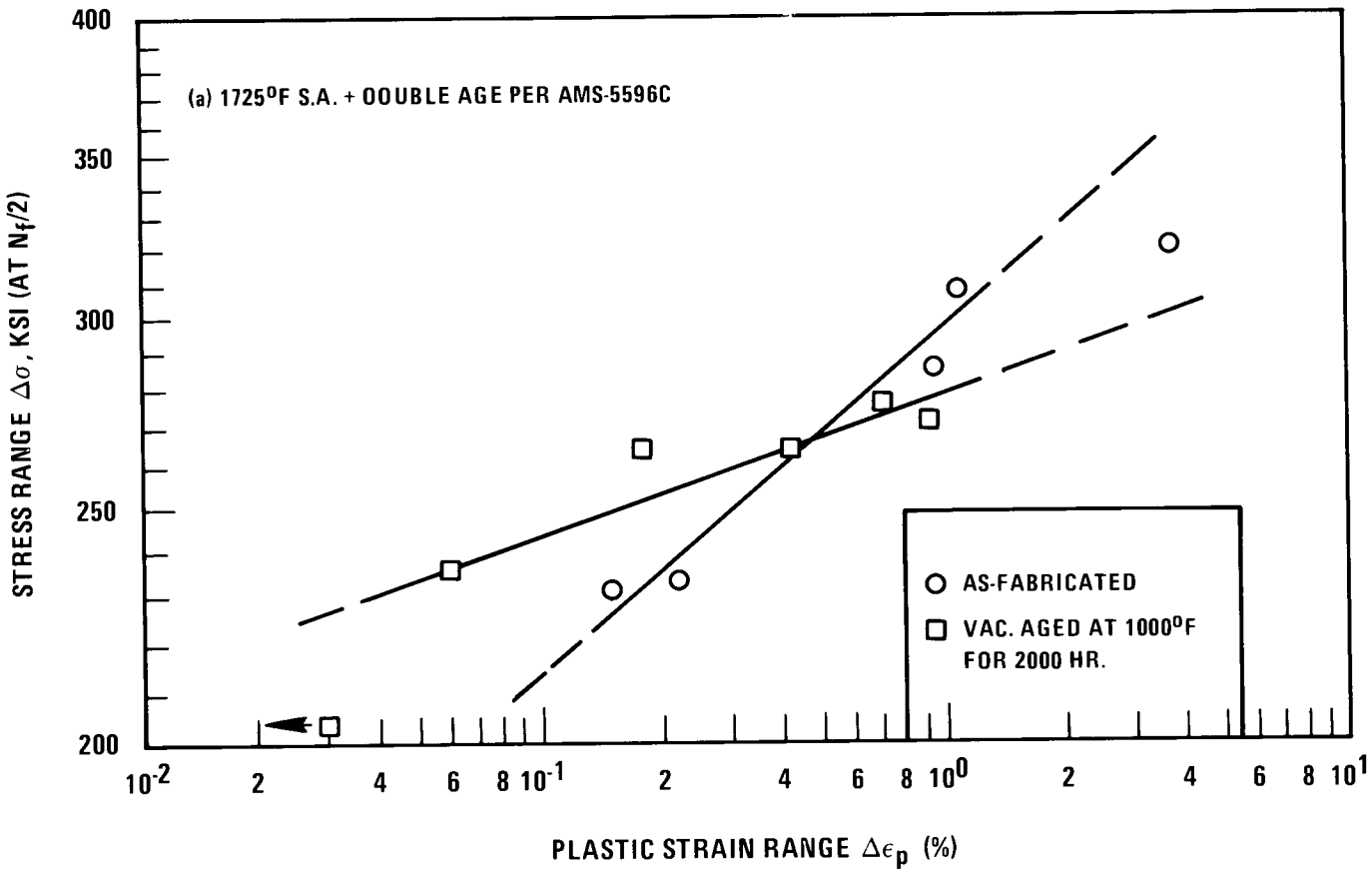


Figure 6.12. Cyclic Stress - Strain Response For Inconel 718 [a] Tested At 1000°F In Air

## 6.5 REFERENCES

1. C. R. Brinkman and G. E. Korth, Low Cycle Fatigue and Hold Time Comparisons of Irradiated and Unirradiated Type 316 Stainless Steel, Metallurgical Transactions, Vol. 5, pp 792, March 1974.

# 7. UNIVERSITIES

## 7.1 UNIVERSITY OF CINCINNATI

J. Moteff and H. Nahm

### 7.1.1 Introduction

The objective of this program is to (a) evaluate the time, temperature and stress-dependent mechanical properties of reactor structural materials, (b) determine the relationship of these properties to the microstructure and (c) show the contribution of the microstructure to the internal stress fields and the subsequent influence on microcracking and the grain boundary sliding behavior during the normal plastic deformation at elevated temperatures. Special consideration is being given to operating conditions typical of nuclear reactor applications, including the knowledge that the radiation environment can influence the substructure of these metals, a circumstance which can lead to significant changes in the conventional mechanical property behavior.

### 7.1.2 Experimental Program

Transmission electron microscopy has been used to study the deformation substructure resulting from creep, fatigue and tensile deformation at elevated temperatures. New work being initiated will also include similar studies on the Commercial, the Developmental and the Fundamental alloys being evaluated in the National Alloy Developmental Program with particular attention on the application of hot-hardness

measurement as a strength microprobe.

A study on difference in fatigue-cracking behavior between bend and push-pull mode of testing is also underway by scanning electron microscopy and the results will be provided in the future reports.

As reported in the previous progress reports[1-4], the substructure formed during strain-controlled push-pull fatigue test of Incoloy 800 has been characterized as part of ongoing research programs at the University of Cincinnati. Observations and the general relationships of subboundary intercept size, dislocation density with fatigue properties are presented. Further analysis and discussions of substructure data will be given in the next report.

### 7.1.2.1 High Temperature Fatigue Substructure for Incoloy 800

Dislocation distribution of undeformed Incoloy 800 was found to be non-uniform, probably as a result of different dislocation generation during heat treatment. Dislocation density was around $2.3 \times 10^9$ $cm^{-2}$. Extended nodes of partial dislocations were not observed, indicating the stacking fault energy (SFE) of Incoloy 800 is higher than that of AISI 304 or 316 stainless steels where nodes were sometimes observed. Using Gallagher's method[5], the SFE for Incoloy 800 is estimated to be $\sim$ 90 ergs/$cm^2$. Since SFE is very sensitive to alloying[5], this estimation is only approximate.

The dislocation structure for Incoloy 800 tested at 538°C is shown in Figs. 1 and 2, and the substructure data are summarized in Table I. Cellular structures were observed in only two out of seven specimens examined which were tested under the large strain range at 538°C. This indicates that the higher dislocation density is needed to form cells at lower temperature. Due to extremely high density, the average mobile dislocation density was not able to be measured in some of the specimens as shown in Table I. The density here was defined previously[4].

Extended cell walls shown in Fig. 1-a were found to be lying parallel to {100} planes from the tilting experiment with the stereographic projection. Well defined cells were formed in specimen #2X72 (See Fig. 1-b). Except for specimens #2R42 and #2X72, all specimens at 538°C exhibited the planar dislocation band structure (See Figs. 1-c, 1-d, and Fig. 2). These bands were often found to be aligned parallel to the low index planes such as {100}, {110}, and {111}. Figs. 1-d and 2 show that band structures mostly consist of dipoles, loops and tangles.

In addition to the second phases such as $M_{23}C_6$ and TiN which were observed in most Incoloy 800 specimens at all testing temperatures, $\gamma'$ precipitates were also observed in specimens with long testing times at 538°C. The details of the TEM identification procedure of second phases formed in Incoloy 800 during fatigue were given before[3]. The influ-

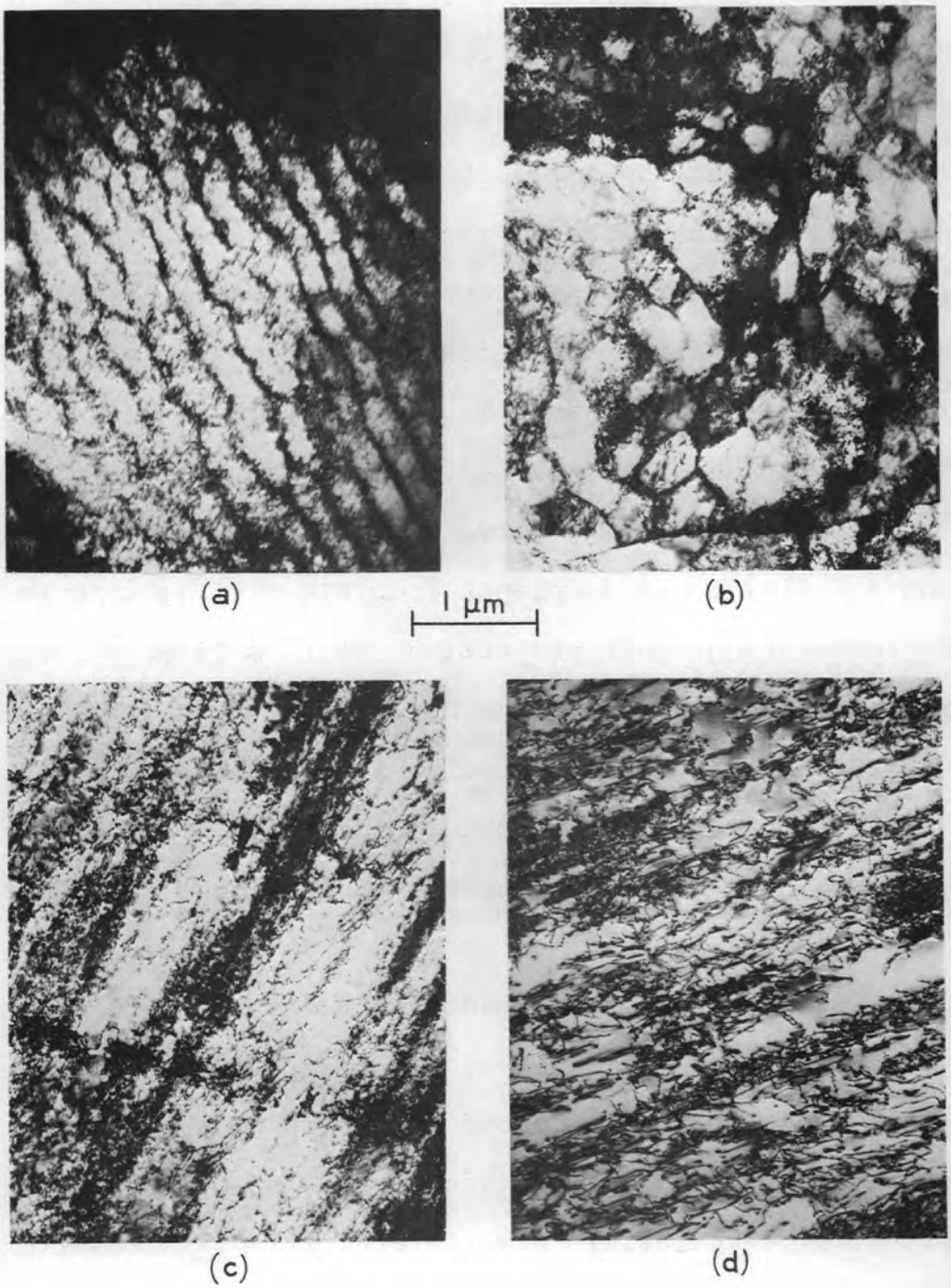


Fig. 1 Fatigue Substructure of Incoloy 800 at 538°C;
(a) Specimen 2R42; (b) Specimen 2X72;
(c) Specimen 2D52; (d) Specimen 2Q41.

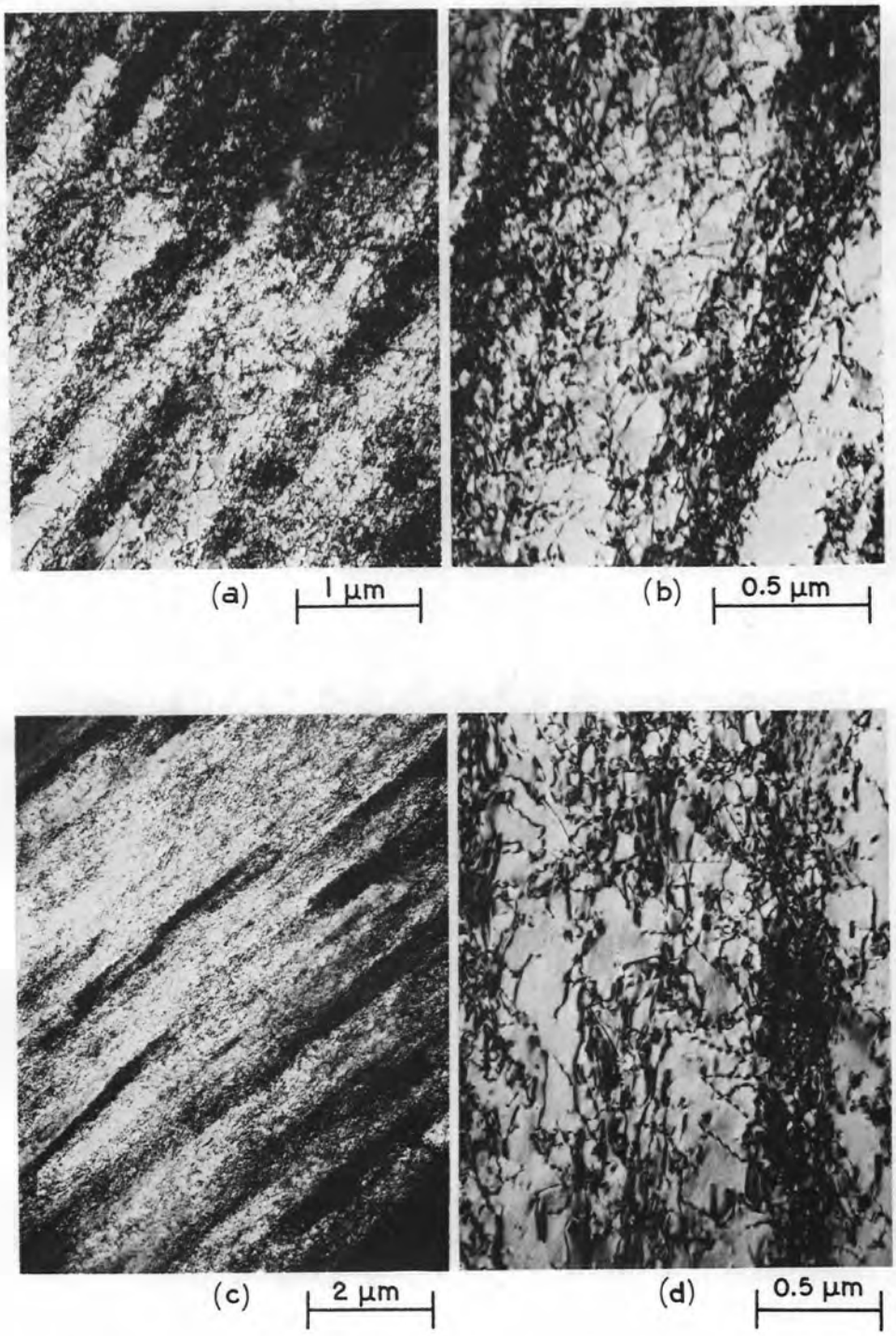


Fig. 2 Fatigue Substructure of Incoloy 800 at 538°C;
(a) Specimen 2H8; (b) Specimen 2H8;
(c) Specimen 2I9; (d) Specimen 2I9.

TABLE I

FATIGUE AND SUBSTRUCTURE PROPERTIES OF INCOLOY 800 AT 538°C

| Spec. No. | Strain Rate $\dot{\varepsilon}$, $sec^{-1}$ | Plastic Strain Range $\Delta\varepsilon_p$, Pct. | Modulus Compensated[a] Saturation Stress $\Delta\sigma/2G$ | $\Delta\sigma/2E$ | Average Subboundary Intercept $\lambda$, μm | Average Mobile Dislocation Density $\rho_m$, $cm^2$ | Sub-boundary Misorientation θ, Degrees |
|---|---|---|---|---|---|---|---|
| 2R42 | $4 \times 10^{-3}$ | 2.35 | $8.53 \times 10^{-3}$ | $3.12 \times 10^{-3}$ | 0.29 ± 0.04 | N.M. | N.M. |
| 2X72 | $4 \times 10^{-3}$ | 1.43 | $7.58 \times 10^{-3}$ | $2.77 \times 10^{-3}$ | 0.37 ± 0.02 | N.M. | N.M. |
| 2D52 | $4 \times 10^{-3}$ | 0.60 | $5.35 \times 10^{-3}$ | $1.96 \times 10^{-3}$ | N.O. | N.M. | ---- |
| 2T44 | $4 \times 10^{-3}$ | 0.17 | $4.42 \times 10^{-3}$ | $1.62 \times 10^{-3}$ | N.O. | $(1.52 \pm 0.63)\times10^{10}$ | ---- |
| 2Q41 | $4 \times 10^{-3}$ | 0.01 | $3.31 \times 10^{-3}$ | $1.21 \times 10^{-3}$ | N.O. | $(9.13 \pm 0.84)\times10^{9}$ | ---- |
| 2H8 | $4 \times 10^{-4}$ | 0.55 | $6.05 \times 10^{-3}$ | $2.21 \times 10^{-3}$ | N.O. | N.M. | ---- |
| 2I9 | $4 \times 10^{-4}$ | 0.12 | $5.16 \times 10^{-3}$ | $1.89 \times 10^{-3}$ | N.O. | $(1.40 \pm 0.19)\times10^{10}$ | ---- |

[a] Elastic Modulus at 538°C ($E=23.58 \times 10^6$, $G=8.60 \times 10^6$ psi) is obtained from the International Nickel Company (Technical Bulletin T-40).

ence of precipitates on the fatigue properties is also discussed there. The second phases formed in Incoloy 800 do not appear to affect the cell or subgrain formation behavior.

The characteristics of the dislocation substructure for Incoloy 800 specimens tested at 649°C are shown in Fig. 3 and Fig. 4, and the substructure data are summarized in Table II. The tendency for subboundary formation at 649°C is more pronounced than that at 538°C, as shown in Fig. 3. Five out of eight specimens studied at 649°C display the cell formation. Cells were found to form in the specimens tested under large strain ranges, which is consistent with the results from the specimens tested at 538°C. Well defined cells, close to subgrains were found in specimen #2N14 which had a longer test time than the others (see Fig. 3-c). The specimens without cell formation often reveal the banded dislocation structures as shown in Fig. 3-d, 3-f and 3-g.

Fig. 4 shows the general features of the free dislocations in the specimens tested at 649°C in which dislocation interactions with second phases are much in evidence. $M_{23}C_6$ particles are often found to form preferentially along the grain boundary, while small TiN particles with high number density are uniformly distributed throughout the matrix.

A summary of the fatigue substructure data for the Incoloy 800 push-pull specimens tested at 704°C is presented in Table III and the characteristics of dislocation substruc-

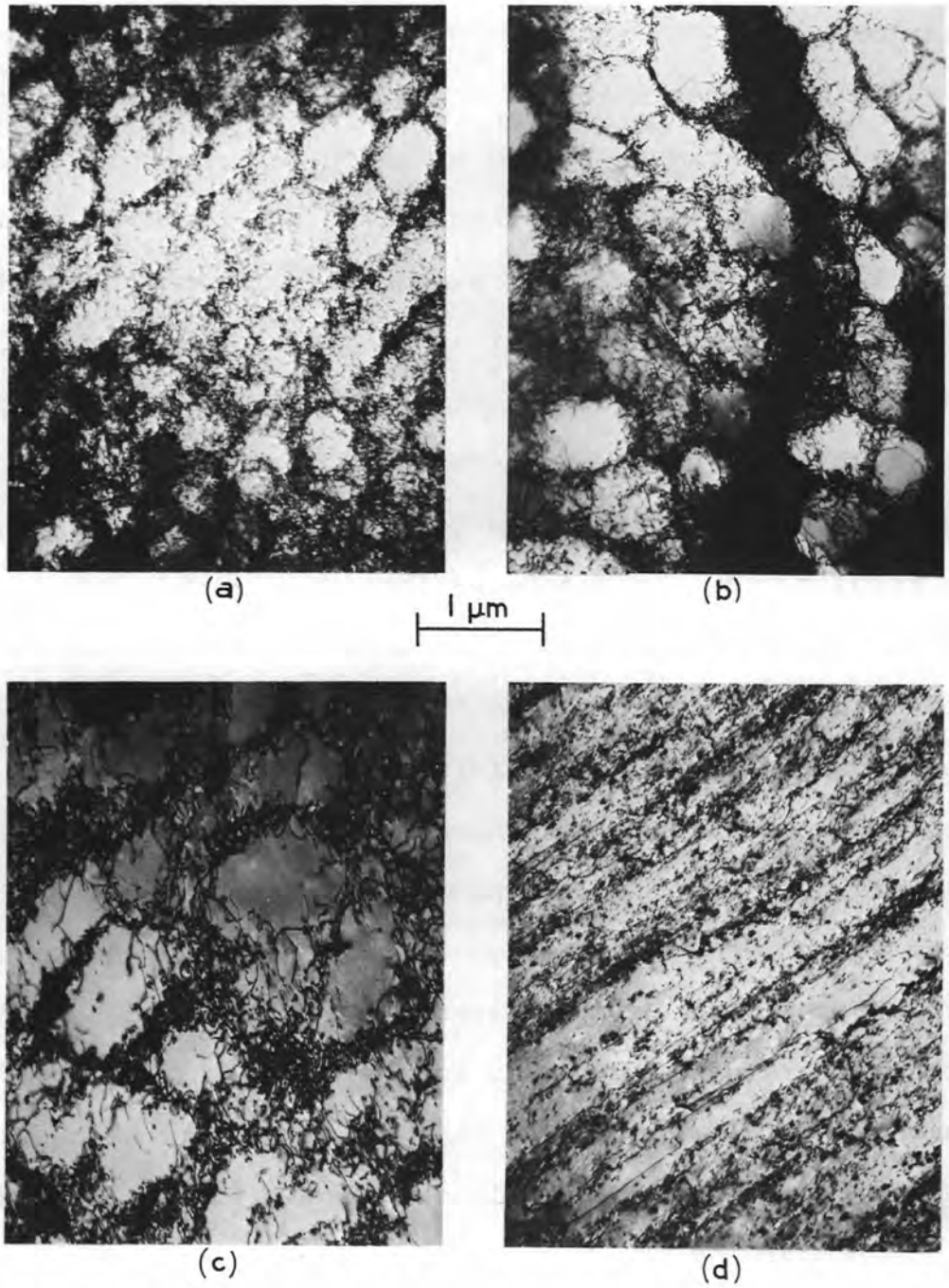


Fig. 3 Fatigue Substructure of Incoloy 800 at 649°C;
(a) Specimen 2E53; (b) Specimen 2A73;
(c) Specimen 2Q40; (d) Specimen 2F54;
(e) Specimen 2N14; (f) Specimen 2M13;
(g) Specimen 2N62.

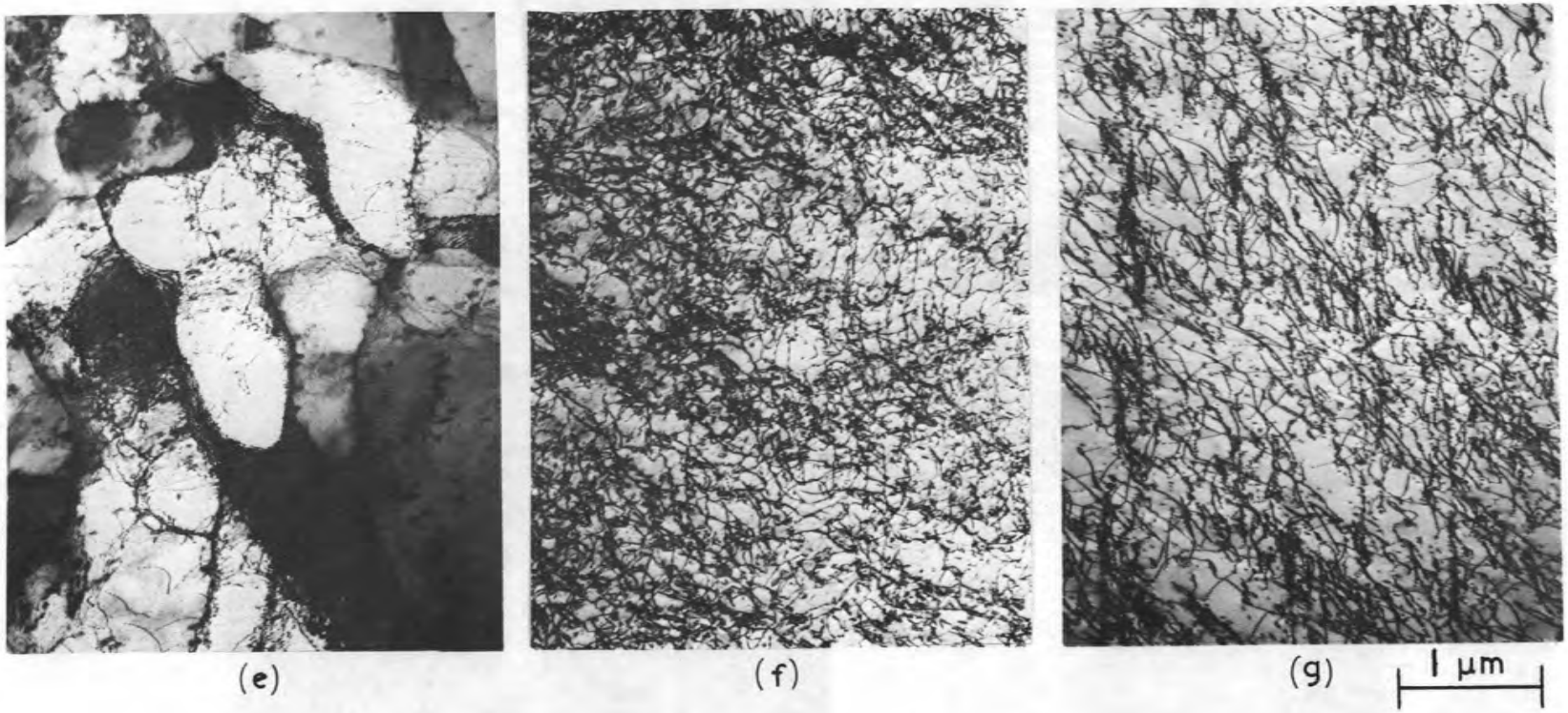


Fig. 3 Cont'd

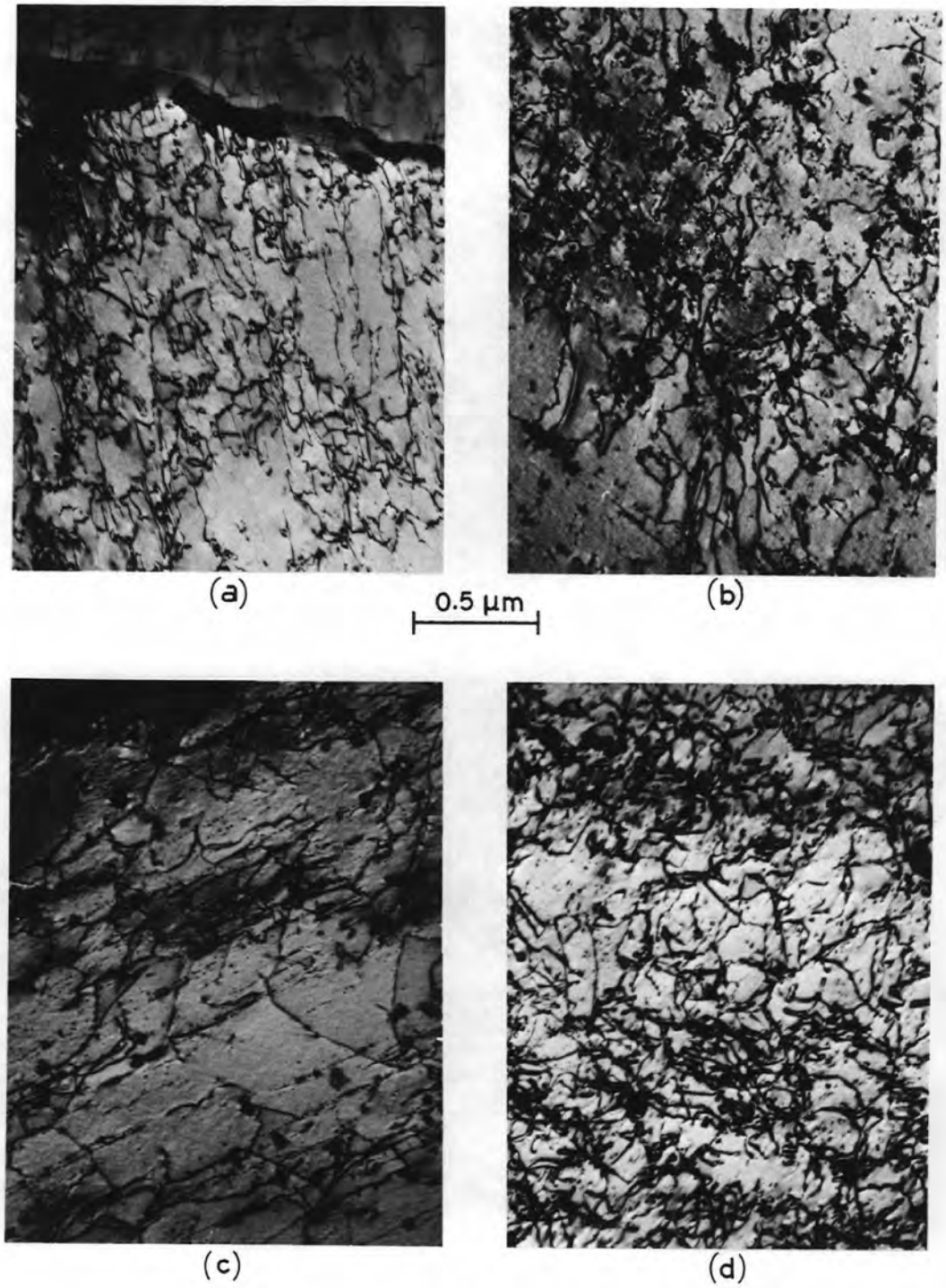


Fig. 4 Fatigue Substructure of Incoloy 800 at 649°C; (a) Specimen 2Q40; (b) Specimen 2F54; (c) Specimen 2N14; (d) Specimen 2M13.

TABLE II

**FATIGUE AND SUBSTRUCTURE PROPERTIES OF INCOLOY 800 AT 649°C**

| Spec. No. | Strain Rate $\varepsilon$ $sec^{-1}$ | Plastic Strain Range $\Delta\varepsilon_p$, Pct. | Modulus Compensated[a] Saturation Stress $\Delta\sigma/2G$ | $\Delta\sigma/2E$ | Average Subboundary Intercept $\lambda$, μm | Average Mobile Dislocation Density $\rho_m$, $cm^2$ | Sub-boundary Misorientation $\theta$, Degrees |
|---|---|---|---|---|---|---|---|
| 2E53 | $4 \times 10^{-3}$ | 3.36 | $8.21 \times 10^{-3}$ | $2.98 \times 10^{-3}$ | 0.40 ± 0.03 | N.M. | N.M. |
| 2A73 | $4 \times 10^{-3}$ | 1.47 | $6.98 \times 10^{-3}$ | $2.53 \times 10^{-3}$ | 0.48 ± 0.03 | $(8.15 \pm 0.90)\times10^{9}$ | 0.66 ± 0.15 |
| 2Q40 | $4 \times 10^{-3}$ | 0.56 | $5.90 \times 10^{-3}$ | $2.14 \times 10^{-3}$ | 0.83 ± 0.05 | $(8.30 \pm 1.20)\times10^{9}$ | 0.17 ± 0.02 |
| 2G55 | $4 \times 10^{-3}$ | 0.19 | $4.21 \times 10^{-3}$ | $1.52 \times 10^{-3}$ | 0.78 ± 0.15 | N.M. | N.M. |
| 2F54 | $4 \times 10^{-3}$ | 0.02 | $3.12 \times 10^{-3}$ | $1.13 \times 10^{-3}$ | N.O. | $(4.49 \pm 0.83)\times10^{9}$ | ---- |
| 2N14 | $4 \times 10^{-4}$ | 0.58 | $5.56 \times 10^{-3}$ | $2.02 \times 10^{-3}$ | 0.82 ± 0.07 | $(4.54 \pm 0.63)\times10^{9}$ | 0.40 ± 0.07 |
| 2M13 | $4 \times 10^{-4}$ | 0.16 | $4.61 \times 10^{-3}$ | $1.67 \times 10^{-3}$ | N.O. | $(1.05 \pm 0.10)\times10^{10}$ | ---- |
| 2N62 | $4 \times 10^{-4}$ | 0.02 | $3.12 \times 10^{-3}$ | $1.13 \times 10^{-3}$ | N.O. | $(8.20 \pm 0.60)\times10^{9}$ | ---- |

[a] Elastic Modulus at 649°C ($E = 22.37 \times 10^6$, $G = 8.12 \times 10^6$ psi) is obtained from the International Nickel Company (Technical Bulletin T-40).

TABLE III

FATIGUE AND SUBSTRUCTURE PROPERTIES OF INCOLOY 800 AT 704°C

| Spec. No. | Strain Rate $\varepsilon$, $sec^{-1}$ | Plastic Strain Range $\Delta\varepsilon_p$, Pct. | Modulus Compensated[a] Saturation Stress $\Delta\sigma/2G$ | $\Delta\sigma/2E$ | Average Subboundary Intercept $\lambda$, $\mu m$ | Average Mobile Dislocation Density $\rho_m$, $cm^2$ | Sub-boundary Misorientation $\theta$, Degrees |
|---|---|---|---|---|---|---|---|
| 2V70 | $4 \times 10^{-3}$ | 3.43 | $7.19 \times 10^{-3}$ | $2.60 \times 10^{-3}$ | 0.48 ± 0.05 | $(9.10 \pm 3.93)\times10^9$ | N.M. |
| 2U21 | $4 \times 10^{-3}$ | 1.53 | $6.18 \times 10^{-3}$ | $2.24 \times 10^{-3}$ | 0.66 ± 0.03 | $(5.50 \pm 1.90)\times10^9$ | 0.44 ± 0.12 |
| 2T20 | $4 \times 10^{-3}$ | 0.60 | $5.32 \times 10^{-3}$ | $1.93 \times 10^{-3}$ | 1.09 ± 0.16 | $(7.41 \pm 1.73)\times10^9$ | 0.48 ± 0.17 |
| 2I57 | $4 \times 10^{-3}$ | 0.20 | $4.06 \times 10^{-3}$ | $1.47 \times 10^{-3}$ | 0.88 ± 0.11 | $(6.66 \pm 0.77)\times10^9$ | 0.53 ± 0.19 |
| 2T68 | $4 \times 10^{-3}$ | 0.06 | $3.20 \times 10^{-3}$ | $1.16 \times 10^{-3}$ | N.O. | $(4.70 \pm 0.58)\times10^9$ | ---- |
| 2P16 | $4 \times 10^{-4}$ | 0.65 | $4.69 \times 10^{-3}$ | $1.70 \times 10^{-3}$ | 1.44 ± 0.32 | $(4.59 \pm 0.50)\times10^9$ | 0.75 ± 0.29 |
| 2B74 | $4 \times 10^{-4}$ | 0.04 | $2.83 \times 10^{-3}$ | $1.02 \times 10^{-3}$ | N.O. | $(2.39 \pm 0.21)\times10^9$ | ---- |

[a] Elastic Modulus at 704°C ($E = 21.74 \times 10^6$, $G = 7.87 \times 10^6$ psi) is obtained from the International Nickel Company (Technical Bulletin T-40).

ture are given in Fig. 5. Well defined subgrains were formed in specimens tested at 704°C. The propensity for subboundary formation at 704°C is greater than that at 649°C. Five out of seven specimens examined were found to have subgrains. This suggests the subboundary formation is strongly temperature dependent. $M_{23}C_6$ particles become larger and incoherent at 704°C as shown in Fig. 5-d.

The fatigue substructure data for Incoloy 800 specimens tested at 760°C is summarized in Table IV and the substructural characteristics are shown in Figs. 6 and 7. The inclination to form subgrains becomes extreme at this temperature. As a matter of fact, all ten specimens examined by TEM showed subgrain formation. In specimen #2B26, which was cycled under a total strain range of 2% at 760°C, the dislocation density was not obtained because the entire volume was occupied by subgrains. Fig. 6 shows that the subgrain intercept increases with decreasing stress range,which is consistent with the results from those specimens tested at 538°C, 649°C and 704°C. $M_{23}C_6$ particles become larger and incoherent and the number density of small TiN particle is decreased in specimens tested for a longer period of time at 760°C.

Similar to case of dislocation bands observed at low testing temperatures, the subboundaries formed at 760°C were often found to lie on the low index crystallographic planes such as {100}, {110} and {111}. In order to study the nature of dislocations comprising the subboundaries, the Burgers

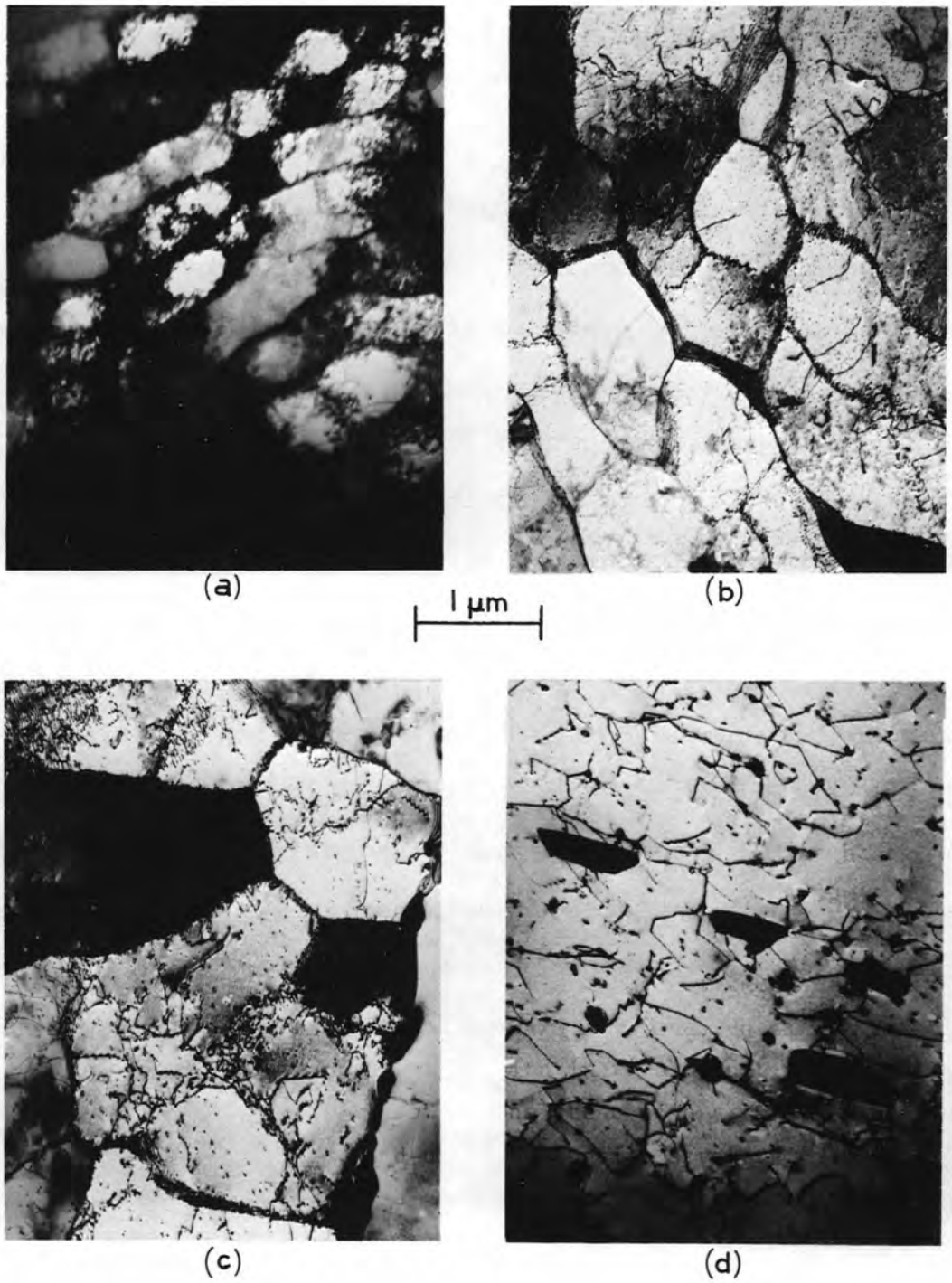


Fig. 5 Fatigue Substructure of Incoloy 800 at 704°C; (a) Specimen 2V70; (b) Specimen 2U21; (c) Specimen 2I57; (d) Specimen 2B74.

TABLE IV

FATIGUE AND SUBSTRUCTURE PROPERTIES OF INCOLOY 800 AT 760°C

| Spec. No. | Strain Rate $\dot{\varepsilon}$, $sec^{-1}$ | Plastic Strain Range $\Delta\varepsilon_p$, Pct. | Modulus Compensated[a] Saturation Stress $\Delta\sigma/2G$ | $\Delta\sigma/2E$ | Average Subboundary Intercept $\lambda$, μm | Average Mobile Dislocation Density $\rho_m$, $cm^{-2}$ | Subboundary Misorientation θ, Degrees |
|---|---|---|---|---|---|---|---|
| 2C75 | $4 \times 10^{-3}$ | 3.53 | $5.69 \times 10^{-3}$ | $2.05 \times 10^{-3}$ | 0.97 ± 0.19 | $(5.23 \pm 2.17) \times 10^{9}$ | 0.67 ± 0.18 |
| 2B26 | $4 \times 10^{-3}$ | 1.61 | $5.08 \times 10^{-3}$ | $1.83 \times 10^{-3}$ | 1.26 ± 0.18 | N.M. | 0.54 ± 0.12 |
| 2F6 | $4 \times 10^{-3}$ | 0.66 | $4.48 \times 10^{-3}$ | $1.61 \times 10^{-3}$ | 1.05 ± 0.05 | $(4.98 \pm 0.95) \times 10^{9}$ | 0.76 ± 0.19 |
| 2W23 | $4 \times 10^{-3}$ | 0.24 | $3.49 \times 10^{-3}$ | $1.53 \times 10^{-3}$ | 1.89 ± 0.41 | $(3.32 \pm 0.80) \times 10^{9}$ | 0.76 ± 0.32 |
| 2D28 | $4 \times 10^{-3}$ | 0.08 | $3.07 \times 10^{-3}$ | $1.11 \times 10^{-3}$ | 1.90 ± 0.40 | $(3.30 \pm 0.40) \times 10^{9}$ | 0.42 ± 0.08 |
| 2G79 | $4 \times 10^{-3}$ | 0.07 | $2.48 \times 10^{-3}$ | $8.93 \times 10^{-4}$ | 2.33 ± 0.19 | $(2.46 \pm 0.51) \times 10^{9}$ | 0.69 ± 0.18 |
| 2K35 | $4 \times 10^{-4}$ | 1.66 | $4.28 \times 10^{-3}$ | $1.54 \times 10^{-3}$ | 1.61 ± 0.10 | $(5.39 \pm 0.31) \times 10^{9}$ | 0.85 ± 0.20 |
| 2H32 | $4 \times 10^{-4}$ | 0.72 | $3.76 \times 10^{-3}$ | $1.35 \times 10^{-3}$ | 2.55 ± 0.24 | $(1.93 \pm 0.23) \times 10^{9}$ | 0.59 ± 0.22 |
| 2I33 | $4 \times 10^{-4}$ | 0.28 | $2.94 \times 10^{-3}$ | $1.06 \times 10^{-3}$ | 1.60 ± 0.16 | $(3.25 \pm 0.30) \times 10^{9}$ | 0.90 ± 0.31 |
| 2H80 | $4 \times 10^{-4}$ | 0.08 | $2.35 \times 10^{-3}$ | $8.46 \times 10^{-4}$ | 2.98 ± 0.56 | $(1.11 \pm 0.25) \times 10^{9}$ | 0.67 ± 0.14 |

[a] Elastic Modulus at 760°C ($E = 21.06 \times 10^6$, $G = 7.58 \times 10^6$ psi) is obtained from the International Nickel Company (Technical Bulletin T-40).

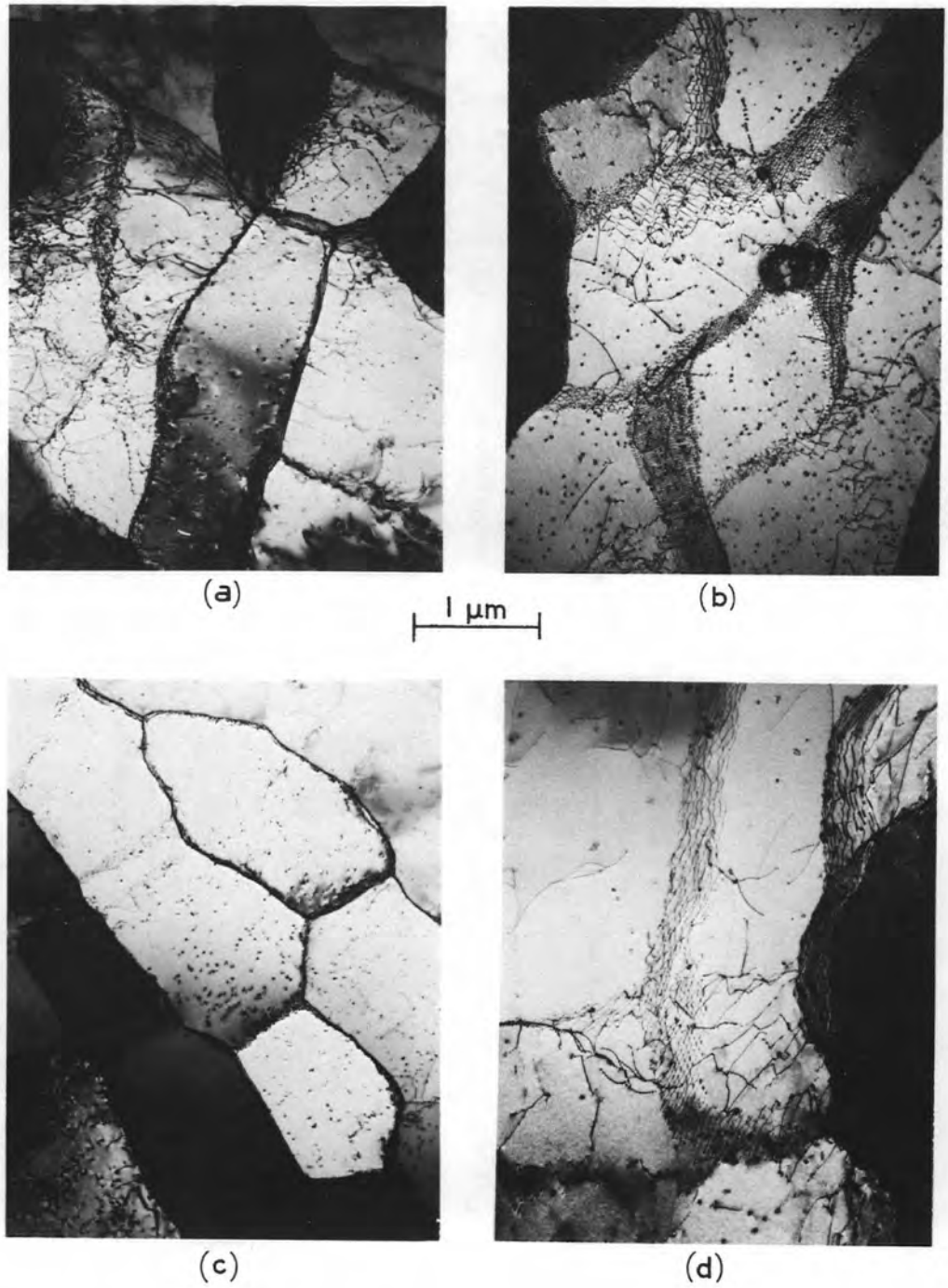


Fig. 6 Fatigue Substructure of Incoloy 800 at 760°C;
(a) Specimen 2C75; (b) Specimen 2B26;
(c) Specimen 2F6; (d) Specimen 2D28;
(e) Specimen 2K35; (f) Specimen 2H32;
(g) Specimen 2H80.

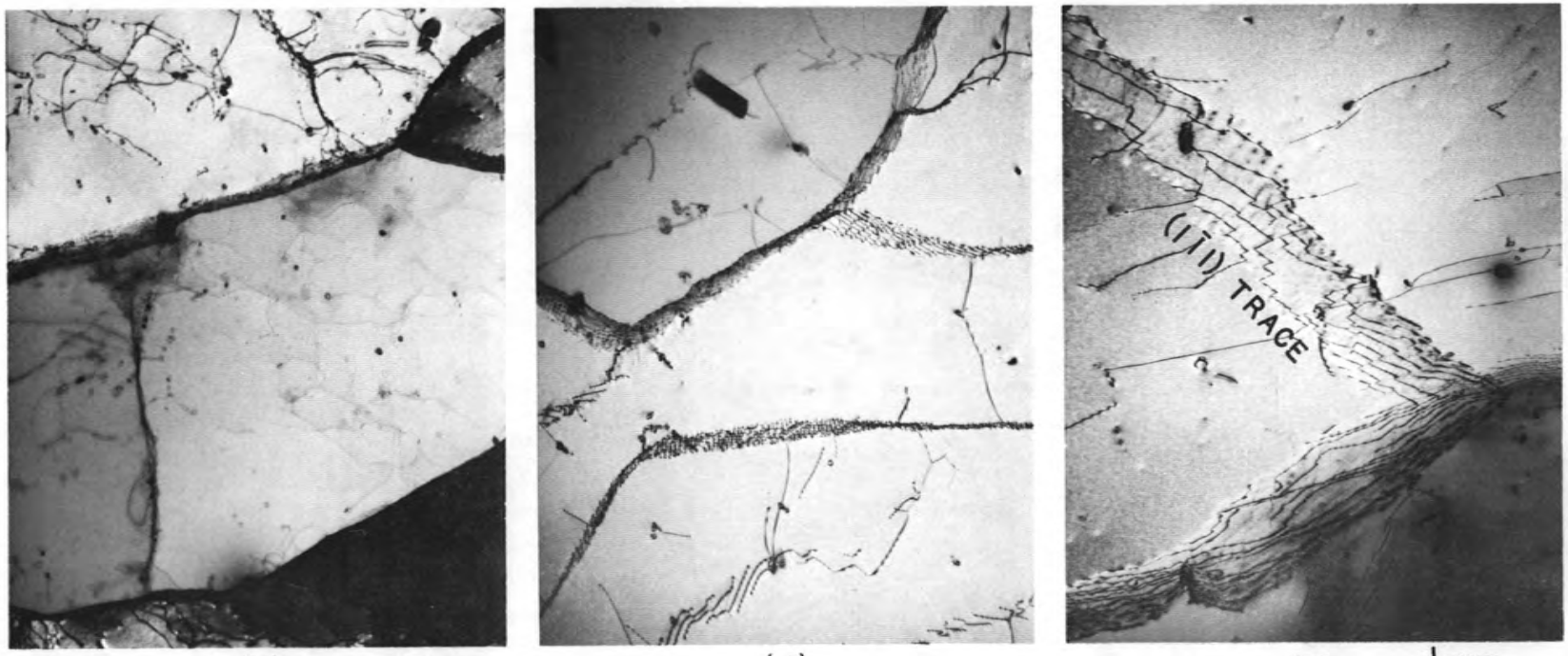


(e) (f) (g)

Fig. 6 Cont'd

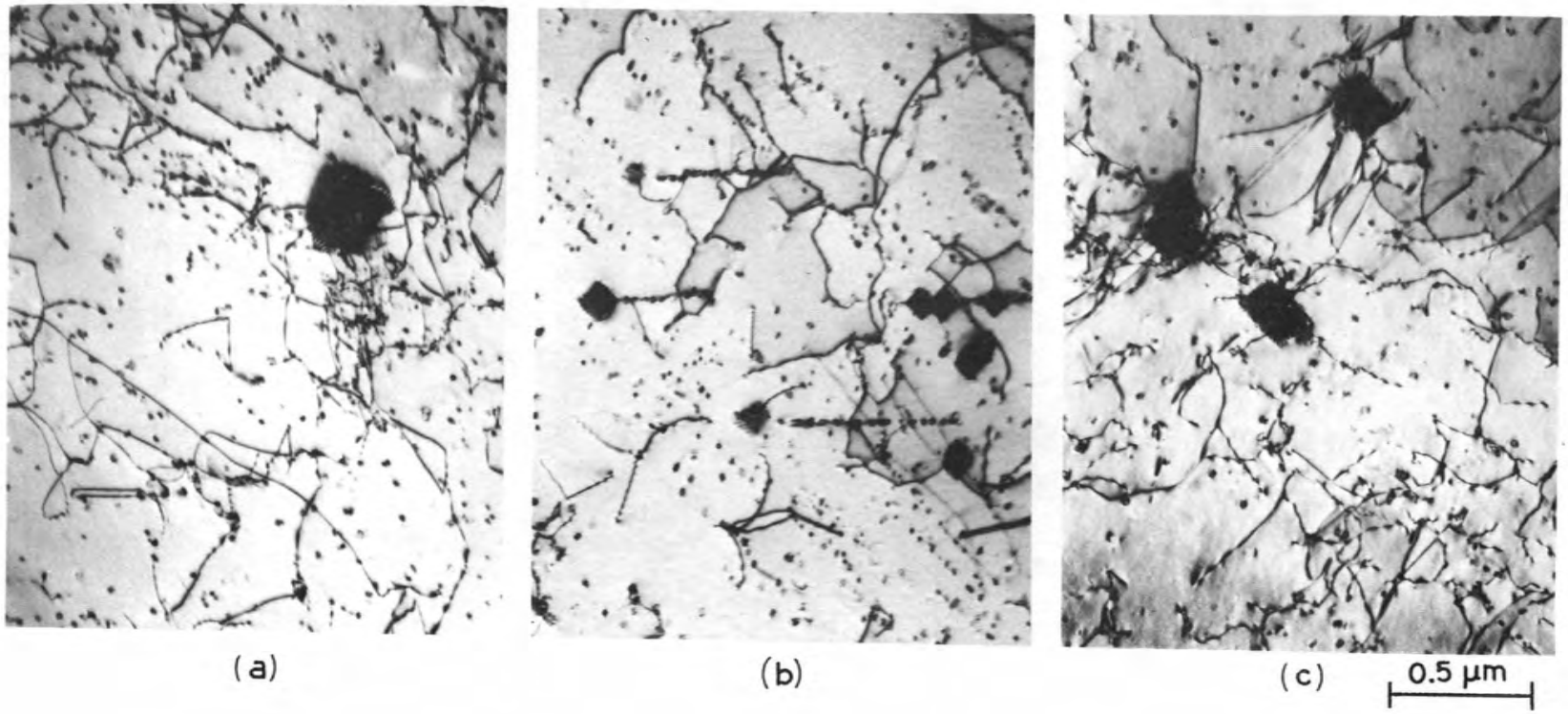


Fig. 7 Fatigue Substructure of Incoloy 800 at 760°C; (a) Specimen 2F6; (b) Specimen 2D28; (c) Specimen 2K35.

vector for the individual dislocations within the subgrain boundaries were determined by using $\bar{g} \cdot \bar{b} = 0$ criterion. A subgrain boundary with crossing dislocations shown in Fig. 6-g was found to be a tilt boundary lying on the $(1\bar{1}1)$ plane. A row of parallel edge dislocations which are out of contrast in Fig. 6-g, have a Burgers vector of $\bar{b}_1 = a/2$ $[10\bar{1}]$ and lie on the $(1\bar{1}1)$ plane, while another set of edge dislocations in contrast have a Burgers vector of $\bar{b}_2 = a/2$ $[\bar{1}0\bar{1}]$ which is perpendicular to the $(1\bar{1}1)$ plane. Thus Burgers vectors of two sets of crossing dislocations are not coplanar.

Fig. 8 gives an insight into the possible role of subboundaries on the high temperature fatigue deformation. Pile-ups of dislocations against subgrain boundaries and grain boundaries are clearly seen in this composite micrograph. The position of the pile-ups suggest that the subboundaries, once formed, might act as barriers to the moving dislocations. It should be mentioned, however , that the pile-ups were rarely observed in this study. Blocky $M_{23}C_6$ precipitates are formed along the grain boundary because of a long fatigue at high temperature (specimen #2H32, $t_f$ = 11.86 hours).

The subboundary intercept, $\lambda$, as a function of the shear modulus compensated stress, $\Delta\sigma/2G$ for Incoloy 800 fatigue tested in push-pull mode is plotted in Fig. 9. Several interesting observaaions can be made from this

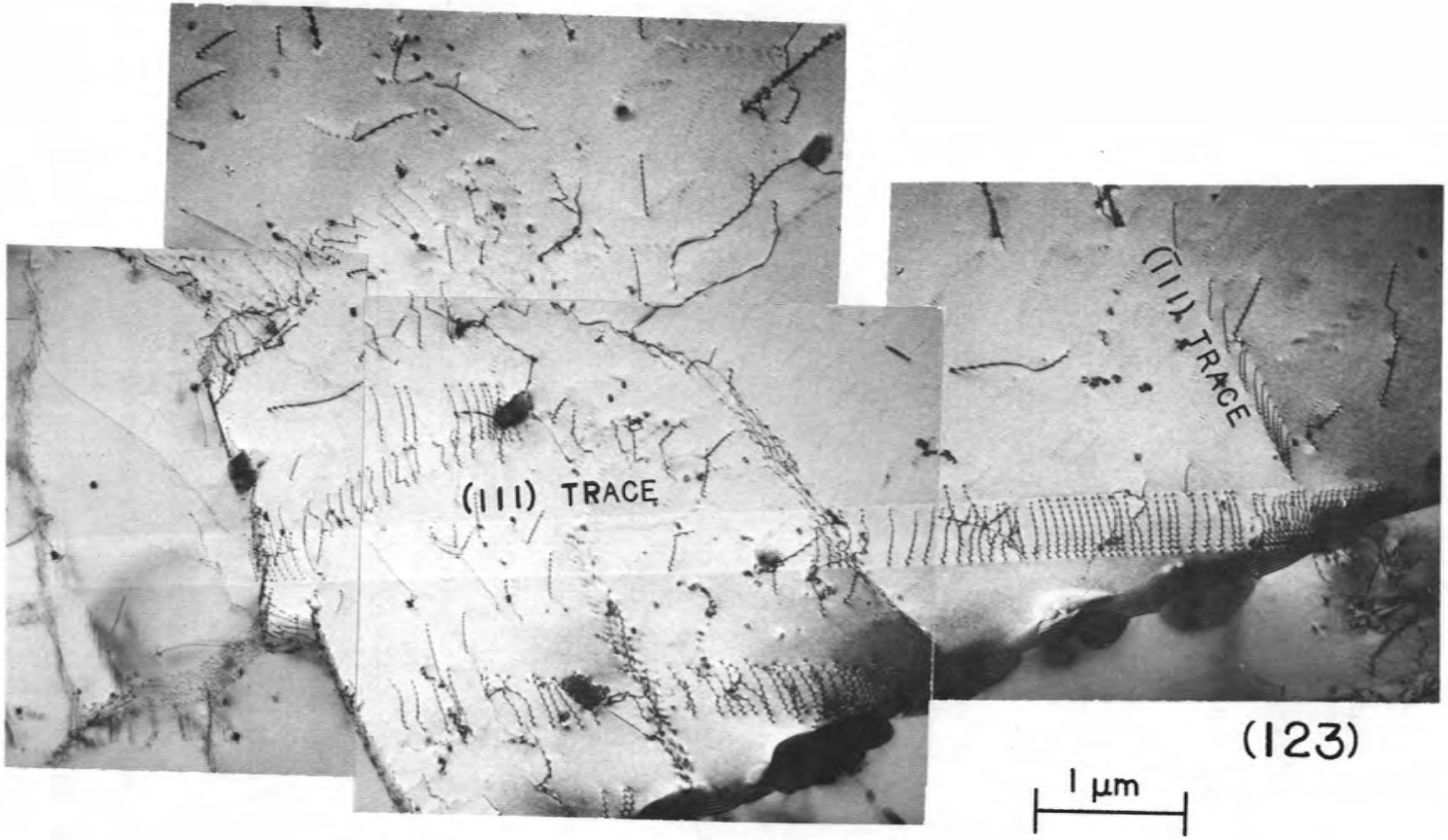


Fig. 8 Fatigue Substructure of Incoloy 800 in Specimen 2H32 at 760°C.

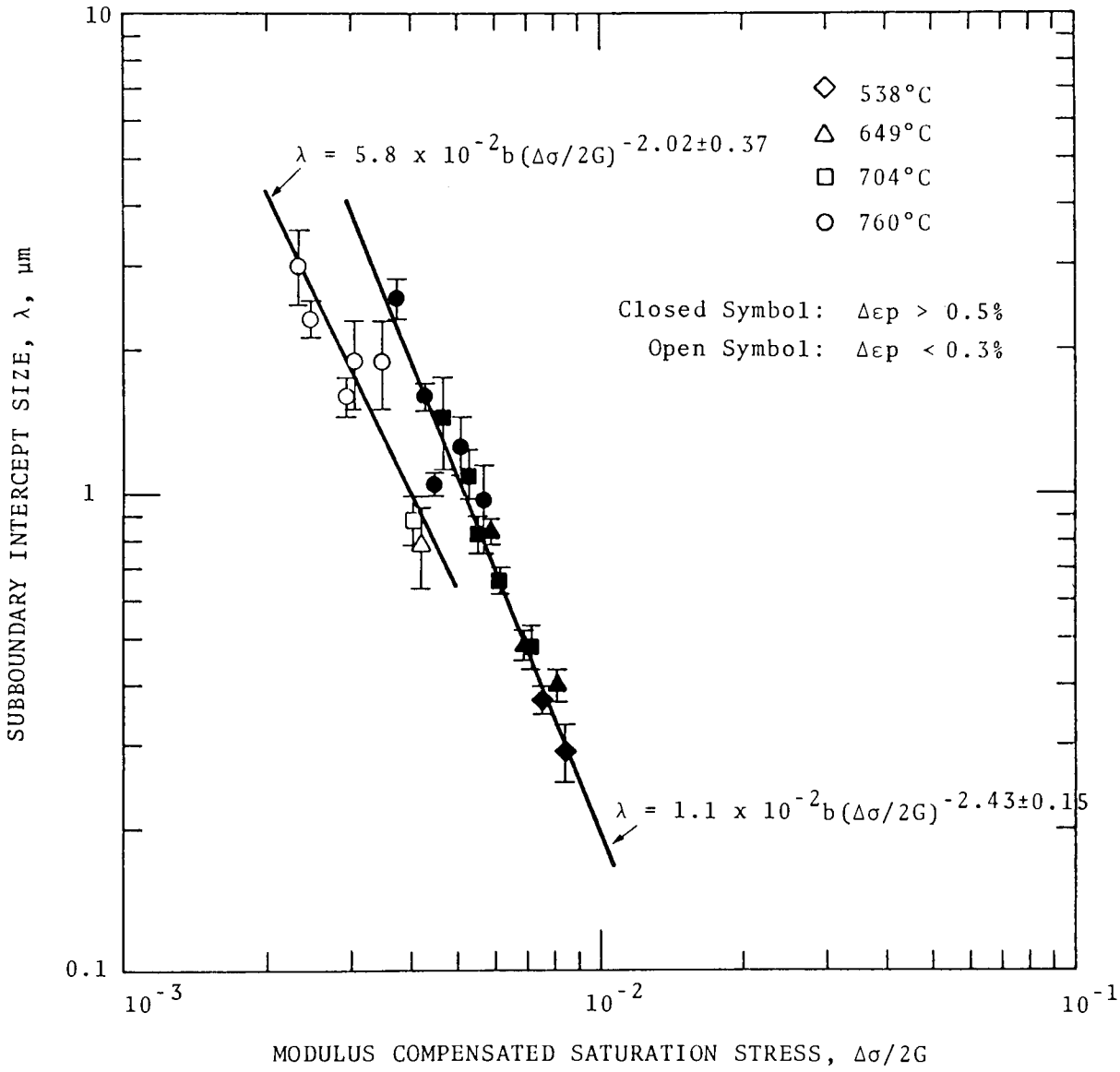


Fig. 9 The Subboundary Intercept Size, λ, as a Function of the Shear Modulus Compensated Saturation Stress Δσ/2G for Incoloy 800.

figure. The general inverse relationship between the subgrain size and stress, which has been observed by many investigators under different modes of plastic deformation, is found to be true for the results of the present investigation. It is also apparent from Fig. 9 that the subboundary intercept, $\lambda$, is strongly dependent on the plastic strain range, $\Delta\varepsilon_p$. The following relationships were obtained for subgrain size as a function of shear modulus compensated saturation stress,

$$\lambda = 1.1 \times 10^{-2} b \left( \frac{\Delta\sigma}{2G} \right)^{-2.43 \pm 0.15} \qquad [7.1]$$

for $\Delta\varepsilon_p > 0.5\%$

$$\lambda = 5.8 \times 10^{-2} b \left( \frac{\Delta\sigma}{2G} \right)^{-2.02 \pm 0.37} \qquad [7.2]$$

for $\Delta\varepsilon_p < 0.3\%$

where b is the Burgers vector ($2.54 \times 10^{-8}$ cm) and the $\Delta\varepsilon_p$ is the plastic range. The subboundary intercept, $\lambda$, appears to reach the saturation value as the plastic strain range increases at the constant shear modulus compensated saturation stress, $\Delta\sigma/2G$.

A plot of the dislocation density, $\rho$, versus the shear modulus compensated saturation stress, $\Delta\sigma/2G$, for Incoloy 800 fatigue tested in push-pull mode is presented in Fig. 10. An equation of the type

$$\rho = A \, (\Delta\sigma/2G)^2 \qquad [7.3]$$

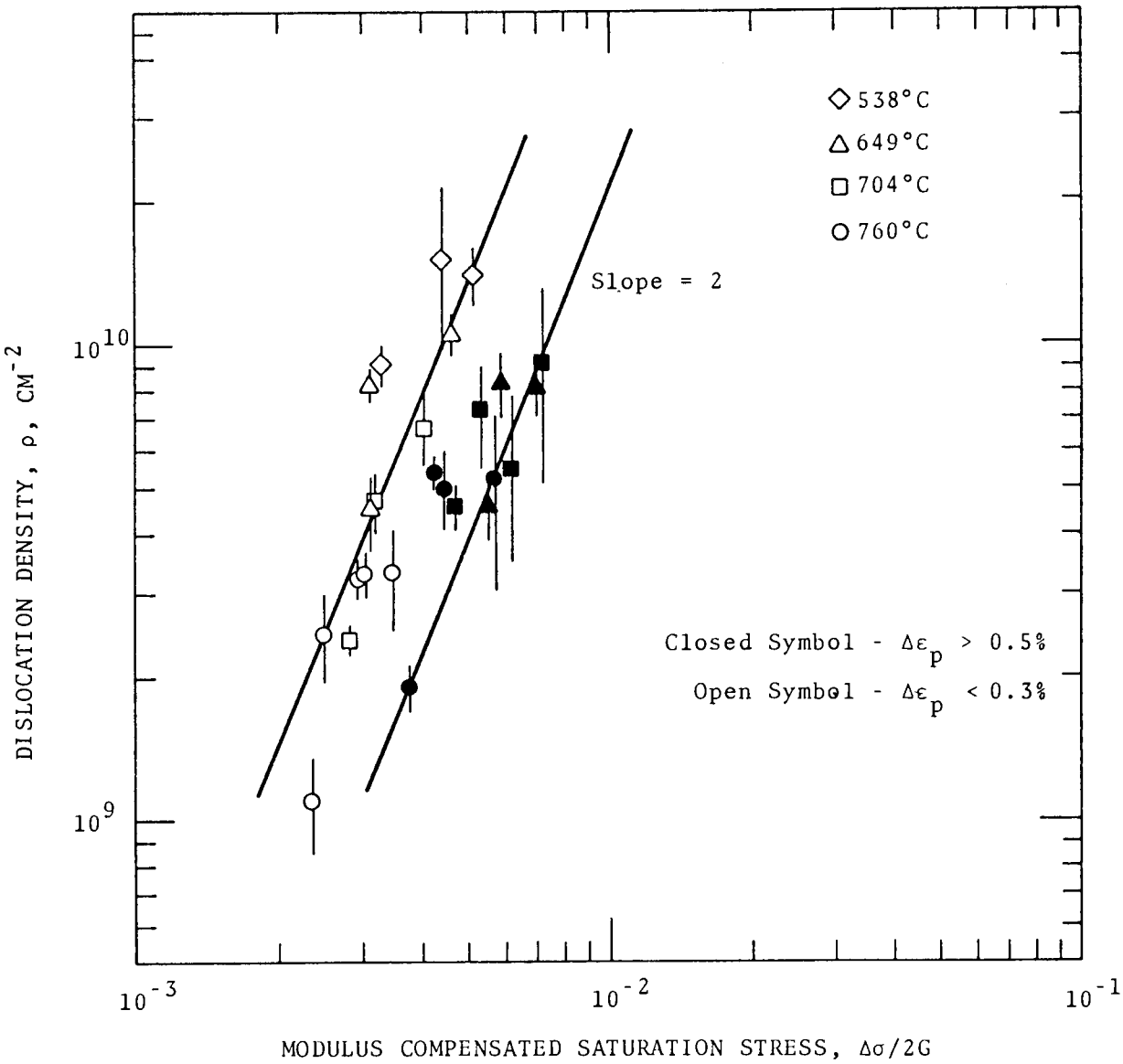


Fig. 10 The Dislocation Density, ρ, as a Function of the Shear Modulus Compensated Saturation Stress, Δσ/2G, for Incoloy 800.

where A is a constant, which was found to satisfactorily describe the relationship between the dislocation density and the flow stress. But the dislocation density is also found to be a function of the plastic strain range with the following equations (See Fig. 11):

$$\tau_s = 1.74 + 0.75\ Gb\sqrt{\rho} \qquad [7.4]$$

for $\Delta\varepsilon_p > 0.5\%$

$$\tau_s = 2.67 + 0.33\ Gb\sqrt{\rho} \qquad [7.5]$$

for $\Delta\varepsilon_p < 0.3\%$

where $\tau_s$ is the saturation shear stress in $kg/mm^2$ as defined elsewhere[6]. This is consistent with the subboundary intercept findings (See Fig. 10). A further analysis and discussion of the data for Incoloy 800 will appear in the next report.

### 7.1.3 References

1. ORNL - 4948, "Mechanical Properties Test Data for Structural Materials", Quarterly Progress Report for Period Ending January 31, 1974, pp. 359-364.
2. ORNL - 4963, "Mechanical Properties Test Data for Structural Materials", Quarterly Progress Report for Period Ending April 30, 1974, pp. 228-241.
3. ORNL - 5105, "Mechanical Properties Test Data for Structural Materials", Quarterly Progress Report for

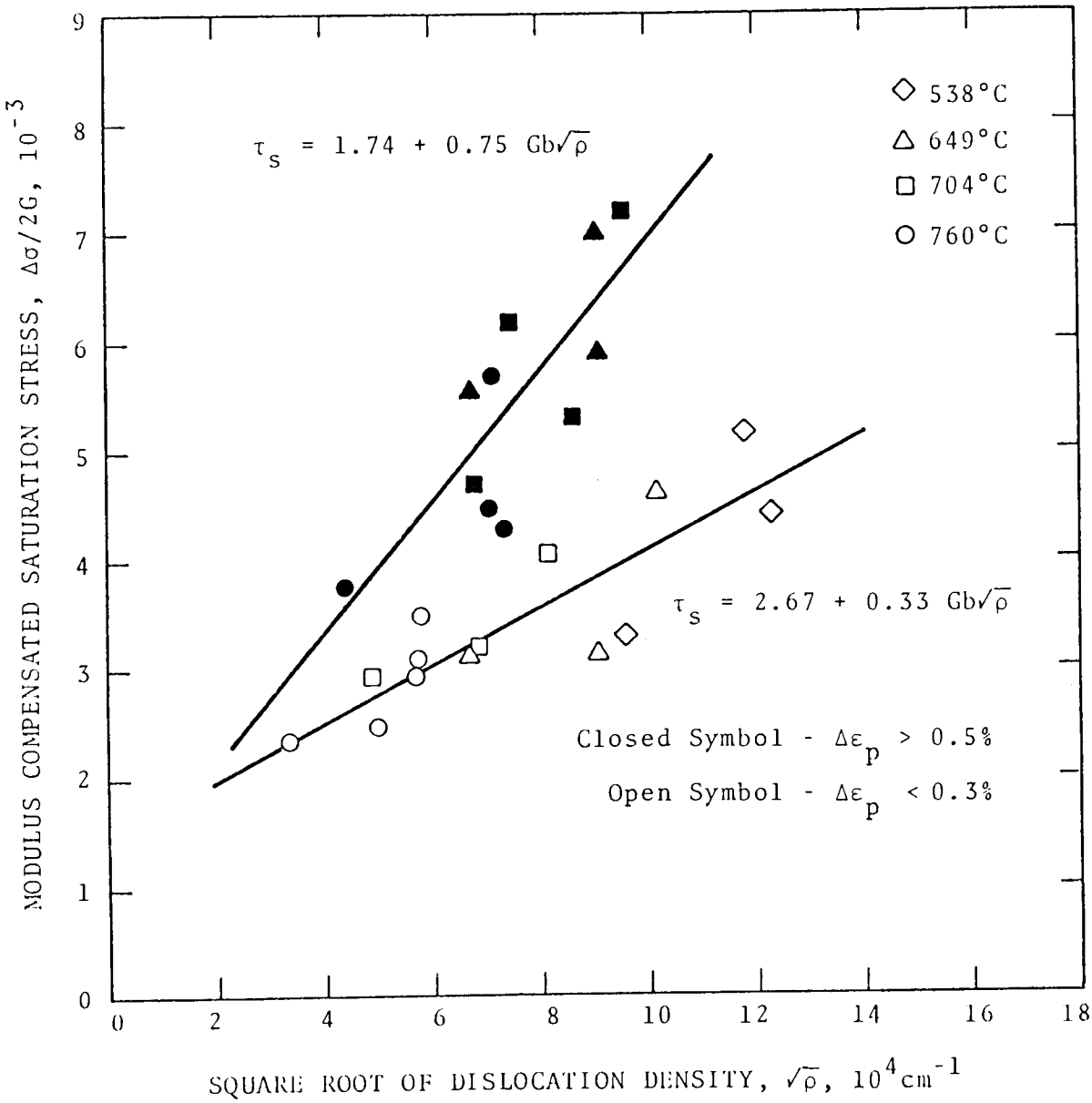


Fig. 11 The Shear Modulus Compensated Saturation Stress, $\Delta\sigma/2G$, as a Function of the Square Root of the Dislocation Density $\sqrt{\rho}$, for Incoloy 800.

Period Ending April 30, 1975, pp. 324-338.

4. ORNL - 5107, "Mechanical Properties Test Data for Structural Materials", Quarterly Progress Report for Period Ending October 31, 1975, pp. 275-287.

5. P. C. J. Gallagher, Met. Trans., 1, (1970) pp. 2429.

6. H. Nahm, Ph.D. Dissertation, 1975, University of Cincinnati.

## 7.2 UNIVERSITY OF CALIFORNIA, LOS ANGELES - A.J. Ardell, K. Ono and A.S. Tetelman

### 7.2.1 The Influence of (0-10%) Cold Work on the Creep Behavior of AISI Type 304 Stainless Steel (O. Ajaja and A.J. Ardell)

### 7.2.2 INTRODUCTION

Several investigators[1-4] have shown that cold work improves the creep strength of a material provided that major structural changes, such as rapid recovery or recrystallization do not take place prior to or during the test. Yim, et al.[1] found that the creep strength is enhanced in Ni prestrained by up to 6%, beyond which partial recrystallization and strain induced boundary migration resulted in a loss of creep resistance. Hazlett, et al.[2] attributed the improvement in strength in Ni and Ni-base alloys partly to the development and stabilization of the substructure which resulted from prestrain and recovery treatments prior to creep testing. They also showed that not only would a sufficient level of cold work ($<4\%$ for their material) totally eliminate transient creep, but that the shape of the creep curve can in fact be changed from a continuously decreasing to a continuously increasing creep rate. The work of Ardell, et al.[3] on Type 316 stainless steels suggests that a critical level of cold work exists for which the rupture life is maximized.

While most of the past research efforts have concentrated mainly on the behavior of the minimum creep rates and rupture lives, very little attention has been paid to understanding the influence of prior cold work on the transient creep kinetics. Since the steady-state creep substructure is fully developed by the end of the transient

creep, it is obvious that most of the structural factors that influence the creep strength have been fully established prior to secondary creep. A detailed analysis of the transient creep seems to be the natural starting point for any investigation of creep behavior as influenced by prior cold work. The present investigation is concentrated on the effect of small amounts (0-10%) of cold work on the creep behavior, with special emphasis on the transient creep, of the Type 304 stainless steels.

### 7.2.3 Materials and Experimental Procedure

The Type 304 stainless steel material used in this study was supplied as 1/4" diameter rods by Atomics International. The material has the following composition (wt. percent):

| C | Mn | P | S | Si | Cr |
|---|---|---|---|---|---|
| 0.056 | 0.85 | 0.027 | 0.027 | 0.41 | 18.36 |

| Ni | Mo | Cu | Co | Fe |
|---|---|---|---|---|
| 9.55 | 0.64 | 0.44 | 0.10 | balance |

Cylindrical tensile creep specimens with a gauge length approximately 1" long and 0.10" in diameter were machined from the rods and solution heated at 1040°C for 1 hr. These were subsequently prestrained by various amounts ranging from 0 to 10% on the Instron tensile tester at room temperature. Constant stress creep experiments were performed at temperatures ranging from 1200-1400°F and stress levels of 15,000-37,000 psi using an Andrade-type constant stress cam assembly as modified by Garofalo, et al.[5] to take account of different

initial specimen lengths. Strain measurement was made using a Linear Variable Differential Transformer (LVDT) attached to the linkage bearing the test specimen. This is connected to a Honeywell chart recorder whose output is displayed in form of a voltage-time plot. Values of creep strain less than $10^{-4}$ have been accurately measured with the LVDT. All tests were conducted in a Helium-furnace whose controller was monitored to limit temperature fluctuations to within ± 1°F of the desired temperature. Most specimens were tested to rupture while a few tests were discontinued prior to the tertiary creep stage.

### 7.2.4 Experimental Results

#### 7.2.4.1 Creep Curves and the Creep Parameters

Figure 1 shows the creep curves for tests performed at 1300°F and 35,000 psi. All our test data are well represented by the Garofalo creep relation:[6,9,10]

$$\epsilon = \epsilon_o + \dot{\epsilon}_s t + \hat{\epsilon}_t (1-e^{-rt}) \qquad (1)$$

where $\epsilon$, $\epsilon_o$ and $\hat{\epsilon}_t$ are the total creep strian at any time t, the instantaneous loading strain and the limiting transient creep strain respectively, $\dot{\epsilon}_s$ is the minimum creep rate and r is a parameter characterizing the rate of exhaustion of transient creep. It is noted in Fig. 1, that all the creep curves run nearly parallel to one another in the steady-state region. This is typical of tests

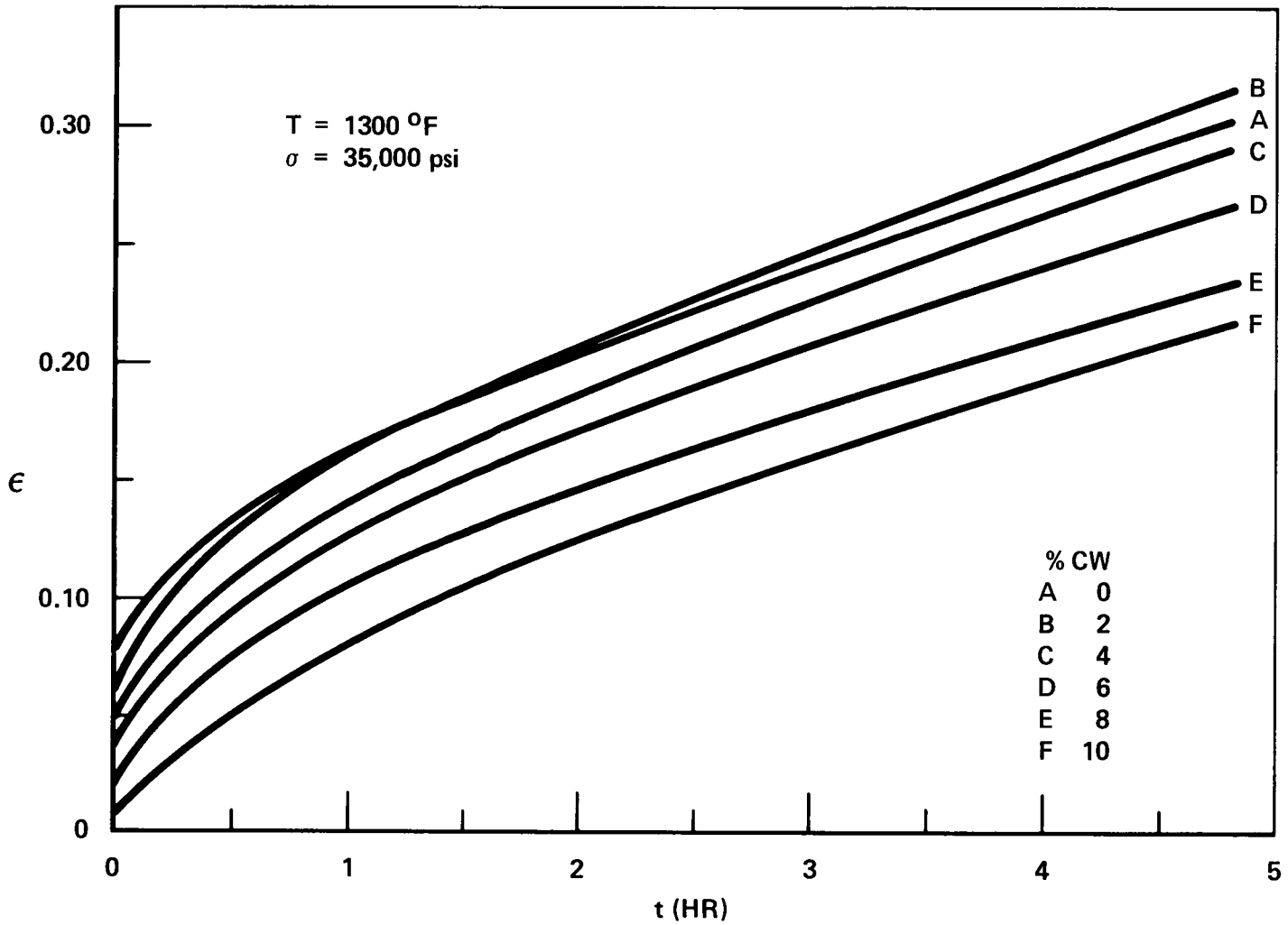


FIG. 1 Creep curves showing the primary and secondary creep stages for various cold work levels for tests performed at 1300°F and 35,000 psi.

TABLE I: Evaluated Creep Parameters At 1300°F

| $\sigma$ (psi) | % COLD WORK | $\varepsilon_o$(%) | $\hat{\varepsilon}_t$(%) | r($hr^{-1}$) | $\dot{\varepsilon}_s$($hr^{-1}$) | $\dot{\varepsilon}_i$($hr^{-1}$) | $t_r$(hr) |
|---|---|---|---|---|---|---|---|
| 35,000 | 0 | 9.07 | 4.65 | 1.711 | $3.40X10^{-2}$ | $1.14X10^{-1}$ | 5.4 |
| | 2 | 7.51 | 5.81 | 1.742 | $3.76X10^{-2}$ | $1.39X10^{-1}$ | 4.9 |
| | 4 | 6.15 | 5.57 | 1.536 | $3.61X10^{-2}$ | $1.22X10^{-1}$ | 4.7 |
| | 6 | 5.02 | 5.40 | 1.582 | $3.35X10^{-2}$ | $1.19X10^{-1}$ | 6.5 |
| | 8 | 3.05 | 6.85 | 1.145 | $2.75X10^{-2}$ | $1.06X10^{-1}$ | 7.2 |
| | 10 | 1.24 | 5.48 | 1.143 | $3.12X10^{-2}$ | $0.94X10^{-1}$ | 7.0 |
| 30,000 | 0 | 5.58 | 5.64 | 0.855 | $8.76X10^{-3}$ | $5.70X10^{-2}$ | 16.6 |
| | 2 | 3.23 | 5.78 | 0.611 | $6.67X10^{-3}$ | $4.20X10^{-2}$ | 20.0 |
| | 4 | 2.89 | 5.26 | 0.501 | $6.84X10^{-3}$ | $3.32X10^{-2}$ | 21.3 |
| | 6 | 0.98 | 6.21 | 0.509 | $11.08X10^{-3}$ | $4.27X10^{-3}$ | 15.2 |
| | 8 | 0.93 | 4.28 | 0.390 | $8.65X10^{-3}$ | $2.53X10^{-2}$ | 16.2 |
| | 10 | 0.74 | 0.66 | 0.344 | $8.43X10^{-3}$ | $1.07X10^{-2}$ | 19.7 |
| 25,000 | 0 | 2.40 | 3.38 | 0.278 | $1.61X10^{-3}$ | $1.10X10^{-2}$ | 69.9 |
| | 2 | 1.67 | 2.04 | 0.236 | $1.00X10^{-3}$ | $5.81X10^{-3}$ | 94.0 |
| | 4 | 0.43 | 1.48 | 0.264 | $1.79X10^{-3}$ | $5.70X10^{-3}$ | 61.6 |
| | 6 | — | 1.13 | 0.176 | $1.40X10^{-3}$ | $3.39X10^{-3}$ | 64.6 |
| | 8 | — | — | — | $4.30X10^{-4}$ | $4.30X10^{-4}$ | 83.1 |
| | 10 | — | — | — | $2.20X10^{-4}$ | $2.20X10^{-4}$ | 72.7 |
| 20,00 | 0 | 1.11 | 0.74 | 0.240 | $2.75X10^{-4}$ | $2.04X10^{-3}$ | 291.5 |
| | 2 | 0.68 | 0.49 | 0.124 | $1.73X10^{-4}$ | $7.86X10^{-4}$ | 305.2 |
| | 4 | 0.70 | 0.09 | 0.143 | $8.93X10^{-5}$ | $2.22X10^{-4}$ | 193.7 |
| | 6 | — | — | — | $7.29X10^{-5}$ | $7.29X10^{-5}$ | 248.7 |
| | 8 | — | — | — | $2.99X10^{-5}$ | $2.99X10^{-5}$ | 336.0* |
| | 10 | — | — | — | $6.89X10^{-6}$ | $6.89X10^{-6}$ | 336.0* |

* Tests Discontinued

carried out at the higher stresses. Table I gives a listing of the various creep parameters which were obtained from a curve-fitting computer program. Note that at the lower stresses, the steady-state creep rate becomes strongly dependent on prestrain.

If we differentiate Eq. (1) w.r.t time, the initial creep rate $\dot{\epsilon}_i$ at t = 0 is

$$\dot{\epsilon}_i = \dot{\epsilon}_s + r\hat{\epsilon}_t \tag{2}$$

The values of $\dot{\epsilon}_i$ computed from Eq. (2) are listed alongside the other parameters in Table I. $\dot{\epsilon}_i$ decreases with increasing cold work levels for all stresses and temperature (Fig. 3). The various parameters, $\dot{\epsilon}_s$, $\dot{\epsilon}_i$, $\hat{\epsilon}_t$ and r are plotted as functions of prestrain for tests performed at 1300°F (Fig. 2-5). While Fig. 2 demonstrates the strong improvement to creep resistance offered by prior cold work (a 10% prestrain decreases the creep rate by more than one order of magnitude), this ehancement is limited only to the lower stresses where the strain rate becomes less than $\sim 10^{-3}$ $hr^{-1}$ (hereafter referred to as "slow tests"). At the higher creep rates (Fig. 3) $\dot{\epsilon}_s$ is not appreciably affected by prestrain.

The transient creep strain varies in a manner similar to the secondary creep rate. For the slow tests ($\sigma$ = 25,000 and 20,000 psi), transient creep is completely eliminated in specimens prestrained more than 8%. $\hat{\epsilon}_t$ is, however, not significantly affected at the higher creep rates (Fig. 4). Although the transient creep parameter r decreases consistently with increasing cold work levels for all test

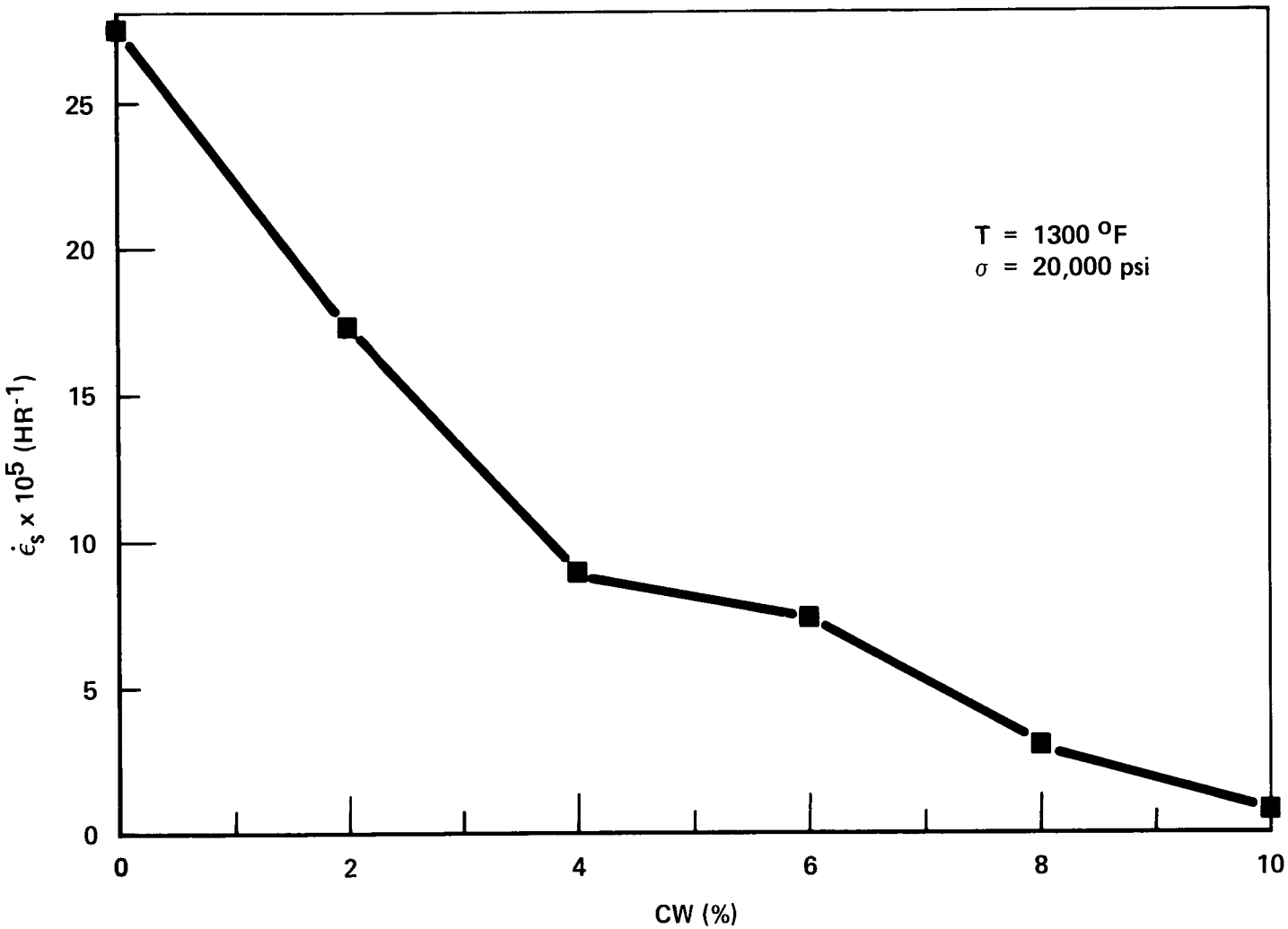


FIG. 2 Plot of steady-state creep rate ($\dot{\epsilon}_s$) vs. cold work level (CW) at 1300°F and 20,000 psi/

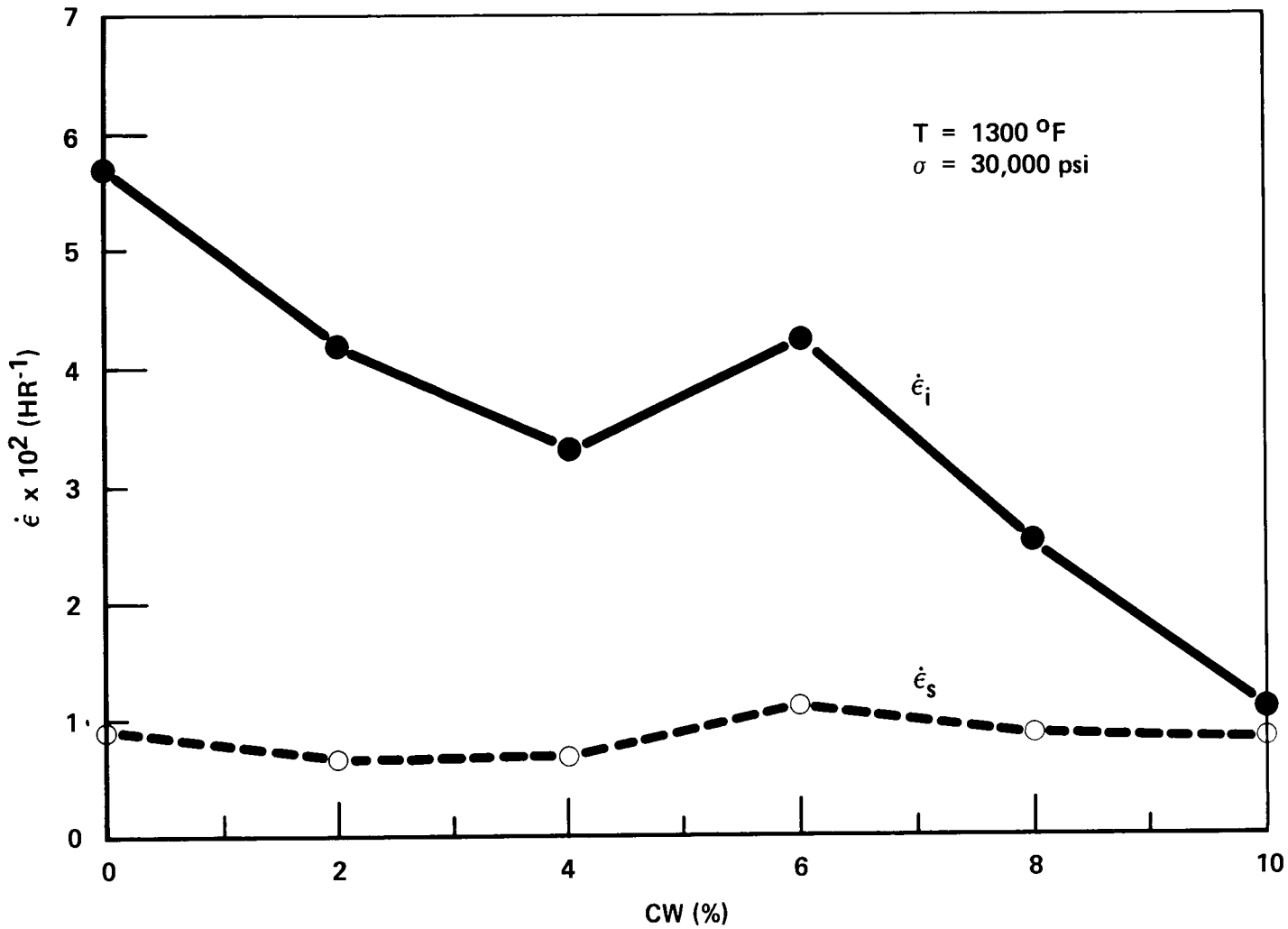


FIG. 3 Illustrating the dependence of the initial creep rate ($\dot{\epsilon}_i$) and the steady-state creep rate ($\dot{\epsilon}_s$) on prior cold work for tests run at 1300°F and 30,000 psi.

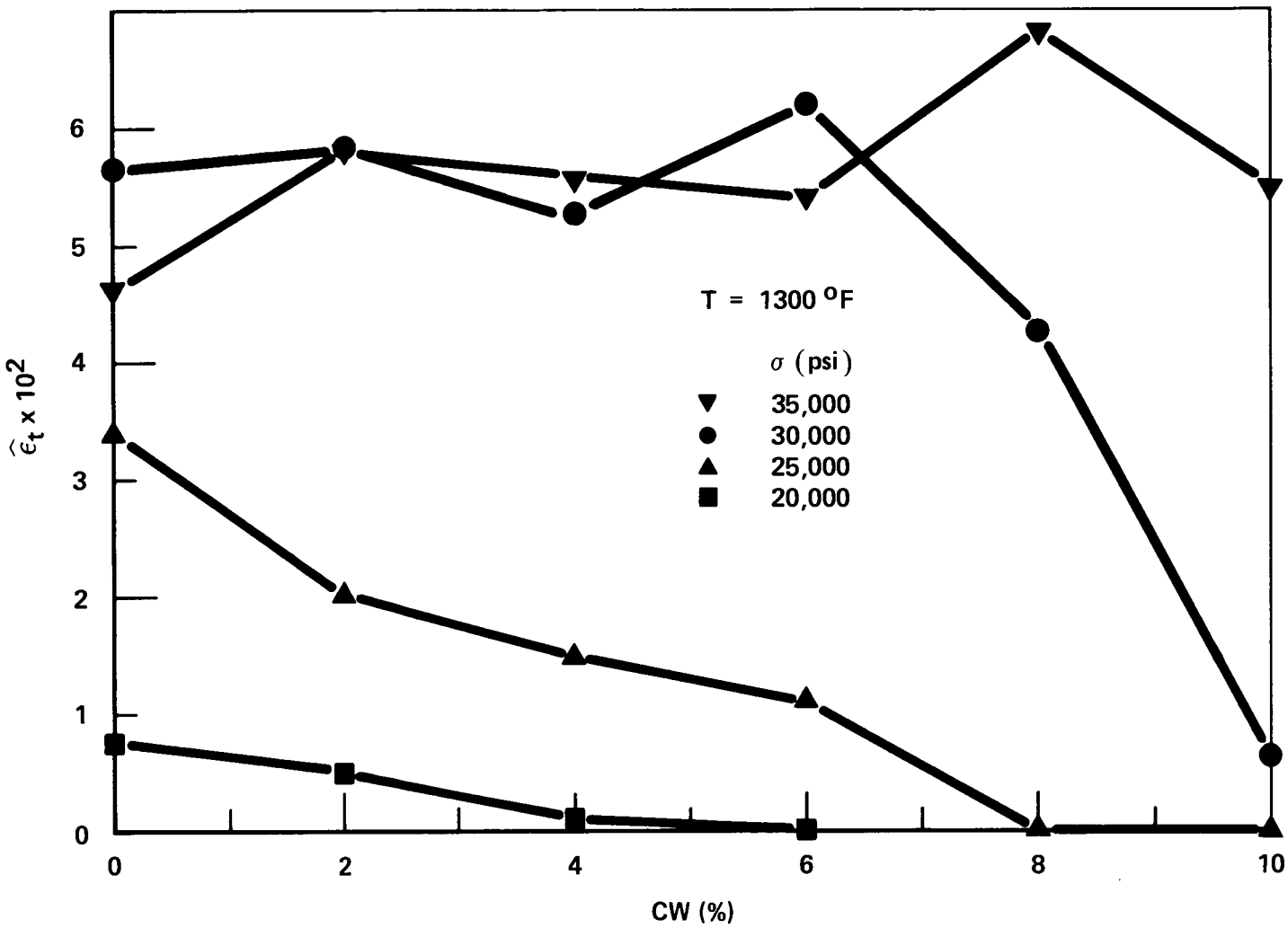


FIG. 4 The relationship between the limiting transient creep strain ($\hat{\epsilon}_t$) and prior cold work at 1300°F for various test stresses.

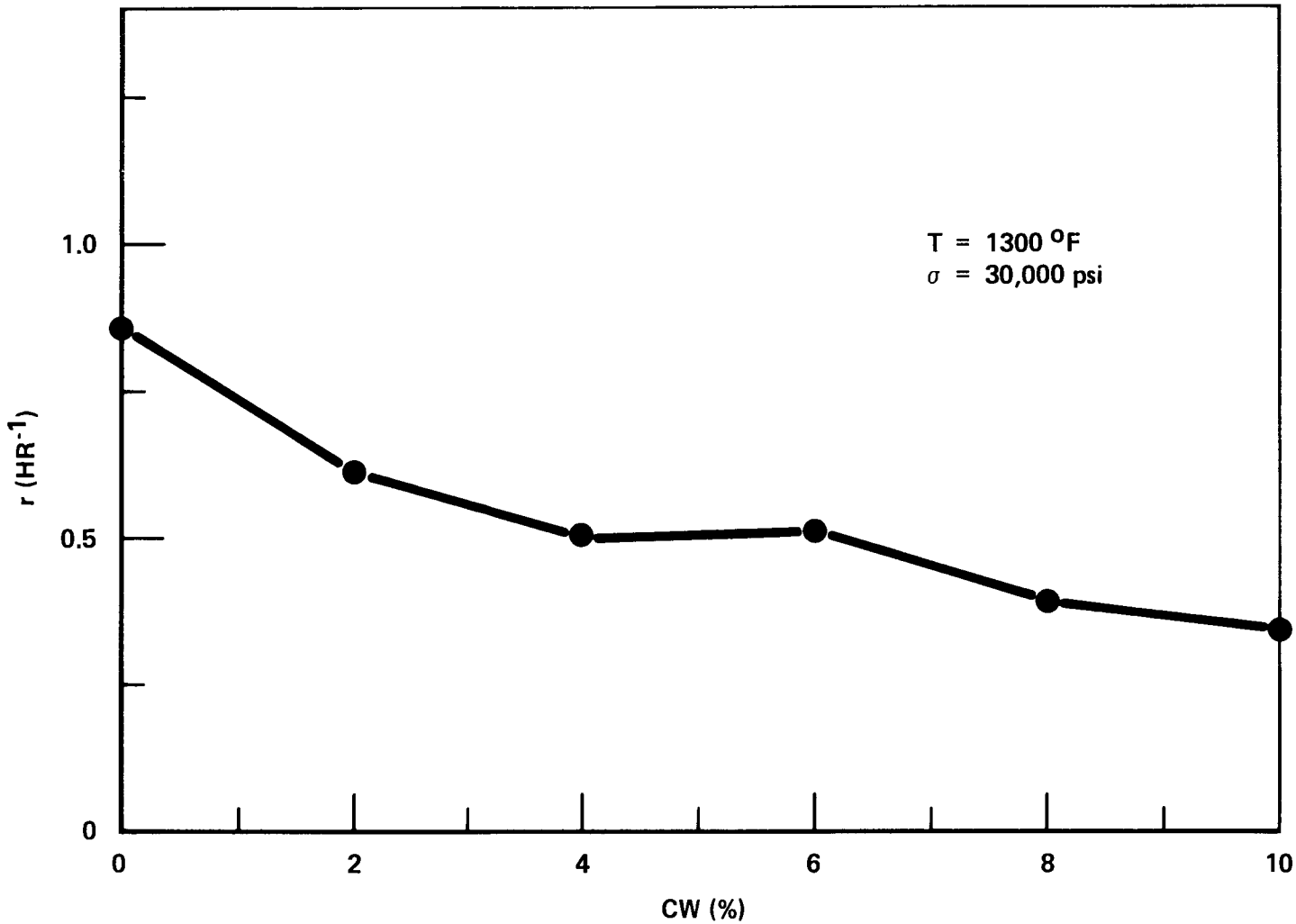


FIG. 5 Illustrating the relationship between the transient creep parameter (r) and prior coldwork at 1300°F and 30,000 psi.

conditions (Fig. 5), both r and $\epsilon_t$ increase with increasing temperature and stress. It appears, however, that the values of $\hat{\epsilon}_t$ obtained for $\sigma$ = 30,000 psi are not significantly altered by a further stress increase to 35,000 psi (Fig. 4). This kind of behavior has been noticed by other investigators where the limiting transient creep strain becomes stress independent after a certain stress level[11] or could even decrease with a further stress increase.[10]

7.2.4.2 Rupture Life, $t_r$

This project is a follow-up of the investigation by Ardell, et al.[3] of the effects of cold work (up to 80%) on the rupture life and minimum creep rates of Type 316 stainless steel. While an optimum level of cold work was observed for which the rupture life was maximized, a somewhat consistent trend was noticed whereby the rupture life initially decreased with increasing cold work up to about 5%, and then increased, appearing to go through a minimum around 4 to 6% cold work. This, in fact, was the main factor in the choice of 0 to 10% cold work levels for the present investigation. The values of rupture life ($t_r$) obtained for tests carried out on Type 304 stainless steel at 1300°F are listed in Table I. As expected, the high temperature and stress tests, in which the minimum creep rates are not significantly prestrain dependent, do not show an appreciable dependence of rupture life on prior cold work. For the slow tests, however, $t_r$ appears to be appreciably lowered for specimens cold-worked 4 and 6%, beyond which an increase in prestrain results in

increased rupture life. More tests will be performed at the slow strain rates in order to fully clarify if this effect is real. If it proves real and significant, then reasons for such behavior will be delineated.

7.2.4.3 Activation Energy

The steady-state creep rate, $\dot{\epsilon}_s$, varies with stress ($\sigma$) and temperature (T) according to the relation:

$$\dot{\epsilon}_s = A_o \exp(\beta_s) \exp(-Q/RT) \qquad (3)$$

where Q is the activation energy for creep and R is the universal gas constant =1.987 cal/mole/°K. $A_o$ and $\beta_s$ are constant at a given temperature. In the present investigation, $\beta$ was found to vary slightly with temperature, its value increasing from $2.67 \times 10^{-4}$ $psi^{-1}$ at 1200°F to $3.2610^{-4}$ $psi^{-1}$ at 1300°F. The fact that $_s$ varies with test temperature for stainless steels had been established by other authors.[4,6]

From Eq. (3),

$$\frac{\dot{\epsilon}_s}{\exp(\beta_s \sigma)} = A_o \exp(-Q/RT) = A'$$

The activation energy for creep was computed from an Arrhenius plot of A' vs. 1/T. The activation energy so obtained for annealed specimens was 76.3 Kcal, in good agreement with established values for stainless steels.[6,10] Further tests at various temperatures and stress levels are required for cold-worked specimens in order to check if the activation energy is affected by prestrain.

### 7.2.5 Discussion of Results

#### 7.2.5.1 Initial Creep Rate, $\dot{\epsilon}_i$

For annealed materials, the initial creep rate had been shown[6,7,8,10] to be related to the secondary creep rate according to the equation:

$$\dot{\epsilon}_i = K\dot{\epsilon}_s \tag{4}$$

where K is a constant.

Figure 6 shows a log-log plot of $\epsilon_i$ vs. $\dot{\epsilon}_s$. For all specimens that exhibit transient creep, our data fit a more general relationship of the type:

$$\dot{\epsilon}_i = k(\dot{\epsilon}_s)^n \tag{5}$$

where n varies from 0.96 for annealed specimens to 1.33 for specimens prestrained 8%. The value of 0.96 is in close agreement with Eq. (4), which predicts a value of n = 1 for unprestrained material. We do not have sufficient transient creep data at this tage to evaluate n for specimens with 10% prior cold work. Figure 6 is also representative of the results obtained for specimens creep tested at 1400°F. For specimens which do not exhibit the transient creep stage, all data points should lie on the line $\dot{\epsilon}_i = \dot{\epsilon}_s$, which has been superposed on the $\dot{\epsilon}_i$ vs. $\dot{\epsilon}_s$ plot. As mentioned earlier, the limiting transient creep strain decreases with decreasing stress, so that it is possible to completely eliminate transient creep, even in annealed materials, by testing at lower stresses. Referring to Fig. 6, the point at which

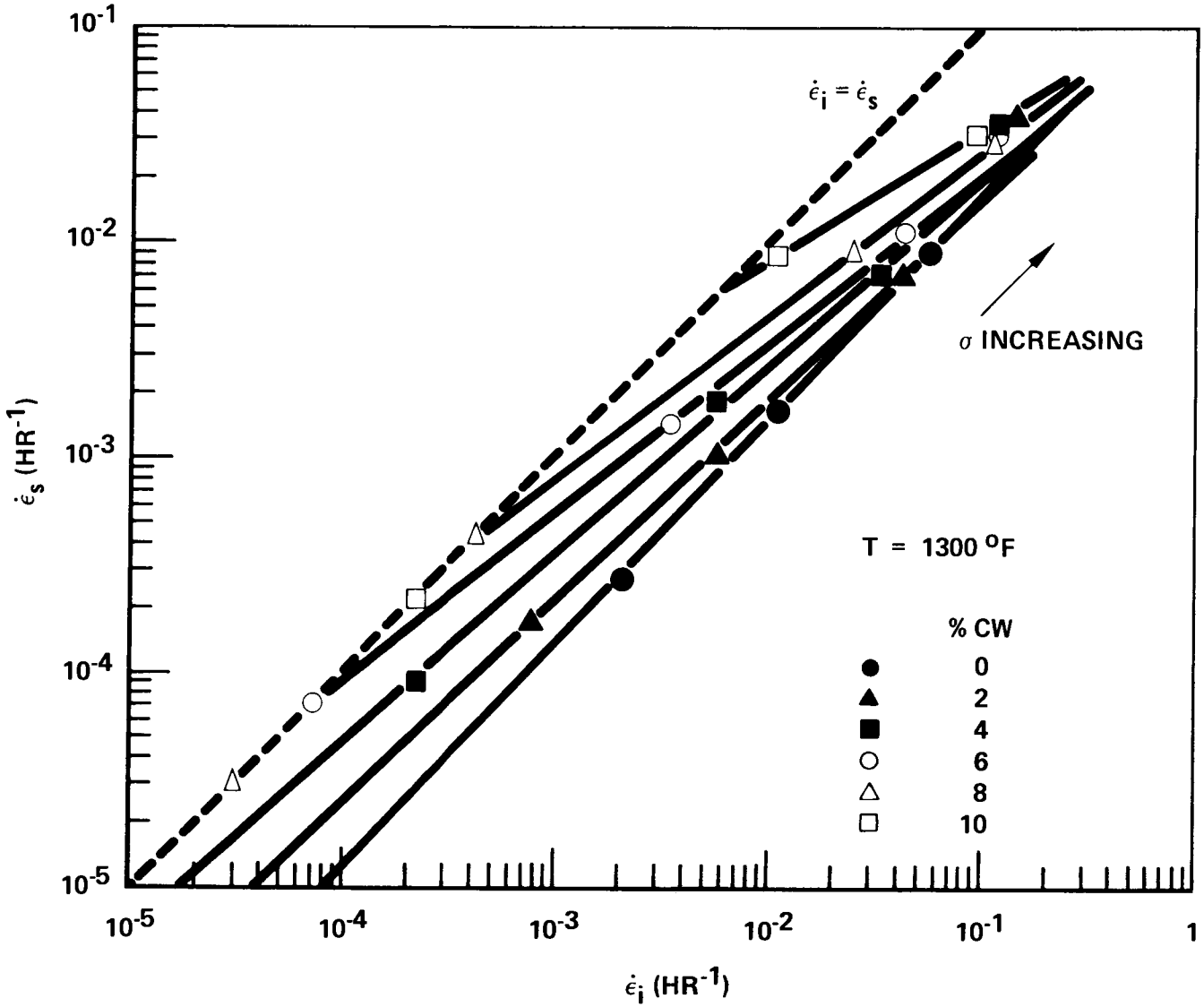


FIG. 6 Plots of the steady-state creep rate ($\dot{\epsilon}_s$) vs. the initial creep rate ($\dot{\epsilon}_i$) for different cold work levels for tests performed at 1300°F and various stress levels ranging from 20,000 - 35,000 psi.

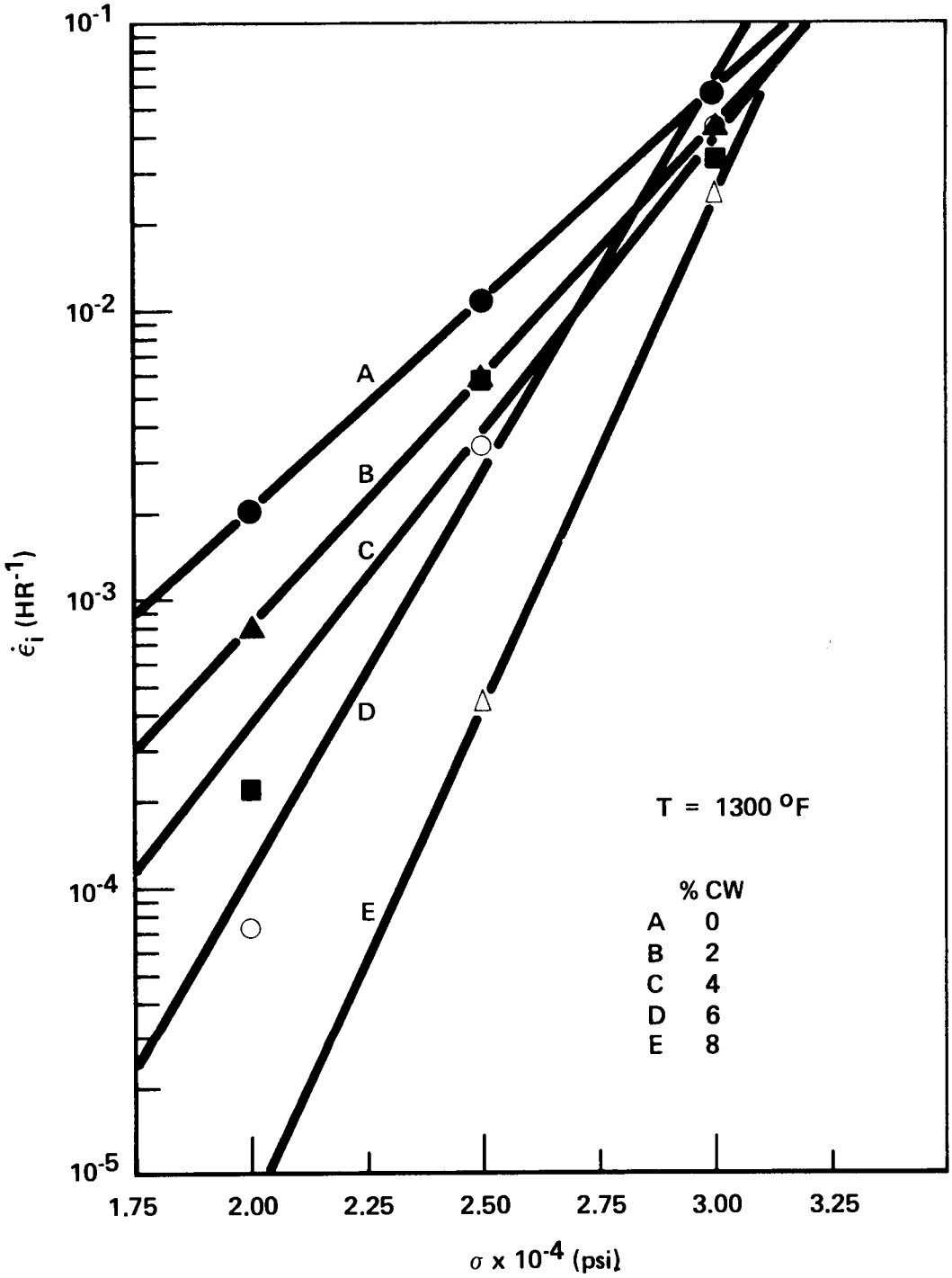


FIG. 7 The dependence of the initial creep rate ($\dot{\epsilon}_i$) on test stress for various cold work levels at 1300°F.

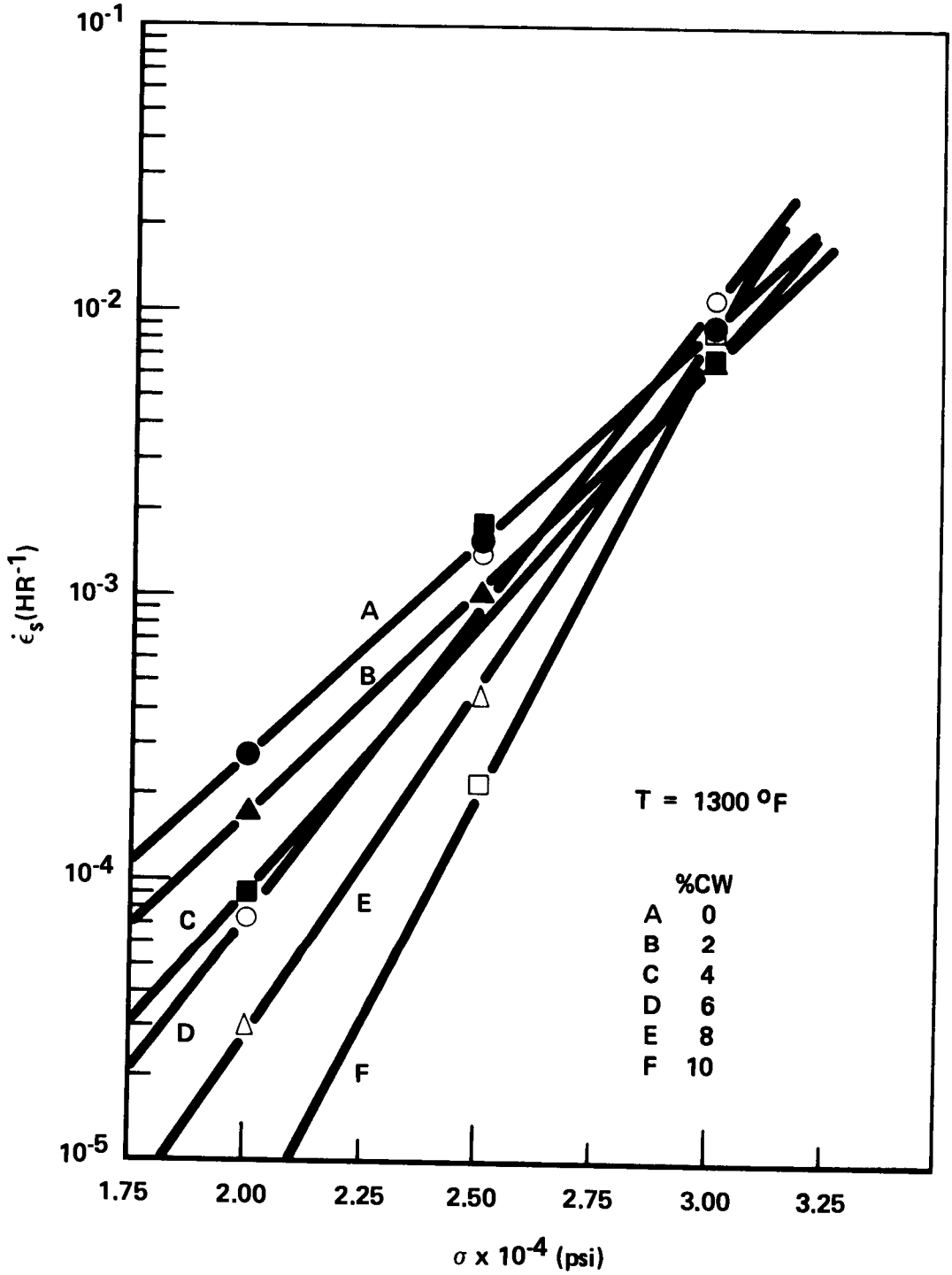


FIG. 8 The dependence of the steady-state creep rate ($\dot{\epsilon}_s$) on test stress for various cold work levels at 1300°F.

the plot of $\dot{\epsilon}_i$ vs. $\dot{\epsilon}_s$ represents the creep-rate below which no transient creep is expected. It becomes apparent that specimens containing higher levels of cold work attain this "Nil-Transient-Creep" condition at higher strain rates, i.e., higher stress levels. While transient creep has been completely eliminated in specimens prestrained 10% at a strain rate of $5 \times 10^{-3}$ $hr^{-1}$, corresponding to a test stress of over 25,000 psi, it is necessary to go down to a creep rate of $7 \times 10^{-5}$ $hr^{-1}$($\sigma \sim$20,000 psi) to wipe out the transient creep in a specimen with 6% prior cold work. This is not surprising since cold working aids in eliminating transient creep.[1,2,10]

Equation (2) can be rewritten as:

$$\dot{\epsilon}_s = B\exp(\beta_s \sigma) \text{ for a given temperature}$$

Combining this with Eq. (5), we obtain

$$\dot{\epsilon}_i = k\left[B\exp(\beta_s \sigma)\right]^n = C\exp(n\beta_s \sigma) \ ,$$

where $C = kB^n$

Therefore, $$\dot{\epsilon}_i = A'' \, e^{\beta_i \sigma} \tag{6}$$

where $$\beta_i \equiv n\beta_s \tag{6-a}$$

$\dot{\epsilon}_i$ and $\dot{\epsilon}_s$ are plotted as functions of stress in Figs. 7 and 8. It is apparent from the plots that $\beta_i$ and $\beta_s$ (the slopes of the lines in Figs. 7 and 8, respectively) are both dependent on prestrain. The values are listed in Table II along with the values of n and k obtained from Fig. 6.

TABLE II: Comparison of the values of 'n' (from Fig. 6) with "$\beta_i/\beta_s$" (from Figs. 7 and 8)

| (%) Cold Work | $\beta_i \times 10^{-4}$ (psi$^-$) | $\beta_s \times 10^{-4}$ (psi$^-$) | $\beta_i/\beta_s$ | n | k |
|---|---|---|---|---|---|
| 0 | 3.33 | 3.26 | 1.02 | 0.96 | 5.44 |
| 2 | 3.98 | 3.65 | 1.09 | 1.09 | 10.17 |
| 4 | 5.01 | 4.33 | 1.16 | 1.14 | 8.98 |
| 6 | 6.38 | 5.03 | 1.27 | 1.27 | 13.46 |
| 8* | --- | --- | --- | 1.33 | 13.20 |

TABLE III: Values of $\sigma_o$, $\chi_o$, $\chi_t$ and $\chi_t$ computed from Figs. 9 and 10

| (%) Cold Work | $\sigma_o \times 10^{-3}$ (psi) | $\chi_o \times 10^{-3}$ (psi) | $\sigma_t \times 10^{-3}$ (psi) | $\chi_t \times 10^{-3}$ (psi) |
|---|---|---|---|---|
| 0 | 12.72 | 74.19 | 14.16 | 64.00 |
| 2 | 14.59 | 77.55 | 16.18 | 58.44 |
| 4 | 21.20 | 54.57 | 18.63 | 50.16 |
| 6 | 25.21 | 44.44 | 20.28 | 39.87 |
| 8 | --- | --- | 25.00 | 27.00 |

*No sufficient data points to evaluate $\beta_i/\beta_s$ for 8 and 10% cold work, and n for 10% cold work.

### 7.2.5.2 The Instantaneous Loading Strain ($\epsilon_0$) and the Limiting Transient Creeep Strain ($\hat{\epsilon}_t$)

The plots of $\sigma$ vs. ($\epsilon_0$) and ($\hat{\epsilon}_t$) in Figs. 9 and 10 indicated that both $\epsilon_0$ and $\hat{\epsilon}_t$ obey a parabolic work-hardening relation for plastic deformation:

$$\sigma = \sigma_0 + \chi_0 \, \epsilon_0^{1/2} \tag{7-a}$$

and

$$\sigma = \sigma_t + \chi_t \, \hat{\epsilon}_t^{1/2} \tag{7-b}$$

where $\sigma_0$, $\sigma_t$ are the threshold stresses $\chi_0$, $\chi_t$ are work-hardening coefficients for the instantaneous and transient creep strains. This behavior had been observed in Type 316 stainless steels,[10] Ni and several other materials.[7] $\sigma_0$ represents the stress level below which no instantaneous strain at loading is expected and $\sigma_t$ has the significance that no transient creep should be observed at lower stress levels. The values of $\sigma_0$, $\chi_0$, $\sigma_t$, and $\chi_t$ are listed in Table III. Both $\sigma_0$ and $\sigma_t$ increase with increasing level of prestrain, as expected, once again confirming the observation in Fig. 6 that lower stresses are necessary to eliminate transient creep in specimens with lower prestrain. $\chi_t$ is less than $\chi_0$ in all cases, demonstrating that appreciably less work-hardening has resulted by the end of the transient creep. Garofalo[10] attributed this effect to the dynamic recovery whic occurs during primary creep. Increasing the prior cold work also results in a lower work-hardening coefficient, apparently due to faster recovery rate induced by higher levels of cold work.

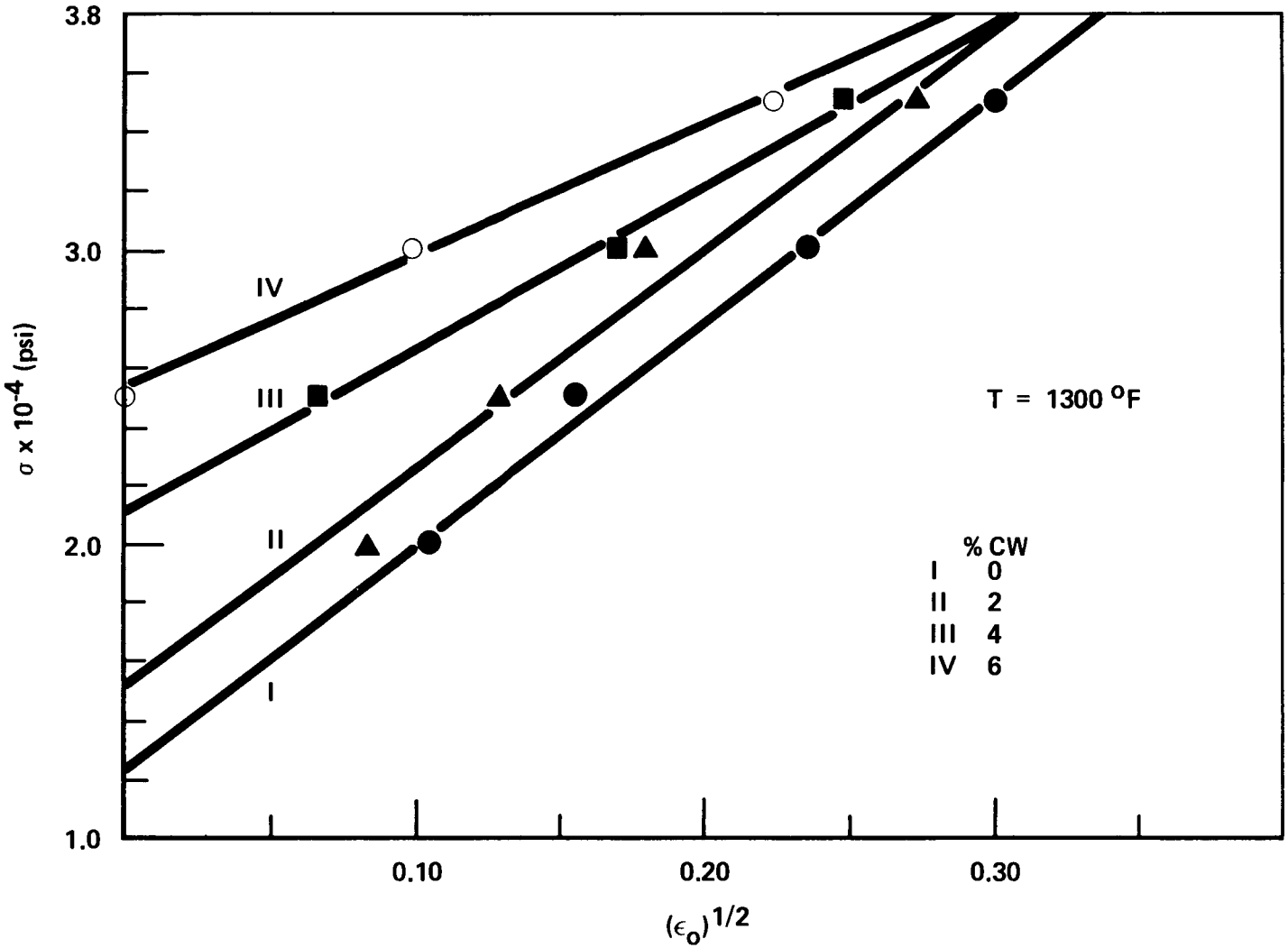


FIG. 9 The relationship between stress ($\sigma$) and the instantaneous loading strain ($\epsilon_0$) for different cold work levels at 1300°F.

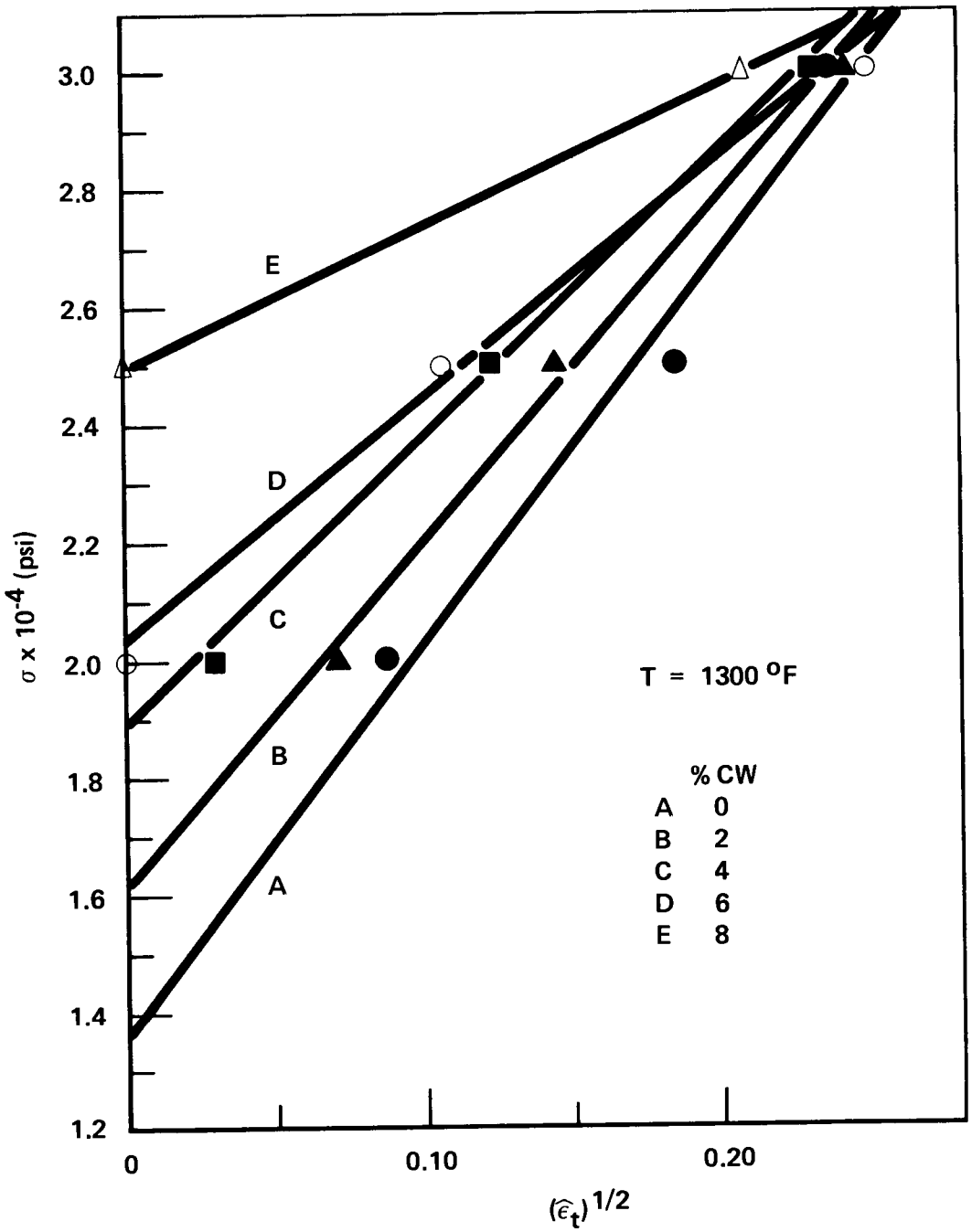


FIG. 10 The relationship between stress ($\sigma$) and the limiting transient creep strain ($\hat{\epsilon}_t$) for different cold work levels at 1300°F.

### 7.2.5.3 The Transient Creep Parameter r

This parameter decreases rather consistently with increasing cold work for all test conditions. Since r represents the rate at which transient creep is exhausted, that is, the rate at which the steady-state creep substructure is developed, it follows that cold work slows down the rate of development and stabilization of this substructure. This is due to the fact that the value of r is determined mainly by the initial creep rates and transient creep strain.

According to Eq. (2),

$$r = \frac{\dot{\epsilon}_i - \dot{\epsilon}_s}{\hat{\epsilon}_t}$$

At higher stress levels, $\dot{\epsilon}_i >> \dot{\epsilon}_s$ so that $r \cong \dot{\epsilon}_i/\hat{\epsilon}_t$. The observation that cold work in fact reduces the initial creep rate (and hence r) can be attributed to the work-hardening (creep resistant) structure introduced in the material by cold working prior to the creep test. The loading duration is short and significant recovery is not expected to have occurred by the beginning of the transient creep.

### 7.2.5.4 The Steady State Creep Rate, $\dot{\epsilon}_s$

At the higher creep rates, the lack of enhancement of creep strength by prestrain can be associated with recovery occurring during the test. The fact that the steady-state creep rates are not prestrain-dependent shows that essentially the same creep substructure had been established in all the specimens by the end of the transient creep.

For the slow tests, recovery is fairly slow and recrystallization is unlikely to occur, hence prestrained specimens are able to retain the creep-resistant structure introduced by cold work.

### 7.2.6 CONCLUSIONS

1) The initial creep rate $\dot{\epsilon}_i$ is related to the steady-state creep rate $\dot{\epsilon}_s$ according to the empirical equation:

$$\dot{\epsilon}_i = k(\dot{\epsilon}_s)^n$$

where n has a value of approximately 1 for annealed specimens, which increases to 1.33 for specimens prestrained 8%.

2) The stress dependence of $\dot{\epsilon}_s$ in the relation

$$\dot{\epsilon}_s = Ae^{\beta\sigma}$$

is influenced by the dependence of $\beta$ on prior cold work. The value of $\beta$ is nearly doubled by a prestrain of 8%.

3) Both the instantaneous loading strain ($\epsilon_0$) and the limiting transient creep strain ($\hat{\epsilon}_t$) obey the parabolic work-hardening relation for plastic deformation. This leads to linear plots of stress vs. $(\epsilon_0)^{1/2}$ and $(\hat{\epsilon}_t)^{1/2}$ from which threshold stresses ($\sigma_0$ and $\sigma_t$) necessary to generate instantaneous loading and transient creep strains could be predicted.

(4) Prior cold work enhances the creep strength only for the low-strain-rate tests where recovery is not rapid enough to eliminate the benefits of cold work.

### 7.2.7 References


1. W. Yim and J. Grant, Trans. Met. Soc. AIME, 227 (1963) 868.
2. T.H. Hazlett and R.D. Hansen, Trans. ASM, 47 (1955) 508.
3. A.J. Ardell, K. Ono and A.S. Tetelman, U.S. Atomic Energy Commission Quarterly Progress Report on Reactor Steels, Contract No. AT(04-3)-34, PA #177, UCLA School of Engineering and Applied Science, January - March, 1973.
4. A.J. Lovell, "Creep of 20% Cold-Worked Type 316 Stainless Steel," Hanford Engineering Development Laboratory (HEDL), Report No. HEDL-TME 73-65, October 1973.
5. F. Garofalo, O. Richmond, W.F. Domis, Journal of Basic Engineering, 84 (1962) 287.
6. F. Garofalo, O. Richmond, W.F. Domis and F. Von Gemmingen, "Joint International Conference on Creep," London, 1963, Institute of Mech. Engineering, p. 1-31.
7. W.J. Evans and B. Wilshire, Trans. Met. Soc. AIME, 242 (1968) 1303.
8. D. Sidey and B. Wilshire, Metal Science Journal, 3 (1969) 56.

9. F. Garofalo, W.F. Domis and F. Von Gemmingen, Trans. Met. Soc. AIME, 230 (1964) 1460.

10. F. Garofalo, Fundamentals of Creep and Creep-Rupture in Metals, Macmillan, New York, 1965.

11. P.L. Threadgill and B. Wilshire, "Creep Strength in Steel and High-Temperature Alloys," Proceedings of a meeting organized by the Iron and Steel Institute, University of Sheffield, England, September 1972, p. 8.

# 8. GENERAL ELECTRIC COMPANY

K. D. Challenger

## 8.1 INTRODUCTION

The principal objective of mechanical properties testing at the General Electric Company is to characterize the behavior of 2¼Cr-1Mo and austenitic stainless steels in sodium environments relevent to LMFBR steam generators and intermediate heat transport systems. Under conditions predicted for the intermediate sodium system of the CRBRP, 2¼Cr-1Mo will lose carbon to the system and be weakened. The carbon will tend to carburize and embrittle stainless steel components in other portions of the system. The effects of a carburizing environment on creep rupture properties of Type 316 stainless steel will be evaluated along with an assessment of creep-fatigue interactions. In addition, studies of fatigue crack propagation rates in carburizing sodium will be performed in order to assess environmental effects under pertinent intermediate sodium loop loading conditions. The loss of carbon from 2¼Cr-1Mo steel components can result in increased creep rates of the decarburized surface layer with the possibility of ratchetting under cyclic straining. These effects will be evaluated for base metal and weld metal in a decarburizing sodium environment. Elastic-plastic fracture mechanics methods, including J-Integral and Crack Opening Displacement (COD) are being employed to determine the toughness ($K_{Ic}$) of 2¼Cr-1Mo steel at relevant temperatures and to compute the critical flaw sizes for the onset of rapid fracture. The effects of welding procedure, flaw location and thermal aging are being evaluated. The effect of melting practice and heat treatment on the mechanical behavior of 2¼Cr-1Mo is being evaluated to confirm that the properties of consumable remelted 2¼Cr-1Mo meet the appropriate requirements of the ASME B&PV Code for LMFBR steam generators.

## 8.2 MECHANICAL PROPERTIES OF STAINLESS STEEL IN CARBURIZING SODIUM

### 8.2.1 Fatigue Crack Growth Studies - J. F. Copeland/G. R. Dodson

The objective of this program is to determine the environmental influence of liquid sodium on the fatigue crack propagation rates for annealed Type 316 stainless steel. To be prototypic of expected LMFBR Intermediate Heat Transport System (IHTS) piping conditions, this testing is being done at low frequency (0.5 cycles per minute (cpm) and at 510°C (950°F). Additionally, the existence of a high carburizing potential in the liquid sodium environment is a distinct possibility.[1] Since the exact carburizing potential of the IHTS sodium has not been determined, this experiment is being run under the most severe conditions, carbon-saturated sodium. The use of carbon-saturated sodium also allows the acceleration of carburization in order to represent design life conditions with a relatively short-term test. Control tests in air are also being performed under the same loading conditions, in order to truly discern environmental effects. These results will show whether or not penalties or allowances for crack growth in secondary system sodium are required or warranted.

ASTM E399, 12.7 mm. (0.5 in.) thick, 3-point bend specimens were machined from annealed 15.9 mm. (5/8 in.) Type 316 plate[1] and fatigue precracked. Specimens to be tested in air were aged at 510°C (950°F) for 1000 hours in air. Those to be fatigued in high carbon sodium were pre-exposed in Loop A sodium with a Grade 1050 carbon steel source at 510°C (950°F) for 1000 hours. The carburization incurred by these specimens during sodium pre-exposure is shown in Figure 8.1, and is typical of that anticipated[1] for a 30-year LMFBR design life with a 2¼Cr-1Mo steel carbon source.

Fatigue crack growth tests were performed in air and flowing, high carbon sodium in two specially designed fatigue test facilities.[1] Three tests could be run concurrently in each facility. After loading for an estimated number of cycles, the specimens were withdrawn and examined for crack growth. When the crack growth approximated 0.76 mm. (30 mils) the specimen was fractured to accurately measure crack growth. A crack

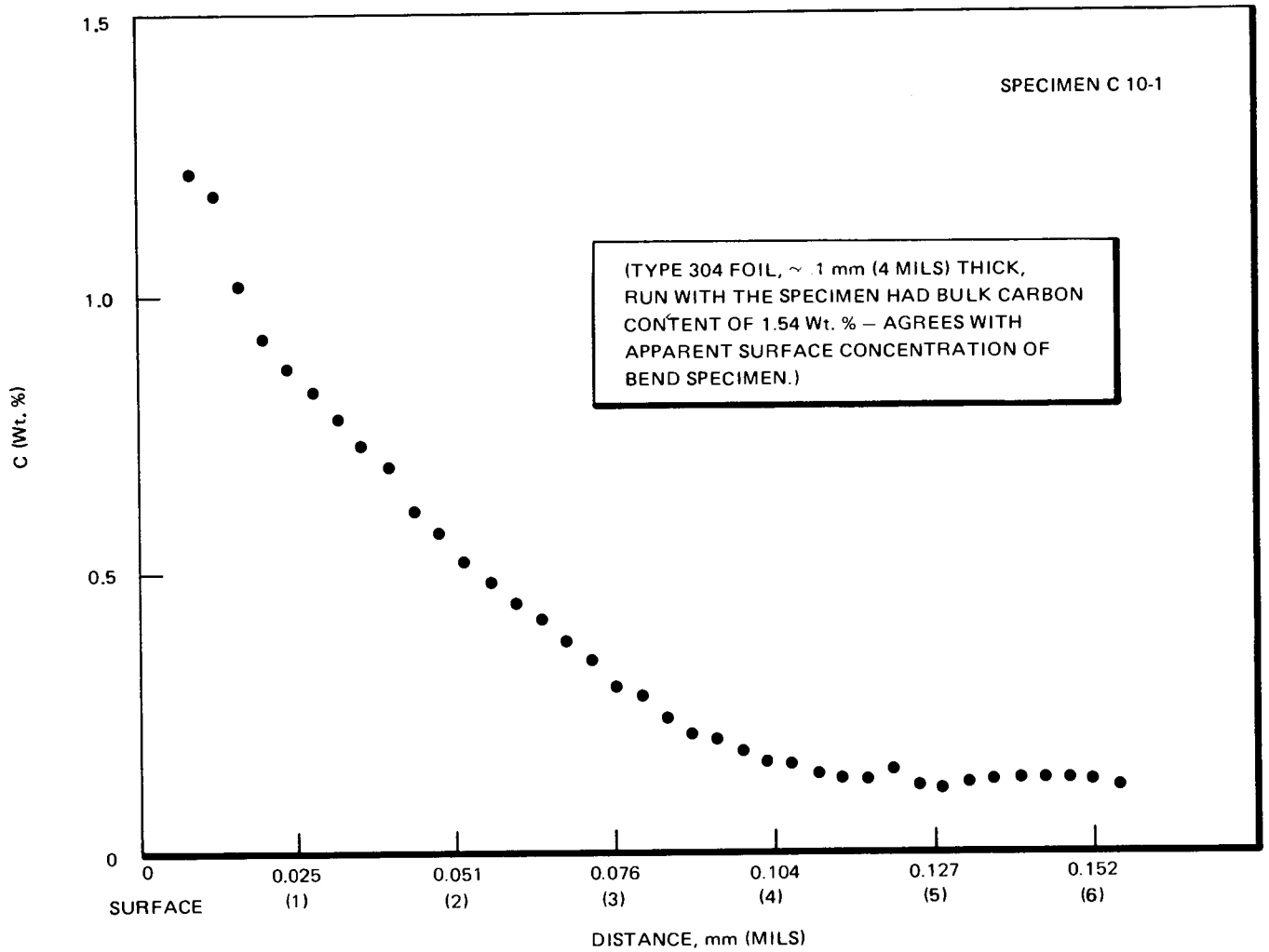


Figure 8.1. *Carbon Profile (Electron Microprobe) on Annealed Type 316 12.7 mm (0.5 in.) Bend Specimen Aged in Loop A for 1000 Hr at 510°C (950° F). 1050 Carbon Steel Source (Carbon – Saturated Sodium)*

growth rate was then computed from the ratio of crack extension to cycles. The stress intensity factor range ($\Delta K$) was calculated at half the crack extension. Preliminary results for tests in air and sodium are shown in Figure 8.2, and compared to other data.[2,3,4,5] The control data (air) is in excellent agreement with previous results.[2,3] Several more tests will be run to more exactly determine this crack growth line. The sodium results fall below the air test values (slower crack growth in sodium) for the low $\Delta K$ values, where crack growth is slower and environment is expected to have more influence. These results fall slightly above the lower carbon sodium results at 427°C (800°F) and 600°C (1112°F) of HEDL and CEGB. This may indicate a slight environmental effect. At higher $\Delta K$ levels there appears to be little environmental influence on crack propagation rates. It should be noted that reference foil monitors indicate a fairly low carburizing potential of the sodium during these six tests. This will be verified and corrected. Further testing is being pursued to verify these preliminary trends. Also, future testing will include slower cycle rates and the influence of hold-times under load. Additional specimens, including some from GTA weldments, are being prepared.

In analyzing the results shown in Figure 8.2, an assessment of fatigue crack growth rate versus carburization rate was performed. Special attention was given to future test planning with hold-times, where carburization could occur during the hold-time period between cycles. Hold-time must be adjusted to allow the diffusion of carbon into the sample to affect crack growth. The carbon must diffuse through the fatigue pre-crack to the surface of the growing crack tip and into the metal. Simple estimates of the time required for carbon diffusion to influence crack growth have been made and hold-times of approximately 1 hour are indicated. The diffusion coefficient for carbon in sodium lies between $10^{-3}$ and $10^{-5}$ $\frac{cm^2}{sec}$ at the testing temperatures. The fatigue pre-crack length of the specimen is approximately 1.4 mm (55 mils). During a time interval of 1 minute, carbon can effectively diffuse from 0.2 to 2.5 mm (7.9 to 98 mils), depending upon the value of the diffusivity of carbon in sodium. In 1 hour this distance is approximately 2 to 20 mm (.079 to .79 in.). Since carbon must diffuse through the sodium in the

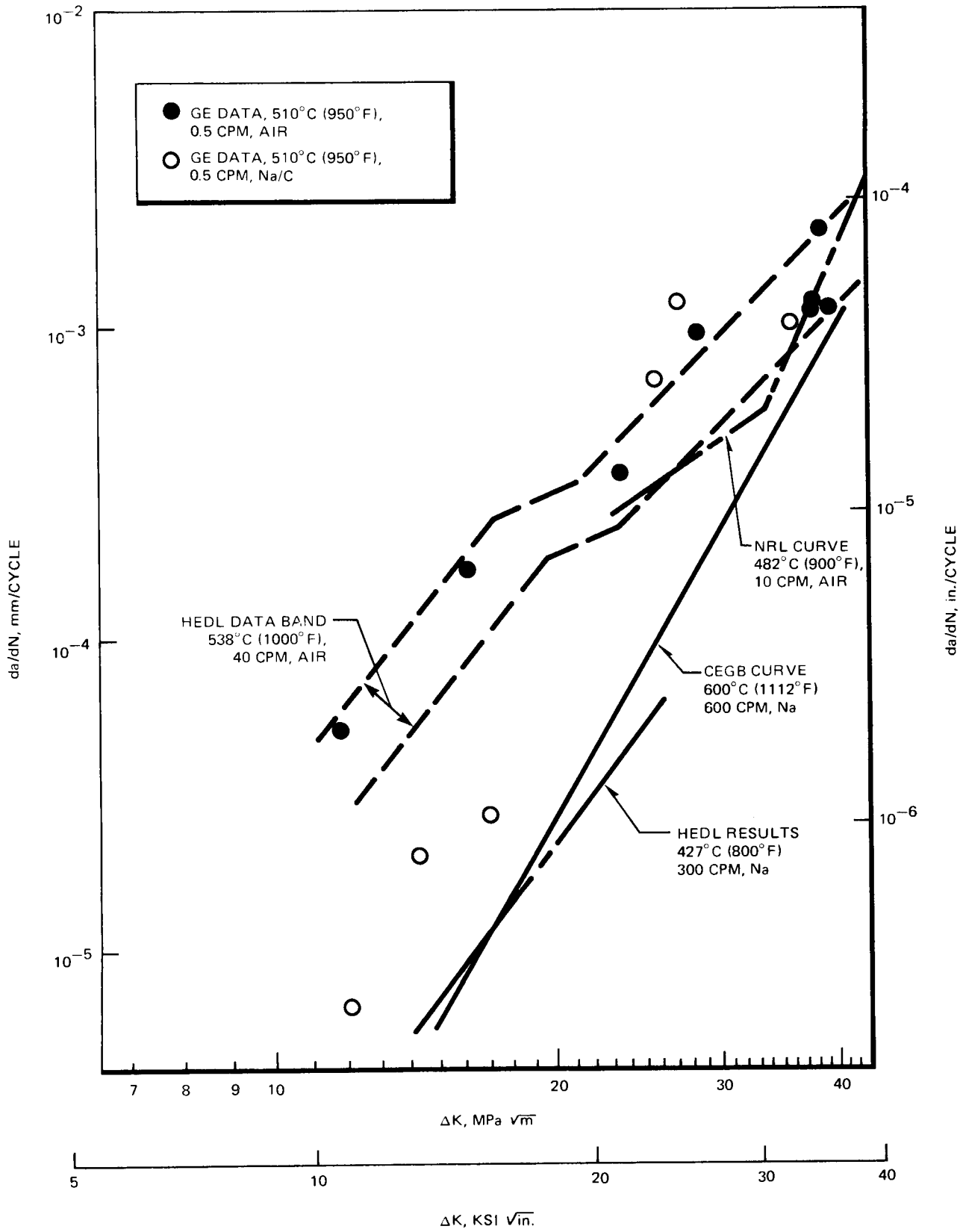


Figure 8.2. Comparison of Fatigue Crack Propagation Rate Results for Annealed Type 316 Stainless Steel in Air and Sodium at Elevated Temperatures.

fatigue crack before it reaches the crack tip, hold-times of approximately 1 hour are required. The effective distance of carbon diffusion into the stainless steel crack tip, provided the sodium can freely supply carbon, is approximately $2X10^{-4}$ mm ($7.9 \times 10^{-6}$ in.) for a hold-time of 1 minute and $1.6 \times 10^{-3}$ mm ($6.3 \times 10^{-5}$ in.) for a hold-time of 1 hour. The value of $10^{-3}$ mm ($3.9 \times 10^{-5}$ in.) is approximately the crack growth distance per fatigue cycle. If hold-times of less than 1 minute are employed, the crack extension should outstrip the diffusion length of the metal and no significant effect of carburization or crack extension will occur. For 1 hour hold-time, the effective diffusion distance of carbon through the fatigue pre-crack and into the stainless steel is theoretically large enough for the effect of carburization on crack growth to appear. For crack growth rates on the order of $10^{-4}$ or $10^{-5}$ mm/cycle ($3.9 \times 10^{-6}$ or $3.9 \times 10^{-7}$ in./cycle), as at lower $\Delta K$ values, even the one or two minute hold-time could reveal the influence of carburization on crack growth rates. Several longer hold-time tests will be run in the near future.

### 8.2.2 Creep/Fatigue Studies - P. P. Pizzo

The objective of this program is to evaluate the tension creep properties of Type 316H stainless steel in a carburizing sodium environment. Particular attention has been given creep behavior under both sustained and cyclic load conditions. Analysis of the preliminary data results has been presented elsewhere.[6] In the following discussion, recently acquired data is presented. Also, previously reported data has been modified to incorporate temperature/stress corrections based on data obtained on instrumented test specimens. The data presented in this discussion supersede data reported in previous GE(FBRD) documents.

Table 8.1 lists the test parameters applicable to the creep-fatigue program. A tubular sample configuration is used to provide a continuously carburizing environment during testing. Specimens are filled with either high purity sodium and a Grade 1095 steel (wire) carbon source, or with Argon for control testing. Tensile test data characterizing the 316H stainless steel test material are included in Table 8.2.

TABLE 8.1

CREEP-FATIGUE TEST PARAMETERS
TUBULAR TENSION SAMPLES

| | |
|---|---|
| Environment | - Carbon-Saturated Na or Argon (Inside Diameter) |
| | - Air (Outside Diameter) |
| Test Temperature | - 502°C (935°F) |
| Material | - Annealed Type 316H Stainless Steel |
| Loading Modes | - Constant Load for Creep<br>Periodic Load Increase of Approximately 69MPa (10 ksi) for Creep Fatigue |
| Load Increase Frequency | - One Cycle Per Hour |
| Hold-Time at Peak Load | - 15s and 1800s |

TABLE 8.2

TEST MATERIAL CHARACTERIZATION
TENSILE TESTS

| 316H Stainless Steel | 0.2% Y.S. MPa | 0.2% Y.S. (Ksi) | U.T.S. MPa | U.T.S. (Ksi) | % El. | % R.A. |
|---|---|---|---|---|---|---|
| One-Quarter Schedule Pipe Tests* | | | | | | |
| Room Temperature | 272 | (39.4) | 623 | (90.4) | 50.0 | 55.3 |
| | 300 | (43.5) | 612 | (88.7) | 44.0 | 48.5 |
| 510°C (950°F) | 173 | (25.1) | 479 | (69.4) | 28.5 | 36.3 |
| | 166 | (24.0) | 491 | (71.2) | 32.5 | 36.6 |

* 8.9 mm (0.35 in.) O.D. x 0.46 mm (0.018 in.) wall x 50.8 mm (2 in.) reduced section.

Table 8.3 is a comprehensive tabulation of creep data obtained at 502°C (935°F). The stress rupture data from this table are graphically presented in Figure 8.3. No definite trend exists for this data. Data representing the main experimental parameters (mode of loading and environment) fall within a common scatter band. All data fall above the minimum expected value for stress rupture approximated from ASME Code Case 1592 data.

Firgure 8.4 is a logarithmic plot of the minimum creep rate as a function of the applied stress. Again, no definite trend exists in distinguishing the data as a function of test parameter. It is to be noted that limited control data is available for comparison. Major effort in the current phase of testing is focused on obtaining control tests (Argon filled) data.

The data of Table 8.3 indicate that a large plastic strain is incurred upon specimen loading. This loading strain is equivalent to that obtained in a standard tensile test, $\dot{\varepsilon} \cong 10^{-3} s^{-1}$, at the test temperature, 510°C (950°F). That is, for the stress conditions of this test program (365 to 565 MPa/53 to 82 ksi), the applied stress is greater than the yield stress at the test temperature (173 MPa/25 ksi). Thus upon loading, the sample deforms (strains), until sufficient work hardening takes place to resist further <u>time independent</u> deformation. Subsequent to this initial strain, time dependent flow (or creep) occurs. These events are illustrated in the strain/time curves of Figure 8.5. Creep strains less than 3% are nominally observed for existing data.

The strain upon loading for control test specimens is plotted in Figure 8.5. Control specimens are found to undergo a larger instantaneous strain than Na/C exposed samples under equivalent test conditions. This information will be used in subsequent testing to isolate potential environmental influences.

TABLE 8.3

CREEP DATA AT 502°C (935°F) FOR
ANNEALED TYPE 316H STAINLESS STEEL

| Specimen | Stress (Ksi) | Stress (MPa) | Peak Stress Hold-Time (Hour) | Pre-Exposure Test Environment(a) | Rupture Time (Hour) | Strain Upon Load Application (%) | Creep Strain (%) | Creep Rate (%/Hour) |
|---|---|---|---|---|---|---|---|---|
| C10 | 57 | 393 | - | Na/C | 2,430 | 4.3 | 1.1 | $3.6 \times 10^{-4}$ |
| C6 | 63 | 434 | - | Na/C | 680 | 7.2 | 0.7 | $7.0 \times 10^{-4}$ |
| C9 | 69 | 476 | - | Na/C | 917 | 9.5 | 0.9 | $8.0 \times 10^{-4}$ |
| C7 | 76 | 524 | - | Na/C | 428 | 13.4 | 0.7 | $1.3 \times 10^{-3}$ |
| C1 | 48/59 | 331/407 | 0 | Ar | (b) | 7.4 | (b) | $2.5 \times 10^{-4}$ |
| C22 | 61/71 | 421/490 | 0 | Ar | 2,584 | 22.0 | 3.2 | $4.7 \times 10^{-5}$ |
| C11 | 54/66 | 372/455 | 0 | Na/C | 2,108 | 9.8 | 0.7 | $3.1 \times 10^{-4}$ |
| C15 | 62/75 | 428/517 | 0 | Na/C | 842 | 10.9 | 3.3 | $9.2 \times 10^{-4}$ |
| C18 | 62/75 | 428/517 | 0 | Na/C | 1,860 | 12.0 | - | - |
| C16 | 63/76 | 434/524 | 0 | Na/C | 4.6 | 15.5 | < .1 | - |
| C13 | 70/82 | 483/565 | 0 | Na/C | 1,585 | 21.2 | 4.9 | $4.6 \times 10^{-3}$ |
| C12 | 53/64 | 365/441 | .5 | Na/C | 904 | 12.3 | 1.0 | $8.8 \times 10^{-4}$ |
| C19 | 60/72 | 414/496 | .5 | Na/C | 2,322 | - | - | - |
| C14 | 60/72 | 414/496 | .5 | Na/C | 423 | 12.3 | 0.9 | $1.3 \times 10^{-3}$ |

(a) All samples pre-exposed to 510C(950F) for 1,000 hours, air.

(b) Test is continued prior to failure.

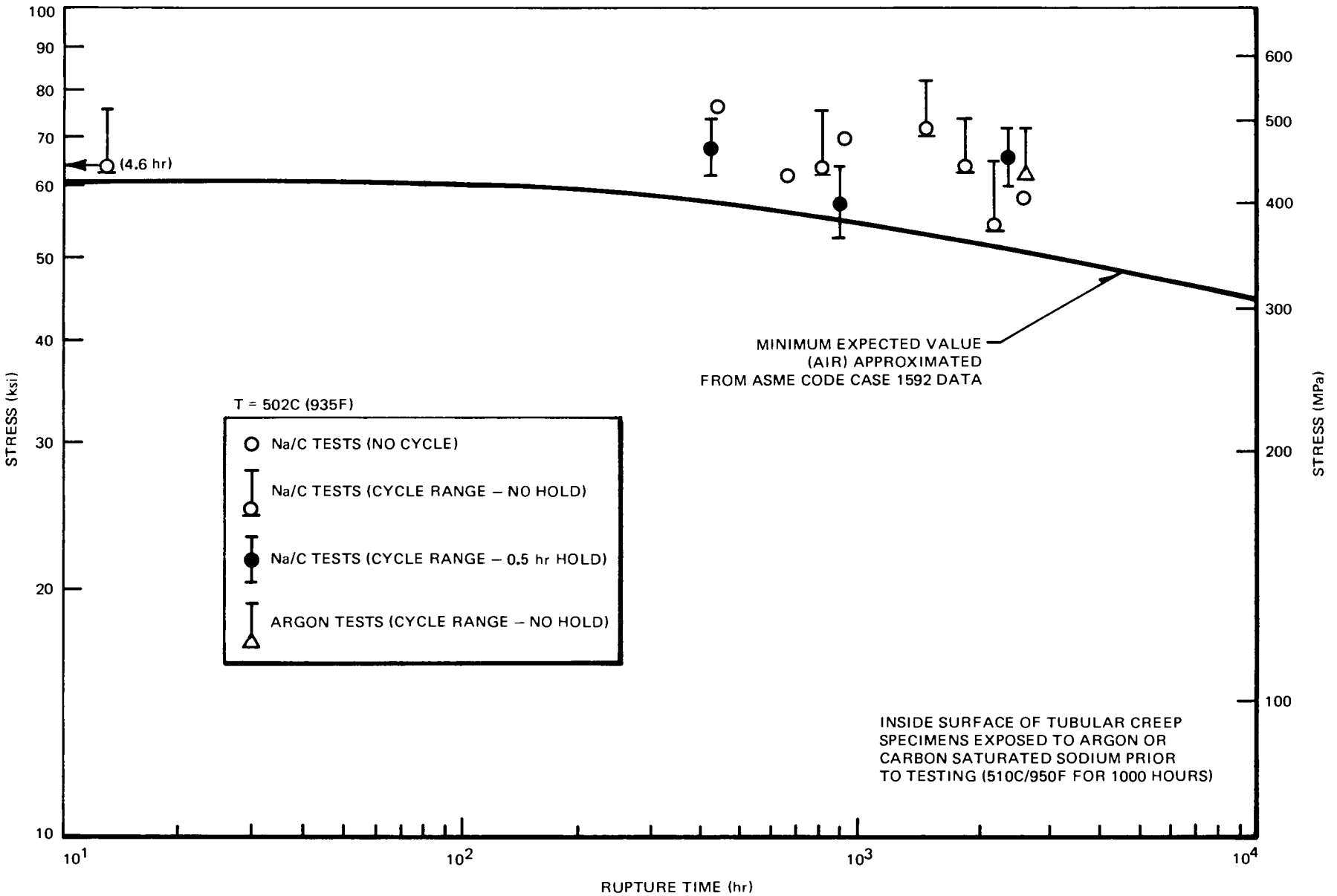


Figure 8.3. Stress Rupture Results for Annealed 316H Stainless Steel Tubular Creep Specimens

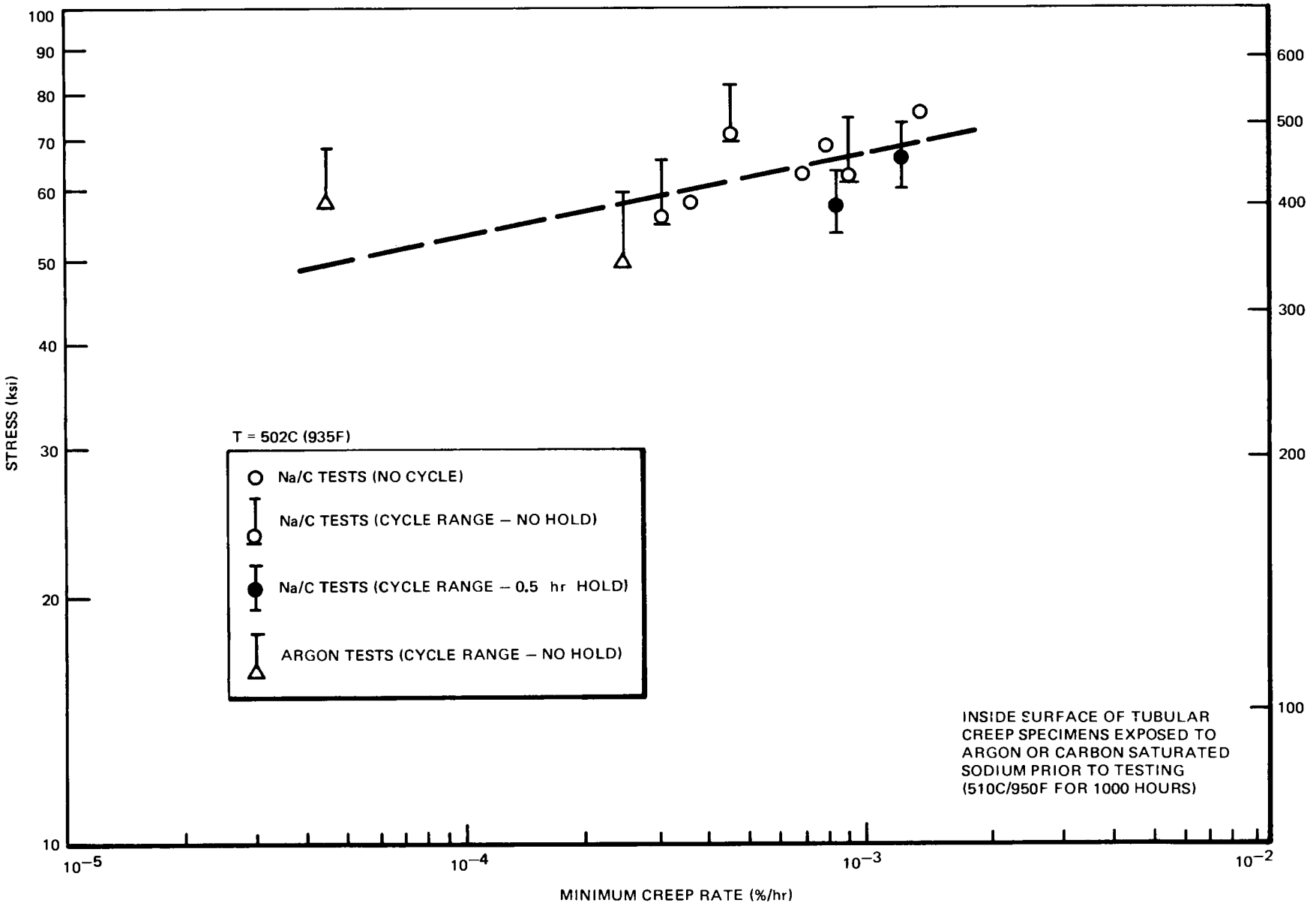


Figure 8.4. Minimum Creep Rate Results for Annealed 316H Stainless Steel Tubular Creep Specimens

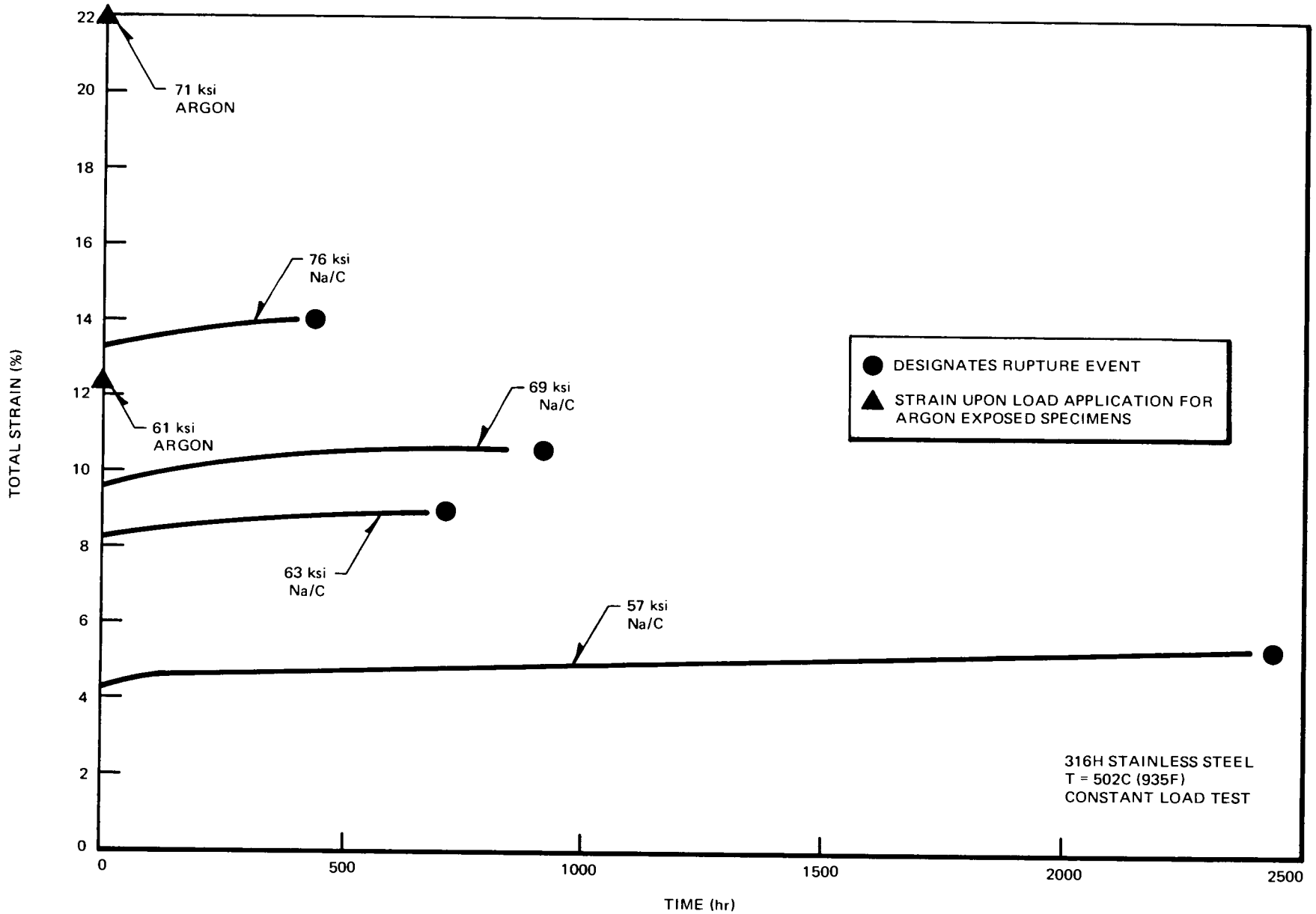


Figure 8.5. Total Strain As A Function of Time. Uniaxial Creep Test

## 8.3 DECARBURIZATION KINETICS AND DESIGN METHODS VERIFICATION TESTING

L. V. Hampton/J. L. Krankota/P. P. Pizzo

### 8.3.1 Objective

The objective of this program is to define the decarburization kinetics of 2¼Cr-1Mo base metal and weld metal exposed to 510°C (950°F) sodium, and to evaluate the response of these materials to interrupted creep loading.

This is necessary because one of the major concerns with the use of 2¼Cr-1Mo for sodium-heated steam generators has been its susceptibility to decarburization. However, it has been shown that the decarburization kinetics of 2¼Cr-1Mo base metal are sufficiently slow to permit its use for steam generator tubing in the LMFBR with only a small (10%) design stress penalty. This small design penalty is possible because the creep/rupture properties of 2¼Cr-1Mo are relatively insensitive to bulk carbon content until the level drops below 0.03-0.04% C, a value which will not be reached in the design life of steam generator tubes under LMFBR secondary sodium conditions. Decarburization tests are being conducted in this task to confirm the predicted rates.

Since the allowable stresses for a welded tube are based on the strength properties of the weakest part of that tube, a "weak" weld in a steam generator tube would govern the allowable stress for the entire tube. Therefore a series of decarburization and creep tests on welds are also being performed to confirm predicted behavior.

### 8.3.2 Decarburization Kinetics

The test matrix to obtain decarburization rate data for 2¼Cr-1Mo base and weld metal in 510°C (950°F) static, titanium-gettered sodium has been completed. With the conclusion of run DP-8, weld metal specimens with 7,000 hours total exposure time and base metal specimens with 12,500 hours exposure have been obtained. Chemical analyses to determine levels of carbon losses of these specimens are in progress.

Weld metal pin specimens (0.318 cm. dia. x 7.62 cm) were fabricated from a 2¼Cr-1Mo linear simulated tube-to-tube sheet weld made at ORNL.[7] After fabrication, the pins were stress-relieved according to Table 8.4.

TABLE 8.4

DECARBURIZATION RATE CONSTANTS FOR
2¼Cr-1Mo EXPOSED TO STATIC SODIUM
510°C (950°F) (TITANIUM-GETTERED)

| | | $K(gmc/cm^2 - sec^{\frac{1}{2}})$ | |
|---|---|---|---|
| | | 10,000 Hrs. | 4,100 Hrs. |
| Annealed* | ½ Hr. - 924°C (1695°F)<br>Fce. Cool to RT | $9.4X10^{-9}$ | $12X10^{-9}$ |
| Normalized and Tempered | ½ Hr. - 924°C (1695°F)<br>AC to RT<br>One Hr. - 677°C (1250°F)<br>AC to RT | $2.5X10^{-9}$ | $3.5X10^{-9}$ |

* Both treatments received a final stress relief anneal one hour at 732°C (1350°F) with subsequent air cooling to room temperature.

Carbon loss data for 1900 and 4500 hour exposures of weld metal specimens yields a rate constant of $5X10^{-8}$ $g/cm^2$-sec for this material. This interim rate is indicated in Figure 8.6, along with previously reported base metal data. Analysis of the 7,000 hour specimens will further improve confidence in the definition of the decarburization kinetics of 2¼Cr-1Mo weld metal.

Figures 8.7a, b, and c show microstructures of exposed base and weld metal. Figures 8.7d and e show microstructures for 2¼Cr-1Mo base metal after annealing (Fig. 8.7d) and normalizing and tempering (Fig. 8.7e). Heat treatment details are shown in Table 8.4. Based on the data of Figure 8.6, the carbide dispersion shown in Figure 8.7 results in a more stable microstructure, as indicated in the last report. After 10,000 hours exposure in 510°C (950°F) sodium, carbides in both specimens tend to coarsen and the annealed material shows evidence of heavy carbide precipitation in the grain boundaries.

Decarburization studies are continuing with vacuum-arc and electroslag remelted (RDT, CRBR reference melt practice) materials, including base metal and weld heat affected zones. These materials are being tested after several different annealing and normalized and tempering treatments in order to further investigate the effect of prior thermal history on the decarburization behavior of 2¼Cr-1Mo. Heat treatment has been found to effect rates of decarburization significantly, both as a result of this work and recent work done in Japan and France.

### 8.3.3 Mechanical Properties of 2¼Cr-1Mo Steel in Decarburizing Sodium

Progress continues in the characterization of the mechanical behavior of isothermal annealed 2¼Cr-1Mo steel in decarburizing sodium. Data for the current phase of the mechanical properties program have been analyzed and the results are presented in this report. The mechanical properties program consists of testing tubular specimens under uniaxial stress creep conditions, and pressure pins (sealed and pressurized cylinders) under biaxial stress test conditions.

Test parameters used in the uniaxial creep/fatigue program are presented in Table 8.5. Both constant load creep tests and cyclic load creep tests are performed. Cyclic tests consist of a sustained monotonic

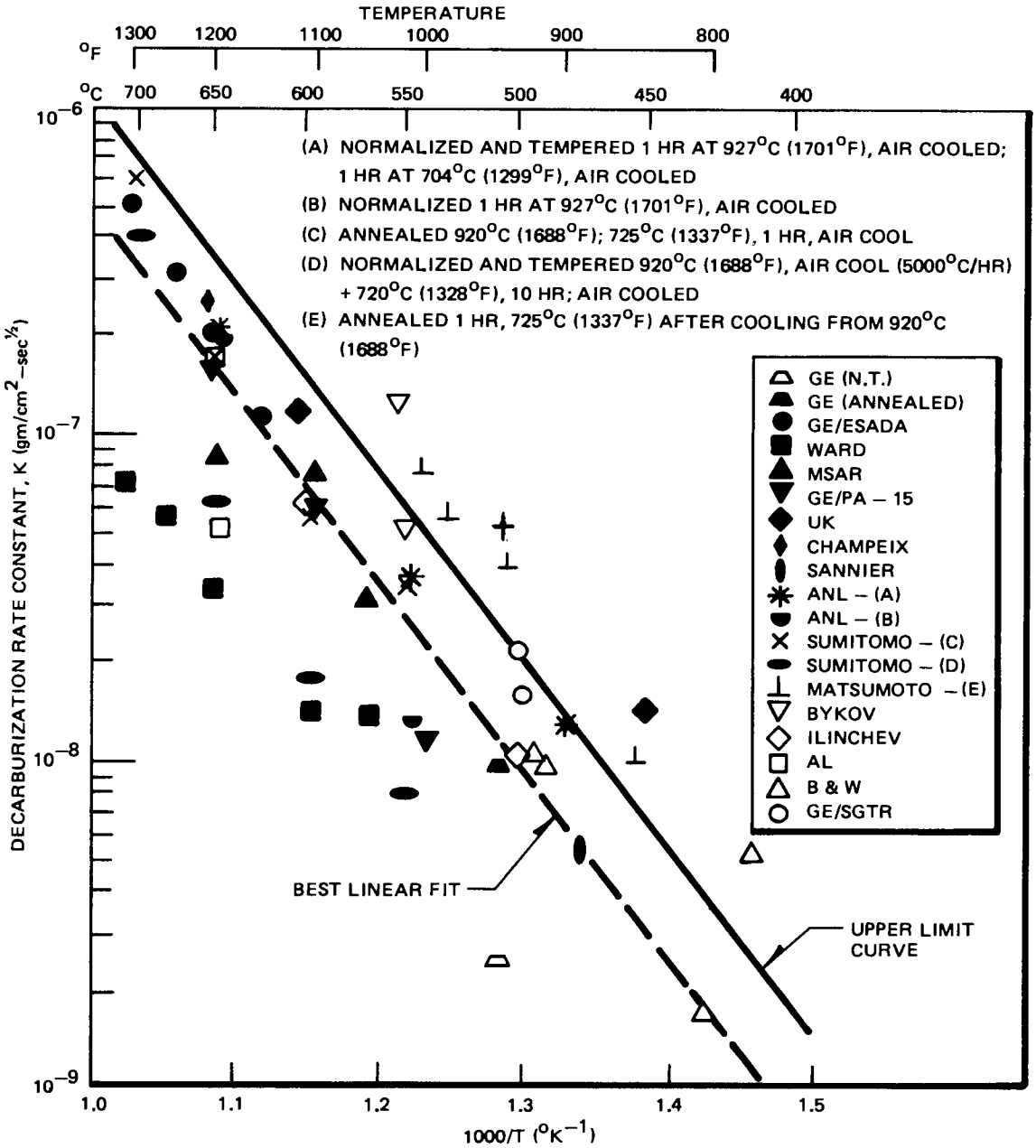


Figure 8.6. Decarburization Rate Constants for All Investigations +GE (Weld Metal-Interim)

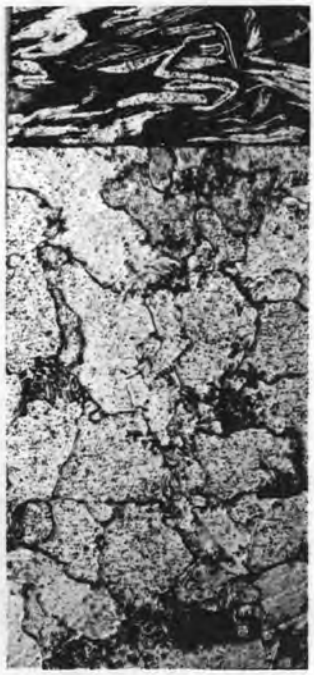

(a) annealed material after 10,000 hours

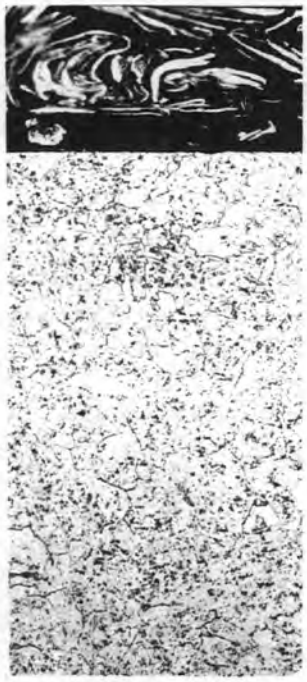

(b) N&T material after 10,000 hours

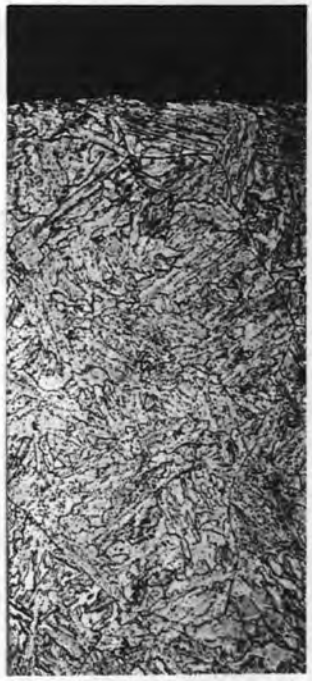

(c) stress-relieved weld metal after 4,500 hours

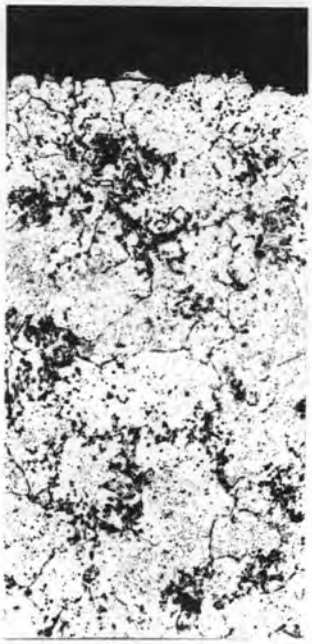

(d) base metal as-annealed

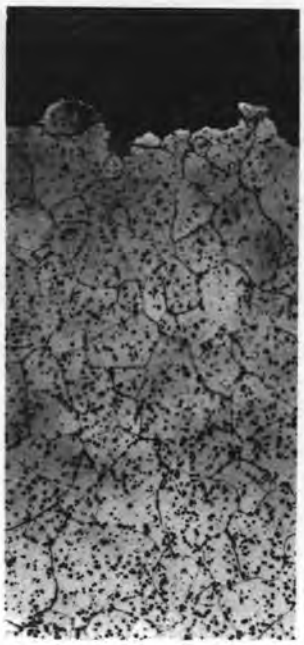

(e) base metal as normalized & tempered

Figure 8.7. Decarburization of 2¼Cr-1Mo Base and Weld Metal, 510°C (950°F) Ti-gettered Sodium (400X)

TABLE 8.5

CREEP FATIGUE TEST PARAMETERS
TUBULAR CREEP SPECIMENS

| | |
|---|---|
| Environment | - Titanium-gettered sodium or helium (inside diameter) |
| | - Air (Outside Diameter) |
| Test Temperature | - 502°C (935°F) |
| Material | - 2¼Cr-1Mo Steel Isothermal Annealed |
| Loading Modes | - Constant Load for Creep |
| | - Periodic load increase of approximately 69 MPa (10 ksi) for creep fatigue |
| Peak Load Frequency | - 1 Cycle Per 24 Hours |
| Hold Time at Peak Load | - 10 Seconds |

load, with a periodic load increase which results in an approximate 69 MPa (10 ksi) stress increment. This peak load is applied once each twenty-four hours, and the load is applied over an approximate 10 second period. The results of the first phase of this test program are tabulated in Table 8.6. Calibration of instrumented tubular test specimens indicated sources of error in earlier analyses of the raw data. The data of Table 8.6 supersede results previously reported.

Minimum creep rates are illustrated in Figure 8.8. No clear differentiation was observed between the decarburized and control test data. Creep rupture data from tubular creep specimens are shown in Figure 8.9. Again, the data are limited, and no clear decarburization effect is apparent. All data lie beyond the minimum expected value of time to rupture for a given applied stress, as approximated from ASME Code Case 1592.

Typical creep curves for both control (Argon) and Na/Ti exposed uniaxial tubular specimens are presented in Figure 8.10. Both specimens were tested at 241 MPa (35 ksi) and at 502°C (935°F). Another Na/Ti specimen (A14) was tested under equivalent conditions, and its fracture time and fracture strain have been plotted in Figure 8.10.

The creep curves of Figure 8.10 allow direct comparison of the behavior of both Na/Ti exposed and control specimens under equivalent creep conditions. On the basis of this isolated datum, a decarburizing effect is observed. The Na/Ti exposed specimens are less creep resistant than the control (helium exposed) specimens. This is true over a broad strain range. A creep strain of 2½% is attained after 180 hours for the Na/Ti exposed sample, while the control sample attains 2½% strain after approximately 1140 hours. If found to be a definite trend in subsequent tests, this would suggest that decarburizing has a direct influence on elevated temperature deformation processes.

Information in Table 8.6 and the creep curves of Figure 8.10 indicate that the fracture strain is essentially constant, irrespective of the test environment. The fracture strain is a common measure of the creep ductility of an alloy. A constant strain to failure suggests that the decarburizing environment does not have a first order effect

TABLE 8.6

UNIAXIAL CREEP/FATIGUE TESTS 502°C (935°F)

| Specimen | Environment | Stress | | Stress Peak | | Rupture Time (Hour) | Rupture Strain (%) | Minimum Creep Rate (MCR) (%/Hour) |
|---|---|---|---|---|---|---|---|---|
| | | MPa | ksi | MPa | ksi | | | |
| A02 | Helium | 310.2 | 45 | - | - | 39.9 | 18.2 | $2.7 \times 10^{-1}$ |
| A04 | Helium | 241.3 | 35 | - | - | 2296 | 29.2 | $1.9 \times 10^{-3}$ |
| A05 [a] | Helium | 172.4 | 25 | - | - | 1000 [a] | | $2.5 \times 10^{-4}$ |
| A13 | Na/Ti | 241.3 | 35 | 310.2 | 45 | 248.5 | 27.0 | - |
| A14 | Na/Ti | 241.3 | 35 | | | 1021.6 | 25.0 | - |
| A15 | Na/Ti | 241.3 | 35 | - | - | 397.3 | 26.8 | $6.9 \times 10^{-3}$ |
| A03 | Helium | 206.8 | 30 | 276 | 40 | 928 | 20.6 | - |

(a) Test of specimen A05 discontinued after 1,000 hours.

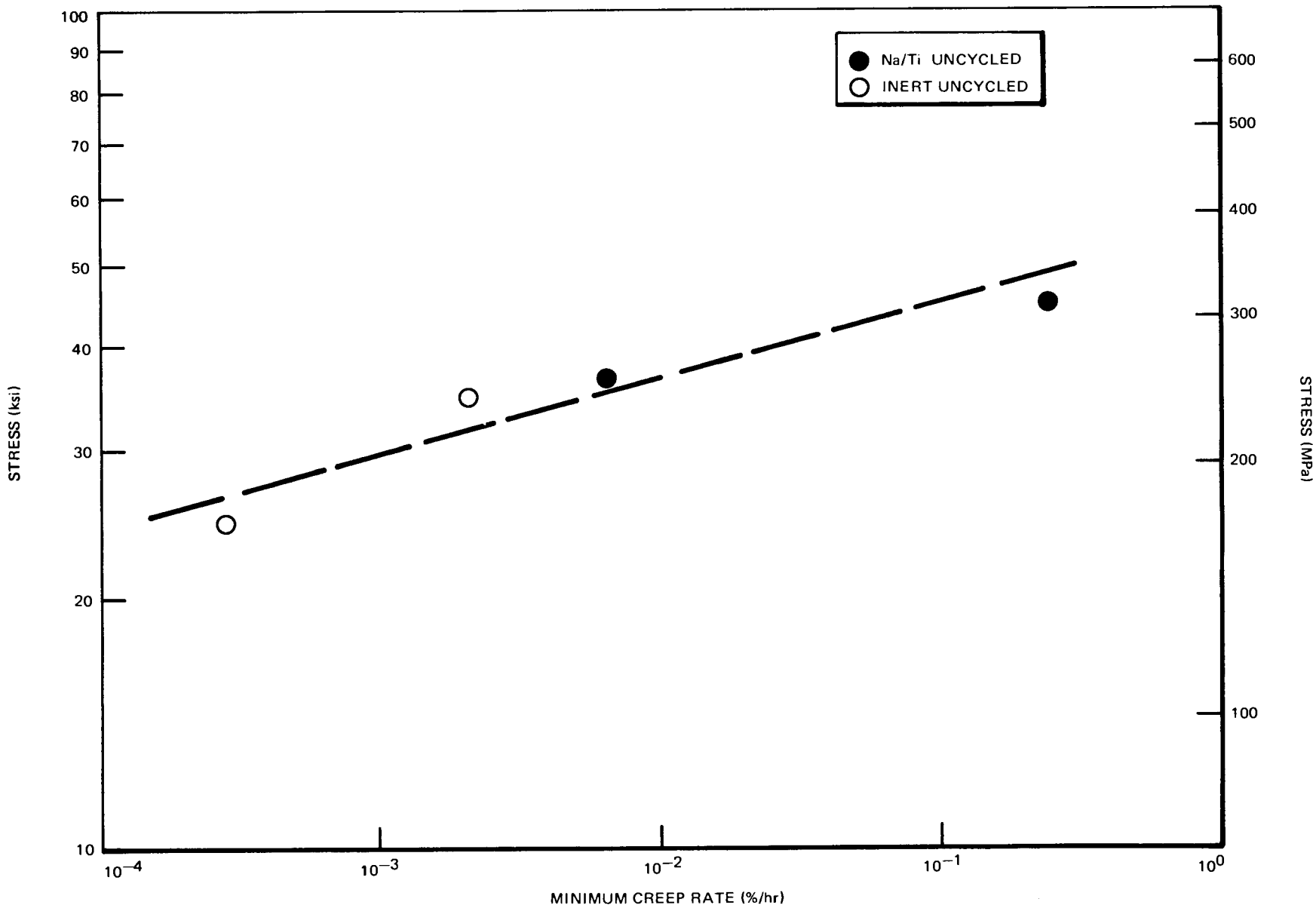


Figure 8.8 Minimum Creep Rate Results for Isothermal Annealed 2¼Cr-1Mo Steel Tubular Creep Specimens

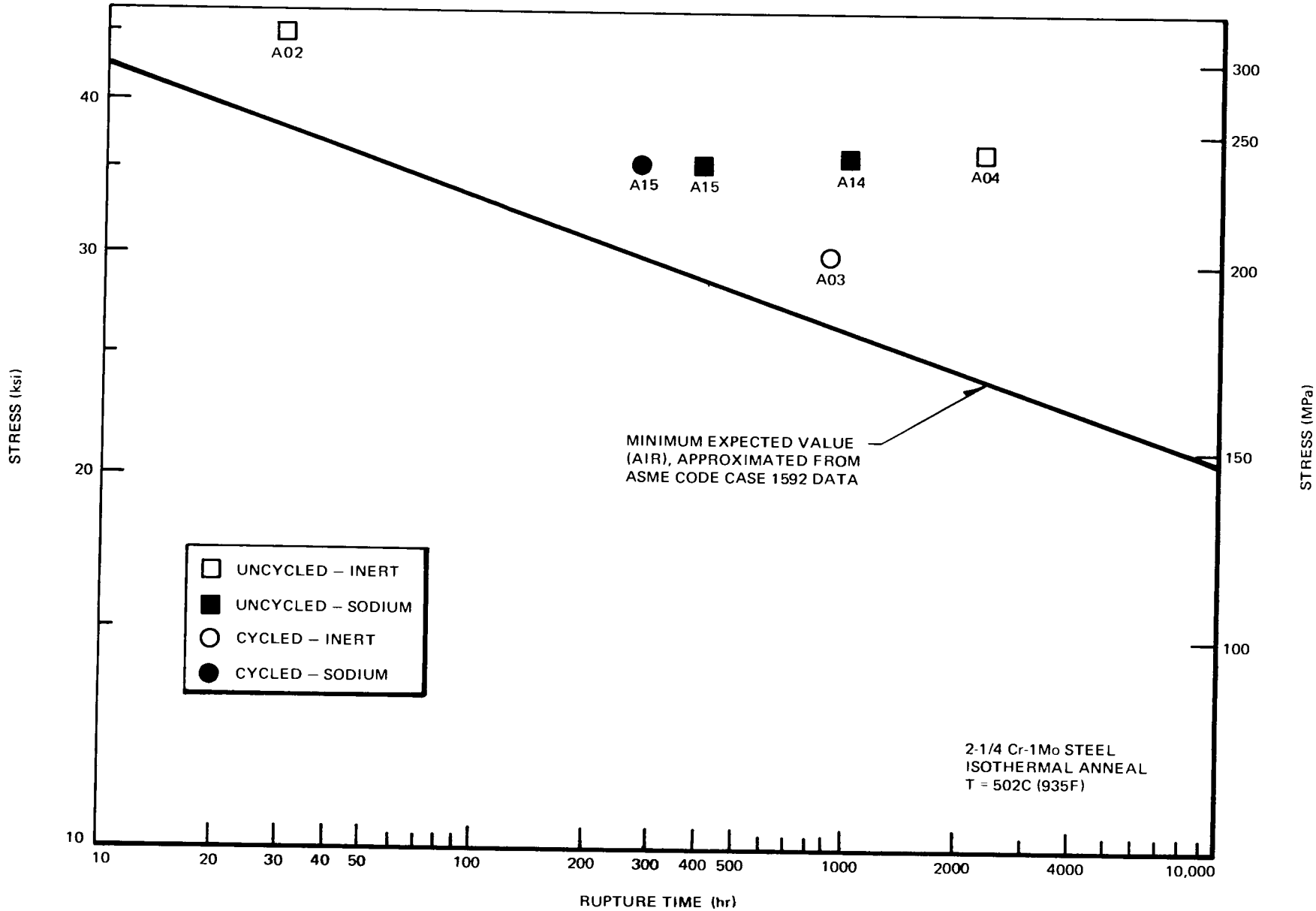


Figure 8.9 Stress Rupture Data for Isothermal Annealed 2¼Cr-1Mo Steel Tubular Creep Specimens

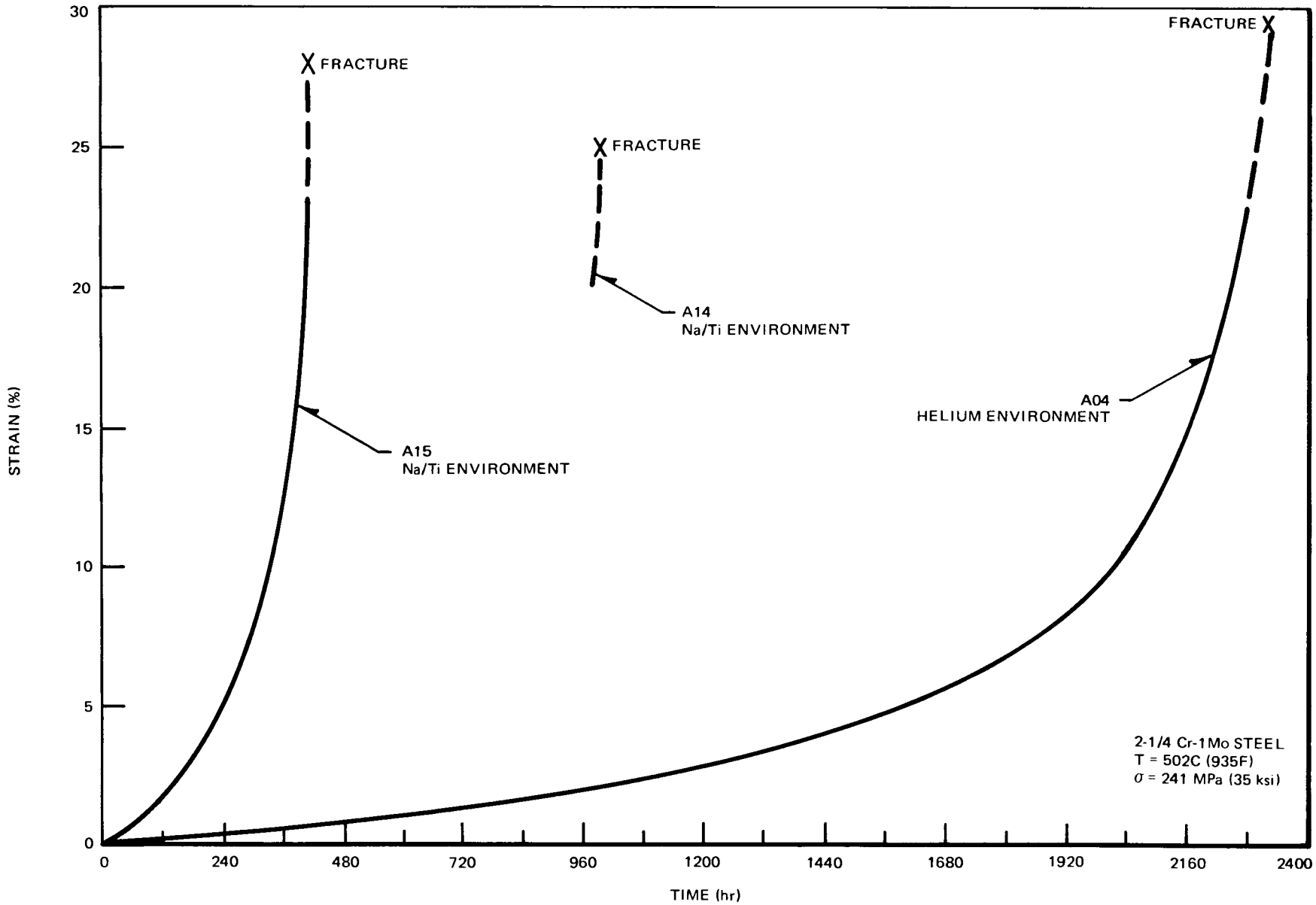


Figure 8.10 Strain versus Time Creep Behavior for Isothermal Annealed 2¼Cr-1Mo Steel

on fracture processes. If however, fracture processes take place over a more limited range of strain (5 to 10%), as would be the case for a more triaxial stress state, important influences on fracture properties may be masked. In subsequent testing, reduction of area at the fracture plane, (known to be more sensitive to fracture processes) will be used to monitor the influence of the decarburizing environment on tertiary creep events and fracture.

In the next phase of creep testing, 2¼Cr-1Mo steel will be tested at 500°C (932°F) and at an applied stress level of 241 MPa (35 ksi). Pre-exposure to the decarburizing environment prior to testing will be introduced as an experimental parameter. Major effort will be concentrated in quantifying decarburizing influence under monotonic creep stress conditions.

Test parameters for the biaxial creep program are summarized in Table 8.7. In this program, cylindrical test specimens 15.9 mn (.625") diameter by 95.4 mn (3.75") long were pre-exposed in decarburizing sodium or exposed to pure argon. The selected test temperature was 510°C (950°F). Both base metal specimens ("B" designation) and weld metal specimens ("W" designation) were tested.

Weld metal specimens were fabricated in the following sequence:

(1) 2¼Cr-1Mo steel weld overlays were deposited on ¼"-Schedule 80, 2¼Cr-1Mo steel pipe.

(2) The I.D. of the specimens was enlarged to remove the base metal/pipe material.

(3) Specimens were further fabricated to meet the established dimensional tolerances and pressure pin configuration.

(4) After fabrication, the specimens were post weld heat treated at 732°C (1350°F) for 4 hours.

The current results of the biaxial stress creep program are tabulated in Table 8.8. The data of Table 8.8 are graphically illustrated in the logarithmic stress versus rupture time plot of Figure 8.11. The trends evident in this test program are as follows:

(1) The rupture life for a given applied stress is found to be displaced to shorter times for the Na/Ti exposed specimens versus control specimens.

TABLE 8.7

BIAXIAL CREEP PARAMETERS
PRESSURE PIN
(CYLINDRICAL) SPECIMENS

| | |
|---|---|
| Environment | - High Pressure Argon 25 MPa/3630 psi (Interior Surface) |
| | - Titanium-Gettered Sodium or Argon (Exterior Surface) |
| Test Temperature | - 510°C (950°F) |
| Material | - 2¼Cr-1Mo Steel Isothermal annealed designated "B" for base metal. |
| | 2¼Cr-1Mo Steel Weld Metal Post weld heat treated (732°C/1350°F for 4 Hours), designated "W" for weld metal. |
| Pre-Exposure Conditions* | - 510°C (950°F) for 950 Hours Control and Na/Ti Specimens |

* Seven of twenty-one tests to date have been pre-exposed prior to testing.

TABLE 8.8

BIAXIAL CREEP PROGRAM (T = 510°C/950°F)

| Specimen | Environment | Stress MPa | Stress ksi | Rupture Time (Hours) |
|---|---|---|---|---|
| B40-07 | Helium | 223.37 | 32.4 | 248.2 |
| B40-08 | Sodium | 223.37 | 32.4 | 98.2 |
| B45-07 | Helium | 251.63 | 36.5 | 116.2 |
| B45-08 | Sodium | 251.63 | 36.5 | 168.5 |
| B40-01 | Helium | 275.76 | 40.0 | 4.0 |
| B40-02 | Sodium | 275.76 | 40.0 | 1.3 |
| B45-01 | Helium | 310.23 | 45.0 | 0.5 |
| B45-02 | Sodium | 310.23 | 45.0 | 0.4 |
| W40-07 | Helium | 223.37 | 32.4 | 200.0 |
| W40-08 | Sodium | 223.37 | 32.4 | 116.2 |
| W45-07 | Helium | 251.63 | 36.5 | 172.5 |
| W45-08 | Sodium | 251.63 | 36.5 | 108.0 |
| W40-01 | Helium | 275.76 | 40.0 | 0.1 |
| W40-02 | Sodium | 275.76 | 40.0 | 0.9 |
| W45-01 | Helium | 310.23 | 45.0 | 0.3 |
| B40-10* | Sodium | 223.37 | 32.4 | 17.1 |
| B40-09* | Helium | 223.37 | 32.4 | 234.5 |
| B40-04* | Sodium | 223.37 | 32.4 | 5.4 |
| B40-03* | Helium | 223.73 | 32.4 | 152.9 |
| B40-06* | Sodium | 223.73 | 32.4 | 5.9 |
| B45-09* | Helium | 251.63 | 36.5 | 154.8 |
| B35-01* | Helium | 195.44 | 28.35 | 473.0 |

B = Base Metal

W = Weld Metal

* Pre-exposed to sodium for 950 hours at 510°C (950°F)

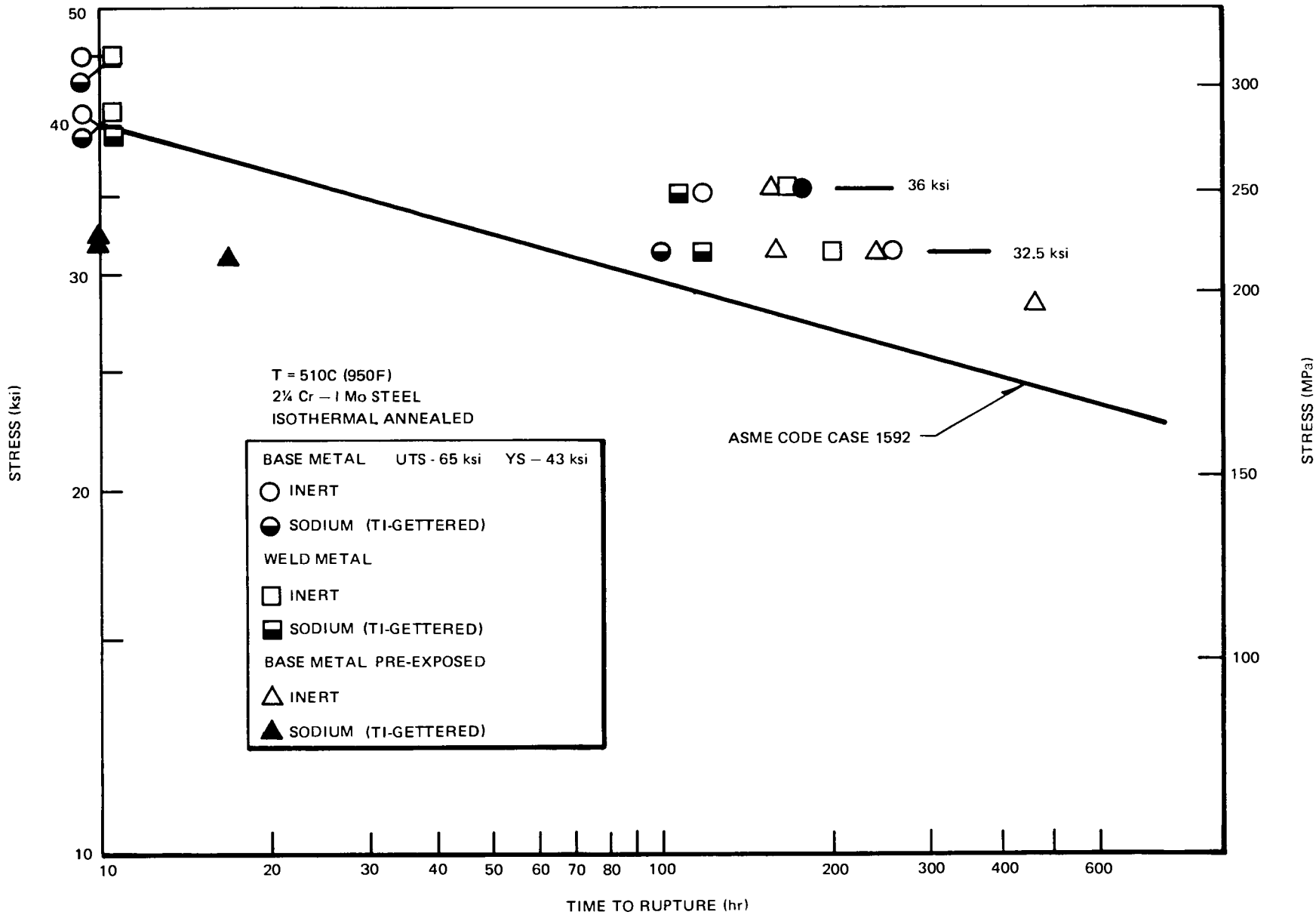


Figure 8.11 Biaxial Creep Tests, 2¼Cr-1Mo Steel: Rupture Data

(2) A ten-fold rupture strength reduction for Na/Ti versus control specimens data is observed for specimens pre-exposed at 510°C (950°F) for 950 hours.

(3) Data from specimens not exposed prior to testing fall above the minimum rupture strength limit established in ASME Code Case 1592, irrespective of test environment.

The biaxial creep data of Figure 8.11 must further be analyzed in order to quantitatively access the loss in rupture strength suffered by the decarburized 2¼Cr-1Mo steel. Metallographic examination and compositional analysis will be conducted on failed pressure pins. Effort will be devoted to determine the critical exposure to Na/Ti (equivalently, the critical bulk carbon content reduction) required for accelerated loss of creep rupture strength. Deformation morphology studies will be correlated with the mechanical properties data in order to investigate the mechanism responsible for creep rupture strength reduction. Mechanical properties data will be compared with the decarburization studies being conducted in this subtask to determine the properties degradation that can be expected in the service life of the LMFBR.

The rupture properties data for the weld metal specimens are inconclusive in the present study. Although the data of Figure 8.11 appear to indicate essentially equivalent behavior for the base metal and weld metal specimens, a variation in failure mode was noted for the weld metal specimens. Base metal failures in the pressurization tests were characterized by longitudinal tearing (the type of the failure mode to be expected in this type of testing). Weld metal specimens failed by <u>either</u> longitudinal tearing <u>or</u> by pinhole perforations through the wall. An example of this latter failure mode is illustrated in Figure 8.12. Figure 8.12a illustrates a failed pressure pin (weld metal specimen). In Figure 8.12b, details of surface perforations are depicted. A transverse section through typical pore-like defects is presented in Figure 8.12c. This section depicts large pores, open in the outer weld overlay (last pass). Reexamination of micrographs obtained during weld overlay characterization indicate that weld porosity was not excessive, however, inclusion particles, approximately 1-2 μm in diameter were

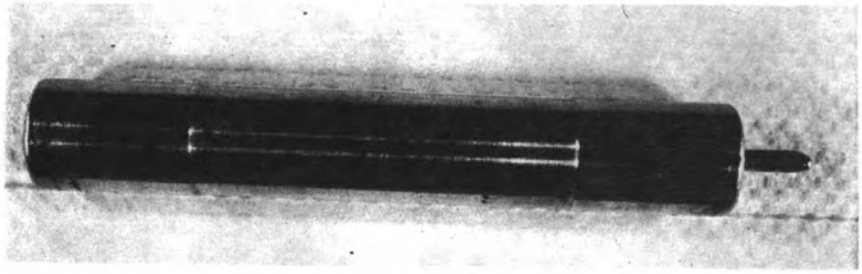

(a) 1X

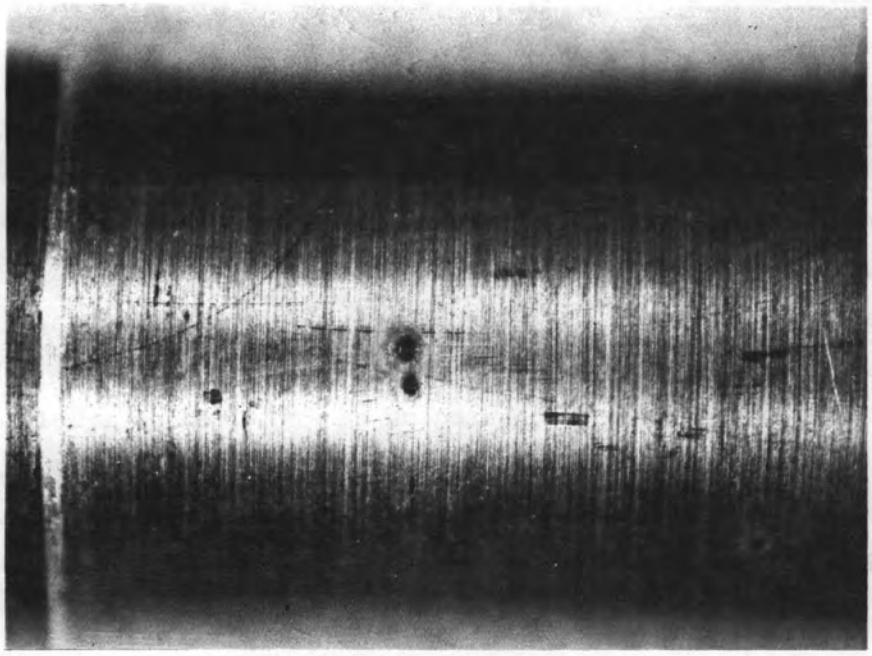

(b) details of surface perferations (5X)

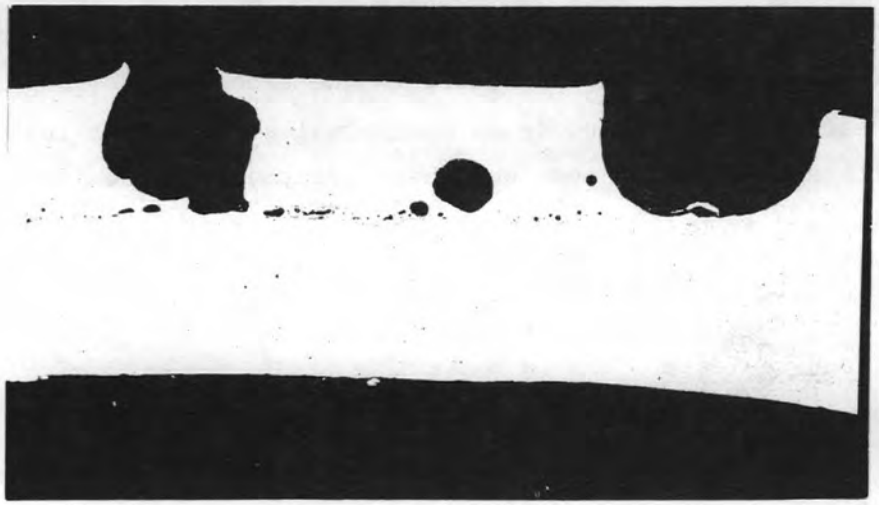

(c) transverse section (80X)

Figure 8.12. 2¼Cr-1Mo All-weld Metal Pressure Pins. Pre-exposed to 950°F (510°C) Static Sodium for 950 Hours.

dispersed throughout the weld metal. Weld metal samples pre-exposed to NA for 950 hours prior to testing leaked upon pressurization. Detailed evaluation of these weld samples has been initiated to determine the cause for the apparent degredation of the weld metal during exposure to Na.

## 8.4 METALLURGICAL CHARACTERIZATION OF VAR AND ESR 2¼Cr-1Mo ALLOY STEEL

H. P. Offer

The objective of this activity is to generate preliminary mechanical property and microstructural characterization data for consumable remelted 2¼Cr-1Mo alloy steel. Vacuum arc remelting (VAR) and electroslag remelting (ESR) will provide high purity material for the critical tube-tubesheet weld region. The mechanical properties resulting from these processing techniques must be shown to meet the applicable ASME Code and RDT Standards, which are based on non-remelted material. Testing and examination conducted and reported earlier[8] include room temperature tensile tests, drop-weight tests, creep-rupture tests, chemical composition,* microcleanliness, grain size and hardness, and isothermal transformation data.

### 8.4.1 Heat Treatment

The heat treatments used in this study closely simulate the various possible heat treatments applicable to the tubesheet forging and tubing. These heat treatments include an isothermal anneal and a full anneal both with and without a post weld heat treatment. Also included is a normalize and temper with post weld heat treatment. The heat treatment parameters are listed in Table 8.9.

### 8.4.2 Tensile Tests

Tensile tests were conducted for VAR heat #55262 and ESR heat #R0110 at 21, 204, 371, 454, 510, and 566°C (70, 400, 700, 850, 950, and 1050°F). The yield and ultimate strength, elongation, and reduction

---

*Please see the end of this section for a corrected analysis.

## TABLE 8.9

### HEAT TREATMENTS* FOR 2 1/4 Cr - 1 Mo STEEL

| | | |
|---|---|---|
| A. | Isothermal Anneal: | 954°C (1750°F) for 1/2 hr.<br>Furnace cool to 710°C (1310°F) for 2 1/2 hr.<br>Air cool to room temperature. |
| | Postweld: | 727°C (1340°F) for 4 hr.<br>Air cool to room temperature. |
| B. | Anneal: | 916°C (1680°F) for 1 1/4 hr.<br>Furnace cool [@ 27.7 to 55.6°C/hr. (@ 50 - 100°F/hr.) to 316°C (600°F)]<br>Air cool to room temperature. |
| | Postweld: | 727°C (1340°F) for 4 hr.<br>Air cool to room temperature. |
| C. | Normalize and Temper: | 954°C (1750°F) for 1 hr.<br>Air cool to room temperature.<br>727°C (1340°F) for 1 3/4 hr.<br>Air cool to room temperature. |
| | Postweld: | 727°C (1340°F) for 4 hr.<br>Air cool to room temperature. |

D. (Same as B without Postweld)

E. (Same as A without Postweld)

* Monitored according to specimen surface temperature.

in area values are reported in Tables 8.10 and 8.11. The yield and ultimate strengths are plotted as a function of temperature in Figures 8.13, 8.14, 8.15 and 8.16, along with the Nuclear Systems Materials Handbook (NSMH) expected value and the 0.95 upper and lower tolerance limits. The expected value of yield strength as a function of temperature given in ASME Code Case 1592 is also shown in Figures 8.13 and 8.14. The yield and ultimate strength for both the VAR and ESR material generally (with the exception of ESR at room temperature) lie between the NSMH expected value and lower tolerance limit at all temperatures tested. The yield strength at 454°C (850°F) and above is generally below the Code Case 1592 expected value for all conditions tested for the ESR material. For the VAR material, only the isothermal anneal produced yield strengths below this expected value above 454°C.

### 8.4.3 Charpy V-Notch Tests

A brief summary of the results of charpy v-notch impact testing was reported earlier.[8] A complete summary of tests to date is given in Table 8.12 for VAR heat #55262, VAR heat #56067, and ESR heat #R0110. The absorbed energy, lateral expansion, and percent shear fracture are plotted as a function of test temperature in Figures 8.18 to 8.27. Of the four heat treatments considered, the full anneal plus post weld heat treatment (PWHT) gives the best assurance of nonductile fracture based on the temperature for 67.8 J (50 ft.-lb.) impact energy and 889 μm (35 mils) lateral expansion. These values are required simultaneously by ASME Code Section III - Division I, Article NB-2300, at the nil-ductility transition temperature (NDT) + 33.3°C (60°F). As previously reported, NDT ranged from -45.6 to -40.0°C (-50 to -40°F) for the ESR material and from -28.9 to -3.9°C (-20 to 25°F) for the VAR material. For full anneal plus PWHT of ESR and VAR material the minimum values are met at -42.8°C (-45°F) and 1.7°C (35°F), respectively. This makes the minimum hydrostatic test temperatures approximately -6.7°C (20°F) for ESR forgings and 29.4°C (85°F) for VAR forgings.

The upper shelf energy of ESR material was observed to be much higher than VAR material. This difference in absorbed energy is attributed primarily to the morphology and distribution of non-metallic

# TABLE 8.10

## TENSILE PROPERTIES OF VAR 2 1/4 Cr - 1 Mo STEEL*

| Temperature °C | Temperature (°F) | Strength, MPa (ksi) Yield 0.2% Offset | Strength, MPa (ksi) Ultimate | Total Elongation, (%) | Reduction in Area, (%) |
|---|---|---|---|---|---|
| **Heat Treatment A - Isothermal Anneal with PWHT**. Longitudinal Orientation** | | | | | |
| 21 | (70) | 221 (32.0) | 465 (67.5) | 29.5 | 72.9 |
| 204 | (400) | 216 (31.3) | 406 (58.9) | 27.6 | 65.2 |
| 371 | (700) | 190 (27.6) | 491 (71.2) | 26.0 | 64.2 |
| 454 | (850) | 165 (24.0) | 405 (58.8) | 26.2 | 62.4 |
| 510 | (950) | 165 (23.9) | 379 (54.9) | 26.6 | 73.0 |
| 566 | (1050) | 157 (22.8) | 317 (46.0) | 32.2 | 81.6 |
| **Heat Treatment B - Full Anneal with PWHT. Longitudinal Orientation** | | | | | |
| 21 | (70) | 241 (34.9) | 441 (63.9) | 32.1 | 65.4 |
| 204 | (400) | 216 (31.3) | 384 (55.7) | 30.1 | 65.2 |
| 371 | (700) | 208 (30.2) | 444 (64.4) | 23.7 | 60.7 |
| 454 | (850) | 179 (25.9) | 423 (61.4) | 27.1 | 68.3 |
| 510 | (950) | 187 (27.1) | 396 (57.4) | 27.2 | 75.2 |
| 566 | (1050) | 168 (24.4) | 352 (51.1) | 33.2 | 74.7 |
| **Heat Treatment D - Full Anneal without PWHT. Longitudinal Orientation** | | | | | |
| 21 | (70) | 243 (35.2) | 472 (68.5) | 33.1 | 66.4 |
| 204 | (400) | 213 (30.9) | 410 (59.5) | 29.7 | 66.4 |
| 371 | (700) | 215 (31.2) | 452 (65.6) | 22.9 | 60.7 |
| 454 | (850) | 214 (31.0) | 449 (65.2) | 26.1 | 61.9 |
| 510 | (950) | 204 (29.6) | 429 (62.2) | 24.6 | 64.8 |
| 566 | (1050) | 200 (29.0) | 372 (54.0) | 30.0 | 72.4 |

* Strain Rate - 6.67 X $10^{-4}$/sec
** PWHT - Post Weld Heat Treatment

# TABLE 8.11

## TENSILE PROPERTIES OF ESR 2 1/4 Cr - 1 Mo STEEL*

| Temperature °C | (°F) | Strength, MPa (ksi) Yield 0.2% Offset | Ultimate | Total Elongation, (%) | Reduction in Area, (%) |
|---|---|---|---|---|---|
| **Heat Treatment B - Full Anneal with PWHT. Longitudinal Orientation** | | | | | |
| 21 | (70) | 225 (37.0) | 480 (69.6) | 36.1 | 74.4 |
| 204 | (400) | - - | - - | - | - |
| 371 | (700) | 192 (27.9) | 421 (61.0) | 29.4 | 66.4 |
| 454 | (850) | 146 (21.2) | 378 (54.8) | 24.8 | 71.9 |
| 510 | (950) | 149 (21.6) | 360 (52.2) | 39.3 | 73.3 |
| 566 | (1050) | 144 (20.9) | 301 (43.7) | 42.1 | 80.8 |
| **Heat Treatment B - Full Anneal with PWHT. Transverse Orientation** | | | | | |
| 21 | (70) | 296 (43.0) | 483 (70.0) | 37.5 | 73.4 |
| 204 | (400) | 242 (35.1) | 405 (58.7) | 33.7 | 72.5 |
| 371 | (700) | 209 (30.3) | 402 (58.3) | 27.1 | 68.1 |
| 454 | (850) | 177 (25.7) | 399 (57.8) | 30.2 | 68.9 |
| 510 | (950) | 174 (25.3) | 370 (53.7) | 33.4 | 69.2 |
| 566 | (1050) | 145 (21.1) | 305 (44.2) | 40.3 | 79.9 |
| **Heat Treatment D - Full Anneal without PWHT. Longitudinal Orientation** | | | | | |
| 21 | (70) | 268 (38.9) | 472 (68.5) | 40.6 | 72.8 |
| 204 | (400) | 226 (32.8) | 403 (58.4) | 27.6 | 74.2 |
| 371 | (700) | 192 (27.9) | 413 (59.9) | 28.3 | 67.7 |
| 454 | (850) | 160 (23.2) | 399 (57.9) | 28.9 | 68.0 |
| 510 | (950) | 148 (21.4) | 360 (52.2) | 34.5 | 73.9 |
| 566 | (1050) | 150 (21.7) | 314 (45.5) | 38.3 | 77.5 |

* Strain rate - $6.67 \times 10^{-4}$/sec

TABLE 8.11 (Cont'd.)

TENSILE PROPERTIES OF ESR 2 1/4 Cr - 1 Mo STEEL*

| Temperature °C | (°F) | Strength, MPa (ksi) Yield 0.2% Offset | Ultimate | Total Elongation, (%) | Reduction in Area, (%) |
|---|---|---|---|---|---|
| Heat Treatment D - Full Anneal without PWHT. Transverse Orientation | | | | | |
| 21 | (70) | 299 (43.4) | 487 (70.6) | 37.5 | 72.1 |
| 204 | (400) | 226 (32.8) | 401 (58.2) | 34.0 | 67.7 |
| 371 | (700) | 195 (28.3) | 459 (66.5) | 25.1 | 65.3 |
| 454 | (850) | 168 (24.3) | 403 (58.5) | 27.6 | 65.6 |
| 510 | (950) | 154 (22.4) | 378 (54.8) | 31.8 | 70.1 |
| 566 | (1050) | 155 (22.5) | 321 (46.5) | 37.8 | 75.8 |
| Requirements of RDT M3-33 (Tubing) | | | | | |
| 21 | (70) | 206 (30)min. | 414 (60) to 586 (85) | 30 min. | -- |
| Requirements of RDT M2-19 (Tubesheet Forging) | | | | | |
| 21 | (70) | 206 (30)min. | 414 (60) to 586 (85) | 20 min. | -- |

* Strain Rate - $6.67 \times 10^{-4}$/sec

# TABLE 8.13

## CREEP-RUPTURE DATA FOR 2 1/4 Cr - 1 Mo STEEL

| SPECIMEN NUMBER | HEAT TREATMENT | STRESS KSI (MPa) | RUPTURE TIME (hr.) | TIME TO THIRD* STAGE (hr.) | STRAIN TO THIRD* STAGE (%) | MINIMUM CREEP* RATE (%/hr.) | ELONGATION (%) | REDUCTION IN AREA (%) | PLASTIC ON LOADING (%) |
|---|---|---|---|---|---|---|---|---|---|
| Heat VAR 55262 | | | | | 850°F (454°C) | | | | |
| C25 | C | 60 (413.7) | ** | -- | -- | -- | 23.4 | 74.4 | 6.9 |
| C1 | A | 55 (379.2) | 6.3 | 3.3 | 2.25 | 0.515 | 24.3 | 71.1 | 3.2 |
| T8 | B | 55 (379.2) | 167.4 | 101.0 | 5.10 | 0.0386 | 27.1 | 71.2 | 4.6 |
| T35** | C | 55 (379.2) | 0.4 | -- | -- | -- | 28.9 | 71.0 | 10.0+ |
| C4 | A | 52 (358.5) | 61.0 | 46.1 | 3.78 | 0.0629 | 24.7 | 73.3 | 5.0 |
| C16 | B | 52 (358.5) | 494.1 | 293.0 | 4.83 | 0.0122 | 28.2 | 73.8 | 3.1 |
| C28 | C | 52 (358.5) | 21.8 | 13.7 | 3.30 | 0.195 | 26.0 | 77.2 | 4.2 |
| C7 | A | 48 (330.9) | 968.4 | 664.0 | 3.40 | 0.0034 | 25.2 | 75.0 | 3.2 |
| C19 | B | 48 (330.9) | 2035.1 | 1175.0 | 4.28 | 0.0025 | 29.1 | 74.5 | 2.3 |
| C31 | C | 48 (330.9) | 119.6 | 57.8 | 2.41 | 0.0318 | 27.9 | 79.0 | 3.0 |
| C10 | A | 40 (275.8) | 2864.8†† | 2450;2200 | 3.23;2.24 | 0.00100;0.000263 | 29.2 | 79.7 | 1.8 |
| C34 | C | 40 (275.8) | 1359.9 | ~810. | ~2.85 | 0.0029† | 31.3 | 82.5 | 1.2 |
| Heat ESR R0110 | | | | | | | | | |
| C51 | B | 52 (358.5) | 2.5 | 1.74 | 8.00 | 3.678 | 31.9 | 73.7 | 6.2 |
| C54 | D | 52 (358.5) | 80.6 | 66.7 | 11.00 | 0.144 | 32.9 | 71.2 | 5.0 |
| T22 | B | 40 (275.8) | 298.4 | 1325.0 | 6.78 | 0.0038 | 36.0 | 75.0 | 0.4 |
| T42*** | D | 40 (275.8) | | | | | | | |

* Determined by 0.2% strain offset
** Specimen failed on loading
*** Specimen on test
† Average for discontinuous behavior
†† Strain discontinuity at 1010 hours

TABLE 8.13 (Cont'd.)

CREEP-RUPTURE DATA FOR 2 1/4 Cr - 1 Mo STEEL

| SPECIMEN NUMBER | HEAT TREATMENT | STRESS KSI (MPa) | RUPTURE TIME (hr.) | TIME TO THIRD* STAGE (hr.) | STRAIN TO THIRD* STAGE (%) | MINIMUM CREEP* RATE (%/hr.) | ELONGATION (%) | REDUCTION IN AREA (%) | PLASTIC ON LOADING (%) |
|---|---|---|---|---|---|---|---|---|---|
| Heat VAR 55262 | | | | | 950°F (510°C) | | | | |
| C26 | C | 40 (275.8) | 20.3 | 5.4 | 1.47 | 0.200 | 34.1 | 81.9 | 1.6 |
| C2 | A | 35 (241.3) | 90.0 | 29.9 | 1.75 | 0.0408 | 41.6 | 80.6 | 1.6 |
| C14 | B | 35 (241.3) | 430.3 | 166.0 | 3.28 | 0.0133 | 39.4 | 83.3 | 1.5 |
| T17 | C | 35 (241.3) | 51.2 | 13.2 | 1.69 | 0.0871 | 42.2 | 83.9 | 0.8 |
| C5 | A | 30 (206.8) | 245.9 | 82.0 | 1.25 | 0.0104 | 50.2 | 83.6 | 1.5 |
| C17 | B | 30 (206.8) | 1398.4 | 427.0 | 2.35 | 0.0041 | 46.6 | 85.5 | 0.6 |
| C29 | C | 30 (206.8) | 226.1 | 55.6 | 1.44 | 0.0201 | 45.9 | 84.2 | 0.3 |
| C8 | A | 25 (172.4) | 721.2 | 198.0 | 0.83 | 0.0032 | 57.5 | 87.3 | 0.3 |
| C20 | B | 25 (172.4) | 2842.8 | 580.0 | 1.46 | 0.0019 | 54.6 | 87.3 | 0.2 |
| C32 | C | 25 (172.4) | 853.3 | 134.0 | 0.41 | 0.0014 | 51.6 | 86.2 | 0.08 |
| C11 | A | 22 (151.7) | 763.6 | 150.0 | 0.76 | 0.0032 | 51.1 | 87.6 | 1.1 |
| C35 | C | 22 (151.7) | 2184.2 | 298.0 | 0.50 | 0.0010 | 55.1 | 88.4 | 0.07 |
| Heat ESR R0110 | | | | | | | | | |
| C52 | B | 30 (206.8) | 387.0 | 172.0 | 9.50 | 0.0466 | 51.2 | 76.2 | 1.3 |
| C55 | D | 30 (206.8) | 895.6 | 274.0 | 5.33 | 0.0150 | 45.5 | 68.8 | 0.8 |
| T23 | B | 22 (151.7) | 3325.4 | 1065.0 | 6.75 | 0.0058 | 48.7 | 61.5 | 0.2 |
| T43*** | D | 22 (151.7) | | | | | | | |

TABLE 8.13 (Cont'd.)

CREEP-RUPTURE DATA FOR 2 1/4 Cr - 1 Mo STEEL

| SPECIMEN NUMBER | HEAT TREATMENT | STRESS KSI (MPa) | RUPTURE TIME (hr.) | TIME TO THIRD* STAGE (hr.) | STRAIN TO THIRD* STAGE (%) | MINIMUM CREEP* RATE (%/hr.) | ELONGATION (%) | REDUCTION IN AREA (%) | PLASTIC ON LOADING (%) |
|---|---|---|---|---|---|---|---|---|---|
| Heat VAR 55262 | | | | | 1050°F (566°C) | | | | |
| C3 | A | 27.5 (189.6) | 9.1 | 2.1 | 2.75 | 1.071 | 24.5 | 70.5 | 12.1 |
| C13 | B | 27.5 (189.6) | ** | -- | -- | -- | 52.6 | 87.2 | 1.1 |
| C15 | B | 27.5 (189.6) | 89.2 | 29.2 | 1.78 | 0.0459 | 43.5 | 85.4 | 0.4 |
| T12 | B | 27.5 (189.6) | 50.1 | 15.0 | 4.23 | 0.235 | 64.1 | 87.5 | 0.6 |
| C27 | C | 27.5 (189.6) | 10.1 | 2.0 | 3.00 | 1.000 | 55.2 | 87.2 | 0.4 |
| C6 | A | 25 (172.4) | 17.3 | 3.9 | 2.28 | 0.456 | 52.7 | 85.7 | 0.3 |
| C18 | B | 25 (172.4) | 76.0 | 16.7 | 2.58 | 0.125 | 61.5 | 87.9 | 0.2 |
| C30 | C | 25 (172.4) | 21.0 | 5.9 | 3.32 | 0.503 | 54.0 | 90.4 | 0.2 |
| C9 | A | 22 (151.7) | 44.6 | 11.6 | 5.10 | 0.422 | 68.0 | 88.3 | 0.4 |
| C21 | B | 22 (151.7) | 168.9 | 24.6 | 1.64 | 0.0483 | 72.5 | 89.2 | 0.06 |
| C33 | C | 22 (151.7) | 73.5 | 9.3 | 1.47 | 0.132 | 62.3 | 89.9 | 0.1 |
| C12 | A | 18 (124.1) | 210.2 | 12.6 | 0.44 | 0.0349 | 68.0 | 90.6 | 0.05 |
| C24 | B | 18 (124.1) | 749.7 | 70.5 | 1.02 | 0.0113 | 68.0 | 90.9 | 0.3 |
| C36 | C | 18 (124.1) | 353.3 | 126.0 | 5.43 | 0.0413 | 63.5 | 90.8 | 0.02 |
| T6 | A | 14 (96.53) | 1259.2 | 475.0 | 7.61 | 0.0152 | 60.8 | 91.3 | 0.01 |
| T18 | C | 14 (96.53) | 2788.5 | 952.0 | 5.35 | 0.0054 | 56.5 | 92.0 | 0.0 |
| Heat ESR R0110 | | | | | | | | | |
| C53 | B | 22 (151.7) | 89.9 | 37.2 | 11.90 | 0.282 | 74.2 | 76.8 | 0.6 |
| C56 | D | 22 (151.7) | 142.5 | 21.0 | 3.80 | 0.138 | 57.4 | 74.4 | 0.2 |
| T24 | B | 14 (96.5) | 1489.3 | 530.0 | 7.90 | 0.0141 | 56.8 | 65.5 | 0.02 |
| T44 | D | 14 (96.5) | 1879.7 | 690.0 | 5.70 | 0.0078 | 46.9 | 62.3 | 0.02 |

## TABLE 8.14

BRINELL HARDNESS VALUES OF 2 1/4 Cr - 1 Mo SPECIMENS
FOR ISOTHERMAL TRANSFORMATION STUDY

| | | | ISOTHERMAL HOLD TIME (minutes) | | | | | | |
|---|---|---|---|---|---|---|---|---|---|
| HEAT # | CARBON | TEMP °C | 30 | 45 | 60 | 90 | 120 | 180 | 300 |
| VAR 56067 | 0.11 | 704 | 195 | 195;185 | 150 | 165;150 | 150;147 | 144 | |
| Air Melt 113632 | 0.15 | 704 | 270 | 265;270 | 210 | 228;200 | 210;234 | 169 | |
| ESR R0110 | 0.10 | 704 | 185 | 159;159 | 144 | 141;139 | 141;144 | 141 | |
| VAR 55262 | 0.09 | 704 | 190 | 151;190 | 162 | 162;139 | 150;150 | 150 | |
| VAR B9783 | 0.165 | 690 | 237 | 305 | 276;276 | 222;255 | 197 | 180 | 170 |
| | | 704 | 294 | 250 | 225;222 | 165;167 | 156 | 162 | 156 |
| | | 718 | 210 | 163 | 159;159 | 148;142 | 140 | 141 | 147 |
| VAR B9784 | 0.153 | 690 | 263 | 248 | 235;234 | 210;228 | 190 | 172 | 170 |
| | | 704 | 245 | 213 | 182;178 | 162;165 | 159 | 159 | 153 |
| | | 718 | 213 | 182 | 154;159 | 144;148 | 151 | 147 | 147 |
| VAR 91506 | 0.10 | 690 | 305 | 273 | 235;250 | 259;228 | 222 | 205 | 185 |
| | | 704 | 293 | 260 | 225;222 | 195;216 | 195 | 167 | 154 |
| | | 718 | 222 | 197 | 178;178 | 148;174 | 165 | 160 | 142 |
| ESR 9796 | 0.153 | 690 | 362 | 352 | 352;322 | 342;342 | 301 | 219 | 192 |
| | | 704 | 347 | 305 | 268;283 | 235;240 | 205 | 165 | 163 |
| | | 718 | 309 | 265 | 234;235 | 185;185 | 159 | 153 | 151 |
| ESR 9797 | 0.155 | 690 | 265 | 235 | 228;228 | 250;245 | 234 | 195 | 176 |
| | | 704 | 313 | 290 | 262;257 | 228;228 | 182 | 169 | 160 |
| | | 718 | 276 | 235 | 213;216 | 172;163 | 157 | 150 | 153 |
| ESR 91505 | 0.088 | 690 | 228 | 234 | 222;216 | 203;200 | 187 | 185 | 163 |
| | | 704 | 205 | 195 | 185;190 | 185;185 | 160 | 157 | 151 |
| | | 718 | 200 | 165 | 176;157 | 137;157 | 147 | 153 | 139 |
| Air Melt 113632 | 0.147 | 690 | 322 | 313 | 287;283 | 260;255 | 237 | 195 | 174 |
| | | 704 | 273 | 237 | 210;219 | 180;180 | 165 | 159 | 154 |
| | | 718 | 228 | 200 | 169;172 | 156;151 | 150 | 147 | 147 |
| Air Melt 279251 | 0.09 | 690 | 205 | 197 | 185;190 | 178;172 | 165 | 160 | 156 |
| | | 704 | 182 | 169 | 159;156 | 160;162 | 157 | 151 | 144 |
| | | 718 | 163 | 153 | 147;151 | 147;147 | 147 | 144 | 137 |
| Air Melt 5P4430 | 0.09 | 690 | 187 | 174 | 162;167 | 151;157 | 154 | 148 | 140 |
| | | 704 | 163 | 156 | 153;150 | 153;150 | 150 | 142 | 141 |
| | | 718 | 144 | 140 | 138;141 | 144;141 | 137 | 139 | 135 |

M3-33 Specification: Maximum Brinell 165 ($R_B$ 85)

690°C = 1275°F; 704°C = 1300°F; 718°C = 1325°F

# TABLE 8.15

## CHEMICAL ANALYSIS OF 2 1/4 Cr - 1 Mo STEEL FOR ISOTHERMAL TRANSFORMATION STUDY

| HEAT NUMBER | Al% | Sb% | As% | C% | Cr% | Co% | Cu% | H% | Mn% | Mo% | Ni% | N% | O% | P% | Si% | S% | Sn% | Ti% | V% |
|---|---|---|---|---|---|---|---|---|---|---|---|---|---|---|---|---|---|---|---|
| VAR 56067 | 0.005 | <0.002 | 0.006 | 0.098 | 2.31 | <0.002 | 0.08 | 0.0007 | 0.42 | 0.99 | 0.17 | 0.006 | <0.001 | 0.010 | 0.28 | 0.015 | <0.002 | 0.002 | 0.006 |
| Air Melt 113632 | | | | 0.15 | 2.39 | | | | 0.45 | 1.10 | | | | 0.011 | 0.23 | 0.021 | | | |
| ESR R0110 | 0.027 | <0.002 | 0.010 | 0.100 | 2.26 | <0.002 | 0.10 | 0.0005 | 0.50 | 0.99 | 0.15 | 0.008 | <0.001 | 0.013 | 0.09 | 0.007 | <0.002 | <0.002 | 0.013 |
| VAR 55262 | <0.005 | <0.002 | 0.008 | 0.099 | 2.26 | <0.002 | 0.09 | 0.0006 | 0.50 | 1.00 | 0.15 | 0.008 | <0.001 | 0.013 | 0.07 | 0.016 | 0.004 | <0.002 | 0.013 |
| VAR B9783 | | | | 0.165* | 2.40 | | | | 0.39 | 1.10 | | | 0.014 | 0.009 | 0.20 | 0.034* | | | |
| VAR B9784 | | | | 0.153* | 2.39 | | | | 0.34 | 1.08 | | | <0.005 | 0.013 | 0.21 | 0.025* | | | |
| VAR 91506 | | | | 0.10 | 2.32 | | 0.05 | | 0.39 | 1.02 | 0.06 | | | 0.011 | 0.39 | 0.005 | | | |
| ESR 9796 | | | | 0.153* | 2.44 | | | | 0.47 | 1.09 | | | 0.008 | 0.009 | 0.14 | 0.016 | | | |
| ESR 9797 | | | | 0.155* | 2.42 | | | | 0.46 | 1.08 | | | 0.008 | 0.007 | 0.19 | 0.017 | | | |
| ESR 91505 | | | | 0.088 | 2.25 | | 0.06 | | 0.46 | 1.02 | 0.05 | | | 0.011 | 0.30 | 0.004 | | | |
| Air Melt 279251 | | | | 0.09 | 2.32 | | | | 0.52 | 0.93 | | | | 0.12 | 0.36 | 0.009 | | | |
| Air Melt 5P4430 | | | | 0.09 | 2.35 | | | | 0.40 | 1.00 | | | | 0.006 | 0.23 | 0.012 | | | |
| RDT M2-19 | Minimum | | | 0.070 | 1.90 | | | | 0.30 | 0.87 | | | | | 0.20 | | | | |
| RDT M3-33 | Maximum | | | 0.110 | 2.60 | | 0.35 | | 0.60 | 1.13 | 0.25 | | | 0.015 | 0.40 | 0.015 | | 0.03 | 0.03 |

* Average Values

TABLE 8.16

COMPACT TENSION SPECIMEN [50.8 mm (2 in) Thick]

FRACTURE TOUGHNESS RESULTS FOR 2 1/4 Cr - 1 Mo VAR HEAT 55262 50.8 mm (2 in) THICK PLATE

TESTS FOR TRANSVERSE ORIENTATION AT 24°C (75°F)

WITH SPECIMEN LOAD POINT DISPLACEMENT RATE OF 1.52 mm/min (0.06 in/min)

| Spec. No. | Stable Crack Extension, Δa, at Unload mm (in) | Remarks | J at Unload $J/mm^2$ ($in\text{-}lb/in^2$) | J at COS, $J_{Ic}$ $J/mm^2$ ($in\text{-}lb/in^2$) | $K_{Ic}$ MPa $\sqrt{m}$ (ksi $\sqrt{in}$) |
|---|---|---|---|---|---|
| GV1 | -- | Pop-in | 9.3 (530) | 9.3 (530) | 145 (132) |
| GV2 | -- | Pop-in | 11.7 (670) | 11.7 (670) | 164 (149) |
| GV3 | -- | Pop-in | 6.5 (370) | 6.5 (370) | 121 (110) |

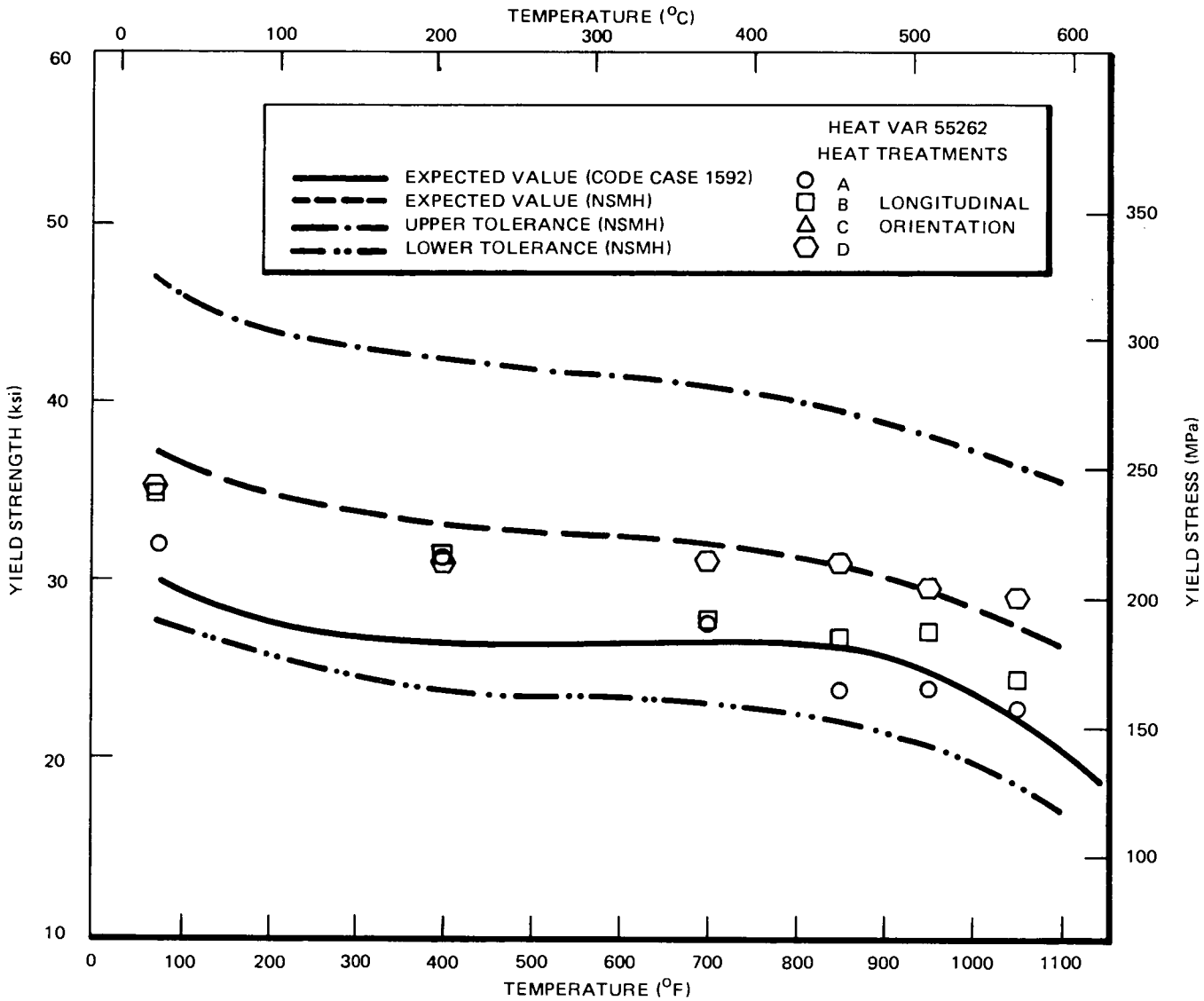


Figure 8.13. *Relationship Between Yield Strength and Temperature for 0.10%C, VAR 2¼ Cr- 1 Mo Steel*

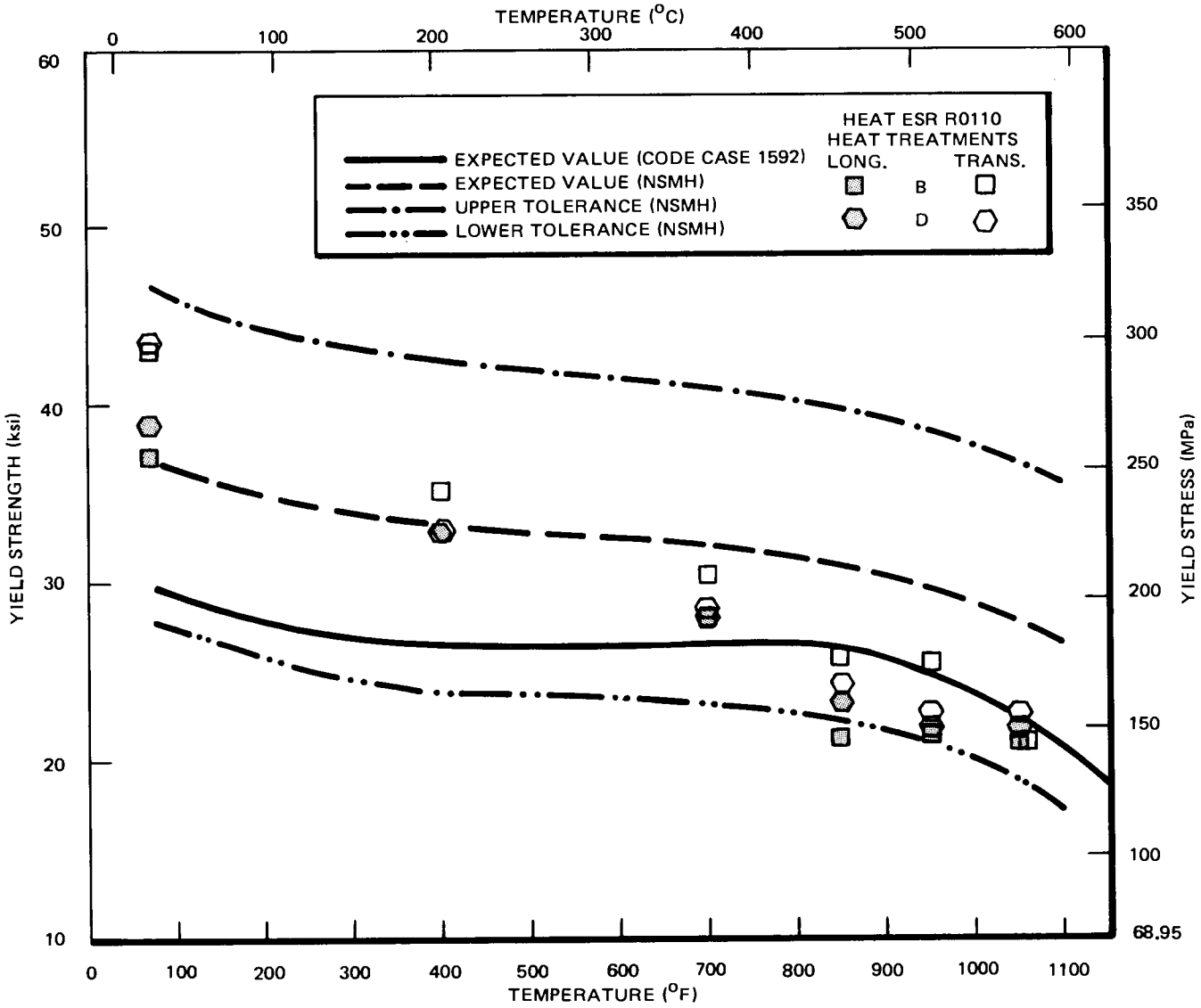


Figure 8.14. *Relationship Between Yield Strength and Temperature for 0.10%C, ESR 2¼ Cr – 1 Mo Steel*

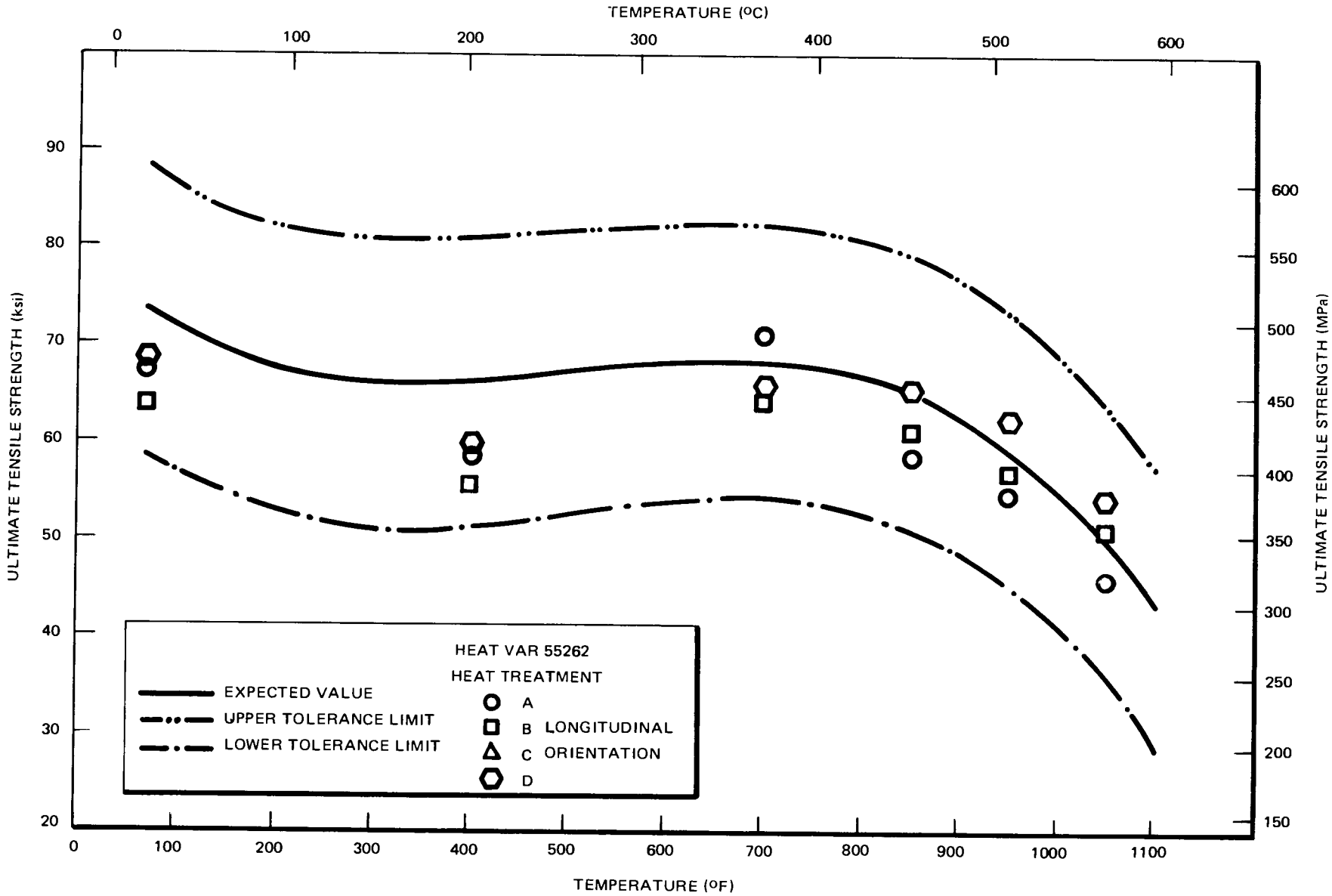


Figure 8.15. *Relationship Between Ultimate Tensile Strength and Temperature for 0.10%C, VAR 2¼ Cr – 1 Mo Steel*

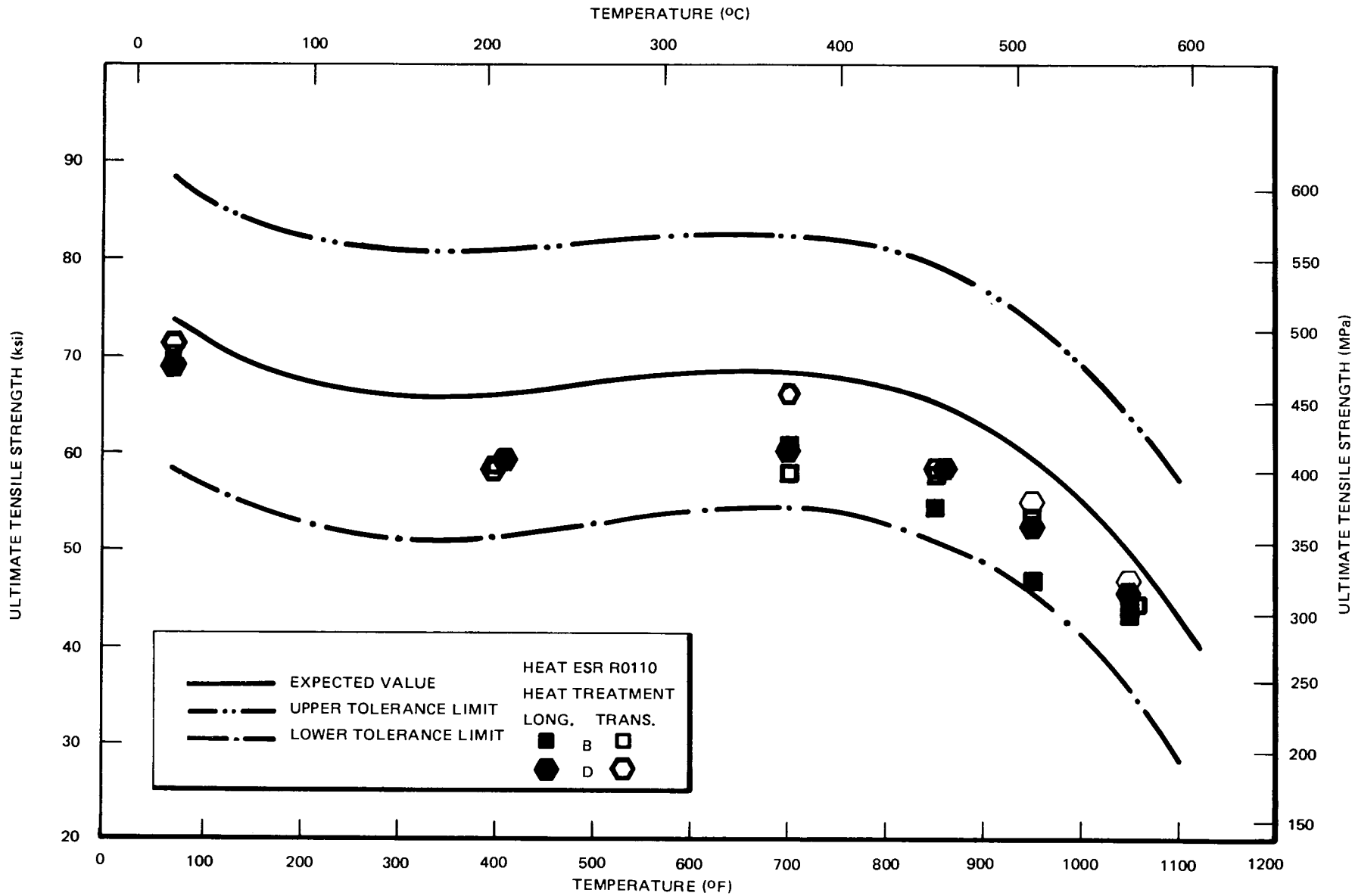


Figure 8.16. *Relationship Between Ultimate Tensile Strength and Temperature for 0.10%C, ESR 2¼ Cr – 1 Mo Steel*

# TABLE 8.12

## CHARPY V-NOTCH RESULTS FOR 2 1/4 Cr - 1 Mo STEEL

| Specimen No. | CVN J (ft.-lb.) | Temp. °C (°F) | Lateral Expansion µm (mils) | Shear Fracture (%) Observation #1 | #2 | #3 | Avg. | Heat** | Heat Treatment | Orientation*** |
|---|---|---|---|---|---|---|---|---|---|---|
| V-10 | 3.5 (2.6) | -45.6 (-50) | 25 (1) | 0 | 1 | 2 | 1 | V-1 | B | L |
| V-3 | 11.5 (8.5) | -40 (-40) | 203 (8) | 2 | 2 | 4 | 3 | V-1 | B | L |
| V-5 | 22.4 (16.5) | -34.4 (-30) | 432 (17) | 8 | 4 | 2 | 5 | V-1 | B | L |
| V-7 | 14.9 (11.0) | -34.4 (-30) | 279 (11) | 5 | 3 | 2 | 3 | V-1 | B | L |
| V-6 | 324.3 (239.2) | -31.7 (-25) | 2390 (94) | 100 | 100 | 100 | 100 | V-1 | B | L |
| V-8 | 6.2 (4.6) | -31.7 (-25) | 0 (0) | 2 | 2 | 2 | 2 | V-1 | B | L |
| V-9 | 4.3 (3.2) | -31.7 (-25) | 25 (1) | 1 | 1 | 2 | 1 | V-1 | B | L |
| V-4 | >324.6 (>239.4) | -28.9 (-20) | 2310 (91) | 100 | 100 | 100 | 100 | V-1 | B | L |
| V-2 | >315.6 (>232.8*) | -17.8 (0) | 2460 (97) | 100 | 100 | 100 | 100 | V-1 | B | L |
| V-1 | >317.8 (>234.4*) | 23.9 (75) | 2260 (89) | 100 | 100 | 100 | 100 | V-1 | B | L |
| V-12 | 4.2 (3.1) | -17.8 (0) | 0 (0) | 2 | 5 | 4 | 4 | V-1 | A | T |
| V-13 | 5.2 (3.8) | -6.67 (20) | 76 (3) | 2 | 4 | 4 | 3 | V-1 | A | T |
| V-14 | 14.9 (11.0) | 15.6 (60) | 356 (14) | 12 | 15 | 5 | 11 | V-1 | A | T |
| V-18 | 12.8 (9.5) | 18.3 (65) | 305 (12) | 8 | 10 | 5 | 8 | V-1 | A | T |
| V-19 | 15.2 (11.2) | 21.1 (70) | 279 (11) | 10 | 14 | 5 | 10 | V-1 | A | T |
| V-11 | 90.8 (67.0) | 23.9 (75) | 1520 (60) | 30 | 20 | 10 | 20 | V-1 | A | T |
| V-15 | 76.7 (56.6) | 37.8 (100) | 1380 (55) | 35 | 25 | 15 | 25 | V-1 | A | T |
| V-17 | 116.6 (86.0) | 65.6 (150) | 1910 (75) | 65 | 65 | 60 | 63 | V-1 | A | T |
| V-16 | 137.8 (101.6) | 98.9 (210) | 1980 (78) | 85 | 80 | 75 | 80 | V-1 | A | T |
| V-20 | 139.6 (103.0) | 176.7 (350) | 1930 (76) | 100 | 99 | 98 | 99 | V-1 | A | T |

* Hammer stopped

** V-1 = VAR 55262, V-2 = VAR 56067, E = ESR R0110

*** L = Longitudinal, T = Transverse

TABLE 8.12 (Cont'd.)

CHARPY V-NOTCH RESULTS FOR 2 1/4 Cr - 1 Mo STEEL

| Specimen No. | CVN J (ft.-lb.) | Temp. °C. (°F) | Lateral Expansion μm (mils) | Shear Fracture (%) Observation | | | | Heat** | Heat Treatment | Orientation*** |
|---|---|---|---|---|---|---|---|---|---|---|
| | | | | #1 | #2 | #3 | Avg. | | | |
| V-24 | 15.2 (11.2) | -28.9 (-20) | 254 (10) | 5 | 10 | 5 | 7 | V-1 | B | T |
| V-22 | 14.9 (11.0) | -17.8 (0) | 330 (13) | 5 | 9 | 1 | 5 | V-1 | B | T |
| V-23 | 46.4 (34.2) | -6.67 (20) | 838 (33) | 10 | 22 | 3 | 12 | V-1 | B | T |
| V-29 | 73.8 (54.4) | 4.44 (40) | 1300 (51) | 20 | 20 | 10 | 17 | V-1 | B | T |
| V-25 | 84.3 (62.2) | 15.6 (60) | 1400 (55) | 25 | 40 | 15 | 27 | V-1 | B | T |
| V-21 | 86.2 (63.6) | 23.9 (75) | 1400 (55) | 35 | 25 | 10 | 23 | V-1 | B | T |
| V-26 | 113.2 (83.5) | 37.8 (100) | 1800 (71) | 80 | 70 | 40 | 63 | V-1 | B | T |
| V-28 | 126.4 (93.2) | 65.6 (150) | 1910 (75) | 95 | 98 | 90 | 94 | V-1 | B | T |
| V-27 | 126.1 (93.0) | 98.9 (210) | 1980 (78) | 100 | 99 | 90 | 96 | V-1 | B | T |
| V-30 | 125.0 (92.2) | 176.7 (350) | 1960 (77) | 100 | 99 | 90 | 96 | V-1 | B | T |
| V-34 | 10.8 (8.0) | -28.9 (-20) | 203 (8) | 2 | 8 | 2 | 4 | V-1 | C | T |
| V-32 | 8.1 (6.0) | -17.8 (0) | 76 (3) | 5 | 10 | 8 | 8 | V-1 | C | T |
| V-33 | 46.8 (34.5) | -6.67 (20) | 787 (31) | 10 | 17 | 10 | 12 | V-1 | C | T |
| V-38 | 50.4 (37.2) | 4.44 (40) | 914 (36) | 15 | 15 | 15 | 15 | V-1 | C | T |
| V-40 | 62.3 (47.4) | 10. (50) | 1120 (44) | 20 | 20 | 15 | 18 | V-1 | C | T |
| V-35 | 81.9 (60.4) | 15.6 (60) | 1420 (56) | 35 | 40 | 20 | 32 | V-1 | C | T |
| V-31 | 90.6 (66.8) | 23.9 (75) | 1470 (58) | 35 | 35 | 20 | 30 | V-1 | C | T |
| V-36 | 100.3 (74.0) | 37.8 (100) | 1570 (62) | 40 | 40 | 25 | 35 | V-1 | C | T |
| V-39 | 108.5 (80.0) | 65.6 (150) | 1650 (65) | 80 | 80 | 75 | 78 | V-1 | C | T |
| V-37 | 118.2 (87.2) | 98.9 (210) | 1780 (70) | 100 | 99 | 95 | 98 | V-1 | C | T |

TABLE 8.12 (Cont'd.)

CHARPY V-NOTCH RESULTS FOR 2 1/4 Cr - 1 Mo STEEL

| Specimen No. | CVN J (ft.-lb.) | Temp. °C (°F) | Lateral Expansion μm (mils) | Shear Fracture (%) Observation #1 | #2 | #3 | Avg. | Heat** | Heat Treatment | Orientation*** |
|---|---|---|---|---|---|---|---|---|---|---|
| V-44 | 4.7 (3.5) | -28.9 (-20) | 25 (1) | 0 | 1 | 1 | 1 | V-1 | D | T |
| V-42 | 9.8 (7.2) | -17.8 (0) | 203 (8) | 5 | 9 | 5 | 6 | V-1 | D | T |
| V-43 | 35.9 (26.5) | -6.67 (20) | 711 (28) | 10 | 15 | 5 | 10 | V-1 | D | T |
| V-48 | 53.1 (39.2) | 4.44 (40) | 991 (39) | 15 | 18 | 15 | 16 | V-1 | D | T |
| V-50 | 66.7 (49.2) | 10. (50) | 1220 (48) | 20 | 20 | 15 | 18 | V-1 | D | T |
| V-45 | 75.1 (55.4) | 15.6 (60) | 1300 (51) | 22 | 25 | 15 | 21 | V-1 | D | T |
| V-41 | 65.6 (48.4) | 23.9 (75) | 1190 (47) | 20 | 25 | 15 | 20 | V-1 | D | T |
| V-46 | 98.3 (72.5) | 37.8 (100) | 1600 (63) | 50 | 50 | 25 | 42 | V-1 | D | T |
| V-49 | 116.6 (86.0) | 65.6 (150) | 1830 (72) | 95 | 95 | 90 | 93 | V-1 | D | T |
| V-47 | 118.0 (87.0) | 98.9 (210) | 1850 (73) | 98 | 98 | 95 | 97 | V-1 | D | T |
| V-52 | 4.7 (3.5) | -17.8 (0) | 51 (2) | 2 | 8 | 2 | 4 | V-1 | E | T |
| V-53 | 9.8 (7.2) | 4.44 (40) | 203 (8) | 5 | 8 | 5 | 6 | V-1 | E | T |
| V-51 | 28.2 (20.8) | 23.9 (75) | 610 (24) | 15 | 17 | 20 | 17 | V-1 | E | T |
| V-54 | 51.5 (38.0) | 37.8 (100) | 1040 (41) | 35 | 25 | 15 | 25 | V-1 | E | T |
| V-57 | 59.4 (43.8) | 48.9 (120) | 991 (39) | 38 | 45 | 40 | 41 | V-1 | E | T |
| V-58 | 66.2 (48.8) | 54.4 (130) | 1270 (50) | 18 | 20 | 15 | 18 | V-1 | E | T |
| V-56 | 103.2 (76.1) | 60. (140) | 1750 (69) | 65 | 75 | 70 | 70 | V-1 | E | T |
| V-60 | 91.1 (67.2) | 65.6 (150) | 1600 (63) | 45 | 55 | 30 | 43 | V-1 | E | T |
| V-55 | 113.2 (83.5) | 98.9 (210) | 1880 (74) | 85 | 90 | 90 | 88 | V-1 | E | T |
| V-59 | 116.9 (86.2) | 176.7 (350) | 1910 (75) | 100 | 99 | 95 | 98 | V-1 | E | T |

TABLE 8.12 (Cont'd.)

CHARPY V-NOTCH RESULTS FOR 2 1/4 Cr - 1 Mo STEEL

| Specimen No. | CVN J (ft.-lb.) | Temp. °C (°F) | Lateral Expansion μm (mils) | Shear Fracture (%) Observation | | | | Heat** | Heat Treatment | Orientation*** |
|---|---|---|---|---|---|---|---|---|---|---|
| | | | | #1 | #2 | #3 | Avg. | | | |
| V-62 | 7.6 (5.6) | -17.8 (0) | 203 (8) | 2 | 5 | 2 | 3 | V-2 | B | T |
| V-63 | 12.2 (9.0) | 4.44 (40) | 305 (12) | 5 | 5 | 5 | 5 | V-2 | B | T |
| V-71 | 24.4 (18.0) | 23.9 (75) | 559 (22) | 10 | 13 | 8 | 10 | V-2 | B | T |
| V-64 | 33.9 (25.0) | 37.8 (100) | 737 (29) | 15 | 15 | 20 | 17 | V-2 | B | T |
| V-67 | 44.5 (32.8) | 48.9 (120) | 914 (36) | 20 | 23 | 30 | 24 | V-2 | B | T |
| V-65 | 54.5 (40.2) | 60. (140) | 1090 (43) | 22 | 22 | 30 | 25 | V-2 | B | T |
| V-66 | 62.6 (46.2) | 71.1 (160) | 1270 (50) | 30 | 40 | 50 | 40 | V-2 | B | T |
| V-68 | 74.6 (55.0) | 82.2 (180) | 1370 (54) | 70 | 75 | 60 | 68 | V-2 | B | T |
| V-69 | 85.6 (63.4) | 93.3 (200) | 1600 (63) | 80 | 85 | 60 | 75 | V-2 | B | T |
| V-61 | 100.3 (74.0) | 98.9 (210) | 1780 (70) | 85 | 90 | 80 | 85 | V-2 | B | T |
| V-72 | 115.0 (84.8) | 121.1 (250) | 1880 (74) | 98 | 98 | 95 | 96 | V-2 | B | T |
| V-70 | 117.7 (86.8) | 176.7 (350) | 2030 (80) | 100 | 99 | 95 | 98 | V-2 | B | T |
| V-73 | 114.4 (84.4) | 176.7 (350) | 2010 (79) | 100 | 99 | 95 | 98 | V-2 | B | T |
| V-75 | 7.6 (5.6) | -17.8 (0) | 152 (6) | 2 | 5 | 5 | 4 | V-2 | D | T |
| V-76 | 14.1 (10.4) | 4.44 (40) | 305 (12) | 5 | 10 | 5 | 7 | V-2 | D | T |
| V-74 | 21.8 (16.1) | 23.9 (75) | 508 (20) | 10 | 13 | 15 | 13 | V-2 | D | T |
| V-77 | 28.5 (21.0) | 37.8 (100) | 711 (28) | 20 | 15 | 18 | 18 | V-2 | D | T |
| V-81 | 41.2 (30.4) | 48.9 (120) | 914 (36) | 25 | 20 | 25 | 23 | V-2 | D | T |
| V-79 | 55.9 (41.2) | 60. (140) | 1090 (43) | 28 | 30 | 25 | 28 | V-2 | D | T |
| V-80 | 62.4 (46.0) | 71.1 (160) | 1270 (50) | 35 | 45 | 30 | 37 | V-2 | D | T |
| V-83 | 70.5 (52.0) | 76.7 (170) | 1300 (51) | 60 | 70 | 50 | 60 | V-2 | D | T |
| V-82 | 79.3 (58.5) | 82.2 (180) | 1450 (57) | 65 | 70 | 50 | 62 | V-2 | D | T |
| V-85 | 78.6 (58.0) | 93.3 (200) | 1520 (60) | 68 | 70 | 50 | 63 | V-2 | D | T |
| V-78 | 103.0 (76.0) | 98.9 (210) | 1780 (70) | 90 | 90 | 80 | 87 | V-2 | D | T |
| V-86 | 112.8 (83.2) | 121.1 (250) | 2010 (79) | 98 | 97 | 95 | 97 | V-2 | D | T |
| V-84 | 116.6 (86.0) | 176.7 (350) | 1980 (78) | 100 | 99 | 95 | 98 | V-2 | D | T |

TABLE 8.12 (Cont'd.)

CHARPY V-NOTCH RESULTS FOR 2 1/4 Cr - 1 Mo STEEL

| Specimen No. | CVN J (ft.-lb.) | Temp. °C (°F) | Lateral Expansion μm (mils) | Shear Fracture (%) Observation | | | | Heat** | Heat Treatment | Orientation*** |
|---|---|---|---|---|---|---|---|---|---|---|
| | | | | #1 | #2 | #3 | Avg. | | | |
| V-94 | 10.6 (7.8) | -56.7 (-70) | 178 (7) | 1 | 3 | 5 | 3 | E | B | L |
| V-90 | 10.6 (7.8) | -51.1 (-60) | 254 (10) | 2 | 8 | 5 | 5 | E | B | L |
| V-96 | 12.9 (9.5) | -48.3 (-55) | 279 (11) | 2 | 8 | 8 | 6 | E | B | L |
| V-91 | 28.5 (21.0) | -45.6 (-50) | 584 (23) | 5 | 10 | 5 | 7 | E | B | L |
| V-93 | 155.6 (114.8) | -42.8 (-45) | 2490 (98) | 40 | 45 | 35 | 40 | E | B | L |
| V-88 | 129.1 (95.2) | -40. (-40) | 2130 (84) | 30 | 33 | 35 | 33 | E | B | L |
| V-97 | 311.6 (229.8) | -37.2 (-35) | 2210 (87) | 100 | 100 | 100 | 100 | E | B | L |
| V-95 | >323.4 (>238.5) | -34.4 (-30) | 2160 (85) | 100 | 100 | 100 | 100 | E | B | L |
| V-92 | >324.0 (>239.0) | -28.9 (-20) | 2130 (84) | 100 | 100 | 100 | 100 | E | B | L |
| V-89 | >319.4 (>235.6) | -17.8 (0) | 2360 (93) | 100 | 100 | 100 | 100 | E | B | L |
| V-87 | >324.7 (>239.5*) | 23.9 (75) | 2210 (87) | 100 | 100 | 95 | 98 | E | B | L |
| V-101 | 11.5 (8.5) | -51.1 (-60) | 279 (11) | 2 | 5 | 5 | 4 | E | B | T |
| V-100 | 123.7 (91.2) | -45.6 (-50) | 1980 (78) | 25 | 30 | 20 | 25 | E | B | T |
| V-98 | >323.9 (>238.9*) | -17.8 (0) | 2210 (87) | 100 | 100 | 100 | 100 | E | B | T |
| V-99 | >317.3 (>234.0) | 10. (50) | 2360 (93) | 100 | 100 | 100 | 100 | E | B | T |
| V-110 | 7.5 (5.5) | -51.1 (-60) | 152 (6) | 0 | 3 | 3 | 2 | E | D | L |
| V-103 | 9.5 (7.0) | -40. (-40) | 203 (8) | 8 | 8 | 5 | 7 | E | D | L |
| V-107 | 63.0 (46.5) | -34.4 (-30) | 1120 (44) | 10 | 20 | 5 | 12 | E | D | L |
| V-108 | 20.6 (15.2) | -34.4 (-30) | 457 (18) | 5 | 8 | 3 | 5 | E | D | L |
| V-106 | 103.3 (76.2) | -28.9 (-20) | 1700 (67) | 20 | 30 | 15 | 22 | E | D | L |
| V-105 | 189.8 (140.0) | -17.8 (0) | 2590(102) | 45 | 50 | 45 | 47 | E | D | L |
| V-109 | 122.6 (90.4) | -12.2 (10) | 1930 (76) | 30 | 30 | 20 | 27 | E | D | L |
| V-111 | >324.6 (>239.4) | -12.2 (10) | 1910 (75) | 100 | 100 | 100 | 100 | E | D | L |
| V-104 | >323.4 (>238.5*) | -6.67 (20) | 2210 (87) | 100 | 100 | 100 | 100 | E | D | L |
| V-102 | >323.8 (>238.8*) | 23.9 (75) | 2260 (89) | 100 | 100 | 100 | 100 | E | D | L |
| V-114 | 60.2 (44.4) | -40 (-40) | 1090 (43) | 5 | 21 | 20 | 15 | E | D | T |
| V-112 | 119.3 (88.0) | -28.9 (-20) | 1850 (73) | 20 | 30 | 20 | 23 | E | D | T |
| V-113 | >323.4 (>238.5*) | 10. (50) | 2180 (86) | 100 | 100 | 100 | 100 | E | D | T |

a.

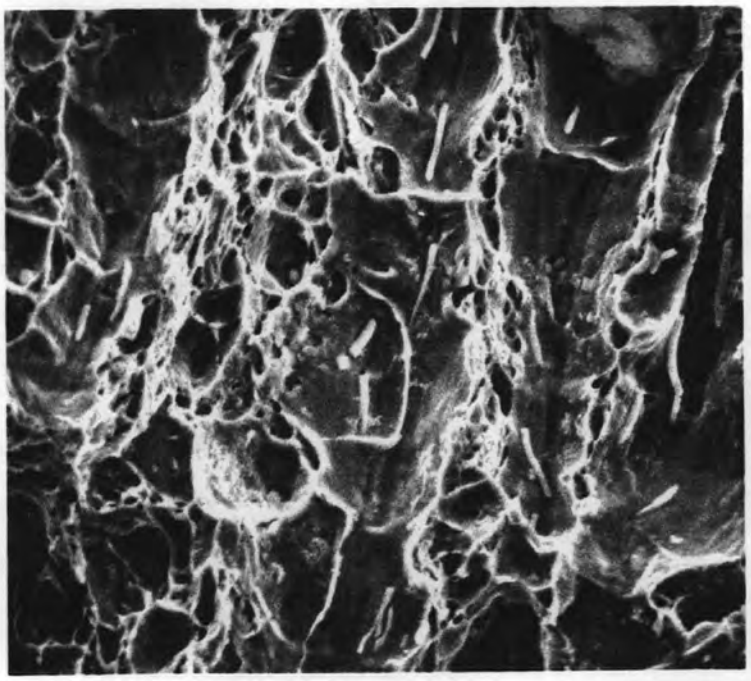

25 µm

b.

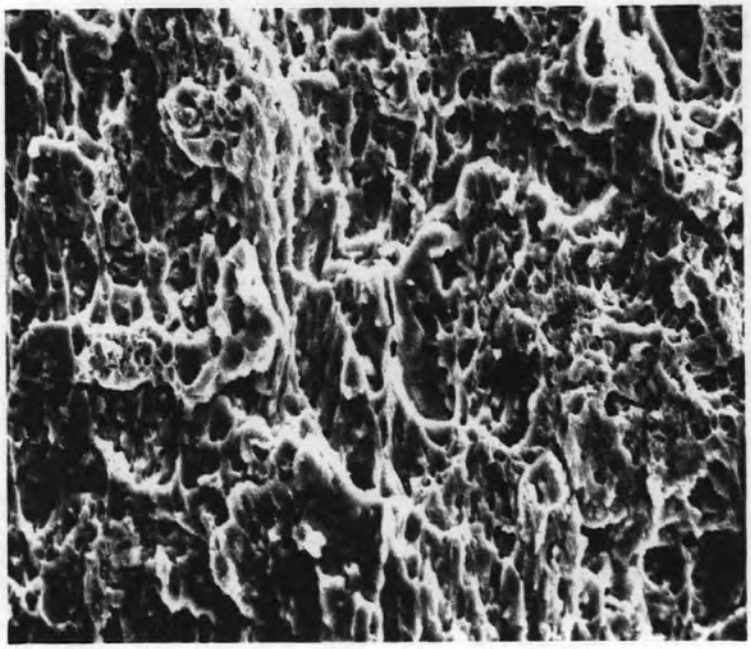

Figure 8.17. *Typical area of fracture surface of Charpy V-Notch specimen broken — the upper shelf temperature range (a) VAR heat 55262 specimen broken at 65.6°C (150°F), (b) ESR heat RO110 Specimen broken at — 17.8°C (0°F)*

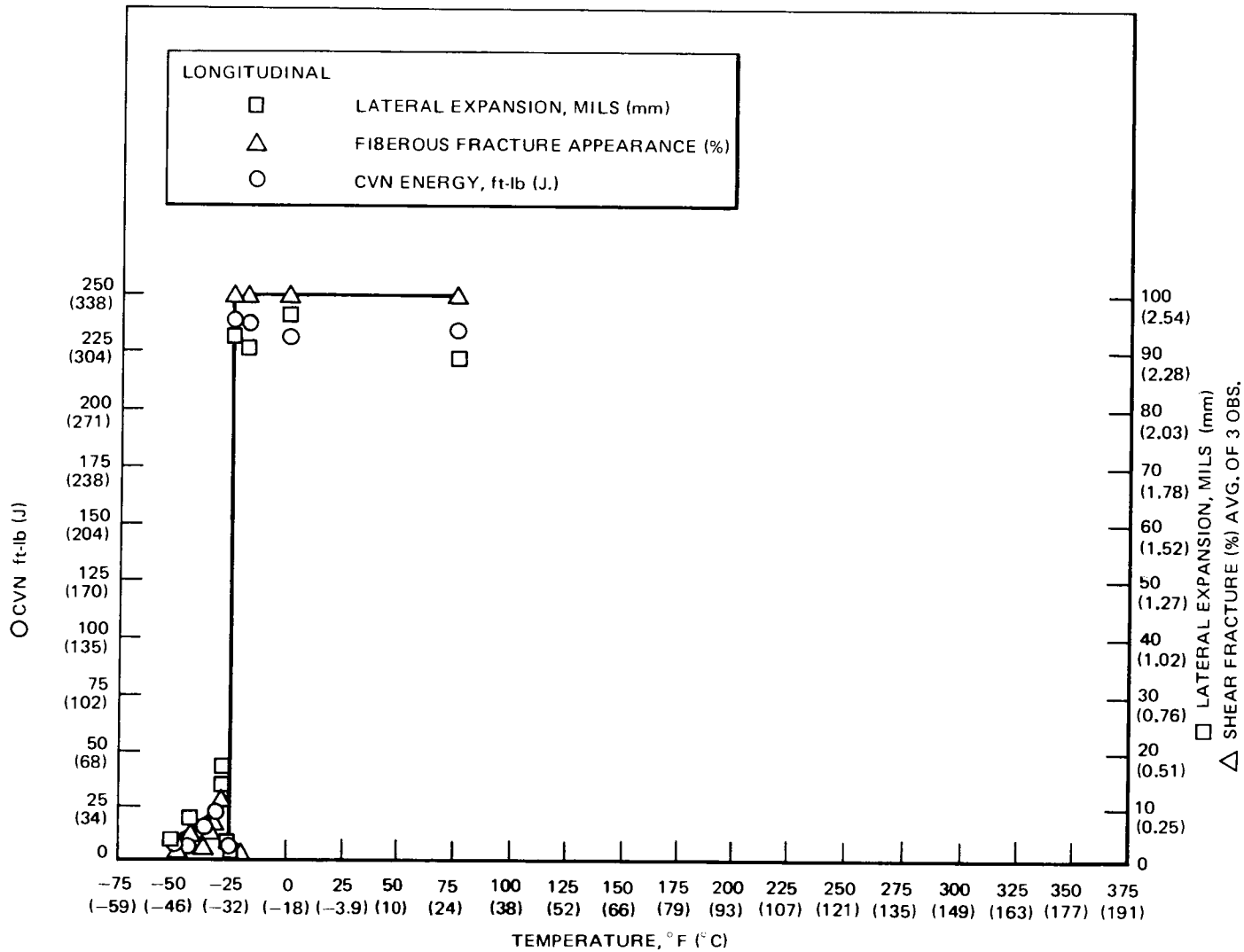


Figure 8.18. *VAR Heat 55262 Longitudinal "B" Heat Treat. V1 to V10*

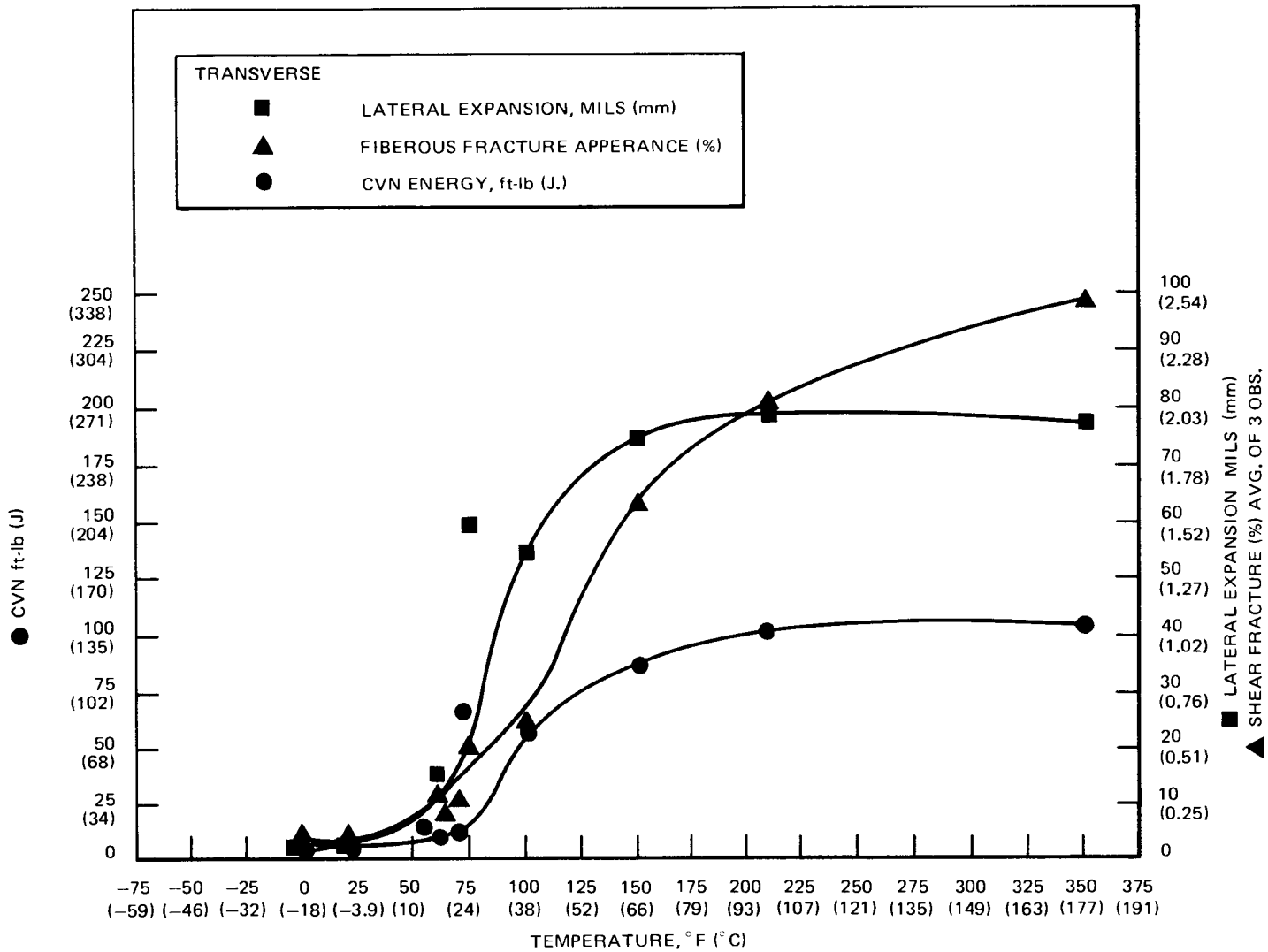


Figure 8.19. *VAR Heat 55262 Transverse "A" Heat Treat. V11 to V20*

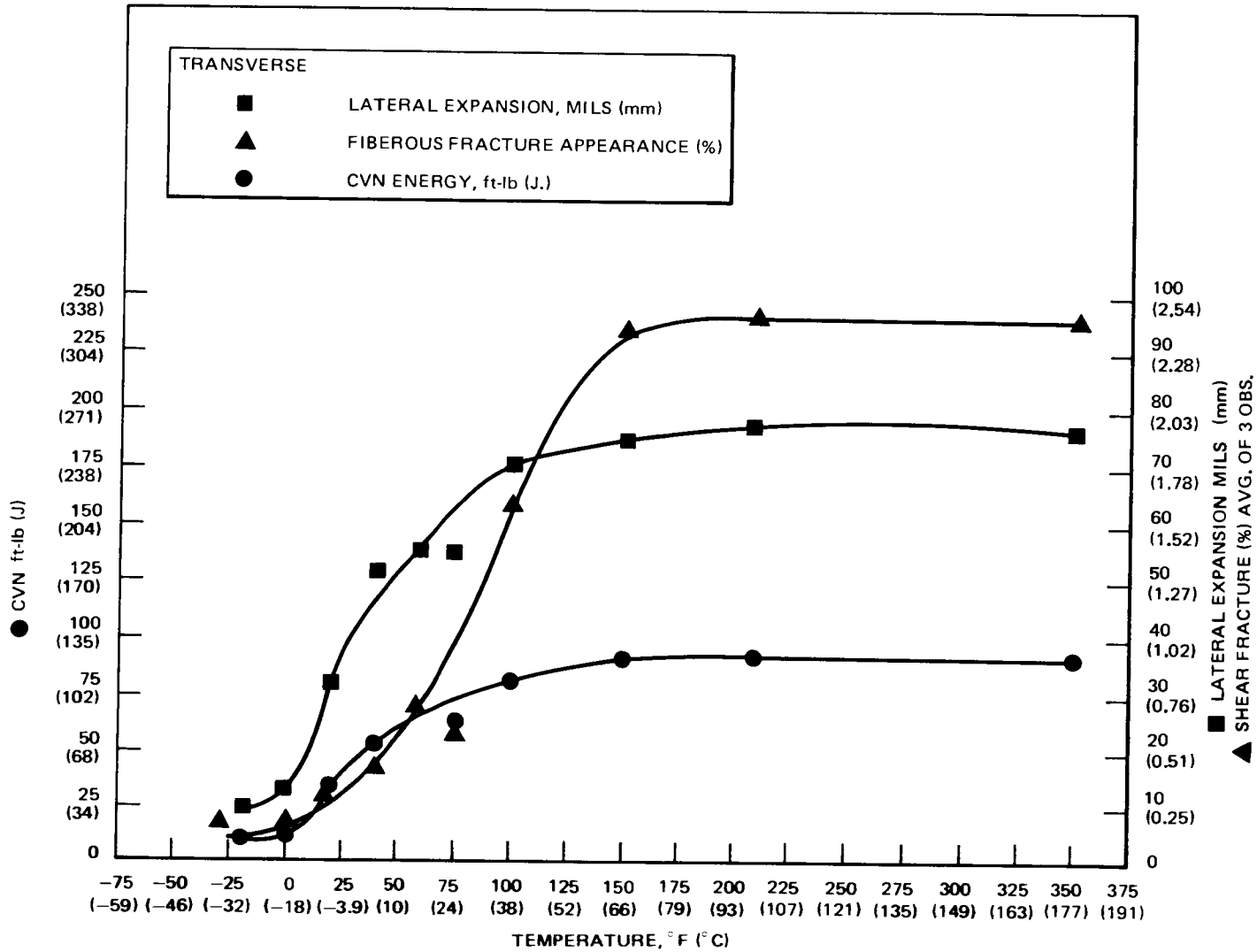


Figure 8.20. *VAR Heat 55262 Transverse "B" Heat Treat. V21 to V30*

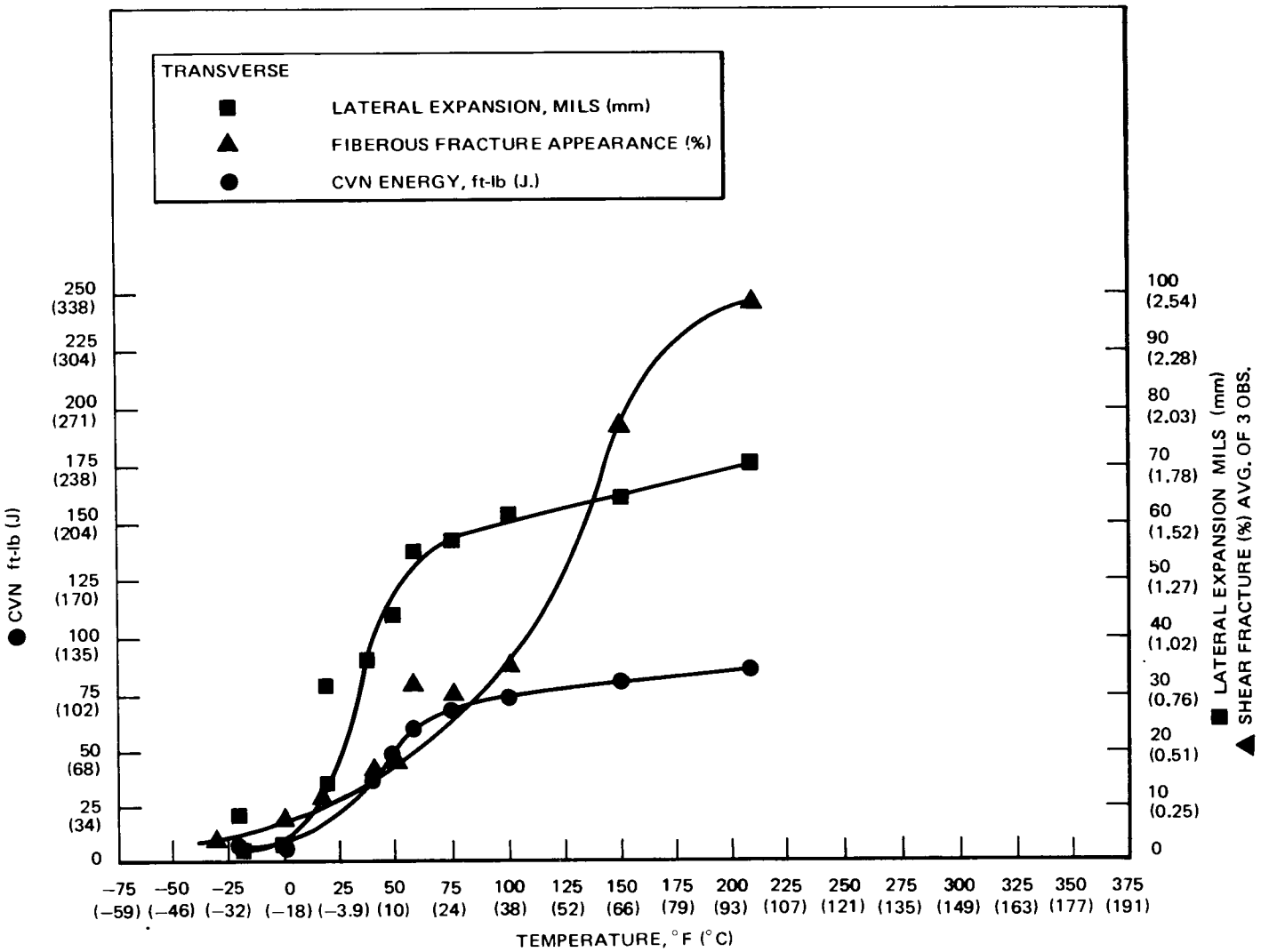


Figure 8.21. *VAR Heat 55262 Transverse "C" Heat Treat. V31 to V40*

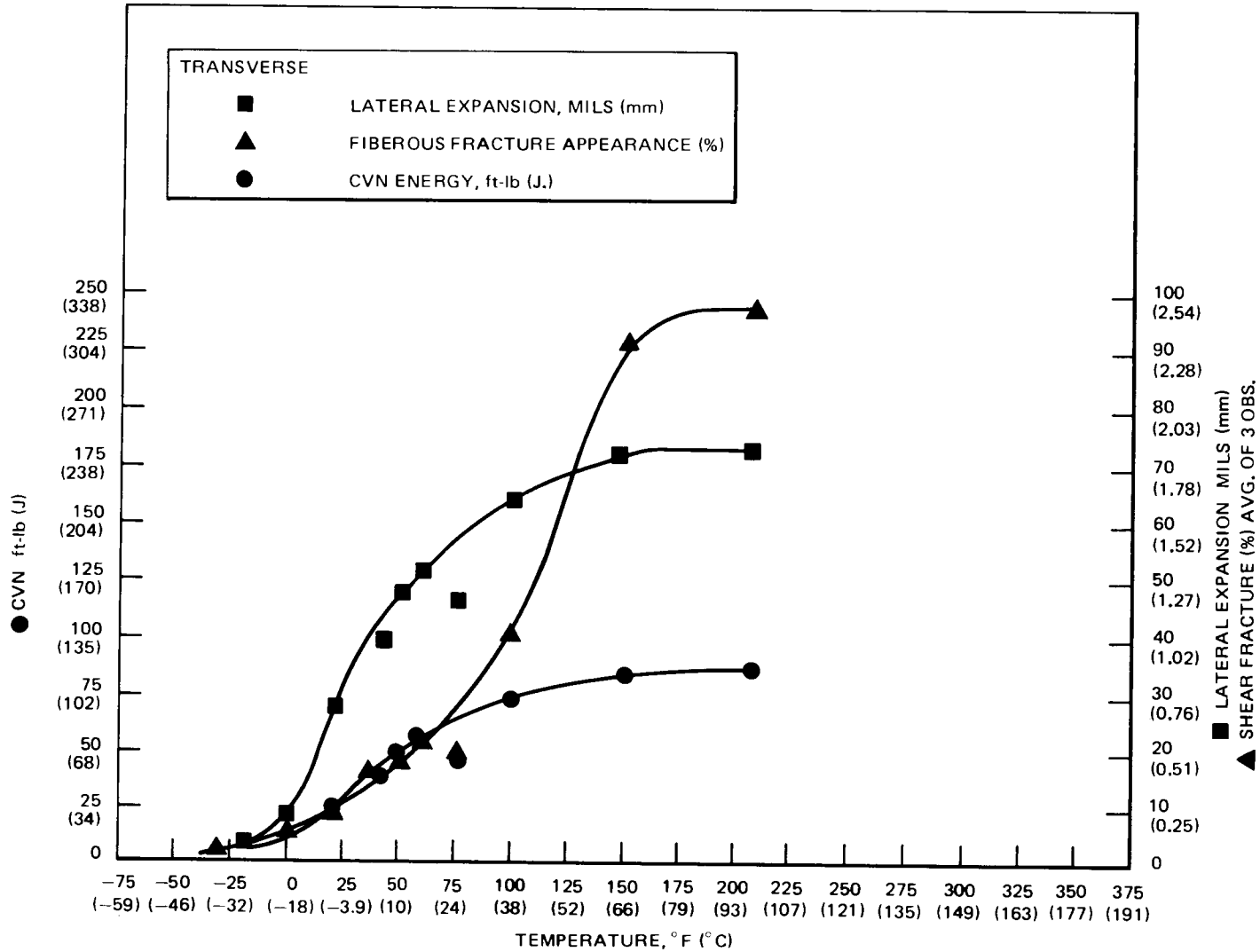


Figure 8.22. *VAR Heat 55262 Transverse "D" Heat Treat. V41 to V50*

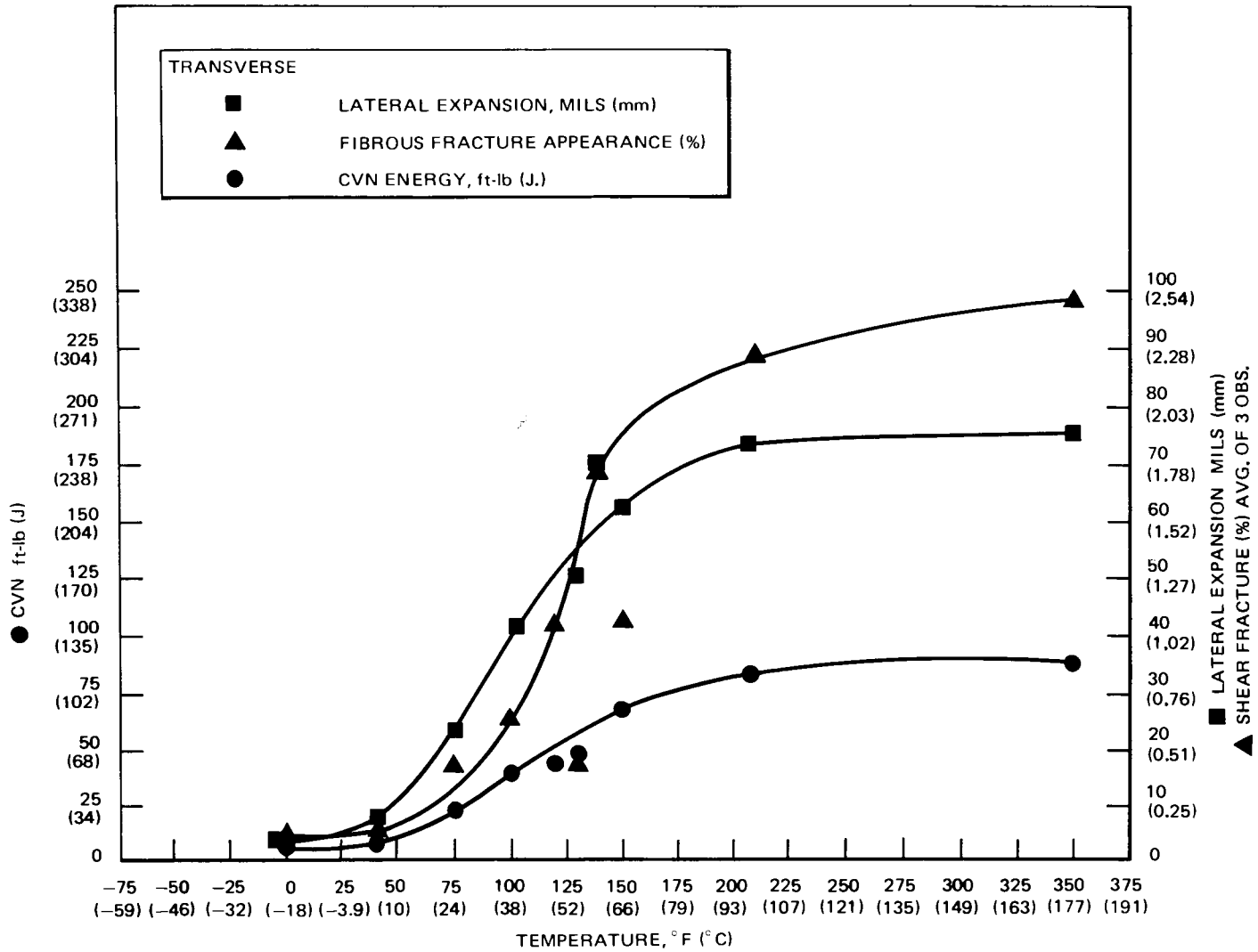


Figure 8.23. *VAR Heat 55262 Transverse "E" Heat Treat. V51 to V60*

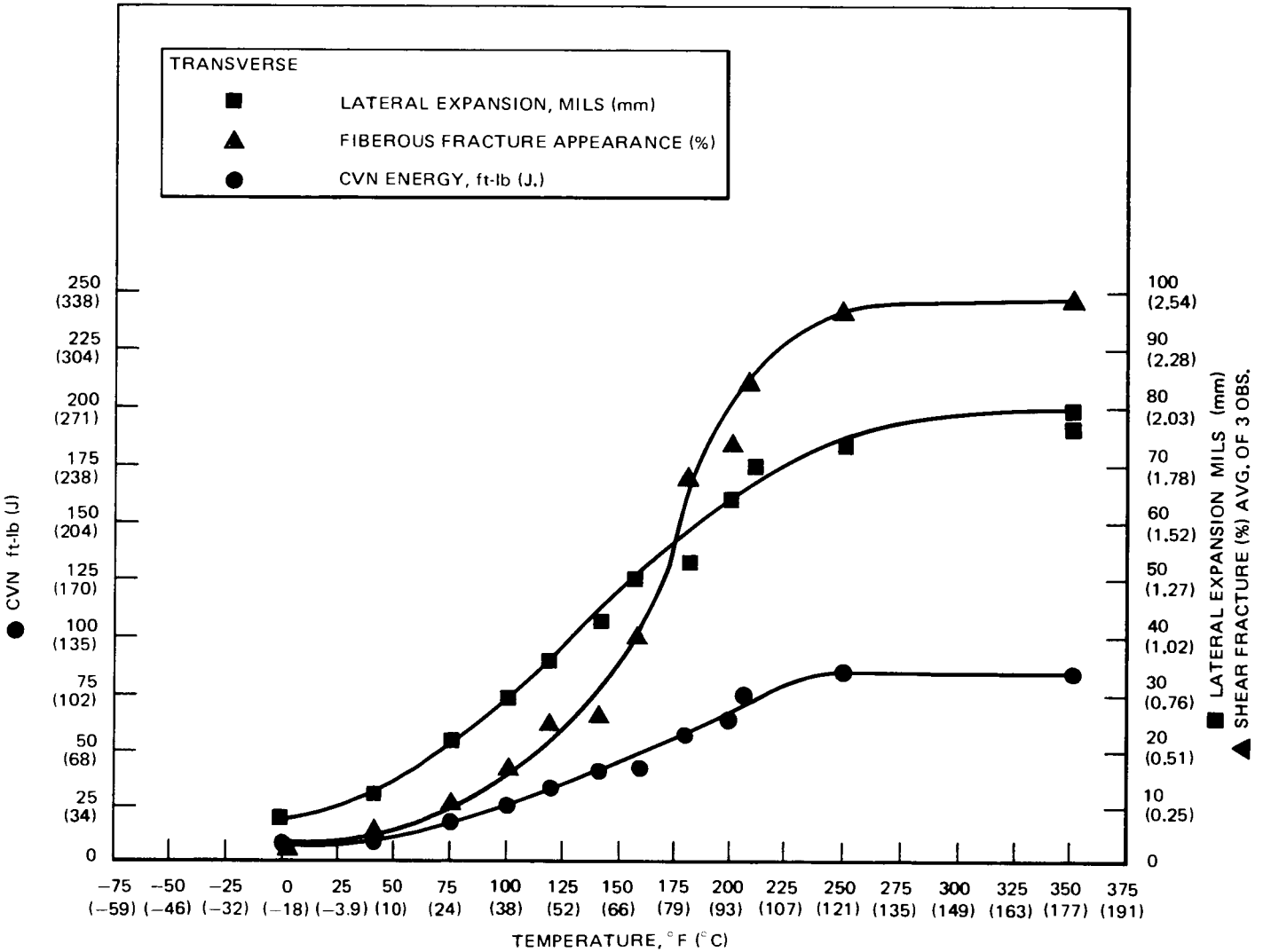


Figure 8.24. *VAR Heat* 56067 *Transverse "B" Heat Treat. V61 to V73.*

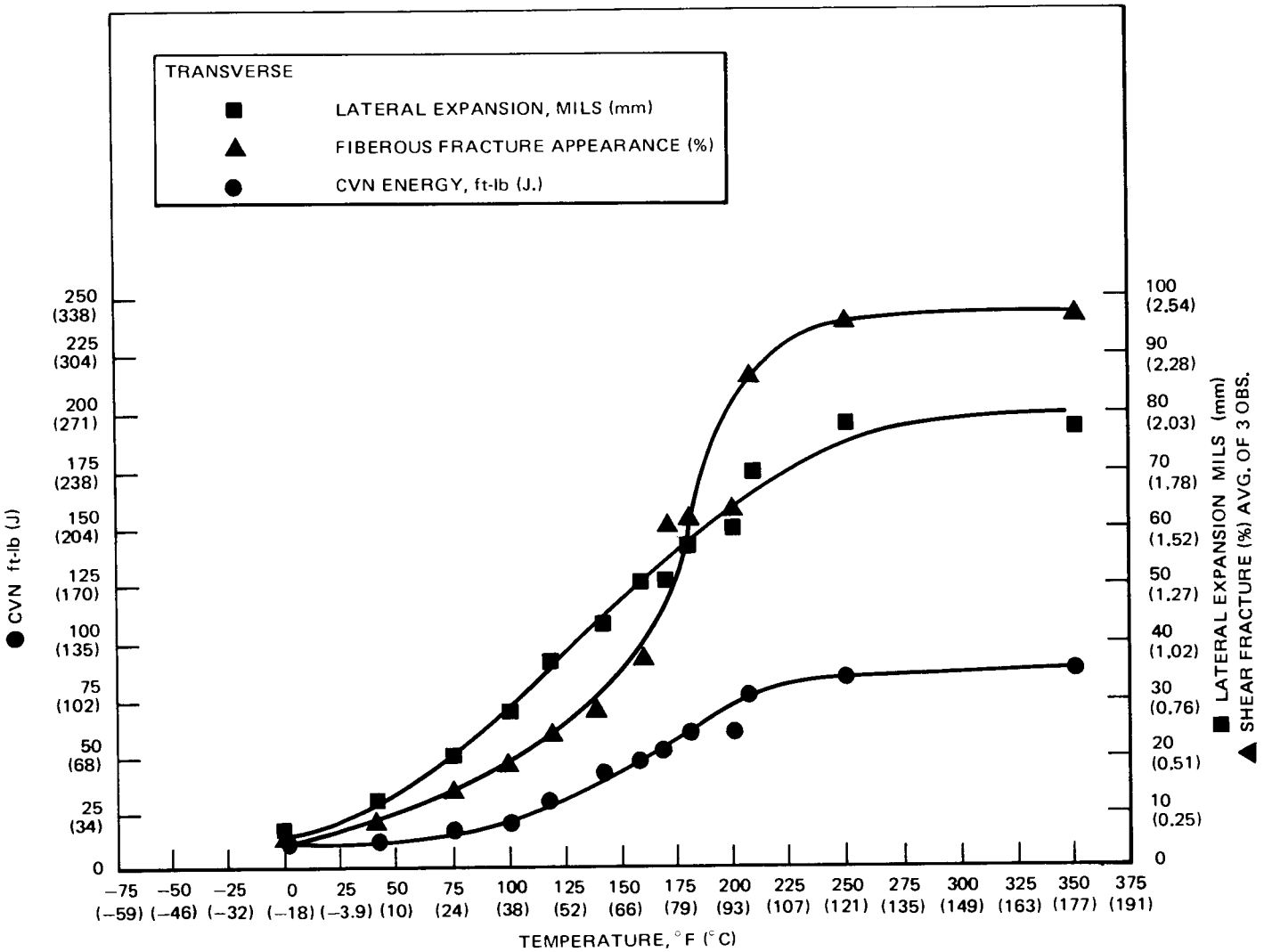


Figure 8.25. *VAR Heat 56067 Transverse "D" Heat Treat. V74 to V86*

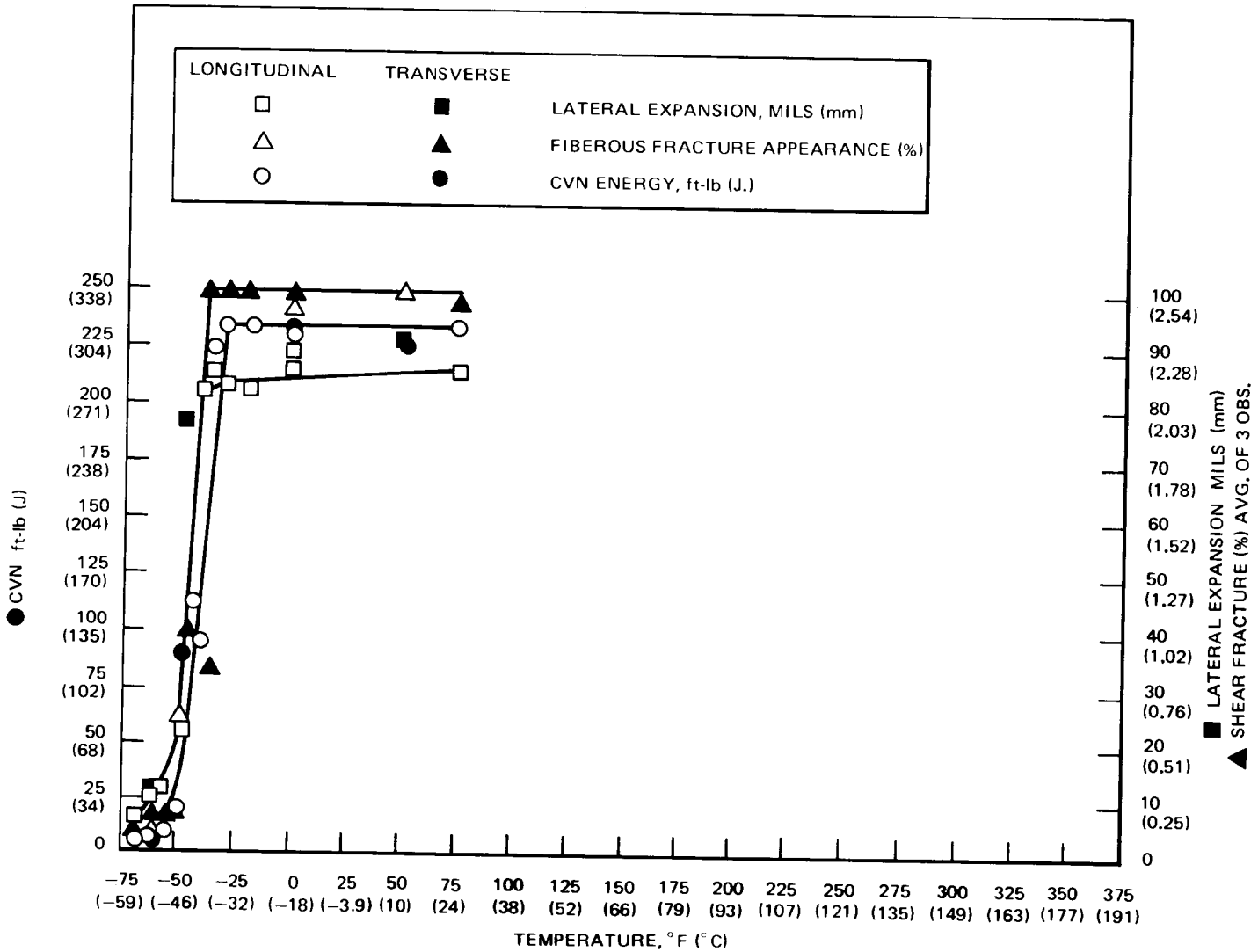


Figure 8.26. *ESR Heat R0110 Longitudinal ○ Transverse ● "B" Heat Treat. V87 to V97 Longitudinal, V98 to V101 Transverse*

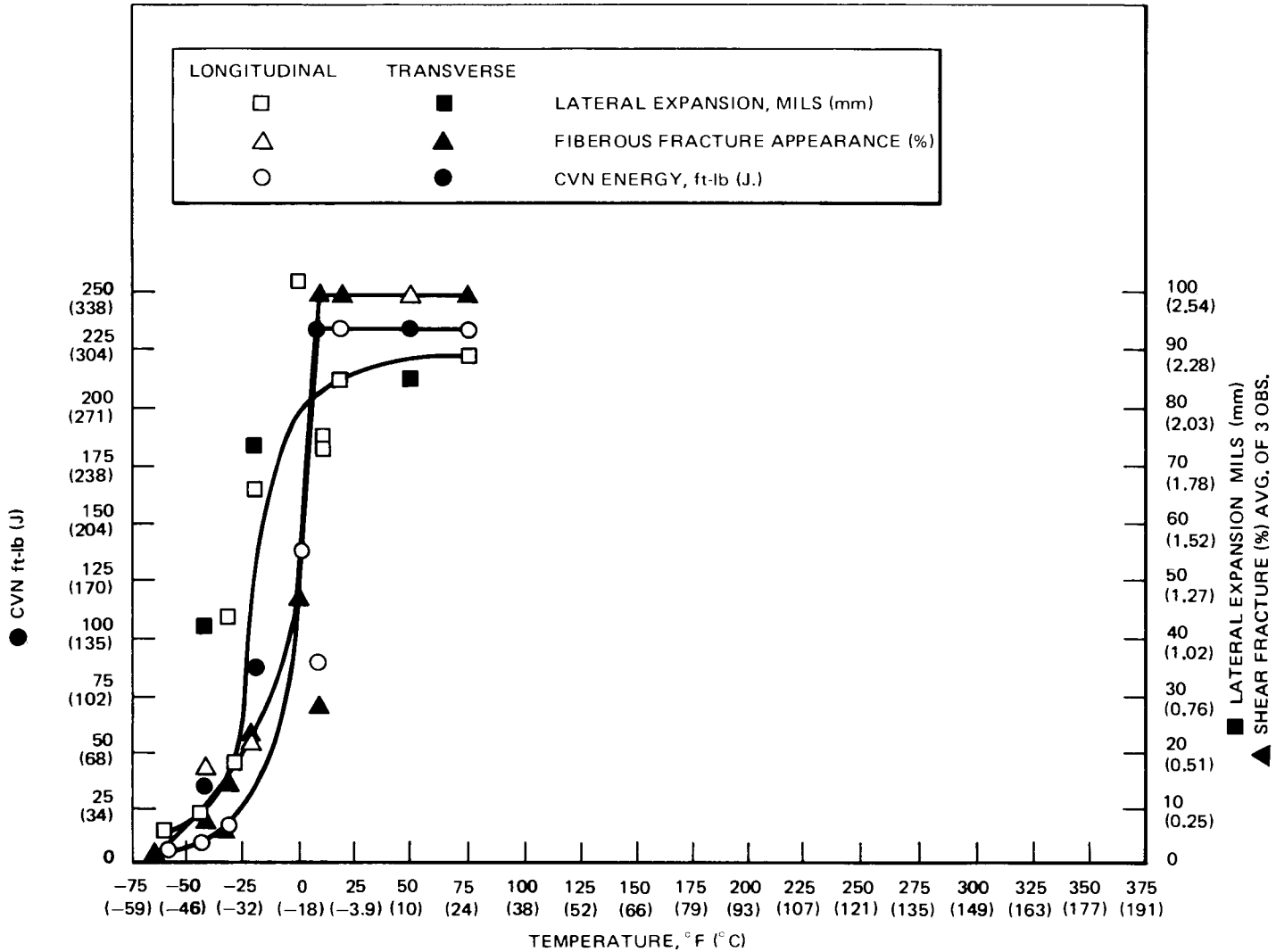


Figure 8.27. *ESR Heat R0110 Longitudinal ○ Transverse ● "D" Heat Treat. V102 to V111 Longitudinal, V112 to V114 Transverse*

inclusions (primarily the sulfide type). The inclusion distributions are different for the ESR and VAR processes. Large cylindrical (~15 μm long, ~1 μm diameter) and spherical (~1 - 2 μm diameter) inclusions were typically observed in the VAR material by scanning electron microscopy. No non-metallic inclusions were visible on the fracture surface of the ESR material. Micrographs of VAR and ESR specimens that were fully annealed with PWHT and fractured in the temperature range of the upper shelf are shown in Figure 8.17.

The effect of the difference in ferrite and prior austenite grain size reported earlier[8] for these two remelting methods is being determined. Grain size has been increased in ESR specimens to match that of the VAR specimens. These will be tested as a function of temperature to verify the effect of grain size on the absorbed energy and fracture appearance transition temperatures.

### 8.4.4 Creep-Rupture Tests

Log stress-log minimum creep rate plots at 454, 510, and 566°C (850, 950, and 1050°F) were reported previously[8] for VAR heat #55262 and ESR heat #R0110. These plots are reproduced in Figures 8.28 to 8.30 with additional data points, along with log stress-log time to tertiary creep and log stress-log rupture time plots in Figures 8.31 to 8.33 and 8.34 to 8.36, respectively. The data are listed in Table 8.13. On the above figures, comparisons are made of remelted steel to air melted steel. The air melt data is in the form of curves of minimum or expected values developed for the ASME Code Case 1592-4 or the Nuclear Systems Materials Handbook. In all cases, the remelted steel data falls within the tolerance limits of the NSMH and above the minimum values established by the Code. That is, the creep-rupture behavior of VAR and ESR is within the variability observed for air melted steels.

### 8.4.5 Isothermal Transformation Study

Four heats of 2¼Cr-1Mo steel were isothermally annealed at 704°C (1300°F) for various times from 30 to 180 minutes after austenitizing at 927°C (1700°F) for ½ hour. The resulting hardness values were

# TABLE 8.17

## FORGING MATERIAL STATUS

| ITEM | MELT PROCESS | SUPPLIER MELTER | SUPPLIER FABRICATOR | NO. | SIZE | SPEC | ANALYSIS % C, Si, P, Other* | DELIVERY STATUS | P/O |
|---|---|---|---|---|---|---|---|---|---|
| LLTI Upper Tubesheet | VAR | CIW | AI | 2 | 58 1/2" Dia. X 16 1/2" Tk. 12,500 lbs. | RDT M2-19 | Meets Spec. | 12/1/75 | C8V09G Item 1 33.5K each |
| Weld Qualification Lower Tubesheet | VAR | CIW | AI | 1 | 48 1/2" Dia. X 13 1/4" Tk. 5,900 lbs. | RDT M2-19 | Meets Spec. | 2/1/76 | C8V10G Item 1 $18,000 each |
| FTTM Tubesheet | VAR | CIW | AI | 6 | 12" Dia. X 8" Tk. 250 lbs. | RDT M2-19 | Meets Spec. | 12/1/75 | C8V09G Item 2 $7,000 each |
| Prototype Upper Tubesheets | VAR | CIW | AI | 2 | 43 1/2" Dia. X 15 3/4" Tk. 7,230 lbs. | RDT M2-19 | Meets Spec. | 4/1/76 | C8V11G Item 1 $21,500 each |
| Prototype Lower Tubesheets | VAR | CIW | AI | 2 | 43 1/2" Dia. X 13 1/4" Tk. 5,900 lbs. | RDT M2-19 | Meets Spec. | 4/1/76 | C8V11G Item 2 $18,000 each |
| Task 10G-2 Tubesheet | VAR | CIW | GE | 1 | 48 1/2" Dia. X 13 1/4" Tk. 5,900 lbs. | RDT M2-19 | Meets Spec. | 2/1/76 | C8V10G Item 1 $18,000 each |
| Weld Development Forging (In process control) | VAR | CIW | AI | 6 | 22" Dia. X 5" Tk. 535 lbs. | RDT M2-19 | Meets Spec. | 2/1/76 | C8V10G Item 2 $2,000 each |
| Weld Development Forging (Weld Qualification) | VAR | CIW | AI | 14 | 8" Dia. X 5" Tk. 70 lbs. | RDT M2-19 | Meets Spec. | 2/1/76 | C8V10G Item 3 $1,000 each |
| Mechanical Property Forging Billets | VAR | CIW | ORML | LOT | 20,000 lbs. | RDT M2-19 | Meets Spec. | 10/75 Delivered | C8V10G Item 4 $19,700 each |

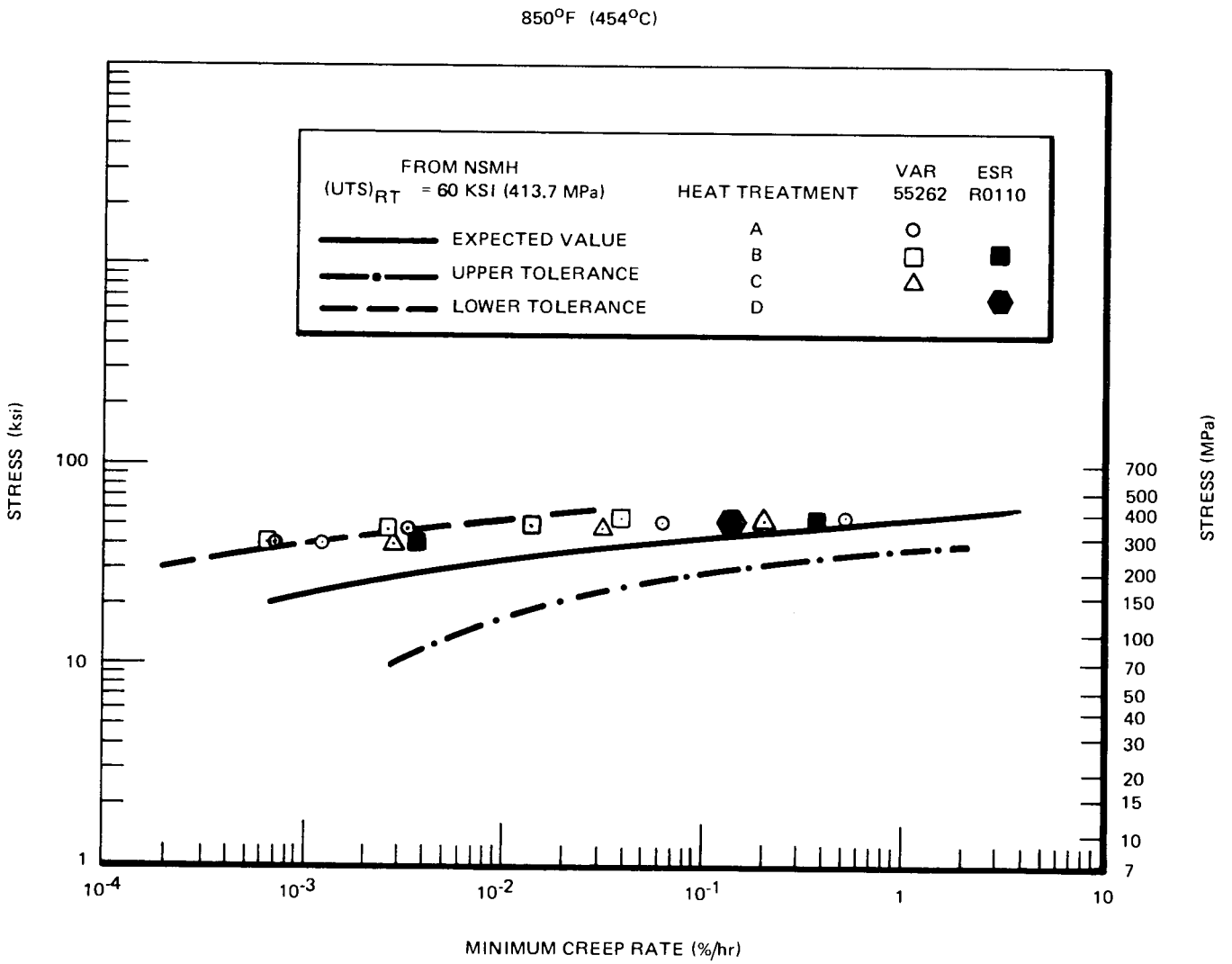


Figure 8.28. *Relationship Between Stress and Minimum Creep Rate for 0.10%C, 2¼ Cr – 1 Mo Steel at 850°F (454°C)*

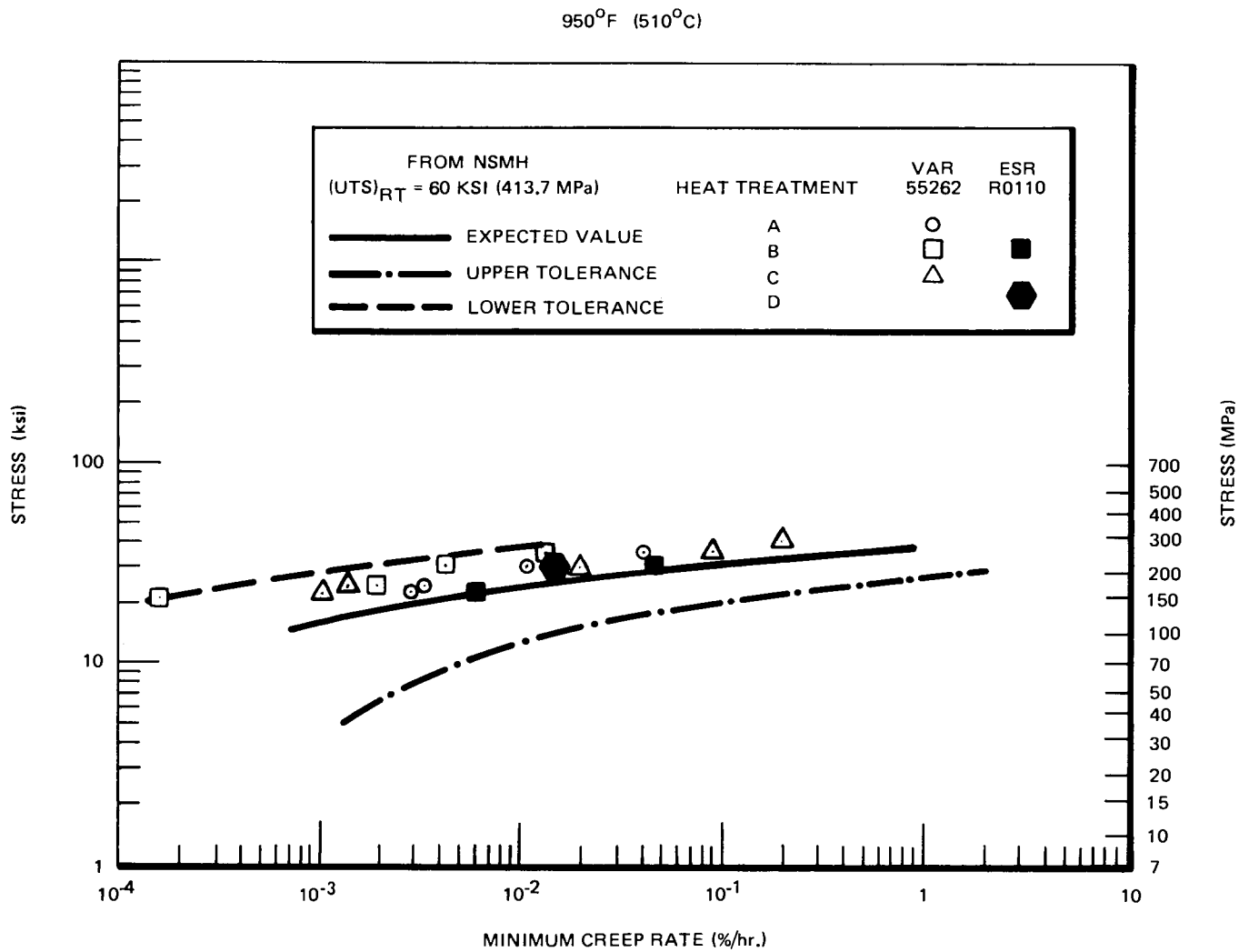


Figure 8.29. *Relationship Between Stress and Minimum Creep Rate for 0.10%C, 2¼ Cr-1 Mo Steel at 950°F (510°C)*

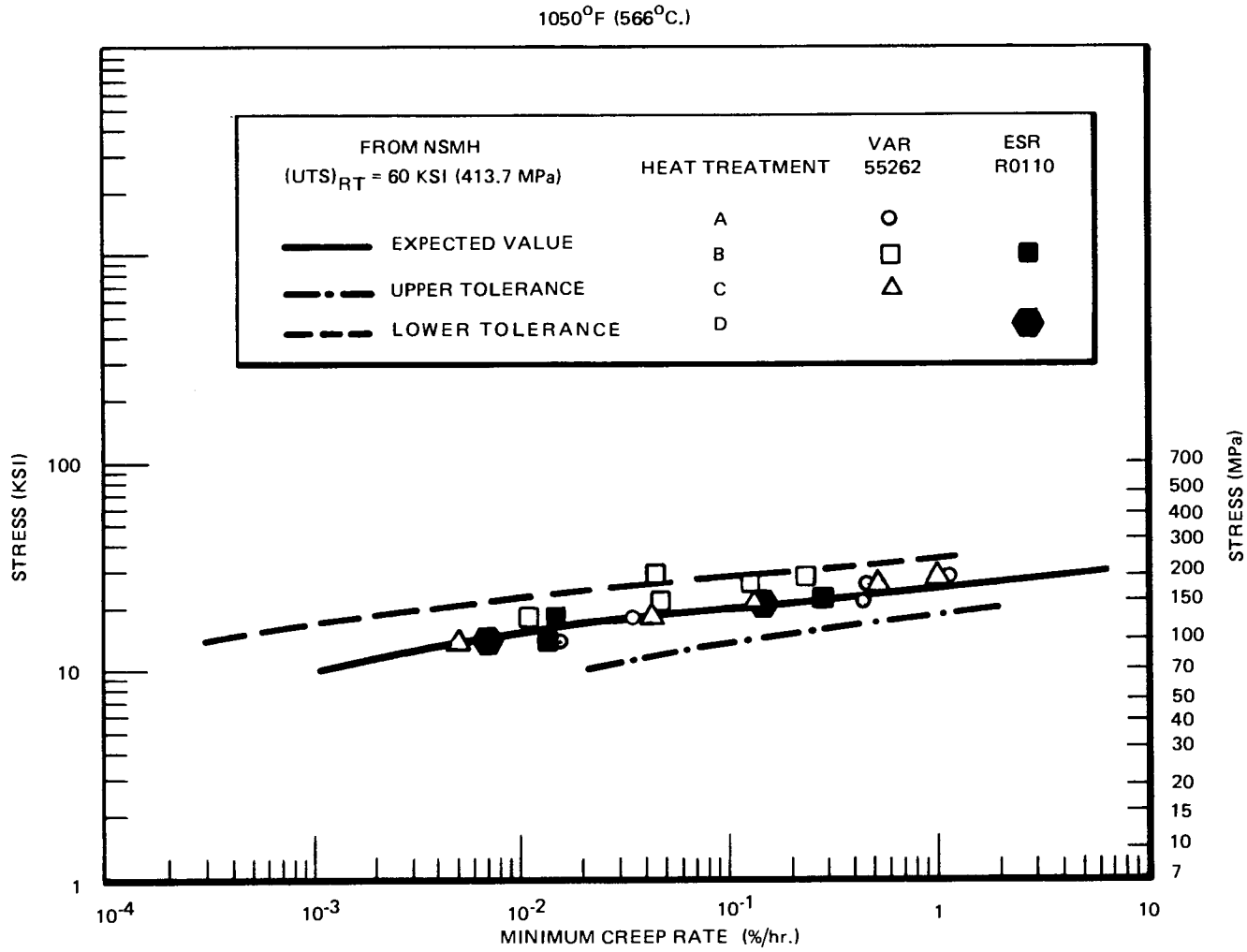


Figure 8.30. *Relationship Between Stress and Minimum Creep Rate for 0.10%C, 2¼ Cr-1 Mo Steel at 1050°F (566°C)*

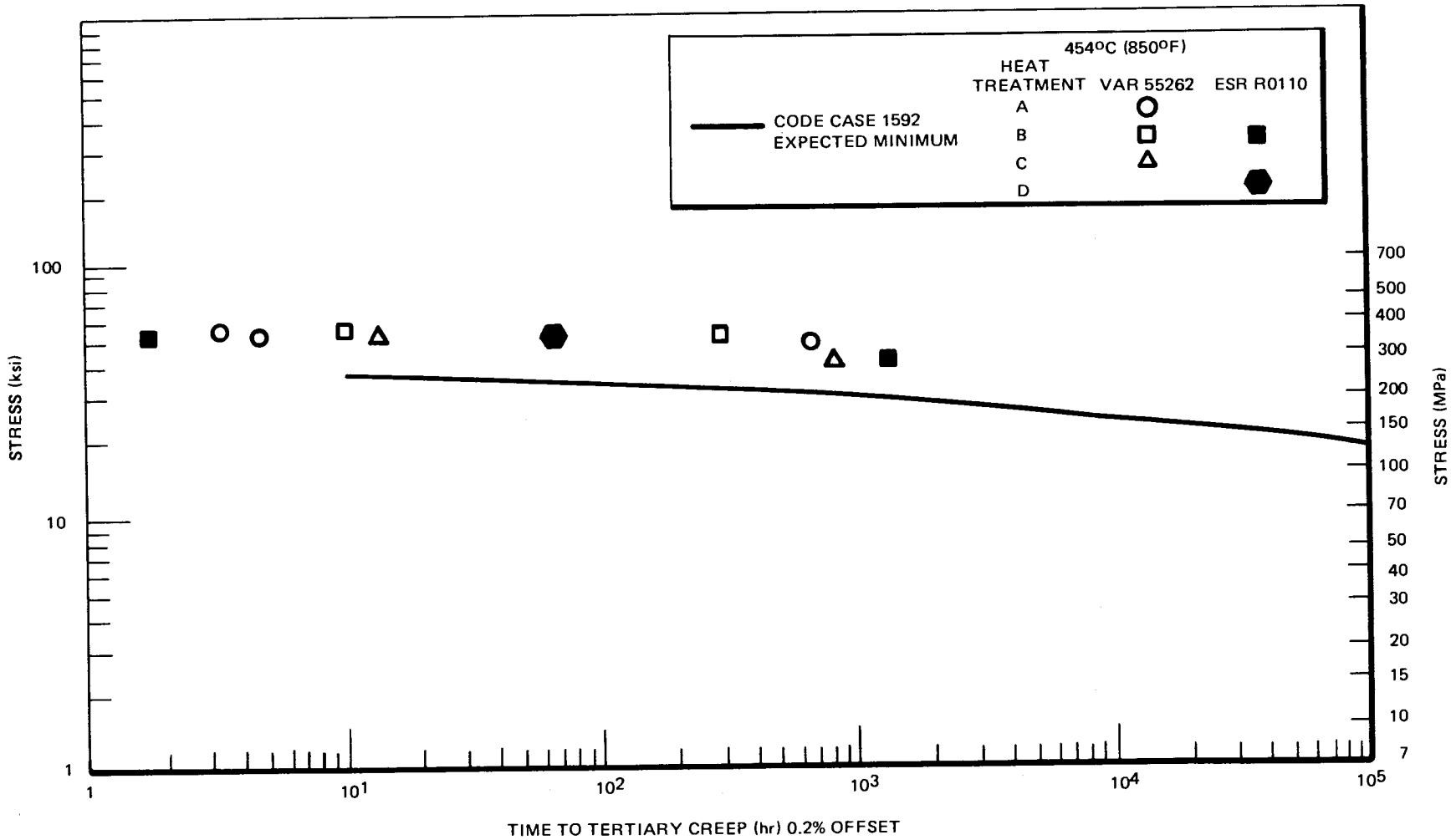


Figure 8.31. *Relationship Between Stress and Time to Tertiary Creep for 0.10%C, 2¼ Cr – 1 Mo Steel at 850°F (454°C)*

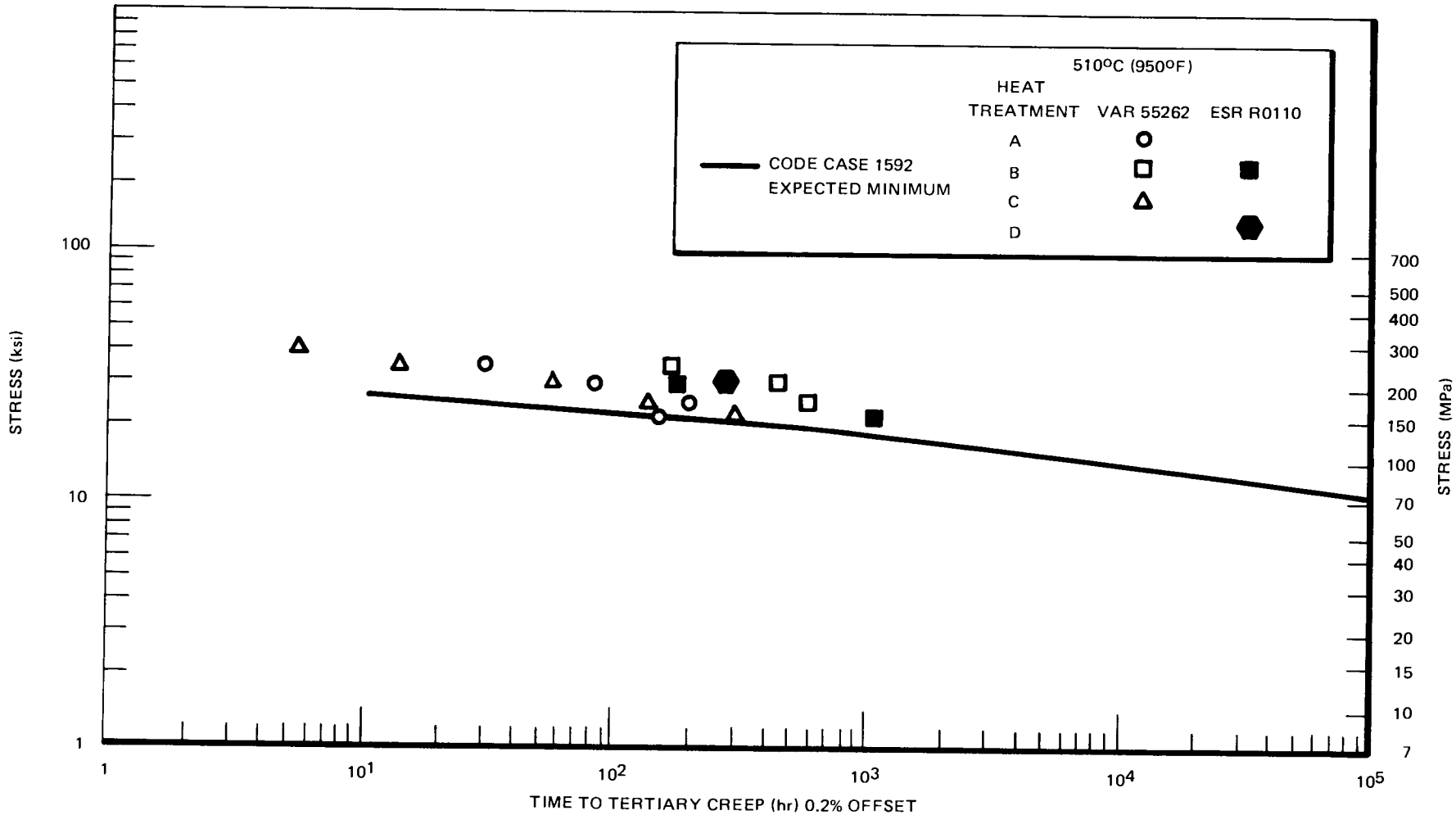


Figure 8.32. *Relationship Between Stress and Time to Tertiary Creep for 0.10%C, 2¼ Cr – 1 Mo Steel at 950°F (510°C)*

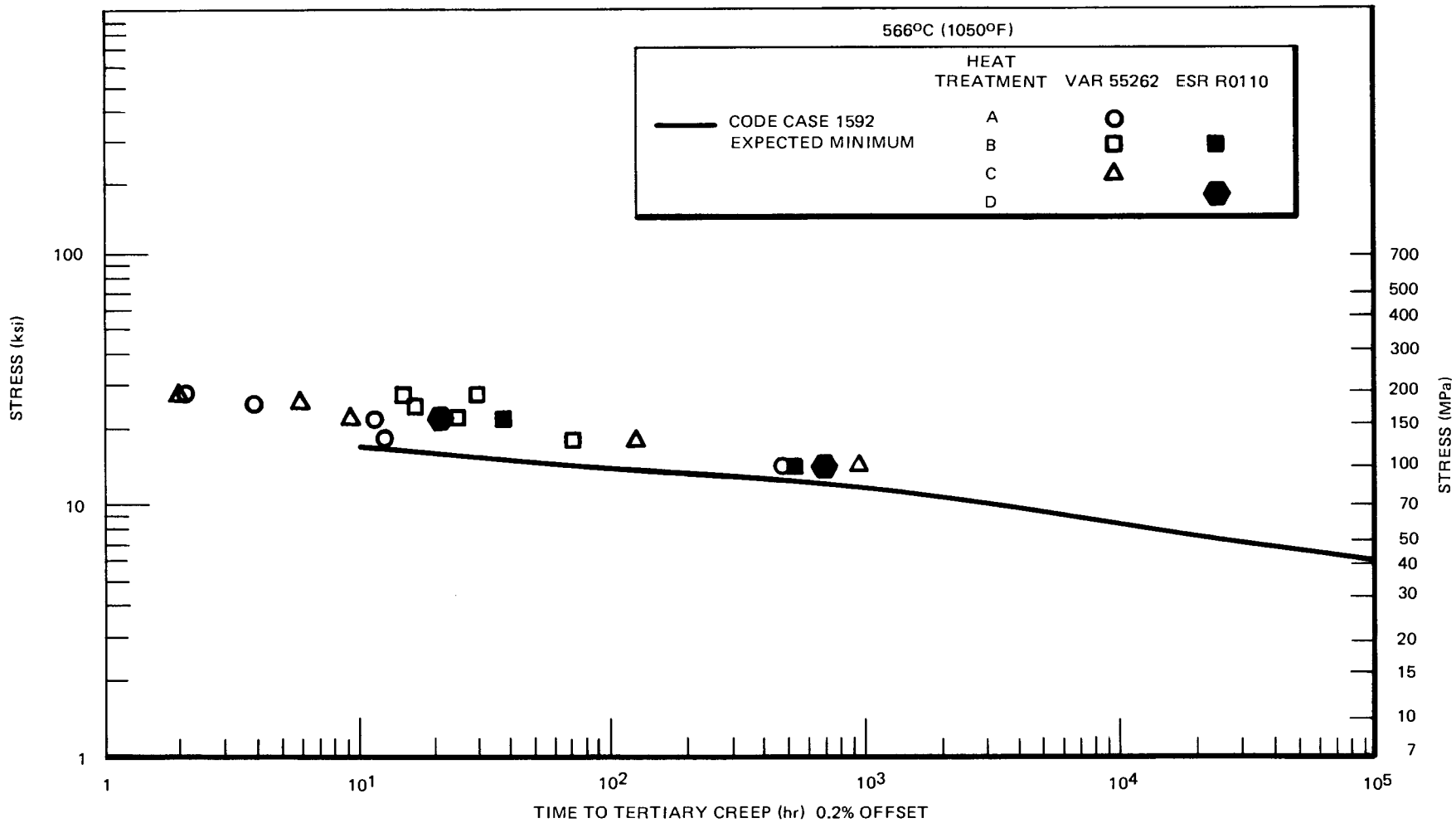


Figure 8.33. *Relationship Between Stress and Time to Tertiary Creep for 0.10%C, 2¼ Cr – 1 Mo Steel at 1050°F (566°C)*

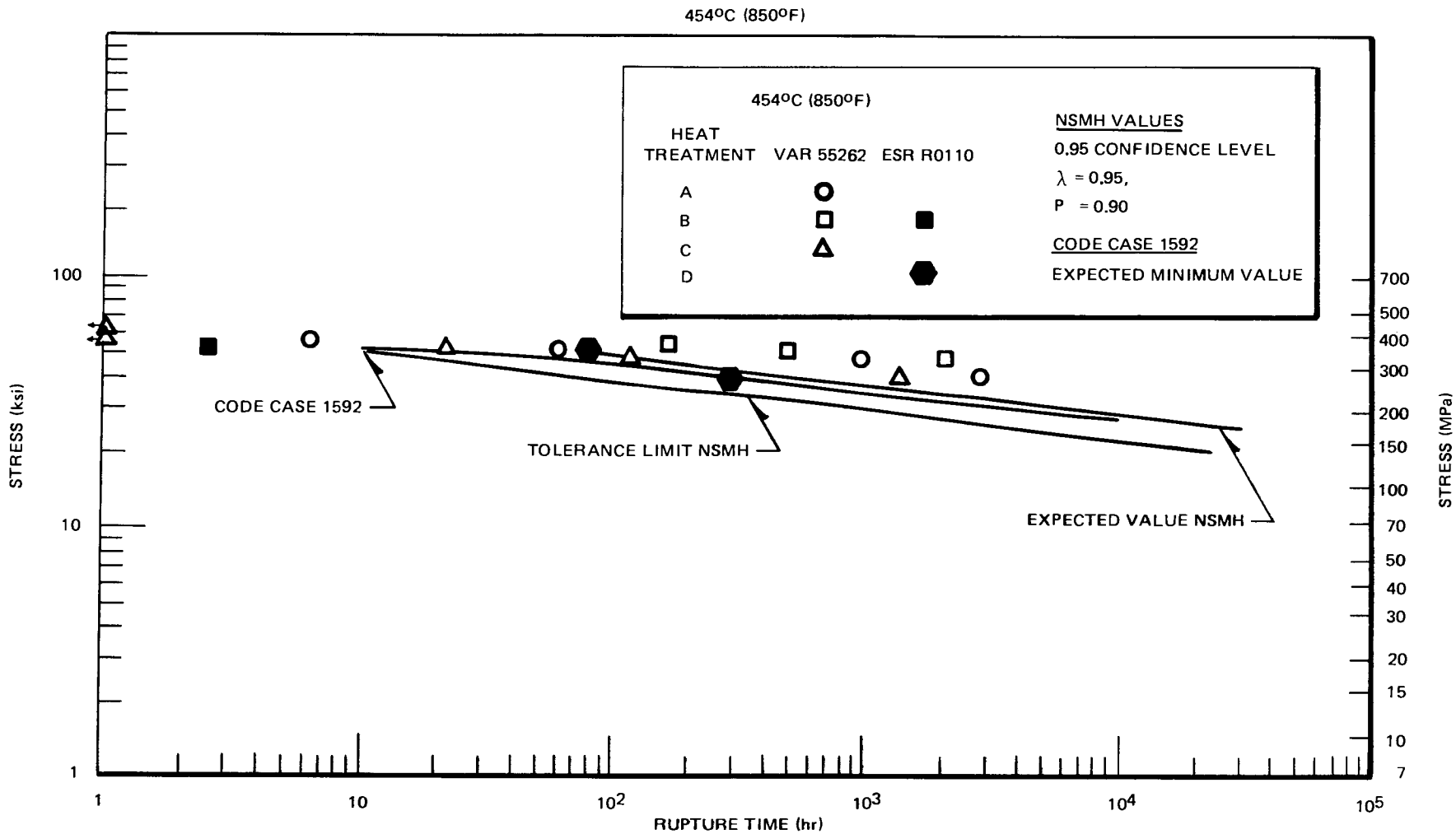


Figure 8.34. *Relationship Between Stress and Rupture Time for 0.10 %C, 2¼ Cr – 1 Mo Steel at 850°F (454°C)*

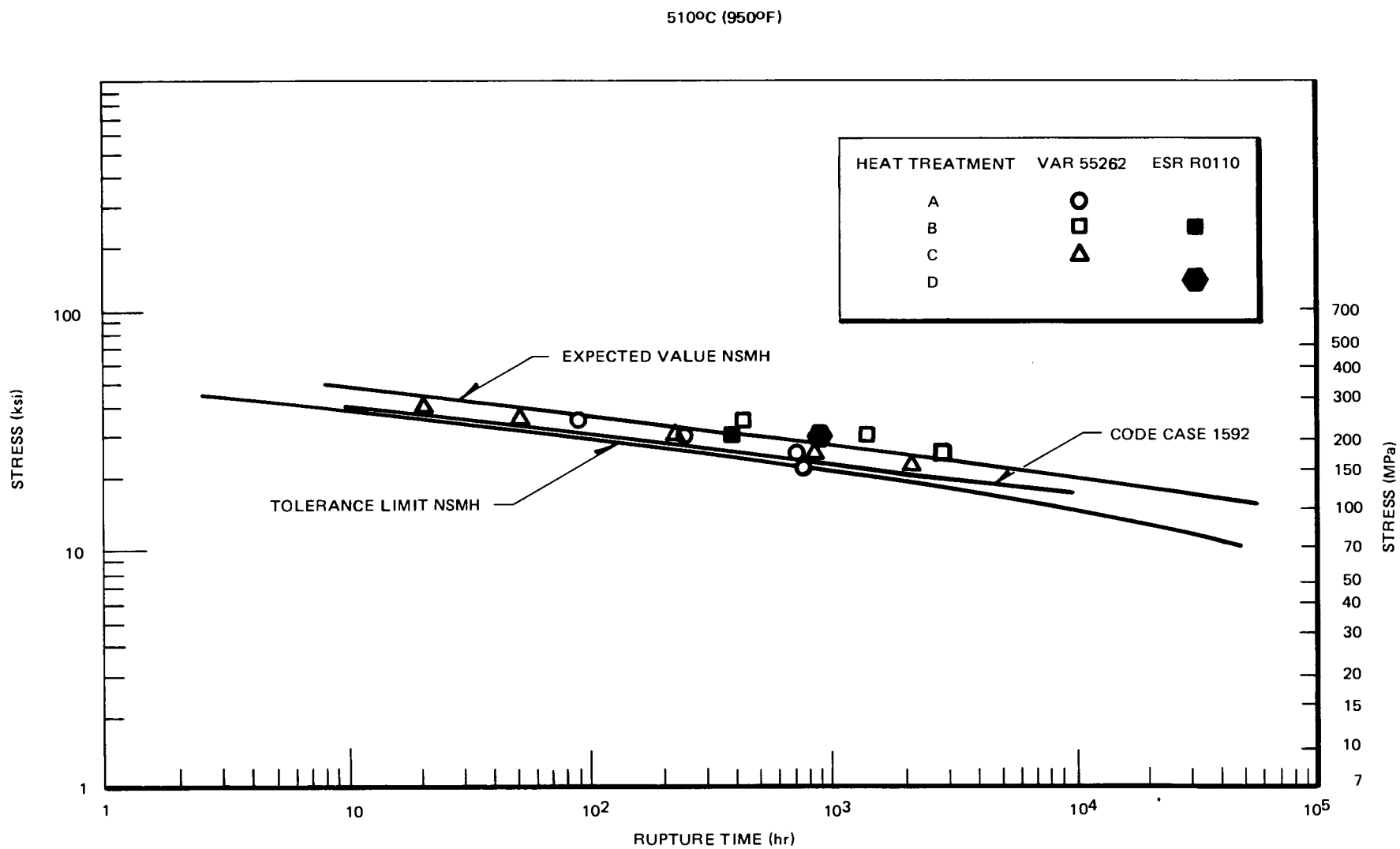


Figure 8.35. *Relationship Between Stress and Rupture Time for 0.10%C, 2¼ Cr – 1 Mo Steel at 950°F (510°C)*

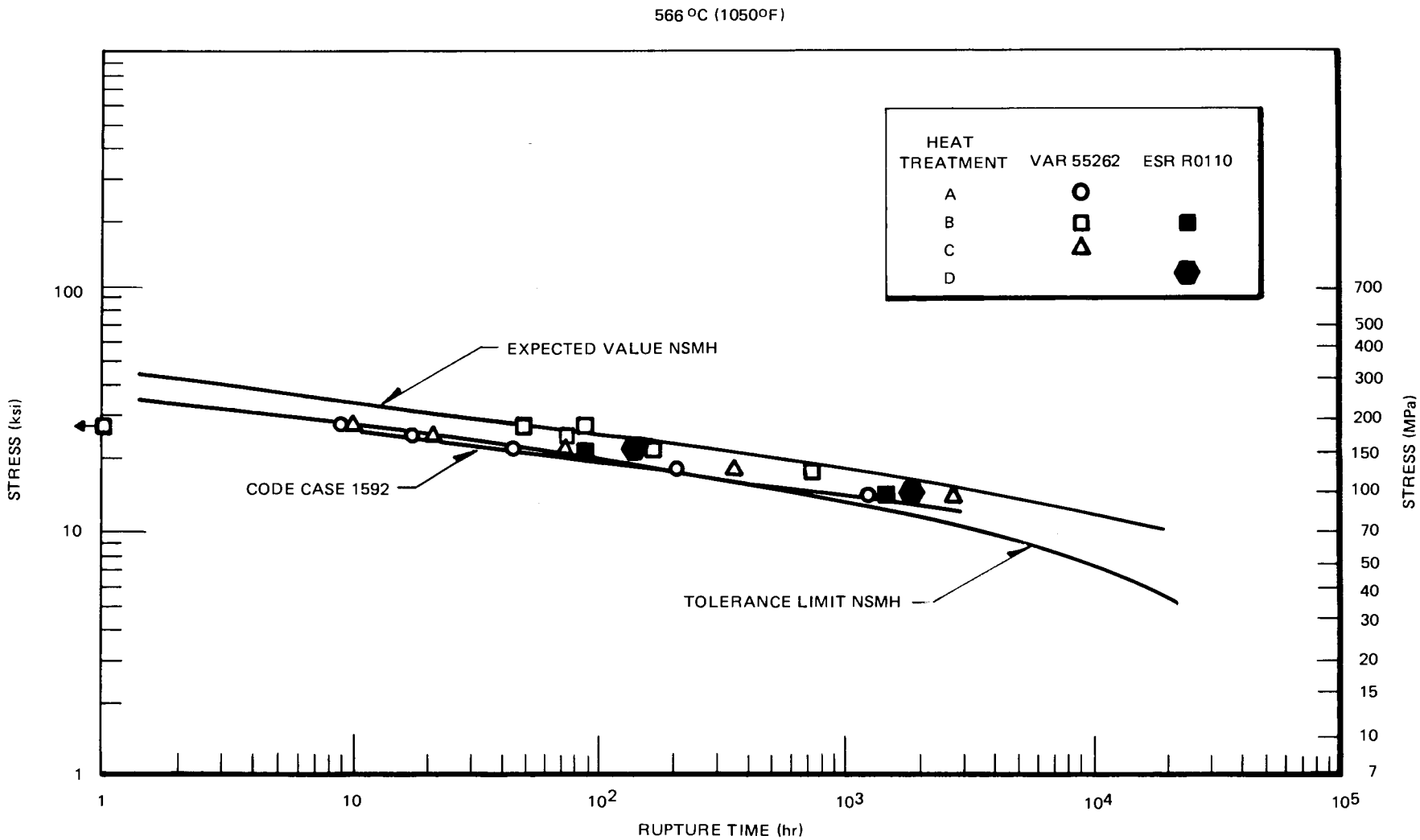


Figure 8.36. *Relationship Between Stress and Rupture Time for 0.10%C, 2¼ Cr – 1 Mo Steel at 1050°F (566°C)*

reported previously.[8] The purpose of this study is to determine the ferrite + carbide phase boundary of the isothermal transformation diagram. The same study has been repeated at 691, 704, and 718°C (1275, 1300, and 1325°F) for 12 heats of 2¼Cr-1Mo steel including air melted, VAR, and ESR material. The resulting hardness values are given in Table 8.14. A chemical analysis for all of these heats is listed in Table 8.15. The carbon content ranged from 0.09 to 0.16%. This exceeds the RDT Standard M3-33 maximum of 0.110%, but it was considered useful to observe the effect of carbon content on transformation time.

The formation of ferrite + carbide as pearlite at 704°C (1300°F) takes approximately 120 minutes. The time for transformation is longer at 691°C (1275°F) than at 718°C (1325°F). This indicates that the nose of the ferrite + carbide phase region on the isothermal transformation diagram for 2¼Cr-1Mo steel is above 704°C (1300°F), the presently accepted temperature for air melted material.[9] This result will be verified by additional isothermal annealing of the same heats at 732°C (1350°F). The microstructures resulting from various hold times at 704°C (1300°F) and water quenching were reported earlier.[8] At approximately 120 minuted hold time, the phases present after water quenching are proeutectoid ferrite, bainite, martensite, discontinuous precipitation, general precipitation, and fine pearlite. All of these phases can be seen in Figure 8.37. It should be noted that the fine pearlite shown is typical in morphology, but occurs only in isolated areas.

### 8.4.6 Fracture Toughness Testing of VAR Materials

The objective of this program is to determine fracture toughness values ($K_{Ic}$) at 24°C (75°F) for steam generator tubesheet materials. These results are then used along with charpy v-notch and drop-weight test values ($RT_{NDT}$ determinations) and tensile test results to evaluate the resistance to fracture. The philosophy of this approach to fracture prevention is set forth in the $K_{IR}$ curve of Appendix G to Section III of the ASME Boiler and Pressure Vessel Code. No toughness data on 2¼Cr-1Mo steel was included in the derivation of this Code $K_{IR}$ curve. Therefore, an important application of these results is to verify the conservatism of the $K_{IR}$ curve for 2¼Cr-1Mo steel.

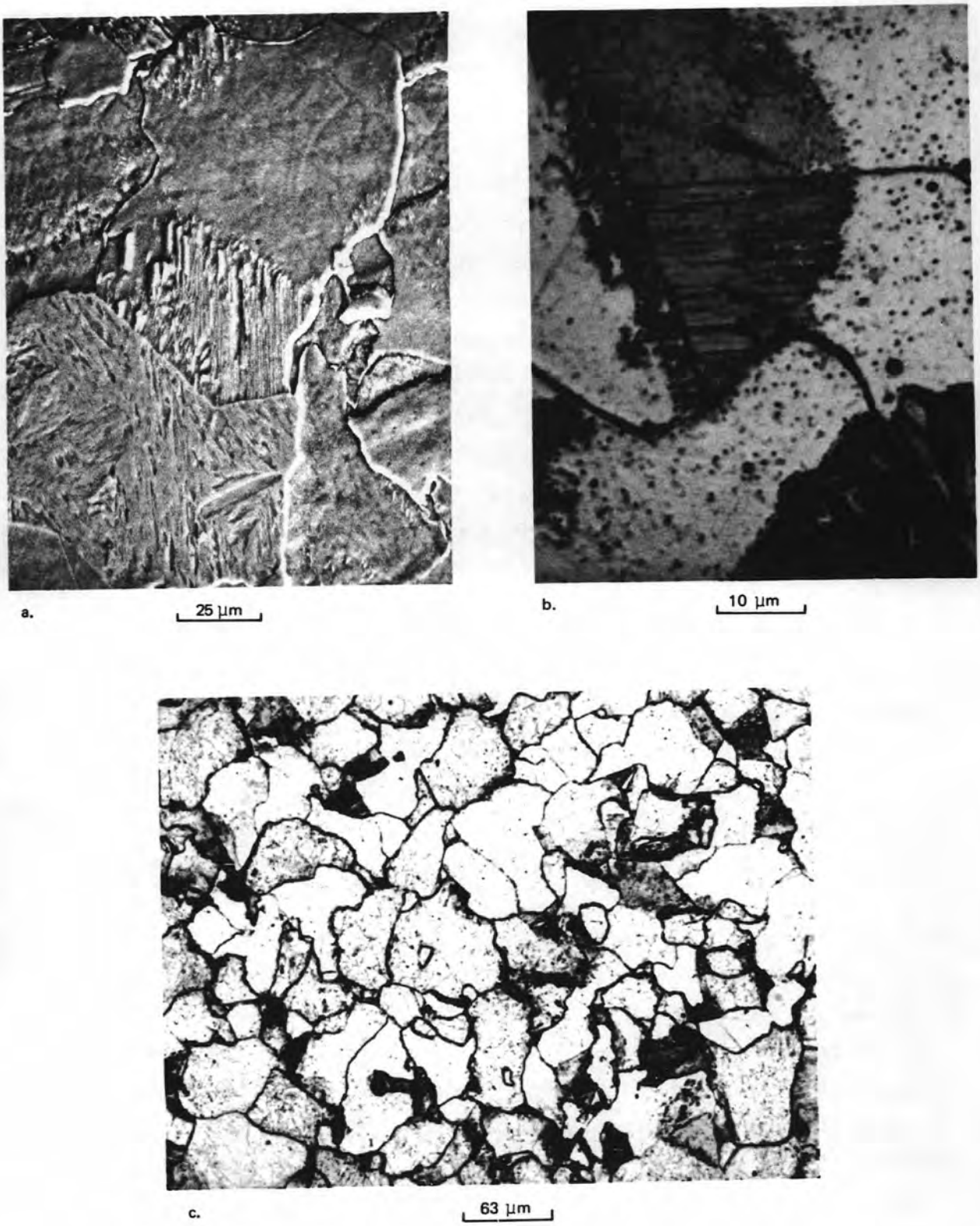


Figure 8.37. *Typical micrographs of VAR heat 55262 isothermally transformed at 704°C (1300°F) for 120 minutes and water quenched (a) scanning electron micrograph, (b) and (c) optical micrographs*

A vacuum arc remelted (VAR) 50.8 mm (2 in.) thick plate (heat #55262) was procured. The chemical composition, tensile test, charpy v-notch, and drop-weight test results have been previously reported for this heat.[8] An $RT_{NDT}$ value of 7°C (20°F) was reported. This plate was heat treated as follows: 927°C (1700°F) for 3 hours, furnace cool to room temperature, plus 727°C (1340°F) for 4 hours, air cool to room temperature. Three 50.8 mm (2 in.) thick ASTM E399 Compact Tension Specimens (CTS) were machined from this plate in the transverse (WR) orientation. The crack lengths were extended by fatigue precracking to a crack length to specimen width ratio (a/w) of approximately 0.65.

These CTS's were tested at 24°C (75°F) under constant stroke control of 1.52 mm/min. (0.06 in./min.). Load versus load-point displacement curves were generated and used to compute $J_{Ic}$ values. These $J_{Ic}$ values, and the $K_{Ic}$ results computed from them, are shown in Table 8.16. The values of $J_{Ic}$ were determined from the points on the load-displacement curves where a brittle pop-in (rapid crack extension) occurred. The brittle pop-in has been shown by Scanning Electron Microscopy (SEM) to be related to cleavage fracture of these specimens. Even with this brittle behavior, the minimum $K_{Ic}$ value of 121 MPa $\sqrt{m}$ (110 ksi $\sqrt{in}$) is above the corresponding $K_{IR}$ curve value of approximately 60 MPa $\sqrt{m}$ (55 ksi $\sqrt{in}$). Further testing would be necessary to determine if this remains the case at higher temperatures relative to the $RT_{NDT}$. Therefore, safe behavior with respect to fracture, for components designed in accordance with the Code $K_{IR}$ curve and Appendix G, is indicated for this material. However, it is recommended that more testing of this type be done to gain statistical confidence in this conclusion, especially in view of the brittle fracture mode. Testing at elevated temperatures is also required to verify that the material toughness is above the $K_{IR}$ curve at service temperatures, and that stable crack extension (ductile) can be achieved.

### 8.4.7 CRBRP Prototype and Plant Tubesheet Forgings

The objective of this activity is to provide the technical support to the procurement of the CRBR prototype, plant, and development tubesheet forgings. These items will be purchased to RDT M2-19.

The order for VAR 2¼Cr-1Mo forgings placed earlier this year for the various CRBRP programs is being processed. Vacuum arc remelting and hot working of remelted ingots has been completed.

Two (2) air melt heats of 2¼Cr-1Mo alloy were made for the GE program. Each air melted heat was for ~45.4 metric tons (50 tons) with a yield of ~38555 kg (85,000 lbs.) per heat. Each air melted heat was conditioned and vacuum arc remelted into 5 VAR ingots. The yield again was ~38555 kg (85,000 lbs.) per heat or 77111 kg (170,000 lbs.) total. The VAR ingots were conditioned and extruded as bars of ~74 cm (29 in.) and 36 cm (14 in.) in diameter. The larger diameter material will be made into the LLTI and prototype forgings; the smaller diameter material will be used for the FTTM and weld development forgings. Therefore, two lots of material were shipped to ORNL from two heats: Lot #1 (~4536 kg; 10,000 lbs.) contained two (2) pieces of 74 cm diameter bar from heat #56448 and Lot #2 (~4536 kg; 10,000 lbs.) contained one (1) piece of 74 cm diameter bar from the other heat. The chemical analysis of heat #56448 met all requirements of RDT M2-19 as shown below:

Chemical Analysis

| Heat No. | C | Mn | P | S | Si | Cr | Ni | Mo | Ti | V | Cu | Co |
|---|---|---|---|---|---|---|---|---|---|---|---|---|
| 56448 | .10 | .56 | .010 | .006 | .26 | 2.15 | .15 | 1.01 | .01 | .01 | .09 | .01 |

The purchase orders have been placed with Cameron Iron Works to forge the 74 cm (29 in.) and 36 cm (14 in.) bars to thicknesses and diameters required for the various tubesheets. The entire order for the prototype, LLTI, FTTM, and weld development forgings is expected to be completed by the end of February 1976. A complete summary of the status of tubesheet purchases is given in Table 8.17.

### 8.4.8 Correction to the Previously Reported Chemical Analysis

The mechanical properties determined in this study indicated that the composition for some of the elements as reported by the chemical analysis vendor were in error. A second product analysis verified this indication. The second chemical analysis is shown below:

Chemical Analysis

| Heat No. | Al | Si | S |
|---|---|---|---|
| VAR 56067 | 0.005 | 0.28* | 0.007* |
| ESR R0110 | 0.027 | 0.18 | 0.006 |

*Same value as reported in first analysis.

## 8.5 FRACTURE TOUGHNESS OF LMFBR STEAM GENERATOR MATERIALS

J. F. Copeland/G. R. Dodson

The objective of this program is to determine fracture toughness values ($K_{Ic}$ at 24°C [75°F]) and higher temperatures, for potential LMFBR Steam Generator shell and tubesheet materials. These results will be combined with Charpy V-notch and drop-weight test values ($RT_{NDT}$) determinations) and tensile test results to evaluate resistance to fracture. The essence of this approach to prevent fracture is set forth in the $K_{IR}$ curve of Appendix G to Section III of the ASME Boiler and Pressure Vessel Code. No toughness data on 2¼Cr-1Mo steel was included in the derivation of the Code $K_{IR}$ curve. Therefore, testing is required at hydrostatic test and at service temperatures to assure that the present $K_{IR}$ curve approach is adequate for this material. In order to evaluate the fracture toughness of 2¼Cr-1Mo above the Nil Ductility Transition Temperature (NDTT), it is necessary to employ elastic-plastic fracture toughness testing methods, such as the J-Integral approach.

Thick section 2¼Cr-1Mo steel plates were procured for this program and heat treated to represent potential LMFBR material conditions. The emphasis is on air-melted material, although some testing was done on Vacuum Arc Remelted (VAR) steel, and these results are presented for comparison. The chemical compositions and heat treatments are given in Tables 8.18 and 8.19. Sulfide inclusion characterization is shown in Figure 8.38 and verifies a lack of directionality (longitudinal versus transverse) for the air-melted plate. Also, as shown in Figure 8.39, there is no significant influence of heat treatment on the microstructural phases present at the quarter thickness (¼ T) location of this 89 mm. (3.5 in.) thick plate.

TABLE 8.18

CHEMICAL COMPOSITIONS OF 2¼Cr-1Mo STEEL PLATES FOR FRACTURE TOUGHNESS TESTING (wt. %)

| Melting Process | Heat No. | | C | Mn | P | S | Si | Cr | Ni | Mo | Al | As | Sb | Sn |
|---|---|---|---|---|---|---|---|---|---|---|---|---|---|---|
| AM | 86693 | Melt | 0.11 | 0.45 | 0.009 | 0.028 | 0.20 | 2.01 | -- | 1.04 | -- | -- | -- | -- |
| | | Check | 0.11 | 0.41 | 0.014 | 0.026 | 0.19 | 2.00 | 0.12 | 1.00 | <0.005 | 0.013 | 0.007 | 0.012 |
| VAR | 55262 | Melt | 0.09 | 0.52 | 0.016 | 0.014 | 0.08 | 2.22 | -- | 0.01 | -- | -- | -- | -- |
| | | Check | 0.10 | 0.50 | 0.013 | 0.016 | 0.07 | 2.26 | 0.15 | 1.00 | <0.005 | 0.008 | <0.002 | 0.004 |

## TABLE 8.19

## HEAT TREATMENT OF 2¼Cr-1Mo STEEL PLATES FOR FRACTURE TOUGHNESS TESTING

A. Anneal (AM)

927°C (1700°F) for 3 hr., furnace cool at max. rate of 55.5°C (100°F) per hr. to room temperature

B. Anneal + Temper (AM)

927°C (1700°F) for 3 hr., furnace cool at max. rate of 55.5°C (100°F) per hr. to room temperature
+727°C (1340°F) for 4 hrs., air cool

C. Anneal + Temper (VAR)

927°C (1700°F) for 3 hr., furnace cool at max. rate of 55.5°C (100°F) per hr. to room temperature

+

727°C (1340°F) for 4 hr., air cool

D. Anneal + Temper + Embrittlement Treatment (AM)

927°C (1700°F) for 3 hr., furnace cool at max. rate of 55.5°C (100°F) per hr. to room temperature

+

727°C (1340°F) for 4 hr., air cool

+

510°C (950°F) for 1000 hr., air cool

E. Normalize + Temper (AM)

927°C (1700°F) for 3 hr., air cool

+

727°C (1340°F) for 4 hr., air cool

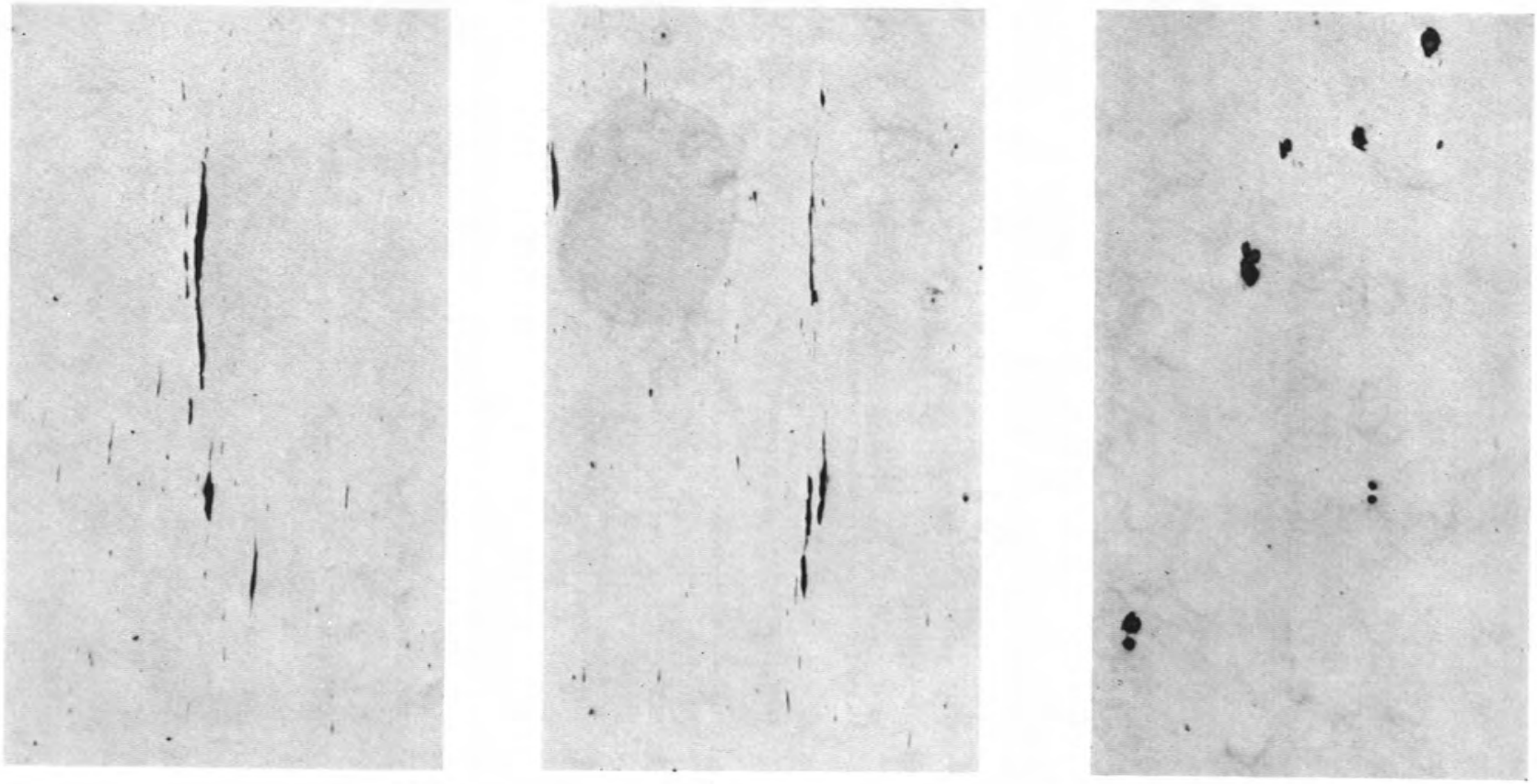

100X

A. VIEW FROM PLATE EDGE

100X

B. VIEW FROM PLATE EDGE AT 90° TO A

100X

C. VIEW FROM PLATE ROLLED SURFACE

Figure 8.38. *Sulfide Inclusion Size and Shape as Related to Plate Orientation, Illustrating Lack of Longitudinal-transverse Directionality Resulting from a Cross-rolling Ratio of 1.0. Heat 86693, 89 mm (3.5 in.) Thick Air Melt Plate at 1/4 T Location. As-polished Specimens*

500X

A. HEAT TREATMENT A.

500X

B. HEAT TREATMENT B.

500X

C. HEAT TREATMENT E.

Figure 8.39. Microstructure as Related to Heat Treatment for Heat 86693, 89mm (3.5 in.) Thick Air Melt Plate at 1/4 T Location. Nital-picral Etch

Table 8.20 gives room temperature tensile test results which, as predicted by the microstructures, reveal no significant effect of heat treatment. One exception is that aging for 1000 hr. at 510°C (950°F) does decrease the room temperature yield strength. Charpy V-notch (CVN) impact test results are tabulated in Table 8.21, and the transition curves for the air-melted steel are given in Figures 8.40 - 8.43. The significant CVN criteria, along with drop-weight test NDTTs are summarized in Table 8.22. The $RT_{NDT}$ values are limited in all cases by the drop-weight NDTTs which are approximately equivalent, at -1°C (30°F), for all five material conditions. Condition B (annealed and tempered air-melt) has the greatest Charpy upper shelf energy.

The CTS design used in the J-Integral fracture toughness tests is illustrated in Figure 8.44. After fatigue precracking, this specimen was loaded monotonically at 24°C (75°F) under constant stroke rate control until rapid, brittle, crack extension (pop-in) occurred or until appreciable deformation resulted in stable, ductile crack extension. The extent of crack extension was determined after the test by examination of the fracture surface, as shown in Figure 8.45. Load versus load-point displacement curves were recorded for each specimen and used to compute J-Integral values at the point of specimen unloading. The results of these tests are given in Table 8.23 and plotted in Figure 8.46 for the determination of $J_{Ic}$ at the onset of real crack extension. $K_{Ic}$ values were then computed from these values of $J_{Ic}$ and are also given in Table 8.23.

The $K_{Ic}$ results of Table 8.23 fall in essentially two groups: The air-melt results which are all at or above 206 MPa $\sqrt{m}$(187 Ksi$\sqrt{in.}$) and are approximately equal, and the VAR results which are at or above 121 MPa $\sqrt{m}$(110 Ksi$\sqrt{in.}$). Scanning Electron Microscopy (SEM) was performed on fracture surfaces to attempt explaining the following phenomena: (a) why the VAR $K_{Ic}$ results were lower than the air-melt results, and (b) why brittle pop-in, as noted in Table 8.23, occurred in some specimens. For heat treatment B, specimens G7 and G6 (which did not and which did, respectively) have brittle pop-in were examined. The results are shown in Figures 8.47a and b. The pop-in region is characterized by quasi-cleavage, which differs from true cleavage in

TABLE 8.20

Tensile Test Properties at 24°C(75°F) for 2¼Cr-1Mo Heat 86693. Air-Melt 89 mm. (3.5 in.) Thick Plate, Properties at ¼ T Location. Strain Rate = 0.04 $min.^{-1}$. Also, results for VAR Heat 55262.

| Heat Treatment | Yield Point MPa (Ksi) | 0.2% Y.S. MPa (Ksi) | U.T.S. MPa (Ksi) | %El (25.4 mm) | % R.A. |
|---|---|---|---|---|---|
| A (Anneal) | 270 (39.2)<br>262 (38.0) | 243 (35.2)<br>243 (35.2) | 472 (68.5)<br>466 (67.6) | 39.6<br>38.2 | 65.3<br>66.1 |
| B (Ann. + Temp.) | 295 (42.8)<br>297 (43.1) | 261 (37.9)<br>267 (38.7) | 466 (67.6)<br>467 (67.7) | 33.3<br>34.6 | 65.9<br>65.1 |
| C, VAR* (Ann. + Temp.) | -- | 275 (39.9) | 439 (63.7) | 36.1 | 51.6 |
| D (Ann. + Temp. + 510°C, 1000 hr.) | 234 (33.9)<br>223 (32.4) | 221 (32.1)<br>220 (31.9) | 459 (66.6)<br>465 (67.4) | 34.8<br>38.1 | 64.4<br>67.2 |
| E (Norm. + Temp.) | 298 (43.2)<br>285 (41.4) | 285 (41.4)<br>264 (38.3) | 462 (67.0)<br>460 (66.7) | 38.4<br>40.0 | 68.7<br>68.8 |

* Results by H. P. Offer (GE) on same VAR Heat No. (55262) - different plate, funded under 189a-SG029.

TABLE 8.21

CHARPY V-NOTCH IMPACT TEST PROPERTIES
FOR 2¼Cr-1Mo HEAT 86693
AIR-MELT 89 MM (3.5 IN.) THICK PLATE, PROPERTIES
AT ¼ T LOCATION, ROLLING RATIO OF 1.0

HEAT TREATMENT A

(ANNEAL)

| Spec. No. | Test Temperature °C (°F) | Fracture Energy J. (Ft.-Lb.) | Lateral Expansion MM (Mils) | Fracture Appearance % Ductile |
|---|---|---|---|---|
| G3-1 | -12 (10) | 8 (6) | 0.20 (8) | 8 |
| -2 | -12 (10) | 30 (22) | 0.61 (24) | 12 |
| -3 | 24 (75) | 73 (54) | 1.40 (55) | 42 |
| -4 | 24 (75) | 52 (38) | 1.09 (43) | 43 |
| -7 | 24 (75) | 64 (47) | 1.24 (49) | 35 |
| -8 | 43 (110) | 58 (43) | 1.17 (46) | 38 |
| -9 | 43 (110) | 95 (70) | 1.70 (67) | 54 |
| -10 | 43 (110) | 77 (57) | 1.47 (58) | 68 |
| -5 | 66 (150) | 87 (64) | 1.60 (63) | 85 |
| -6 | 66 (150) | 130 (96) | 2.14 (84) | 95 |
| -11 | 66 (150) | 109 (80) | 1.73 (68) | 83 |
| -12 | 93 (200) | 103 (76) | 1.83 (72) | 93 |
| -13 | 93 (200) | 127 (94) | 2.06 (81) | 99 |

HEAT TREATMENT B

(ANNEAL + TEMPER)

| | | | | |
|---|---|---|---|---|
| G5-1 | -12 (10) | 39 (29) | 0.69 (27) | 13 |
| -2 | -12 (10) | 76 (56) | 1.22 (48) | 20 |
| -3 | 24 (75) | 22 (163) | 2.11 (83) | 91 |
| -4 | 24 (75) | 107 (79) | 1.75 (69) | 53 |
| -8 | 43 (110) | 172 (127) | 2.16 (85) | 97 |
| -9 | 43 (110) | 153 (113) | 2.31 (91) | 97 |
| -5 | 66 (150) | 175 (129) | 2.26 (89) | 96 |
| -6 | 66 (150) | 195 (144) | 2.34 (92) | 99 |
| -11 | 93 (200) | 195 (144) | 2.08 (82) | 98 |

TABLE 8.21 (Cont'd.)

HEAT TREATMENT D

(ANNEAL + TEMPERATURE + 510°C, 1,000 HOURS)

| Spec. No. | Test Temperature °C (°F) | Fracture Energy J. (Ft.-Lb.) | Lateral Expansion MM (Mils) | Fracture Appearance % Ductile |
|---|---|---|---|---|
| G12-13 | -12 (10) | 11 (8) | 0.25 (10) | 5 |
| -14 | -12 (10) | 11 (8) | 0.15 (6) | 5 |
| -1 | 24 (75) | 61 (45) | 1.17 (46) | 30 |
| -2 | 24 (75) | 56 (41) | 1.07 (42) | 30 |
| -8 | 24 (75) | 46 (34) | 0.89 (35) | 30 |
| -10 | 43 (110) | 71 (52) | 1.27 (50) | 40 |
| -11 | 43 (110) | 75 (55) | 1.40 (55) | 40 |
| -3 | 66 (150) | 79 (58) | 1.52 (60) | 75 |
| -4 | 66 (150) | 87 (64) | 1.52 (60) | 70 |
| -12 | 66 (150) | 88 (65) | 1.57 (62) | 80 |
| -5 | 93 (200) | 107 (79) | 1.78 (70) | 99 |
| -6 | 93 (200) | 98 (72) | 1.63 (64) | 99 |
| -7 | 93 (200) | 107 (79) | 1.73 (68) | 95 |

HEAT TREATMENT E

(NORMALIZE + TEMPER)

| | | | | |
|---|---|---|---|---|
| G13-1 | -12 (10) | 11 (8) | 0.23 (9) | 10 |
| -2 | -12 (10) | 14 (10) | 0.36 (14) | 11 |
| -3 | 24 (75) | 131 (97) | 1.96 (77) | 98 |
| -4 | 24 (75) | 69 (51) | 1.22 (48) | 32 |
| -7 | 24 (75) | 77 (57) | 1.40 (55) | 37 |
| -8 | 43 (110) | 88 (65) | 1.55 (61) | 53 |
| -9 | 43 (110) | 117 (86) | 1.91 (75) | 82 |
| -5 | 66 (150) | 121 (89) | 1.78 (70) | 90 |
| -6 | 66 (150) | 127 (94) | 1.93 (76) | 89 |
| -10 | 66 (150) | 126 (93) | 1.98 (78) | 99 |
| -11 | 93 (200) | 123 (91) | 2.01 (79) | 99 |
| -12 | 93 (200) | 130 (96) | 1.98 (78) | 99 |

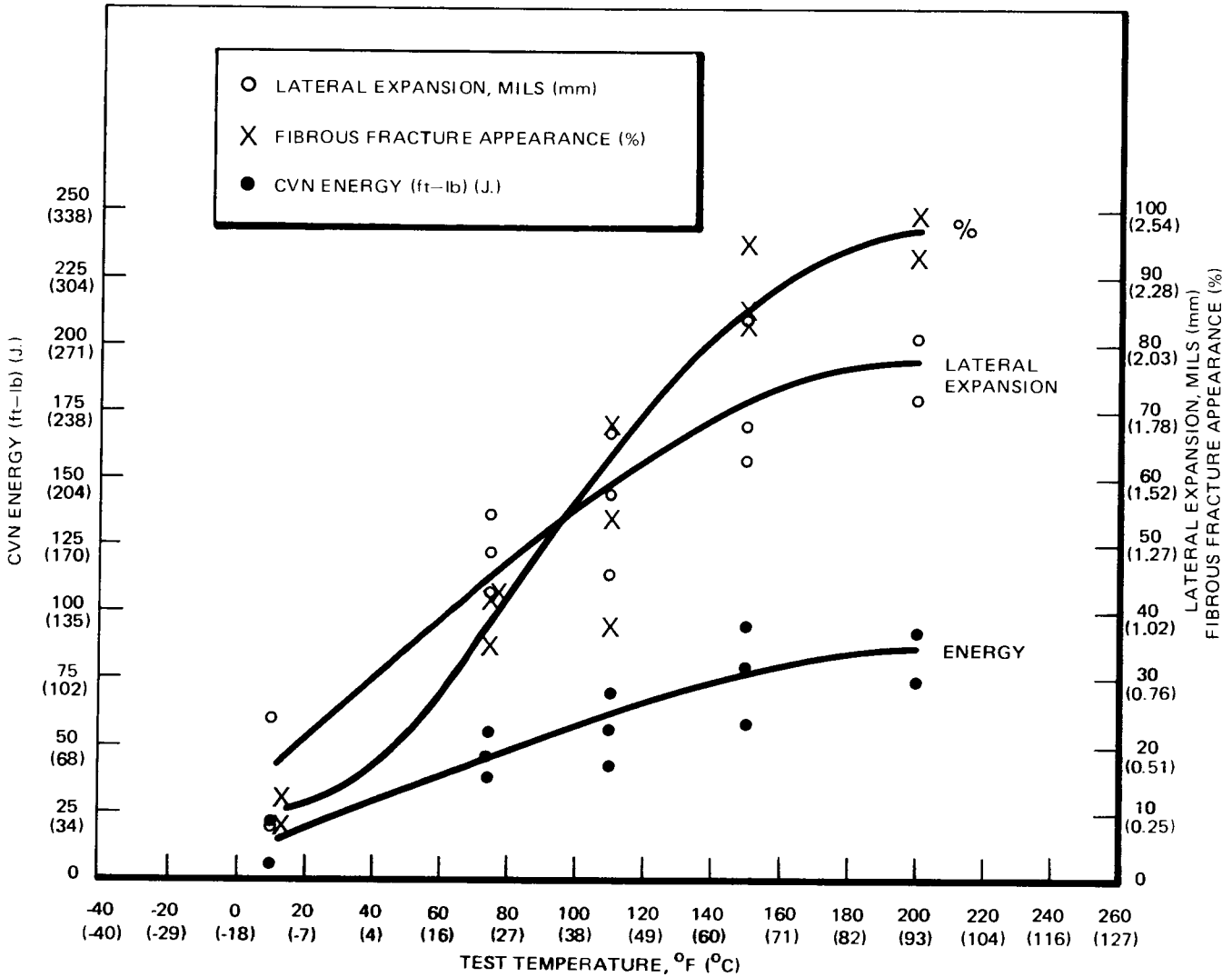


Figure 8.40. *Charpy V-Notch Transition Curves for 2¼ Cr-1 Mo Heat 86693, Air Melt 89mm (3.5 in.) Thick Plate, Properties at Quarter Thickness, Rolling Ratio = 1.0, Heat Treatment A.*

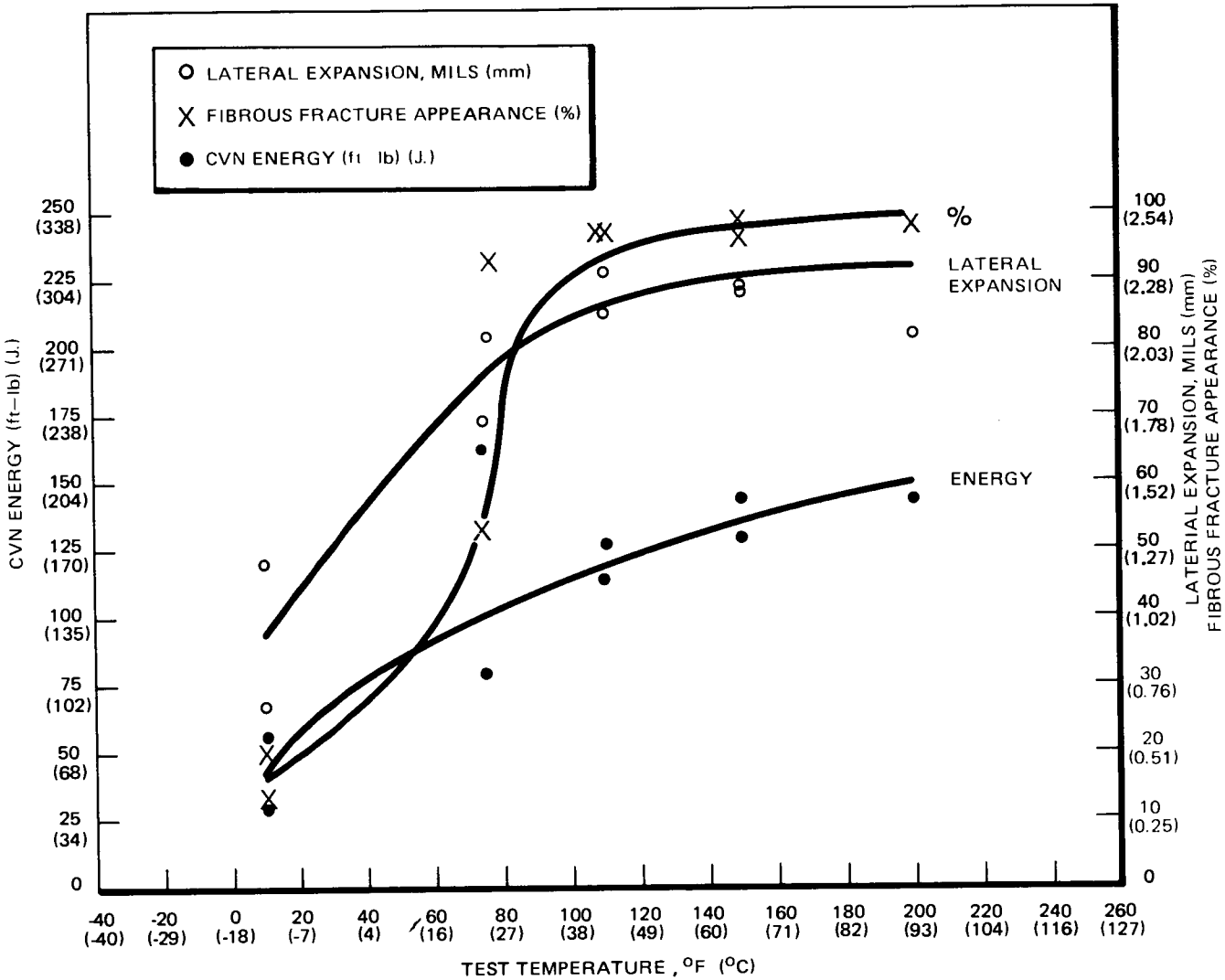


Figure 8.41. *Charpy V-Notch Transition Curves for 2¼ Cr-1 Mo Heat 86693, Air Melt, (89 mm) 3.5 in. Thick Plate, Properties at Quarter Thickness, Rolling Ratio = 1.0, Heat Treatment B.*

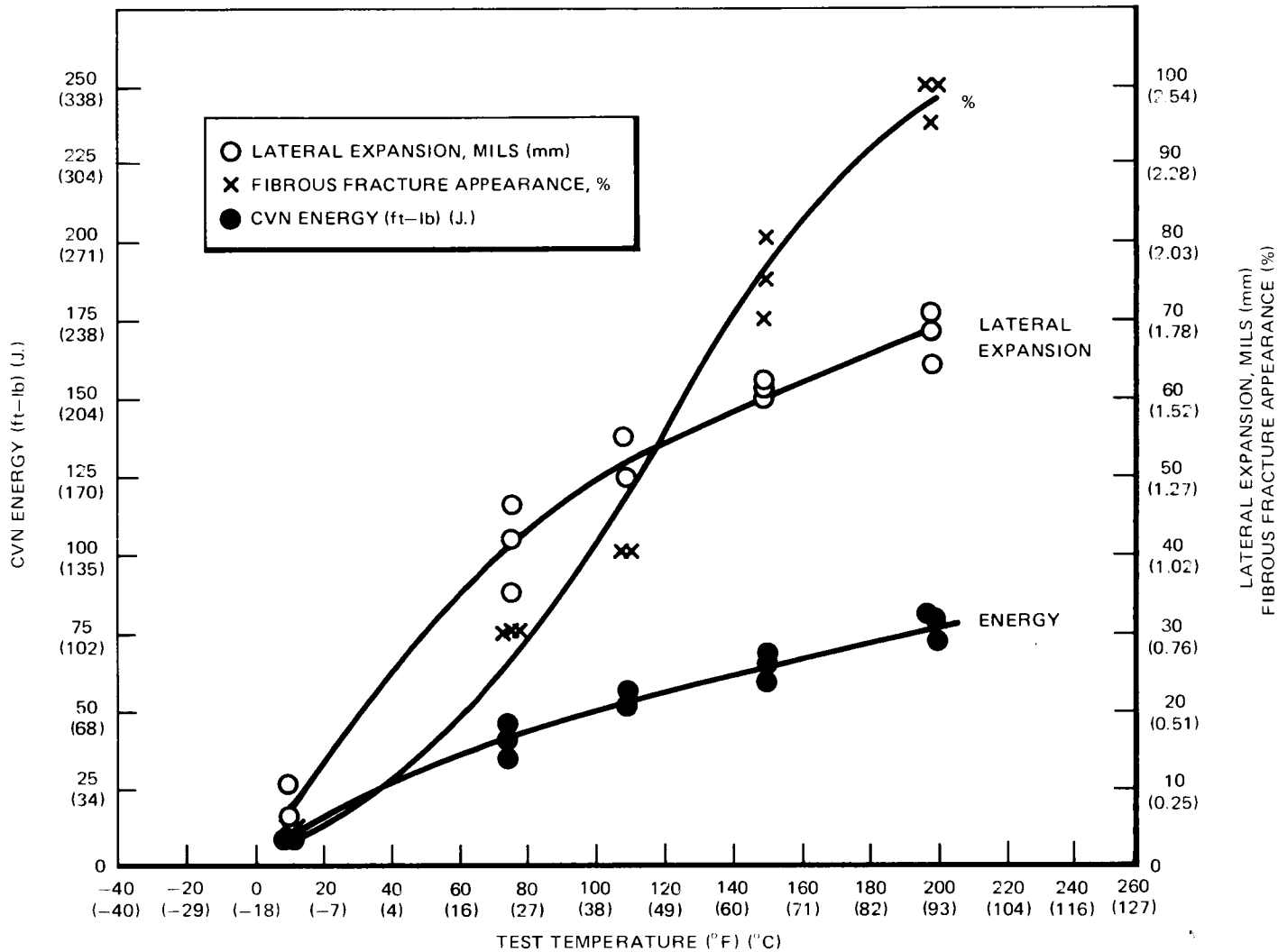


Figure 8.42. *Charpy V-Notch Transition Curves for 2 1/4 Cr-1 Mo Heat 86693, Air Melt, 89 mm (3.5 in.) Thick Plate, Properties at Quarter Thickness, Rolling Ratio = 1.0, Heat Treatment D*

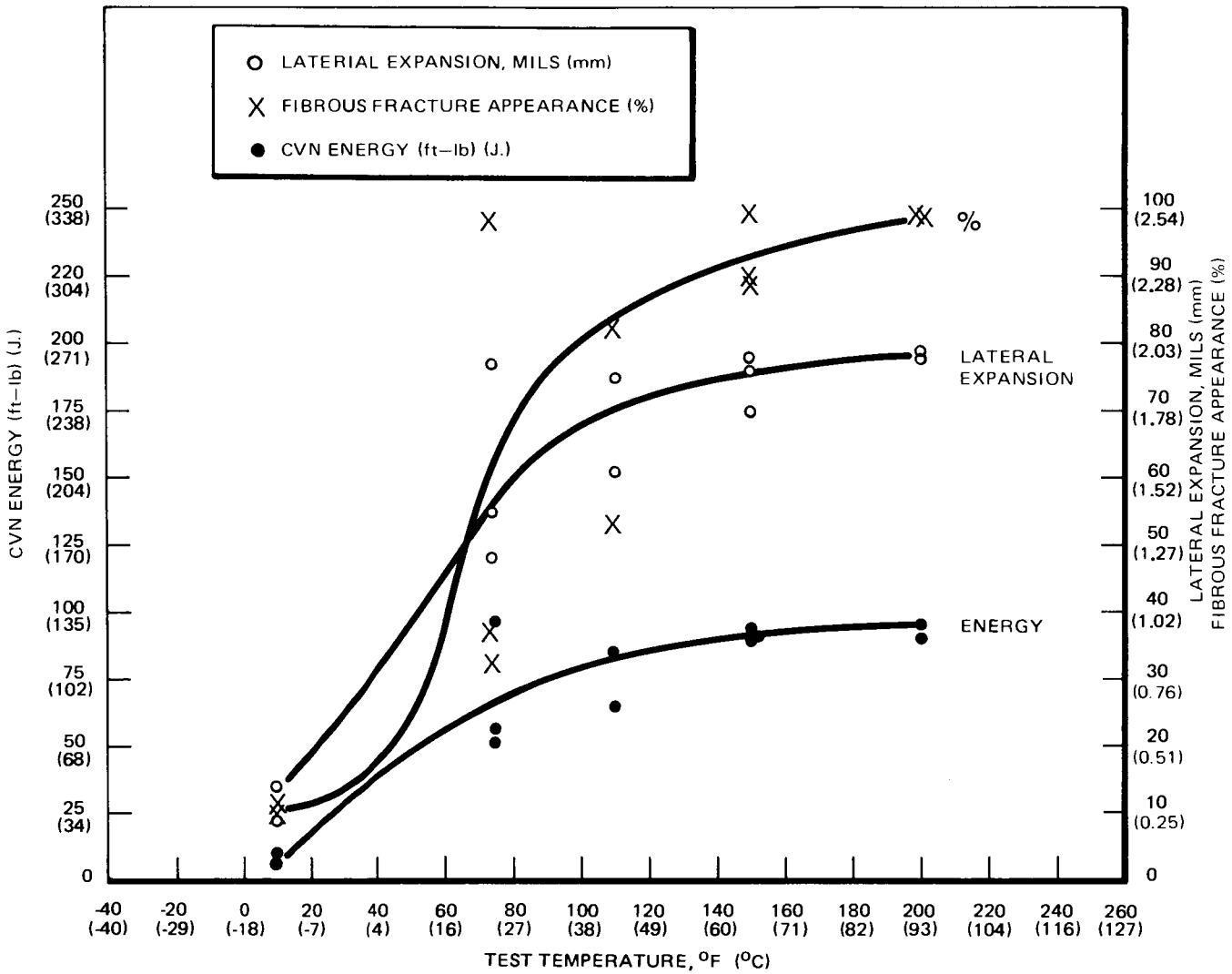


Figure 8.43. *Charpy V-Notch Transition Curves for 2¼ Cr-1 Mo Heat 86693, Air Melt, 3.5 in. (89 mm.) Thick Plate, Properties at Quarter Thickness, Rolling Ratio = 1.0, Heat Treatment E*

TABLE 8.22

CHARPY V-NOTCH TOUGHNESS CRITERIA AND P-3 DROP-WEIGHT NIL DUCTILITY TRANSITION (NDT) RESULTS FOR 2¼Cr-1Mo HEAT 86693, AIR-MELT (3.5 IN.) THICK PLATE, PROPERTIES AT ¼ T LOCATION, ROLLING RATIO OF 1.0, ALSO, TRANSVERSE RESULTS FOR VAR HEAT 5562

| Heat Treatment | 68 J. (50 Ft.-Lb.) Transition Temperature | | 0.89 MM (35 Mils) Lateral Expansion Transition Temperature | | 50% Fracture Appearance Transition Temperature | | NDT | Reference NDT | Upper Shelf CVN Fracture Energy (93°C {200°F}) | |
|---|---|---|---|---|---|---|---|---|---|---|
| | °C | (°F) | °C | (°F) | °C | (°F) | °C (°F) | (RT, NDT)* | J. | (Ft.-Lb.) |
| A | 29 | (84) | 11 | (52) | 32 | (90) | (30) | (30) | 118 | (87) |
| B | -10 | (14) | -13 | (8) | 22 | (72) | (30) | (30) | 203 | (150) |
| C (VAR)** | 2 | (35) | -4 | (25) | 29 | (85) | (20) | (20) | 125 | (92) |
| D | 36 | (96) | 14 | (58) | 46 | (114) | (20) | (20) | 102 | (75) |
| E | 13 | (56) | 7 | (45) | 19 | (66) | (30) | (30) | 129 | (95) |

* Determined according to the ASME B&PV Code, Section III, No. NB-2300.

** Results by H. P. Offer (G.E.) on the same VAR Heat No. (55262), different plate. Funded under 189a-SG029.

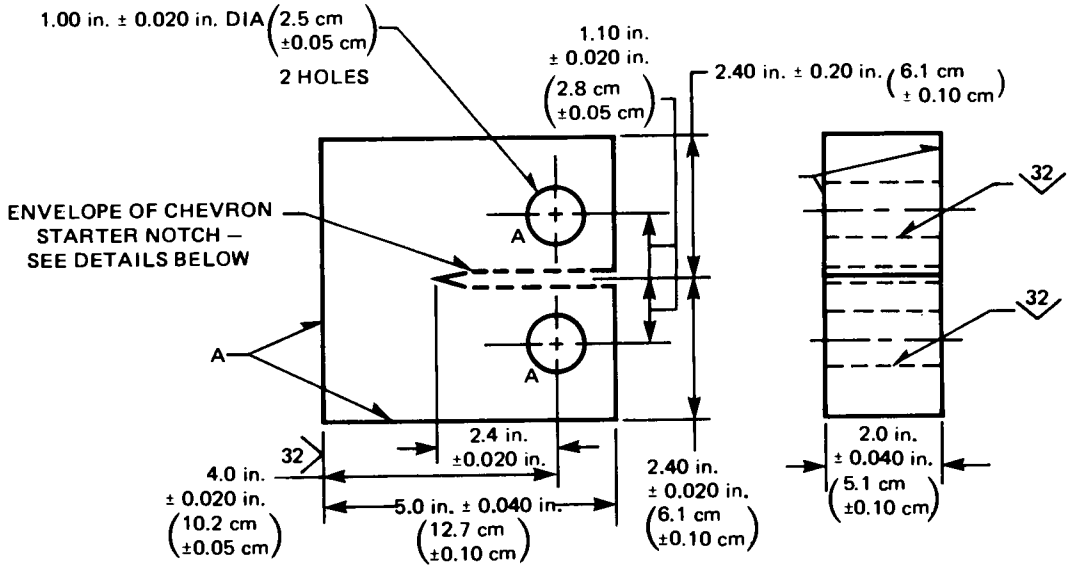


NOTE 1 – A SURFACES SHALL BE PERPENDICULAR AND PARALLEL WITHIN 0.001 in. (0.0025 cm) TIR

NOTE 2 – CRACK STARTER PERPENDICULAR TO SPECIMEN LENGTH AND THICKNESS TO WITHIN ± 2 DEG

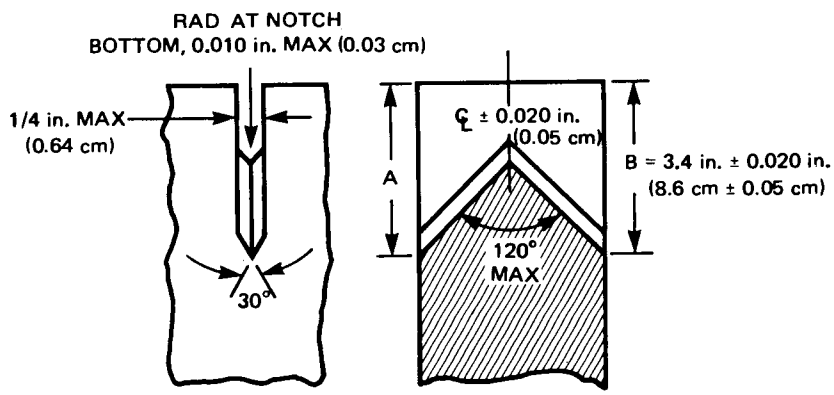


CHEVRON NOTCH CRACK STARTER DETAILS

NOTE 1 – A = B TO WITHIN 0.040 in. (0.10 cm)

Figure 8.44. *50.8 mm (2 in.) Thick Compact Tension Specimen for Fracture Toughness. Drawing Dimensions in Inches (mm).*

Figure 8.45. *Typical 50.8 mm (2 in.) Thick Compact Tension Specimen Fracture Surface After $J_{ic}$ Test, Heat Treatment A, 24°C (75°F). Shows (From Top) Machined Chevron Notch, Fatigue Precrack, Crack Extension During Test (Dark Cresent), and Brittle Separation Fracture (−196°C [−320°F] for Convenience).*

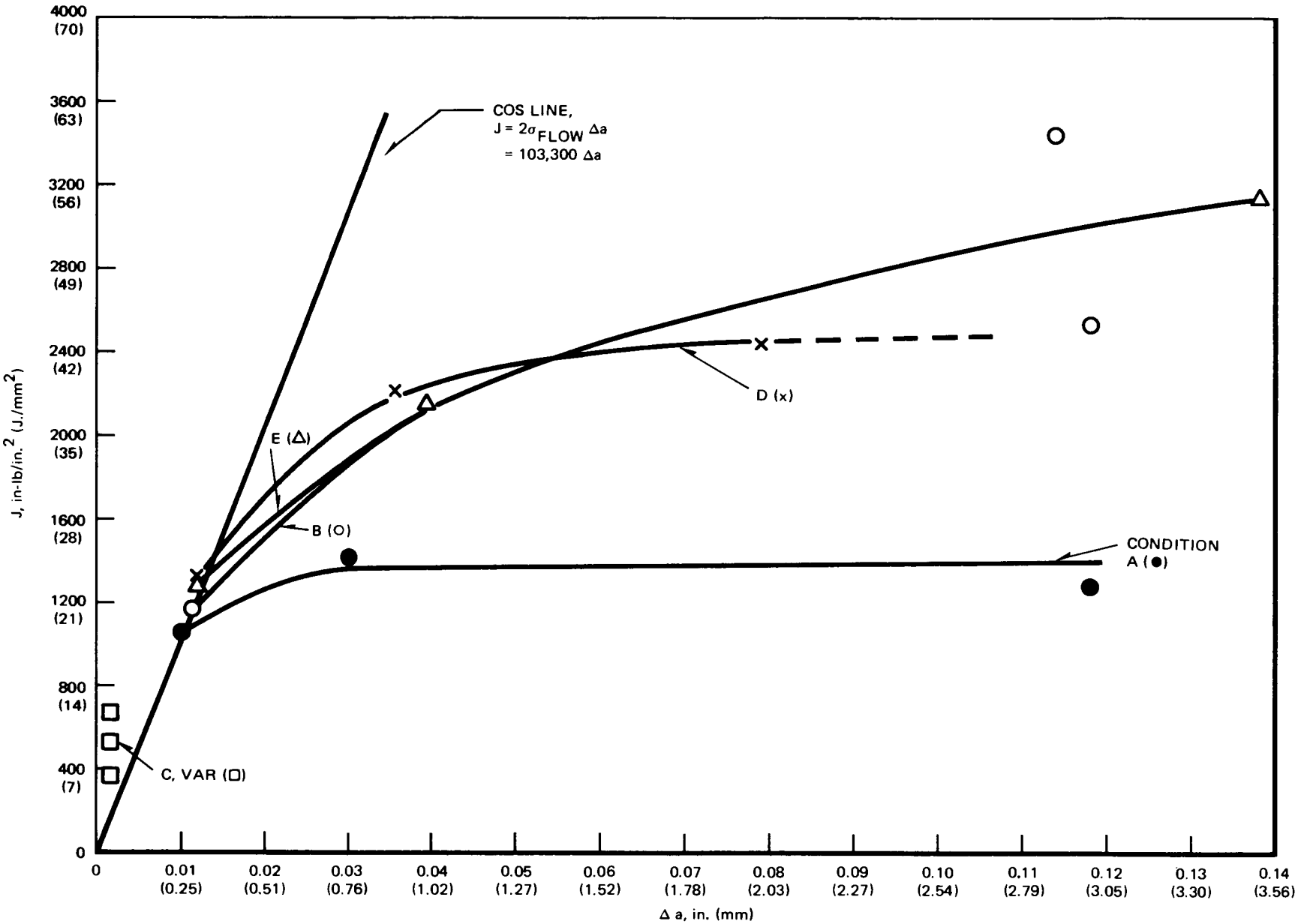


Figure 8.46. J-Integral Resistance Curves for 2¼Cr-1Mo Material Conditions at 24°C (75°F) Showing J-Integral Values (J) Versus Crack Extension (Δa) at Specimen Unloading.

# TABLE 8.23

Compact Tension Specimen (50.8 mm. (2 in.) Thick)
Fracture Toughness Results for 2¼Cr-1Mo Heat 86693.
Air-Melt 89 mm. (3.5 in.) Thick Plate with Rolling
Ratio of 1.0. Also, Transverse Results for VAR
Heat 55262, 50.8 mm. (2 in.) Thick Plate. Specimen
Load Point Displacement Rate of 1.52 mm/min. (0.06 in./min.).
All tests at 24°C (75°F).

| Spec. No. | Heat Treatment | Stable Crack Extension, Δa, at Unload. mm. | (in.) | Remarks | J at Unload J./mm² | (in-lb/in.²) | J at COS*, $J_{Ic}$ J./mm² | (in-lb/in.²) | $K_{Ic}$ MPa $\sqrt{m.}$ | (Ksi $\sqrt{in}$ |
|---|---|---|---|---|---|---|---|---|---|---|
| G1 | | 0.25 | (0.0099) | COS* only. | 18.4 | (1050) | | | | |
| G2 | A | 3.00 | (0.1180) | Stable Δa. | 22.6 | (1290) | 18.4 | (1050) | 206 | (187) |
| G3 | | 0.76 | (0.030) | Δa, Pop-in. | 24.9 | (1425) | | | | |
| G6 | | 0.70 | (0.0276) | Δa, Pop-in. | 20.3 | (1160) | | | | |
| G7 | B | 3.00 | (0.1180) | Stable Δa. | 44.5 | (2540) | 20.3 | (1160) | 216 | (196) |
| G8 | | 2.90 | (0.1140) | Stable Δa. | 60.2 | (3440) | | | | |
| GV1 | | ——— | | Pop-in. | 9.3 | (530) | 9.3 | (530) | 145 | (132) |
| GV2 | C (VAR) | ——— | | Pop-in. | 11.7 | (670) | 11.7 | (670) | 164 | (149) |
| GV3 | | ——— | | Pop-in. | 6.5 | (370) | 6.5 | (370) | 121 | (110) |
| G10 | | 0.30 | (0.0118) | Δa, Pop-in. | 23.1 | (1320) | | | | |
| G11 | D | 0.90 | (0.0355) | Δa, Pop-in. | 38.8 | (2220) | 24.5 | (1400) | 236 | (215) |
| G12 | | 2.00 | (0.0790) | Stable Δa. | 42.8 | (2450) | | | | |
| G14 | | 0.30 | (0.0118) | Δa, Pop-in. | 22.6 | (1290) | | | | |
| G15 | E | 1.00 | (0.0394) | Stable Δa. | 37.6 | (2150) | 22.9 | (1310) | 229 | (208) |
| G16 | | 3.50 | (0.1380) | Stable Δa. | 54.9 | (3140) | | | | |

* Crack Opening Stretch - No Real Crack Extension

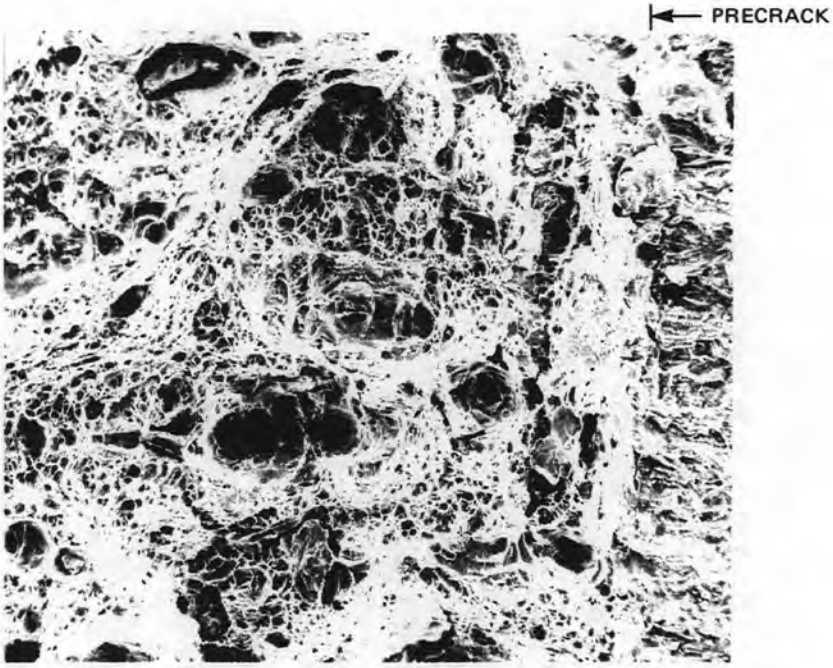


100X

A. SPECIMEN G7 (TREATMENT B), CTS, SHOWING FATIGUE PRECRACK (RIGHT) AND DUCTILE, STABLE CRACK EXTENSION ZONE

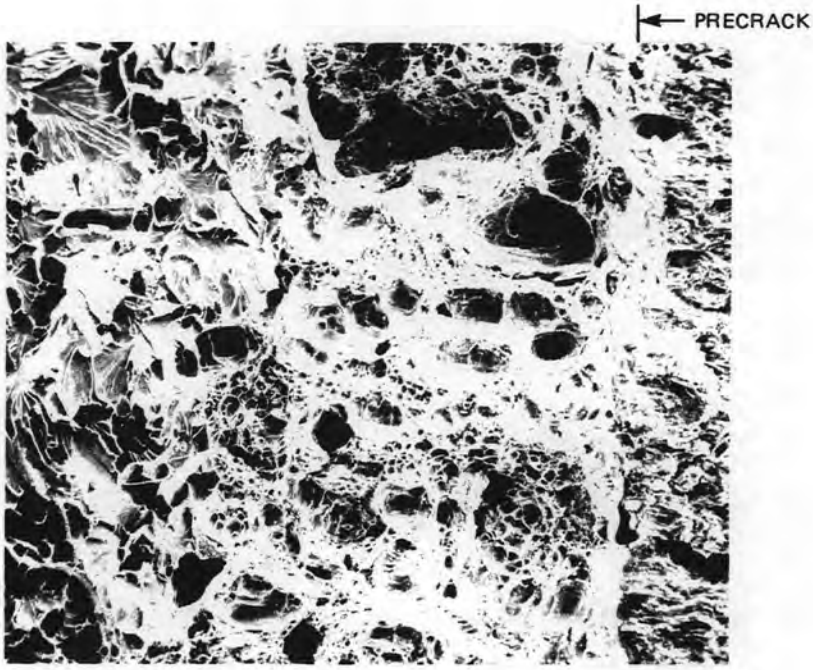


100X

B. SPECIMEN G6 (TREATMENT B), CTS, SHOWING PRECRACK (RIGHT), DUCTILE, STABLE CRACK EXTENSION AND QUASI-CLEAVAGE (LEFT) WHICH CHARACTERIZES BRITTLE POP-IN.

Figure 8.47. *Scanning Electron Micrographs Characterizing Specimens for Various Material Conditions Which Did and Did Not Experience Brittle Pop-in*

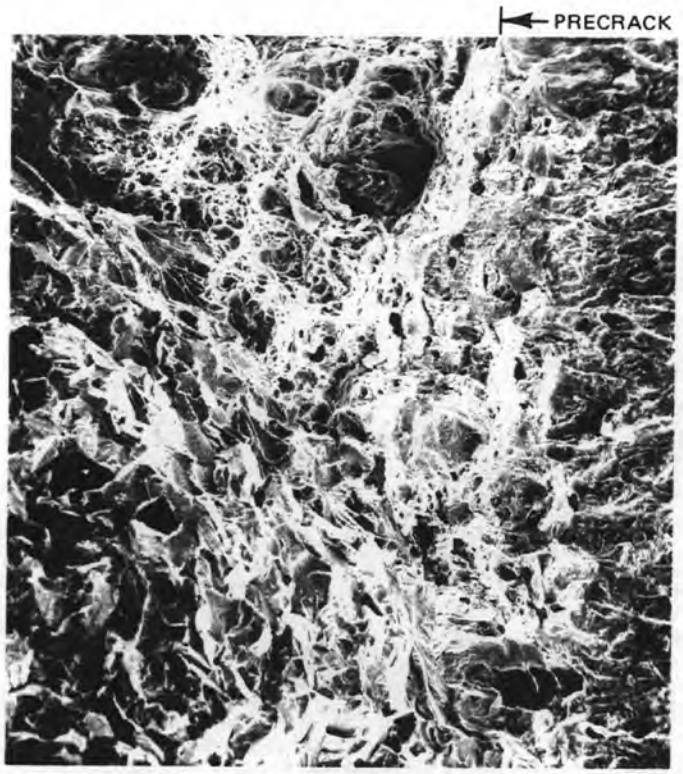


C. SPECIMEN G14 (TREATMENT E), CTS, SHOWING FATIGUE PRECRACK (RIGHT), SMALL REGION OF DUCTILE, STABLE CRACK EXTENSION (TOP, LEFT), AND QUASI-CLEAVAGE (BOTTOM, LEFT) CHARACTERIZING POP-IN.

D. SPECIMEN G14 (TREATMENT E), CTS, SHOWING FATIGUE PRECRACK (RIGHT) AND QUASI-CLEAVAGE (LEFT) CHARACTERIZING BRITTLE POP-IN. DIFFERENCE IN ELEVATION BETWEEN PRECRACK AND QUASI-CLEAVAGE ZONES INDICATES CRACK OPENING STRETCH PRIOR TO CRACK GROWTH.

Figure 8.47. Scanning Electron Micrographs Characterizing Specimens for Various Material Conditions Which Did and Did Not Experience Brittle Pop-in. (Continued)

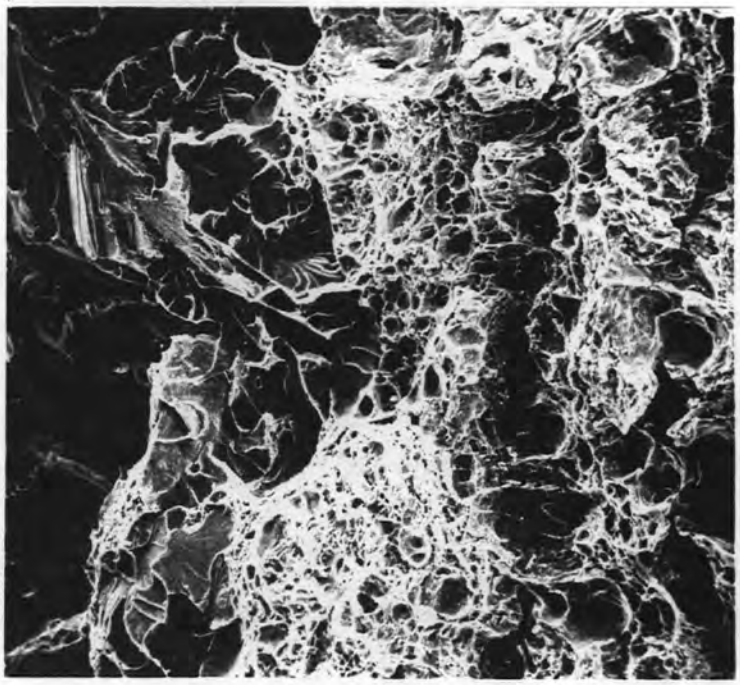

250X

E. CHARPY SPECIMEN (TREATMENT D) FRACTURED AT 43°C (110°F), SHOWING DUCTILE ZONE (MICROVOID COALESCENCE) AT EDGE OF SPECIMEN (RIGHT) AND QUASI-CLEAVAGE (LEFT)

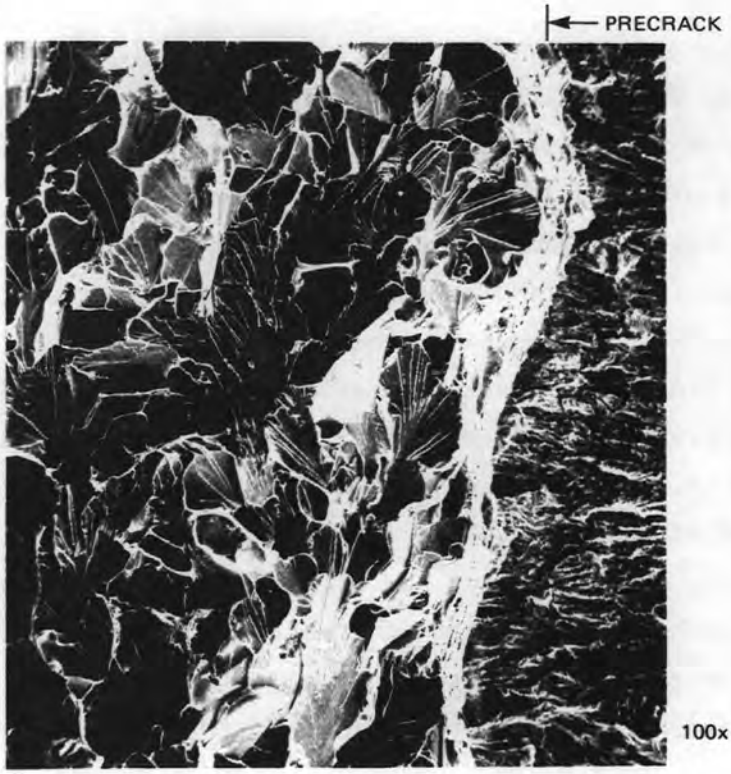


100x

F. SPECIMEN GV1 (TREATMENT C), CTS, SHOWING FATIGUE PRECRACK (RIGHT) AND CLEAVAGE ZONE (LEFT) CHARACTERISTIC OF BRITTLE POP-IN

Figure 8.47. Scanning Electron Micrographs Characterizing Specimens for Various Material Conditions Which Did and Did Not Experience Brittle Pop-in. (Continued)

that: (a) some ductility is seen, as with microvoid coalescence, (b) river patterns tend to radiate from the center of the cleavage facets, and (c) fracture is not confined to strictly cleavage planes. Large sulfide inclusions were found in the ductile crack extension regions of both specimens. No reason for the difference in behavior of the two specimens was apparent, except that the test temperature was very close to the CVN 50% Fracture Appearance Transition Temperatures (Table 8.23), and statistical scatter in the fracture mode would be expected. Figures 8.47c and d illustrate similar behavior for a condition E specimen which had pop-in. Figure 8.47e shows a CVN fracture for condition D, a potential temper embrittlement treatment. Although the CVN values are lower for D than for B, no intergranular fracture (characteristic of temper embrittlement) is observed. These CVN values are being rechecked. Figure 8.47f, representing the VAR material, shows no stable crack extension on the microscopic scale, but illustrates the immediate initiation of cleavage fracture. CVN specimens will be run from this plate (broken CTS piece) to determine the transition temperatures.

The $K_{Ic}$ results of this study are shown in comparison to the Code $K_{IR}$ curve in Figure 8.48. The values all fall above the curve for this temperature, and indicate safe performance when Appendix G and the $K_{IR}$ curve, design, loading and inspection approaches are followed. Thus must also be verified at the higher service temperatures. Also, further statistical confidence (especially heat-to-heat variation) is desired at the hydrotest temperature of approximately room temperature. Figure 8.49 illustrates the effect of fracture toughness and applied stress on the maximum crack size allowed to prevent fast fracture. For applied stresses above 138 MPa (20 Ksi), inspection for flaws becomes critical, especially for the lower fracture toughness.

Further specimens are currently being machined for elevated temperature J-Integral tests of air-melt material. SMAW weldments are also being prepared for weld metal and HAZ testing.

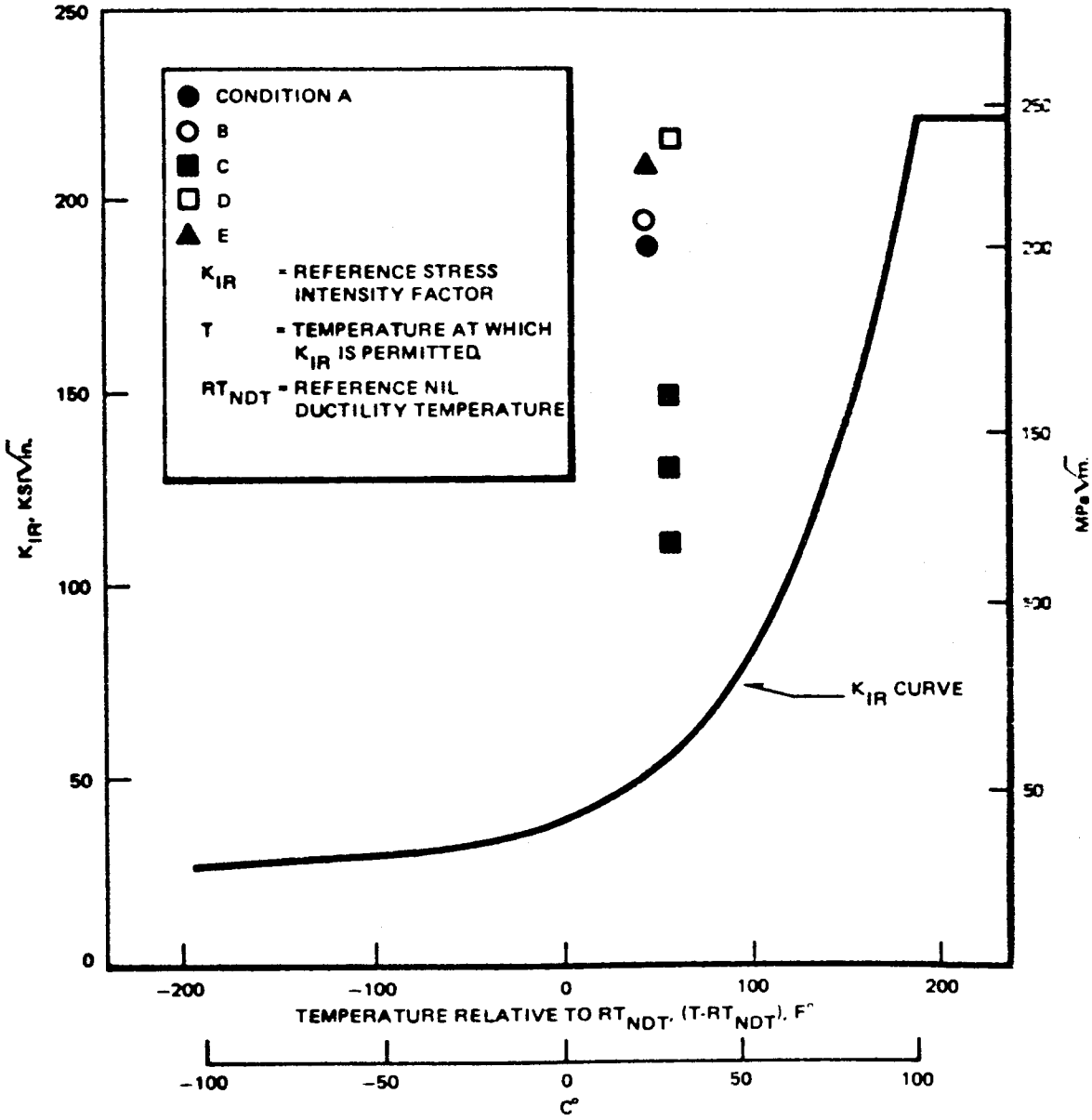


Figure 8.48. *Comparison of Fracture Toughness Data with ASME Code Section III $K_{IR}$ Curve*

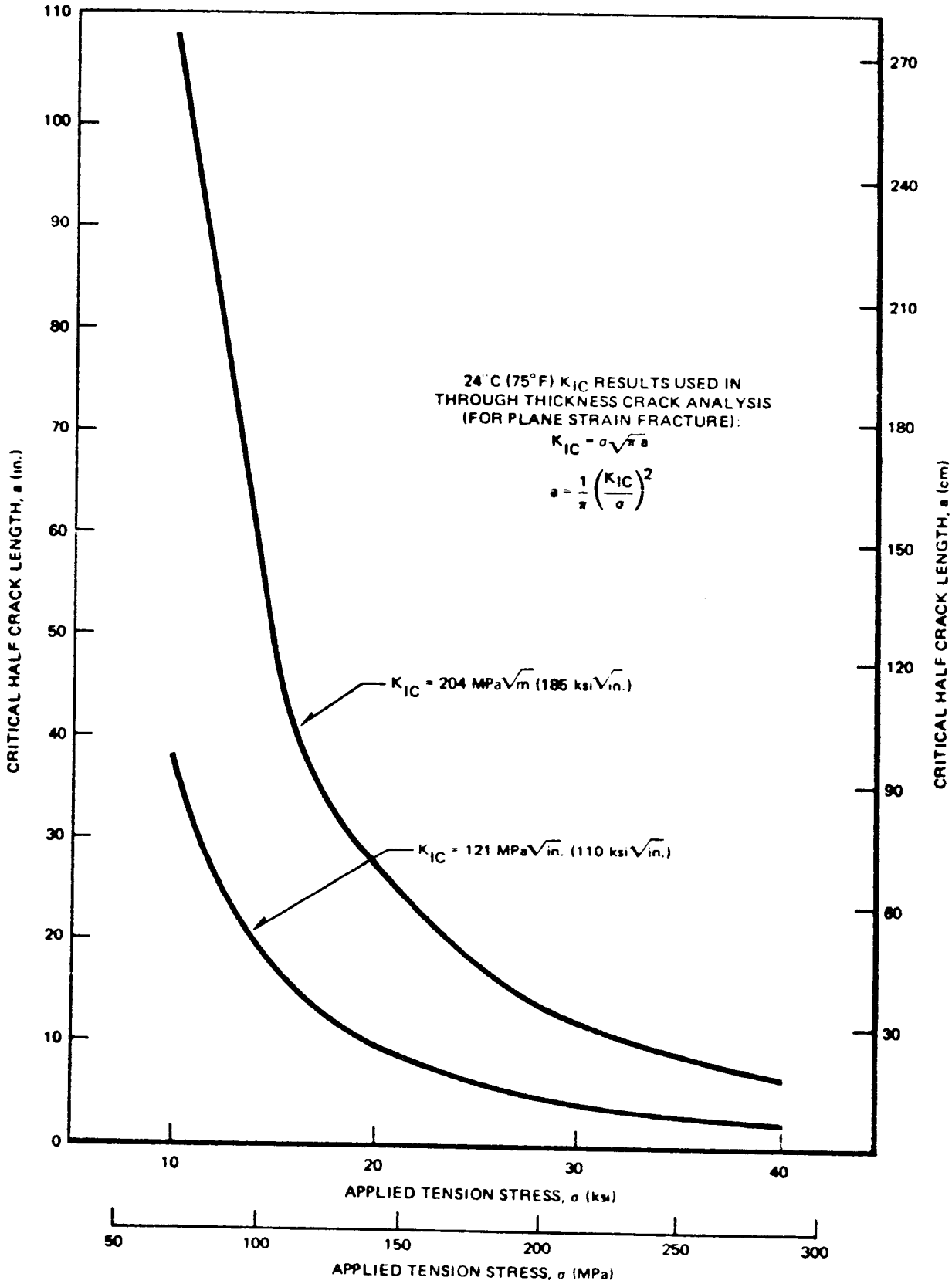


Figure 8.49. *Half Critical Flaw Length (for Through Thickness Crack in Tension) as Related to 24°C (75°F) Fracture Toughness and Applied Stress.*

## 8.6 REFERENCES


1. "Program for the Development of Design Data - LMFBR Steam Generator Materials" prepared for the ERDA under contract at (04-3)-893 Task 10-G and Task 18, July 16 & 17, 1975
2. L. A. James, "Effect of Thermal Aging Upon the Fatigue-Crack Propagation of Austenitic Stainless Steels", Met. Trans., Vol. 5, Apr. 1974, pp. 831-838
3. P. Shahinian et al, "Fatigue Crack Growth in Type 316 Stainless Steel at High Temperature", Trans. ASME, Nov. 1971, pp. 976-980
4. P. Marshall, "The Fatigue Behavior of Annealed AISI 316 Stainless steel in Air and High Temperature Sodium: Review and Preliminary Results", Central Electricity Generating Board, Report RD/B/N 3236, Nov. 1974.
5. L. A. James and R. L. Knecht, "Fatigue-Crack Propagation Behavior of Type 304 Stainless Steel in a Liquid Sodium Environment", Met. Trans., Vol. 6A, Jan. 1975, pp. 109-116.
6. Fifth Quarterly Report, Steam Generator Materials Engineering, July - September 1975, GEAP-14029-5, U.S. ERDA Contract E (04-3)-893 Task 18, Oct. 1975
7. Communication, P. Patriara to D. Weinstein, "Linear-Simulated 2¼Cr-1Mo Steel Tube-to-Tube Sheet Weldment", May 16, 1974
8. LMFBR Steam Generator Materials - Program for the Development of Design Data, July 16 - 17, 1975, prepared for ERDA under Contract AT(04-3)-893, Task 10-G and 18.
9. J. F. Copeland, "Factors Influencing the Notch Toughness and Transition Temperature of ASTM A542 Steel", PhD Dissertation, Department of Metallurgy and Materials Science, Lehigh University, 1973.

INDEX


| Test | Material | Page |
|---|---|---|
| Creep Test Data | | |
| Base-Line Data | | |
| | type 304 SS . . . . . | 21–30 |
| | type 304 SS, Na preexposed. . . | 21–30 |
| | type 304 SS bar . . . . . | 151–153 |
| | type 304 SS plate . . . . . | 37–44, 198 |
| | type 304 SS tube . . . . . | 206 |
| | type 304 SS welded bar . . . . | 206 |
| | type 304 SS welded plate. . . . | 200 |
| | type 304-308 SS weld . . . . . | 142–143 |
| | type 316 SS . . . . . | 147 |
| | type 316 SS tube. . . . . | 206, 280–286 |
| | 2 1/4 Cr-1 Mo steel . . . . . | 304–355 |
| | 2 1/4 Cr-1 Mo weld metal. . . . | 287–304 |
| Base-Line (INEL Ht Tr) | | |
| | alloy 718 . . . . . | 11–18 |
| Correlations | | |
| | type 304 SS . . . . . | 30–34, 44–56, 67–75 |
| | type 304 SS Na preexposed . . . | 30–34 |
| | 2 1/4 Cr-1 Mo . . . . . | 103–125, 127–132 |
| Effect of Aging | | |
| | type 304 SS . . . . . | 63–67 |
| Effect of Cold Work | | |
| | type 304 SS . . . . . | 249–272 |
| Effect of Cyclic Loading | | |
| | type 304 SS . . . . . | 144–146 |
| | 2 1/4 Cr-1 Mo . . . . . | 150 |
| Effect of Cycling | | |
| | type 316 SS tube . . . . . | 280–286 |
| | 2 1/4 Cr-1 Mo tube, weld metal. | 287–304 |

| Test | Material | Page |
|---|---|---|
| Creep Test Data (Continued) | | |
| Effect of Heat Treatment | | |
| | type 308 SS weld metal. . . . . | 80–85 |
| Effect of HTGR Coolant | | |
| | Hastelloy X . . . . . | 161–162 |
| Effect of Hold Time | | |
| | type 316 SS . . . . . | 278–280 |
| Effect of Mechanical Pretreatment | | |
| | type 304 SS . . . . . | 144–146 |
| Effect of Sodium Exposure | | |
| | type 316 SS tube (carburizing). . | 280–286 |
| | 2 1/4 Cr-1 Mo weld metal. . . . . | 287–304 |
| Heat-to-Heat Variation | | |
| | type 304 SS . . . . . | 44–56 |
| Interrupted Tests | | |
| | type 304 SS bar . . . . . | 154 |
| Multiaxial Tests | | |
| | type 304 SS bar . . . . . | 151–161 |
| Elastic Constants | | |
| Static Measurements | | |
| | type 304 SS . . . . . | 77–80 |
| | 2 1/4 Cr-1 Mo . . . . . | 77–80 |
| Distribution in Weld Metal | | |
| | type 308 SS . . . . . | 85–91 |
| Dynamic Measurements | | |
| | Inconel 82 weld metal . . . . . | 133–141 |
| | Inconel 666 . . . . . | 133–141 |
| | type 16-8-2 SS weld metal . . . . | 133–141 |
| Fatigue Test Data | | |
| Base and Weld (INEL Ht Tr) | | |
| | alloy 718 . . . . . | 1–6 |
| Crack Growth Rate | | |
| Base-Line Data | | |
| | type 316 SS plate . . . . . | 276–280 |

| Test | Material | Page |
|---|---|---|
| Crack Growth Rate (Continued) | | |
| Effect of Frequency | | |
| | 2 1/4 Cr-1 Mo | 168–170 |
| | type 316 SS | 276–280 |
| Effect of Environment | | |
| | 2 1/4 Cr-1 Mo | 170–172 |
| Effect of Hold Time | | |
| | type 316 SS | 186–191 |
| | type 316 SS plate | 276–280 |
| Effect of Specimen Thickness | | |
| | type 304 SS | 179–185 |
| Effect of Stress Intensity Factor | | 276–280 |
| Heat-to-Heat Variation | | |
| | 2 1/4 Cr-1 Mo | 168–170 |
| Cyclic Fatigue Tests Data | | |
| Effect of Sodium Environment | | |
| | type 304 SS | 19–21 |
| | type 304 SS, Na preexposed | 19–21 |
| Data Analysis | | |
| | 2 1/4 Cr-1 Mo | 101–108 |
| Dislocation Microstructure | | |
| | Incoloy 800 | 224–248 |
| Effect of Aging Hold Time | | |
| | Inconel 718 plate | 216–221 |
| Effect of Sodium Environment | | |
| | type 304 SS | 19–21 |
| | type 304 SS, Na preexposed | 19–21 |
| | type 316 SS plate | 209–216 |
| Mean Stress Effects | | |
| | alloy 718 | 6–11 |
| Microstructure | | |
| | Incoloy 800, fatigue tested | 224–248 |

| Test | Material | Page |
|---|---|---|
| Fatigue Test Data (Continued) | | |
| Strain-Controlled Tests | | |
| | Hastelloy X | 162–168 |
| Hardness Data | | |
| Correlations | | |
| | 2 1/4 Cr-1 Mo | 127–128 |
| Relaxation Data | | |
| | type 316 SS | 147–148 |
| | 2 1/4 Cr-1 Mo | 148–150 |
| Tensile Test Data | | |
| Base-Line Data | | |
| | 2 1/4 Cr-1 Mo | 304–351 |
| Correlations | | |
| | 2 1/4 Cr-1 Mo | 124–128 |
| Effect of Aging | | |
| | type 304 SS | 56–63 |
| | type 316 SS | 56–63 |
| Effect of Heat Treatment | | |
| | 2 1/4 Cr-1 Mo | 92–101 |
| Effect of Strain Rate | | |
| | 2 1/4 Cr-1 Mo | 91–92 |
| | type 316 SS | 146–147 |
| Toughness | | |
| Charpy V-Notch | | |
| | 2 1/4 Cr-1 Mo | 304–374 |
| J-Integral | | |
| | 2 1/4 Cr-1 Mo | 351–374 |
| Drop Weight NDT | | |
| | 2 1/4 Cr-1 Mo | 304–374 |

ORNL-5112
UC-79b, -h, -k
(Liquid Metal Fast
Breeder Reactors)

INTERNAL DISTRIBUTION

1–2. Central Research Library
3. Document Reference Section
4–8. Laboratory Records Department
9. Laboratory Records, ORNL RC
10. ORNL Patent Office
11. R. J. Beaver
12. R. G. Berggren
13. J. J. Blass
14. M. K. Booker
15. C. R. Brinkman
16. D. A. Canonico
17. J. Corum
18. W. R. Corwin
19. F. L. Culler
20. J. E. Cunningham
21. J. H. DeVan
22. D. P. Edmonds
23. G. Fee
24. M. H. Fontana
25. W. R. Gall
26. B. L. Greenstreet
27. J. C. Griess, Jr.
28. J. P. Hammond
29. W. O. Harms
30. R. L. Heestand
31–33. M. R. Hill
34. D. O. Hobson
35. H. Inouye
36. P. R. Kasten
37. J. F. King
38. R. T. King
39. R. L. Klueh
40. K. C. Liu
41. C. T. Liu
42. A. L. Lotts
43–63. W. R. Martin
64. W. J. McAfee
65. H. E. McCoy
66. H. C. McCurdy
67. C. J. McHargue
68. J. Merkle
69. P. Patriarca
70. S. Peterson
71. H. Postma
72. C. E. Pugh
73. P. L. Rittenhouse
74. D. N. Robinson
75. T. Roche
76. J. L. Scott
77. Myrtleen Sheldon
78. V. K. Sikka
79. G. M. Slaughter
80. W. J. Stelzman
81. J. P. Strizak
82. R. W. Swindeman
83. D. B. Trauger
84. T. N. Washburn
85. J. R. Weir, Jr.
86. G. D. Whitman
87. T. Yahr
88. W. C. Leslie (consultant)
89. John Moteff (consultant)
90. Hayne Palmour III (consultant)
91. J. W. Prados (consultant)
92. N. E. Promisel (consultant)
93. G. V. Smith (consultant)
94. D. F. Stein (consultant)

EXTERNAL DISTRIBUTION

95–96. USERDA DIVISION OF NUCLEAR FUEL CYCLE AND PRODUCTION, Washington, DC 20545

Director

97–98. USERDA DIVISION OF REACTOR RESEARCH AND DEVELOPMENT, Washington, DC 20545

Director

99–100. USERDA OAK RIDGE OPERATIONS OFFICE, P.O. Box E, Oak Ridge, TN 37830

Research and Technical Support Division
Director, Reactor Division

101-354. USERDA TECHNICAL INFORMATION CENTER, Office of Information Services, P.O. Box 62, Oak Ridge, TN 37830

For distribution as shown in TID-4500 Distribution Category, UC-79b (Fuels and Materials Engineering Development); UC-79h (Structural Materials Design Engineering); UC-79k (Components)

☆ U.S. GOVERNMENT PRINTING OFFICE: 1976-748-189/269